ACS SYMPOSIUM SERIES [illegible]

Degradable Polymers and Materials

Principles and Practice

EDITED BY
Kishan Khemani and Carmen Scholz

Degradable Polymers and Materials

Downloaded by 89.163.35.42 on August 9, 2012 | http://pubs.acs.org
Publication Date: September 23, 2006 | doi: 10.1021/bk-2006-0939.fw001

Downloaded by 89.163.35.42 on August 9, 2012 | http://pubs.acs.org
Publication Date: September 23, 2006 | doi: 10.1021/bk-2006-0939.fw001

Downloaded by 89.163.35.42 on August 9, 2012 | http://pubs.acs.org
Publication Date: September 23, 2006 | doi: 10.1021/bk-2006-0939.fw001

ACS SYMPOSIUM SERIES **939**

Degradable Polymers and Materials

Principles and Practice

Kishan C. Khemani, Editor
Plantic Technologies Limited

Carmen Scholz, Editor
University of Alabama in Huntsville

Sponsored by the
ACS Division of Polymer Chemistry, Inc.

American Chemical Society, Washington, DC

Library of Congress Cataloging-in-Publication Data

American Chemical Society. Meeting (229th : 2005 : San Diego, Calif.)
Degradable polymers and materials : principles and practice / Kishan C. Khemani, editor, Carmen Scholz, editor.

p. cm.—(ACS symposium series ; 939)

"Developed from a symposium sponsored by the Division of Agricultural and Food Chemistry, Inc. at the 229th National Meeting of the American Chemical Society, San Diego, California, March 13–17, 2005"—T.p. verso.
"Sponsored by the ACS Division of Agricultural and Food Chemistry, Inc.

Includes bibliographical references and index.

ISBN-13: 978–0–8412–3972–2 (alk. paper)

1. Polymers—Biodegradation—Congresses.

I. Khemani, Kishan C., 1955– II. Scholz, Carmen, 1963– III. American Chemical Society. Division of Agricultural and Food Chemistry, Inc. IV. Title. V. Series.

QP801.P64A44 2005
620.1'90423—dc22 2006042722

The paper used in this publication meets the minimum requirements of American National Standard for Information Sciences—Permanence of Paper for Printed Library Materials, ANSI Z39.48–1984.

Copyright © 2006 American Chemical Society

Distributed by Oxford University Press

All Rights Reserved. Reprographic copying beyond that permitted by Sections 107 or 108 of the U.S. Copyright Act is allowed for internal use only, provided that a per-chapter fee of $33.00 plus $0.75 per page is paid to the Copyright Clearance Center, Inc., 222 Rosewood Drive, Danvers, MA 01923, USA. Republication or reproduction for sale of pages in this book is permitted only under license from ACS. Direct these and other permission requests to ACS Copyright Office, Publications Division, 1155 16th Street, N.W., Washington, DC 20036.

The citation of trade names and/or names of manufacturers in this publication is not to be construed as an endorsement or as approval by ACS of the commercial products or services referenced herein; nor should the mere reference herein to any drawing, specification, chemical process, or other data be regarded as a license or as a conveyance of any right or permission to the holder, reader, or any other person or corporation, to manufacture, reproduce, use, or sell any patented invention or copyrighted work that may in any way be related thereto. Registered names, trademarks, etc., used in this publication, even without specific indication thereof, are not to be considered unprotected by law.

PRINTED IN THE UNITED STATES OF AMERICA

Downloaded by 89.163.35.42 on August 9, 2012 | http://pubs.acs.org
Publication Date: September 23, 2006 | doi: 10.1021/bk-2006-0939.fw001

Downloaded by 89.163.35.42 on August 9, 2012 | http://pubs.acs.org
Publication Date: September 23, 2006 | doi: 10.1021/bk-2006-0939.fw001

Foreword

The ACS Symposium Series was first published in 1974 to provide a mechanism for publishing symposia quickly in book form. The purpose of the series is to publish timely, comprehensive books developed from ACS sponsored symposia based on current scientific research. Occasionally, books are developed from symposia sponsored by other organizations when the topic is of keen interest to the chemistry audience.

Before agreeing to publish a book, the proposed table of contents is reviewed for appropriate and comprehensive coverage and for interest to the audience. Some papers may be excluded to better focus the book; others may be added to provide comprehensiveness. When appropriate, overview or introductory chapters are added. Drafts of chapters are peer-reviewed prior to final acceptance or rejection, and manuscripts are prepared in camera-ready format.

As a rule, only original research papers and original review papers are included in the volumes. Verbatim reproductions of previously published papers are not accepted.

ACS Books Department

In Degradable Polymers and Materials; Khemani, K., et al.;
ACS Symposium Series; American Chemical Society: Washington, DC, 2006.

Preface

A revolution is in the making in the world, where scientists are working very hard to discover viable biodegradable and natural renewable resource-based alternatives to the fossil-fuel-based, non-degradable polymers and materials. This movement is driven by the growing general awareness among the consumers and governmental agencies in most countries that conventional plastic products, although useful, are doing tremendous damage to their environment, marine and animal life, water supplies, sewer systems, and the rivers and streams. This is further exasperated by the more obvious eyesore of the littering problems that are associated with these non-degradable products, which have created a public outcry that something must be done about it.

The modern petrochemicals-based plastics industry realized more than 20 years ago that it is unsustainable in the long run, because of the limited and rapidly depleting raw material source. Combined with the growing discontent of worldwide plastics-consuming communities with their plastic litter problems, it did not take long before most major plastics manufacturers had launched research programs aimed at developing biodegradable polymers. Although the initial efforts were mostly aimed at making hydrolysable polymers, such as polyesters and polyamides, biodegradable via the use of aliphatic monomers, the recent shift has been toward the use of renewable resource raw materials, such as starches and proteins.

The 22 main chapters in this symposium series book describe various aspects of current research and development related to design, synthesis, properties, processing, applications, degradation, and biodegradation of a variety of novel polymers and materials. This book was developed from the more than 65 papers presented at the spring meeting of the American Chemical Society (ACS) that was held in San

Downloaded by 89.163.35.42 on August 9, 2012 | http://pubs.acs.org
Publication Date: September 23, 2006 | doi: 10.1021/bk-2006-0939.pr001

Diego, California in March 2005. The tremendous success of the symposium and the lively discussions that followed every presentation attested to the growing interest in this area. A need for a book such as this was quite apparent at the conclusion of the symposium. Because we were restricted by the size of the book by our publisher, the ACS Books Department, we had to make a careful and judicious selection of symposium presentations that were to be included in this book and that could benefit the R&D community. We sincerely regret that we were unable to include all of the symposium presentations in this book. In the end, we selected chapters that highlight the key areas of activities in this fascinating field. The contributing authors, from all around the world, are recognized leaders in their respective fields.

The authors and the editors of this book sincerely hope that the workers, researchers, scientists and engineers working in this and related fields will find this book very useful and helpful in their work and pursuit of novel, environmentally benign, as well as degradable and biodegradable polymers and materials.

Kishan C. Khemani
Chief Science Officer
PolymerResource.com
4751 Amarosa Street
Santa Barbara, CA 93110

Carmen Scholz
Associate Professor
Department of Chemistry
University of Alabama
in Huntsville
John Wright Drive, MSB 333
Huntsville, AL 35899

Downloaded by 89.163.35.42 on August 9, 2012 | http://pubs.acs.org
Publication Date: September 23, 2006 | doi: 10.1021/bk-2006-0939.pr001

Overview

People in developed countries have enjoyed a modern, highly industrialized society since the middle of the last century. Many convenient and industrial products are available at low costs. These products (such as synthetic polymers including plastics, fibers, rubber, and other chemicals) are derived mainly from a petroleum source. In such a society, everything is governed by the economic factors for maintaining a convenient daily life. As a result, however, a serious problem arose: an environmental problem of the Earth! This is more or less related with natural resources, energy (including global warming), foods, and population problems, which we now face.

In the area of polymers, the best possible ways to solve the above problem is definitely the use of degradable polymers and related materials. As a simple example, non-degradable waste plastics brought about a serious damage to the environment, which is a white pollution. Reducing the consumption of crude petroleum and other fossil resources will help us to realize a green sustainable society. Recently, many polymer scientists are pursuing studies in this direction and are designing and preparing various degradable polymers. As shown in this book, degradable commodity polymers, ideally derived from renewable resources are expected to gradually replace petroleum-based polymers. A typical example is poly(lactic acid), which is actually used in the packaging industry and in automobiles. Natural polymers will find new practical applications in various ways. Degradable fine polymers will contribute to better materials for biomedical and drug-delivery applications.

Finally, I highly appreciate the organizers for their very timely contributions to this symposium and for the publication of the presented papers. This book suggests to the readers an important direction of future research into polymeric materials. Polymer scientists should always take into account the environmental problems, which are one of the most important and serious problems confronting the 21st century.

Shiro Kobayashi
Distinguished Professor
R & D Center for Biobased Materials
Kyoto Institute of Technology
Matsugasaki, Sakyo-ku
Kyoto 6068585
Japan

Downloaded by 89.163.35.42 on August 9, 2012 | http://pubs.acs.org
Publication Date: September 23, 2006 | doi: 10.1021/bk-2006-0939.pr001

Chapter 1

Introduction

Carmen Scholz[1] and Kishan Khemani[2]

[1]Department of Chemistry, University of Alabama in Huntsville,
301 Sparkman Drive, Huntsville, AL 35899
[2]Plantic Technologies Ltd., Unit 2, Angliss Park Estate, 227–231 Fitzgerald
Road, Laverton North, Victoria 3026, Australia

Downloaded by 89.163.35.42 on August 9, 2012 | http://pubs.acs.org
Publication Date: September 23, 2006 | doi: 10.1021/bk-2006-0939.ch001

Introduction

This book describes some recent developments in natural and synthetic degradable and biodegradable polymers and materials, including their synthesis and assembly, characterization and degradation studies, as well as the design and exploration of such materials for specific and alternative eco-friendly and sustainable applications to conventional polymers and materials. The twenty five chapters in this book have been written by world's leading researchers in their respective areas. Here, these chapters have been organized in the order such that they describe advances in natural polymers, natural and synthetic polymers, polymer synthesis, characterization and finally degradation mechanisms.

Several chapters of this book are dedicated to natural polymers, which are inherently biodegradable due to their natural origin. Chemical modifications of natural polymers lead to enhanced properties, typically tailored to specific applications and it is often possible to sustain biodegradability despite chemical conversions of the natural polymers. Since ester bonds readily undergo hydrolysis, various polyesters are considered (bio)degradable and are the focus of many studies that aim at the synthesis of novel, environmentally benign materials, from biomedical materials to lubricants and packaging. In many cases the judicious placement of selected co-monomers within the polyester backbone guarantees a controlled, time-dependent degradability. While it is easy to claim

In Degradable Polymers and Materials; Khemani, K., et al.;
ACS Symposium Series; American Chemical Society: Washington, DC, 2006.

degradability for a particular polymer based on its chemical nature, it is more challenging to actually prove degradability. In particular the question of the degradation timeframe has given rise to arguments and discussions. Polymeric materials can degrade physically due to the influence of heat and/or electromagnetic radiation or biologically under the impact of degrading enzymes. Recently, it became possible to identify biochemical pathways for enzymatically catalyzed polymer degradation. Several chapters are dedicated to the characterization of degradable materials, including rules and legislature that define and govern degradable materials. Known polymer analysis techniques have recently been adopted to detect the early onset of polymer disintegration and to make themselves particularly useful to natural polymers and chemically modified natural polymers.

Plastic materials are used worldwide for a multitude of applications, in fact it is very difficult, if not impossible, to imagine life without plastics today. The application range for plastics is extremely wide and includes such high-performance and high-tech applications as Kevlar in bulletproof vests and low-end applications such as garbage and shopping bags. Some of the manufacturing processes for common polymers that we use on a daily basis are known for more than a century, for instance, the making of polystyrene and polyvinylchloride is known since the 1830's. But it was only after World War II that plastics quickly conquered the materials market. Plastic materials were, and still are, appreciated for their durability, impact and tensile strength, reliability and the ability to adjust their properties to match intended uses and in addition, plastics show virtually no corrosion and age slowly. However, with a worldwide increase of plastic waste build-up, paired with a better understanding of the impact of human action on the environment and new and growing environmental awareness, new demands have arisen for plastic materials, specifically their ability to degrade according to a specific, pre-set timetable. Thus, there is a growing general awareness among consumers and government agencies in most countries around the world that conventional plastic products, although useful, are causing tremendous damage to the environment, water supplies, sewer systems as well as to the rivers and streams. While by no means all currently used plastics ought to be replaced by degradable materials, and certainly no plastics in high-performance applications should be degradable. It is paramount to take into account new procedures for plastics production that are based on renewable resources and/or lead to degradable products especially for materials in single-use applications. This book reflects on the latest developments in the area of degradable materials by summarizing new trends in the synthesis, characterization, physical, chemical and degradation behavior as well as information on legislative regulations.

Downloaded by 89.163.35.42 on August 9, 2012 | http://pubs.acs.org
Publication Date: September 23, 2006 | doi: 10.1021/bk-2006-0939.ch001

Every year more than one hundred million tons of plastics are produced worldwide. In 2004, the United States alone produced about 52 million tons of plastics [1,2]. The packaging industry is a major area of interest when considering degradable plastic materials, primarily due to the package's limited life of usage. High and low density polyethylene, polypropylene, polystyrene, polyethylene terephthalate, and polyvinyl chloride and polyvinylidene chlorides cover almost the entire packaging market. While plastics production grew slightly over the past several years, plastics used in the packaging industry stayed constant at approximately 30%, or currently 16 million tons. [2] 70% of all the plastic packaging material, which is roughly 11 million tons, is used for food packaging, thus intended explicitly for short term or single use application. The packaging industry, while it could be the largest consumer of degradable materials, is rather conservative in adopting new technologies. Partially, this is due to the fact that olefin-based polymeric materials have been well established in the industries, both from the manufacturing as well as engineering points of view. Due to the nearly hundred years of process optimization experience, the production of polymers for packaging is highly efficient, stable and hence the resulting polymers are cost-effective and difficult to replace.

By contrast, the manufacturing of naturally derived polymers into packaging materials is a rather novel approach in the industry. Early attempts, dating back to the early 1990's, included embedding of starch granules into polyethylene in an effort to produce a (bio)degradable material. The production of fully biodegradable materials, as defined by the new standards (ASTM D6400, EN 13432, ISO 14855) and certified by agencies such as the Biodegradable Products Institute, the DIN Certico or the AIB Vincotte is still a niche market, with a share of less than 1% of the total market. Some large chemical companies, such as DuPont, Cargill Dow, Monsanto, Eastman and BASF have successfully pursued the development of polyester-based degradable materials. A short list of several biodegradable polymers and their basic properties as well as approximate costs currently available in the market place is given in Table 1.

Smaller and start-up companies, for example Novamont, EarthShell and Plantic are more focused on converting natural renewable resource polymers, such as starch and soy-derivatives, into degradable materials. Due to low volumes and curtailed process optimization, (bio)degradable materials are currently still comparatively expensive as compared to conventional plastics. Whilst consumers in European countries seem to be more agreeable to pay extra price for environmentally friendly products, their American and Japanese

Downloaded by 89.163.35.42 on August 9, 2012 | http://pubs.acs.org
Publication Date: September 23, 2006 | doi: 10.1021/bk-2006-0939.ch001

Downloaded by 89.163.35.42 on August 9, 2012 | http://pubs.acs.org
Publication Date: September 23, 2006 | doi: 10.1021/bk-2006-0939.ch001

Table 1: Biodegradable polymers and their manufacturers

Producer	**Polymer / Class**	**Product Name**	**Approx. Price [USD/kg]**	**Tm [°C]**	**Tg [°C]**	**Sp. Gravity [g/cm3]**
BASF	Aliphatic-Aromatic Polyester	Ecoflex F Ecoflex S Ecoflex U	4.00	105-115	-33	1.25
Bayer	AliphaticPolyester-amide	BAK 1095	4.00	125		1.15
		BAK 2195		175		1.18
Cargill / NatureWorks	Aliphatic Polyester	PLA	3.00	175	57-65	1.25
DuPont	Aromatic Polyester	Biomax PET	3.00	208	50	1.35
Eastman Chemical / Novamont	Aliphatic-aromatic Polyester	EastarBio 14766	4.00			
		GP		112	-30	1.20
		Ultra		115	-30	1.25
IRe	Aliphatic Polyester	Enpol	5.00	90-150	varies	1.20-1.30
Mitsui Chemicals	Aliphatic Polyester	PLA	4.00	173	74	1.26
Novamont	Starch-Polyester – Blend	Mater-Bi	4.00	61 115	-60	1.20
Showa High Polymer	Aliphatic Polyester	Bionolle	6.00	114	-30	1.26
				95	-35	1.23
				102	-4	1.30
Solvay	Aliphatic Polyester	PCL	4.00	60	-60	1.20
Union Carbide	Aliphatic Polyester	Tone / PCL	4.00	61	-60	1.20

counterparts are less inclined to do so. Of course, the imposition of the green-dot disposal fees in several European countries has a lot to do with this trend. At present, use and disposal of non-degradable plastic products is either banned or discouraged through government laws and imposed fees in several countries, and countries such as Germany, The Netherlands, Switzerland, Italy, Ireland etc. have levied taxes on all non-degradable plastic goods. Similar laws are under consideration throughout other European countries. Canada, Japan, Taiwan and South Africa have banned the use of plastic bags. Other developed nations, such as USA, Singapore, Hong Kong, as well as developing nations such as India, China, Mexico are all moving towards legislation discouraging the use of conventional plastic products by levying "disposal tax" for all non-degradable products. The State of Orissa in India banned the use and manufacture of non-biodegradable plastics that is less than 20 microns thick in 2004 and plans on strongly enforcing this law under the Environment Protection Act of 1986. Even in parts of the US, the use of non-degradable plastic bags is either being banned or levied a disposal fee, thereby discouraging their usage. For instance, in Michigan, the use of plastic lawn bags for bagging fallen leaves has been banned. Similarly, in California a legislature last year considered imposing a two-cent tax on retail non-degradable plastic bags but didn't take action. It is very likely that this legislation will be reconsidered sometime in the near future. Other U.S. states will likely follow suit in due course as well. The very high landfill tipping fees in Europe, Japan and other countries also have a positive impact on the development of the biodegradable products and markets in these countries. Some optimistic estimates predict a market share of 10% for biodegradable materials by 2010. While it would certainly be of environmental benefit, it remains to be seen whether this estimate holds up.

After their usability has been exhausted, packaging materials and especially food packaging materials are discarded and end-up as municipal waste. In fact, the extent of plastics production is mirrored by waste generated. In 2001, a total of 229 million tons of municipal waste were collected in the United States [3]. Of all the municipal solid waste, 11% or 25 million tons were plastics. Only 5.5% of this plastic waste was recycled, the remainder was disposed of by combustion or landfill disposal. Despite many efforts made by communities, the recycling efficiency of plastics is still very low and ranges well below the average 30% recycling of the total municipal solid waste. Considering that almost half of the amount of plastics produced every year is discarded and is likely to be permanently deposited in a landfill, it becomes even more urgent to consider replacing current petroleum-based plastics with (bio)degradable materials. The situation is even more dire in developing countries, which often

Downloaded by 89.163.35.42 on August 9, 2012 | http://pubs.acs.org
Publication Date: September 23, 2006 | doi: 10.1021/bk-2006-0939.ch001

lack the means and technologies for an effective waste removal, thus leaving plastic waste to litter entire communities and industrial sites, but also beaches and non-industrialized zones, a phenomenon that has became infamously known as "white litter". For instance in China, the "white line" along its railway lines could be seen from the space and has in fact been identified as the discarded polystyrene lunch boxes thrown out of the moving trains.

Types of Degradable Materials

Natural Polymers

Nature provides a chemically diverse variety of degradable polymers. These polymers were the first materials used by humankind. Early men dressed themselves in hides (proteins, polysaccharides), later in cotton (polysaccharide), silk and wool (proteins). Early men used wood (polysaccharides, polyphenols) for tools and construction materials. Where available natural rubber (polyisoprene) was used for a variety of daily-life functions, from construction to water-proofing storage containers.

Due to their natural origin, that is, an enzyme catalyzed synthesis, all natural polymers are inherently biodegradable. For every polymerase enzyme whose action leads to a natural polymer there is a depolymerase capable of catalyzing the degradation of that natural polymer. In other words, in nature, "if there is a process to make it, there is also a process to break it." Thus, nature keeps a balance in the generation and degeneration of materials. Depolymerase enzymes for individual natural polymers are either present in the polymer-generating species itself, with poly(hydroxyalkanoate) being a prime example, where the natural polymer actually serves as an internal carbon and energy source, or the depolymerase enzyme resides in other species for which the respective natural polymer serves as food source. Fungi and molds are examples for species that are able to degrade, eventually, all natural polymer s and even lignins.

We use the following natural polymers either directly or after physical and/or chemical conversions that aim at improving upon their properties or adding to characteristics. Natural polymers are derived from plants, animals and microorganisms, besides finding extensive use as food, many natural polymers are used as materials in applications ranging from construction and clothing to biomedical materials.

Downloaded by 89.163.35.42 on August 9, 2012 | http://pubs.acs.org
Publication Date: September 23, 2006 | doi: 10.1021/bk-2006-0939.ch001

Polysaccharides are available from plants (starch, cellulose, alginate), animals (chitin), fungi (pullulan) and bacteria (dextran, emulsan, pectin). For a summary on industrial polysaccharides see Stivala et al. [4, 5]. Proteins are produced by all living species in order to maintain their metabolic functions, but from a materials point of view it is the fibrous proteins from plants (soy), animals (wool, silk) [6] and bacteria (polyglutamic acid) that are exploited. Lignin, a polyphenolic compound, [7] and natural rubber, a polyisoprene, [8] are synthesized by plants. Finally, poly(hydroxyalkanoates) are synthesized naturally exclusively by bacteria [9]. Bacterial polymerase genes have also been successfully transferred to plants [10].

Downloaded by 89.163.35.42 on August 9, 2012 | http://pubs.acs.org
Publication Date: September 23, 2006 | doi: 10.1021/bk-2006-0939.ch001

Polymers from Renewable Resources

Polymers from renewable resources are distinct from natural polymers by the fact that their synthesis has been purposely initiated, either a microbial cascade has been triggered or chemical means were employed. Renewable resources are of biological origin and are distinguished by their ability of seasonal (agricultural) renewal or triggered (animal, microbial) renewal. When considering renewable resources for the manufacturing of plastic materials two distinctly different approaches can be taken: *(i) direct conversion of renewable resources into finished polymeric products, and (ii) renewable resources are first converted into small molecules, not unlike an oil refinery, and are subsequently converted by chemical means into plastic materials.* One of the prime example for the first approach is the bacterial production of poly(hydroxyalkanoates). A renewable resource, often a sugar, is converted by enzymatic actions directly into the polymer. The physical properties of this polymer depend upon the polymerization characteristics of the bacterial strain. Every bacterial synthesis leads to one distinct polymer with a microbiologically pre-determined set of physical properties. Another example of this type of use of renewable resource raw material is the water dispersible and biodegradable chocolate trays produced from the use of 90% renewable resource material, corn starch, that are produced and marketed by an Australian start-up company, Plantic Technologies, Ltd. The second approach allows a large variety of polymeric materials with a broad spectrum of physical properties. Given the versatility provided by the second approach, this is, undoubtedly, the more viable option for the future.

Currently, there is no industrial process in place yet that produces plastic materials solely from renewable resources. However, there are hybrid processes that are either chemical processes that use in part renewable resources in their syntheses or combine strictly - biotechnological procedures, that is, fermentation, with organic chemical syntheses to yield polymeric materials.

Sorona, a polyester marketed by DuPont Staley Bio Products Co., LLC [11] is a good example of this. 1,3-Propanediol is the key building block for the synthesis of this polyester. Sorona, that is currently on the market is still made from petroleum-derived 1,3-propanediol, but a joint venture consisting of DuPont and Tate & Lyle PLC, was formed that is developing the technology for the fermentation of corn sugar to yield 1,3-propanediol. Thus, a polymer that is based in part on a renewable resource was developed and it is projected that by 2006 Sorona production will be converted to agriculturally derived 1,3-propanediol.

Poly(lactic acid), produced by NatureWorks LLC, is another example for a hybrid process, in which the monomer, lactic acid is produced by fermentation of corn using lactobacilli. The subsequent polymerization is accomplished either by anionic ring-opening polymerization of the lactide dimer, or more recently by an azeotropic dehydration condensation, a chemical process. Cargill Dow now has shown that the polylactic acid produced by it's subsidiary NatureWorks LLC, is fully competitive with its synthetic counterparts, and fibers can also be melt-spun from this polymer. These Ingeo fibers are "world's first man made fiber made from 100% annually renewable resources." [12].

Degradable Materials from Petroleum

In addition to using natural polymers as degradable materials or making use of renewable resources, (bio)degradability can also be induced in chemically synthesized polymers. Polymers, mostly polyesters, polyorthoesters and polyanhydrides, especially for specialty applications, have been designed in such a way that these materials readily undergo chemical reactions, often hydrolysis, that lead to their chemical and physical disintegration. By tailoring the chemical structure of the building blocks and/or the ratio of chemically different repeat units in copolymers, it is possible to control exactly the degradation behavior and times. Naturally, this chemical approach to degradable materials allows for the largest variety in products and their properties, simply because of the rich diversity of chemical building blocks and the chemical means of their

Downloaded by 89.163.35.42 on August 9, 2012 | http://pubs.acs.org
Publication Date: September 23, 2006 | doi: 10.1021/bk-2006-0939.ch001

combination. The development of degradable polymers for biomedical applications is currently one of the most active research areas. Copolymers of polylactic acid and polyglycolic acid were the first polymers considered for resorbable sutures and fixtures. Lactel Absorbale Polymers, formerly Birmingham Polymers, is one of the oldest manufacturers of biodegradable polymers for biomedical devices using polylactide, polyglycolide and polycaprolactone [13].

While the packaging industry could have a remarkable impact on the development of degradable materials, simply due to its consumption of about 16 million tons annually, there are other driving forces that are furthering the development of degradable materials. Biomedical materials research continues to be one of the pioneers in the development of degradable materials. The development and investigation of degradable materials for biomedical applications has always been on the forefront of degradable materials research, and some of the latest developments from this area together with chapters on the synthesis, characterization, physical, chemical and degradation behavior as well as information on legislative regulations constitute this book.

Downloaded by 89.163.35.42 on August 9, 2012 | http://pubs.acs.org
Publication Date: September 23, 2006 | doi: 10.1021/bk-2006-0939.ch001

References

1. Chemical and Engineering News 2005. 83 (28), 74
2. www.americanplasticscouncil.org
3. EPA document EPA530-R-03-011
4. Industrial Polysaccharides: The Impact of Biotechnology and Advanced Methodologies ed.: S.S. Stivala, V. Crescenti, I.C.M. Dea, Gordon and Breach Science Publishers, **1987**
5. Polysaccharides I : Structure, Characterisation and Use (Advances in Polymer Science), ed.: T.T. Heinze Springer Verlag **2005**
6. Silk Polymers Materials Science and Biotechnology, ed.: D. Kaplan, W. W. Adams, B. Farmer, C. Viney ACS Symposium Series 544 **1994**
7. Lignin: Properties and Materials, ed.: W. Glaser ACS Symposium Series 742 **1989**
8. Immobilized Biocatalysts to Isoprene, Volume A14, Ullmann's Encyclopedia of Industrial Chemistry ed.: H.-J. Arpe Wiley-VCH 1989 5th edition
9. Doi, Y. *Microbial Polyesters* VCH Publishers, Inc., New York, Weinheim, Cambridge, **1990**

10. Snell, K.D., Peoples, O. P. "Polyhydroxyalkanoate Polymers and Their Production in Transgenic Plants" Metabolic Engineering, 4, 29-40, 2002
11. http://www.Dupont.com/sorona
12. http://www.natureworksllc.com
13. http://www.birminghampolymers.com

Downloaded by 89.163.35.42 on August 9, 2012 | http://pubs.acs.org
Publication Date: September 23, 2006 | doi: 10.1021/bk-2006-0939.ch001

Downloaded by UNIV OF ARIZONA on August 10, 2012 | http://pubs.acs.org
Publication Date: September 23, 2006 | doi: 10.1021/bk-2006-0939.ch002

Chapter 2

Emulsan–Alginate Microspheres as a New Vehicle for Protein Delivery

Guillermo R. Castro[1,2], Emilia Bora[1], Bruce Panilaitis[1], and David L. Kaplan[1]

[1]**Department of Biomedical Engineering, Bioengineering and Biotechnology Center, Tufts University, Medford, MA 02155**
[2]**Laboratory of Biocatalysis, PROIMI, Av. Belgrano y Caseros, 4000 Tucuman, Argentina**

A solution containing emulsan, a lipoheteropolysaccharide, and calcium was used to produce emulsan-alginate microspheres (EAMs). Optical, scanning electron microscopy and EDX (Energy Dispersive X-ray) analysis of the microspheres suggested different morphologies and compositions, respectively, when compared with microspheres prepared only from alginate. The EAMs were twice as stable in phosphate solution compared to alginate alone when assessed with blue dextran encapsulation. The EAMs were able to adsorb about twice the amount of BSA (Bovine Serum Albumin) compared to alginate alone. When azo-BSA was adsorbed on the emulsan-alginate microspheres, protein release could be triggered with enzymes. BSA released from the EAMs retained about of 78% of the α-helix structure.

In Degradable Polymers and Materials; Khemani, K., et al.;
ACS Symposium Series; American Chemical Society: Washington, DC, 2006.

Downloaded by UNIV OF ARIZONA on August 10, 2012 | http://pubs.acs.org
Publication Date: September 23, 2006 | doi: 10.1021/bk-2006-0939.ch002

In recent years with the emergence of the fields of biotechnology and biomedicine there has been growing interest in the development of systems able to transport, capture or deliver molecules. Biocompatible gels have become an important topic for encapsulation of living cells, drug delivery systems and implants (*1*). Alginate, a linear polysaccharide of ß-D-mannuronic (M) and α-L-guluronic (G) acids found in algae and some bacteria, can be gelled by calcium and others bivalent cations. Alginate gels are considered safe and currently used in many biotechnology applications (*1*). However alginate gels are unstable in the presence of cation chelating agents such as phosphate and/or competing non-gelling cations such as sodium or potassium which are present in biological fluids (*2*).

In order to prevent alginate microsphere swelling, polymers like chitosan, poly-L-lysine, polyacrylates and others have been added to stabilize alginate gels by crosslinking or co-gelation (*3,4*). Chitosan, a cationic copolymer of N-acetylglucosamine and glucosamine, is water soluble and biodegradable polymer often used in the pharmaceutical industry as an excipient because of is biocompatibility and lack of toxicity in mammals (*1*). However, the degree of acetylation of chitosan, which correlates with its biological and chemical properties, depends on the chemical treatment of chitin by alkaline N-deacetylation. In addition, sometimes extra chemical steps are required in order to improve the mucoadhesive properties of chitosan for drug delivery purposes (*5*). Also, the major source of chitin is the exoskeleton of crustaceans, which can lead to problems in terms of contamination from heavy metals, a serious disadvantage for human consumption (*1*), along with the variability in source supply of the chitin, impacting molecular weight and degree of deacetylation.

Emulsan, a polysaccharide of ~1x106 Da., is produced by *Acinetobacter venetianus* RAG-1 and composed by D-galactosamine, D-galactosaminuronic acid, and 2,4-diamino-6-deoxy-D-glucosamine linked with fatty acids by N- and O-acyl bonds to the sugar backbone with interesting biological and chemical properties (*6*). Studies in our laboratory have shown that both physiological control of the biosynthesis process or genetic manipulation of the organism changes the structure and thus function of this amphiphilic polymer can be altered toward specific goals (*7, 8*). Interestingly, crude emulsan secreted by the bacterium harbors up to 23% by weight of adsorbed protein in the native state (*7*), a property that could be useful for protein delivery. The disadvantage of the emulsan is that the polymer does not easily form stabilized gel systems.

In order to study the ability of emulsan as protein delivery the polymer was combined with alginate in gel form. Bovine serum albumin (BSA) was selected for adsorption studies because it is well characterized and responsible for 99% of free fatty acid transport in cows, with equilibrium constants on the order of $10_7 M_{-1}$ (*9*).

Downloaded by UNIV OF ARIZONA on August 10, 2012 | http://pubs.acs.org
Publication Date: September 23, 2006 | doi: 10.1021/bk-2006-0939.ch002

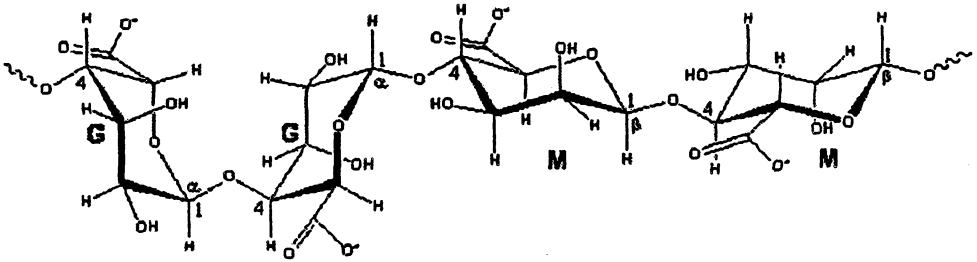

Figure 1. Chemical structure of alginate. G and M are β-D-mannuronic and α-L-guluronic acids respcetively.

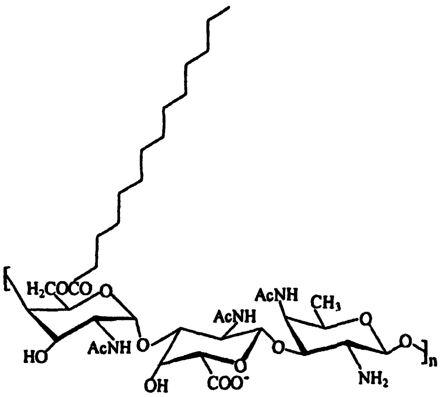

Figure 2. Chemical structure of emulsan.

The aim of the present work was to characterize a new biogel system based on the combination of emulsan-alginate for protein delivery. Analysis of biogel surfaces was conducted using optical microscopy, scanning electron microscopy and energy dispersive X-ray mapping, and the vesicles were assessed for gel integrity and chemical and biocatalyzed protein release. The BSA before and after release was compared for structural features by circular dichroism. The results suggest these hybrid systems offer important options in the adsorption and delivery of proteins, mimicking the native function of emulsan as a carrier of large amounts of protein in the environment,

Experimental methods

Materials

Chemical reagents were of analytical grade and microbiological media were of highest available grade (Aldrich Milwaukee, WI; Difco, Franklin Lakes, NJ). Low viscosity alginate (average M_n~ $1x10_5$ Da) , blue dextran ($2x10_6$ Da), acid blue 2, BSA (fraction V), azo BSA, subtilisin Carlsberg (from *B. licheniformis*), and *C. rugosa* lipase were purchased from Sigma (St. Louis, MO).

Bacterial cultures and emulsan purification

Emulsan (average M_n $1x10_6$ Da) synthesis by *A. venetianus* strain RAG-1 (ATCC 31012) was produced in saline medium supplemented with ethanol, and purified according to our previously reported procedures (*8*).

Downloaded by UNIV OF ARIZONA on August 10, 2012 | http://pubs.acs.org
Publication Date: September 23, 2006 | doi: 10.1021/bk-2006-0939.ch002

Optical Microscopy (OM) and Scanning Electron Microscopy (SEM).

OM was performed with an Axiovert S-100 inverted microscope (Carl Zeiss, Jena, Germany). SEM was performed with a Leo 982 (Noran, Germany) using lyophilized microsphere samples with no previous treatment.

Microsphere formation.

Sodium alginate (1.5 to 5.0 %) was dropped into a solution containing 20 to 100 mM CaCl2, with or without emulsan (0.22 to 3.0 mg/ml) under continuous stirring in order to avoid coalescence of gel beads. Fresh microspheres were incubated in the respective calcium chloride solutions for 48 hours in a rocker at 25 rpm at 5°C for aging, followed by filtration on paper (Whatman #1). Filtered microspheres were kept in solution containing CaCl2 and 10 μM NaN3 at 5°C until use. For polymer release studies, 1.0 mg/ml blue dextran or acid blue 2 were loaded into 2.0% alginate solution and stirred until total dissolution, followed the gelation procedure mentioned above. For protein experiments, typically 500 μg/ml of BSA or azo-BSA were incubated with 200 μg of gel microspheres at 37°C for one hour. The microspheres were centrifuged, washed with 150 mm NaCl, and stored at 5°C until use.

Downloaded by UNIV OF ARIZONA on August 10, 2012 | http://pubs.acs.org
Publication Date: September 23, 2006 | doi: 10.1021/bk-2006-0939.ch002

Energy Dispersive X-ray mapping (EDX).

Microspheres were mounted on an environmental scanning electron microscope (ESEM) plate without any previous treatment for EDX-ray analysis consisting in Falcon System running Genesis 1.1 software and a super ultra thin window). The X-ray spectra were obtained in ESEM mode with a 20 kV accelerating voltage and a 35-degree take-off angle. Elemental micro-probe and elemental distribution mapping techniques were used for analyzing the elemental composition. The spectra were collected for 100 seconds with a dead time between 20-30%. Spectra major peaks were identified by X-ray energies characteristic of each element.

Circular dichroism (CD)

The CD spectra were recorded on a spectropolarimeter (Jasco J-710, Tokyo, Japan) with a 0.1 mm cell path length at 25°C. Scans were obtained in a 200 to 250 nm with 1-nm bandwidth and 4-seconds integration time. Four scans were accumulated for each sample at a scan rate of 100 nm min-1. The α-helix BSA content was estimated considering a molecular weight of 66,700 Da, and 582 amino acid residues with equations described elsewhere (*10*).

Release studies

The release of blue dextran from the microspheres was studied in 25 mM buffer phosphate solution (pH 7.5) incubated in a rotatory shaker at 200 rpm and 37°C. Biocatalytic release of azo-BSA and sulfanilic acid from the microspheres was performed with subtilisin or lipase in 25 mM Tris-ClH buffer solution (pH=7.8) incubated at 200 rpm and 37°C. Azo-BSA and sulfanilic acid were determined spectrophotometrically at 334 nm. The presence of sulfanilic acid in the supernatant was assayed after precipitation of azo-BSA with 5% TCA for 15 minutes at 0°C, followed by centrifugation (10,000 xg, 20 minutes at 4°C). Controls without enzymes, and with protease previously inhibited with 1.0 mM diisopropyl fluorophosphate, or thermal inactivate lipase (heated at 100°C) were included. Chemical release of BSA from the microspheres was performed by incubating the microspheres in a buffer phosphate (100 mM, pH=7.4) until total microsphere disintegration. For CD analysis of BSA, samples were filtered through 100 kDa. MWCO devices (Centricon, Millipore, Billerica, MA, USA).

Downloaded by UNIV OF ARIZONA on August 10, 2012 | http://pubs.acs.org
Publication Date: September 23, 2006 | doi: 10.1021/bk-2006-0939.ch002

Results and discussion

Gelation and characterization of alginate microspheres mixed with other polymers are well described previously in the literature (*1,2*). However, no references for the interaction of emulsan and other polymers were found. Comparative optical microscopy of alginate and emulsan-alginate microspheres showed different surface morphologies (Figure 3). The results were confirmed by SEM (Figure 4).

Alginate gel microspheres showed smooth surfaces compared to the emulsan-alginate microspheres suggesting surface interactions due to the presence of the emulsan likely influence the localized calcium interactions in gel formation. Also, the presence of fatty acid acyl residues on the emulsan main chain, and the lack of these side chains on alginate likely contribute to the observed differences in surface homology. Concentrations ranging from 20 to 100 mM of calcium chloride combined with 1.5% to 5.0% alginate which modify the gelation rate did not change the morphology of the emulsan-alginate microspheres observed by microscopy (data not shown). Another advantage of the system is that size of the microspheres can be modified by changing the speed of the pump, which is able to produce homogenous sizes between 300 μm to 2.5 mm diameter.

Downloaded by UNIV OF ARIZONA on August 10, 2012 | http://pubs.acs.org
Publication Date: September 23, 2006 | doi: 10.1021/bk-2006-0939.ch002

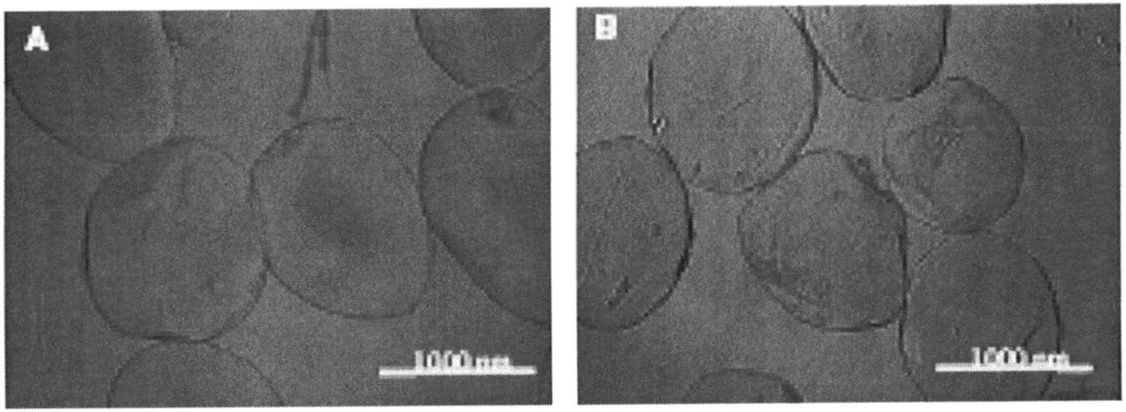

Figure 3. Optical microscopy (16x) of microspheres: A, alginate, and B emulsan-alginate.

Downloaded by UNIV OF ARIZONA on August 10, 2012 | http://pubs.acs.org
Publication Date: September 23, 2006 | doi: 10.1021/bk-2006-0939.ch002

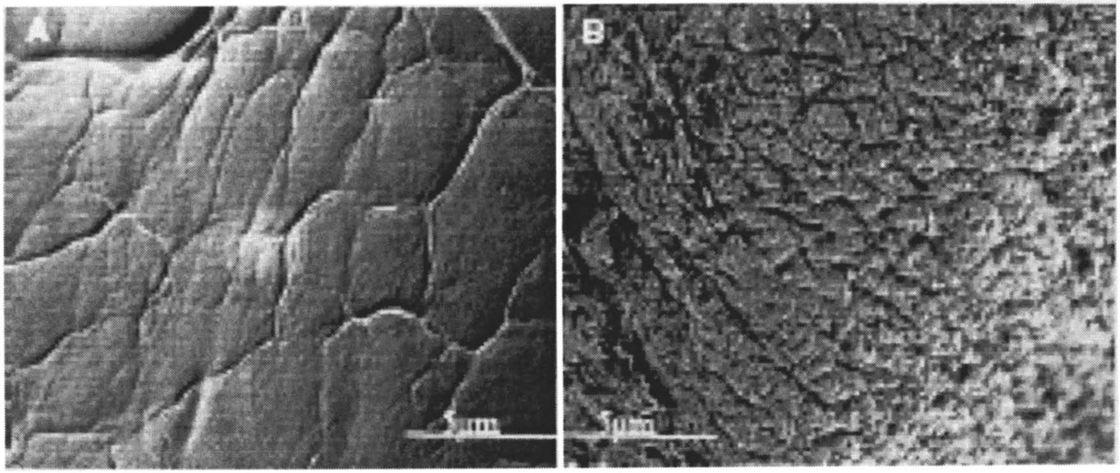

Figure 4. SEM (x 5,000) of alginates (A), and emulsan-alginate microspheres (B).

Downloaded by UNIV OF ARIZONA on August 10, 2012 | http://pubs.acs.org
Publication Date: September 23, 2006 | doi: 10.1021/bk-2006-0939.ch002

Alginate crosslinking and gelation are provided by the exchange of monovalent ions, like sodium, from α-L-guluronic acid residues with divalent cations, such as calcium and magnesium (*1*). Alginate crosslinking is produced when two adjacent α-L-guluronic acid residues interact cooperatively forming a binding cage for polyvalent cations. If 20 or more monomer units from different chains interact a gel network is formed. The gelation and strength can be correlated with the presence of α-L-guluronic (G) blocks in the alginate chain. The increase of the length of G block content implies more calcium crosslinking which has direct relevance to the functionality, stability and structure of alginate gels (*2*). Interferences that reduce the complexation between divalent ions and α-L-guluronic residues therefore also decrease the strength and stability of the gel. If emulsan interferes within calcium-alginate crosslinking of the microspheres and consequently with gel formation, emulsan-alginate microspheres would have a weaker structure and disintegrate more easily in phosphate solutions compared to alginate microspheres without emulsan. Conversely, if emulsan forms a coating on the alginate microspheres, perhaps due to the differences in chain chemistry and thus solubility, the time release of tracer molecules retained or adsorbed in the microsphere core will be delayed compared to alginate alone microspheres. In order to test this hypothesis, blue dextran or acid blue 2 (dye covalently attached to dextran) were loaded into 2.0 % alginate solutions and dropped into the calcium solution for gelation. Typically 30 mM was used, and the time release for these compounds was studied in terms of release from both alginate and emulsan-alginate microspheres. Acid blue 2 was totally release in less than 15 minutes without any differences in the time release profiles in both types of microspheres (data not shown). At pH 7.5 the 2 x106 Da MW blue dextran released from alginate microspheres showed a hyperbolic profile and the process was completed in 1 hour. The blue dextran release profile from emulsan-alginate microspheres was sigmoid and the process was completed in about 2 hours (Figure 5). The time-release for dextran was strongly influenced by the disintegration of the microspheres which increased with pH (data not shown). These results suggest that there was no interference from emulsan in the alginate gelling process and probably little diffusion of the emulsan to the inside the alginate gel core. This interpretation is also supported by previous data showing that 1.5 to 3.0% alginate gels had 170 to 147 Å pore sizes (*11*), with an approximately exclusion pore size of 21-25 kDa. (*12*). Considering that alginate gelation proceed by diffusion of calcium ions and crosslinking from the microsphere surface to the microsphere core, and the emulsan is 1x106 Da, which is about 40 times larger than the exclusion pore size, diffusion of significant amounts of emulsan to the inside the gel core is not likely. On the contrary, the presence of emulsan apparently reinforced the microsphere structure probably because of the hydrophobic nature conferred by the fatty acid side chains.

Downloaded by UNIV OF ARIZONA on August 10, 2012 | http://pubs.acs.org
Publication Date: September 23, 2006 | doi: 10.1021/bk-2006-0939.ch002

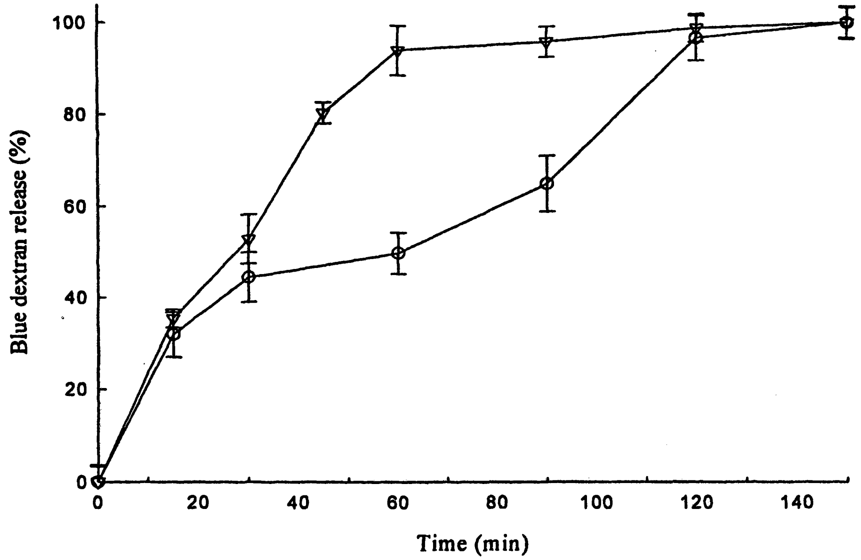

Figure 5. Release of blue dextran from Alginate (∇), and emulsan-alginate microspheres (O) incubated at 200 rpm at 37°C.

EDX analysis of both microspheres (alginate and emulsan-alginate) revealed the presence of four major elements: carbon, oxygen, chloride and calcium (Figure 6). Semiquantitative chemical analysis of both types of microspheres provided different oxygen/carbon ratios of 1.09 and 1.20 for emulsan-alginate and alginate microspheres, respectively. An approximately 10% difference between calcium: carbon ratios for both types of microspheres was found with values of 0.43 and 0.34 for emulsan-alginate and alginate respectively. Chloride was constant in both types of microspheres, suggesting the enhanced amount of calcium in emulsan-alginate microspheres was because of the presence of emulsan since calcium chloride is the only source of both ions.

In order to determine the effect of emulsan on BSA adsorption by the microspheres, solutions containing different amounts of emulsan were used to coat alginate microspheres followed by BSA adsorption. The results in Figure 7 showed that the increase of emulsan concentration in the microspheres was proportional to the increase in BSA adsorption by the microspheres. The BSA adsorption kinetics on the emulsan-alginate microspheres was more than twice that for BSA adsorption to the alginate microspheres at 37°C (Figure 8). However, saturation levels of BSA in the alginate microspheres was reached in about 10 minutes, while in the emulsan-alginate microspheres this process required about 20 minutes.

Downloaded by UNIV OF ARIZONA on August 10, 2012 | http://pubs.acs.org
Publication Date: September 23, 2006 | doi: 10.1021/bk-2006-0939.ch002

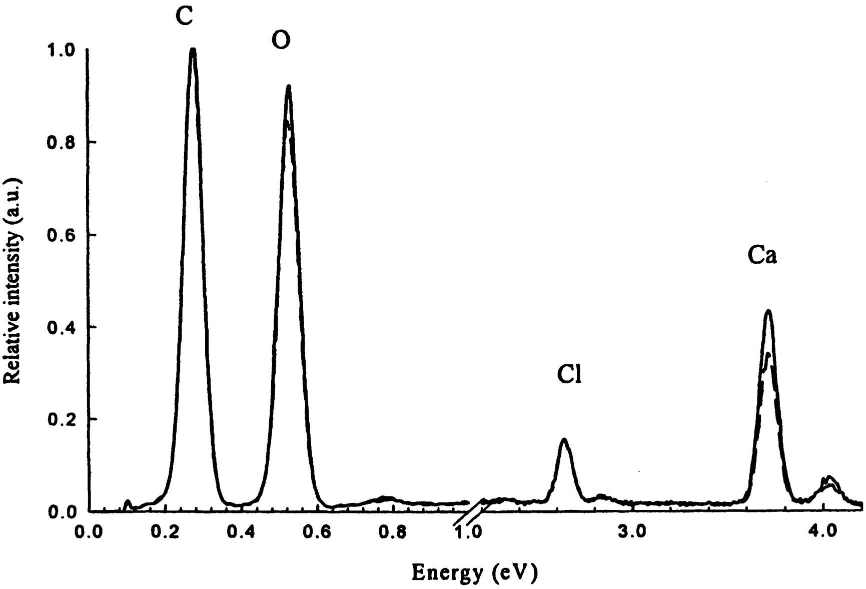

Figure 6. EDX spectra of alginate (dashed line), and emulsan-alginate microspheres (continuous line).

Downloaded by UNIV OF ARIZONA on August 10, 2012 | http://pubs.acs.org
Publication Date: September 23, 2006 | doi: 10.1021/bk-2006-0939.ch002

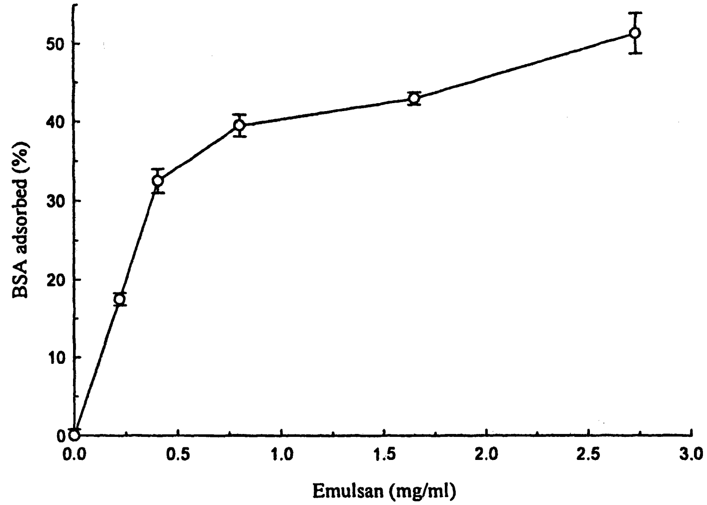

Figure 7. Effect of emulsan concentration on BSA adsorption by emulsan-alginate microspheres incubated at 37°C for 25 minutes.

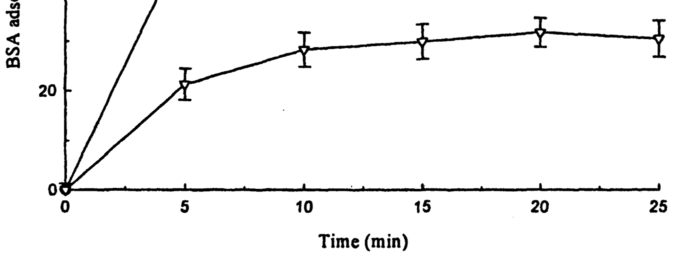

Figure 8. Adsorption of BSA by alginate (∇) and emulsan-alginate microspheres (○).

Based on the results of blue dextran release from emulsan-alginate microspheres using calcium complexing agents such as phosphate, and taking in account the potential use of these systems in oral drug delivery, enzyme triggered release methods from these systems was explored. Two scenarios were considered, the use of pre-proteins adsorbed in the microspheres with subsequent cleavage by a protease (e.g. insulin), which would trigger biological activity. A scheme of this model is displayed in **Figure 9**. BSA covalently linked to sulfanilic acid, azo-BSA, was used as a model substrate for the catalysis and adsorbed by the emulsan-alginate microspheres. Studies of sulfanilic acid release by biocatalysis from the emulsan-alginate microspheres was performed with subtilisin. Subtilisin, a common serine protease belonging to the same family as trypsin and chymotrypsin, which are most abundant proteases present in mammalian intestine.

Downloaded by UNIV OF ARIZONA on August 10, 2012 | http://pubs.acs.org
Publication Date: September 23, 2006 | doi: 10.1021/bk-2006-0939.ch002

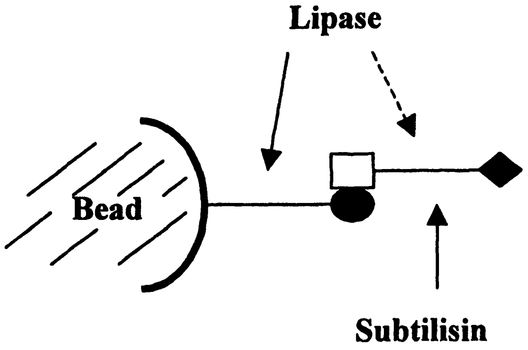

Figure 9. Diagram of enzymatic release of azo-BSA from emulsan-alginate microspheres. Symbols: □——◆, azo-BSA; ——●, fatty acid; □, BSA; and ◆ sulfanilic acid respectively.

The azo-BSA release from the microspheres is induced by the hydrolysis of the fatty acid ester side chains on the emulsan. *Candida rugosa* lipase was used to follow the release of azo-BSA by specific enzymatic cleavage of the fatty acids, and the nonspecific enzymatic cleavage of azo-BSA into sulfanilic acid. The results are displayed in **Table I**.

In enzymatic cleavage from the microspheres either with subtilisin or lipase, the release of the substrate was greater than 60%. Impressively, the release of azo-BSA from the microspheres catalyzed by lipase was greater than 90%. However, nonspecific hydrolysis of azo-BSA by lipase was detected, probably attributed to the similarities between the ester and amide bonds. Also, both reactions were performed in closed systems, contrary to the biological environment in the digestive track which is an open and dynamic system where the presence of end-products from biocatalysis affects reaction kinetic as well as the conversion of substrate and side products.

Table I. Enzymatic release of azo-BSA from emulsan-alginate microspheres incubated 20 minutes at 37°C.

Treatment	*Percentage of total release*	
	Azo-BSA	*Sulfanilic acid*
Subtilisin	0	62.9 ± 2.3
Lipase	82.6± 3.1	15.2 ± 1.2
No enzyme	0	0

Another question to be addressed is the status of the protein structure after release from the microspheres. Secondary structure can provide a qualitative estimate of function and reflects to some extent biological activity. Protein inactivation by unfolding is one of the major obstacles in drug delivery. For this purpose, analysis of BSA structure by circular dichroism before and after the release from the microspheres was assessed. After release from the emulsan-alginate microspheres, BSA showed some loss in helix content based on the decrease of negative elipcticity at 222 nm typical of α-helix (Figure 10).

In the experimental conditions utilized, native BSA dissolved in phosphate buffer at pH 7.4 had 56.0±1.4% α-helix content and 43.9±3.2% for the desorbed-filtered BSA without any other excipient. In previous work with poly(lactic-co-glycolic acid) microspheres the BSA α-helix content was 21% without any excipient and the α-helix value reported was 39.0% in the presence of additives (*13*). These values are between 27 to 60 % loss of the total α-helix content for PLGA microspheres compared to roughly 22% α-helix loss using the emulsan-alginate microspheres.

Conclusions

Microscopy studies revealed the presence of emulsan likely on the surface of the emulsan-alginate microspheres. The presence of emulsan on the microsphere surface increased the stability of the gels in comparison to alginate alone based on the release of blue dextran, the amount of protein adsorbed and the delayed time of about two fold for the release of the carbohydrate to

Downloaded by UNIV OF ARIZONA on August 10, 2012 | http://pubs.acs.org
Publication Date: September 23, 2006 | doi: 10.1021/bk-2006-0939.ch002

Downloaded by UNIV OF ARIZONA on August 10, 2012 | http://pubs.acs.org
Publication Date: September 23, 2006 | doi: 10.1021/bk-2006-0939.ch002

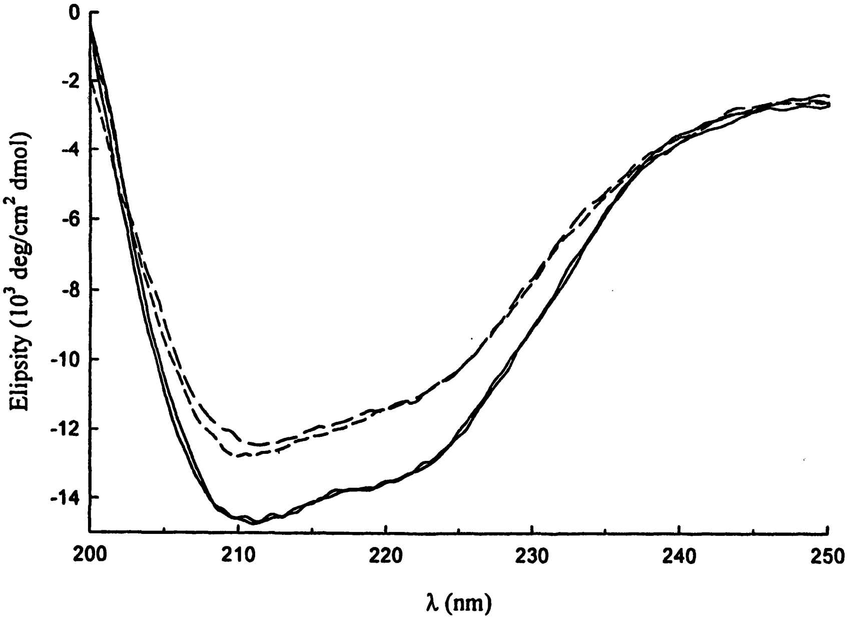

Figure 10. Circular dichroism spectra of BSA after adsorption (continuous line), and before release (dashed line) from emulsan-alginate microspheres.

solution. This study also demonstrated that triggered release of adsorbed protein from emulsan-alginate microspheres was feasible and the protein adsorbed and then released retained its native state. The higher preservation of BSA structure after adsorption and desorption from emulsan-alginate microspheres compared to PLGA microspheres suggests a potential use of these systems in protein drug delivery. Also, the option to tailor emulsan hydrophobicity and molecular weight for the delivery of specific proteins with different structures and complexities suggests new possibilities for the field of controlled release.

Acknowledgements

The SEM work was performed at the Center for Imaging and Mesoscale Structures from instrumentation funded by NSF grant number 0099916, Division of Biological Infrastructure, Harvard University. We thank Richard Schalek for technical assistance. Support from the USDA (Grant #99-355504-7915) and CONICET (Argentina) is gratefully acknowledged, as is support from the NIH P41 Center for Tissue Engineering.

References

1. Dornish, M.; Kaplan, D.; Skaugrud, Ø. *Ann N. Y. Acad. Sci.* **2001**, 944, 388-397.
2. Smidsrød, O.; Skjåk-Bræk G. *Trends Biotechnol.* **1990**, **8**, 71–78.
3. Toshiya, T; Takayama K.; Machida, Y.; Nagai, T. *Int. J. Pharm.,* **1990**, 61, 35-41
4. Thu, B.; Bruheim, P.; Espevick, T.; Smidsrød, O; Soon-Shiong, P.; Skjåk-Bræk, G. *Biomaterials*, 1996, **17**, 1031-1040.
5. Borchard, G.; Lueßen H. L., de Boer, A. G.; Verhoef J. C.; Lehr C. M.; Junginger H. E. *J. Control. Release*, **1996**, 39, 131-138.
6. Rosenberg, E.; Ron, E.Z. *Biopolymers* **2002**, 5, 91-111.
7. Gorkovenko, A.; Zhang, J.; Gross, R. A.; Kaplan, D. L. *Carbohydr. Pol.,* **1999**, *39,* 79-85.
8. Johri, A.; Blank, W.; Kaplan, D. *Appl. Microbiol. Biotechnol.* **2002**, 59, 217-223.
9. Peters Jr, T. All about albumin. Biochemistry, genetics and medical applications. Academic Press, New York, 1996.
10. Greenfield, N.; Fasman G. D. *Biochemistry* **1969**, 4108-4116.
11. Li, R. H.; Altreuter, D. H.; Gentile, F. T. *Biotechnol. Bioeng.* **1996**, 50, 365-373.
12. Dembczynski, R.; Jankowski, T. *J. Biomat. Scie. Polym. Ed.* **2001**, 12, 1051-1058.
13. Fu K., Griebenow K., Hsieh L., Klibanov A.L., Langer R. *J. Control Release* **1999**, 58, 357-366.

Downloaded by UNIV OF ARIZONA on August 10, 2012 | http://pubs.acs.org
Publication Date: September 23, 2006 | doi: 10.1021/bk-2006-0939.ch002

Downloaded by COLUMBIA UNIV on August 28, 2012 | http://pubs.acs.org
Publication Date: September 23, 2006 | doi: 10.1021/bk-2006-0939.ch003

Chapter 3

Metabolic Engineering of *Escherichia coli* for Short Chain Length–Medium Chain Length Polyhydroxyalkanoate Biosynthesis

Christopher T. Nomura and Yoshiharu Doi

Polymer Chemistry Laboratory, RIKEN Institute, 2–1 Hirosawa, Wako-shi, Saitama 351–1098, Japan

Polyhydroxyalkanoates (PHA)s are microbially produced polyesters that are biodegradable and have a wide variety of uses. PHAs can be divided into three groups dependent on the size of the monomers incorporated into the polymer. Short-chain-length (SCL) PHAs are composed of C3-C5 monomers and are thermoplastic in nature, while medium-chain-length (MCL) PHAs are composed of C6-C14 monomers and are elastomeric in nature. SCL-MCL PHAs are composed of monomers C3-C14 in length and where the properties of the polymer vary based on the mol% composition of SCL and MCL monomers. This study compares various monomer-supplying pathways in recombinant *Escherichia coli* used for PHA production from non-related carbon sources to supply SCL and MCL PHA monomers. In addition, data describing the composition and thermal properties of polymers produced in recombinant *E. coli* using engineered PHA synthases and fatty acid biosynthesis enzymes are presented.

In Degradable Polymers and Materials; Khemani, K., et al.;
ACS Symposium Series; American Chemical Society: Washington, DC, 2006.

Introduction

Polyhydroxyalkanaotes (PHA)s are microbially produced polyesters that are produced by some bacteria as a carbon and energy sink when grown under nutrient stress in the presence of excess carbon (*1*). PHAs may be attractive alternatives for petroleum-based plastics because they are biodegradable, and, unlike peteroleum-based plastics, can be produced from renewable resources such as plant oils and sugars. The properites of PHAs are determined by their monomer composition. Short-chain-length (SCL) PHAs consist of monomer units C3-C5 in length and are generally classified as thermoplastics, while medium-chain-length (MCL) PHAs consist of monomer units C6-C14 in length and fall into the category of elastomers. SCL-MCL PHAs consist of monomers of C3-C14 in length and have a potentially wide range of properties dependent on the mol ratio of SCL to MCL monomer units. SCL-MCL PHAs with a relatively high mol% of SCL monomers have properties similar to the bulk commodity plastic, polypropylene (*2*). The monomeric composition of PHA polymers is determined by several factors, including the carbon source that the cells are grown on and how that carbon source is metabolized in the cells, the types of monomer-supplying enzymes used, and the type of PHA synthase used to synthesize the polymer. Although SCL and MCL PHA monomers can be derived from related carbon sources such as fatty acids and oils, the use of these carbon sources is limited to organisms with an intact and active β-oxidation pathway. PHA monomer supply from the β-oxidation pathway is oxygen dependent and may present limitations during large-scale bacterial fermentations for PHA production. Therefore it is important to elucidate new metabolic pathways capable of prodcuing a wide variety of monomers for PHA production from non-related carbon sources. *Escherichia coli* represents a model strain to study PHA production because it can easily be genetically modified, has a known genomic sequence, and does not possess enzymes which would degrade PHA that are present in native PHA producing bacterial strains. This study will summarize previous efforts to dictate the polymer composition by manipulating the monomer-supplying enzymes used for the production of the PHAs from non-related carbon sources, such as sugars, and compare them to our current efforts to use fatty acid biosynthesis enzymes as PHA monomer-supplying enzymes for the production of SCL-MCL PHA copolymers from glucose.

Experimental Section

Bacterial strains, plasmids, and culture conditions for PHA production. Transformations and DNA manipulations were carried out with *Escherichia coli* JM109 as the host strain [recA1 endA1 gyrA96 thi-1 hsdR17 (rK- mK+) supE44 relA1 λ-lac[F'proAB lacIq ZΔM15]]. JM109 was also used for the production of PHA. Strains were grown at 30 °C in Luria-Bertani (LB) medium supplemented with glucose to a final concentration of 2 mg ml^{-1}. In order to

Downloaded by COLUMBIA UNIV on August 28, 2012 | http://pubs.acs.org
Publication Date: September 23, 2006 | doi: 10.1021/bk-2006-0939.ch003

supplemented with glucose to a final concentration of 2 mg ml^{-1}. In order to maintain and select for plasmids within the recombinant *E. coli,* 100 μg ml^{-1} of ampicillin and 50 μg ml^{-1} of kanamycin were used when necessary. Plasmids harboring both genetically engineered *fabH* and *phaC1* genes as described in previous studies (*3-5*) were used to transform *E. coli* JM109 cells. The cells were grown for a total of 96 h before harvesting by centrifugation. PHA contents were determined by gas chromatography (GC) analysis of lyophilized cells as previously described (*4*).

Gel permeation chromatography (GPC) analysis of PHA polymers. Polymers were isolated from cells as described previously (*4*) and molecular mass data of polyesters were obtained by GPC analysis using a Shimadzu 10A system fitted with a RID-10A refractive-index detector with serial columns of ShodexK802 and K806M as described previously (*6*). Polystyrene standards with a low polydispersity were used to make a calibration curve.

Determination of PHA polymer composition by nuclear magnetic resonance (NMR). Twenty mg of each polymer was dissolved in 1 ml of $CDCl_3$ and subjected to both ^1H and ^{13}C NMR analysis. ^1H NMR spectra were recorded using a JEOL α-400 spectrometer with a 5.0 μs pulse width (45° pulse angle), 3-s pulse repetition, 7500-Hz spectra width, and 16K data points. For ^{13}C NMR analysis, data were collected using a JEOL ECP-500 spectrometer with a 7.0-μs pulse width (45° pulse angle), 5-s pulse repetition, 25000-Hz spectra width, and 64K data points. Tetramethylsilane (Me_4Si) was used as an internal chemical shift standard.

Determination of thermal properties of SCL-MCL PHA polymers produced by recombinant *E. coli*. The thermal data were recorded on a Perkin-Elmer Pyris 1 differential scanning calorimeter (DSC) equipped with a liquid nitrogen-cooling accessory. Data were collected under a nitrogen flow of 20 ml min^{-1}. The polyester samples (ca. 3 mg) were encapsulated in aluminum pans and quenched from the melt at -30 °C and then heated to 200 °C at a rate of 20 °C min^{-1}, during which the heat flow curves were recorded. The observed melting temperatures and enthalpies of fusion were determined from the positions of the endothermic peaks. The glass transition temperatures were taken as the midpoints of the heat capacity change.

Results and Discussion

PHA produced from non-related carbon sources in recombinant *E. coli*. Non-related carbon feedstocks such as simple sugars represent inexpensive carbon feedstocks that can be used to produce PHAs in recombinant bacteria. An understanding of the metabolic pathways that could enable a recombinant organism to produce monomers for PHA polymerization from non-related carbon sources is important for further increasing the efficiency of PHA production. Table I summarizes data for the production of SCL-PHA in various *E. coli* strains grown on non-related carbon sources.

Downloaded by COLUMBIA UNIV on August 28, 2012 | http://pubs.acs.org
Publication Date: September 23, 2006 | doi: 10.1021/bk-2006-0939.ch003

Downloaded by COLUMBIA UNIV on August 28, 2012 | http://pubs.acs.org
Publication Date: September 23, 2006 | doi: 10.1021/bk-2006-0939.ch003

Table I. SCL-PHA from non-related carbon sources in recombinant *E. coli*

Strain	*Introduced genes*	*Carbon source*	*PHA content (wt%)*	*Monomer composition (mol%)*		*Ref.*
				3HB	*4HB*	
LE392	$phaCAB_{Re}$	gluconate (LB)	20	100	ND	(*7*)
DH5α	$phaCAB_{Re}$	gluconate (LB)	54	100	ND	(*7*)
LM83	$phaCAB_{Re}$	glucose (LB)	26	100	ND	(*8*)
K12	$phaCAB_{Re}$	glucose (LB)	30	100	ND	(*8*)
DH5α	$phaCAB_{Re}$	glucose (LB)	50	100	ND	(*8*)
XL1-Blue	$phaCAB_{Re}$	glucose (LB)	81	100	ND	(*9*)
B	$phaCAB_{Re}$	glucose (LB)	76	100	ND	(*9*)
JM109	$phaCAB_{Re}$	glucose (LB)	85	100	ND	(*9*)
HB101	$phaCAB_{Re}$	glucose (LB)	75	100	ND	(*9*)
MC4100	$phaCAB_{Re}$	glucose	95	100	ND	(*10*)
DH5α	$phaCAB_{Re}$, $4hbD_{Ck}$, $sucD_{Ck}$, $orfZ_{Ck}$	glucose	45	99	1	(*11*)
GCSC6576	$phaCAB_{Re}$	lactose + whey	80	100	ND	(*12*)
S17-1	$phaE_{Syn}$, $phaC_{Syn}$	glucose (LB)	13	100	ND	(*13*)
BL21	$phaCAB_{Al}$	glucose	52	100	ND	(*14*)
XL1-Blue	$phaCAB_{Pd}$, $phaP_{Pd}$	lactate (LB)	43	100	ND	(*15*)
XL1-Blue	$phaCAB_{Pd}$, $phaP_{Pd}$, $phaR_{Pd}$	lactate (LB)	44	100	ND	(*15*)
XL1-Blue	$phaCAB_{Al}$	glucose	77	100	ND	(*16*)
XL1-Blue	$phaCAB_{Re}$	soy waste	28	100	ND	(*17*)
CGSC4401	$phaCAB_{Al}$	lactose + whey	76	100	ND	(*18*)
XL10	$phaE_{Syn}$, $phaCAB_{Syn}$	glucose	13	100	ND	(*19*)
HB101	$fabD_{Ps}$, $phaC_{Ac}$	glucose (LB)	11.4	100	ND	(*20*)
HB101	$fabD_{Ec}$, $phaC_{Ac}$	glucose (LB)	4.6	100	ND	(*20*)
HB101	$fabH_{Ec}$, $phaC_{Ac}$	glucose (LB)	6.5	100	ND	(*20*)
JM109	$fabH_{Ec}$, $phaC_{Ac}$	glucose (LB)	9.8	100	ND	(*4*)

Re, *Ralstonia eutropha*; Al, *Alcaligenes latus*; Ck, *Clostridium acetobutylicum*; Pd, *Paracoccus denitrificans*; Syn, *Synecocystis* sp. PCC 6803; Ec, *Escherichia coli*; Ac, *Aeromonas caviae;* LB, Luria-Bertani medium; 3HB, 3-hydroxybutyrate; 4HB, 4-hydroxybutyrate are as indicated for the polymer monomer composition. ND, not determined.

Downloaded by COLUMBIA UNIV on August 28, 2012 | http://pubs.acs.org
Publication Date: September 23, 2006 | doi: 10.1021/bk-2006-0939.ch003

Table I shows that production of SCL-PHA from non-related carbon sources is robust in recombinant bacteria, with some strains capable of producing up to 95% of the cell dry weight as polymer. Table I also shows that the fatty acid biosynthesis enzyme FabH is capable of supplying monomers for SCL-PHA production.

The most common SCL monomer in SCL-PHA polymers is P(3HB). However, incorporation of other SCL monomers, such as 3HV and 4HB, into PHAs can improve the properties of the polymer that broaden the number of applications that SCL PHA polymers can be used for. Figure 1 depicts the demonstrated and potential SCL-PHA monomer supplying pathways from a non-related carbon source in *E. coli.* Figure 1A shows the production of (*R*)-3-hydroxybutyryl-CoA via the fatty acid biosynthesis enzymes FabD, FabH (*20*), and FabG (*3*). The classic (*R*)-3-hydroxybutyryl-CoA monomer-supplying pathway proceeds via either the PhaA or BktB ketothiolase enzymes, converting two molecules of acetyl-CoA to acetoacetyl-CoA which is then converted to (*R*)-3-hydroxybutryl-CoA by PhaB as shown in 1B.

Poly-3-hydroxybutyrate-*co*-3-hydroxyvalerate [P(3HB-*co*-3HV)] copolymers have a variety of uses as single use, bulk-commodity plastics, in the marine environment and in biomedical applications (*21*). Normally, P(3HB-*co*-3HV) is synthesized in bacteria grown on a mixture of glucose and propionate (*22*). Although demonstrated in plants, Figure 1C shows a pathway which could potentially be used in bacteria for the conversion of threonine (derived from the TCA cycle) to 3-hydroxyvalerate by threonine deaminase, IlvA, to 2-ketobutyrate, followed by reduction to propionyl-CoA by pyruvate dehydrogenase. BktB then catalyzes the formation of the 3-(*R*)-hydroxyvaleryl-CoA substrate which can be polymerized into a P(3HB-*co*-3HV) copolymer (*23*).

P(3HB-*co*-3HV) has been studied for potential biomedical applications (*23*), but recently, poly-4-hydroxybutyrate [P(4HB)] and poly-3-hydroxybutyrate-*co*-4-hydroxybutyrate [P(3HB-*co*-4HB)] have also been studied for their potential use as biomedical polymers(*24*). These potential uses stress the importance of developing metabolic pathways for the economic production of 4HB monomers. Figure 1D shows a monomer-supplying pathway for 4-hydroxybutyryl-CoA production via succinyl-CoA from the citric acid cyle. Succinate dehydrogenase (SucD) catalyzes the formation of succinate-semialdehyde from succinyl-CoA, which is further reduced to 4-hydroxybutyrate by 4-hyroxybutyrate dehydrogenase (4HbD). This 4-hydroxybutryate is then converted to 4-hydroxybutyryl-CoA by 4-hydroxybutyric acid-CoA transferase [either Cat1 or Cat2] (*25,26*).

All of the aforementioned pathways may be targeted for enhanced metabolic flux via carbon source supply, protein engineering, and other forms of regulation in order to enhance SCL-PHA production.

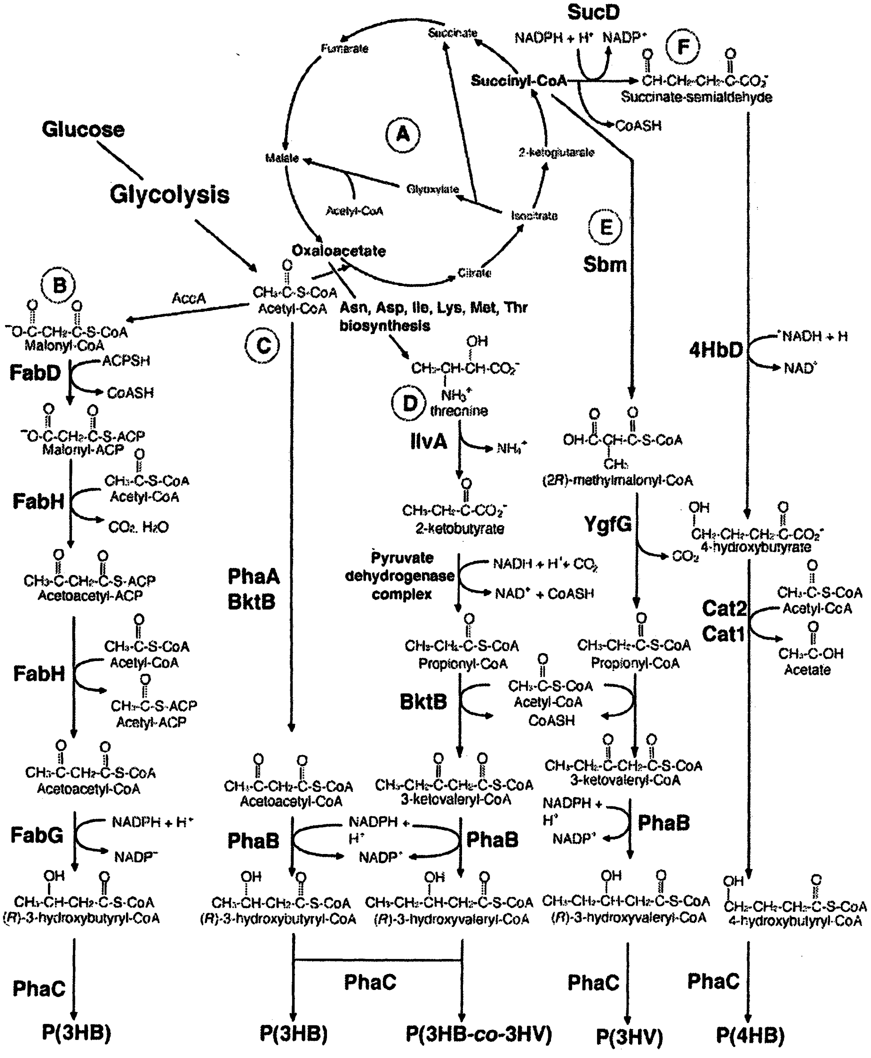
SucD
NADPH + H⁺ NADP⁺
F
Succinate
Fumarate
Succinyl-CoA
CH-CH₂-CH₂-C-CO₂⁻
Succinate-semialdehyde
CoASH
Glucose
A
Malate
2-ketoglutarate
Glyoxylate
Glycolysis
Acetyl-CoA
Isocitrate
E
Oxaloacetate
Sbm
Citrate
B
AccA
CH₃-C-S-CoA
Acetyl-CoA
Asn, Asp, Ile, Lys, Met, Thr biosynthesis
⁻O-C-CH₂-C-S-CoA
Malonyl-CoA
C
OH
CH₃-CH-CH-CO₂⁻
NH₃⁺
threonine
4HbD
NADH + H
NAD⁺
FabD
ACPSH
CoASH
D
⁻O-C-CH₂-C-S-ACP
Malonyl-ACP
IlvA
NH₄⁺
OH-C-CH-C-S-CoA
CH₃
(2R)-methylmalonyl-CoA
FabH
CH₃-C-S-CoA
Acetyl-CoA
CO₂, H₂O
CH₃-CH₂-C-CO₂⁻
2-ketobutyrate
YgfG
OH
CH₂-CH₂-CH₂-C-CO₂⁻
4-hydroxybutyrate
CO₂
CH₃-C-CH₂-C-S-ACP
Acetoacetyl-ACP
PhaA
BktB
Pyruvate dehydrogenase complex
NADH + H⁺+ CO₂
NAD⁺ + CoASH
CH₃-C-S-CoA
Acetyl-CoA
Cat2
Cat1
CH₃-C-OH
Acetate
FabH
CH₃-C-S-CoA
Acetyl-CoA
CH₃-C-S-ACP
Acetyl-ACP
CH₃-CH₂-C-S-CoA
Propionyl-CoA
CH₃-CH₂-C-S-CoA
Propionyl-CoA
BktB
CH₃-C-S-CoA
Acetyl-CoA
CoASH
CH₃-C-CH₂-C-S-CoA
Acetoacetyl-CoA
CH₃-C-CH₂-C-S-CoA
Acetoacetyl-CoA
CH₃-CH₂-C-CH₂-C-S-CoA
3-ketovaleryl-CoA
CH₃-CH₂-C-CH₂-C-S-CoA
3-ketovaleryl-CoA
FabG
NADPH + H⁺
NADP⁺
PhaB
NADPH + H⁺
NADP⁺
PhaB
NADPH + H⁺
NADP⁺
PhaB
CH₃-CH-CH₂-C-S-CoA
(R)-3-hydroxybutyryl-CoA
CH₃-CH-CH₂-C-S-CoA
(R)-3-hydroxybutyryl-CoA
CH₃-CH₂-CH-CH₂-C-S-CoA
(R)-3-hydroxyvaleryl-CoA
CH₃-CH₂-CH-CH₂-C-S-CoA
(R)-3-hydroxyvaleryl-CoA
CH₂-CH₂-CH₂-C-S-CoA
4-hydroxybutyryl-CoA
PhaC
PhaC
PhaC
PhaC
P(3HB)
P(3HB)
P(3HB-co-3HV)
P(3HV)
P(4HB)

Figure 1. SCL-PHA production from non-related carbon sources. A. The tricarboxylic acid cycle. B. Poly-3-hydroxybutyrate [P(3HB)] monomer supply via the fatty acid biosynthesis enzymes, FabD, FabH, and FabG. C. P(3HB) monomer supply mediated by the beta-ketothiolase enzymes, PhaA or BktB, and the NADPH-reductase, PhaB. D. Poly-3-hydroxyvalerate (P3HV) monomer supply mediated by threonine deaminase (IlvA), pyruvate dehydrogenase, BktB, and PhaB. E. Poly-4-hydroxybutyrate monomer supply mediated by succinate dehydrogenase (SucD), 4-hydroxybutyrate dehydrogenase (4HbD), and acetyl transferase (Cat1 or Cat2).

Downloaded by COLUMBIA UNIV on August 28, 2012 | http://pubs.acs.org
Publication Date: September 23, 2006 | doi: 10.1021/bk-2006-0939.ch003

The incorporation of MCL monomers into PHA dramatically changes their properties and it has been shown in previous studies that a SCL-MCL PHA copolymer has properties similar to polypropylene (*2*). Therefore, the development of pathways capable of supplying MCL monomers for copolymerization with SCL monomer units is very important for the future use of these polymers as bulk commodity plastics. Table II summarizes data for the production of MCL containing PHA polymers from non-related carbon sources.

Figure 2 depicts MCL-PHA monomer supplying pathways from non-related carbon sources such as glucose. In all three pathways, monomers are derived from the fatty acid biosynthesis pathway.

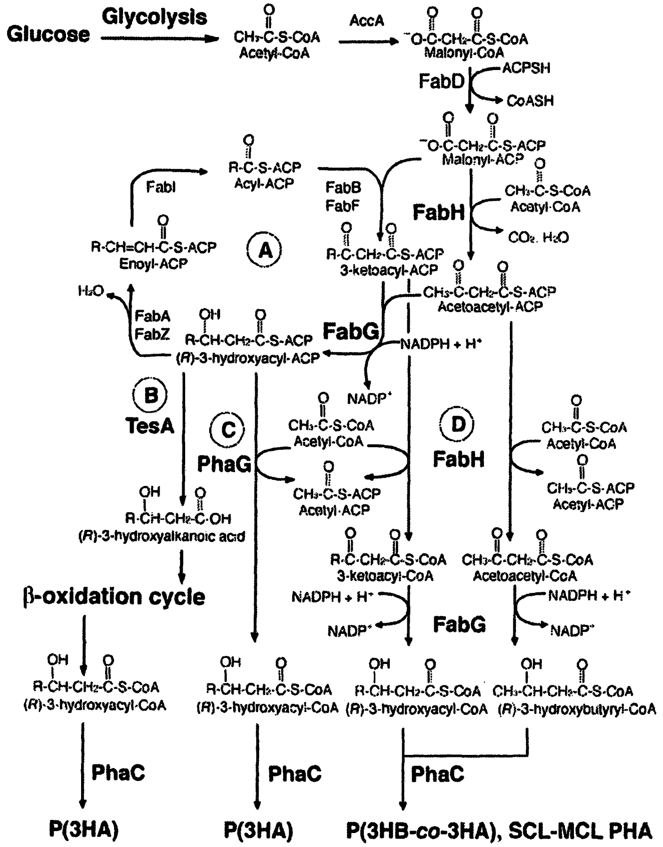
Glucose
Glycolysis
Acetyl-CoA
AccA
Malonyl-CoA
FabD
ACPSH
CoASH
Malonyl-ACP
Acyl-ACP
FabI
FabB
FabF
FabH
Acetyl-CoA
CO2, H2O
Enoyl-ACP
A
3-ketoacyl-ACP
H2O
Acetoacetyl-ACP
FabA
FabZ
FabG
NADPH + H+
(R)-3-hydroxyacyl-ACP
NADP+
B
TesA
C
PhaG
Acetyl-CoA
Acetyl-ACP
D
FabH
Acetyl-CoA
Acetyl-ACP
(R)-3-hydroxyalkanoic acid
3-ketoacyl-CoA
Acetoacetyl-CoA
β-oxidation cycle
NADPH + H+
NADP+
FabG
NADPH + H+
NADP+
(R)-3-hydroxyacyl-CoA
(R)-3-hydroxyacyl-CoA
(R)-3-hydroxyacyl-CoA
(R)-3-hydroxybutyryl-CoA
PhaC
PhaC
PhaC
P(3HA)
P(3HA)
P(3HB-co-3HA), SCL-MCL PHA

Figure 2. Medium-chain-length (MCL) PHA production from non-related carbon sources. A. The fatty acid biosynthesis pathway. B. FabH and FabG mediated SCL-MCL PHA monomer supply. C. 3-hydroxyacyl-ACP:CoA transacetylase (PhaG) mediated MCL PHA monomer supply. D. Thioesterase A (TesA) mediated MCL PHA monomer supply (via the β-oxidation pathway).

Downloaded by COLUMBIA UNIV on August 28, 2012 | http://pubs.acs.org
Publication Date: September 23, 2006 | doi: 10.1021/bk-2006-0939.ch003

Table II. MCL-PHA from non-related carbon sources in recombinant *E. coli*

Strain	*Introduced genes*	*Media*	*PHA content (wt%)*	*Monomer composition (mol%)*				*Ref.*
				3HB	*3HHx*	*3HO*	*3HD*	
JMU193	*tesA*$_{\text{Ec}}$, *phaC*$_{\text{Pa}}$	gluconate (LB)	0.1-2.0	ND	21-33	62-71	3-8	(*27*)
S17-1	*phaG*$_{\text{Pp}}$, *phaC*$_{\text{Pa}}$	gluconate (LB), triclosan	1.5-3.3	ND	ND	ND	100	(*28*)
LS1298	*tesA*$_{\text{Ec}}$, *phaC*$_{\text{Pa}}$	gluconate (LB)	3.2	ND	ND	ND	100	(*29*)
RS3097	*tesA*$_{\text{Ec}}$, *phaC*$_{\text{Pa}}$	gluconate (LB)	3.4	ND	ND	ND	100	(*29*)
JM109	*fabH(F87T)*$_{\text{Ec}}$, *phaC*$_{\text{Ac}}$	glucose (LB)	1.8	97	3	ND	ND	(*4*)
JM109	*fabH(F87T)*$_{\text{Ec}}$, *phaC1*$_{\text{Ps}}$	glucose (LB)	0.8	76	24	ND	ND	(*4*)
JM109	*fabH(F87T)*$_{\text{Ec}}$, *phaAB*$_{\text{Re}}$, *phaC1(STQK)*$_{\text{Ps}}$	glucose (LB)	23	99	1	ND	ND	(*5*)
JM109	*fabH(F87T)*$_{\text{Ec}}$, *fabG*$_{\text{Ec}}$, *phaC1*$_{\text{Ps}}$	glucose (LB)	0.6	67	23	7	3	(*3*)
JM109	*fabH(F87T)*$_{\text{Ec}}$, *fabG*$_{\text{Ps}}$, *phaC1*$_{\text{Ps}}$	glucose (LB)	0.1	96	4	ND	ND	(*3*)
JM109	*fabH(F87T)*$_{\text{Ec}}$, *phaC1(STQK)*$_{\text{Ps}}$	glucose (LB)	1.0	91	6	2	1	(*3*)
JM109	*fabH(F87T)*$_{\text{Ec}}$, *fabG*$_{\text{Ec}}$, *phaC1(STQK)*$_{\text{Ps}}$	glucose (LB)	4.5	94	5	1	ND	(*3*)
JM109	*fabH(F87T)*$_{\text{Ec}}$, *fabG*$_{\text{Ps}}$, *phaC1(STQK)*$_{\text{Ps}}$	glucose (LB)	0.7	94	5	1	ND	(*3*)

Re, *Ralstonia eutropha*; Al, *Alcaligenes latus*; Ck, *Clostridium acetobutylicum*; Pd, *Paracoccus denitrificans*; Syn, *Synecocystis* sp. PCC 6803; Ec, *Escherichia coli*; Ac, *Aeromonas caviae*; LB, Luria-Bertani medium; 3HB, 3-hydroxybutyrate; 4HB, 4-hydroxybutyrate.

Downloaded by COLUMBIA UNIV on August 28, 2012 | http://pubs.acs.org
Publication Date: September 23, 2006 | doi: 10.1021/bk-2006-0939.ch003

Only the FabH-FabG mediated PHA monomer supplying pathway is capable of supplying both SCL and MCL-PHA monomers for polymerization without the aid of either the β-oxidation pathway [TesA derived MCL-PHA monomers (*24*)] or the aid of fatty acid biosynthesis inhibitors [PhaG derived MCL-PHA monomers (*25*)]. In the current study, FabH (F87T) was used to supply both SCL and MCL PHA monomers from glucose in *E. coli* JM109. Because *E. coli* JM109 is normally used for standard cloning procedures it is unlikely to make spurious mutations caused by recombination, since it is *recA*-deficient and has limited DNA recombination mechanisms. This *recA* deficiency is an important genotype for the stability of the introduced genes in recombinant PHA production systems; recombinant genes introduced into *recA* harbouring strains may be genetically unstable. In addition, there was no need to add fatty acid biosynthesis inhibitors to generate the monomers necessary for SCL-MCL PHA production as was done in other studies.

Because fatty acid biosynthesis is an anabolic rather than a catabolic process, a wide array of carbon sources can be potentially transformed to PHA using these enzymes as monomer suppliers. This would be important for the transfer of this PHA producing pathway to other recombinant organims, such as plants, whereby the cost of the carbon feedstock can be bypassed by photosynthetic conversion of carbon dioxide to the biopolymer. Only *E. coli* strains harboring recombinant *fabH* genes have been shown to be capable of producing SCL-MCL PHA copolymers from non-related carbon sources. Although the amounts are too low for commercial production of PHAs, these enzymes and their monomer supplying pathway provide a starting point for enhancing the production of monomers from non-related carbon sources. By coexpressing fatty acid biosynthesis enzymes with engineered PHA synthases (*30-32*) it is hoped that economical yields and SCL-MCL PHA copolymers with desired properties could be produced.

Downloaded by COLUMBIA UNIV on August 28, 2012 | http://pubs.acs.org
Publication Date: September 23, 2006 | doi: 10.1021/bk-2006-0939.ch003

Physical characterization of a SCL-MCL PHA copolymer produced from glucose in recombinant *E. coli* expressing fatty acid biosynthesis enzymes and PHA synthase. The isolated polymer produced by fatty acid biosynthetic enzymes and a mutant PHA synthase was characterized by NMR, gel permeation chromatography (GPC), and differential scanning calorimetry (DSC). In order to determine the structure of the isolated polymer and to show that the polymer was a true copolymer rather than a blend of polymers, NMR was used. The mol% fractions of the secondary (C6) and tertiary (C8) monomer units were determined from the intensity ratio of the main-chain methylene proton resonance to methyl proton resonance in the ^{1}H NMR spectra (Figure 3A). Supporting information for tertiary (C8) monomer units were obtained by ^{13}C NMR analysis. As shown in Figure 3B, the ^{13}C NMR spectrum was used to show that the polymer was a random copolymer rather than a blend of polymers.

Figure 3 also shows the chemical shift assignments for each of the carbonyl resonances. In a previous study by Shimamura et al., (*33*) the degree of randomness for P(3HB-*co*-3HH) was determined based on peak intensities for four carbonyl resonance lines (i.e., 3HB monomer next to 3HB, 3HB monomer next to 3HH, 3HH monomer next to 3HB, and 3HH monomer next to 3HH). However, the randomness value could not be estimated using this method since the 3HH resonance line adjacent to the 3HB resonance was too small to be observed clearly. Accordingly, the experimentally obtained spectra and simulated spectra were compared in which random distribution was assumed. The R-factor was found to be 0.998 (near 1.000) as determined by the least-square method, in which the experimentally obtained spectra and the simulated spectra were compared. This result indicates that the polymer isolated from this strain was a random copolymer. The ^1H NMR and ^{13}C NMR spectra of polymer isolated from *E. coli* JM109 harboring the pTrcFabH(F87T) and pBBRGEC plasmids revealed that the polymer was composed of 95.1 mol% 3HB, 3.6 mol% 3HHx, and 1.3 mol% 3HO.

The thermal properties of the SCL-MCL PHA copolymer isolated from recombinant *E. coli* harboring the pTrcFabH(F87T) and pBBRGEC plasmids were determined by differential scanning calorimetry (DSC) analysis and compared with the thermal properties of P(3HB) homopolymer. All data were determined from the endotherm profiles (Figure 4).

For the SCL-MCL PHA copolymer, two melting temperature peaks were observed as opposed to the single melting temperature peak observed for the P(3HB) homopolymer. The lower temperature melting peaks observed for the SCL-MCL PHA copolymers are from their respective original crystals, while the higher temperature melting peaks arose from the recrystallization that occurred during the heating process.

The weight-average molecular weight (M_w) of the polymer was determined by GPC which revealed that the M_w of the SCL-MCL PHA copolymer was slightly lower than that of the P(3HB) homopolymer, but that the polydispersity indices (M_w/M_n) were similar for the SCL-MCL PHA copolymer and P(3HB). As determined by NMR analysis, the SCL-MCL PHA copolymer consisted of 95.1 mol% 3HB, 3.6 mol% 3HHx, and 1.3 mol% 3HO monomer units as determined by NMR analysis. The addition of 4.9 mol% 3HHx and 3HO MCL-monomer units to the PHA copolymer lowered the melting temperature to 150 °C from 170 °C compared to the P(3HB) homopolymer sample. In addition, the enthalpy of fusion was lowered to 32 J/g compared to 52 J/g for the P(3HB) homopolymer. These results indicate that the polymer is an SCL-MCL PHA copolymer and that the additional pendant groups within the copolyester dramatically alter the thermal properties of the polymer. These differences in thermal properties may translate into enhanced physical properties, leading to the production of biodegradable polymers with a wider array of applications.

Downloaded by COLUMBIA UNIV on August 28, 2012 | http://pubs.acs.org
Publication Date: September 23, 2006 | doi: 10.1021/bk-2006-0939.ch003

Downloaded by COLUMBIA UNIV on August 28, 2012 | http://pubs.acs.org
Publication Date: September 23, 2006 | doi: 10.1021/bk-2006-0939.ch003

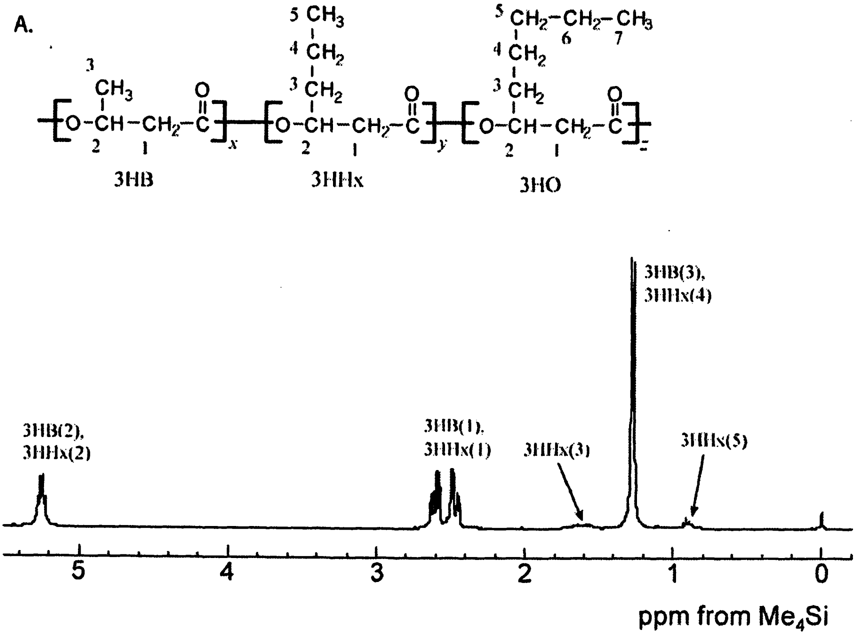

Figure 3. ^{1}H- and ^{13}C-NMR spectra of SCL-MCL PHA polymer isolated from E. coli *JM109 harboring the pTrcFabH(F87T) and pBBRSTQKECG plasmids grown in the presence of glucose. A. ^{1}H-NMR spectrum. B. ^{13}C-NMR with expanded carbonyl carbon resonances; 3HB, 3-hydroxybutyrate; 3HHx, 3-hydroxyhexanoate; 3HO, 3-hydroxyoctanoate.*

Downloaded by COLUMBIA UNIV on August 28, 2012 | http://pubs.acs.org
Publication Date: September 23, 2006 | doi: 10.1021/bk-2006-0939.ch003

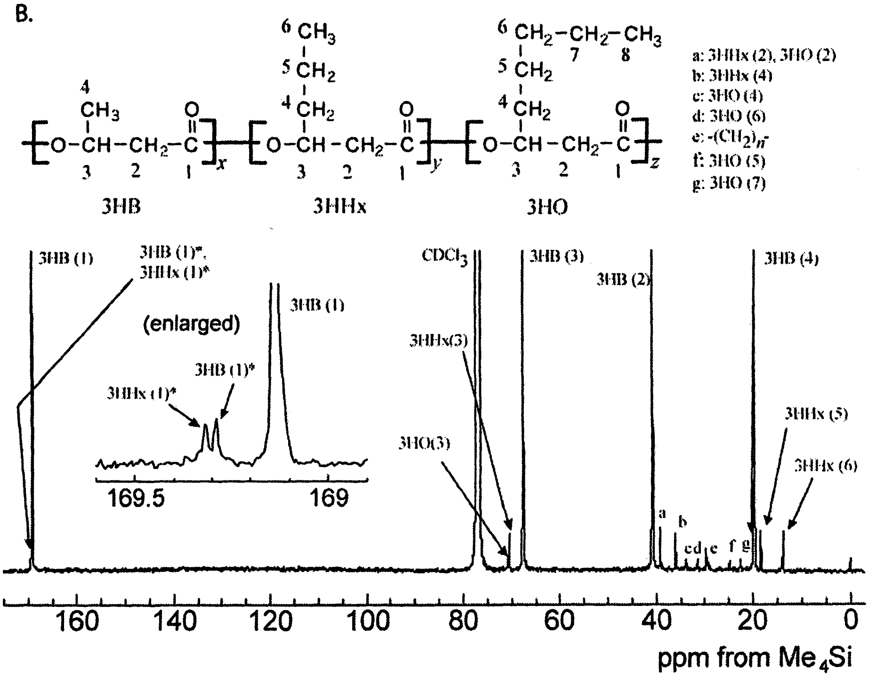

Figure 3. *Continued.*

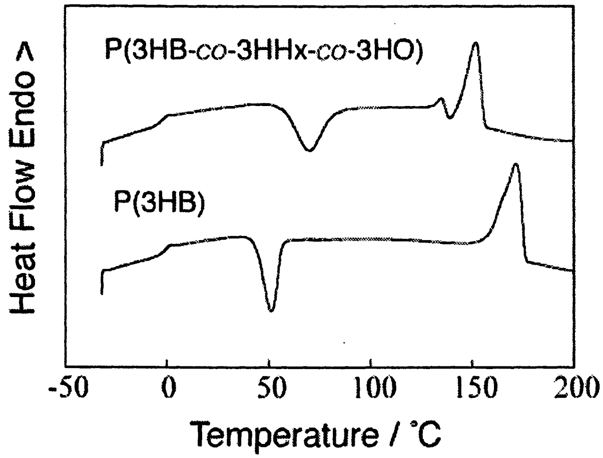

*Figure 4. DSC endotherm profiles for P(3HB-*co*-3.6% 3HHx-*co*-1.3% 3HO) copolymer and P(3HB) homopolymer.*

Conclusions

This study has shown that SCL and MCL PHA monomer supply from glucose is enhanced by overexpression of genes for the fatty acid biosynthesis enzymes (*fabH* and *fabG*) in recombinant *E. coli.* SCL-MCL PHA copolymers with a relatively low mol% of MCL monomer incorporated were produced by recombinant *E. coli* and the resultant T_m was dramatically reduced compared to that of P(3HB) homopolymer. The use of the fatty acid biosynthesis pathway for SCL and MCL PHA monomer supply provides a foundation from which more robust methods for the production of SCL-MCL PHA copolymers from non-related carbon sources can be developed.

Acknowledgements

C.T. Nomura is supported by a fellowship from the Japan Society for the Promotion of Science (JSPS). Additional financial support for this study was provided by a grant for Ecomolecular Science Research from RIKEN. The authors thank the following scientists for their contributions and technical advice regarding this study: T. Tanaka, K. Kuwabara, H. Abe, K. Takase, K. Taguchi, and Z. Gan. We would also like to thank J.J. Hull for critical reading of the manuscript.

Downloaded by COLUMBIA UNIV on August 28, 2012 | http://pubs.acs.org
Publication Date: September 23, 2006 | doi: 10.1021/bk-2006-0939.ch003

References

1. Sudesh, K.; Abe, H.; Doi, Y. *Prog Polym Sci* **2000**, *25*, 1503-1555.
2. Abe, H.; Doi, Y. *Biomacromolecules* **2002**, *3*, 133-138.
3. Nomura, C. T.; Taguchi, K.; Gan, Z.; Kuwabara, K.; Tanaka, T.; Doi, Y. *Appl Environ Microbiol* **2005**, *71,* 4297-4306.
4. Nomura, C. T.; Taguchi, K.; Taguchi, S.; Doi, Y. *Appl Environ Microbiol* **2004**, *70*, 999-1007.
5. Nomura, C. T.; Tanaka, T.; Gan, Z.; Kuwabara, K.; Abe, H.; Takase, K.; Taguchi, K.; Doi, Y. *Biomacromolecules* **2004**, *5*, 1457-1464.
6. Kusaka, S.; Abe, H.; Lee, S. Y.; Doi, Y. *Appl Microbiol Biotechnol* **1997**, *47*, 140-143.
7. Slater, S. C.; Voige, W. H.; Dennis, D. E. *J Bacteriol* **1988**, *170*, 4431-4436.
8. Schubert, P.; Steinbuchel, A.; Schlegel, H. G. *J Bacteriol* **1988**, *170*, 5837-5847.
9. Lee, S. Y.; Chang, H. N. *Can J Microbiol* **1995**, *41 Suppl 1*, 207-215.
10. Kalousek, S.; Lubitz, W. *Can J Microbiol* **1995**, *41 Suppl 1*, 216-221.
11. Valentin, H. E.; Zwingmann, G.; Schonebaum, A.; Steinbuchel, A. *Eur J Biochem* **1995**, *227*, 43-60.
12. Wong, H. H.; Lee, S. Y. *Appl Microbiol Biotechnol* **1998**, *50*, 30-33.
13. Hein, S.; Tran, H.; Steinbuchel, A. *Arch Microbiol* **1998**, *170*, 162-170.
14. Choi, J. I.; Lee, S. Y.; Han, K. *Appl Environ Microbiol* **1998**, *64*, 4897-4903.
15. Maehara, A.; Ueda, S.; Nakano, H.; Yamane, T. *J Bacteriol* **1999**, *181*, 2914-2921.
16. Lee, S. Y.; Choi, J.; Han, K.; Song, J. Y. *Appl Environ Microbiol* **1999**, *65*, 2762-2764.
17. Hong, K.; Leung, Y. C.; Kwok, S. Y.; Law, K. H.; Lo, W. H.; Chua, H.; Yu, P. H. *Appl Biochem Biotechnol* **2000**, *84-86*, 381-390.
18. Ahn, W. S.; Park, S. J.; Lee, S. Y. *Appl Environ Microbiol* **2000**, *66*, 3624-3627.
19. Taroncher-Oldenburg, G.; Stephanopoulos, G. *Appl Microbiol Biotechnol* **2000**, *54*, 677-680.
20. Taguchi, K.; Aoyagi, Y.; Matsusaki, H.; Fukui, T.; Doi, Y. *Biotech Lett* **1999**, *21*, 579-584.
21. Asrar, J.; Gruys, K. J. In *Biopolymers*; Doi, Y.; Steinbuchel, A., Eds.; WILEY-VCH: Weinheim, Germany, 2002; Vol. 4, pp 53-90.
22. Holmes, P. A. *Phys Technol* **1985**, *16*, 32-36.
23. Slater, S.; Houmiel, K. L.; Tran, M.; Mitsky, T. A.; Taylor, N. B.; Padgette, S. R.; Gruys, K. J. *J Bacteriol* **1998**, *180*, 1979-1987.

Downloaded by COLUMBIA UNIV on August 28, 2012 | http://pubs.acs.org
Publication Date: September 23, 2006 | doi: 10.1021/bk-2006-0939.ch003

24. Williams, S. F.; Martin, D. P. In *Biopolymers*; Doi, Y.; Steinbuchel, A., Eds.; WILEY-VCH: Weinheim, Germany, 2002; Vol. 4, pp 91-127.
25. Hein, S.; Sohling, B.; Gottschalk, G.; Steinbuchel, A. *FEMS Microbiol Lett* **1997**, *153*, 411-418.
26. Saito, Y.; Doi, Y. *Int J Biol Macromol* **1994**, *16*, 99-104.
27. Klinke, S.; Ren, Q.; Witholt, B.; Kessler, B. *Appl Environ Microbiol* **1999**, *65*, 540-548.
28. Rehm, B. H.; Mitsky, T. A.; Steinbuchel, A. *Appl Environ Microbiol* **2001**, *67*, 3102-3109.
29. Rehm, B. H.; Steinbuchel, A. *Appl Microbiol Biotechnol* **2001**, *55*, 205-209.
30. Takase, K.; Matsumoto, K.; Taguchi, S.; Doi, Y. *Biomacromolecules* **2004**, *5*, 480-485.
31. Takase, K.; Taguchi, S.; Doi, Y. *J Biochem* **2003**, *133*, 139-145.
32. Matsumoto, K.; Takase, K.; Aoki, E.; Doi, Y.; Taguchi, S. *Biomacromolecules* **2005**, *6*, 99-104.
33. Shimamura, E.; Kasuya, K.; Kobayashi, G.; Shiotani, T.; Doi, Y. *Macromolecules* **1994**, *27*, 878-880.

Downloaded by COLUMBIA UNIV on August 28, 2012 | http://pubs.acs.org
Publication Date: September 23, 2006 | doi: 10.1021/bk-2006-0939.ch003

Downloaded by UNIV OF GUELPH LIBRARY on August 10, 2012 | http://pubs.acs.org
Publication Date: September 23, 2006 | doi: 10.1021/bk-2006-0939.ch004

Chapter 4

Physical Properties, Structure Analysis, and Enzymatic Degradation of Poly[(*R*)-3-hydroxybutyrate-*co*-(*R*)-3-hydroxyvalerate] Films and Fibers

Tadahisa Iwata[1], Toshihisa Tanaka[1], Norihito Adachi[2], Masashi Hasegawa[2], Shinya Teramachi[2], and Yoshiharu Doi[1]

[1]Polymer Chemistry Laboratory, RIKEN Institute, 2–1 Hirosawa, Wako-shi, Saitama 351–1098, Japan
[2]Department of Applied Chemistry, Kogakuin University, Hachiouji, Tokyo 192–0015, Japan

High tensile strength films and fibers of poly[(*R*)-3-hydroxybutyrate-*co*-8mol%-(*R*)-3-hydroxyvalerate] were prepared by cold-drawing from amorphous preforms at a temperature near the glass transition temperature (T_g). High tensile strength fibers of over 1 GPa were processed by onestep-drawing with small crystal nuclei grown near T_g. Meltquenched films in a rubber state could be stretched reproducibly to a draw ratio of 16, and subsequent annealing under tension led to the improvement of the tensile strength and Young's modulus. The highly-ordered structure of films and fibers was investigated by wide- and small-angle X-ray diffractions in synchrotron radiation of SPring-8. The mechanical properties remained unchanged after storing for 6 months at room temperature, suggesting that a high crystallnity of the stretched-annealed films avoids a process of secondary crystallization. Cold-drawn films were enzymatically degraded with an extracellular PHB depolymerase purified from *Ralstonia pickettii* T1, and it was revealed that the stretched films had the shish-kebab structure.

In Degradable Polymers and Materials; Khemani, K., et al.;
ACS Symposium Series; American Chemical Society: Washington, DC, 2006.

Downloaded by UNIV OF GUELPH LIBRARY on August 10, 2012 | http://pubs.acs.org
Publication Date: September 23, 2006 | doi: 10.1021/bk-2006-0939.ch004

Introduction

Poly[(*R*)-3-hydroxybutyrate-*co*-(*R*)-3-hydroxyvalerate] (P(3HB-*co*-3HV)) is accumulated by a wide variety of microorganisms as intracellular carbon and energy storage material, and has been extensively studied as a biodegradable and biocompatible thermoplastics.[1,2] P(3HB-*co*-3HV) is successful copolyester, which has been produced commercially under the trade name of Biopol$^{\text{TM}}$. While P(3HB-*co*-3HV) has attracted much attention as textile products such as fishing line or surgical suture, etc., it has not been recognized as practical because of its stiffness and brittleness.[3] Furthermore, P(3HB-*co*-3HV) is a relatively unusual copolymer because 3HB and 3HV units are isodimorphous, that is, due to their similarity in shape and size, the 3HV units are incorporated into poly[(*R*)-3-hydroxybutyrate] (P(3HB)) crystal lattice.[4]

Recently, we succeeded in obtaining strong fibers and films from P(3HB) and its copolymers by hot-drawing and cold-drawing techniques.[5-15] The structure of P(3HB) fibers with high tensile strength of 1.32 GPa was analyzed by micro-beam X-ray diffraction with synchrotron radiation, and it was revealed that the P(3HB) fiber has a new core-sheath structure consistent with two types of molecular conformations: a 2_1 helix conformation (□-form) in the sheath region and a planar zigzag conformation (β-form) in the core region.[10,14]

In this paper, we describe the processing of P(3HB-*co*-3HV) films and fibers with high tensile strength by cold-drawing from amorphous perform. The highly-ordered structures were investigated by X-ray diffractions, and the fiber structure of mono-filament was revealed by micro-beam X-ray diffraction with synchrotron radiation at SPring-8, Japan.[15] Furthermore, the enzymatic degradability of P(3HB-*co*-3HV) films by using an extracellular PHB depolymerase purified from *Ralstonia pickettii* T1 is also addressed.

Experimental

Materials

Bacterial poly[(*R*)-3-hydroxybutyrate-*co*-8mol%-(*R*)-3-hydroxyvalerate] (P(3HB-*co*-8%-3HV)) was supplied by Monsanto Japan Co. M_w and polydispersity of P(3HB-*co*-8%-3HV) are 1.0×10^6 and 2.8, respectively. Samples after dissolution in chloroform at 100 °C were purified by precipitation in *n*-hexane and dried in vacuum. Melting temperature (T_m) and glass transition temperature (T_g) of the P(3HB-*co*-8%-3HV) powder are 143 °C and –4 °C, respectively, as measured by differential scanning calorimetry (DSC). The composition of 3HV unit determined by ^{1}H nuclear magnetic resonance (^{1}HNMR) in $CDCl_3$ was 7.7 mol%.

Downloaded by UNIV OF GUELPH LIBRARY on August 10, 2012 | http://pubs.acs.org
Publication Date: September 23, 2006 | doi: 10.1021/bk-2006-0939.ch004

Processing of films with high tensile strength

The films of P(3HB-*co*-8%-3HV) were prepared by a conventional solvent-casting technique from chloroform solution using glass petri dishes as casting surface. The amorphous preforms of films were prepared by melting of solvent-cast films in a hot press at 180 °C for 30 s and subsequently quenching into ice water. These amorphous preforms were oriented by cold-drawing 200% -1600% of their initial length in ice water and annealed in an autoclave at 50 °C -125 °C with weak tension to increase the crystallinity. All samples were used after aging for at least 3 days at room temperature.

Processing of fibers with high tensile strength

Melt-spinning of P(3HB-*co*-8%-3HV) was carried out using a laboratory-size extruder equipped with a single nozzle with an inner diameter of 1 mm. P(3HB-*co*-8%-3HV) was extruded at 170 °C, which was 10-20 °C higher than T_m. The extruder was taken up at 50-60 mm/s by roll and directly quenched into ice water placed 15 cm below the nozzle to obtain the amorphous fibers. The extrusion rate was 0.1-0.2 mm/s. One-step-drawing was performed against the quenched amorphous fibers by using a stretching machine at room temperature after isothermal crystallization for 24 h in ice water of near the T_g. Drawing rate by stretching machine was 4.5-5.0 mm/s. All drawn fibers to increase the crystallinity were annealed at 60 °C in an autoclave under constant tension for 30 min. All samples after aging for at least one week at room temperature were used to analyze.

Stress-strain test

Mechanical properties of films and fibers were evaluated by using a tensile testing machine (SHIMADZU EZTest). An initial specimen length of 10 mm was used. Tests were carried out a cross-head speed of 20 mm/min at room temperature. These results obtained were averaged over five samples for each condition.

Wide- and small-angle X-ray diffraction

The two dimensional wide-angle X-ray diffraction (WAXD) and smallangle X-ray scattering (SAXS) were carried out at beam line BL45XU with wavelength of 0.09 nm in synchrotron radiation at SPring-8, Harima, Japan. The diffraction patterns were recorded with a CCD camera (C7330-12-NR, Hamamatsu Photonics, Japan) with exposure time of 76-1058 ms. The pixel size of CCD camera was 125 μm ×125 μm. The camera length for WAXD and SAXS were 110 and 2337 mm, respectively.

Micro-beam X-ray diffraction

The micro-beam wide-angle X-ray diffraction was carried out at beam line BL47XU with wavelength of 0.15497 nm at 8 keV of synchrotron radiation at SPring-8, Harima, Japan. The experimental focus beam size was obtained as 0.5 μm by using Fresnel Zone Plate technique. Measurement for highly-ordered structure of strong P(3HB-*co*-8%-3HV) fiber with isothermal crystallization was linearly scanned perpendicular to the fiber axis with a step width of 4 μm between the individual frames. The diffraction patterns were recorded with a CCD camera (C4880-10-14A, Hamamatsu Photonics, Japan) with exposure time of 10 s. The camera length was 110 mm.

Enzymatic degradation

Polyhydroxybutyrate (PHB) depolymerase purified from *Ralstonia pickettii* T1 (200 μg/ml in phosphate buffer) was used for enzymatic degradation of P(3HB-*co*-8%-3HV) films. For enzymatic degradation tests of films, samples of 1 cm^2 film and 5 μl of *R. pickettii* T1 PHB depolymerase in 1 ml of potassium phosphate-buffer (pH 7.4) were incubated at 37 °C. Onset of degradation was measured as weight-loss over time. For weight-loss measurement, films were periodically removed, washed twice with distilled water, and dried to constant weight before analysis. Weight measurements of solvent-cast and stretched P(3HB-*co*-8%-3HV) films were performed every 1 h over a period of 6 h. Samples incubated without enzyme showed no weight loss even after 4 days.

Downloaded by UNIV OF GUELPH LIBRARY on August 10, 2012 | http://pubs.acs.org
Publication Date: September 23, 2006 | doi: 10.1021/bk-2006-0939.ch004

Scanning electron microscopy

Scanning electron micrographs (SEM) for the surface on samples were taken by using a JEOL JSM-6330F microscope, operated at an acceleration voltage of 5 kV, after samples were coated with gold using a SANYU DENSHI SC-701 quick coater.

Results and Discussion

Structure and mechanical properties of films

The cold-drawing of melt-quenched films (amorphous preform) of P(3HB-*co*-8%-3HV) succeeded easily and reproducibly at a temperature below, but near to, the glass transition temperature of 4 °C in ice water. The films were easily drawn at very low stress by 16 times against their initial length, but elastic recovery occurred on release from stretching machine. Accordingly, the annealing procedure is required for fixing the extended polymer chains. The maximum values of tensile strength were obtained at annealing temperature of 75 °C. Figure 1 shows the tensile strength and crystal orientation of P(3HB-*co*-8%-3HV) cold-drawn and annealed film. The tensile strength of P(3HB-*co*-8%-3HV) films was drastically increased up to 117 MPa, when the film was stretched at the draw ratio of 10. At the draw ratio of over 12, the tensile strength was almost identical as near 170 MPa, suggesting that the chain orientation parallel to the stretching direction is a limit at the draw ratio of over 12. This phenomenon can be explained by the fact that crystal orientation has already reached ca. 0.95, when the film was stretched at the draw ratio of over 10, as shown in Figure 1. Mechanical properties of cold-drawn and annealed films of P(3HB-*co*-8%-3HV) are summarized in Table 1, together with crystal orientation and X-ray crystallinity.

All reflections of wide-angle X-ray fiber diagram (WAXD) of 10 times cold-drawn film as shown in Figure 2A were indexed with orthorhombic unit cell parameters of P(3HB) homopolymer (α-form: a = 0.576 nm, b = 1.320 nm and c(fiber axis) = 0.596 nm, $P2_12_12_1$ space group) as reported by Yokouchi et al.[16] and by Okamura and Marchessault.[17] However, one sees a new reflection on the equatorial line in X-ray fiber diagram (Figure 2B) obtained from 16 times cold-drawn film, derived from the planar zigzag conformation (β-form), together with α-form reflections. Two kinds of molecular structures of P(3HB) were presented in Figure 2E. This β-form has been already confirmed in P(3HB-*co*-3HV) film by Orts et al.[18] and in P(3HB) fibers and films by Iwata et al.[8-10,12-15] Until now, it was considered that β-form is generated from the molecular chains in amorphous region between lamellar crystals by two-step drawing.[8-10,12,15,18] However, it is of interest that the β-form is clearly observed in X-ray fiber diagram of 16 times one-step cold-drawn film. This result indicates that the high orientation leads directly to the β-form from amorphous state of molecular

Downloaded by UNIV OF GUELPH LIBRARY on August 10, 2012 | http://pubs.acs.org
Publication Date: September 23, 2006 | doi: 10.1021/bk-2006-0939.ch004

chains. Thus, the generation of β-form supports the increase in tensile strength of cold-drawn films with the draw ratio of over 10, in spite of the crystal orientation being limited.

The small-angle X-ray scatterings (SAXS) of 10 times and 16 times cold-drawn films are shown in Figure 2C and 2D, respectively. The long periods of 10 times and 16 times cold-drawn films are 6.7 nm and 7.8 nm, respectively. Two spots along the meridian were clearly observed in SAXS pattern of 10 times cold-drawn film (Figure 2C), suggesting that this film consists of two regions of lamellar crystal (α-form crystal) and amorphous between lamellar crystals. However, in the case of 16 times cold-drawn film, the intensities of two reflections decreased, indicating that whole regions have almost same densities along the stretching direction. Based on the results that 16 times cold-drawn film has two kinds of crystalline domains (α-form and β-form) as shown in Figure 2B, it is concluded that the crystal densities of both crystalline domains are almost same.

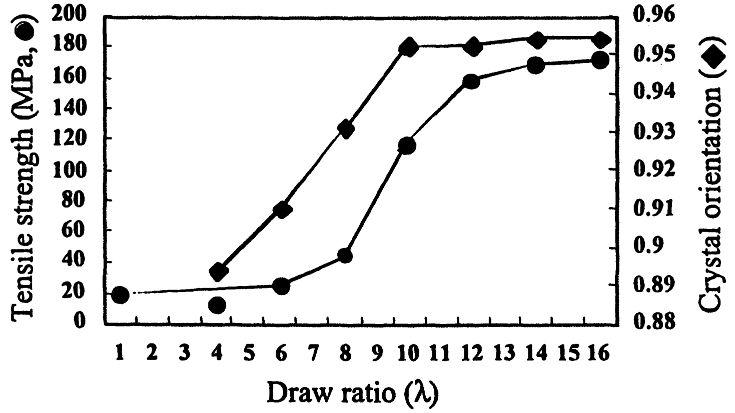

*Figure 1. Tensile strength (●) and crystal orientation (■) of P(3HB-*co*-8%-3HV) cold-drawn and annealed films, as functions of draw ratio. The crystal orientation was obtained from azimuthal scans of the (020) reflection in 2D WAXD pattern.*

Table I. Mechanical properties, crystal orientation, and crystallinity of cold-drawn and annealed P(3HB-*co*-8%-3HV) films, stored for 10 days or 6 months.

Draw ratio (λ)	Aging time (days)	Tensile strength (MPa)	Elongation to break (%)	Young's modulus (GPa)	Crystal orientation	Xc (%)
1	10	19±1.3	35±2	0.3±0.0	-	53
10	10	117±17	109±31	0.5±0.1	0.950	77
16	10	172±24	74±13	1.1±0.2	0.954	78
10	180	109±14	101±20	1.9±0.1	0.951	80

Downloaded by UNIV OF GUELPH LIBRARY on August 10, 2012 | http://pubs.acs.org
Publication Date: September 23, 2006 | doi: 10.1021/bk-2006-0939.ch004

Downloaded by UNIV OF GUELPH LIBRARY on August 10, 2012 | http://pubs.acs.org
Publication Date: September 23, 2006 | doi: 10.1021/bk-2006-0939.ch004

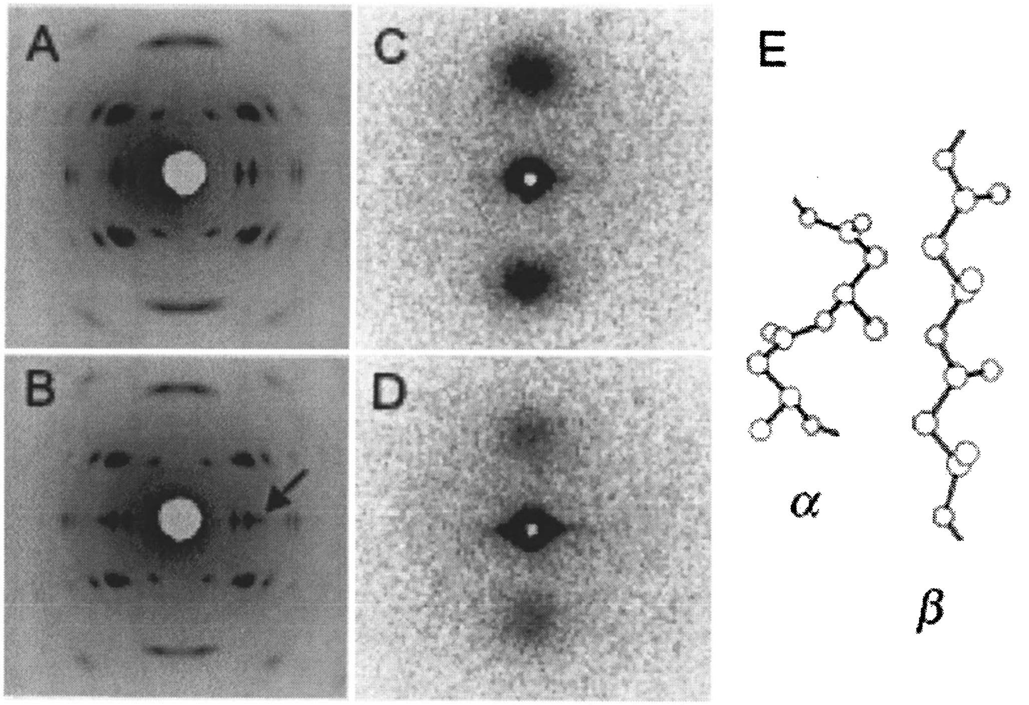

*Figure 2. WAXD and SAXS patterns of P(3HB-*co*-8%-3HV) cold-drawn and annealed films: (A and B) 10 times drawn film, and (C and D) 16 times drawn film. (E) Two kinds of molecular conformations (2_1 helix (α-form) and planar zigzag (β-form) conformations) of P(3HB) built by using the atomic coordinates reported in ref. 16 and ref. 18, respectively. Arrow indicates a reflection derived from β-form.*

Downloaded by UNIV OF GUELPH LIBRARY on August 10, 2012 | http://pubs.acs.org
Publication Date: September 23, 2006 | doi: 10.1021/bk-2006-0939.ch004

Structure and mechanical properties of fibers

P(3HB-*co*-8%-3HV) fiber was prepared by one-step-drawing procedure of amorphous fiber with small crystal nuclei at room temperature.[15] Amorphous fibers were obtained by quenching of the melt-spun fibers of P(3HB-*co*-8%-3HV) into ice water. Isothermal crystallization of amorphous P(3HB-*co*-8%-3HV) fibers was held in ice water for a certain period to prevent rapid crystallization and to grow small crystal nuclei. One-step-drawing after isothermal crystallization was performed by the stretching machine at room temperature, and then annealed at 60 °C for 30 min in an autoclave for fixing the extended polymer chains. One-step-drawn fibers with isothermal crystallization for 24 h were opaque and maximum total draw ratio was *ca.* 10 times.

The mechanical properties of one-step-drawn fibers of P(3HB-*co*-8%-3HV) are summarized in Table 2.[15] While the tensile strength of non-drawn fibers was ca. 30 MPa, the tensile strength of 5 times one-step-drawn fiber with isothermal crystallization increased to 710 MPa. Moreover, the tensile strength of 10 times one-step-drawn fiber increased to 1,065 MPa. The isothermal crystallization near glass transition temperature is considered to grow many small crystal nuclei.

Drawing with isothermal crystallization leads to the high orientation of molecular chains in amorphous region between small crystal nuclei. Figure 3 shows the WAXD and SAXS patterns of one-step-drawn P(3HB-*co*-8%-3HV) fibers without and with isothermal crystallization. The WAXD and SAXS patterns of as-spun fiber without isothermal crystallization showed the ring and four-point patterns, respectively, indicating that α-form crystals are not oriented and inclined (Figures 3A and 3B). On the other hand, the WAXD pattern of 10 times one-step-drawn fiber without isothermal crystallization showed the arc reflections of α-form and a weak reflection of β-form (Figure 3C), indicating the low orientation of α-form crystals along the drawing direction. The SAXS pattern of 10 times one-step-drawn fiber showed clear two-spot reflections corresponding to oriented lamellae along the meridian (Figure 3D).

The WAXD pattern of non-drawn fiber with isothermal crystallization showed only ring pattern contributed to unoriented α-form crystal (Figure 3E) as

Table II. Mechanical properties of cold-drawn and annealed P(3HB-*co*-8%-3HV) fibers[15].

Draw ratio (λ)	Tensile strength (MPa)	Elongation to break (%)	Young's modulus (GPa)
1 (as-spun)	27+3	15+5	1.2+0.2
5	710±126	50±6	6.8±1.4
10	1065±187	40±12	8.0±1.1

Downloaded by UNIV OF GUELPH LIBRARY on August 10, 2012 | http://pubs.acs.org
Publication Date: September 23, 2006 | doi: 10.1021/bk-2006-0939.ch004

the case of as-spun fiber without isothermal crystallization. On the other hand,the WAXD patterns of 10 times one-step-drawn fibers with isothermal crystallization showed the sharp reflections of α-form and a strong reflection of *β*-form (Figure 3G). The orientation of *α*-form crystals and the intensity of *β*-form reflection increased with increasing draw ratio for one-step-drawn fiber with isothermal crystallization. The (020) and (110) reflections are observed on the ring patterns in the WAXD patterns of one-step-drawn fibers as shown in Figure 3G. These ring patterns are considered to be derived from pseudohexagonal crystals oriented perpendicular to the fiber axis, as reported by Furuhashi *et al.*[19]

The SAXS patterns of 10 times one-step-drawn fibers with isothermal crystallization (Figure 3H) showed clear streak scatterings along the equator and weak reflections along the meridian, while the SAXS pattern of non-drawn fiber showed only ring pattern by unoriented lamellae (Figure 3F). The clear streak scatterings along the equator suggest that many voids seem to exist in one-step drawn fibers. The weak reflection along the meridian is considered to indicate that one-step-drawn fibers with isothermal crystallization have highly-oriented structure with almost same crystal densities of lamellar crystals (*α*-form) and planar zigzag chains (*β*-form).

Micro-diffraction techniques have been developed mainly at the ID13 beamline of the European Synchrotron Radiation Facility (ERSF) with a beam size of 3-10 μm for viscose rayon fibers,[20] spider silk,[21] spherulites of P(3HB),[22] and a poly(lactic acid)/(atactic-P(3HB)) blend.[23] Recently, we developed the micro-diffraction techniques with 0.5 μm beam size for analysis ultra-high-molecular-weight-P(3HB) mono-filament[10] and P(3HB) copolymer spherulites.[24] To reveal the detail fiber structure and the distribution of two types of molecular conformations in drawn P(3HB-*co*-8%-3HV) mono-filament, a micro-beam X-ray diffraction experiment was performed with synchrotron radiation at SPring-8, Japan. The beam size was focused to 0.5 μm with the Fresnel Zone Plate technique and the P(3HB-*co*-8%-3HV) mono-filament was scanned linearly perpendicular to the fiber axis with a step of 4 μm.

Figure 4 shows a series of micro-beam X-ray diffraction patterns of one-step-drawn P(3HB-*co*-8%-3HV) fiber with isothermal crystallization scanned perpendicular to the fiber axis. All micro-beam X-ray diffraction patterns of one-step-drawn fiber showed the reflections of both *α*- and *β*-forms. These reflections were not changed throughout fiber except for intensities. This result indicates that one-step-drawn P(3HB-*co*-8%-3HV) fiber with isothermal crystallization has not a core-sheath structure such as cold-drawn and two-step-drawn UHMW-P(3HB) fiber.[10] In the other word, one-step-drawn P(3HB-*co*-8%-3HV) fibers with isothermal crystallization is an uniform structure throughout fiber consistent with both *α*- and *β*-form crystals. This structure supports the result that one-step-drawn fiber with isothermal crystallization has a high tensile strength in spite of low draw ratio.

Downloaded by UNIV OF GUELPH LIBRARY on August 10, 2012 | http://pubs.acs.org
Publication Date: September 23, 2006 | doi: 10.1021/bk-2006-0939.ch004

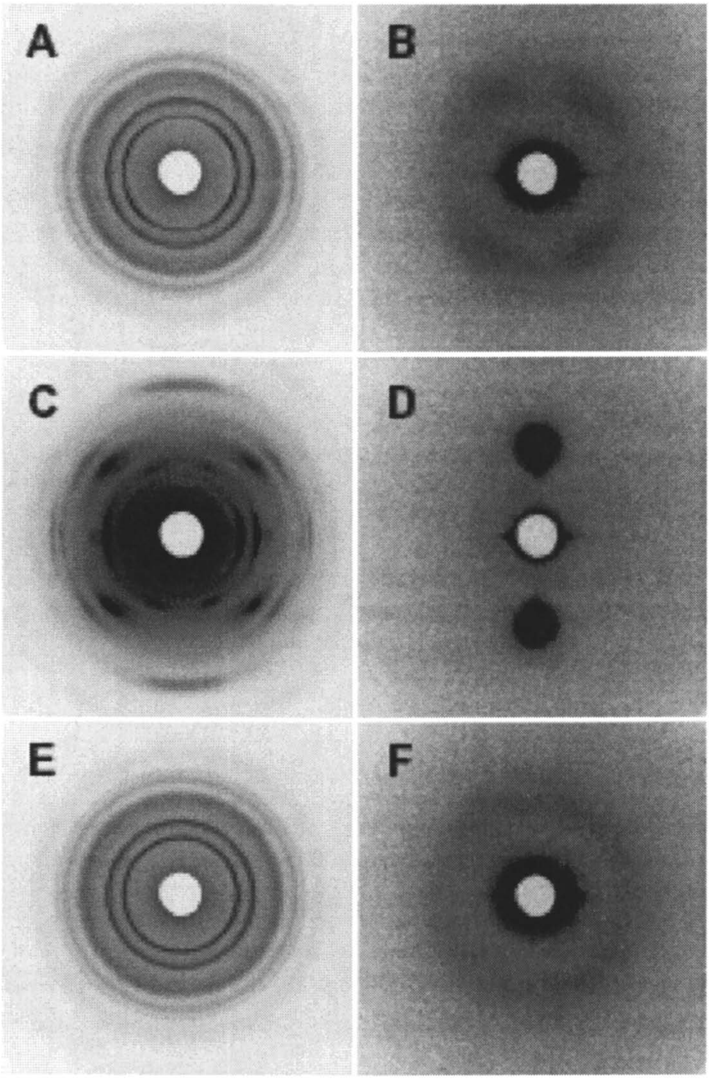

*Figure 3. WAXD and SAXS patterns of P(3HB-*co*-8%-3HV) fibers: (A and B) non-drawn fibers without isothermal crystallization, (C and D) 10 times one-step-drawn fibers without isothermal crystallization, (E and F) non-drawn fibers with isothermal crystallization, (G and H) 10 times one-step-drawn fibers with isothermal crystallization*[15].

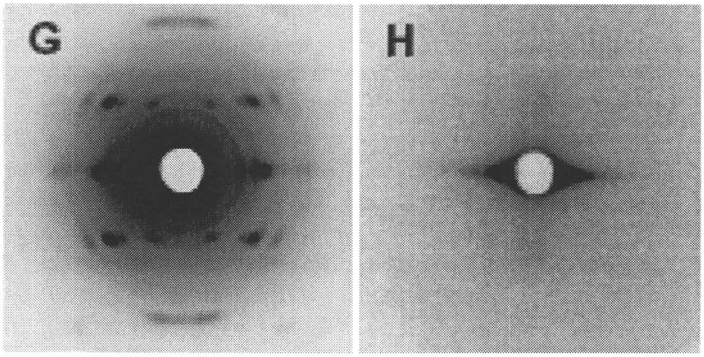

Figure 3. Continued.

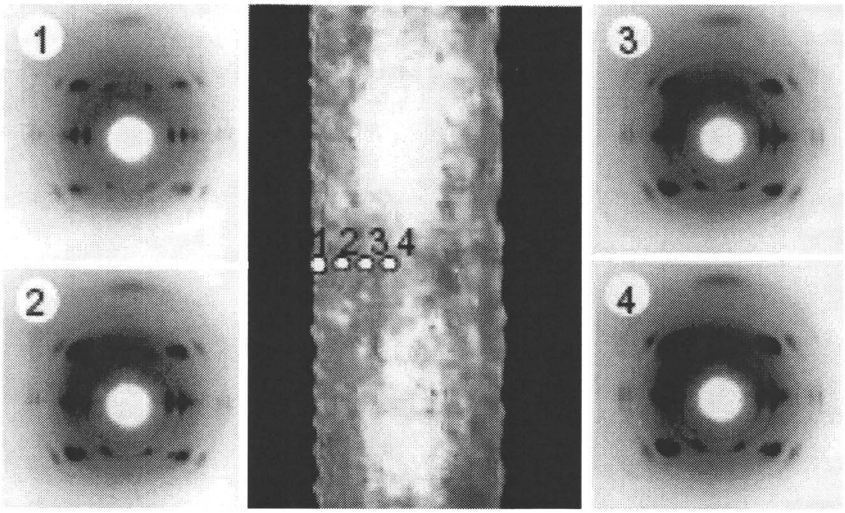

*Figure 4. Microbeam X-ray fiber diagrams of 10 times one-step-drawn P(3HB-*co*-8%-3HV) mono-filament with isothermal crystallization, recorded from the point in the microscope image*[15].

Downloaded by UNIV OF GUELPH LIBRARY on August 10, 2012 | http://pubs.acs.org
Publication Date: September 23, 2006 | doi: 10.1021/bk-2006-0939.ch004

Effect of storage time on mechanical properties

It is well known that the mechanical properties of P(3HB-*co*-8%-3HV) films markedly deteriorate to stiffness and brittleness by a process of secondary crystallization. The cold-drawn and annealed films of P(3HB-*co*-8%-3HV) were stored for 6 months at room temperature to study the time dependent change of the mechanical properties, and the stress-strain test was performed. The tensile strength and elongation to break of cold-drawn and annealed films remained unchanged for 6 months as summarized in Table 1. It is of importance to note that the mechanical properties of the cold-drawn and annealed film did not deteriorate during 6 months. It is concluded that a highly oriented and crystallized P(3HB) film keeps superior mechanical properties for long periods.

It is interesting to note that Young's modulus increased after the storage for 6 months. This result relates to the glass transition temperature (T_g) of P(3HB-*co*-8%-3HV). P(3HB-*co*-8%-3HV) molecules can move at room temperature during the storage because T_g of P(3HB-*co*-8%-3HV) is below room temperature. This molecular mobility causes the secondary crystallization and deterioration. However, in the case of cold-drawn and annealed film, since the entanglements of molecular chains are considered as less in amorphous region, the scission of molecular chains caused by the incorporation of molecular chains from amorphous region to crystal domain does not occur. Furthermore, the crystallinity measured by X-ray diffraction remained unchanged during the storage. Based on these results, the increase of Young's modulus of P(3HB-*co*-8%-3HV) cold-drawn and annealed film after the storage is due to the improvement of the stability for the chain-packing state of P(3HB-*co*-8%-3HV) molecules in crystal region.

Downloaded by UNIV OF GUELPH LIBRARY on August 10, 2012 | http://pubs.acs.org
Publication Date: September 23, 2006 | doi: 10.1021/bk-2006-0939.ch004

Enzymatic degradation

The enzymatic degradation of three kinds of P(3HB-*co*-8%-3HV) films, solvent-cast, 10 times cold-drawn film, and 16 times cold-drawn film, were performed in 0.1M phosphate buffer (pH 7.4) using an extracellular PHB depolymerase from *Ralstonia pickettii* T1 at 37°C. Figure 5 shows the rate of erosion profiles of P(3HB-*co*-8%-3HV) films as a function of time.

The amount of film erosion increased proportionally with time for all the samples. The rate of erosion of solvent-cast film of P(3HB-*co*-8%-3HV) was 0.50 mg/h/cm^2, and this value is five times faster than that of P(3HB) homopolymer solvent-cast film (0.10 mg/h/cm^2).[6] On the other hand, the rates of erosion of the 10 times and 16 times cold-drawn films were 0.38 and 0.32 mg/h/cm^2, respectively, suggesting the effect of the crystallinity and long period on the rate of erosion. We reported the effect of crystallinity and solid state structure on enzymatic erosion of P(3HB) stretched films.[6] In the case of P(3HB-*co*-8%-3HV), the enzymatic erosion rate seems to be strongly affected by the crystallinity and long period, as the case of P(3HB).

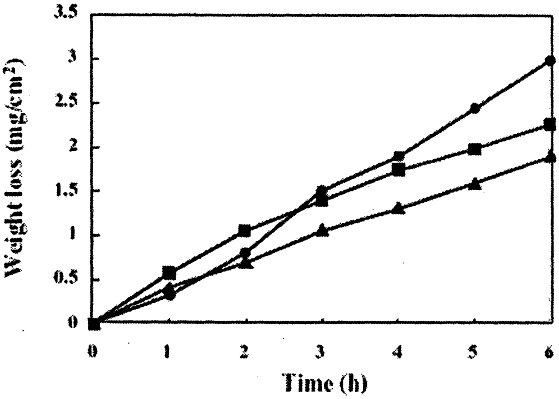

*Figure 5. Enzymatic degradation of P(3HB-*co*-8%-3HV) films in an aqueous solution of extracellular PHB depolymerase from* Ralstonia pickettii *T1 at 37 °C; (●) solvent-cast film, (■) 10 times cold-drawn and annealed film, and (▲) 16 times cold-drawn and annealed film.*

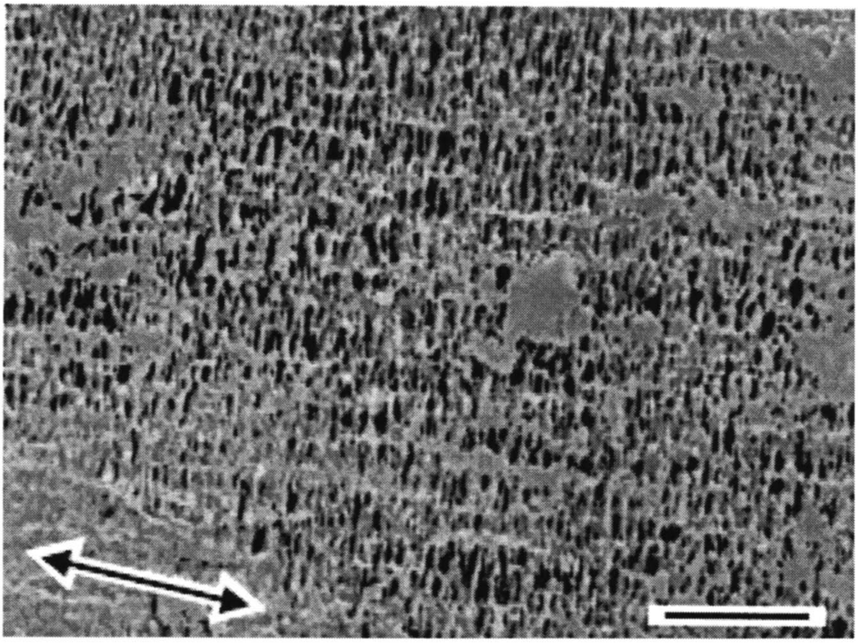

*Figure 6. Scanning electron micrograph of the cold-drawn and annealed P(3HB-*co*-8%-3HV) film after partial enzymatic degradation in an aqueous solution of extracellular PHB depolymerase from* Ralstonia pickettii *T1 at 37 °C. The scale bar represents 10 μm and the arrow indicates the stretching direction.*

Downloaded by UNIV OF GUELPH LIBRARY on August 10, 2012 | http://pubs.acs.org
Publication Date: September 23, 2006 | doi: 10.1021/bk-2006-0939.ch004

Figure 6 shows a scanning electron micrograph of 10 times cold-drawn film of P(3HB-*co*-8%-3HV) after partial enzymatic degradation using an extracellular PHB depolymerase from *R. pickettii* T1 at 37°C for 3 h. It is well known that the amorphous region is etched faster than the crystal one. Accordingly, this micrograph expresses the unetched core along the draw direction and lamellar crystals perpendicular to the core. The P(3HB-*co*-8%-3HV) at the surface of the film seems to have a shish-kebab morphology similar as found P(3HB) stretched films. The high tensile strength of both films might be due to a stretched chain core in the shish-kebab morphology, together with the generation of planar zigzag conformation.

Downloaded by UNIV OF GUELPH LIBRARY on August 10, 2012 | http://pubs.acs.org
Publication Date: September 23, 2006 | doi: 10.1021/bk-2006-0939.ch004

Conclusions

Uniaxially oriented films of P(3HB-*co*-8%-3HV) were prepared by cold-drawing from amorphous preform at a temperature near to the glass transition temperature (T_g). High tensile strength fibers of P(3HB-*co*-8%-3HV) were produced from amorphous states by one-step-drawing at room temperature after isothermal crystallization at T_g to grow small crystal nuclei. The colddrawn films had acceptable mechanical properties with high tensile strength and elongation to break, and showed hardly any variation after storing for 6 months at room temperature. It has been suggested that the embrittlement of P(3HB-*co*-8%-3HV) films due to secondary crystallization is avoided by its high crystallinity and high degree of orientation. The rate of enzymatic degradation of cold-drawn films by using an extracellular PHB depolymerase purified from *Ralstonia pickettii* T1 decreased with increasing in draw ratio, and it was revealed that the cold-drawn films had the shish-kebab structure.

The tensile strength of 10 times one-step-drawn fiber was over 1.0 GPa, which corresponded to those of common plastics such as polyethylene and poly(ethylene terephthalate). The molecular and highly ordered structure of mono-filament was analyzed by a micro-beam X-ray diffraction with synchrotron radiation at SPring-8, Japan.

Both stretched films and fibers had two kinds of molecular conformations, 2_1 helix (α-form) and planar zigzag (β-form) conformations. The improvement of mechanical properties is due to the generation of β-form that exists between α-form lamellar crystals. In SAXS patterns of highly stretched films and fibers, the intensities of reflections along the stretching direction, which indicate the long period of lamellar crystals, remarkably decreased, suggesting that two crystalline forms have almost same crystal densities.

Acknowledgments

This work has been supported by a Grant-in-Aid for Young Scientists (A) from the Ministry of Education, Culture, Sports, Science and Technology (MEXT) of Japan (No. 15685009) (to T. Iwata) and by a grant for Ecomolecular Science Research provided by RIKEN Institute. The synchrotron radiation experiments were performed at the SPring-8 with the approval of the Japan Synchrotron Radiation Research Institute (JASRI) (Proposal No. 2003B0054-NL2b-np and No. 2004B0016-ND1b-np).

Downloaded by UNIV OF GUELPH LIBRARY on August 10, 2012 | http://pubs.acs.org
Publication Date: September 23, 2006 | doi: 10.1021/bk-2006-0939.ch004

References

1. Doi, Y. In *Microbial Polyesters*; VCH Publishers: Weinheim, 1990.
2. Yoshie, N.; Inoue, Y. *Biopolymers*, *Vol. 3b*, *Polyesters II*; Doi, Y.; Steinbüchel, A., Eds.; Wiley-VCH: Weinheim, 2002; pp 133-156.
3. Holmes, P. A. *Developments in Crystalline Polymers Vol. 2*; Bassett, D.C., Ed.; Elsevier Applied Science: London, 1988; pp 1-65.
4. Yoshie, N.; Saito, M.; Inoue, Y. *Macromolecules* **2001**, *34*, 8953.
5. Kusaka, S.; Iwata, T.; Doi, Y. *J. Macromol. Sci. - Pure Appl. Chem.* **1998**, *35*, 319.
6. Kusaka, S.; Iwata, T.; Doi, Y. *Int. J. Biol. Macromol.* **1999**, *25*, 87.
7. Iwata, T.; Kusaka, S.; Doi, Y. *Polymer from Renewable Resources: Biopolyesters and Biocatalysis*; Scholz, C.; Gross, R. A. Eds.; *ACS Symp. Ser., 76*; Washington, 2000; pp. 67-76.
8. Aoyagi, Y.; Doi, Y.; Iwata, T. *Polym. Degrad. Stab.* **2003**, *79*, 209.
9. Iwata, T.; Tsunoda, K.; Aoyagi, Y.; Kusaka, S.; Yonezawa, N.; Doi, Y. *Polym. Degrad. Stab.* **2003**, *79*, 217.
10. Iwata, T.; Aoyagi, Y.; Fujita, M.; Yamane, H.; Doi, Y.; Suzuki, Y.; Takeuchi, A.; Uesugi, K. *Macromol. Rapid Commun.* **2004**, *25*, 1100.
11. Fischer, J. J.; Aoyagi, Y.; Enoki, M.; Doi, Y.; Iwata, T. *Polym. Degrad. Stab.* **2004**, *83*, 453.
12. Iwata, T.; Fujita, M.; Aoyagi, Y.; Doi, Y.; Fujisawa, T. *Biomacromolecules* **2005**, *6*, 1803.
13. Iwata, T.; Doi, Y. *Macromol. Symp.* **2005**, *224*, 11.
14. Iwata, T. *Macromol. Biosci.* **2005**, *5*, 689.
15. Tanaka, T.; Fujita, M.; Suzuki, Y.; Takeuchi, A.; Uesugi, K.; Ito, K,; Fujisawa, T.; Doi, Y.; Iwata, T. submitted to *Biomacromolecules*.
16. Yokouchi, M.; Chatani, Y.; Tadokoro, H.; Teranishi, K.; Tani, K. *Polymer* **1973**, 14, 267.

17. Okamura, K.; Marchessault, R. H. *Conformation of Biopolymers*, *Vol. 2*, Ramachandra, G. N., Ed.; Academic Press: New York, 1967; pp. 709-720.
18. Orts, W. J.; Marchessault, R. H.; Bluhm, T. L.; Hamer, G. K. *Macromolecules* **1990,** *23*, 5368.
19. Furuhashi, Y.; Ito, H.; Kikutani, T.; Yamamoto, T.; Kimizu, M.; Cakmak, M. *J. Polym. Sci., Part B: Polym. Phys.* **1998,** *36*, 2471.
20. Muller, M.; Riekel, C.; Vuong, R.; Chanzy, H. *Polymer* **2000,** *41*, 2627.
21. Riekel, C.; Madsen, B.; Knight, D.; Vollrath, F. *Biomacromolecules* **2000,** *1*, 622.
22. Gazzano, M.; Focarete, M. L.; Riekel, C.; Scandola, M. *Biomacromolecules* **2000,** *1*, 604.
23. Gazzano, M.; Focarete, M. L.; Riekel, C.; Scandola, M. *Biomacromolecules* **2004,** *5*, 553.
24. Tanaka, T.; Fujita, M.; Takeuchi, A.; Suzuki, Y.; Uesugi, K.; Doi, Y.; Iwata, T. *Polymer* **2005,** *46*, 5673.

Downloaded by UNIV OF GUELPH LIBRARY on August 10, 2012 | http://pubs.acs.org
Publication Date: September 23, 2006 | doi: 10.1021/bk-2006-0939.ch004

Downloaded by OHIO STATE UNIV LIBRARIES on August 28, 2012 | http://pubs.acs.org
Publication Date: September 23, 2006 | doi: 10.1021/bk-2006-0939.ch005

Chapter 5

Bacterial Poly(β-hydroxybutyrate): Hydrophilized and Colored

K. Busse[1], H. Budde[1], C. Scholz[2], and J. Kressler[1]

[1]Department of Engineering Science, Martin-Luther-University,
Halle-Wittenberg, D–06099 Halle, Saale, Germany
[2]Department of Chemistry, University of Alabama in Huntsville,
Huntsville, AL 35899

This study described synthesis and investigation of physical properties of hydrophilized and colored poly(β-hydroxybutyrate) (PHB) copolymers obtained by modulated fermentation of *Azotobacter vinelandii UWD* and *Wautersia eutropha.* During fermentation, poly(ethylene glycol) (PEG), di(ethylene glycol) (DEG), pentaerythritol ethoxylate (PEE) and ethoxylated anthraquinone dye were used to modulate the bacterial synthesis of PHB. Small-angle X-ray scattering (SAXS) showed that lamellar distances decreased for modulated PHB when compared to neat PHB. Furthermore, the contact angle of water on the PHB/PEG or PHB/DEG polymer surfaces decreased when compared to that of PHB, which corresponds to an increase in surface tension, and therefore to hydrophilization. The ethoxylated anthraquinone dye (alizarin) was chemically linked to the PHB chain and led to a change of the color from white to yellow or orange, depending on the pH-value of the environment.

In Degradable Polymers and Materials; Khemani, K., et al.;
ACS Symposium Series; American Chemical Society: Washington, DC, 2006.

Poly(β-hydroxyalkanoate)s, PHAs, the term is generally reserved for microbial polyesters, are a family of biopolyesters with varying side-chain lengths. PHAs were shown to be biocompatible, in particular in the realm of treatment of bone related deseases. Specifically, poly(β-hydroxybutyrate), PHB, is the most widely investigated PHA and has been studied for a variety of bone-replacement applications (1-5). However, due to its hydrophobicity, PHB is not blood compatible and the exposure of blood to PHB-surfaces leads to platelet adhesion and subsequent thrombi formation (6). It has been shown, that end-capping a growing PHB-chain with PEG will increase the surface tension of bulk samples (7). PEG is able to penetrate the cell walls of polyester-producing microorganisms and in small concentration (below 10%) does not deter their growth. PEG-modulated fermentation has been shown in the past to produce natural-synthetic hybrid block copolymers (8-11). The microorganisms carry out the PEG-ylation of nascent PHB chains via a competition reaction at the active site of the polymerase enzyme thus guaranteeing the formation of isotactic PHB in *R*-configuration and its subsequent end-capping with PEG (12). The *R*-configuration is known to be responsible for the bone-compatibility (13,14). Pentaerythritol ethoxylate (PEE) can be regarded as a starlike PEG oligomer (Fig. 1) and can also be used for modified fermentation (15).

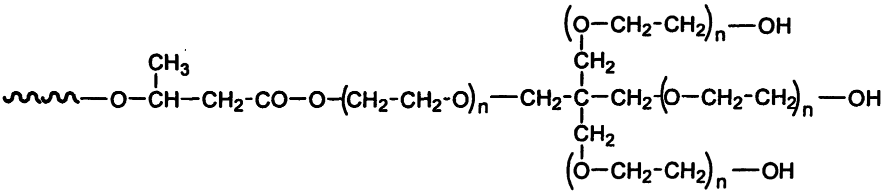

Figure 1. Pentaerythritol ethoxylate, a starlike PEG oligomer linked to PHB via ester bond

The present study focuses on elucidating and quantifying the physical changes in the polymers that were induced by the PEG-modulation of the PHB-synthesis. PEG is a polyether that is known for its exceptional blood and tissue compatibility, it is used extensively as stealth material in a variety of drug delivery vehicles and is also under investigation as surface coating for biomedical implants. PEG, when dissolved in water, has a low interfacial free energy, exhibits rapid chain motion, and its large excluded volume leads to steric repulsion of approaching molecules (16, 17). These properties are responsible for the superb biocompatibility of PEG. However, PEG is not a thermoplastic material and therefore not moldable. Furthermore, a PEG-modified alizarin dye is used for modulated fermentation in order to synthesize colored bacterial PHB.

Downloaded by OHIO STATE UNIV LIBRARIES on August 28, 2012 | http://pubs.acs.org
Publication Date: September 23, 2006 | doi: 10.1021/bk-2006-0939.ch005

Colored PHB might replace normal PHB in fields where pH sensitivity is required or when absorption in the range of visible light is preferred. Furthermore, colored PHB's may be attractive alternatives for petroleum based plastics, since they are biodegradable and produced from renewable resources.

In previous works, PEG-modified fermentations of *Wautersia eutropha* (syn. *Alcaligenes eutrophus,* ATCC 17697) and *Azotobacter vinelandii UWD* (ATCC 53799) were conducted and PHB was end-capped with diethyleneglycol (DEG), pentaerythritol ethoxylate (PEE, molecular weigth 270 and 800 g/mol), and PEG's of varying molecular weight (400, 2000 and 3400 g/mol PEG) (7,12,15). Previous characterization of the polymers included molecular weight analysis by GPC, static light scattering, and viscometry. In addition, the chemical structure of the polymer was characterized by ^{1}H-NMR and heteronuclear multiple bond correlation (HMBC) spectroscopy. The results verified a covalent bond for the PHB/DEG copolymers. In subsequent cell adhesion experiments, it was shown that the naturally hydrophobic PHB-surface could be modified to a more cell-deterring surface by modification with PEG of varying molecular weights. Contact angles of PHB, PHB/DEG, and PHB/PEG block copolymers with water were compared. Wide angle X-ray scattering (WAXS) studies of PHB have shown the chains to be in a helical conformation (whether right or left-handed is still debatable) (18-20). PHB has lath-shaped lamellar crystals, meaning they are folded chain crystals in which the fiber axis is normal to the lamellar surface (21). This is a common feature of crystalline morphology, especially when the polymer is precipitated from dilute solution (22). PHB has a great propensity for assuming this lamellar morphology; therefore, it is a prime candidate for identification studies (23, 24). It is this definitive nature of PHB that allowed for X-ray comparable studies using small angle X-ray scattering (SAXS) to determine the interplane or lamellar distance. The dye modified PHB was analyzed by UV-Vis spectroscopy and colored bulk samples were produced.

Downloaded by OHIO STATE UNIV LIBRARIES on August 28, 2012 | http://pubs.acs.org
Publication Date: September 23, 2006 | doi: 10.1021/bk-2006-0939.ch005

Experimental Section

Materials

PEGs of different molecular weight (400, 2000 and 3400 g/mol) were used as received. PEEs of different molecular weight (270 and 800 g/mol) were purchased from Sigma Aldrich and used as received.

The ethoxylated dye was synthesized anionically from alizarin dye according to the following reaction scheme (Figure 2) in a pressurized steel reactor. After chromatographic purification from side products, the structure of the dye was confirmed by NMR spectroscopy and the molecular weights were measured by GPC. As the main product α-hydroxy,β-hydroxy-oligoethoxy anthraquinone (eth. dye; Fig. 2 b) is formed, since the OH group at β-position is most acidic and can readily be transformed to the alcoholate. As a side product, α,β-hydroxy-oligoethoxy anthraquinone (Fig. 2 c) can be observed, whereas α-hydroxy-oligoethoxy,β-hydroxy anthraquinone (Fig. 2 d) is not formed.

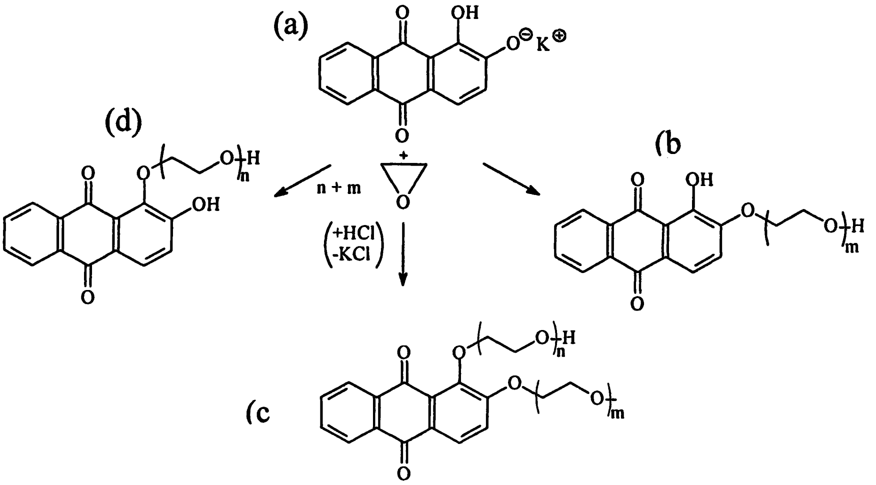

Figure 2. Formation of various ω-hydroxy-oligoethoxy-9,10-anthraquinones (b-d) from 1,2-dihydroxy-9,10-anthraquinone potassium salt(a)

Synthesis of Block Copolymers

A. vinelandii UWD and *W. eutropha* were grown in a two-step process, employing a pre-culture and a polymer medium. For PEG and DEG modulated fermentation, *A. vinelandii UWD* was used. After 48 h of growth, 10 vol.% of the pre-culture were used as inoculum for the polymer medium, which was harvested after 24 h (12). Both media were amended with 2.0 wt % of the respective PEGs. It is noteworthy that *A. vinelandii UWD* must be grown in the presence of 20 mg/L rifampicin, in order to prevent the back mutation of the engineered strain to the *A. vinelandii UW* parental strain genotype, which is not resistant to the antibiotic. All fermentation experiments were conducted in a shaker-incubator (New Brunswick Scientific) at 30 °C and 180 rpm. Cells were

Downloaded by OHIO STATE UNIV LIBRARIES on August 28, 2012 | http://pubs.acs.org
Publication Date: September 23, 2006 | doi: 10.1021/bk-2006-0939.ch005

harvested by centrifugation and lyophilization yielded biomass pellets. The polymer was extracted from these pellets by refluxing for 8 h with methylene chloride, concentrating the solution in a rotary evaporator, and precipitating the polymer into chilled methanol. After collecting by filtration and drying under vacuum, the polymer was purified by recrystallization, i.e. redissolving in methylene chloride, concentrating, and precipitating into chilled methanol (15). The hydrophilic PEG and DEG are expected to wash out of the polymer if they were not covalently linked.

For PEE and dye modulated fermentation, *W. eutropha* was used. Five cultures of 50 mL were prepared in 200 mL shake flasks for the inoculation. The cultures grew for 5 h. These pre-cultures were used as inoculum for batch fermentation with an initial volume of 4 L. A specific culture broth formulation was used: 20 g/L fructose, 6.7 g/L $Na_2HPO_4{\cdot}7H_2O$, 2 g/L $(NH_4)_2SO_4$, 1.5 g/L $MgSO_4{\cdot}7H_2O$, 6 mg/L KH_2PO_4, 7.5 mg/L $Fe(NH_4)$citrate, 7.5 mg/L $CaCl_2$. All broth formulations were prepared in deionized water. The pH was kept constant at 7.0 by continuously adding aqueous ammonia (20 wt %) solution and 1 M H_3PO_4 at a temperature of 30 °C. The growth of *W. eutropha* was initiated in a fermenter Biostat C in nutrient-rich broth under aerobic conditions for 24 h. The cells were then harvested aseptically by centrifugation (5900g, 10 min). Typically, the cell dry mass (CDM) of the first-stage *W. eutropha* cultivations was approximately 9 g/L. The cells were aseptically transferred into four fermenters (Sixfors) containing 400 mL of nitrogen-free broth and 30 g/L sterile fructose as the polymer-producing substrate with different amounts of PEE and of ethoxylated anthraquinone dye. The organisms were cultivated at 30 °C and a pH value of 7.0. At the end of the fermentations, the cells were separated, washed, and freeze dried. The CDM (approximately 8 g) was then extracted with 250 mL of methylene chloride, and the polymers were recovered by precipitation in an excess of cooled methanol, filtration, and drying.

The characteristics of the samples investigated are given in Table I.

Polymer Analyses

The chemical structure of the biopolymers was determined using a nuclear magnetic resonance spectrometer (Varian Unity Inova). Molecular weights of the polymers were determined by gel permeation chromatography (GPC) in chloroform using a Biorad system equipped with a Styragel HR4E column (Waters). The molecular weight data obtained by GPC were verified by static light scattering using a He-Ne laser with a wavelength of 632.8 nm and by viscometry using a Cannon-Ubbelohde viscometer. Samples were dissolved in chloroform with concentrations ranging between 0.1 and 2.5 mg/mL and solution flow times were recorded to the nearest 0.01 s. Molecular weights were

Downloaded by OHIO STATE UNIV LIBRARIES on August 28, 2012 | http://pubs.acs.org
Publication Date: September 23, 2006 | doi: 10.1021/bk-2006-0939.ch005

determined using the Kuhn-Mark-Houwink formula with $K = 7.7 \times 10^{-3}$ mL/g and $\alpha = 0.82$ (25).

Table I. Description of Investigated Samples.

Sample (abbrev)	*Sample*	*M_w by GPC [kg/mol]*
PHB-1	PHB (*A. vinelandii UWD*)	630
DEG	PHB-1 + DEG	650
PEG4	PHB-1 + PEG 400	140
PEG20	PHB-1 + PEG 2000	n.d.
PEG34	PHB-1 + PEG 3400	500
PHB-2	PHB (*W. eutropha*)	1220
PEE-270	PHB-2 + 2 vol% PEE (270 g/mol)	500
PEE-270b	PHB-2 + 5 vol% PEE (270 g/mol)	260
PEE-800	PHB-2 + 2 vol% PEE (800 g/mol)	890
eth. dye	α-hydroxy-β-hydroxyethyl-oligoethoxy anthraquinone	0.8
Col.-PHB	PHB-2 + ethoxylated anthraquinone dye	100

n.d.: not determined

SAXS data for PEG and DEG modified PHBs were obtained in the θ range of 0.2-5° from measurements with a two-dimensional (2D) detector (SIEMENS HI star) installed on a rotating anode (Rigaku) X-ray instrument with fine focus source. SAXS measurements for PEE modified PHB were performed in a Kratky camera (Anton Paar). The PEE modified samples were isothermally crystallized at 140 °C for 1 week. The SAXS data are background corrected and Fourier transformed to obtain the one dimensional correlation function. The PHB crystallinity was determined by wide-angle X-ray scattering (WAXS) using a Rigaku RU-200 (50kV/180mA) in the θ range of 5-50°.

The AFM experiments were carried out using a Nanoscope IIIa (Digital Instruments). The dried material was pressed between cover glasses on a hot stage, annealed at 180 °C for several minutes and rapidly quenched to the crystallization temperature of 140 °C. After the crystallization was completed, the samples were placed in distilled water in order to remove the cover glass from the film surface.

Downloaded by OHIO STATE UNIV LIBRARIES on August 28, 2012 | http://pubs.acs.org
Publication Date: September 23, 2006 | doi: 10.1021/bk-2006-0939.ch005

The light microscope was equipped with a hot stage for isothermal annealing experiments. Photographs of spherulites were taken after isothermal crystallization at 130 °C.

The contact angles were measured using the sessile drop method on a polymer film. The films were obtained by dissolving the polymers in methylene chloride (~ 2 wt.% solution), putting drops of the solution on a glass slide, and then spinning the slide using a Micro-Bit (Model PWM32) for 30 sec at 2000 rpm. This provided a uniform and thin polymer surface suited for contact angle analysis. A drop of 30 μl of freshly bidistilled water was placed on each sample. The sessile drop analyses were performed with an OCA 20 (DataPhysics Instruments GmbH) contact angle instrument, employing both digital imaging and drop-shape analysis. The advancing contact angle was measured for 8 drops on both sides at a temperature of 20°C and the average was calculated from the data. In this study, the surface tension or free energy (γ) is calculated from the contact angle (θ) using an iterative method due to Li and Neumann (26, 27), based on results of Good and Girifalco (28).

UV-Vis spectra were obtained using a Cary 5000 spectrometer (Varian). The samples were dissolved in chloroform.

Downloaded by OHIO STATE UNIV LIBRARIES on August 28, 2012 | http://pubs.acs.org
Publication Date: September 23, 2006 | doi: 10.1021/bk-2006-0939.ch005

Results and Discussion

The modification of PHB during fermentation is frequently carried out using PEG-like oligomers, since OH containing molecules terminate the polymerization reaction and the terminating reagent can be covalently incorporated into the polymer chain. Thus it seems reasonable, that an ethoxylated dye will lead to colored PHB when used as terminating reagent during fermentation.

Figure 3 shows the ^{1}H-NMR spectra of initial alizarin and its oligoethoxylated product, eth. dye. From the broadening and appearance of additional peaks, it can be concluded, that the ethoxylation was successful.

A characteristic ^{1}H NMR spectrum of the PEE-modified PHBs is shown in Figure 4. The sample PEE-270b showed the characteristic peaks of PHB, and additionally signals indicating the presence of covalently bound PEE were observed. Signals in the range of 3.6 ppm (inset a) were caused by the methylene protons of PEE, and the signal at 4.25 ppm (inset b) can unambiguously assigned to the methylene protons adjacent to the ester group that linked the PHB terminal carboxyl group to the PEE moiety (10). Similar NMR spectra were observed for the other modified PHB samples.

As described in the experimental part, one fermentation of PHB in the presence of eth. dye was carried out. After extensive purification of the polymer, by dissolution and precipitation processes, it can be assumed, that the original eth. dye was completely removed. Nevertheless, the polymer remained a yellow

Downloaded by OHIO STATE UNIV LIBRARIES on August 28, 2012 | http://pubs.acs.org
Publication Date: September 23, 2006 | doi: 10.1021/bk-2006-0939.ch005

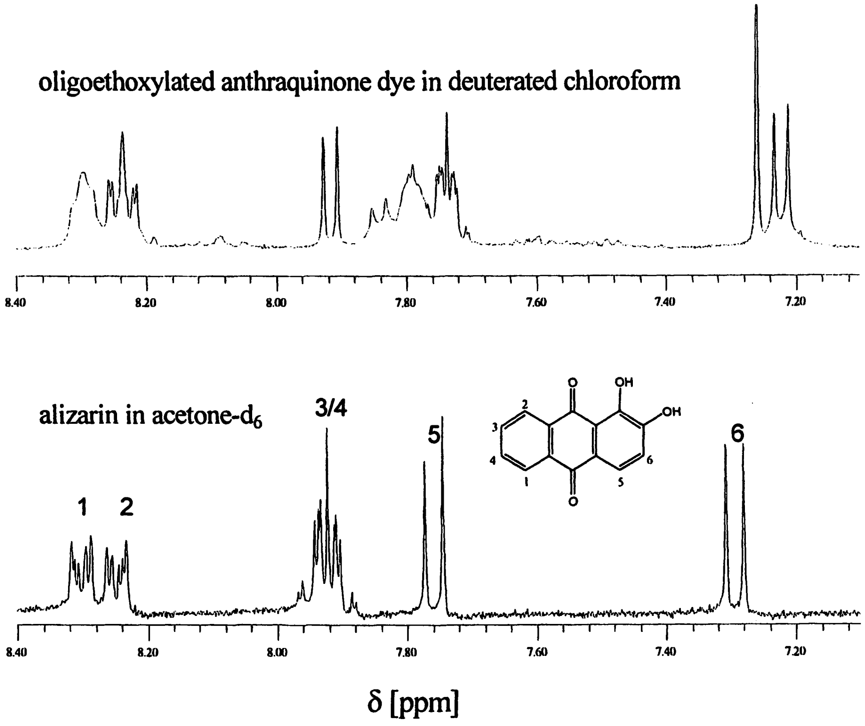

Figure 3: ^{1}H-NMR-spectroscopy of eth.-dye in deuterated chloroform (top) and original alizarin dye in deuterated acetone (bottom)

Downloaded by OHIO STATE UNIV LIBRARIES on August 28, 2012 | http://pubs.acs.org
Publication Date: September 23, 2006 | doi: 10.1021/bk-2006-0939.ch005

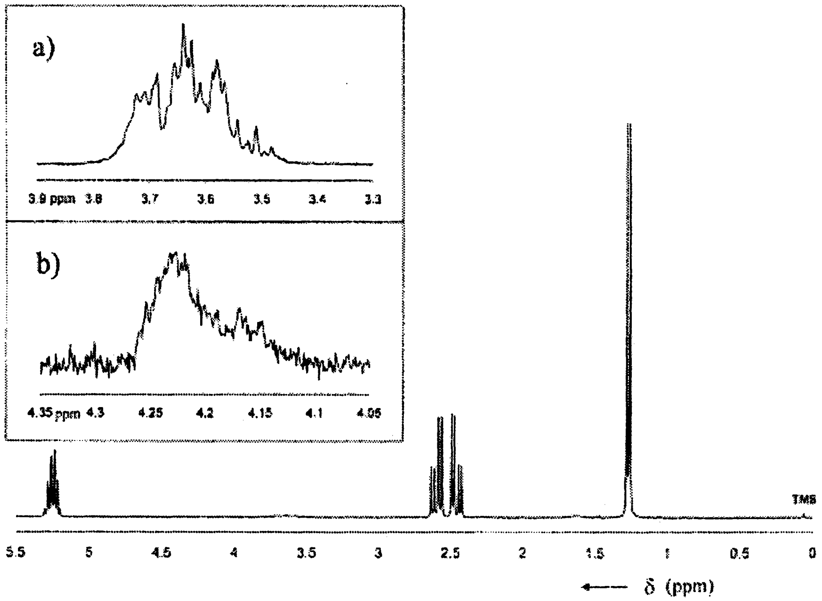

Figure 4: ^1H NMR spectrum of PEE-modified PHB. The insets show the region of the methylene protons of PEE (a) and the methylene protons indicating the ester linkage between PEE and PHB (b) (Reproduced from reference 15. Copyright 2001 American Chemical Society.)

color after precipitation. This is also demonstrated in the UV-Vis spectrum, depicted in Figure 5.

When the pH value of the environment is changed to larger than 7, the polymer changes its color to red. This is the typical behavior of alizarin obviously maintained when the dye is covalently attached to PHB via the oligoethylene oxide spacer.

During PHB crystallization, the attached end units cannot be included into the crystal lattice of PHB. Thus, PEG, DEG or PEE moieties are enriched in the amorphous phase of the lamella staples. Observing the initiation and growth of PHB-2 and PEE modified PHB spherulites, differences in the crystallization behaviour were detected. Whilst the spherulite growth rate *R* was comparable for all samples, i.e. the expelling of PEE from the crystalline phase did not hinder the spherulite growth, the sphrulite initiation time was different. Spherulites of PEE-270, PEE-270b, and PEE-797 were observed immediately after starting the measurement, i.e. immediately after reaching the crystallization temperature between 120 and 140 °C. First spherulites in neat PHB-2 appeared later, in case of a crystallization temperature of 130 °C, a delay of 800 sec was observed. This effect can be explained by a nucleating effect of the incorporated PEE.

Downloaded by OHIO STATE UNIV LIBRARIES on August 28, 2012 | http://pubs.acs.org
Publication Date: September 23, 2006 | doi: 10.1021/bk-2006-0939.ch005

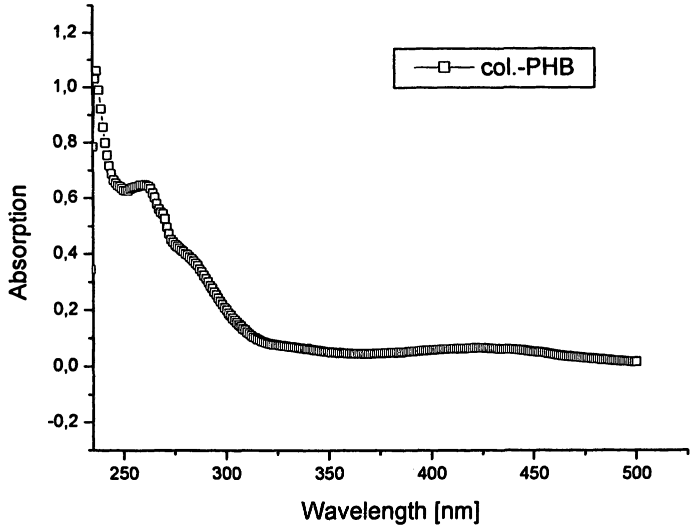

Figure 5: UV-Vis spectrum of colored PHB dissolved in chloroform

These results were supported by the fact that after isothermal crystallization at 120 °C PEE-270b had clearly the highest degree of crystallinity for PEE modified PHB (58%) and even higher than the crystallinity of neat PHB-2, crystallized at this temperature. Again, this indicated the nucleating effect of the PEE units incorporated into the polyester. On the other hand, after crystallization from solution of PHB-1 and PEG and DEG modified samples, the neat PHB-1 samples have shown highest crystallinity (~80%) and the modified ones are slightly lower in crystallinity. The reason can be found in the higher amount of amorphous matter in the modified samples due to their PEG and DEG parts.

The desmeared SAXS data of PEE modified PHB are depicted in Figure 6. Generally, the scattering trace can be assigned to a lamellar system with first and higher order reflections. The first maximum at q^* can be used for the calculation of the long period L_p using the Bragg relation ($L_p = 2\pi/q^*$) where q^* is the scattering vector at the first maximum. According to the measurements, L_p decreased with the amount of PEE incorporated into the polymer. PEO-2 had a long period of 11.6 nm, PEE-270 and PEE-797 had a value of 11.2 nm, and the long period of PEE-270b was 10.8 nm.

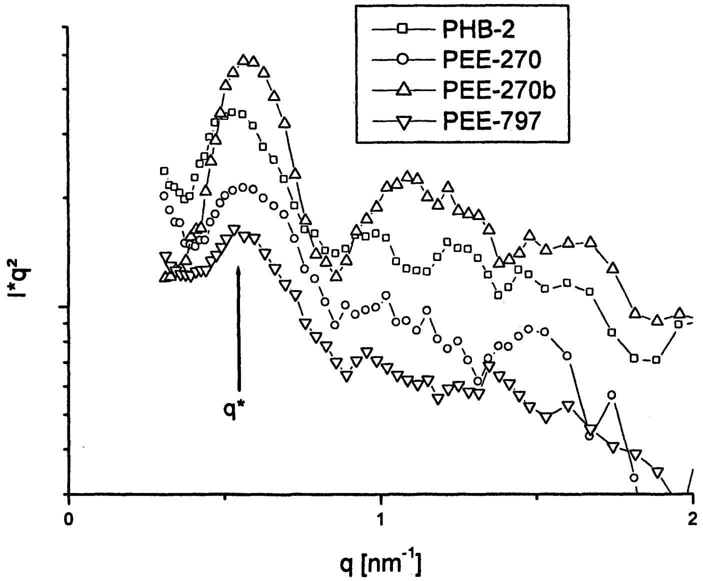

Figure 6. SAXS measurements of PHB-2 and PEE modified samples isothermally crystallized at 140 °C for 8 days.

Observing the crystallization process in a polarized light microscope, in neat PHB samples only unstructured spherulites can be seen, whereas the copolymers show the occurrence of banded spherulites as a microstructure (Figure 7a) (15). The twist-banding of lamellar ribbon crystals caused by chainfolding in different directions on opposite faces of lamellae (29) lead typically to band spacings of 10 µm or above in the temperature range under investigation. Therefore, the neat PHB sample seems to be unstructured as the band spacing is larger than the observed spherulite radius. The occurrence of banded spherulites with a typical band spacing of 3 µm in the case of the copolymers in therefore caused by the non-crystallizable PEE polymer units that force the lamellae to bend (30). The periodicity of the rings in the banded spherulites can be related to the amount of impurities of excluded polymer units. In AFM measurements after isothermal crystallization at 140 °C (Figure 7b) staples of lamellae can be observed. Obviously the growth of lamellae is stopped by spherical entities, that can be seen. This might be the reason for the initiation of the bending process.

Downloaded by OHIO STATE UNIV LIBRARIES on August 28, 2012 | http://pubs.acs.org
Publication Date: September 23, 2006 | doi: 10.1021/bk-2006-0939.ch005

Downloaded by OHIO STATE UNIV LIBRARIES on August 28, 2012 | http://pubs.acs.org
Publication Date: September 23, 2006 | doi: 10.1021/bk-2006-0939.ch005

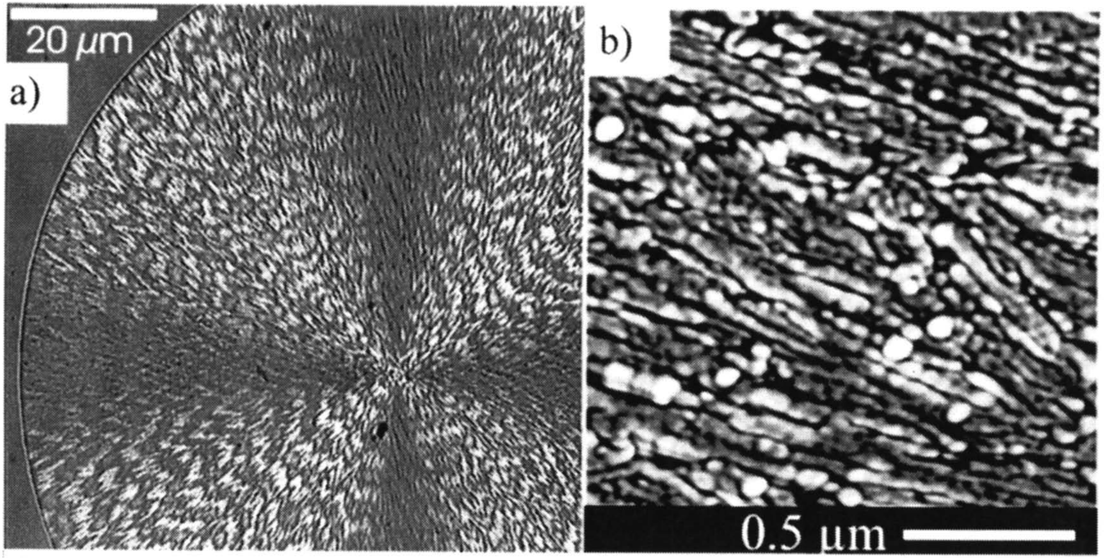

Figure 7. PEE-270b isothermally crystallized at 130 °C observed by polarized light microscopy (a) and crystallized at 140 °C observed by AFM (b) (15)

In surface tension studies the contact angles for sessile drops of water on the PHB, PHB/DEG, and PHB/PEG surfaces were determined (Table II). As expected, the contact angle for the hydrophobic PHB was with 89° the highest. Contact angles for the PHB/DEG and PHB/PEG were expected to be decreased due to the hydrophilic modification with PEG and DEG, respectively. The modified samples with higher masses, DEG and PEG 3400, show a significantly stronger decrease in contact angle (~76°), compared to the lower mass sample, PEG 400 with 83.4°. The surface tension γ_{sv} was calculated via Neumann iteration (26) from the contact angles. PHB has the lowest surface tension with a 29.8 mN/m value and the PHB/DEG and PHB/PEG samples ranged from 33 – 38 mN/m.

Table II. Water contact angle and surface tension of some samples

Sample	*Contact angle* θ *[°]*	*error*	*Surface tension* γ_{sv} *[mN/m]*
PHB-1	89.0	± 0.9	29.8
DEG	75.7	± 0.8	38.2
PEG4	83.4	± 0.7	33.4
PEG34	76.0	± 1.1	38.0

Data are taken from Ref. 7.

Conclusion

The reaction between the alizarin mono potassium salt and ethylene oxide gave α-hydroxy-β-hydroxy-oligoethoxy anthraquinone as main product and α,β-hydroxy-oligoethoxy anthraquinone as side product. The content of PEG with anthraquinone end groups as segment in poly(β-hydroxybutyrate) was qualitatively confirmed by UV-Vis spectroscopy. Thus it is possible to synthesize colored PHB already during the fermentation process. Using PEG-like oligomers in modulated fermentation leads to PHBs with improved wettability and thus better properties for many biomedical applications, especially in the field of bone replacement.

Acknowledgment

We gratefully acknowledge the German Academic Exchange Service (DAAD), Deutsche Forschungsgemeinschaft (DFG, SFB 418), and VolkswagenStiftung (AZ: 77742) for financial support.

Downloaded by OHIO STATE UNIV LIBRARIES on August 28, 2012 | http://pubs.acs.org
Publication Date: September 23, 2006 | doi: 10.1021/bk-2006-0939.ch005

References

1. Gogolewski, S.; Jovanovich, M.; Perren, S. M.; Dillon, J. G.; Hughes, M. K. *J. Biomed. Mat. Res.* **1993**, 27, 1135-1148.
2. Doyle, C.; Tanner, E. T.; Bonfield, W. *Biomat.* **1991**, 12, 841-847.
3. Yagmurlu, M. F.; Korkusuz, F.; Gürsel, I.; Korkusuz P.; Örs, Ü.; Hasirci, V. *J. Biomed. Mater. Res.* **1999**, 46, 494-503.
4. Sendil, D.; Gursel, I.; Wise, D. L.; Hasirci, V. *J. Control. Rel.* **1999**, 59, 207-217.
5. Scholz, C. In: *Polymers from Renewable Resources - Biopolyesters and Biocatalysis;* Scholz, C.; Gross, R.A. Eds.; ACS series 764, American Chemical Society: Washington, DC, 2000, 328-334.
6. van der Giessen, W. J.; Lincoff, A. M.; Schwartz, R .S.; van Beusekom, H. M.; Serruys, P. W.; Holmes Jr., D. R.; Ellis, S. G.; Topol, E. J. *Circulation,* **1996**, 94, 1690-1697.
7. Townsend, K. J.; Busse, K.; Kressler, J.; Scholz, C. *Biotechnol. Progr.* **2005**, 21, 959-964.
8. Ashby, R. D.; Shi, F.; Gross, R. A. *Biotechnol. Bioeng.* **1999**, 62, 106-113.
9. Shi, F.; Ashby, R.; Gross, R. A. *Macromolecules* **1996**, 29, 7753-7758.
10. Shi, F.; Gross, R. A.; Rutherford, D. R. *Macromolecules* **1996**, 29, 10-17.
11. Shi, F.; Scholz, C.; Deng, F.; Gross, R. A. *Polymer Preprints* **1998**, 39(2), 102-103.
12. Zanzig, J.; Scholz, C. *J. Polym. Environm.* **2003**, 11, 145-154.
13. Doyle, C.; Tanner, E. T.; Bonfield, W. *Biomaterials,* **1991**, 12, 841-847.
14. Holland, S. J.; Yasin, M.; Tighe, B. J. *Biomaterials,* **1990**, 11, 206-215.
15. Jenzsch M.; Volk, N.; Kressler, J.; Scholz, C. *Biomacromolecules* **2001**, 2, 1055-1060.
16. Lee, J. H.; Andrade, J. D. In: *Polymer Surface Dynamics;* Andrade, J.D., Ed.; Plenum Publishing Press New York, NY, 1988; 119-136.
17. Lee, J.H.; Kopecek, J.; Andrade, J.D. *J. Biomed. Mat. Res.* **1989**, 23, 351-368.
18. Okamura, K.; Marchesaault, R. H. In *Conformation of Biopolymers;* Ramachandran, G. M. Ed.; Academic Press, New York, NY, 1967; Vol.2, pp 709-720.
19. Cornibert, J.; Marchessault, R.H. *J. Mol. Biol.* **1972**, 71,735.
20. Yokouchi, M.; Chatani, Y.; Tadokoro, H.; Teranishi, K.; Tani, H. *Polymer* **1973**, 14, 267.
21. Alper, R.; Lundgren, D.G.; Marchessault, R.H.; Cote, W.A. *Biopolymers* **1963**, 1, 545.
22. Geil, P.H. *Polymer Single Crystals;* Wiley: New York, NY, 1963.
23. Lundgren, D.G.; Alper, R.; Schnaitman, C.; Marchessault, R.H. *J. Bacteriol.* **1965**, 89, 245.

Downloaded by OHIO STATE UNIV LIBRARIES on August 28, 2012 | http://pubs.acs.org
Publication Date: September 23, 2006 | doi: 10.1021/bk-2006-0939.ch005

24. Barham, P.J.; Selwood, A. US Patent 4,391,766, 1983.
25. *Polymer Handbook;* Mark, J. E., Ed.; Oxford University Press: New York, NY, 1999.
26. Li., D.; Neumann, A.W. *J. Coll. Interf. Sci.* **1990**, 137, 304.
27. Grundke, K.; Bogumil, T.; Gietzelt, T.; Jacobasch, H.-J.; Kwok, D.Y.; Neumann, A.W. *Progr. Coll. Polym. Sci.* **1996**, 101, 58-68.
28. Girifalco, L.A.; Good, R.J. *J. Phys. Chem.* **1957** 61, 904-909.
29. Owen, A.J. *Polymer* **1997**, 38, 3705-3708.
30. Wang, C.; Thomann, R.; Kressler, J.; Craemer, K.; Stuehn, B.; Svobode, P.; Inoue, T. *Acta Polymer.* **1997**, 48, 354-362.

Downloaded by OHIO STATE UNIV LIBRARIES on August 28, 2012 | http://pubs.acs.org
Publication Date: September 23, 2006 | doi: 10.1021/bk-2006-0939.ch005

Downloaded by PENNSYLVANIA STATE UNIV on August 10, 2012 | http://pubs.acs.org
Publication Date: September 23, 2006 | doi: 10.1021/bk-2006-0939.ch006

Chapter 6

Modifications of Soybean Oil Using Novel Ozone-Based Chemistry

Daniel Graiver[1,2], Phuong Tran[1], Laura Patrick[1], Ken Farminer[2], and Ramani Narayan[1,2]

[1]Department of Chemical Engineering and Material Science, Michigan State University, East Lansing, MI 48824
[2]Bioplastic Polymers and Composites LLC, 4275 Conifer Circle, Okemos, MI 48864

Soybean oil is an abundant annually renewable resource. It is composed of triglycerides with long chain saturated and unsaturated fatty acids. The presence of these unsaturated fatty acids results in poor oxidative stability. However, this enhanced reactivity also allows for chemical modification to introduce new functionalities to the oil. A novel single-step catalytic ozonolysis and in-situ reaction will be described. The reaction proceeds rapidly and efficiently at room temperature in the absence of solvents. The catalytic ozonolysis reaction has been used to reduce the unsaturation in soybean oil, and successfully prepare a number of potentially useful materials such as bio-lubricants with good thermal/oxidative stability, bio-diesel with thermal properties comparable to that of Diesel Fuel #2, and bio-plastic intermediates such as polyols, polyesters, and polyamides. This new class of soy-based materials is competitive both in cost and performance to petroleum based materials and offers the added advantage of being environmentally friendly and sustainable.

In Degradable Polymers and Materials; Khemani, K., et al.;
ACS Symposium Series; American Chemical Society: Washington, DC, 2006.

Introduction

Biobased products have made a significant inroad in recent years as a source of raw materials. They are commonly found as fuels, chemicals, construction materials, lubricants, fibers, coatings, oils, and a host of other products. The U.S. Government has set the goal of tripling U.S. use of bioenergy and biobased products by the year 2010. It is estimated that this goal will create an additional $15-20 billion a year in new income for farmers and people in rural America. Furthermore, meeting this goal will reduce the environmental impact associated with annual greenhouse gas emission by as much as 100 million metric tons of carbon, provide a stable source of raw materials for continuous economic growth, and alleviate the dependence on foreign oil reserves[1]. Indeed, the recently signed Presidential Orders 13101 and 13123 as well as the Farm Security and Rural Investment Act of 2002 intend to promote usage of biobased materials.

One readily available source of annually renewable biomaterials is vegetable oil. In the US soybeans provided 80 percent of the edible consumption of fats and oils. Soybeans were planted on 75.2 million acres (30.4 million hectares) in 2004, producing a record 3.141 billion bushels (85.49 million metric tons) of soybeans with a total 2004 crop value exceeding $17.7 billion[2]. Although most of the total U.S. Soybean oil production in 2004 (17,604 million pounds) was consumed in edible products, a significant portion of it (628 million pounds) was used for industrial products. In many of these applications soybean oil was used successfully with little or no modification provided extreme conditions were not encountered. Typical examples include printing ink, candles and waxes, low temperature lubricants and hydraulic fluids, industrial cleaners and metalworking fluids, crayons, personal care lotions, paint additives, processing aids, etc. However, much broader use of soy oil (and other vegetable oils) can be realized if the stability and the reactivity of the oil can be manipulated and economically controlled without adversely affecting the "good" properties of the oil.

Of particular concern is the presence of double bonds in the fatty acid residues of the triglycerides. These double bonds are susceptible to premature oxidation at elevated temperatures, or even upon storage at ambient temperatures, preventing the use of these biobased oils as engine lubricants and hindering their use as biofuels. Simple hydrogenation of these double bonds is not feasible as the resulting saturated products are waxy with higher melting points than the original oils, detracting their use as such due to poor low temperature flow properties. In other applications, soy oil and other vegetable oils are not sufficiently reactive and cannot be converted to high molecular weight polymers and resins unless they are chemically modified.

Here, we wish to present our recent results related to a novel catalytic ozonation as a platform for modifications of soy oil. Unlike a typical ozonation

Downloaded by PENNSYLVANIA STATE UNIV on August 10, 2012 | http://pubs.acs.org
Publication Date: September 23, 2006 | doi: 10.1021/bk-2006-0939.ch006

reaction where ozone attacks the double bonds to yield ozonide intermediates, which spontaneously decompose to a mixture of carboneouceous hydrocarbons, we employ a catalyst and direct the reaction of the ozonide intermediates to the desired product.

Catalytic Ozonation Process

Ozone is known as a very powerful oxidation agent and its reactivity toward double bonds has been well documented[3]. One of the more significant properties of oxidation reactions with ozone is the fact that the production of ozone is relatively simple and consists of passing oxygen (or a gas mixture containing oxygen) near high electrical potential electrodes and into the reaction mixture. It does not require special packaging or expensive transportation protocols. At the end of the oxidation reaction, unused ozone leaves no by-products and dissociates back to oxygen. Since the early ozonolysis experiments[4] it was realized that no other oxidation agent is capable of reacting with double bonds as fast and with as great efficiency as ozone. Furthermore, great advances were realized in the last few years in the design and production of ozone generators. The availability of efficient, low cost ozone generators enhances the possibility of preparing new functional groups directly from the ozonide intermediate.

The intermediate from this initial attack on a double bond is an ozonide as shown generally in Figure 1. Due to the high oxygen content of this intermediate, it is not stable and spontaneously decomposes to a mixture of carbonyl compounds. Various carboxylic acid[5] and aldehyde[6] derivatives of vegetable oils have been prepared in the past by such ozonolysis reactions and this process was commercialized by Emery Industries to manufacture azelaic and pelargonic acids from oleic acid[7].

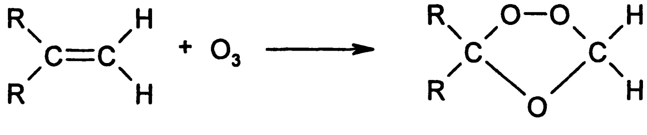

Figure 1: Initial attack of ozone on a double bond

More recently various olefins were converted in a single-step reaction to methyl esters by ozonolysis in the presence of sodium methoxide. Such reactions were previously demonstrated with unsaturated ethers, esters, and amides[8] including the reaction of methyl oleate to methyl nonanoate and dimethyl nonanedioate (Figure 2). It was concluded that this one-step conversion of olefins to methyl esters in basic methanol solution appears to be general and does not depend on a required structure or a strained bond of the reactants.

Downloaded by PENNSYLVANIA STATE UNIV on August 10, 2012 | http://pubs.acs.org
Publication Date: September 23, 2006 | doi: 10.1021/bk-2006-0939.ch006

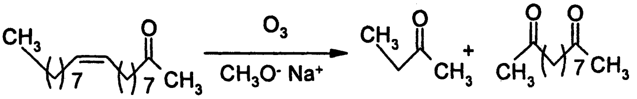

Figure 2: Ozonolysis of methyl oleate in sodium methoxide solution

This reaction was shown to proceed smoothly at −15°C in a solvent to give high yields of the methyl esters when five equivalents of NaOH in MeOH were used. Unfortunately, attempts to use soy oil instead of methyl oleate under the same conditions led to undesired hydrolysis of the triglyceride esters. However, we have found that using $CaCO_3$ as a catalyst also yields methyl esters directly from the ozonide intermediates without the undesirable hydrolysis of the fatty acids from the triglycerides. Furthermore, the reaction could be run between 0°C and 25°C without additional solvent and, in general, produced a mixture of triglycerides as well as low molecular weight esters and diesters as shown in Figure 3.

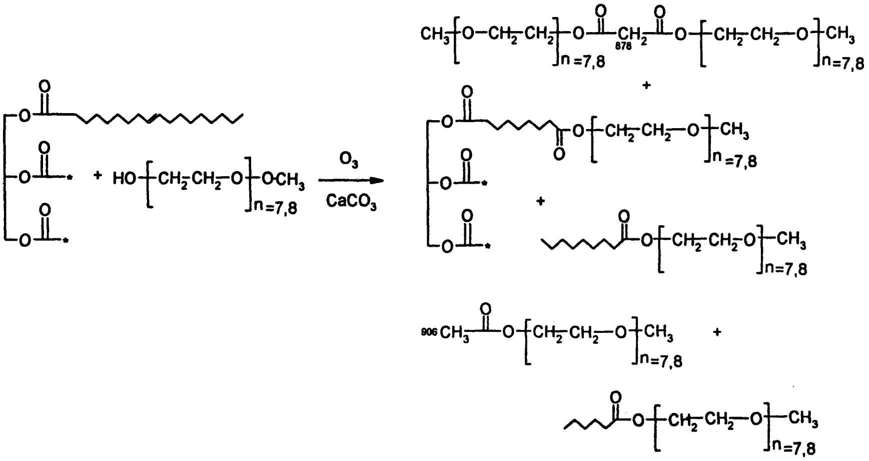

Figure 3: Thermally stable lubricant from soy oil and MPEG 350

The particular product mixture from this catalytic ozonolysis depends on the composition of the starting oil. In the case of soy oil, ozone attacks and cleaves the double bonds in the oleic, linoleic and linolenic acid residues, designated here as O, L1, and L2 respectively. Thus, oleic acid in the triglyceride would be cleaved at the double bond in the 9th carbon leaving methoxy nonanoate ester on the triglyceride (designated as N) and methoxy nonanoate fragment (designated E1). Similarly, linoleic acid would be cleaved at the double bonds to yield the same methoxy nonanoate residue on the triglyceride as well as methoxy hexanoate (E2) and bis-methoxy malonate (EE) fragments. Linolenic acid, which

Downloaded by PENNSYLVANIA STATE UNIV on August 10, 2012 | http://pubs.acs.org
Publication Date: September 23, 2006 | doi: 10.1021/bk-2006-0939.ch006

contains multiple unsaturations at the 9th, 12th, and 15th positions would yield methoxy nonanoate residue attached to the triglyceride as well as methoxy propionoate (E3) and bis-methoxy malonate (EE) fragments. The saturated fatty acids (e.g. palmitic and stearic, P and S, respectively) are not cleaved by the ozone and remain intact. It is apparent from the structure of the unsaturated fatty acids that irrespective of the acid, cleavage occurs at the 9th carbon to yield methoxy nonanoate attached to the glycerol.

It is possible to determine the composition of the triglycerides in the oil by calculating all the possible permutations of the 5 fatty acid residues in groups of 3 knowing their relative abundance (11 wt.% palmitic acid, 4 wt.% stearic acid, 23 wt.% oleic acid, 51 wt.% linoleic acid, and 7 wt.% linolenic acid). Thus, a typical soy oil composition contains a product mixture as shown in Figure 4.

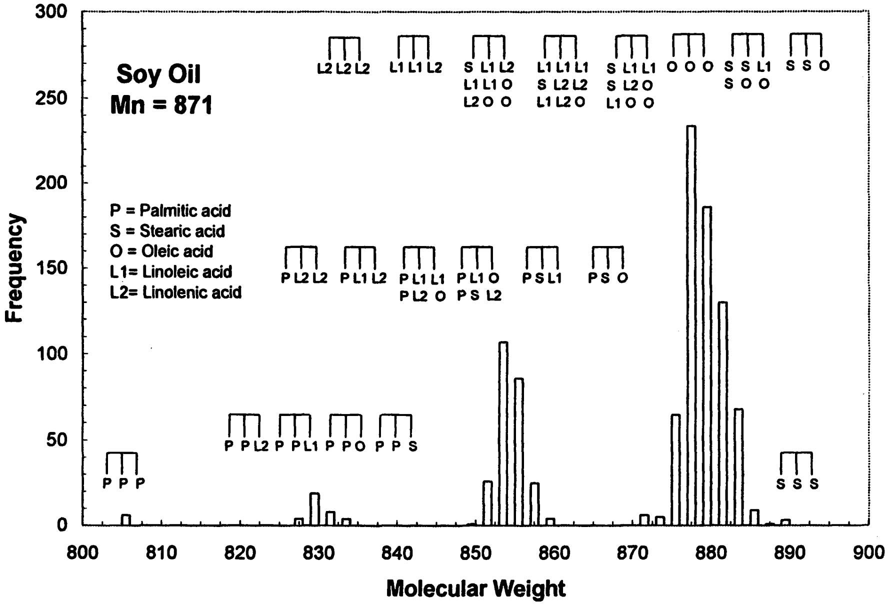

Figure 4: calculated molecular weight distribution of soy oil

Similarly, the product composition after ozonolysis can be calculated as shown in Table I.

It is apparent from this statistical analysis that the triglyceride mixture after ozonolysis is much more uniform than the original soy triglyceride mixture as

Downloaded by PENNSYLVANIA STATE UNIV on August 10, 2012 | http://pubs.acs.org
Publication Date: September 23, 2006 | doi: 10.1021/bk-2006-0939.ch006

Table I. Calculated composition of soy oil before and after catalytic ozonolysis with methanol

Unmodified Soy – Oil						*Methanol modified Soy - Oil*		
Triglyceride	*Frequency*	*MW*	*Triglyceride*	*Frequency*	*MW*	*Triglyceride*	*Frequency*	*MW*
L1L1O	0.1965	880	OOS	0.0085	886	NNN	0.2352	644
L1L1L1	0.1367	878	PSO	0.0082	860	NNP	0.1008	698
L1L1P	0.0902	854	PPO	0.0082	832	NNS	0.0336	727
OOL1	0.0888	882	SL2O	0.0059	882	PPP	0.0007	807
PL1O	0.0849	856	L2L2O	0.0042	876	PPN	0.0007	753
L1L1L2	0.0656	876	SSL1	0.0032	886	PPS	0.0144	835
L1L2O	0.0617	878	PSL2	0.0027	856	SSS	0.0000	891
L1L1S	0.0410	882	PPL2	0.0027	828	SSN	0.0016	809
SL1O	0.0386	884	L2L2P	0.0019	850	SSP	0.0002	863
PL1L2	0.0283	852	PPS	0.0017	834	NPS	0.0096	781
OOP	0.0188	858	SSO	0.0015	888	*Fragments*		
PSL1	0.0177	858	PPP	0.0010	806	EE	0.2698	132
PPL1	0.0177	830	L2L2S	0.0009	878	E1	0.0952	172
OOL2	0.0137	880	L2L2L2	0.0007	872	E2	0.2063	130
PL2O	0.0131	854	SSP	0.0007	862	E3	0.0317	88
SL1L2	0.0129	880	SSL2	0.0005	884			
OOO	0.0125	884	SSS	0.0001	890			
L2L2L1	0.0090	874						

only 3 fatty acid residues (instead of 5) are present (nonanoate, palmitate, and stearate) and about half of these triglycerides are composed of the same acid residue (NNN). Furthermore, about half of the product mixture is composed of triglycerides and the other half is composed of low molecular weight esters (E1, E2, and E3) and diester (EE). If needed, these low molecular weight species can be removed and separated from the triglycerides mixture although, in most cases this is not necessary.

The catalytic ozonation set-up is shown schematically in Figure 5. Ozone was produced by passing dry oxygen (0.25 ft^3/min) through Praxair Trailigaz ozone generator (Cincinnati, OH) model number OZC-1001. The output ozone concentration was approximately 6 wt.%. The exit port of the ozone generator

Downloaded by PENNSYLVANIA STATE UNIV on August 10, 2012 | http://pubs.acs.org
Publication Date: September 23, 2006 | doi: 10.1021/bk-2006-0939.ch006

was connected to the bottom of the reaction bottle such that ozone was introduced into the reaction through a fritted disc as fine bubbles. The very small gas bubbles allowed good dispersion of the ozone within the reaction medium. Excess gas and unreacted ozone were vented through the top of the reaction bottle through aqueous KI solution to destroy any unreacted ozone. Unless noted all the ozonolysis reactions were run at 0°C and maintained at this temperature with an ice/water bath.

Downloaded by PENNSYLVANIA STATE UNIV on August 10, 2012 | http://pubs.acs.org
Publication Date: September 23, 2006 | doi: 10.1021/bk-2006-0939.ch006

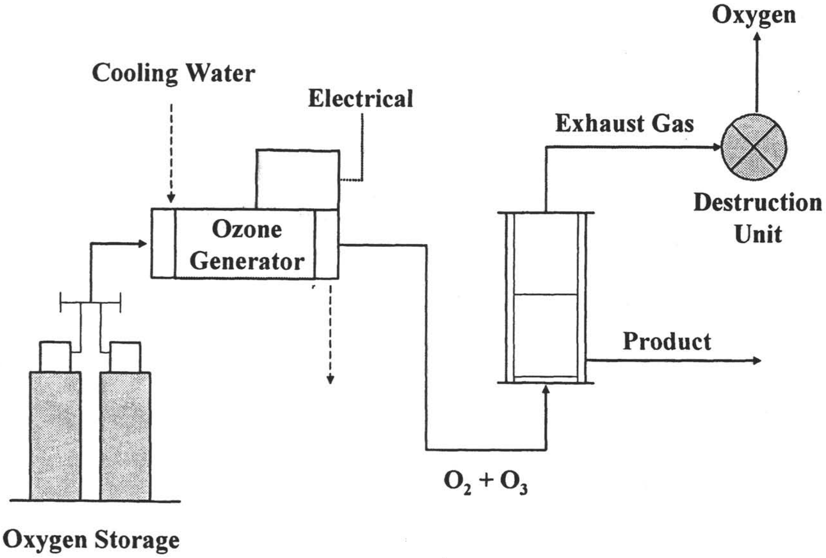

Figure 5 : Schematic ozonolysis process

A typical procedure consisted of placing the soybean oil, alcohol (methanol, butanol, octanol, dodecanol, or methoxy terminated poly-ethylene glycol [MPEG]) and known amounts of a $CaCO_3$ in a 500 ml reactor. The reaction mixture was cooled to 0°C in an ice water bath, ozone was then introduced, and the reaction was run for a predetermined period of time. At the end of the reaction $CaCO_3$ was filtered out, and the product was washed several times with excess distilled water in order to remove any excess alcohol. The product was then dried over molecular sieves for 48 hours prior to testing.

The number of double bonds was determined using iodine number testing, according to ASTM test method D1959[9]. The iodine number in this test is defined as centigrams of I_2 per gram of sample.

The acid number was determined according to ASTM test method D1980[10]. The acid number in this test is defined as milligrams of KOH per gram of sample.

Functional groups were identified using Perkin-Elmer FTIR model 1000 using at least 64 scans. Prior to recording a spectrum, the sample holder was flushed with nitrogen to remove moisture and CO_2 and the background was recorded. The spectra were obtained after dissolving the samples in chloroform and placing a drop of the solution between sodium chloride crystals. The solvent was allowed to evaporate leaving a thin film on the surface of the crystal. The sample cell was constantly purged with dry nitrogen while the signal was acquired.

Thermo-gravimetric analysis (TGA) was carried out with a TA Instruments (New Castle, DE) Model TGA 2950 thermobalance. The instrument was operated in the dynamic mode with a heating rate of 5°C/min, where 40°C and 350°C were the initial and final temperatures, respectively. On average, 4 mg was the initial mass of each sample analyzed. Air was used instead of inert atmosphere, to study the effect of thermal oxidation.

NMR spectra were obtained on a 500 MHz model INOVA 500 instrument. Samples were dissolved in deuterated chloroform, and the ^{1}H NMR and ^{13}C NMR spectra were obtained at room temperature.

Downloaded by PENNSYLVANIA STATE UNIV on August 10, 2012 | http://pubs.acs.org
Publication Date: September 23, 2006 | doi: 10.1021/bk-2006-0939.ch006

Thermally stable soy-based lubricants

The need for lubricants from soy and other vegetable oils is driven by environmental concerns due to millions of gallons of petroleum-based oils, greases and hydraulic fluids that leak into the environment every year as well as costly waste disposal and clean-up issues from large quantities of after-use oils[11,12]. The chemical structure of all these oils is similar and consists mainly of triglyceride mixtures obtained by the reaction of different fatty acids with glycerol. Inherently, these biobased oils are non-toxic and biodegradable and they are readily extracted from abundant renewable resources. Furthermore, as lubricants they are characterized by a high viscosity index, low evaporation loss, good boundary lubrication with metal surfaces, and excellent miscibility with other fluids or additives. At present they are primarily suited for use as base stock in pumps, switches and ropes that operate close to room temperature and where the lubricants directly move into the environment during their use. Unfortunately, their use as common industrial lubricants is limited due to their limited thermal, hydrolytic and oxidative stability[13]. These poor thermal and oxidative properties are directly related to the presence of unsaturated double bonds in the residual fatty acids[14], which under high temperature, pressure, and shear stress, and contact with a metal surface are susceptible to premature oxidative degradation.

Several approaches have been used in the past to improve the thermal stability and expand the use of vegetable oils to more demanding applications.

These approaches can be divided into three broad categories; chemical additives such as antioxidants, genetic modification and hybridization to yield triglycerides with fewer double bonds, and various chemical modifications to the structure of the oil to replace the double bonds with a more stable functional groups. Our catalytic ozonation falls into the last category. There are numerous patented technologies and publications based on these chemical modification approaches. Some notable examples include selective or partial hydrogenation[15], epoxidation[16,17,18], hydroxylation[19], transesterification[20], esterification[21], sulfurization and phosphate modification[22,23]. Unfortunately, hydrogenation of the double bonds leads to oils that tend to solidify at higher temperatures than the oils containing unsaturated fatty acids, which limits the use of such lubricants in cold weather (poor pour point characteristics). The other chemical modifications were shown to improve the thermal and oxidative stability with various degrees of success. However, they are relatively expensive, some require specialized equipment and uncommon reagents to complete the reaction, and all of them are based on multi-step processes. We have used our *one-step*, catalytic ozonation of soy oil in the presence of alcohols to enhance the thermal and oxidative stability of the oil by replacing the double bonds with ester linkages (Figure 6) in a relatively simple and fast process.

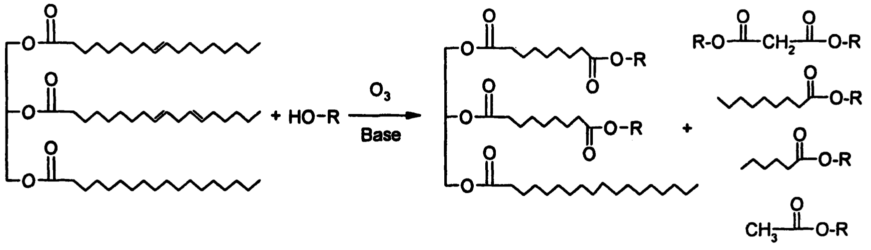

Figure 6: Catalytic ozonolysis of triglycerides in the presence of an alcohol

It is apparent that running the catalytic ozonation in the presence of methanol will produce a mixture with lower overall molecular weight (and viscosity) than the original oil due to cleavage of C3, C6, and C9 fragments beyond the double bonds and their replacement with methoxy esters. Even more potentially problematic is the fact that these low molecular weight fragments will adversely impact the volatility of the oil (indeed, these fragments can be separated and removed by distillation, but this will negatively impact the cost the product). Instead, we have found[24] that the molecular weight and viscosity of the oil after ozonolysis is essentially unchanged provided octanol is used. The best results were obtained with mono-methoxy polyethyleneglycol (MPEG 350) having an average molecular weight of 350 (about 7-8 ethylene oxide units per chain) as shown in Figure 7. This alcohol is water soluble, which makes it easy

Downloaded by PENNSYLVANIA STATE UNIV on August 10, 2012 | http://pubs.acs.org
Publication Date: September 23, 2006 | doi: 10.1021/bk-2006-0939.ch006

to recover and reuse in subsequent runs by simple water washing. It has an adequate freezing point (-10°C), which is lower than soy oil, low volatility, good lubricity characteristics, and high thermal stability.

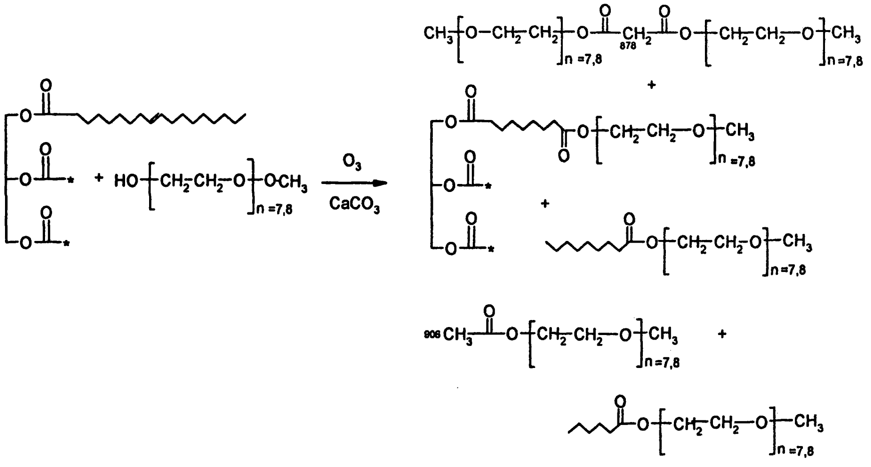

Figure 7: Thermally stable lubricant from soy oil and MPEG 350

The progress of the reaction was followed by the disappearance of the double bond peak in the FTIR (3005 cm^{-1}) and was quantified by deconvolution of the peak complex around 2800-3100 cm^{-1} (Figure 8). This procedure allowed us to separate the double bond peak, which appears as a shoulder on the -C-H stretching peak and determine the area under this peak. Thus, setting the ratio of the area under the double bond peak to the C-H peak area as 1.0 for soy oil, the progress of the reaction can be determined from this ratio as a function of the reaction time (Figure 9). It is apparent from these data that under these experimental conditions essentially all the double bonds were consumed after about 5 min per gr. sample. It should further be mentioned here that the

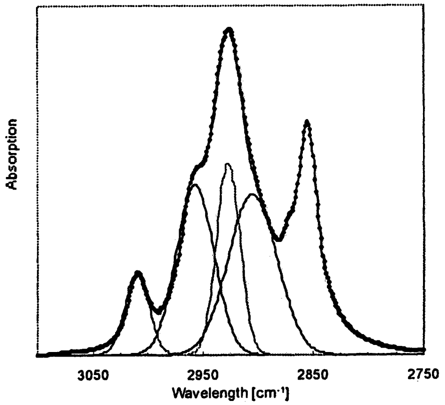

Figure 8: Partial FTIR spectrum indicating peak deconvolution to determine the disappearance of the double bonds

Downloaded by PENNSYLVANIA STATE UNIV on August 10, 2012 | http://pubs.acs.org
Publication Date: September 23, 2006 | doi: 10.1021/bk-2006-0939.ch006

direct conversion to ester is evident by the changes in the carbonyl region of the spectrum and the lack of adsorption peaks due to hydroxyl groups as no other peaks were observed that should be apparent if a carboxylic acid or its salts were formed.

Downloaded by PENNSYLVANIA STATE UNIV on August 10, 2012 | http://pubs.acs.org
Publication Date: September 23, 2006 | doi: 10.1021/bk-2006-0939.ch006

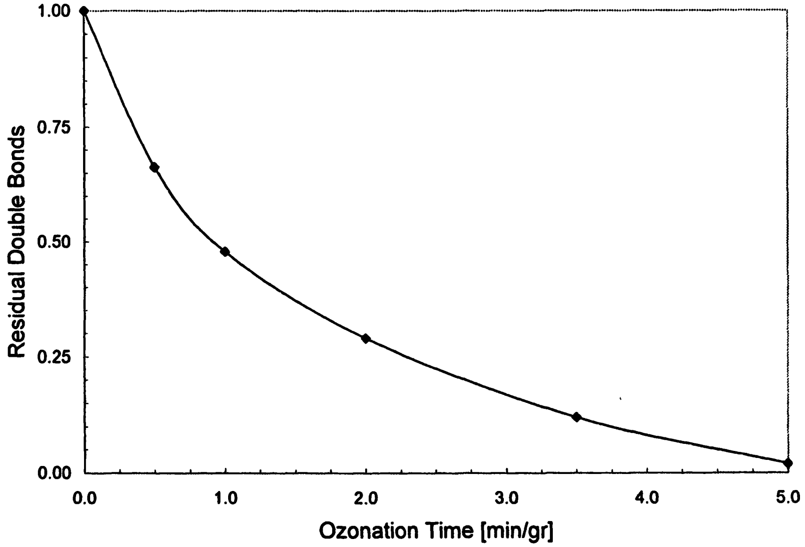

Figure 9: Consumption of double bonds during the ozonolysis process

Lubrication Properties

Thermo-oxidation Engine Oil Simulation Test (TEOS) was used to simulate oxidation in moderately high temperature deposit conditions in the piston ring zone of modern smaller, more highly stressed engines. Due to the known poor oxidation stability of soy oil in this test, a sample was run for only 10 hours at 285°C rather than the normal 24 hours. Accordingly, 8.5 g of oil was circulated continuously over a special steel rod heated to 285°C. Air was also circulated continuously over the rod to increase exposure to oxygen. In addition, any volatile material was caught by the walls of a surrounding mantle and collected separately, thus increasing the stress on the remaining oil. The weight of the rod before and after the test was then determined as the main criterion of the extent of oxidation. The results showed that the amount of deposits was reduced from 1590 mg for soy oil to 6 mg for the MPEG 350 treated soy oil.

Scanning Brookfield Technique (SBT) was used to determine the low temperature profile of the lubricant by continuously measuring the viscosity as the temperature is slowly (1°C/hr) decreased from 0°C to the maximum viscosity of the viscometer head. Any build-up of structure in the sample would cause an increase in the viscosity above the exponential relationship expected from a Newtonian fluid, which by definition, is free of gel-forming tendencies. The presence of any such structures can easily be observed from the change in the viscosity-temperature curve. The temperature range in these studies was chosen from 0°C down to the lowest temperature possible of the viscometer head. It is apparent from the data in Figure 10 that the cold flow properties of the modified soy oil are much better than the original soy oil and are approaching the typical low temperature characteristics of mineral oils.

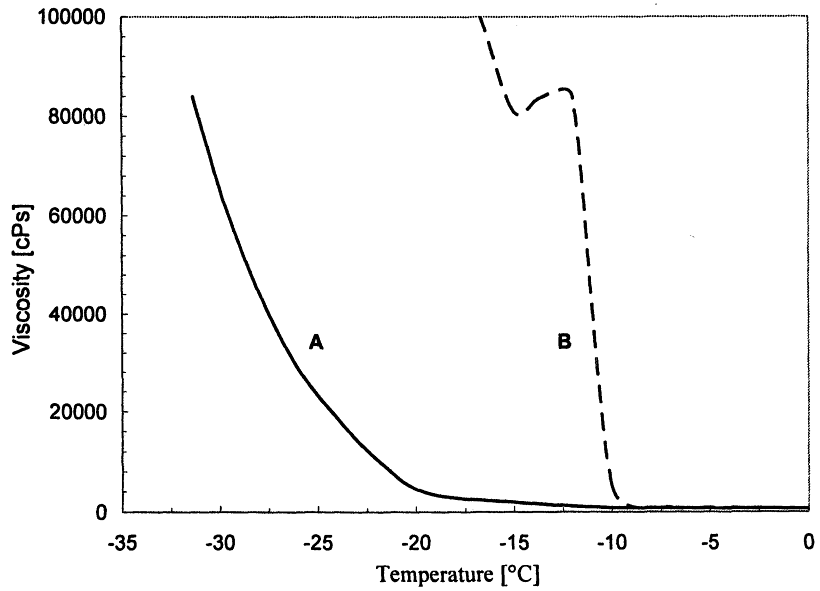

Figure 10: Cold flow properties of (A). MPEG350 modified soy and (B). soy oil

Friction and wear were measured by a modified Falex pin and V-block test. In this test, two V-blocks press against a rotating pin from opposite sides, 'pinching' the pin between them with a force that is progressively increased in steps by the test operator. The contact between the V-blocks and the pin are four straight lines and permit evaluation of the lubricant tested in the so-called quasihydrodynamic region of lubrication. This region can produce wear and ultimate seizure of the contiguous contacting surfaces. The test was conducted with increasing 50 lb steps of force with five minutes residence time at each step. Wear, friction and pin temperature were measured at each step. Typical wear profile for the MPEG 350 modified soy oil is shown in Figure 11. It is observed that the cumulative wear before failure is significantly higher than soy oil. This is

Downloaded by PENNSYLVANIA STATE UNIV on August 10, 2012 | http://pubs.acs.org
Publication Date: September 23, 2006 | doi: 10.1021/bk-2006-0939.ch006

the case simply due to the fact that this oil withstood failure longer than typical soy oil.

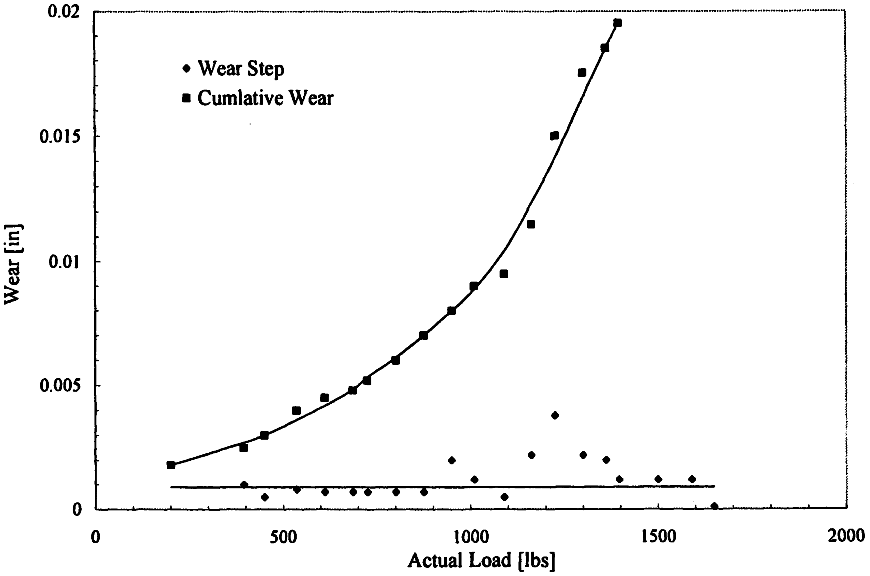

Figure 11: Typical wear plot of MPEG 350 modified soy oil (Reproduced with permission from reference 42. Copyright 2005 American Chemical Society.)

The ozonation process to modify a soy oil with MPEG 350 did not impact the viscosity index of the oil and it remained essentially unchanged (229 for soy oil and 212 for MPEG 350 modified soy oil).

Bioplastics derived from chemically modified soy oil

A growing awareness of the environment has led to the emergence of biodegradability and/or the usage of renewable resources as being important design criteria. In contrast to petroleum-based materials, agricultural-based materials are not depleted and are readily regenerated by photosynthesis. In previous work, we have reported on the rationale, design, and engineering of bio-based materials[25,26]. Unfortunately, soybean oil does not contain reactive functional groups that can be polymerized directly to yield useful high molecular weight plastic materials, resins and composites. Of particular interest here is to use modified soy oil in the preparation of polyurethanes and polyesters through polycondensation.

Downloaded by PENNSYLVANIA STATE UNIV on August 10, 2012 | http://pubs.acs.org
Publication Date: September 23, 2006 | doi: 10.1021/bk-2006-0939.ch006

Downloaded by PENNSYLVANIA STATE UNIV on August 10, 2012 | http://pubs.acs.org
Publication Date: September 23, 2006 | doi: 10.1021/bk-2006-0939.ch006

One of the early methods to prepare polyols from various vegetable oils is based on transesterification of the fatty acids in the triglycerides with a polyol such as glycerol, glycerin, pentaerytol, α-methylglucoside or sucrose[27,28]. Unfortunately, premature degradation occurs by this process due to the high temperatures and the relatively long period of time in this reaction. Another method is based on reacting vegetable oils with peroxyacid acid to yield epoxidized fatty acids. The epoxide rings are then open[29,30] or hydroxylated[31] with polyfunctional alcohols to yield secondary alcohols. Epoxidized soy oil is available commercially but the reactivity of this oil is low due to the nature of the secondary alcohols. Furthermore, several hydroxyl groups per fatty acid residue are obtained (at least these fatty acids that contain more than one double bond). Consequently, multiple numbers of hydroxyl groups having varying reactivity are present, which tend to complicate subsequent reactions and could lead to premature gelation. Hydroformylation offers another method to prepare polyols whereby an aldehyde functional vegetable oil is first obtained, which is then hydrogenated to alcohols[32,33]. Polyurethanes prepared from these polyols had different mechanical properties depending on the hydroformylation catalyst that was used. Thus, rigid materials at room temperature were obtained with a rhodium catalyst while a cobalt catalyzed hydroformylation led to rubbery materials[34]. An alternative method to prepare primary polyols is based on oxidizing an olefin having a carbonyl group with molecular oxygen followed by hydrolysis and reduction of the acetal (or ketal) to an alcohol[35]. Although this method appears somewhat complicated and must run at high pressure, good yields were reported. A somewhat less complicated method, also based on an oxidation process to yield polyols, is based on catalytic oxidation using an organic hydroperoxide in the presence of OsO_4 and a NaBr cocatalyst[36]. An alternative process is to use ozone to cleave and oxidize the double bonds in the vegetable oil and then reduce the decomposing ozonides to alcohols using $NaBH_4$ or similar reducing agents.

It is apparent that there is a need to improve the chemistry as well as the process and devise a more efficient method to prepare vegetable oils containing primary alcohols. Our catalytic ozonation is suitable for the production of such primary polyols in a single-step process. Our method takes advantage of the ease and efficiency of the oxidation methods mentioned earlier but it is relatively simple, fast and gives high yields.

Significant results

Soy oil-based polyols were prepared by catalytic ozonation in the presence of various di- and tri-alcohols. An example of this reaction with ethylene glycol is shown in Figure 12. Here, the double bonds are cleaved and the new chain-ends react with one hydroxyl group of the ethylene oxide leaving the other hydroxyl as a new, primary hydroxyl chain-end. As described in the previous section, the product mixture contains polyol terminated triglycerides as well as hydroxyl terminated linear fragments obtained from the hydrocarbon fragments beyond the cleaved double bonds.

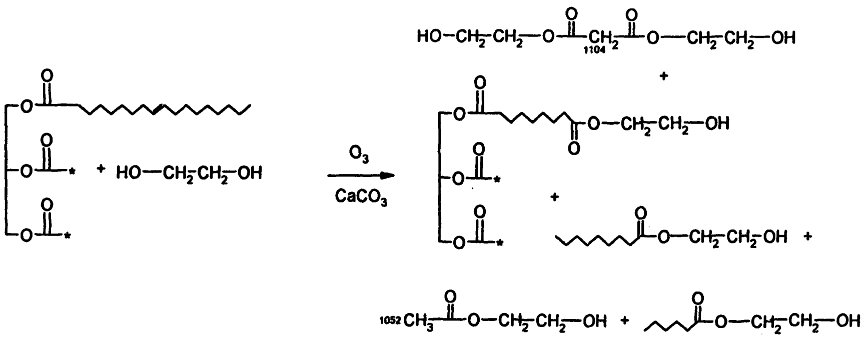

Figure 12: Preparation of soy polyol by catalytic ozonation in ethylene glycol

Statistical analysis of the product mixture indicates that about 24 wt.% of the product mixture contains triols (NNN), 13 wt.% contains diols (NNP and NNS), less than 3 wt.% contains mono functional alcohols (NPS, PPN and SSN). Most importantly, only a very small component (less than 0.2 wt.%) of unreactive triglycerides having no hydroxyl groups is present in the mixture.

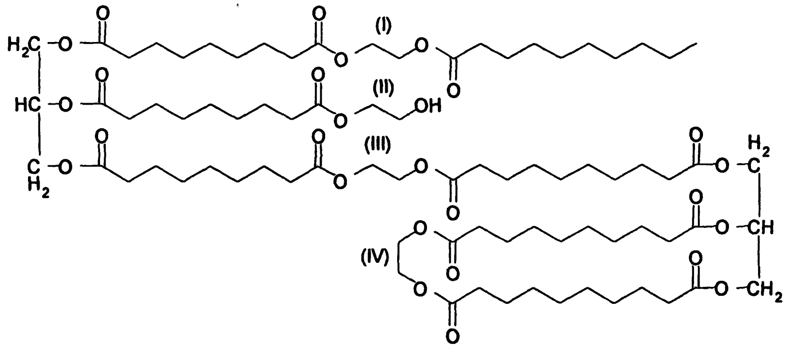

Figure 13: Possible side-reactions involving inter- and intramolecular

Downloaded by PENNSYLVANIA STATE UNIV on August 10, 2012 | http://pubs.acs.org
Publication Date: September 23, 2006 | doi: 10.1021/bk-2006-0939.ch006

Downloaded by PENNSYLVANIA STATE UNIV on August 10, 2012 | http://pubs.acs.org
Publication Date: September 23, 2006 | doi: 10.1021/bk-2006-0939.ch006

Furthermore, about half of the polyols product mixture is composed of triglycerides and the other half is composed of linear diols and mono functional alcohols fragments. If needed, these low molecular weight species can be removed and separated from the polyol triglycerides. However, in most cases, this is not necessary as these species still participate in the polymerization. It is also important to note that all these polyols are composed of primary hydroxyls, which are more desirable than secondary alcohols in the preparation of polyurethanes and polyesters.

This statistical analysis did not take into account possible complications as shown in Figure 13 involving the reactions of both hydroxyl groups in ethylene glycol. Thus, when a hydroxyl terminated fragment (instead of ethylene glycol) reacts with an ozonide (case I) the product will be a higher molecular weight adduct on the triglyceride than the reaction with an ethylene glycol molecule (case II). The terminal group of this adduct could be primary alcohol or a non-functional methyl group depending on the functionality of the reacting fragment. Alternatively, a high molecular weight product is expected if one ethylene glycol molecule reacts with two triglycerides (case III) or, similarly, if hydroxyl terminated triglycerides react with each other. Intramolecular weight reaction are also possible, where ethylene glycol reacts with two fatty acids in the same triglyceride (case IV), which will lead to cyclization and loss of the hydroxyl functionality. Similar complications could arise when any of the hydroxyl terminated fragments reacts with another triglyceride instead of ethylene glycol. However, we have observed that most of these complications can be avoided, or at least greatly minimized, by using excess ethylene glycol in the reaction mixture.

The soy polyol mixture is characterized by a broad hydroxyl stretching peak around 3500 cm^{-1}, the complete disappearance of the C=C band at 3005 cm^{-1} and the C=C stretch at 1650 cm^{-1} (Figure 14). The FTIR spectra further indicate that at the end of the ozonolysis reaction the carbonyl stretch at 1743 cm^{-1} became broader suggesting the formation of new carbonyl compounds. A significant increase in the 1105 cm^{-1} band was also observed and that was assigned to C---O stretching. It is important to note here that no adsorptions were noted around 2900–2700 cm^{-1} related to the C-H stretch adjacent to the carbonyl, indicating the absence of aldehyde groups.

Further confirmation of the soy polyol structure is obtained from ^{13}C NMR (Figure 15). The characteristic double bond double peak at 130 ppm, related to the unsaturated fatty acid in the soy oil, does not appear in the soy polyol spectrum indicating complete cleavage of the double bonds. The carbonyl ester peaks (177 ppm) and the various methylene peaks (between 25 and 36 ppm) remained unchanged as did the glycerol carbons (64 and 69 ppm).

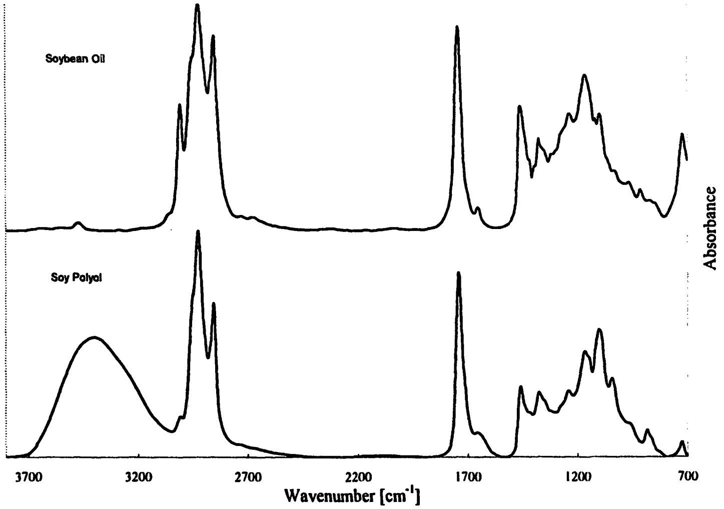

Figure 14: FTIR spectra of (A) soy oil and (B)soy polyol obtained by $CaCO3$ catalyzed ozonolysis of soy oil with ethylene glycol

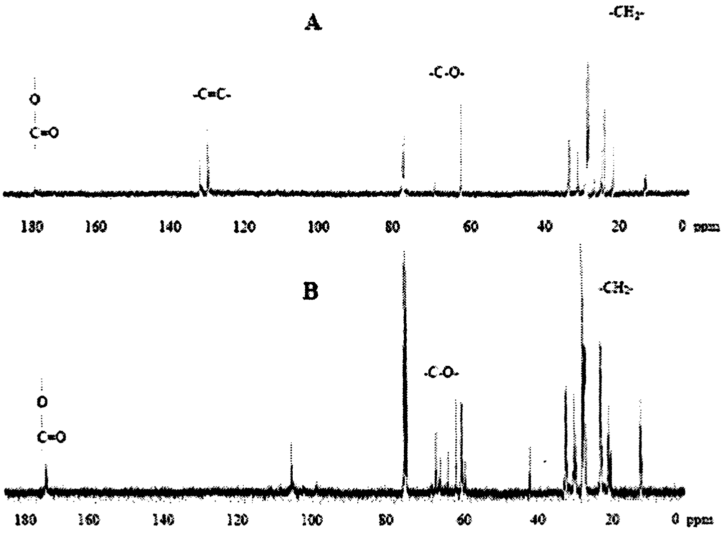

Figure 15: ^{13}C NMR of (A) soy oil and (B) soy polyol obtained by $CaCO3$ catalyzed ozonolysis of soy oil with ethylene glycol

Downloaded by PENNSYLVANIA STATE UNIV on August 10, 2012 | http://pubs.acs.org
Publication Date: September 23, 2006 | doi: 10.1021/bk-2006-0939.ch006

Additionally, new resonance peaks appear at 66 ppm related to ethylene oxide carbons as well as peaks at 60 ppm related to the new C-OH functional groups. It is apparent from the NMR data that the hydroxylation of soybean oil progressed as expected to yield the desired polyols.

These soy polyols were further formulated to polyurethanes and polyesters. Their properties and structural characterization are currently being studied.

Downloaded by PENNSYLVANIA STATE UNIV on August 10, 2012 | http://pubs.acs.org
Publication Date: September 23, 2006 | doi: 10.1021/bk-2006-0939.ch006

Soy-based biodiesel

Biodiesel is a general term referred to alkyl monoesters derived from vegetable oils or animal fats, which are prepared by transesterification of these triglycerides with a low molecular weight alcohol (usually, methanol or ethanol). The most common "biodiesel" is methyl soyate, which is a mixture of products from the transesterification reaction of soy oil and methanol.

In general, biodiesel has superior cetane number and lubricity characteristics with respect to petroleum middle distillates; it also has comparable heats of combustion and kinematic viscosities, and it is non-flammable (making it safer to store and handle). Biodiesel is renewable and can help reduce our dependence on imported petroleum. It is environmentally friendly, biodegradable and its combustion reduces most harmful exhaust emissions, including carbon monoxide, particulate matter, and polyaromatic hydrocarbons. These and other benefits of biodiesel have been well documented[37]. However, problems related to fuel quality, filter plugging, injector failure, material compatibility, and fuel economy still remain and must be resolved before wide spread use of biodiesel can be addressed[38]. Some of these problems are inter-related, but all are inherent to the composition of the biodiesel itself. In particular, the presence of double bonds in the fatty esters and the relatively high average molecular weight of the mixture affect the stability, flow and compatibility of biodiesel compared with a petroleum-based diesel. These inherent problems require blending biodiesel with petroleum-based fuel, hinder its use in cold temperatures, negatively affect fuel economy, increase particulate emission, and lead to power loss.

The catalytic ozonation process offers a potentially simple and efficient chemical modification whereby the methyl soyate species are cleaved at the double bonds, thus eliminating all unsaturation and reducing the overall molecular weight of the fuel. This one-step process is fast, selective and simple and is expected to provide an economical route to improve the quality of vegetable-based biodiesel fuels.

It is well known that the oxidation and thermal stability of fatty acids is directly related to the number of double bonds present[39]. It was clearly shown that the double bond is the initial point of attack during autoxidation and the rate of oxygen absorption is much higher in fatty acids containing multiple double bonds. For example, the relative autoxidation rate of methyl stearate, methyl oleate, methyl linoleate, and methyl linolenate was found to be 1:11:114:170 at comparable temperatures[40]. Based on the mechanism, it was further concluded that the rate of oxidation of nonconjugated polyunsaturated fatty acids is the highest because of the activation of methylene groups between the two double bonds[41]. However, irrespective of the oxidation rate, the general mechanism in every unsaturated fatty acid involves the formation and decomposition of hydroperoxides, which is an autocatalytic reaction in nature, and eventually leads to crosslinking and chain scission reactions. The autoxidation of saturated fatty acids is much slower and these compounds are essentially inert at temperatures below 100°C. The cleavage of the unsaturated fatty esters in methyl soyate biodiesel was achieved by ozonolysis in methanol as described in the previous section. The products from this reaction are methyl esters and diesters as shown in Figure 16.

Downloaded by PENNSYLVANIA STATE UNIV on August 10, 2012 | http://pubs.acs.org
Publication Date: September 23, 2006 | doi: 10.1021/bk-2006-0939.ch006

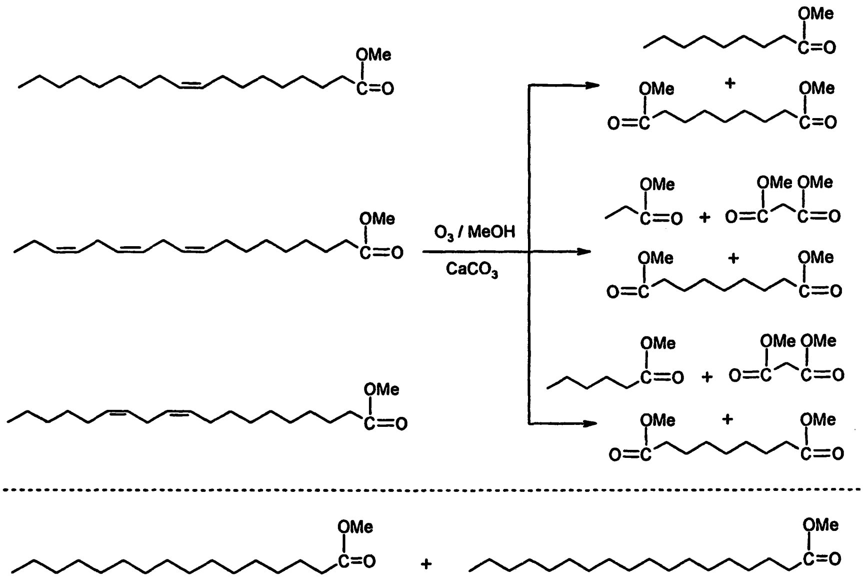

Figure 16: Composition of methyl soyate biodiesel after the catalytic ozonation with methanol

Closer examination of the ozonolysis products shows that the calculated mixture composition consists primarily of dimethyl nonanedioate, dimethyl propanedioate and methyl hexanoate (Table II). Since methyl stearate and methyl palmitate have no double bonds, they are not affected by the ozonolysis process and are present in the product mixture with no change. It is expected that the molecular weight after ozonolysis will be lower than the original methyl soyate due to the cleavage of the double bonds and indeed, the calculated number average molecular weight after ozonolysis is 169 compared with 292 for methyl soyate. This average molecular weight is much closer to diesel No.2 than methyl soyate.

Table II. Expected Composition of the Biodiesel after ozonolysis

Methyl Ester	*Relative Composition [wt. %]*	*MW*
dimethyl nonanedioate	34.5	216
dimethyl propanedioate	24.7	132
methyl hexanoate	21.6	130
methyl palmitate	4.7	270
methyl nonanoate	9.8	172
methyl propanoate	3.0	88
methyl stearate	1.7	298

Significant properties

FTIR, NMR and GC-MS confirmed the cleavage of the double bonds and the reaction of the new chain ends with methanol to yield a methyl esters and diesters[42] as listed in table II. The lower average molecular weight of the ozone treated biodiesel compared with untreated biodiesel is also more volatile than the untreated biodiesel (Figure 17). The volatilization temperature is fundamentally important for fuel as it has a major impact on the vapor-air ratio in the cylinder and therefore influences the ignition quality of the fuel. It is clearly evident from this figure that the volatility characteristics of the resulting ester mixture approached that of diesel fuel as the reaction time is increased. Since the boiling points of fatty acid methyl esters increase with the length of the hydrocarbon tail (or with molecular weight), it is not surprising that volatility increased as the heavier, long chain, unsaturated components are fragmented to shorter, lighter, saturated components, shifting its TGA profile towards diesel fuel.

Downloaded by PENNSYLVANIA STATE UNIV on August 10, 2012 | http://pubs.acs.org
Publication Date: September 23, 2006 | doi: 10.1021/bk-2006-0939.ch006

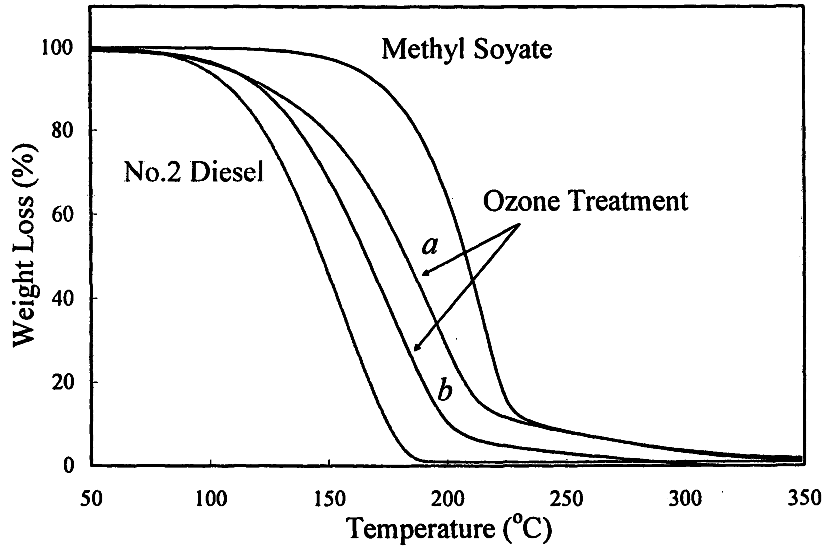

Figure 17: TGA profile of methyl soyate, ozone treated methyl soyate for(a) 40 and (b) 120 min, and No.2 diesel fuel.

The stability of the ozone treated biodiesel toward oxidation has been markedly improved as indicated from the Rancimat test results in Figure 18. This oxidation stability test has been used extensively in the food industry. Typically, a 10 gram oil sample is aged at a constant temperature (120°C) with an airflow passing through at the rate of 10 l/h. The airflow is then exhausted into a cell filled with distilled water. There the conductivity of the water is monitored continuously. During the oxidation process volatile acids are formed and are blown into the water and are detected by the conductivity of the aqueous solution. It is apparent from Figure 18 that within about 1 hr (induction period) a marked increase in the conductivity of the untreated biodiesel is observed and the conductivity is continuously increased as the test progresses. Conversely, the ozone treated biodiesel sample appears much more stable toward oxidation. Initially, some volatile (most likely the volatile methyl propionate) is blown into the water but then the conductivity remains constant over an extended period of time, confirming the resistance to oxidation.

Unfortunately, the catalytic ozonation process does not improve the flow properties of biodiesel at low temperatures (Figure 19).

Downloaded by PENNSYLVANIA STATE UNIV on August 10, 2012 | http://pubs.acs.org
Publication Date: September 23, 2006 | doi: 10.1021/bk-2006-0939.ch006

Downloaded by PENNSYLVANIA STATE UNIV on August 10, 2012 | http://pubs.acs.org
Publication Date: September 23, 2006 | doi: 10.1021/bk-2006-0939.ch006

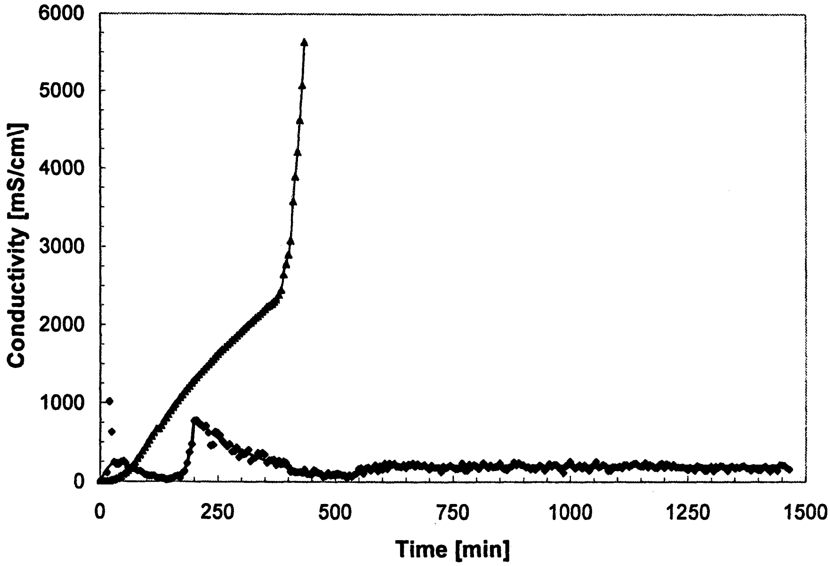

Figure18: Rancimat tests of (▲). Biodiesel(methyl soyate) and (♦). treated biodiesel (ozone/methanol)

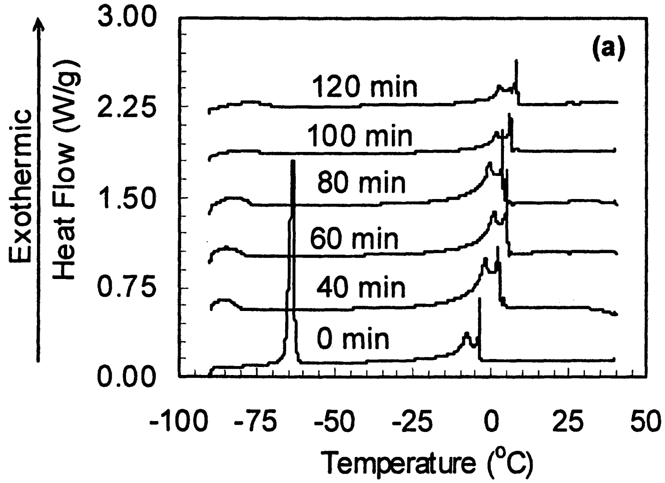

Figure 19: DSC of methyl soyate at different reaction times

These DSC data show that the low temperature crystallization peak (-70°C), related to the unsaturated fatty esters) is absent but the high temperature peak (around 0 to 10°C), related to the saturated ester is still present. This deficiency is directly related to the crystallization of the saturated fatty esters in the mixture (methyl stearate and methyl palmitate) upon cooling. Since the catalytic ozonation process does not affect these saturated esters, their crystallization must be suppressed by other means in order to use the biodiesel in cold climates.

Downloaded by PENNSYLVANIA STATE UNIV on August 10, 2012 | http://pubs.acs.org
Publication Date: September 23, 2006 | doi: 10.1021/bk-2006-0939.ch006

Conclusions

We have developed a novel catalytic ozonation process whereby unsaturated fatty acids are cleaved by the ozone and the resulting new chain-ends are reacted with an alcohol through an ester linkage. Although any alkaline catalyst is suitable for this process, we have used primarily $CaCO_3$ as it is stable to ozone, easily removed from the reaction mixture by filtration and it is readily available and economical. The ozonation process itself is relatively fast, simple, and unlike typical ozonation process, is a single-step process. All the reactions were run between 0°C and room temperature with no additional solvent. Furthermore, this process can be scaled-up to a continuous production.

The catalytic ozonation process is fairly general and provides us with a broad platform for modifications of vegetable oils. In this article we have used it to enhance the thermal stability of soy-based lubricants, chemically modified soy oil to introduce primary alcohol groups which can then be further condensed to yield polyurethanes and polyester, and to resolve the oxidative and storage stability of biodiesel.

Acknowledgements

This work was done under generous support from the USB contract numbers SB-3417, SB-2432, and SB-4413; as well as SBIR 2004-00525.

References

---

1. *The technology roadmap for plant/crop-based renewable resources 2020.* DOE/GO-10099-706; Feb. **1999** www.oit.doe.gov/agriculture.
2. http://www.soystats.com/2005/Default-frames.htm
3. *Ozonation in Organic Chemistry*, Bailey, P.S., Ed. Academic Press, New York, NY, 1978

4. *Ozonation in Organic Chemistry*, Bailey, P.S., Ed. Academic Press, New York, NY, 1978
5. Harris, C.D. *Ber. Disc. Chem. Ges.* **1903**, 36, 1993.
6. Merion, A.M. US Patent 2,865,937 **1958**
7. Beal R.E. US Patent 3,504, 038 **1970**
8. Chem. Eng. (N.Y) 59, No. 9, 246 **1952**
9. Marshall, J.A.; Garofalo, A.W. *J. Org. Chem.* **1993**, 58(14), 3675-80
10. ASTM D1959, Standard Test Method for Iodine Value of Drying Oils and Fatty Acids, Annual Book of ASTM Standards 06.03: 399-401 **2000**
11. ASTM D1980, Standard Test Method for Acid Value of Fatty Acids and Polymerized Fatty Acids, Annual Book of ASTM Standards 06.03: 418-419 **2000**.
12. Randles, S.J.;Wright, M. *J. Synth. Lub.* **1992**, 9, 145-16.
13. Dick, R.M. *Manuf. Eng. Mater. Proc.* **1994**, 41, 339-365.
14. *Biobased Industrial Fluids and Lubricants*, Erhan, S.Z.; Perez, J.P. Eds. AOCS Press, Champaign, IL. **2002**.
15. *Autoxidation and Antioxidants,* Lundberg, W.O. Ed., Interscience Publishers: New York, **1961**; Vol. I.
16. Johansson, L.E.; Lundin, S.T. *J. Am. Oil. Chem. Soc.* **1979**, 56, 974-980.
17 Adhvaryu, A.; Erhan, S.Z. *Ind. Crops Prod.* **2002**, 15, 247-254.
18. Tao, T.; Zhu, H.L.; Hu, Z.M. *Lubr. Sci.* **1996**, 8, 397-407.
19. Watanabe, S.; Fujita, T.; Sakamota, M. *J. Am. Oil. Chem. Soc.* **1988**, 65, 1311-1312.
20. Adhvaryu, A.; Erhan, S.Z.;Perez, J.M. *Wear* **2004**, 257, 359-367.
21. Uosukainen, E.; Linko, Y.Y.; Lamasa, M.; Tervakangas T. *J. Am. Oil Chem. Soc.* **1998**, 75, 1557-1563.
22. Kadesch, R.G. *J. Am. Oil Chem. Soc.* **1979**, 56, 845A-849A.
23. Schwab A.W. and Gast L.E. *J. Am. Oil Chem. Soc.* **1970**, 47, 371-373.
24. Schwab A.W., Gast L.E., and Rohwedder W.K. *J. Am. Oil Chem. Soc.* **1975**, 52, 236-239.
25. Phuong T.; Vicary, R.; Graiver, D.; Narayan, R. “Enhanced Thermal-Oxidative Stability of Biobased Lubricants”, *unpublished*
26. Narayan, R. *Kunstoff* **1989**, 79, 1022-1028.
27. Narayan, R. *In Polymeric Materials from Agricultural Feedstocks, Polymers from Agricultural Coproducts* Ed. Fishman, M.L.; Friedman, R.B.; Huang S.J., Am. Chem. Soc. Symp. Ser. **1994**, 575, 2.
28. Stanton, J.M. *J. Am. Oil Chem. Soc.* **1959**, 36: 503.
29. Wells, E.R.; Hixenbaugh, J.C. *Am. Paint J.***1962**, 46: 88.
30. Sherringham, J.A.; Clark, A.J.; Keene, B.R.T. *Lipid Technology*. **2000**, 12: 129-132.
31. Gruber, B.; Hoefer, R.; Kluth, H.; Meffert, A. *Fett Wissenschaft Technologie* **1987**, 89: 147-51.

Downloaded by PENNSYLVANIA STATE UNIV on August 10, 2012 | http://pubs.acs.org
Publication Date: September 23, 2006 | doi: 10.1021/bk-2006-0939.ch006

32. Heidbreder, A.; Gruetzmacher, R.; Nagorny, U.; Westfechtel, A. DE Patent 96-19646424 **1998**.
33. Frankel, E.N.; Pryde, E.H. *J. Am. Oil Chem. Soc.* **1977**, 54: 873-81.
34. Khoe, T.H.; Otey, F.H.; Frankel, E.N. *J. Am. Oil Chem. Soc.* **1972**, 49: 615-618.
35. Guo, A.; Demydov, D.; Zhang, W.; Petrovic, Z.S., *J. of Polym. and the Environ. 10*: **2002**, 49-52.
36. Takahara, J.; Setoyama, T. WO Application Patent 2002049999 **2002**.
37. Michaelson, R.G.; Austin, R.C. US Patent 4314088 **1982**.
38. Holmberg, W.C. *Biodiesel: A technology, performance, and regulatory overview*, American Biofuels assoc. inf. resources, inc. **1994**, pp 1-52
39. Schumacher, L.G.; Gerpen, J.V. "*Research Needs Resulting from Experiences of Fueling of Diesel Engines with Biodiesel*", Proceeding of the 3rd Fuel Conf. Nashville, TN **1996**.
40. *Autoxidation and antioxidants*, . Lundberg, W.O. ed. Interscience Pub., John Wiley and Sons, New York **1961**, Volume 1, pp. 10-48
41. Stirton, A.J.; Turner, J.; Riemenschneider, R.W. *Oil & Soaps* **1945**, 22, 81.
42. Farmer, E.H.; Sutton, D.A. *J. Chem. Soc.* **1942**, 139.
43. Baber, T. M.; Graiver, D.; Lira, C. T.; Narayan, R. *Biomacromolecules* **2005**, 6, 1334-1344.

Downloaded by PENNSYLVANIA STATE UNIV on August 10, 2012 | http://pubs.acs.org
Publication Date: September 23, 2006 | doi: 10.1021/bk-2006-0939.ch006

Downloaded by UNIV OF GUELPH LIBRARY on August 28, 2012 | http://pubs.acs.org
Publication Date: September 23, 2006 | doi: 10.1021/bk-2006-0939.ch007

Chapter 7

Poly(lactic acids): A Brief Review

J. R. Dorgan[1], B. Braun[1], J. R. Wegner[2], and D. M. Knauss[2]

**Departments for [1]Chemical Engineering and [2]Chemistry and Geochemistry,
Colorado School of Mines, Golden, CO 80401**

The family of bioplastics known as polylactic acids, or PLA, encompasses the set of polymers of lactide, a cyclic dimer produced by the dehydration of lactic acid, that represents a highly promising and versatile category of biomaterials. The development of PLA into a commodity polymer has spanned over six decades of research and design from inception to the present commercial utility. This review discusses the history of PLA synthesis and applications, as well as its degradation and environmental impact. The physical properties, that lead to the increasing interest in PLA, especially for packaging applications, as well as processing and fundamental chain properties are also summarized.

In Degradable Polymers and Materials; Khemani, K., et al.;
ACS Symposium Series; American Chemical Society: Washington, DC, 2006.

1. Introduction

The development of PLA into a commodity polymer has spanned over six decades of research and design from inception to the present commercial utility. The recorded history of PLA development began in 1932 when Wallace H. Carothers, et al. documented the earliest attempted polymerization and depolymerization of oligomeric lactides in the Journal of the American Chemical Society (1). In 1954, the Dupont Corporation synthesized high molecular weight PLA with improved lactide purification techniques, as well as antimony trioxide and antimony trihalide as polymerization catalysts (2). Later, methods were developed to produce high molecular weight PLA with properties sufficient for competition with traditional oil-derived polymers, but its production was prohibitively expensive. In the 1960's, several researchers investigated relationships between the chemical structures of lactide monomers and the configurations and crystalline structures of resulting PLAs (3-7). Because of its inherent biodegradability, PLA was one of the earliest polymers used in biomedical applications; Kulkarni, et al. demonstrated the human body's ability to absorb PLA-based sutures in 1966 (8). Work in the 1970's and 80's focused primarily on discovery of new catalyst systems for polymerization, improving characterization with new analytical techniques, and investigation of new medical applications (9).

Recently, the need for more biofriendly polymers has led to the study of additional catalyst systems, new types of copolymers, and polymerization mechanisms. In the early 1990's, methods were developed for the continuous production of both lactide and PLA. A major step in the commercialization of PLA occurred when Cargill Corporation developed its method to produce PLA in a continuous process (10-13). A joint venture of Cargill with Dow Polymers (CDP) was then formed in 1997 to develop further the potential of PLA as a commodity polymer. A production facility, opened in 2002, was built in Blair, Nebraska with the capability of producing approximately 300 million lbs of PLA per year. Large-scale production of PLA has dramatically decreased the cost of PLA resins and is now enabling it to compete with established petroleum-based materials (Wall Street Journal, "One Word of Advice: Now its Corn", October 12, 2004). Dow Chemical recently exited the joint venture and the Blair works is operated by a wholly owned subsidiary of Cargill called NatureWorks (www.NatureWorksllc.com), which is now producing and selling large quantities of resins for products ranging from clothing to food packaging.

2. PLA Biosynthesis, Biodegradation, and Environmental Impact: Overview

PLA is commercially produced utilizing corn as the feedstock according to the process diagramed in Fig. 1. Corn first undergoes the traditional milling

Downloaded by UNIV OF GUELPH LIBRARY on August 28, 2012 | http://pubs.acs.org
Publication Date: September 23, 2006 | doi: 10.1021/bk-2006-0939.ch007

Downloaded by UNIV OF GUELPH LIBRARY on August 28, 2012 | http://pubs.acs.org
Publication Date: September 23, 2006 | doi: 10.1021/bk-2006-0939.ch007

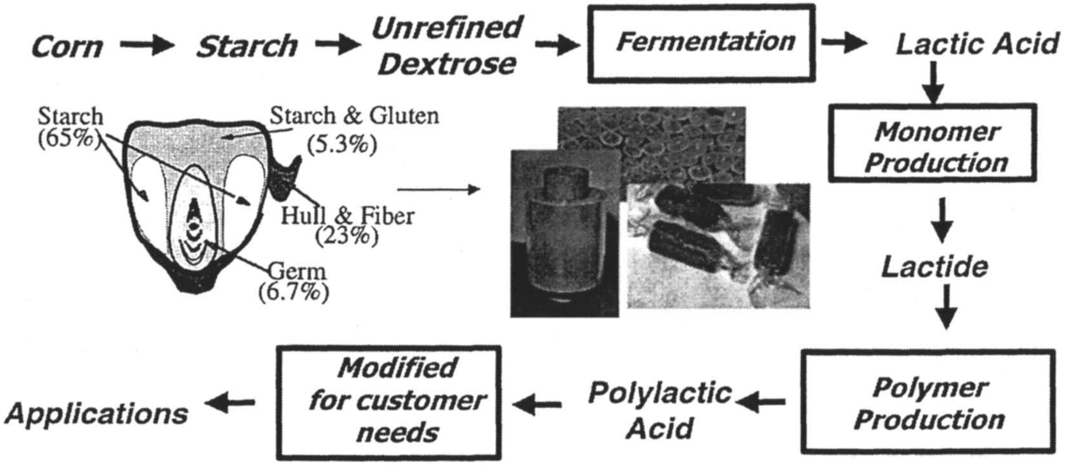
Corn
Starch
Unrefined Dextrose
Fermentation
Lactic Acid
Starch (65%)
Starch & Gluten (5.3%)
Hull & Fiber (23%)
Germ (6.7%)
Monomer Production
Lactide
Polymer Production
Polylactic Acid
Modified for customer needs
Applications

Figure 1. Commercial route to biobased PLA plastics.

process to produce unrefined glucose (dextrose), after which microorganisms ferment the glucose to lactic acid. Importantly, this fermentation process is anaerobic: a wide variety of literature suggests that anaerobic fermentations hold great advantage over aerobic fermentations when CO_2 balance is of concern (discussed further below).

After fermentation, the resulting lactic acid is formed into cyclic lactide through dimerization using reactive distillation. The lactide ring is then polymerized to produce PLA.

The degradation of polymeric materials in the environment is a critical area of concern due to the large quantity of plastics generated. Each year, over 70 million tons of polymers are produced which end up in landfills (14,15). Breakdown of PLA in the environment can occur biotically or abiotically (16); in the absence of sufficient microbial activity or oxygen, hydrolysis becomes the predominant pathway for degradation, while in aerated composting environments, biotic processes can degrade PLA rapidly (within weeks) and completely (17,18), these parameters are subject to the form and purity of the PLA (19). As an alternative to biodegradation, waste PLA can be recycled into lactic acid, which can then be reformed into lactide and repolymerized (16,17).

To assess the environmental impact of PLA synthesis and use, a comprehensive Life Cycle Inventory (LCI) enabling "apples-to-apples" comparisons with petrochemical-based thermoplastics was recently undertaken (Fig. 2) (20). Among the most notable benefits of PLA shown were reductions in both fossil fuel use and global warming potential, even assuming use of fossil-based energy sources for agriculture and processing. Compared to most traditional hydrocarbon-based polymers, PLA uses 30-50% less fossil fuel energy and results in lower CO_2 emission by 50-70%. Whereas conventional thermoplastic polymers require oil as their source of monomers (fossil feedstock) and additional fossil fuels for processing, solar energy provides approximately 1/3 of the Gross Energy Requirement in PLA production; in addition, processing of oil into conventional plastics releases even greater amounts of CO_2 than does PLA production (20).

3.1. Physical Properties

The bulk properties of PLA are greatly affected by the molecular weight of the polymer, the chain architecture (branched vs. linear), and the degree of crystallinity in the polymer (21,22). The acheivable crystallinity of PLA is determined by the relative proportions of L- and D-lactide in the polymer backbone; the greater the optical purity, the higher the crystallinity.

Downloaded by UNIV OF GUELPH LIBRARY on August 28, 2012 | http://pubs.acs.org
Publication Date: September 23, 2006 | doi: 10.1021/bk-2006-0939.ch007

Downloaded by UNIV OF GUELPH LIBRARY on August 28, 2012 | http://pubs.acs.org
Publication Date: September 23, 2006 | doi: 10.1021/bk-2006-0939.ch007

E.T.H Vink et. al. / Polymer Degradation and Stability 80 (2003) 403-419

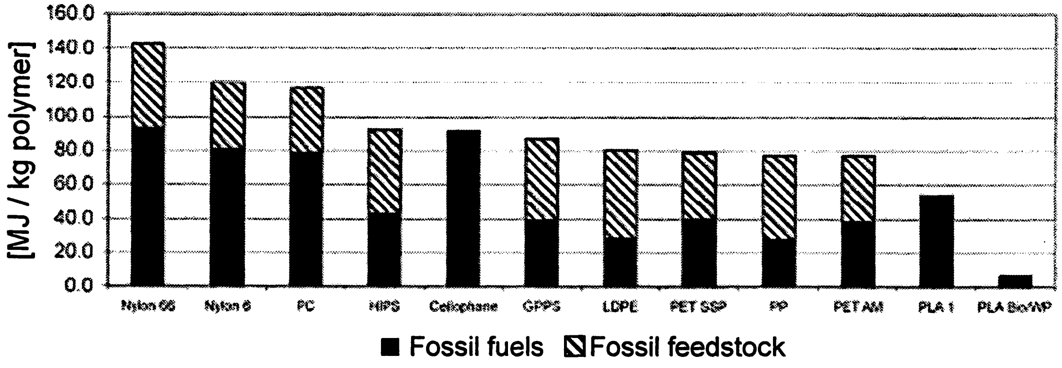

Figure 2. Life cycle analysis results for energy content of various thermoplastic polymers. PLA1 represents present technology; PLA Bio/WP is the projection for the production of PLA from agricultural waste using wind power.
(Reproduced with permission from reference 20. Copyright 2003 Elsevier.)

PLA samples containing 87.5% L-lactide are reported as being completely amorphous, while samples with 92% L-lactide possess some crystallinity (14). Polymers from 100% L -lactide can be nearly half-crystalline (16). The melting point (T_m) range of crystalline PLA is 145-186°C (21), although a blend of 100% D-lactide and 100% L-lactide polymers in a "stereo-complex" form a closely packed crystalline structure that increases the T_m to 230°C (23). The appearance of the PLA is also affected by the crystalline content. Amorphous PLA and low-crystalline PLA are clear materials with high gloss, while highly crystalline PLA is an opaque white material.

The molecular weight, structure, and crystallinity of PLA play important roles in its mechanical properties as well, including tensile strength, tensile modulus, and percent elongation to break. These properties are comparable to those of poly(ethylene terephthalate) (PET), polypropylene (PP), and polystyrene (PS), presenting the possibility that PLA variations may replace thermoplastics in many applications. Investigation of such applications is an active area of research in Japan, North America, and Europe (17,21,22).

Downloaded by UNIV OF GUELPH LIBRARY on August 28, 2012 | http://pubs.acs.org
Publication Date: September 23, 2006 | doi: 10.1021/bk-2006-0939.ch007

3.2. Applications

A wide range of products can be produced from PLA and PLA derivatives, including structural support and drug delivery in medical applications, tough fibers in woven and non-woven products, and molded or extruded consumer products.

In initial medical applications, lactide and glycolide copolymers were used to make absorbable sutures capable of replacing denatured collagen or catgut (14). Materials based on PLA and PLA copolymers have also been designed to replace metal and other non-absorbable polymers as therapeutic aids in surgery, including pins (24), plates (25), screws (25,26), suture anchors (27), and intravascular stents (9,28). The advantages of PLA and PLA glycolide copolymers for these applications come from the ability of the body both to degrade the polymers and to metabolize the degradation products over time, leaving no residual foreign material in the body (8). The ability to tune PLA degradation times is also relevant to the field of drug delivery, as drugs encapsulated in polymers can be released based on the known degradation time of PLA (29) or PLA copolymers (30,31), even allowing the specific targeting of organs (32). Other medical applications currently being pursued include dressings for burn victims (33), substrates for skin grafts (24), and dental applications (9). Medical usage in devices, sutures and drug delivery systems, while technologically important, nevertheless represents only a small opportunity for displacing less environmentally benign plastics.

Downloaded by UNIV OF GUELPH LIBRARY on August 28, 2012 | http://pubs.acs.org
Publication Date: September 23, 2006 | doi: 10.1021/bk-2006-0939.ch007

Fortunately, PLA also has properties suitable for commercial fiber products. Fibers can be produced from either pure liquid polymer, in a "melt-spun" process (34,35), or from polymer dissolved in an organic solvent, in a "solution-spun" process (36,37). Advantageously, fibers produced from PLA have lower processing temperatures than PET fibers and therefore require lower energy input during processing. In applications, non-woven fibers are able to wick moisture without absorbing it and can therefore be used in products such as diapers. Materials produced from woven fibers have additional desirable properties, including favorable hand and touch, drape, wrinkle resistance, rapid wicking, and low moisture absorbance. Woven PLA fiber-based materials are highly resilient to wear, have excellent UV resistance, and low inflammability. Applications for the PLA fibers or blends of PLA fibers with other natural fibers, such as silk, cotton, or wool, therefore include clothing, carpets, upholstery, and draperies (38).

The greatest opportunity for PLA to displace less environmentally benign materials is in the area of packaging. This is because the properties of PLA often improve function as well as diminish environmental impact. PLA can be used in traditional polymer processing operations such as injection molding, blow molding, extrusion, and extrusion coating; as a result, lids, trays, and clamshells used in food handling can be thermoformed from extruded sheet PLA, even yielding products with higher flex-crack resistance in living hinges (thin sections of plastic that bridge two parts) than those made of polystyrene. Disposable cutlery can also be produced using injection molding of PLA. In addition, thin sheets of many PLA variants possess high gloss, excellent heat sealability, and clarity, allowing extruded thin sheets of PLA to replace cellophane and PET in transparent packaging (39). Bags for yard and/or food wastes form another set of applications in which the physical properties as well as the biodegradable nature of PLA can be used to advantage; bags are tough and puncture resistant but are completely degraded within 4-6 weeks in a composting environment (39).

Extrusion coating of PLA for paper products is another set of applications with several benefits. For example, paper coated with PLA does not require pretreatment for ink adherence, whereas polyethylene (PE) paper coatings often do. PLA coatings also possess higher gloss, greater clarity, lower coefficients of friction, and greater stiffness than PE, allowing thinner paper to be used (18).

Some limitations do still exist, however, to the use of PLA in polystyrene-like applications. These include primarily the low melt strength (extensibility without breaking of the molten state) and the relatively low temperature at which heat distortion begins to occur. The drawbacks of PLA are overshadowed by its advantages in products with short product cycle lifetimes (39).

3.3. Synthesis

The two general synthetic routes for PLA include the condensation polymerization of lactic acid and the ring-opening polymerization of lactide. Condensation polymerization methods have produced high molecular weight PLA through chain extension and, more recently, through dehydration using azeotropic high-boiling (b.p. >150°C) aprotic solvents and vacuum techniques. Polymerization utilizing a ring opening mechanism is the preferred method of synthesis, however, and is the basis of the commercial NatureWorks process.

Condensation polymerization has recently become a reliable method for production of high molecular weight PLA. Attempts as recently as the mid-1990s to produce high molecular weight PLA through simple dehydration without catalysis were unsuccessful, primarily due to side reactions among free lactic acid, water, and short-chained polyesters, as well as side reactions forming monomeric lactide (40). As a result, these efforts yielded only oligomeric PLA with a maximum average molecular weight (M_n) of 5,000g/mol (16). To reduce the interfering side reactions, two methods are currently available. The first, developed by Ajioka et al. in 1995 (40), involves the dehydration of lactic acid using high-boiling aprotic solvents, such as diphenyl ether, that form azeotropes with water under vacuum conditions, as well as a catalyst. The second method for reducing side reactions, producing relatively high molecular weight PLA, was developed by Moon et al. in 2000 (41). This technique involved the use of a dual catalyst system in the presence of a 10 torr vacuum. Other methods have been attempted with the goal of producing high molecular weight PLA directly from lactic acid monomers, but to date have yielded only moderate molecular weight materials (42,43).

Chain extension of oligomeric PLA is another approach, within the category of condensation polymerization, used to produce higher molecular weight PLA. Two basic methodologies have been developed: one uses an additive to promote esterification of two PLA chains into one continuous chain, (44,45). while the other uses a linking agent to couple two or more chains together. Chain linking agents such as diisocyanates (46,47), thiirane (47), and diacidchlorides (44) are more economical than esterification promoting agents due to fewer purification steps and the important ability to run the reactions in the bulk. Problems associated with linking agents, however, include the persistence of unreacted chain linking agents, residual metals, and the non-biodegradability of the linking agent, all of which diminish the environmental advantages of the resultant PLA.

Although the straight dehydration of lactic acid does not produce high molecular weight polymers, the process is important in the production of lactide, as noted above. The amount of lactide produced is influenced by temperature,

Downloaded by UNIV OF GUELPH LIBRARY on August 28, 2012 | http://pubs.acs.org
Publication Date: September 23, 2006 | doi: 10.1021/bk-2006-0939.ch007

Downloaded by UNIV OF GUELPH LIBRARY on August 28, 2012 | http://pubs.acs.org
Publication Date: September 23, 2006 | doi: 10.1021/bk-2006-0939.ch007

pressure, and the types of catalysts added to the system (48). Commercially, lactide is produced from lactic acid prepolymers. Multiple purification methods are used industrially, including Cargill's multiple reflux controlled columns (11,12), multi-step recrystallization reactors (49-56), and direct vapor-phase reaction of lactic acid (57,58). Formation of lactide occurs through a "back-biting" reaction involving two lactic acid monomers to form the six-member lactide ring. Three types of lactide can be formed: L-lactide or D-lactide with m.p.= 97°C, or meso-lactide with m.p.= 52°C, depending on the composition of the starting material and extent of racemization (Fig. 3). A fourth type, D,L-lactide, is formed when a racemic stereocomplex of D and L-lactide are crystallized together; this form has a much higher melting point of 126-127°C (16). Crystallinity in the PLA can be adjusted by changing the ratio of D- to L-lactide in the monomer feed.

Lactide, once formed, can be polymerized by three general mechanisms: anionic, (33,59-61) cationic, (33,62,63). and coordination insertion (see below). Of these, coordination-insertation is the most prevalent and industrially most important. Polymerization reactions may be performed in bulk or in solution. The type of lactide, reaction temperature, and catalyst system determine the stereochemistry at each carbon-carbon bond along the backbone of PLA, in turn determining the properties of the resulting material, while impurities present in the lactide such as water, lactic acid, and lactyl-lactic acid decrease the molecular weight of the end polymer (64,65).

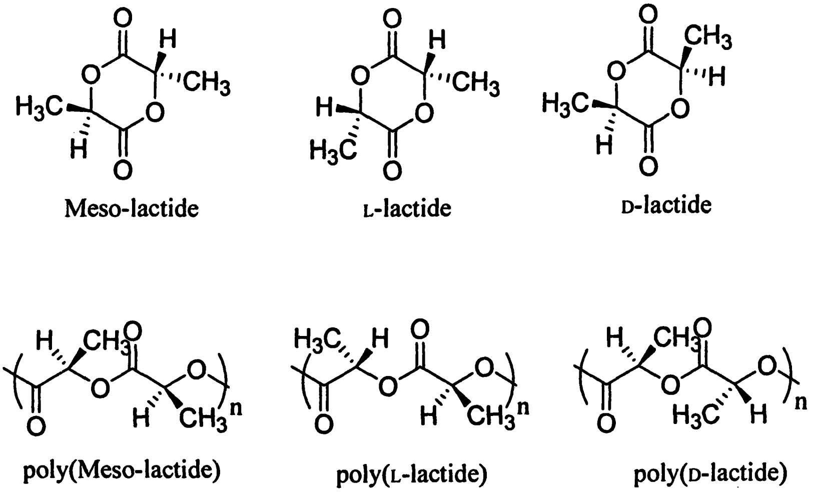
Meso-lactide L-lactide D-lactide

poly(Meso-lactide) poly(L-lactide) poly(D-lactide)

Figure 3. Types of lactide (meso-lactide, L-lactide, and D-lactide) and their corresponding polymers (poly(meso-lactide), usually atactic, poly(L-lactide) and poly(D-lactide)).

Polymerization of lactide through a coordination insertion mechanism is the most common method used to produce high molecular weight PLA with high optical purity and crystallinity. Many catalytic or initiator systems have been developed for the coordination insertion polymerization of lactide. Oxides, halides, and alkoxides of metals possessing free p-, d-, or f- orbitals such as Mg (66-68), Zn (66,69-73), Al (74-83), Sn (64,65,73,80,82,84-94), and Y (95,96) effectively catalyze the ring-opening polymerization of lactide. In general, the most useful catalysts possess highly covalent metal-ligand bonds (33).

The general catalytic mechanism involves coordination of the lactide carbonyl group to the catalyst metal, followed by cleavage of the ring acyl-oxygen bond and attachment of the growing, catalyst-attached polymer. The terminally bound catalyst then promotes the addition of successive monomers. Because each catalyst (or initiator) molecule facilitates the extension of a single polymer chain, molecular weights of PLA are controlled by varying the proportion of catalyst/initiator to lactide. Polymerization temperatures used vary from ambient to >200°C. Unlike ionic initiators, insertion catalysts do not cause racemization at temperatures up to 150°C (33).

Among the coordination insertion catalysts, tin 2-ethylhexanoate (tin octoate, or $Sn(Oct)_2$) is the most widely used and studied due to its ability to produce highly crystalline PLA in relatively short periods of time with high conversion and low racemization up to 180°C. It has also been approved by the United States Food and Drug Administration for food contact (16), making it ideal for many packaging applications.

Debate about the nature of the initiating species and the mechanism of tin octoate catalyzed polymerizations can be found in the literature.(64,73,88,93,97-102) Water, alcohol, lactic acid, and lactyl lactate can form other species with tin octoate, including tin oxide, tin hydroxides, tin alkoxides, tin lactate, all of which have been suggested to catalyze the ring opening of lactic acid (65,101,103). Most recent work has established the initiating species in the presence of added alcohol initiator to be tin (II) alkoxide produced from exchange reactions between the 2-ethylhexanoic acid on the tin octoate and the alcohol.(88,98-100)

Aluminum alkoxides are another class of highly-studied catalysts and initiators for PLA polymerization. One of the most popular aluminum initiators, aluminum isopropoxide, has three initiation sites (76). Polymerization proceeds by a coordination insertion mechanism; as with the tin catalyst, the reaction is first order with respect to the lactide monomer and polymerization rates decrease as extents of conversion become higher (81,104,105). Living polymerizations are those in which the chain end remains reactive and can therefore reinitiate polymerization with another monomer to make block copolymers. For PLAs this has been accomplished using aluminum alkoxides at temperatures $\leq$ 70°C (79,106) with molecular weights < 90,000g/mol (104). Above 90,000g/mol, at extended polymerization times, or at higher polymerization temperatures, transesterification increases, forming cyclics and lower molecular weight materials leading to broader polydispersities (77,83).

Downloaded by UNIV OF GUELPH LIBRARY on August 28, 2012 | http://pubs.acs.org
Publication Date: September 23, 2006 | doi: 10.1021/bk-2006-0939.ch007

Recently, single-site catalysts prepared by the addition of bulky side groups to metals have produced PLA with stereochemically-controlled structures. (107). Highly syndiotactic PLA has been formed from meso-lactide using bulky racemic aluminum catalysts (108). Using the same catalyst, D,L-lactide was polymerized to form "stereoblocks" of PLA, possessing blocks of isotactic D- and L-PLA (109). The stereoblock copolymer had a T_g slightly higher than isotactic L- or D-PLA, but lower than the stereocomplex formed between D- and L-PLA. Similar results were observed for the polymerization of D,L-lactide (110) using the same catalyst. Single-site catalyst work thus demonstrates a method to produce PLA with good control of the polymer backbone stereochemistry. This is a promising development, now opening the possibility of forming stereocomplexes between copolymer blocks that can withstand higher temperatures before heat distortion occurs at the interfaces between blocks.

3.4. Architectural Variations

Using techniques developed for polymerization of linear PLA, it has been possible to synthesize random copolymers, block copolymers, and branched polymers to modify the properties of the materials produced.

Random copolymers are produced by polymerization of two or more species together using a catalyst functional with both. Monomers that fit the criteria for ring-opening copolymerizations with lactide are glycolide (111-113), glycolide derivatives (114-117), lactones (30,118-120), cyclic amide ethers (121), cyclic amide esters (122,123), cyclic ether esters (31,124,125), cyclic phosphates (126), cyclic anhydrides (127) or cyclic carbonates (128-130). Additional copolymers have been made through transesterification reactions of PLA with other polyesters, including PET (131). By adjusting the proportions of each monomer, properties such as T_g, ease of biodegradation, and backbone flexibility can be altered (31,125).

Block copolymers can also be produced. In one method, a ring-opening polymerization mechanism is employed using either coordination insertion catalysis or anionic catalysis (132). Monomer addition sequence is important in this method: those that produce primary hydroxyl groups, such as lactones (97,106,121,133-135), trimethylene carbonate (TMC) (130,135), and 1,5-dioxepan-2-one (DXO) (136) must generally be polymerized first. Exceptions to the order of addition involve both glycolide (137) and D,L-3-methyl glycolide (MG) (117), which can be polymerized sequentially before or after PLA to form block copolymers because they possess the same type of propagating chain end as lactide. Ring-opening polymerization from polymeric initiators, a second method to produce block copolymers, employs polymeric initiators that possess

Downloaded by UNIV OF GUELPH LIBRARY on August 28, 2012 | http://pubs.acs.org
Publication Date: September 23, 2006 | doi: 10.1021/bk-2006-0939.ch007

hydroxyl groups on their chain ends. These groups initiate polymerization with the same catalysts used in polymerization of linear PLA. Effective polymeric initiators include poly(ethylene glycol) (132,138-146), poly(ethylene glycol-co-propylene glycol) (147), poly(propylene glycol) (113), poly(tetrahydrofuran) (139,148), poly(dimethyl siloxane) (139,149-151), hydroxyl functionalized polyethylene (152), and hydroxyl functionalized poly(isoprene) (153,154). Dendritic molecules with a single hydroxyl group have also been used to produce linear / dendritic di-block copolymers (155).

Several methods for synthesis of highly branched polymers through the ring opening of lactones have likewise been developed. Star formations are produced either by divergence, where polymer chains grow from a central core, or through convergence in which a termination reaction couples together individual chains (156-158). Comb-shaped copolymers consisting of linear backbones with pendent linear chains may also be produced (159-165). Lactides have also been polymerized into hyperbranched structures, in which many branch points lead to other branch points (166-170). Star-shaped copolymers are generally produced in a similar manner to star-shaped homopolymers, with hydroxyl groups on a multifunctional initiator used to initiate polymerization (171).

Downloaded by UNIV OF GUELPH LIBRARY on August 28, 2012 | http://pubs.acs.org
Publication Date: September 23, 2006 | doi: 10.1021/bk-2006-0939.ch007

3.5. Fundamental Chain Properties

The characterization of PLA depends on the accurate knowledge of its fundamental properties. These include such parameters as Mark-Houwink (MH) constants that relate intrinsic viscosity to molecular weights, theta-condition front factors (K) used to calculate single chain properties, and characteristic ratios (C_∞) that give an indication of the bonding structure of polymers. Unfortunately, each of these is reported inconsistently in the literature (5,6,156,172-178).

A recent study (179) has addressed these inconsistencies experimentally. PLA homopolymers and copolymers spanning wide ranges of molecular weight and stereoisomer proportion were prepared by ring-opening polymerizations of L- and D-lactides using tin octoate as the catalyst. Samples were then characterized by means of dilute-solution viscometry in three different solvents, size-exclusion chromatography, static multiangle light scattering, variable-angle spectroscopic ellipsometry, and melt rheology. Data provided by these experiments include values of C_∞ as well as Schulz-Blaschke and Mark-Houwink constants, all of which show consistently that polylactides are typical linear flexible polymers, in excellent agreement with recently published theoretical simulation results (180).

3.6. Processing Properties

Plastics are typically fabricated into useful articles in the molten state, thereby causing the melt flow, or rheological, properties of a polymer to be of great importance. As discussed above, PLAs have physical properties useful in fibers, packaging, and other applications traditionally dominated by petroleum-based resins. Although the general literature on polylactides is extensive, only a few articles (181-185) have considered rheological properties. Measurements of dynamic, steady, and transient shear viscosities have been presented and the extensional data on PLA showed a strong strain hardening behavior (185). These studies did not, however, capture a systematic description of PLA rheology across a broad range of stereooptical composition, as materials studied to date have usually possessed high (>90%) L-stereochemical center content. However, a recent study (186) has provided a comprehensive evaluation of the linear viscoelastic properties of PLA across a wide range of molecular weights and stereochemical compositions. The rheology of blends of linear and branched poly(lactic acid) (PLA) architectures has also been comprehensively investigated (184,187). The results suggest that excellent control over rheological behavior of PLA is possible through blending chain architectures without compromising mechanical properties.

Mechanical properties of solution-spun (36,37,188,189) and melt-spun (34,36,190-193) PLA fibers have been thoroughly investigated. It has been found that these properties are roughly equivalent to other polyesters meaning that PLA can replace textiles based on non-renewable resources. In addition, scanning electron microscopy (SEM) (34,37,188,190) and wide-angle X-ray scattering (WAXS) (36,194) have been useful in examining surface structure with respect to roughness and fracture surfaces. Understanding surface properties is important for dying and other textile finishing operations. Cicero et al. have provided a complete characterization of the hierarchical fiber morphology from linear PLAs (35,195), determining thermal, mechanical, and morphological properties of the fibers and showing that properties can be widely manipulated through a combination of processing temperature and draw ratio. Maximum tensile strength and modulus of 0.38 GPa and 3.2 GPa, respectively, were obtained. Atomic force microscopy showed that the fiber morphology was found to be highly fibrillar with microfibril diameters of ~40 nm in diameter. The same researchers have studied the effects of branching on fiber properties and morphology (196) and investigated the improvement of fiber properties specifically when thermally stabilized PLA is used (197). These research studies provide several routes for optimizing the performance of PLA when used as a textile fiber in place of conventional, fossil resource based polyesters.

Downloaded by UNIV OF GUELPH LIBRARY on August 28, 2012 | http://pubs.acs.org
Publication Date: September 23, 2006 | doi: 10.1021/bk-2006-0939.ch007

3.7. Permeation Properties

Because of the desirability of using PLA in packaging applications, understanding the permeation properties of PLA with respect to various gases and vapors, especially those of interest to the food industry, is extremely important. PLA is, unfortunately, a relatively poor barrier to water vapor and CO_2, with a water-vapor transmission rate significantly higher than those of PET, PP or PVC, (198) with the result that some highly environmentally beneficial applications of PLA to packaging are being limited. For example, PLA's high permeability to water prevents it from being used to bottle water, despite the fact that increasing sales of bottled water have created considerable pressure on landfill space, particularly in California.

In response, NatureWorks has developed several biaxially-oriented PLA films to improve PLA barrier properties, including two with trade names of PLA 4030-D and PLA 4040-D. Permeation of nitrogen, oxygen, carbon dioxide, and methane in very thin (5 μm) amorphous films of various grades of PLA (L:D ratios from 95:5 to 98:2) cast from solution have also been examined (199). Notably, changes in polymer chain branching and L:D ratios had no effect on the permeation properties of PLA with respect to small gases.

4. Conclusions

PLA is an established material for medical applications. Recently, the progression towards more sustainable industrial practices has led to its development as an environmentally benign replacement of various fossil based polymers. However, in order to guide ongoing research in the field of bioplastics further evaluation and standardization of Life Cycle Impact Analysis tools are needed.

Presently, PLA and other biopolyesters suffer from two important deficiencies that limit their use, of which the first is the low heat distortion temperature. The second is their relatively high permeabilities toward a number of substances, particularly water. Recently, copolymerization of cellulose acetate with PLA, both originating from renewable resources, resulted in a material with increased heat distortion temperature (200). In addition, nanocomposite technologies hold promise for improving both temperature distortion and permeation characteristics, as they have in conventional plastics.

Beyond issues of heat distortion and permeability described above, the greatest current obstacle to greater market penetration of PLA is its cost. Increasingly higher oil prices are enabling PLA to compete directly with petroleum-based plastics despite the fact that PLA is a new entity in the plastics marketplace, but cost reductions would nevertheless allow greater utilization.

Downloaded by UNIV OF GUELPH LIBRARY on August 28, 2012 | http://pubs.acs.org
Publication Date: September 23, 2006 | doi: 10.1021/bk-2006-0939.ch007

Accordingly, renewable materials such as starches, cellulose, and wood flours and fibers that could be used in PLA blends to decrease costs without significantly degrading performance are of great commercial interest. New technical developments involving architectural variation, copolymeriztion, blends and nanocomposites of PLA are rapidly appearing further strengthening the possibility of replacing petroleum based plastics with biopolymers from renewable resources for many applications.

6. References

1. Carothers, W. H.; Dorough, G. L.; Van Natta, F. J. *The Journal of American Chemical Society* 1932, *54*, 761-772.
2. Lowe, C. E. In United States Patant and Trademark Office; E.I. du Pont de Nemours and Company: United States of America, 1954.
3. Goodman, M.; D'Alagni, M. *Polymer Letters* 1967, *5*, 515-521.
4. Schulz, R. C.; Guthmann, A. *Polymer Letters* 1967, *5*, 1099-1102.
5. Tonelli, A. E.; Flory, P. J. *Macromolecules* 1969, *2*, 225-227.
6. Tonelli, A. E.; Flory, P. J.; Brant, D. A. *Macromolecules* 1969, *2*, 227.
7. Schulz, V. R. C.; Schwaab, J. *Die Makromolekulare Chemie* 1965, *87*, 90-102.
8. Kulkarni, R. K.; Pani, K. C.; Neuman, C.; Leonard, F. *Archives of Surgery* 1966, *93*, 839-843.
9. Middleton, J. C.; Tipton, A. J. In Medical Plastics and Biomaterials Magazine, 1998.
10. Gruber, P. R.; Hall, E. S.; Kolstad, J. J.; Iwan, M. L.; Benson, R. D.; Borchardt, R. L. In US Patent and Trademark Office, USP 5,247,058; Cargill, Incorporated: United States of America, 1993.
11. Gruber, P. R.; Hall, E. S.; Kolstad, J. J.; Iwen, M. L.; Benson, R. D.; Borchardt, R. L. In US Patent and Trademark Office, USP 5,247,059; Cargill, Incorporated: United States of America, 1993.
12. Gruber, P. R.; Hall, E. S.; Kolstad, J. J.; Iwen, M. L.; Benson, R. D.; Borchardt, R. L. In US Patent and Trademark Office, USP 5,274,073; Cargill, Incorporated: United States of America, 1993.
13. Gruber, P. R.; Hall, E. S.; Kolstad, J. J.; Iwen, M. L.; Benson, R. D.; Borchardt, R. L. In US Patent and Trademark Office, USP 5,357,035; Cargill, Incorporated: United States of America, 1994.
14. Vert, M.; Schwarch, G.; Coudane, J. *J.M.S.-Pure Appl. Chem.* 1995, *A32*, 787-796.
15. Dorgan, J. R. 3rd Annual Green Chemistry and Engineering Conference Proceedings, Washington, D.C., 1999, pp 145-149.
16. Hartman, M. H.High Molecular Weight Polylactic Acid Polymers In Biopolymers from renewable Resources; Kaplan, D. H., Ed.; Springer-Verlag: Berlin, 1998, pp 367-411.

Downloaded by UNIV OF GUELPH LIBRARY on August 28, 2012 | http://pubs.acs.org
Publication Date: September 23, 2006 | doi: 10.1021/bk-2006-0939.ch007

17. Naitove, M. H. *Plastics Technology* 1995, *March*, 15-17.
18. Riggle, D. *Biocycle: Journal of Composting and Recycling* 1997, *38*, 65.
19. Zhang, X.; Wyss, U. P.; Pichora, D.; Goosen, M. F. A. *Journal of Bioactive and Compatible Polymers* 1994, *9*, 81-100.
20. Vinka, E. T. H.; Ra′bago, K. R.; Glassner, D. A.; Gruber, P. R. *Polymer Degradation and Stability* 2003, *80*, 403–419.
21. Lu, L.; Mikos, A. G.Poly(lactic acid) In Polymer Data Handbook; Mark, J. E., Ed.; Oxford University Press: New York, 1999, pp 627-633.
22. Engelberg, I.; Kohn, J. *Biomaterials* 1991, *12*, 292-304.
23. Ikada, Y.; Jamshidi, K.; Tsuji, H.; Hyon, S.-H. *Macromolecules* 1987, *20*, 904-906.
24. Vainionpää, S.; Rokkanen, P.; Törmälä, P. *Progress in Polymer Science* 1989, *14*, 679-708.
25. Eitenmüller, J.; David, A.; Pommer, A.; Muhr, G. *Der Chirurg* 1996, *67*, 413-418.
26. Viljanen, J. T.; Pihlajamäki, H. K.; Törmälä, P. O.; Rokkanen, P. U. *Journal of Orthopaedic Research* 1997, *15*, 398-407.
27. Richardson, J. B.; Jones, R.; Hunt, A.; Brat, S. J. t. In Orthopeadic Product News: Online Edition: http://www.opnews.com/ole/archives/articles/mar.may00/items.html, 2000.
28. Pétas, A.; Talja, M.; Tammela, T. L. J.; Taari, K.; Välimaa, T.; Törmälä, P. *British Journal of Urology* 1997, *80*, 439-443.
29. Vert, M. *Die Makromolekulare Chemie, Macromolecular Symposia* 1986, *6*, 109-122.
30. Ge, H.; Hu, Y.; Yang, S.; Jiang, X.; Yang, C. *Journal of Applied Polymer Science* 2000, *75*, 874-882.
31. Edlund, U.; Albertsson, A.-C. *Journal of Polymer Science: Part A: Polymer Chemistry* 1999, *37*, 1877-1884.
32. Griffith, L. G. *Acta Materialia* 2000, *48*, 263-277.
33. Kricheldorf, H. R.; Kreiser-Saunders, I.; Jürgens, C.; Wolter, D. *Macromolecular Symposium* 1996, *103*, 85-102.
34. Yuan, X.; Mak, A. F. T.; Kwok, K. W.; Yung, B. K. O.; Yao, K. *Journal of Applied Polymer Science* 2001, *81*, 251-260.
35. Cicero, J. A.; Dorgan, J. R. *J. Polymers and Environ.,* 2001, 1-15.
36. Eling, B.; Gogolewski, S.; Pennings, A. J. *Polymer* 1982, *23*, 1587-1593.
37. Fambri, L.; Pegoretti, A.; Migliaarsesi, C. *Journal of Material Science. Materials in Medi.* 1994, *5*, 679-683.
38. Rudie, R. In International Fiber Journal, 2000.
39. Auras, R. A.; Harte, B.; Selke, S.; Hernandez, R. J. Worldpak-IAPRI, East Lansing, MI. 48824-1224. USA, 2002.
40. Ajioka, M.; Enomoto, K.; Suzuki, K.; Yamaguchi, A. *Bulletin of the Chemical Society of Japan* 1995, *68*, 2125-2131.
41. Moon, S. I.; Lee, C. W.; Miyamoto, M.; Kimura, Y. *Journal of Polymer Science: Part A: Polymer Chemistry* 2000, *38*, 1673-1679.

Downloaded by UNIV OF GUELPH LIBRARY on August 28, 2012 | http://pubs.acs.org
Publication Date: September 23, 2006 | doi: 10.1021/bk-2006-0939.ch007

42. Otera, J.; Kawada, K.; Yano, T. *Chemistry Letters* 1996, 225-226.
43. Hiltunen, K.; Seppal, J. V.; Harkonen, M. *Macromolecules* 1997, *30*, 373-379.
44. Buchholz, B. In US Patent and Trademark Office; Ingelheim, Boehringer: United States of America, 1994.
45. Aharoni, S. M.; Masilamani, D. In US Patent and Trademark Office; Allied Chemical Corporation: United States of America, 1986.
46. Woo, S. I.; Kim, B. o.; Jun, H. S.; Chang, H. N. *Polymer Bulletin* 1995, *35*, 415-421.
47. Bonsignore, P. V. In US Patent and Trademark Office, USP 5,470,944; ARCH Development Corporation: United States of America, 1995.
48. Bellis, H. E. In US Patent and Trademark Office, USP 4,727,163; E. I. Du Pont de Nemours and Company: United States of America, 1988.
49. Bhatia, K. K. In US Patent and Trademark Office, USP 5,023,349; E. I. Du Pont de Nemours and Company: United States of America, 1991.
50. Bhatia, K. K. In US Patent and Trademark Office, USP 5,023,350; E. I. Du Pont de Nemours and Company: United States of America, 1991.
51. Bhatia, K. K. In US Patent and Trademark Office, USP 5,043,458; E. I. Du Pont de Nemours and Company: United States of America, 1991.
52. Bhatia, K. K. In US Patent and Trademark Office, USP 5,091,544; E. I. du Pont de Nemours and Company: United States of America, 1992.
53. Bhatia, K. K. In US Patent and Trademark Office, USP 5,266,706; E. I. Du Pont de Nemours & Company: United States of America, 1992.
54. Bhatia, K. K.; Drysdale, N. E.; Kosak, J. R. In US Patent and Trademark Office, USP 5,117,008; E. I. Du Pont de Nemours and Company: United States of America, 1992.
55. Bhatia, K. K.; Tarbell, J. V. In US Patent and Trademark Office, USP 5,196,551; E. I. du Pont de Nemours and Company: United States, 1993.
56. Fridman, I. D.; Kwok, J. In US Patent and Trademark Office, USP 5,264,592; Camelot Technologies Inc.: United States of America, 1993.
57. Benecke, H. P.; Cheung, A.; Cremeans, G. E.; Hillman, M. E. D.; Lipinsky, E. S.; Markle, R. A.; Sinclair, R. G. In US Patent and Trademark Office, USP 5,319,107; BioPak Technology, Ltd.: United States of America, 1994.
58. Sinclair, R. G.; Markle, R. A.; Smith, R. K. In US Patent and Trademark Office, USP 5,274,127; BioPak Technology, Ltd.: United States of America, 1993.
59. Kleine, V. J.; Kleine, H.-H. *Die Makromolekulare Chemie* 1959, *30*, 23-38.
60. Kricheldorf, H. R.; Kreiser-Saunders. *Die Makromolekulare Chemie* 1990, *191*, 1057-1066.
61. Kricheldorf, H. R.; Boettcher, C. *Die Makromolekulare Chemie* 1993, *194*, 1665-1669.

Downloaded by UNIV OF GUELPH LIBRARY on August 28, 2012 | http://pubs.acs.org
Publication Date: September 23, 2006 | doi: 10.1021/bk-2006-0939.ch007

62. Kricheldorf, H. R.; Dunsing, R. *Die Makromolekulare Chemie* 1986, *187*, 1611-1625.
63. Dittrich, W.; Schulz, R. C. *Angew. Makromol. Chem.* 1971, *15*, 109-126.
64. Kricheldorf, H. R.; Kreiser-Saunders, I.; Boettcher, C. *Polymer* 1995, *36*, 1253-1259.
65. Kricheldorf, H. R.; Kreiser-Saunders, I.; Stricker, A. *Macromolecules* 2000, *33*, 702-709.
66. Kricheldorf, H. R.; Kreiser-Saunders, I.; Damrau, D.-O. *Macromolecular Symposium* 2000, *159*, 247-258.
67. Kricheldorf, H. R.; Lossin, M. *Journal of Macromolecular Science. Pure and Applied Chemistry* 1997, *34*, 179-189.
68. Kricheldorf, H. R.; Lee, S.-R. *Polymer* 1995, *36*, 299-307.
69. Kricheldorf, H. R.; Damrau, D.-O. *Macromolecular Chemistry and Physics* 1997, *198*, 1753-1766.
70. Kricheldorf, H. R.; Damrau, D.-O. *Macromolecular Chemistry and Physics* 1998, *199*, 1747-1752.
71. Kricheldorf, H. R.; Damrau, D.-O. *Macromolecular Chemistry and Physics* 1998, *199*, 1089-1097.
72. Kricheldorf, H. R.; Boettcher, C. *Journal of Macromolecular Science. Pure and Applied Chemistry* 1993, *30*, 441-448.
73. Nijenhuis, A. J.; Grijpma, D. W.; Pennings, A. J. *Macromolecules* 1992, *25*, 6419-6424.
74. Huang, C.-H.; Wang, F.-C.; Ko, B.-T.; Yu, T.-L.; Lin, C.-C. *Macromolecules* 2001, *34*, 356-361.
75. Cameron, P. A.; Jhurry, D.; Gibson, V. C.; White, A. J. P.; Williams, D. J.; Williams, S. *Macromolecular Rapid Communications* 1999, *20*, 616-618.
76. Emig, N.; Nguyen, H.; Krautscheid, H.; Réau, R.; Cazaux, J.-B.; Bertrand, G. *Organometallics* 1998, *17*, 3599-3608.
77. Dubois, P.; Jacobs, C.; Jérôme, R.; Teyssié, P. *Macromolecules* 1991, *24*, 2266-2270.
78. Eguiburu, J. L.; Fernandez Berridi, M. J. *Polymer* 1995, *36*, 173-179.
79. Kricheldorf, H. R.; Berl, M.; Scharnagl, N. *Macromolecules* 1988, *21*, 286-293.
80. Kohn, F. E.; Van Ommen, J. G.; Feijen, J. *European Polymer Journal* 1983, *19*, 1081-1088.
81. Eguiburu, J. L.; Fernandex-Berridi, M. J.; San Roamn, J. *Macromolecules* 1999, *32*, 8252-8258.
82. Kricheldorf, H. R.; Serra, A. *Polymer Bulletin* 1985, *14*, 497-502.
83. Montaudo, G.; Montaudo, M. S.; Puglisi, C.; Samperi, F.; Spassky, N.; LeBorgne, A.; Wisniewski, M. *Macromolecules* 1996, *29*, 6461-6465.
84. Kricheldorf, H. R.; Eggerstedt, S. *Macromolecular Chemistry and Physics* 1999, *200*, 587-593.
85. Kohn, F. E.; Berg, J. W. A. V. D.; Ridder, G. V. D.; Feijen, J. *Journal of Applied Polymer Science* 1984, *29*, 4265-4277.

Downloaded by UNIV OF GUELPH LIBRARY on August 28, 2012 | http://pubs.acs.org
Publication Date: September 23, 2006 | doi: 10.1021/bk-2006-0939.ch007

Downloaded by UNIV OF GUELPH LIBRARY on August 28, 2012 | http://pubs.acs.org
Publication Date: September 23, 2006 | doi: 10.1021/bk-2006-0939.ch007

86. Kricheldorf, H. R.; Lee, S.-R.; Bush, S. *Macromolecules* 1996, *29*, 1375-1381.
87. Möller, M.; Kånge, R.; Hedrick, J. L. *Journal of Polymer Science: Part A: Polymer Chemistry* 2000, *38*, 2067-2074.
88. Kowalski, A.; Libiszowski, J.; Duda, A.; Penczek, S. *Macromolecules* 2000, *33*, 1964-1971.
89. Schindler, A.; Gaetano, K. D. *Journal of Polymer Science: Part C: Polymer Letters* 1988, *26*, 47-48.
90. Kricheldorf, H. R.; Sumbél, M. *European Polymer Journal* 1989, *25*, 585-591.
91. Kricheldorf, H. R.; Boettcher, C.; Tönnes, K.-U. *Polymer* 1992, *33*, 2817-2824.
92. Dahlmann, J.; Rafler, G. *Acta Polymerica* 1993, *44*, 103-107.
93. Leenslag, J. W.; Pennings, A. J. *Die Makromolekulare Chemie* 1987, *188*, 1809-1814.
94. Witzke, D. R.; Narayan, R.; Kolstad, J. J. *Macromolecules* 1997, *30*, 7075-7085.
95. Aubrecht, K. B.; Chang, K.; Hillmyer, M. A.; Tolman, W. *Journal of Polymer Science: Part A: Polymer Chemistry* 2001, *39*, 284-293.
96. Chamberlain, B. M.; Jazdzewski, B. A.; Pink, M.; Hillmyer, M. A.; Tolman, W. B. *Macromolecules* 2000, *33*, 3970-3977.
97. In't Veld, P. J. A.; Velner, E. M.; Van De Witte, P.; Hamhuis, J.; Dijkstra, P. J.; Feijen, J. *Journal of Polymer Science: Part A: Polymer Chemistry* 1997, *35*, 219-226.
98. Kowalski, A.; Duda, A.; Penczek, S. *Macromolecular Rapid Communications* 1998, *19*, 567-572.
99. Kowalski, A.; Duda, A.; Penczek, S. *Macromolecules* 2000, *33*, 689-695.
100. Penczek, S.; Duda, A.; Kowalski, A.; Libiszowski, J.; Majerska, K.; Biela, T. *Macromolecular Symposia* 2000, *157*, 61-70.
101. Schwach, G.; Coudane, J.; Engel, R.; Vert, M. *Journal of Polymer Science: Part A: Polymer Chemistry* 1997, *35*, 3431-3440.
102. Zhang, X.; MacDonald, D. A.; Goosen, M. F. A.; McAuley, K. B. *Journal of Polymer Science: Part A: Polymer Chemistry* 1994, *32*, 2965-2970.
103. Storey, R. F.; Taylor, A. E. *Journal of Macromolecular Science, Pure and Applied Chemistry* 1998, *35*, 723-750.
104. Dubois, P.; Degee, P.; Jerome, R.; Teyssie, P. *Macromolecules* 1993, *26*, 2730-2735.
105. Duda, A. *Macromolecules* 1996, *29*, 1399-1406.
106. Jacobs, C.; Dubois, P.; Jerome, R. *Macromolecules* 1991, *24*, 3027-3034.
107. Cheng, M.; Attygalle, A. B.; Coates, G. W. *Journal of the American Chemical Society* 1999, *121*, 11583-11584.

108. Ovitt, T. M.; Coates, G. W. *Journal of the American Chemical Society* 1999, *121*, 4072-4073.
109. Ovitt, T. M.; Coates, G. W. *Journal of Polymer Science: Part A: Polymer Chemistry* 2000, *38*, 4686-4692.
110. Radano, C. P.; Baker, G. L.; Smith, M. R. I. *Journal of the American Chemical Society* 2000, *122*, 1552-1553.
111. Joziasse, C. A. P.; Grablowitz, H.; Pennings, A. J. *Macromolecular Chemistry and Physics* 2000, *201*, 107-112.
112. Rafler, G.; Dahlmann, J. *Acta Polymerica* 1990, *41*, 611-617.
113. Farnia, S. M. F.; J., M.-R.; Sarbolouki, M. N. *Journal of Applied Polymer Science* 1999, *73*, 633-637.
114. Hile, D. D.; Pishko, M. V. *Macromolecular Rapid Communications* 1999, *20*, 511-514.
115. Yin, M.; Baker, G. L. *Macromolecules* 1999, *32*, 7711-7718.
116. Dong, C.-M.; Qiu, K.-Y.; Gu, Z.-W.; Feng, X.-D. *Journal of Polymer Science: Part A: Polymer Chemistry* 2000, *38*, 4179-4184.
117. Dong, C.-M.; Qiu, K.-Y.; Gu, Z.-W.; Feng, X.-D. *Journal of Polymer Science: Part A: Polymer Chemistry* 2001, *39*, 357-367.
118. Nakayama, A.; Kawasaki, N.; Maeda, Y.; Aravanitoyannis, I.; Aiba, S.; Yamamoto, N. *Journal of Applied Polymer Science* 1997, *66*, 741-748.
119. Kasperczyk, J.; Bero, M. *Makromo. Chem.* 1993, *194*, 913-925.
120. Hiljanen-Vainio, M.; Karjalainen, T.; Seppälä, J. *Journal of Applied Polymer Science* 1996, *59*, 1281-1288.
121. Deng, X.; Yao, J.; Minglong, Y.; Li, X.; Xiong, C. *Macromolecular Chemistry and Physics* 2000, *201*, 2371-2376.
122. Ouchi, T.; Nozaki, T.; Ishikawa, A.; Fujimoto, I.; Ohya, Y. *Journal of Polymer Science: Part A: Polymer Chemistry* 1997, *35*, 377-383.
123. Ouchi, T.; Seike, H.; Nozaki, T.; Ohya, Y. *Journal of Polymer Science: Part A: Polymer Chemistry* 1998, *36*, 1283-1290.
124. Albertsson, A.-C.; Edlund, U.; Stridsberg, K. *Macromolecular Symposium* 2000, *157*, 39-46.
125. Stridsberg, K.; Gruvegard, M.; Albertsson, A.-C. *Macromolecular Symposium* 1998, *130*, 367-378.
126. Wen, J.; Zhuo, R.-X. *Polymer International* 1998, *47*, 503-509.
127. Zhu, K. J.; Lei, Y. *Polymer International* 1997, *43*, 210-216.
128. Keul, H.; Höcker, H. *Macromolecular Rapid Communications* 2000, *21*, 869-883.
129. Storey, R. F.; Mullen, B. D.; Melchert, K. M. *Polymer Preprints* 2001, *42*, 553-554.
130. Kricheldorf, H. R.; Stricker, A. *Macromolecular Chemistry and Physics* 1999, *200*, 1726-1733.

Downloaded by UNIV OF GUELPH LIBRARY on August 28, 2012 | http://pubs.acs.org
Publication Date: September 23, 2006 | doi: 10.1021/bk-2006-0939.ch007

131. Haderlein, G.; Schmidt, C.; Wendorff, J. H.; Greiner, A. *Polymers for Advanced Technologies* 1997, *8*, 568-573.
132. Deng, X.; Zhu, Z.; Xiong, C.; Zhang, L. *Journal of Polymer Science: Part A: Polymer Chemistry* 1997, *35*, 703-708.
133. Qing, C.; Bei, J.; Wang, S. *Polymers for Advanced Technologies* 2000, *11*, 159-166.
134. Song, C. X.; Feng, X. D. *Macromolecules* 1984, *17*, 2764-2767.
135. Grijpma, D. W.; Van Hofslot, R. D. A.; Supèr, H.; Nijenhuis, A. J.; Pennings, A. J. *Polymer Engineering and Science* 1994, *34*, 1674-1684.
136. Stridsberg, K.; Albertsson, A.-C. *Journal of Polymer Science: Part A: Polymer Chemistry* 2000, *38*, 1774-1784.
137. Barakat, I.; Dubois, P.; Grandfils, C.; Jérôme, R. *Journal of Polymer Science: Part A: Polymer Chemistry* 2001, *39*, 294-306.
138. Kricheldorf, H. R.; Boettcher, C. *Die Makromolekulare Chemie. Macromolecular Symposia* 1993, *73*, 47-64.
139. Spinu, M.; Jackson, C.; Keating, M. Y.; Gardner, K. H. *Journal of Macromolecular Science. Pure and Applied Chemistry* 1996, *33*, 1497-1530.
140. Cho, K. Y.; Kim, C.-H.; Lee, J.-W.; Park, J.-K. *Macromolecular Rapid Communications* 1999, *20*, 598-601.
141. Fujiwara, T.; Kimura, Y.; Teraoka, I. *Journal of Polymer Science: Part A: Polymer Chemistry* 2000, *38*, 2405-2414.
142. Salem, A. K.; Cannizzaro, S. M.; Davies, M. C.; Tendler, S. J. B.; Roberts, C. J.; Williams, P. M.; Shakesheff, K. M. *Biomacromolecules* 2001, *2*, 575-580.
143. Kricheldorf, H. R.; Meier-Haack, J. *Die Makromolekulare Chemie* 1993, *194*, 715-725.
144. Zhu, K. J.; Xiangzhou, L.; Shilin, Y. *Jounal of Applied Polymer Science* 1990, *39*, 1-9.
145. Du, Y. J.; Lemstra, P. J.; LNijenhuis, A. J.; Aert, H. A. M. v.; Bastiaansen, C. *Macromolecules* 1995, *28*, 2124-2132.
146. Yuan, M.; Wang, Y.; Li, X.; Xiong, C.; Deng, X. *Macromolecules* 2000, *33*, 1613-1617.
147. Yamaoka, T.; Takahashi, y.; Ohta, T.; Miyamoto, M.; Murakami, A.; Kimura, Y. *Journal of Polymer Scince: Part A: Polymer Chemistry* 1999, *37*, 1513-1521.
148. Kricheldorf, H. R.; Langanke, D. *Macromolecular Chemistry and Physics* 1999, *200*, 1183-1190.
149. Zhang, S.; Hou, Z.; Gonsalves, K. E. *Polymer Preprints* 1996, *38*, 853-854.
150. Zhang, S.; Hou, Z.; Gonsalves, K. E. *Journal of Polymer Science: Part A: Polymer Chemistry* 1996, *34*, 2737-2742.
151. Riffle, J. S.; Steckle, W. P., Jr.; White, K. A.; Ward, R. S. *Polymer Preprints* 1985, *26*, 251-252.

Downloaded by UNIV OF GUELPH LIBRARY on August 28, 2012 | http://pubs.acs.org
Publication Date: September 23, 2006 | doi: 10.1021/bk-2006-0939.ch007

152. Wang, Y.; Hillmyer, M. A. *Journal of Polymer Science: Part A: Polymer Chemistry* 2001, *39*, 2755-2766.
153. Frick, E. M.; Hillmyer, M. A. *Macromolecular Rapid Communications* 2000, *21*, 1317-1322.
154. Frick, E. M.; Hillmyer, M. A. *Polymer Preprints* 2001, *42*, 534.
155. Mecerreyes, D.; Dubois, P.; Jerome, R.; Hedrick, J. L.; Hawker, C. J. *Journal of Polymer Science: Part A: Polymer Chemistry* 1999, *37*, 1923-1930.
156. Kim, S. H.; Han, Y.-K.; Kim, Y. H.; Hong, S. I. *Makromol. Chem.* 1992, *193*, 1623-1631.
157. Kim, S. H.; Han, Y.-K.; Ahn, K.-D.; Kim, Y. H.; Chang, Y. *Makromol. Chem.* 1993, *194*, 3229-3236.
158. Lee, S.-H.; Kim, S. H.; Han, Y.-K.; Kim, Y. H. *Journal of Polymer Science: Part A: Polymer Chemistry* 2001, *39*, 973-985.
159. Breitenbach, A.; Kissel, T. *Polymer* 1998, *39*, 3261-3271.
160. Breitenbach, A.; Pistel, K. F.; Kissel, T. *Polymer* 2000, *41*, 4781-4792.
161. Kim, J.-B.; Wang, C.; Bruening, M. L.; Baker, G. L. *Polymer Preprints* 2001, *42*, 551-552.
162. Li, Y.; Nothnagel, J.; kissel, T. *Polymer* 1997, *38*, 6197-6206.
163. Donabedian, D. H.; McCarthy, S. P. *Macromolecules* 1998, *31*, 1032-1039.
164. Wallach, J. A.; Huang, S. J. *Biomacromolecules* 2000, *1*, 174-179.
165. Lim, D. W.; Choi, S. H.; Park, T. G. *Macromolecular Rapid Communications* 2000, *21*, 464-471.
166. Trollsås, M.; Hawker, C. j.; Remenar, J. F.; Hedrick, J. L.; Johansson, M.; Ihre, H.; Hult, A. *Journal of Polymer Science: Part A: Polymer Chemistry* 1998, *36*, 2793-2798.
167. Trollsås, M.; Hedrick, J.; Mecerreyes, D.; Jérôme, R.; Dubois, P. *Journal of Polymer Science: Part A: Polymer Chemistry* 1998, *36*, 3187-3192.
168. Hedrick, J. L.; Trollsås, M.; Hawker, C. J.; Atthoff, B.; Claesson, H.; Heise, A.; Miller, R. D. *Macromolecules* 1998, *31*, 8691-8705.
169. Trollsås, M.; Hedrick, J. L.; Mecerreyes, D.; Dubois, P.; Jérôme, R.; Ihre, H.; Hult, A. *Macromolecules* 1998, *31*, 2756-2763.
170. Carnahan, M. A.; Grinstaff, M. W. *Journal of the American Chemical Society* 2001, *123*, 2905-2906.
171. Grijpma, D. W.; Joziasse, C. A. P.; Pennings, A. J. *Die Makromoleculare Chemie, Rapid Communications* 1993, *147*, 155-161.
172. Garlotta, D. *J. Polym. Environ.* 2001, *9*, 63-84.
173. Kratochvil, P.; Suter, U. W. *Pure Appl. Chem.* 1989, *61*, 211-241.
174. Ren, J.; Urakawa, O.; Adachi, K. *Polymer* 2003, *44*, 847-855.
175. Schindler, A.; Harper, D. *J. Polym. Sci., Polym. Chem. Ed.* 1979, *17*, 2593-2599.

Downloaded by UNIV OF GUELPH LIBRARY on August 28, 2012 | http://pubs.acs.org
Publication Date: September 23, 2006 | doi: 10.1021/bk-2006-0939.ch007

176. Joziasse, C. A. P.; Veenstra, H.; Grijpma, D. W.; Pennings, A. J. *Macromol. Chem. Phys.* 1996, *197*, 2219-2229.
177. Kang, S.; Zhang, G.; Aou, K.; Pekrul, R. L.; Hsu, S. L.; Yang, X. *Polym. Preprints* 2002, *43*, 896-897.
178. Ren, J.; Urukawa, O.; Adachi, K. *Macromolecules* 2003, *36*, 210-219.
179. Dorgan, J. R.; Janzen, J.; Hait, S. B.; Knauss, D. K.; Limoges, B. R.; Hutchinson, M. H. *J. Polym. Sci. B: Polym. Phys.* 2005, *43*, 3100-3111.
180. Blomqvist, J. *Polymer* 2001, *42*, 3515-3521.
181. Biresaw, G.; Carriere, C. J. *J. Polym. Sci., Part B: Polym. Phys.* 2002, *40*, 2248-2258.
182. Cooper-White, J. J.; Mackay, M. E. *J. Polym. Sci., Part B: Polym. Phys.* 1999, *37*, 1803-1814.
183. Dorgan, J. R.; Williams, J. S. *J. Rheology* 1999, *43*, 1141-1155.
184. Lehermeier, H. J.; Dorgan, J. R. *Polymer and Engineering Science* 2001, *41*, 2172-2184.
185. Palade, L. I.; Lehermeier, H. J.; Dorgan, J. R. *Macromolecules* 2001, *34*, 1384-1390.
186. Dorgan, J. R.; Janzen, J.; Clayton, M. P.; Knauss, D. M.; Hait, S. B. *Journal of Rheology* 2005, *49*, 607-619.
187. Lehermeier, H. J. MS Thesis, Chemical Engineering; Colorado School of Mines: Golden, Colorado, 2000.
188. Leenslag, J. W. G., S.; Pennings, A.J. *J. Appl. Polym. Sci.* 1984, *29*, 2829-2842.
189. Leenslag, J. W.; Pennings, A. J. *Polymer Communications* 1987, *28*, 92-94.
190. Fambri, L. P., A.; Fenner, R.; Incardona, S.D.; Migliaresi, C. *Polymer* 1997, *38*, 79-85.
191. Incardona, S. D. F., L.; Migliaresi, C. *J. Mater. Sci. Mater. Med.* 1996, *7*, 387-391.
192. Schmack, G. T., B.; Vogel, R.; Beyreuther, R.; Jacobsen, S.; Fritz, H.-G. *J. Appl. Polym. Sci.* 1999, *73*, 2785-2797.
193. Mezghani, K. S., J.E. *J. Polym. Sci. Part B: Polym. Phys.* 1998, *36*, 1005-1012.
194. Hoogsteen, W.; Postema, A. R.; Pennings, A. J. *Macromolecules* 1990, *23*, 634-642.
195. Cicero, J. A.; Dorgan, J. R.; Janzen, J.; Garrett, J.; Runt, J.; Lin, J. S. *J. Appld. Polym Sc* 2002, *86*, 2828-2838.
196. Cicero, J. A.; Dorgan, J. R.; Garrett, J.; Runt, J.; Lin, J. S. *J. Appld. Polym Sci.* 2002, *86*, 2839-2846.

Downloaded by UNIV OF GUELPH LIBRARY on August 28, 2012 | http://pubs.acs.org
Publication Date: September 23, 2006 | doi: 10.1021/bk-2006-0939.ch007

197. Cicero, J. A.; Dorgan, J. R.; Dec, S. F.; Knauss, D. M. *Polymer Degradation and Stability* 2002, *78*, 95-105.
198. Siparsky, G. L.; Voorhees, K. J.; Dorgan, J. R.; Schilling, K. *Journal of Environmental Polymer Degradation* 1997, *5*, 125-136.
199. Lehermeier, H. J.; Dorgan, J. R.; Way, J. D. *J. Memb. Sci.* 2001, ***190***, 243-251.
200. Teramoto, Y.; Nishio, Y. *Polymer* 2003, *44*, 2701-2709.

Downloaded by UNIV OF GUELPH LIBRARY on August 28, 2012 | http://pubs.acs.org
Publication Date: September 23, 2006 | doi: 10.1021/bk-2006-0939.ch007

Downloaded by NORTH CAROLINA STATE UNIV on August 10, 2012 | http://pubs.acs.org
Publication Date: September 23, 2006 | doi: 10.1021/bk-2006-0939.ch008

Chapter 8

Biocatalytic Synthesis of Ricinoleic Acid Star Polymers: "Green" Manufacturing of Potentially Valuable Lubricant Additives and Drug Delivery Materials

Douglas G. Hayes

Department of Biosystems Engineering and Soil Science, University of Tennessee, 2506 E. T. Chapman Drive, Knoxville, TN 37996–4531

Bulk-phase polymerization catalyzed by lipases has been employed to synthesize oligomers of ricinoleic acid, a renewable material derived from castor oil, and to covalently attach the oligomeric chains to polyols such as pentaerythritol, producing novel star polymers possessing desirable physical properties for bio-based lubricants. For instance, pentaerythritol-tetra[poly(ricinoleic acid)], produced at 87% purity, possessed a value of the number-averaged molecular weight, M_n, of 4.8 *kDa*, a high viscosity index (155), and a low melting point temperature (< -15°C). A targeted viscosity value can be readily achieved by controlling the product's M_n, since viscosity versus M_n for star polymers is a linear relationship. Lipase-catalyzed polymerization provides an environmentally-friendly processing alternative to chemical synthesis since the former employs mild temperatures and pressures, the absence of solvents, and frequently requires little or no downstream purification. This chapter consists of an assessment of poly(hydroxy acids) and their derivatives as biolubricants and a review of the enzymatic synthesis and modification of poly(hydroxyl acids), including star polymer formation. Recent results on the lipase-catalyzed synthesis of ricinoleic acid copolymers in the author's laboratory are presented.

In Degradable Polymers and Materials; Khemani, K., et al.;
ACS Symposium Series; American Chemical Society: Washington, DC, 2006.

Downloaded by NORTH CAROLINA STATE UNIV on August 10, 2012 | http://pubs.acs.org
Publication Date: September 23, 2006 | doi: 10.1021/bk-2006-0939.ch008

Ricinoleic acid oligomers are potentially valuable biolubricants

Ricinoleic acid, *R*-9-*cis*,11-hydroxy octadecenoic acid (R-18:1^{9c}-OH^{12}), which comprises ~90% of the oil from the castor plant (*Ricinus comminus*), has been a well- utilized chemical synthon for many centuries. A patent search of ricinoleic acid produced 1733 hits for the period 1907-2005, including U.S. patents dating back to the first decade of the 20th Century. The numerous applications of ricinoleic acid (*RA*) and its derivatives, reviewed elsewhere (*1-3*), include production of sebacic (1,10-decanedioic) acid as a monomer for nylon-11, polyesters, polyurethanes, laxatives, disinfectants and cleaning fluids, emulsifiers and other food products, lipstick and other cosmetic products, paints and coatings, and lubricants. Global demand for castor oil was reported to be 1 billion pounds annually in 2003, with an economic value of $500 million (*4,5*). World annual production of castor beans was reported to be 14 million metric tons (MMT) in 2003, with the majority produced by India, Brazil, and China (*5*). The European Union and US imported 6.3 and 0.13 MMT of castor beans, respectively, in 2003 (*5*). The presence of ricin, a toxin that has raised Homeland Security concerns worldwide, and allergens are problems that will need to be corrected through genetic modification of castor.

In addition to *RA*, nature produces other hydroxy fatty acids with similar potential applications (*6,7*) (Table I). Microbial transformations have also produced a myriad of hydroxy acids that differ in chemical structures (*8*). Polymers (oligomers) of hydroxy acids, or *pHAs*, also referred to as estolides, and their derivatives, may be useful materials for cosmetics, coatings, and food-related applications (*9,10*). For instance, the monoester of poly(*RA*), or *pRA*, and polyglycerol, "polyglycerol polyrcinoleate", is a common ingredient of cake mixes, toppings, and low-fat salad dressings, serves as a viscosity-reducing agent for chocolate, and is commonly used to lubricate cooking tins (*11*).

However, the major potential market for hydroxy acid oligomers is lubricants (*12-15*). The lubricant market is significantly large; the global demand for lubricants was 37.1 MT in 2003 (*16*). The North American market, accounting for approximately 30% of the lubricant market, had a value of $3.8 billion in 2003; market sizes for Europe and Asia/Pacific Rim were nearly as large (*16*).

Most lubricants used today are based on mineral oils, which are poorly biodegradable and toxic, and derived from petroleum, and thus, are nonsustainable. The need for environmentally-friendly lubricants is evidenced by recent studies that attribute oil or lubricant spills to 40% of the 5-10 MT of petroleum that are "leaked" into the environment; for instance, at least 70% of hydraulic fluid employed enter the environment through leakage (*17*).

"Biolubricants," lubricants derived from vegetable oils and other natural resources, provide an eco-friendly alternative. Typically, a biolubricant consists of vegetable oil as a base fluid and a relatively high proportion of eco-friendly additives (corrosion inhibitors, antioxidants, pour point depressants, viscosity index modifiers, etc; 2-5% overall), resulting in a high-cost material that performs or often outperforms common mineral oil lubricant products (*18*).

Table I. Selected hydroxy fatty acids derived from nature

Hydroxy Acid	*Chemical Structure*	*Source*
Auricolic	R-20:2^{11c,17c}-OH^{14}	*Lesquerella fendleri* (4% in oil)
Dimorphocolic	S-18:2^{10t,12t}-OH^{9}	*Dimorphotheca pluvialis* (62% in oil)
Ipurolic	14:0-OH^{3,11}	*Ipomoea purga* (tubers)
α-Kamlolenic	18:3^{9c,11t,13t}-OH^{18}	*Mallotus philippinensis*, or "kamala" (70% in oil)
Lesquerolic	R-20:1^{11c}-OH^{14}	*Lesquerella fendleri* (55% in oil)
Phelloniclic	22:0-OH^{13}	Cork
Ricinoleic	R-18:1^{9c}-OH^{12}	*Ricinus comminus* (90% in oil)

SOURCE: Reproduced from Reference (*6*). Copywrite 1996 AOCS Press.

Biolubricants are potentially a $5.1 billion market according to a recent study (*19*). Currently, about 40 MT of biolubricants are sold in each Europe and the US (*18*). Due to stringent ecological policies, biolubricants are expected to capture a higher fraction of the lubricant market in Europe, perhaps as high as 35% (*20*). In the US, biolubricants are projected to assume over 70% of the market share of hydraulic, marine, drip, bar chain, wire rope fluids, and perhaps high-performance automobiles (*21*). Niche markets have already been established for hydraulic fluids, mold release agents, two-cycle engine oils, and lubricants for forestry, agricultural, and off-highway equipment, among others (*17,22*). Table II projects potential market growth for specific lubricant types (*22*). The enthusiasm for biolubricant growth must be balanced by the realization that plant oil-based lubricants cannot be produced at a rate that meets current demands, and that a significant gap in production costs remains despite the recent increase of crude oil prices (*23*).

Table II. Potential market size for biolubricants

Lubricant Type	*Potential Market Size, MT yr^{-1}*
Greases for agricultural, mining, and railroad machinery	1,000,000
Metalworking fluids	540,000
Hydraulic fluids	350,000
Gear oils for marine, agriculture, and food machinery equipment	90,000
Two-cycle engine oils	70,000
Textile lubricants	45,000
Chain saw lubricants	45,000

Source: Data taken from Reference (*22*).

Downloaded by NORTH CAROLINA STATE UNIV on August 10, 2012 | http://pubs.acs.org
Publication Date: September 23, 2006 | doi: 10.1021/bk-2006-0939.ch008

Downloaded by NORTH CAROLINA STATE UNIV on August 10, 2012 | http://pubs.acs.org
Publication Date: September 23, 2006 | doi: 10.1021/bk-2006-0939.ch008

When one compares the physical properties of *pHAs* and their derivaties with mineral oils, the former generally match or outperform the latter (*12,22,24,25*) (Table III), due in part to their highly branched structure, common to many lubricant materials (*26*). Moreover, due to their low melting point and high viscosity and viscosity index, or *VI* [a measure of the resistance to viscosity increase with decreasing temperature (*27*)], *pHAs* may be valuable lubricant materials. pHAs achieve the same viscosity targets as mineral oils, and can be "tuned" via their chemical structure to achieve a high or low value (discussed below); thus, they may be applicable as "thin" lubricants such as transmission fluid and "thick" lubricants such as greases. A typical *VI* target value for lubricants would be 150. Whereas mineral oils fall well short of this target, hence requiring the addition of "*VI* modifiers" additives, ester derivatives of *pHAs* meet or exceed this value (Table III). In terms of pour point, referring to the minimum temperature at which fluids freely flow when subjected to a hydrostatic driving force, *pHA* derivatives meet or outperform mineral oils (Table III). As would be expected, based on similarity in chemical structure to ester synthetic lubricants, high biodegradability for *pHAs* can be anticipated (*26*), in contrast to poorly-biodegradable mineral oils-based lubricants (*13*).

However, issues exist with regard to the stability of *pHAs*. A trade-off exists in relation to the oligomers' double bonds: the hydrogenation of double bonds (e.g., 12-hydroxy stearic acid formed upon hydrogenation of *RA*) results in a more oxidative stable lubricant that possesses a higher pour point (*12*). Additives would probably be required to achieve sufficient thermostability since oligomers can decompose as temperature is increased (*12,28*). In addition, although biolubricants possess high biodegradability, they are often poorly bioresistant to microorganisms that can occur in the lubricant handling system, and thus may require a biocide additive (*29*).

Table III. Lubricant-related properties of mineral oils and pHA esters

Measurement	*Mineral Oils*	*Hydroxy acid oligomers and their derivatives*
Kinematic viscosity at 40°C, cSt	65.6	50-800
Kinematic viscosity at 100°C, cSt	8.4	15-70
Viscosity Index (*VI*)	97	130-165
Pour Point, °C	-18	-15 to -42

Source: Data taken from References (*12,22,24,25*).

Eco-Friendly Biocatalytic Synthesis of Poly(Hydroxy Acids)

pHAs are traditionally formed via catalysis; moreover, acidic catalysts such as *p*-toluene sulfonic acid catalyze the condensation of hydroxy acids at elevated temperatures (*9,30*). Alternatively, fatty acids containing double bonds can be converted catalytically into *pHAs* at ca. 30-70% yield with degree of polymerization (*DP*) of 3-6 (*14,31*). The resultant oligomers possessed monomeric units with a broad distribution of hydroxyl and *cis* and *trans* double bond positions (*32,33*).

It has been suggested that *pRA* be prepared enzymatically (using lipases) to avoid problems of discoloration, odor, and high energy costs that occur in high-temperature chemical processes (*34*). Also, dehydration of *RA* can occur in chemical processes (*11*). Moreover, hydroxy acid oligomers produced chemically often require multiple downstream purification steps (*31*). Lipases that are not 1,3-positional selective (i.e., can utilize both primary and secondary acyl acceptors, the latter represented by the hydroxyl group at C_{12} for *RA*) have been employed successfully in the bulk oligomerization of *RA*. Hayes and coworkers conducted bulk polymerization of *RA* using a thermophilic, immobilized lipase from *Candida antarctica* ("Novozym," from Novozymes, Inc., Franklinton, NC, to be referred to here as *CAL*) at ~80°C to accelerate the reaction rate and allow for the free evaporative removal of the reaction product water (thus improving the reaction's equilibrium position), achieving 97% conversion, a number-averaged molecular weight, or M_n, value of 1040, equivalent to a *DP* of 3.7 (*25*). Similar values were reported by Yamaguchi et al. (*35,36*). A packed bed bioreactor connected in series to flash evaporator achieved 7 batches of 75 *g* of ricinoleic acid within a 700 *hr* period, with products possessing *DP* values near 5.0 (*37*).

Reviewed elsewhere (*38-40*), biocatalyst-directed synthesis of polymers has received increased interest due to its low energy usage, environmentally-friendliness, and the ability of enzymes to limit the product distribution through their inherent substrate, regio- and stereo-selectivity. Most of the reported research involving lipase-catalyzed polymerization has involved the esterification of diacids and α,ω-diols and the ring-opening polymerization of lactones, the latter producing unbranched polymers of ω-hydroxy acid and carbonate monomeric units that often possess crystalline morphology and are poor lubricants. Product molecular weight (*MW*) in the 10-100 *kDa* range has been reported for the latter using lactones of carbon chain length 3-16, as well as polylactides (*41*). Many experimental parameters control the *DP* and product distribution, such as water content, liquid phase polarity, temperature, and the diffusional mass transfer of the liquid phase through the pores of the solid, biocatalyst-containing, phase (*38,40*). As an example of the sustainability of the biocatalytic approach to polyester synthesis, Matusmura employed lipase-catalyzed reactions for both synthesis and hydrolysis of poly(ε-caprolactone), or *pCL* (*42*). First, ε-caprolactone was polymerized in bulk at 99% conversion, yielding *pCL* with M_n ~ 25 *kDa* (*42*). Subsequently, *pCL* was hydrolyzed by lipase to yield small oligomers with M_n ~ 1.1 *kDa* (*42*). The oligomers were then esterified using lipase to produce *pCL* with M_n ~ 79 *kDa* (*42*).

Downloaded by NORTH CAROLINA STATE UNIV on August 10, 2012 | http://pubs.acs.org
Publication Date: September 23, 2006 | doi: 10.1021/bk-2006-0939.ch008

Lipase-Catalyzed Synthesis of Poly(Hydroxy Acid) Esters

The esterification of the free -COOH terminus of *pHAs* by fatty alcohol enhances their physical properties, namely, the viscosity is lowered and *VI* increased with low melting temperature characteristics retained (*12,24*). The formation of an ester bond between a *pHA* chain and fatty alcohol can occur chemically (*12,30*) or enzymatically without destruction of the *pH*A's ester bonds (*24*). In addition, Hayes and Kleiman successfully esterified di- and poly(hydoxy acid) synthesized chemically to the hydroxyls of 1,10-decanediol via biocatalysis at high yield (*24*). The resultant materials had melting point temperatures < -17°C and *VI* values > 150 (*24*). Also, Gross and co-workers synthesized a star polymer containing a ethyl glucoside core and *pCL* and poly(lactide) arms via a chemo-enzymatic approach (*43*).

Motivated by the desirable lubricant-related properties obtained for diol diesters of *pHAs* discussed above and the desirable properties (low pour point and high *VI*) and biodegradability of polyol-fatty acid ester lubricants (*26,44-46*), star polymers consisting of a polyol core [e.g., pentaerythritol (*PE*), trimethylolpropane (TMP), or dimer diol (*DD*)] and *pRA* arms (Figure 1) were synthesized in bulk at 70°C using *CAL* as biocatalyst in our laboratory within a 1-week period. *DD* is a biolubricant material derived chemically from unsaturated fatty acids.

Several synthesis protocols were screened for synthesis of TMP-*pRA* star polymers, with the main comparison being a "divergent" versus "convergent" approach. The former refers to the outward growth of the star polymer from the core; moreover, a single *RA* unit was attached to the primary hydroxyl groups of the polyol without the occurrence of polymerization, taking advantage of the 1,3-positional selectivity of immobilized *Rhizomucor miehei* lipase. The second step of the "divergent" approach is the *CAL*-catalyzed growth of hydroxyl acid oligomeric chains on the star polymer. Alternatively, "convergent" involves the lipase-catalyzed covalent attachment of *pRA* to polyol hydroxyls, with the former produced from biocatalytically. The highest *MW* and conversion of monomer occurred using the "divergent" approach (*25*). Kinetic analysis demonstrated the rate-limiting step in the formation of *pRA*, propagation, was first-order with respect to monomer (ricinoleyl acyl groups), similar to lipasecatalyzed ring-opening polymerization of ε-caprolactone (*47,48*); and, chain-transfer reactions were absent (*25*).

Such a procedure yielded pentaerythritol-*pRA* tetraester with an average MW of 4.5-4.9 *kDa* according to ^{1}H-NMR and gel permeation chromatography (GPC) analyses (*25*). Matrix-assisted laser desorption ionization-time of flight-mass spectroscopy, or MALDI-TOF-MS, and ^{13}C-NMR confirmed the NMR- and GPC-derived molecular structure and composition of the product (*25*). Esterification of the polyol acyl acceptor's hydroxyl groups occurred at 78%,

Downloaded by NORTH CAROLINA STATE UNIV on August 10, 2012 | http://pubs.acs.org
Publication Date: September 23, 2006 | doi: 10.1021/bk-2006-0939.ch008

Downloaded by NORTH CAROLINA STATE UNIV on August 10, 2012 | http://pubs.acs.org
Publication Date: September 23, 2006 | doi: 10.1021/bk-2006-0939.ch008

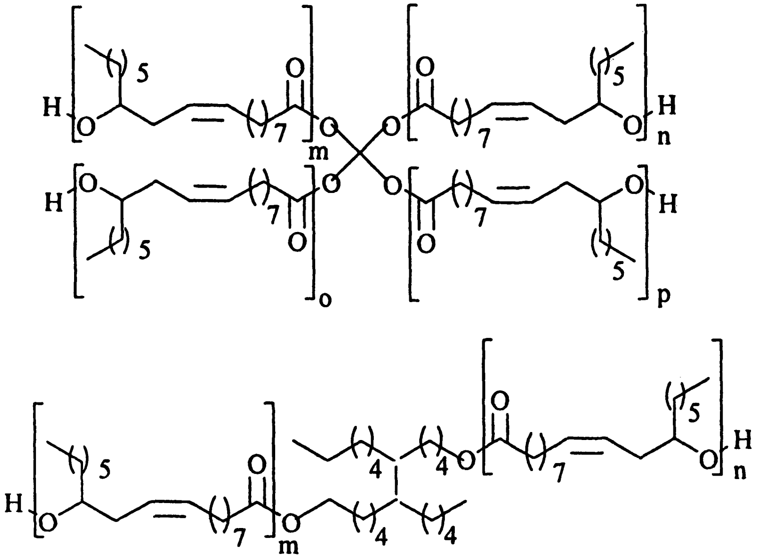
H
O
5
O
7
m
O
O
O
7
5
O
H
n
H
O
7
5
O
o
O
O
7
O
5
H
p
H
O
5
O
7
m
O
4
4
4
4
O
O
7
5
O
H
n

Figure 1. PE- and DD-pRA star polymers; m,n,o,and p are arbitrary numbers

with the average *DP* for its *pRA* chains being 5.4 (*25*). The final product consisted of 83% PE star polymer and 17 wt. % non-esterified linear *pRA* (*25*). The unpurified, technical grade, products possessed high viscosity and *VI* (155 for the *PE* star polymer) and melting point temperatures < -7.5°C, suggesting their use as environmentally-friendly lubricant materials (*25*). Figure 2 demonstrates that logarithm of viscosity increased linearly with the inverse of temperature for *pRAs* and their star polymers, suggesting the materials obey the Andrade Equation (*49*). Esterification of *pRA* to *DD* greatly improved the physical properties of the latter, providing a material whose viscosity changes much less with temperature (Figure 2), demonstrated by the increase of *VI* from 24 to 155 (*25*). Viscosity increased linearly with M_n for star polymers (Figure 2); also, star polymers shared similar trends with respect to the change in viscosity with temperature (i.e., nearly similar values of the slope for the Andrade Equation) (*25*).

Downloaded by NORTH CAROLINA STATE UNIV on August 10, 2012 | http://pubs.acs.org
Publication Date: September 23, 2006 | doi: 10.1021/bk-2006-0939.ch008

Curent Research: Ricinoleic Acid Copolymers

Recent work in the author's laboratory has focused upon lipase-catalyzed synthesis of *RA* copolymer to achieve two goals (Figure 3). The first is the elongation of *pRA* chains through copolymerization with pentadecyl lactone (*PDL*), an "activated" form of ω-hdyroxypentadecanoic acid. *PDL* has been successfully used as a monomer in the formation of lipase-catalyzed synthesis of random co-polymers (*50-52*). The second goal is the "end-capping" of the "free" hydroxyl termini of *pRA* chains with lauric acid, to improve the pour point and *VI* characteristics of *pHAs* (*12,30,31*).

Reactions were analyzed GPC (Styragel HR-5E column, 300 mm x 7.8 mm ID, from Waters, Milford, MA, using tetrahydrofuran at 1.0 $mL\ min^{-1}$ as mobile phase) using either *RA* and its oligomers or *PE-pRA* star polymers as standards. As demonstrated previously, elution of *RA/pRA* analytes was delayed, apparently due to the interaction of their carboxylic acid groups with the GPC stationary phase (*25*). Thus, partial separation of *RA*, its dimers, trimers, and oligmers, and star polymers readily occurred (*25*). Hence, GPC allowed for calculation of the percent conversion of monomer, and detection of *pRA* not esterified to polyol. Also, estimates of M_n provided by GPC and ^{1}H-NMR strongly agreed with each other (*25*). For the reactions described herein, GPC was equally as valuable, due to its partial resolution of *PDL*, lauric acid, *RA*, and the latter's monomer and dimer (Figure 4). The retention time of *PDL* corresponded to the value predicted using star polymer standards; but, the *pPDL* product, which apparently contained mono- and di-ω-pendadecanoic acid, and lauric acid corresponded closely with pRA standards. Thus, *pRA* standards were employed to calculate *MW* except for *PDL*'s GPC peak.

Downloaded by NORTH CAROLINA STATE UNIV on August 10, 2012 | http://pubs.acs.org
Publication Date: September 23, 2006 | doi: 10.1021/bk-2006-0939.ch008

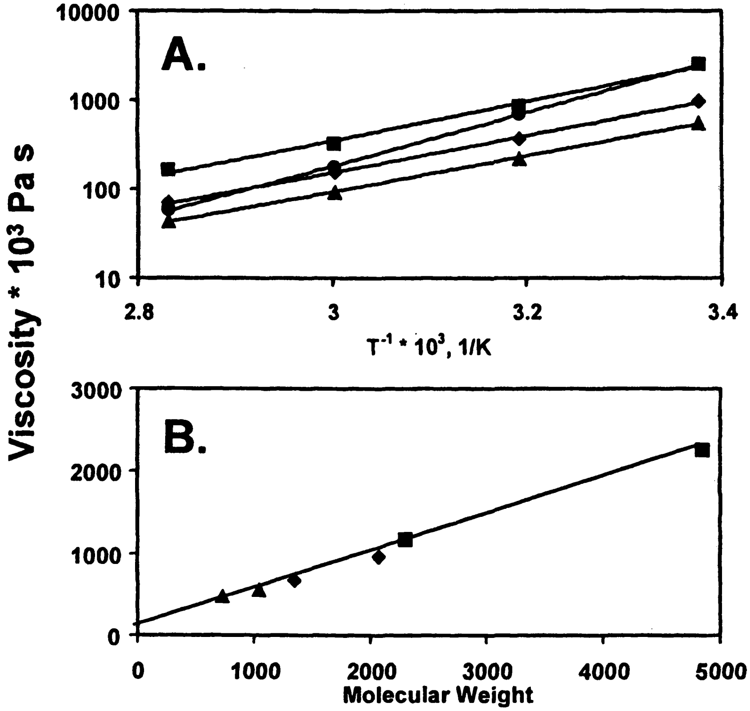

Figure 2. A. Andrade Equation plot; B. Plot of molecular weight versus viscosity at 23°C for (■)PE- and (◆) DD-pRA star polymers, (▲) pRA, and (●) DD. Errors for viscosity and molecular weight are within 5% and 10% of values indicated in the plots, respectively. Data from reference (25).

Also employed for characterization was the use of two different detectors, refractive index and evaporative light scattering, RID and ELSD, respectively. Whereas *RA*, lauric acid, and their oligomers each produced nearly identical RID- and ELSD-based chromatograms, a chromatogram for *pPDL* was detected using the ELSD but not the RID. Product from reactions between *RA* and *PDL* produced similar RID and ELSD-based chromatograms, which suggest that the resultant polymers are co-polymers rather than a mixture of homopolymers, and that the co-polymers are detected by both RID and ELSD. Response factors for all analytes were nearly identical for the RID.

Downloaded by NORTH CAROLINA STATE UNIV on August 10, 2012 | http://pubs.acs.org
Publication Date: September 23, 2006 | doi: 10.1021/bk-2006-0939.ch008

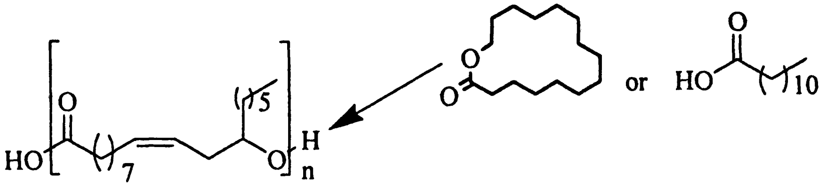

Figure 3. Elongation of pRA by ω-pentadecyl lactone or lauric acid

Table IV. Results from reaction of *RA* and *pRA* with *PDL* and lauric acid[a]

Rxn. No.	*Substrates*	*t, hr*	M_n	*DP*	*PDI*	*%Conv*
A.	PDL	4.0	855	3.6	2.8	60.3[b]
B.	RA/pRA (DP = 2.2)	172	979	3.5	1.5	95.4
C.	PDL + RA/pRA[c] 2.35 $mol\ mol^{-1}$	80	2490	9.9	3.7	95.8[d], 84.1[e]
D.	PDL + pRA[f] 1.15 $mol\ mol^{-1}$	70	3430	9.0	2.1	100[d], 100[e]
E.	Lauric Ac + pRA[f] 1.14 $mol\ mol^{-1}$	138	1640	6.3	2.1	34.0[g], 100[e]

[a]Reaction conducted in bulk at 80°C under ~300 rpm magnetic stirring, catalyzed by *CAL* at 4 wt%. M_n, *DP*, and *PDI* determined via gel permeation chromatography using a Abbreviations: *t* = reaction time, *PDI* = polydispersity index, *%Conv* = percent conversion; others explained in text; [b]monomer present in the form of ω-hydoxypentanoic acid; [c]monomer from Rxn. B; [d]with respect to *PDL*; [e]with respect to *RA*, [f]product from Rxn. B; [g]with respect to lauric acid.

CAL-catalyzed polymerization of each monomer was performed as a control. *pPDL* was produced rapidly, yielding a broad product distribution (Figure 4) and a *DP* value of 3.5 (Table IV, Rxn A). The reaction was stopped at 4.0 *hr.* when the resultant product became a solid-phase, apparently due to the high melting point temperature of *pPD*L (97°C) and 15-hydroxy pentadecanoic acid formed via hydrolysis, which melts at 85°C. Significantly higher M_n values were achieved in bulk and in solvent (22 and 86 *kDa*, respectively) when the medium's water content was reduced to < 1% (*51*), which was not performed herein. Polymerization of *RA* occurred to the same degree as discussed above (Table IV, Rxn. B). Using either *RA* or *pRA* as substrate, co-polymerization with *PDL* led to an increase of M_n and yielded high conversion of monomers

(Table IV, Rxns. C and D). However, the resultant polymeric products were solids at room temperature, making them impractical for lubrication.

The lipase-catalyzed "end-capping" of *pRA* by lauric acid occurred successfully, demonstrated by the 34% conversion of lauric acid (Table IV, Rxn E). This allowed for an increase of *MW* beyond that of a laruic acyl group, suggesting that further polymerization of *RA* groups occurred, perhaps due to the decrease of viscosity that probably occurred as a result of end-capping (*12,30,31*), which would improve the mass transport of polymers to the active site of lipases.

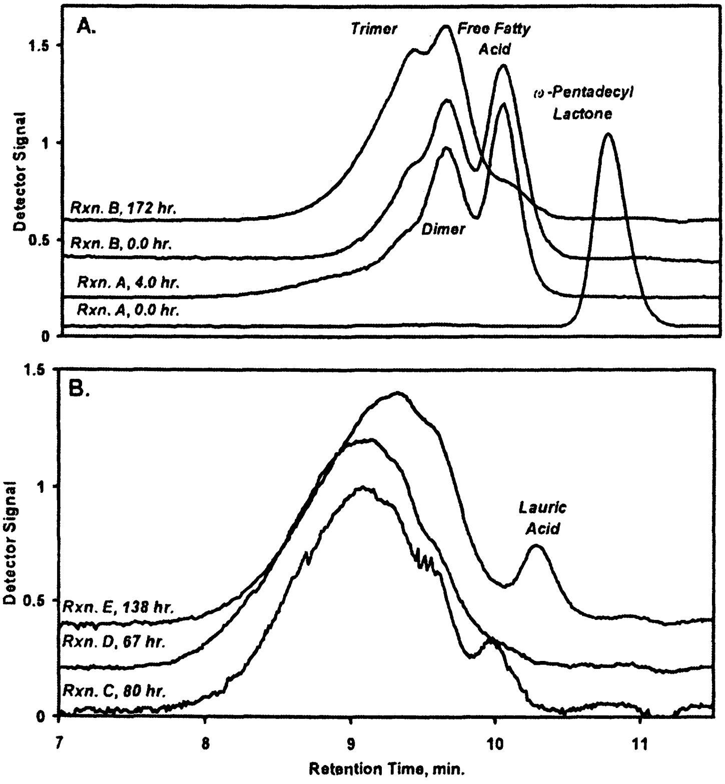

Figure 4. GPC Chromatograms of CAL-catalyzed polymerization of (A.) homopolymers and (B.) copolymers involving RA, PDL, and lauric acid monomers. Captions refer to reaction number indicated in Table IV.

Downloaded by NORTH CAROLINA STATE UNIV on August 10, 2012 | http://pubs.acs.org
Publication Date: September 23, 2006 | doi: 10.1021/bk-2006-0939.ch008

Summary and Future Research

Lipase-catalyzed synthesis of *pHAs* and their ester derivatives, such as star polymers, presents an eco-friendly means of producing effective bio-based lubricant materials for use in environmentally-sensitive applications. Moreover, the process is simple and does not involve harsh reaction conditions or organic solvents. The future increase of demand for bio-based lubricants is expected to make a biocatalytic route for synthesis more cost-competitive. Improvement of thermostability and bioresistance, among other properties, is required to improve the applicability of star polymers as biolubricants. Recent work has involved the lipase-catalyzed chain elongation of *pRA* using co-polymerization. Inclusion of *PDL* as co-monomer resulted in a co-polymer with a melting point too high for practical use as a lubricant. Lauric acid was employed to successfully to "end-cap" the free hydroxy group of *pRA*.

Future research planned by our group includes chemo-enzymatic modification of star polymers for their use as vehicles for oral or parenternal drug delivery. To fulfill this application, the free hydroxyls of the star polymer molecule's linear chains will be covalently attached to hydrophilic groups such as poly(ethylene glycol), resulting in a molecule that closely resembles unimeric polymeric micelles, or *UPMs*. In solution, *UPMs* form nanodroplets containing a hydrophobic core and a hydrophilic exterior, useful for solubilizing hydrophobic drugs in aqueous solution. Unlike micelles formed by small molecules or micelles, *UPMs* remain stable upon dilution, even to parts per million concentrations. Chemical synthesis has produced *UPMs* useful for *in vivo* delivery of lipophilic drugs (*53*). The use of an enzymatic route for their synthesis is expected to simplify the synthetic procedure and improve product and process biocompatibility.

Downloaded by NORTH CAROLINA STATE UNIV on August 10, 2012 | http://pubs.acs.org
Publication Date: September 23, 2006 | doi: 10.1021/bk-2006-0939.ch008

References

1. Gaginella, T. S.; Capasso, F.; Mascolo, N.; Perilli, S. *Phytother. Res.* **1998**, *12*, S128-S130.
2. Achaya, K. T. *J. Am. Oil Chem. Soc.* **1971**, *48*, 758-763.
3. Schwitzer, M. K. In *Proceedings World Conference on Oleochemicals: Into the 21st Century*; Applewhite, T. H., Ed.; AOCS Press: Champaign, IL, 1991; pp 111-118.
4. Hodges, R. M. *Genomics & Proteomics* **2003**, *3*, 46.
5. *FAO Statistical Databases*, http://faostat.fao.org/.
6. Hayes, D. G. *J. Am. Oil Chem. Soc.* **1996**, *73*, 543-549.
7. Smith, C. R., Jr. In *Progress in the Chemistry of Fats and Other Lipids*; Holman, R. T., Ed.; Pergamon Press: Oxford, UK, 1970.

8. Hou, C. T. *SIM News* **2003**, *53*, 56-61.
9. Baker, A. S.; Walbridge, D. J. US Patent 3,669,939, 1972
10. Yamaguchi, C.; Tooyama, A.; Asaoka, S.; Ogata, F. *Yushi* **1989**, *42*, 230-233.
11. Wilson, R.; Van Schie, B. J.; Howes, D. *Food Chem. Toxicol.* **1998**, *36*, 711-718.
12. Cermak, S.; Isbell, T. A. *INFORM* **2004**, *15*, 515-517.
13. Lyons-Johnson, D. *Agric. Res.* **1998**, *46*, 9.
14. Isbell, T. A.; Abbott, T. A.; Asadauskas, S.; Lohr, J. E. US Patent 6,018,063, 2000
15. Lawate, S. S. US Patent 05,427,704, 1995
16. Freedonia, I. *Fredonia Focus on Lubricants*; Freedonia, Inc.: Cleveland, OH, 2004.
17. Miller, S.; Scharf, C.; Miller, M. In *Trends in New Crops and New Uses*; Janick, J.; Whipkey, A., Eds.; ASHS Press: Alexandria, VA, 2002; pp 26-28.
18. Cunningham, B.; Battersby, N.; Wehrmeyer, W.; Fothergill, C. *J. Ind. Ecol.* **2004**, *7*, 179-192.
19. Nibe, K. *BioEconomy Update* **2004**, *2*, 1-2.
20. Agriculture and Agri-Food Canada. *Non-Food/Non-Feed Industrial Uses for Agricultural Products: Phase 1*; Agriculture and Agri-Food Canada: Ottawa, CA, 2002.
21. Johnson, D. L.; Rhodes, B.; Allen, R. In *Trends in New Crops and New Uses*; Janick, J.; Whipkey, A., Eds.; ASHS Press: Alexandria, VA, 2002; pp 29-33.
22. Gawrilow, I. *INFORM* **2004**, *15*, 702-704.
23. Landis, P. S.; Shanahan, A. *INFORM* **1994**, *5*, 689-691.
24. Hayes, D. G.; Kleiman, R. *J. Am. Oil Chem. Soc.* **1995**, *72*, 1309-1316.
25. Kelly, A. R.; Hayes, D. G. *J. Appl. Polym. Sci.* **2005**, *99*, in press.
26. Shubkin, R. L. *Synthetic Lubricants and High-Performance Functional Fluids*: New York, 1992.
27. ASTM. *1981 Annual Book of ASTM Standards*; American Society for Testing and Materials: Philadelphia, 1981.
28. Lakshimarayana, G.; Subbarao, R.; Sastry, Y. S. R.; Kale, V.; Rao, T. C. *J. Am. Oil Chem. Soc.* **1984**, *61*, 1204-1206.
29. Biresaw, G. *INFORM* **2004**, *15*, 148-149.
30. Cermak, S.; Brandon, K. B.; Isbell, T. A. *Ind. Crops Prod.* **2005**, *53*, in press.
31. Cermak, S.; Isbell, T. A. *J. Am. Oil Chem. Soc.* **2004**, *81*, 297-303.
32. Isbell, T. A.; Kleiman, R.; Erhan, S. M. *J. Am. Oil Chem. Soc.* **1992**, *69*, 1177-1183.
33. Isbell, T. A.; Kleiman, R. *J. Am. Oil Chem. Soc.* **1996**, *73*, 1097-1107.

Downloaded by NORTH CAROLINA STATE UNIV on August 10, 2012 | http://pubs.acs.org
Publication Date: September 23, 2006 | doi: 10.1021/bk-2006-0939.ch008

34. Yoshida, Y.; Kawase, M.; Yamaguchi, C.; Yamane, T. *Yukagaku* **1994**, *44*, 328-333.
35. Yamaguchi, C.; Tooyama, A.; Asaoka, S.; Ogata, F. Japanese Patent 02013387, 1990
36. Yamaguchi, C.; Akita, M.; Asaoka, S.; Osada, F. Japanese Patent 01016591, 1989
37. Yoshida, Y.; Kawase, M.; Yamaguchi, C.; Yamane, T. *J. Am. Oil Chem. Soc.* **1997**, *74*, 261-267.
38. Kobayashi, S.; Uyama, H.; Kimura, S. *Chem. Rev.* **2001**, *101*, 3793-3818.
39. Akkara, J.; Ayyagari, M. s. R.; Bruno, F. F. *Trends Biotechnol.* **1999**, *17*, 67-73.
40. Gross, R. A.; Kumar, A.; Kalra, B. *Chem. Rev.* **2001**, *101*, 2097-2124.
41. Matsumura, S.; Tsukada, K.; Toshima, K. *Int. J. Biol. Macromol.* **1999**, *25*, 161-167.
42. Matsumura, S.; Ebata, H.; Toshima, K. *Makromol. Chem., Rapid Commun.* **2000**, *21*, 860-863.
43. Deng, F.; Bisht, K. S.; Gross, R. A.; Kaplan, D. L. *Macromolecules* **1999**, *32*, 5159-5161.
44. Basu, H. N.; Robley, E. M.; Norris, M. E. *J. Am. Oil Chem. Soc.* **1994**, *71*, 1227-1230.
45. Yunus, R.; Fakhru'l-Razi, A.; Ooi, T. L.; Iyuke, S. E.; Perez, J. M. *Eur. J. Lipid Sci. Technol.* **2004**, *106*, 52-60.
46. Willing, A. *Fette/Lipid* **1999**, *101*, 192-198.
47. Mei, Y. M.; Kumar, A.; Gross, R. A. *Macromolecules* **2003**, *36*, 5530-5536.
48. Henderson, L. A.; Svirkin, Y. Y.; Gross, R. A.; Kaplan, D. L.; Swift, G. *Macromolecules* **1996**, *29*, 7759-7766.
49. Andrade, E. N. d. C. *Nature (London)* **1930**, *125*, 309-310.
50. Ceccorulli, G.; Scandola, M.; Kumar, A.; Kalra, B.; Gross, R. A. *Biomacromolecules* **2005**, *6*, 902-907.
51. Kumar, A.; Kalra, B.; Dekhterman, A.; Gross, R. A. *Macromolecules* **2000**, *33*, 6306-6309.
52. Kumar, A.; Garg, K.; Gross, R. A. *Macromolecules* **2001**, *34*, 3527-3533.
53. Liu, M.; Kono, K.; Frechet, J. M. J. *J. Controlled Release* **2000**, *65*, 121-131.

Downloaded by NORTH CAROLINA STATE UNIV on August 10, 2012 | http://pubs.acs.org
Publication Date: September 23, 2006 | doi: 10.1021/bk-2006-0939.ch008

Downloaded by STANFORD UNIV GREEN LIBR on August 28, 2012 | http://pubs.acs.org
Publication Date: September 23, 2006 | doi: 10.1021/bk-2006-0939.ch009

Chapter 9

Multifunctional Polyester-Based Materials with Controlled Degradability

Daniel Grande, Estelle Renard, Valérie Langlois, Géraldine Rohman, Laurianne Timbart, and Philippe Guérin

Laboratoire de Recherche sur les Polyméres, UMR 7581 CNRS–Université Paris XII, 2, rue Henri Dunant, 94320 Thiais, France

Hydrolytic degradability can be fine-tuned in polyester-based materials by controlling the nature and placement of comonomers introduced within the polymer structures. This contribution describes how D,L-lactide-, ε-caprolactone-, and β-hydroxyoctanoate-containing polyesters can be used to design nanostructured drug delivery vehicles and mesoporous polymeric materials. In the first part, the efficient synthesis of poly(β-hydroxyoctanoate)-based block and graft copolymers is addressed. A versatile and straightforward approach toward mesoporous functional polymers *via* the partial hydrolysis of poly(D,L-lactide)-based Interpenetrating Polymer Networks (IPNs) is discussed in a second part.

In Degradable Polymers and Materials; Khemani, K., et al.;
ACS Symposium Series; American Chemical Society: Washington, DC, 2006.

Downloaded by STANFORD UNIV GREEN LIBR on August 28, 2012 | http://pubs.acs.org
Publication Date: September 23, 2006 | doi: 10.1021/bk-2006-0939.ch009

The need for well-defined macromolecular architectures with either totally or partially hydrolyzable character is increasing, in the context of the development of new hydrolyzable and biocompatible materials for targeted applications, especially temporary applications (therapeutic or environmental ones). In this regard, we have recently synthesized a large variety of polyester-based materials *via* chemical or biological processes (*1*). The control of the polymer structure is crucial to fine-tune the physico-chemical properties of the polymers synthesized, and more particularly their hydrolytic degradability, so as to reach specific applications. This will be illustrated through different systems recently investigated in our group.

The first part of this contribution is devoted to the design and synthesis of graft and block copolyesters based on poly(3-hydroxyoctanoate) (PHO) meant for controlled drug delivery. Poly(β-hydroxyalkanoate)s (PHAs) are biodegradable and biocompatible polymers produced by a wide range of microorganisms; the properties of these biopolyesters mainly depend on the side-chain length (*2, 3*).

In the second part, we report on the preparation of mesoporous materials derived from partially hydolyzable Interpenetrating Polymer Networks (IPNs). Mesoporous materials are of particular interest because of their diverse applications in many areas, including separation techniques, biomolecule immobilization, as well as template-assisted synthesis of nanomaterials (*4*). This work presents the synthesis and characterization of poly(D,L-lactide) (PLA)-based IPNs, as well as the effective strategy developed to engineer mesoporous networks from such novel precursors, by taking advantage of the hydrolytic degradability of PLA.

Experimental Section

Materials

PHO with a M_n of 80,000 g.mol^{-1} (M_w/M_n = 2) was produced by using *Pseudomonas sp* Gpo 1 (CERMAV-CNRS, France). Dihydroxy-telechelic PLA (M_n = 1,700 g.mol^{-1}; M_w/M_n = 1.2) was synthesized according to a literature method (*5*). ε-caprolactone and methyl methacrylate (Aldrich) were dried over CaH_2, and distilled under vacuum prior to use. Triethylaluminum ($AlEt_3$, Fluka) and dibutyltin dilaurate (DBTDL, Fluka) were used as received. 4,4',4"-triisocyanato-triphenylmethane (Desmodur® RU 1.25 mol.L^{-1} in dichloromethane solution) was provided by Bayer. Bisphenol A dimethacrylate (BADMA) and diurethane dimethacrylate (DUDMA) were purchased from Aldrich and used as received. AIBN (Merck) was purified by recrystallization in methanol.

PHO Methanolysis

High-molar mass PHO (250 mg) was dissolved in 10 mL of dichloromethane. 10 mL of methanol was mixed with the solution containing

PHO and 0.75 mL of H_2SO_4 was added. The solution was stirred with a magnetic stirrer at 100 °C for a given time to obtain the desired molar mass. After cooling to room temperature, 5 mL of distilled water was added, and after decantation, the organic layer was washed again with distilled water, dried under $MgSO_4$ and filtered. The solvent was evaporated and the product was dried under vacuum at 40 °C.

Diblock Copolymer Synthesis

160 mg of PHO oligomer (M_n = 1,100 $g.mol^{-1}$; M_w/M_n = 1.9) was dried by three successive azeotropic distillations with dried toluene (3 x 2 mL). Then, the dried polymer was reacted with 1.2 mole equivalents ($1.6 \cdot 10^{-4}$ mol, $88 \cdot 10^{-3}$ mL) of $AlEt_3$ compared to the concentration of hydroxyl chain-end groups in toluene at 50 °C for 2 h. After cooling to room temperature, ε-caprolactone ($5.9 \cdot 10^{-3}$ mol, 0.67 mL) was added and polymerized for 24 h. After addition of a few drops of a 0.1 $mol.L^{-1}$ HCl aqueous solution, the polymer solution was precipitated twice in a 10-fold excess of heptane (20 mL). The resulting copolymer was recovered by filtration and dried under reduced pressure at 40 °C. Yield: 73 %.

Synthesis of PLA/PMMA IPNs

IPNs constituted of PLA and PMMA sub-networks (50/50 wt %) were synthesized by the *in situ* sequential method, i.e. by mixing all the precursors homogeneously, and then forming both networks via two successive and noninterfering cross-linking reactions. Hence, the PLA sub-network was first generated at room temperature for 20 h by DBTDL-catalyzed cross-linking of dihydroxy-telechelic PLA oligomer with Desmodur® RU as a triisocyanate cross-linker. Subsequently, the methacrylic sub-network was created at 65 °C by AIBN-initiated copolymerization of MMA and a dimethacrylate (2 h), and finally cured at 110 °C for 2 h to ensure a near completion of the cross-linking processes.

Partial Hydrolysis of IPNs

In different vials containing 3 mL of a phosphate buffer solution (pH = 8.2) and 3 mL of ethanol, 0.2 g of network samples were immersed at 60 °C. After a given period of time, the reaction medium was neutralized by a 0.1 $mol.L^{-1}$ NaOH aqueous solution, and the residual network was rinsed with distilled water up to neutral pH. Two characteristic parameters were assessed, namely mass loss (Δm) and water absorption (Q_{H2O}), as follows: $\Delta m = (m_0 - m_d) / m_0$ and $Q_{H2O} = (m_w - m_d) / m_d$, where m_0, m_d, and m_w stand for the initial mass of the samples, their residual mass after vacuum drying, and their wet mass after wiping, respectively.

Downloaded by STANFORD UNIV GREEN LIBR on August 28, 2012 | http://pubs.acs.org
Publication Date: September 23, 2006 | doi: 10.1021/bk-2006-0939.ch009

Instrumentation

^1H and ^{13}C NMR spectra were run at room temperature using a Bruker AC 200 spectrometer at resonance frequencies of 200 and 50 MHz, respectively. Solid-state ^{13}C NMR spectra were recorded at a resonance frequency of 75 MHz on a Bruker Avance 300 spectrometer. The Size Exclusion Chromatography (SEC) equipment comprised a Spectra Physics P100 pump, two PLgel 5 μm mixed-C columns (Polymer Laboratories), and a Shodex RI 71 refractive index (RI) detector. The eluent was tetrahydrofuran (THF) at a flow rate of 1 mL min^{-1}; the calibration was effected with polystyrene (PS) standards from Polymer Laboratories. FTIR spectra were recorded between 4000 and 450 cm^{-1} on a Bruker Tensor 27 DTGS spectrometer in Attenuated Total Reflection (ATR) mode. Glass transition temperature (T_g) and thermoporometry analyses were performed by Differential Scanning Calorimetry (DSC) with a Perkin Elmer DSC 4 calorimeter under a nitrogen atmosphere. The samples were scanned from -100 to 200 °C for T_g analyses and from -50 to 5 °C for thermoporometry, at a heating rate of 20 °C min^{-1} and 1 °C min^{-1}, respectively. Scanning Electron Microscopy (SEM) analyses were performed with a LEO 1530 microscope equipped with a high-vacuum (10^{-10} mmHg) Gemini column. The accelerating tensions ranged from 1 to 5 kV; two types of detectors (Inlens and Secondary Electron) were used. Prior to analyses, the samples were cryofractured and coated with a Pd/Au alloy in a Cressington 208 HR sputter-coater.

Design of PHA-Based Degradable Materials

PHAs constitute an important class of biodegradable polyesters that are produced as intracellular energy and carbon storage materials by a wide variety of bacteria (*2, 3*). Besides biodegradability by enzymes, such as PHA depolymerase and hydrolase, a common feature to PHAs is their chirality: indeed, they are characterized by highly stereoregular linear polymer chains with R configuration. Moreover, these bacterial polyesters are biocompatible, and their physico-chemical properties make them suitable for biomedical applications, including controlled drug delivery and tissue engineering. Among bacteria able to produce medium-chain length (mcl) PHAs, *Pseudomonas sp* Gpo 1 has the particularity to create functional mcl-PHAs with side-chain C=C double bonds (*6*). Such unsaturations can be chemically modified for further functionalization with the possibility to modulate the solubility and the hydrophilic/hydrophobic balance. Micelles and nanoparticles have then been prepared. These aspects will be developed in the following sections.

Design and Properties of Graft Copolymers

As mentioned previously, a bacterial copolyester (poly(3-hydroxyoctanoate-*co*-3-hydroxyundecenoate), PHOU) containing repeating units with terminal

Downloaded by STANFORD UNIV GREEN LIBR on August 28, 2012 | http://pubs.acs.org
Publication Date: September 23, 2006 | doi: 10.1021/bk-2006-0939.ch009

Downloaded by STANFORD UNIV GREEN LIBR on August 28, 2012 | http://pubs.acs.org
Publication Date: September 23, 2006 | doi: 10.1021/bk-2006-0939.ch009

alkene substituents at the 3-position was produced by *Pseudomonas sp* Gpo 1 using sodium octanoate and 10-undecenoic acid as carbon sources. The polymer composition was fine-tuned by the initial substrate composition. Chemical modifications were successfully completed on the double bonds under conditions in which negligible chain scission reactions were noticed, thus affording novel functional biopolyesters. Unsaturated groups were transformed into carboxylic acid groups by oxidation using $KMnO_4$ to generate poly(3-hydroxyoctanoate-*co*-9-carboxy-3-hydroxydecanoate) (PHOD) (*7*). Alcohol functions were also introduced by hydroboration-oxidation of PHOU (*8*) (Figure 1). Through such means, it is possible to control the hydrophilic/hydrophobic balance, and to improve the water solubility so as to enhance significantly the hydrolytic degradability of PHAs. For instance, at 37 °C and pH = 10, a PHO sample did not undergo any degradation in a buffered aquous solution, whereas a PHOD sample of equivalent molar mass was totally hydrolyzed within 2 h (*9*). The latter sample was even substantially degraded at pH = 7.

Moreover, the resulting copolyesters with pendant carboxylic groups (PHOD) can further be modified by binding bioactive molecules and either hydrolyzable or hydrophilic oligomers. Thus, graft copolymers constituted of a PHO main chain and either PLA or poly(ethylene glycol) (PEG) short grafts were respectively synthesized by direct esterification of PLA or PEG oligomers (M_n = 350 $g.mol^{-1}$) with side-chain carboxylic groups (*10*). Graft copolyesters contained around 10-15 mol % of residual unmodified carboxylic acid groups (Figure 2). Nanoparticles were derived from these copolyesters by solvent displacement (i.e. nanoprecipitation of acetone solution in water, followed by evaporation of acetone) without any stabilizer. They were obtained quantitatively as indicated by the absence of precipitation. Stable nanoparticles were formed in water, and the suspensions remained stable for several weeks without visible aggregation. The potential applications in biological medium involve the presence of salts in aqueous medium. Consequently, we investigated the stability of particle suspensions under different NaCl concentrations through turbidity measurements. Turbidity was calculated according to the following Beer-Lambert extinction law: $\tau = \ln(A) / e$, where A is the sample absorbance measured by UV spectroscopy and e the sample thickness.

As a general rule, $\tau = \lambda^{-\gamma}$, where the gradient γ is the slope of the turbidity variation *vs.* the wavelength λ. The gradient decreases when the particle size increases. In Figure 3, we compare the nanoparticle stability in the presence of different salt concentrations as a function of the PHO-based structure. It has to be stressed that the gradient usually decreased with an increase of salt composition, which is associated with aggregate formation and precipitation. Interestingly, for PHOD-*g*-PEG nanoparticles, the gradient decreased slightly, but no major aggregation was observed. PEG grafts actually acted as surfactants and contributed to the prevention of particle coalescence.

Downloaded by STANFORD UNIV GREEN LIBR on August 28, 2012 | http://pubs.acs.org
Publication Date: September 23, 2006 | doi: 10.1021/bk-2006-0939.ch009

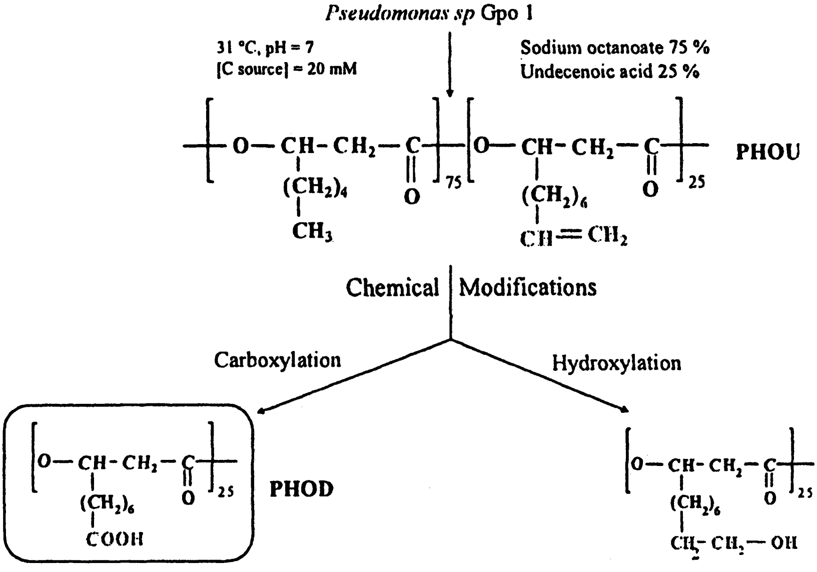
Pseudomonas sp Gpo 1
31 °C, pH = 7
[C source] = 20 mM
Sodium octanoate 75 %
Undecenoic acid 25 %
PHOU
Chemical Modifications
Carboxylation
Hydroxylation
PHOD

Figure 1. Design of functional polyesters by chemical modifications on PHOU.

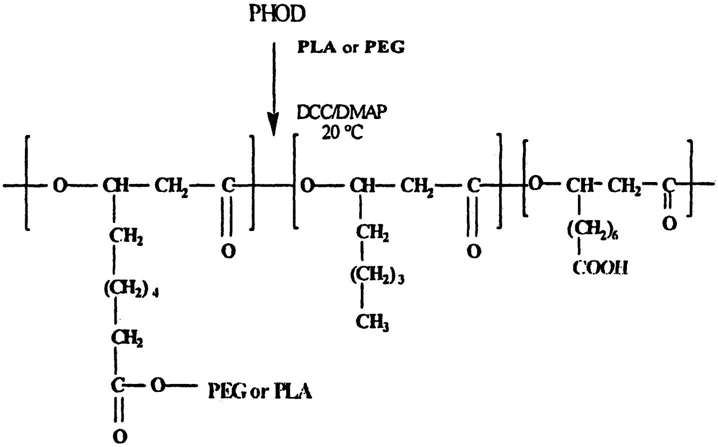
PHOD
PLA or PEG
DCC/DMAP
20 °C
PEG or PLA

Figure 2. Design of bacterial graft copolymers from PHOD.

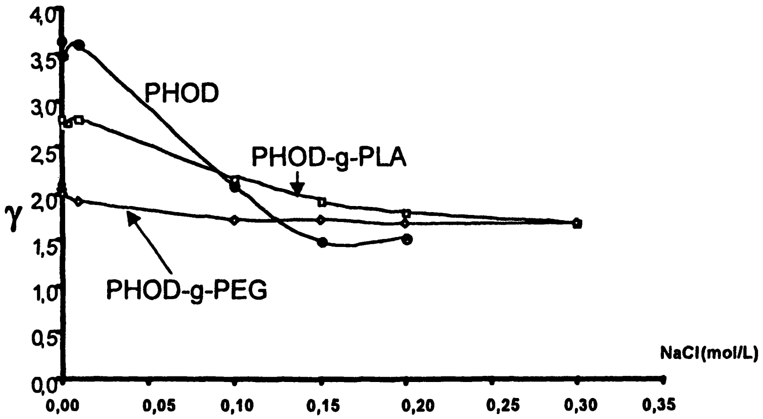

Figure 3. Dependence of γ on salt concentration for PHO-based nanoparticles.

Downloaded by STANFORD UNIV GREEN LIBR on August 28, 2012 | http://pubs.acs.org
Publication Date: September 23, 2006 | doi: 10.1021/bk-2006-0939.ch009

Synthesis and Properties of Block Copolyesters

The amorphous character of the graft copolyesters have limited their potential applications. We then turned our attention on the design and synthesis of block copolyesters constituted of a soft PHO block and a more crystalline poly(ε-caprolactone) (PCL) block (*11*). For this purpose, a two-step process was designed: the first step consisted in the preparation of hydroxy-terminated PHO oligomers, and in the second step, these oligomers were used as macroinitiators for the ring-opening polymerization of ε-caprolactone to generate the desired diblock copolymers.

The effective one-step synthesis of PHO oligomers containing a hydroxyl end group at one side and an ester end group on the other side was achieved by exposing a PHO sample of high molar mass to an acid-catalyzed methanolysis. Such a reaction led to the control of the molar masses of the samples. Thus, the methanolysis reaction was allowed to proceed for a period of time ranging from 10 to 60 min to produce well-defined PHO oligomers with a M_n value varying from 20,000 to 800 g.mol^{-1}, respectively. The polydispersity indices were as high as that of the PHO precursor ($M_w/M_n \approx 2$). The hydroxy-functionalized PHO oligomers with different molar masses were used to trigger the polymerization of ε-caprolactone to generate PHO-*b*-PCL diblock copolymers. As depicted in Figure 4, the block polymerization process was carried out using $AlEt_3$ as a catalyst (*12*).

The physico-chemical characteristics of block copolyesters are listed in Table I. It is interesting to point out that the DSC thermograms only revealed the presence of PCL segments wit a T_g value around -60 °C and a T_m value at about

Downloaded by STANFORD UNIV GREEN LIBR on August 28, 2012 | http://pubs.acs.org
Publication Date: September 23, 2006 | doi: 10.1021/bk-2006-0939.ch009

60 °C, and high degrees of crystallinity as indicated by the values of ΔH_m. The presence of PHO phase was detected for the sample containing the highest molar mass PHO block (copolymer 5). Thus, it is clear that such copolyesters developed macrophase separation with domain sizes larger than a few hundreds of nanometers.

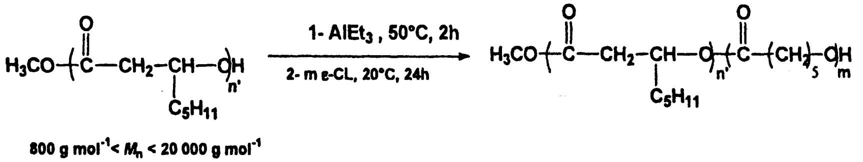

*Figure 4. Synthesis of PHO-*b*-PCL diblock copolymers from PHO oligomers.*

Table I. Characteristics of PHO-b-PCL Diblock Copolyesters

Copolymer	$M_n{}^a$ (g.mol^{-1}) PHO block	$M_n{}^a$ (g.mol^{-1}) PCL block	$T_g{}^b$ (° C)	$T_m{}^b$ (° C)	$\Delta H_m{}^b$ (J.g^{-1})
1	800	16,000	-58	63	89
2	2,500	13,500	-58	63	106
3	5,300	18,000	-58	63	106
4	8,600	18,000	-59	55	52
5	20,000	18,000	-63 / -41	62	51

[a] values determined by ^{1}H NMR. [b] values determined by DSC.

All these biodegradable PHO-based copolymers may represent useful model systems to investigate the encapsulation of doxorubicin inside nanoparticles and the drug delivery thereby. This bioactive molecule is an important agent involved in bladder cancer treatment.

Porous Networks Derived from Partially Hydrolyzable IPNs

Over the last decade, much attention has been paid to the design of porous polymeric materials as they find a large variety of applications in many areas, including separation and filtration techniques, enzyme immobilization, supported catalysis, as well as controlled drug release (*4*). Obtaining mesoporous polymeric materials with controlled porosity is not a trivial task. In this context, the preparation of ordered mesoporous polymers through the selective degradation of one block from self-organized annealed block copolymers has well been established by many groups (*13*). However, an alternative approach for generating porous cross-linked materials has been put forward only by a handful number of research teams through the utilization of partially degradable IPNs as precursors (*14, 15*).

Synthesis and Characterization of PLA-Based IPNs

IPNs represent an intimate combination of two independently cross-linked polymers, at least one being obtained in the immediate presence of the other (*16*). Interestingly, if one of the sub-networks is degradable under peculiar conditions, and the other one is stable under identical conditions, mesoporous networks can be designed from such IPNs by resorting to selective degradation methods (*14, 15*). In this context, IPNs based on an hydrolyzable polyester, such as PLA, and a polymer containing a non-hydrolyzable skeleton, such as PMMA, can be considered as appropriate precursors. Furthermore, PMMA is a rigid matrix with a high T_g, while PLA has a lower T_g, and both polymers are characterized by a low interaction parameter ($\chi = 0.017$), which ensures a good compatibility.

In this work, IPN systems constituted of PLA and PMMA sub-networks were prepared by the *in situ* sequential method as explained in the Experimental Section. For the PMMA sub-network generation, two different dimethacrylates were employed: BADMA, a "rigid" dimethacrylate, and DUDMA, a "softer" one (*17*). The influence of cross-link density on the structure and properties of the resulting networks was also probed by varying the initial dimethacrylate content from 1 to 10 mol %. All IPN samples were subjected to a dichloromethane extraction for 24 h at 40 °C; the amounts of soluble fractions were lower than 10 wt % as long as cross-linking of dihydroxy-telechelic PLA oligomer was carried out with a 40 mol % excess of isocyanate functions compared to alcohol functions. It is most noteworthy that IPNs were transparent, before and after extraction, suggesting good chain interpenetration of both constitutive sub-networks. Indeed, considering that the difference between the refractive indices of both partners is significant (n_D^{25} (PLA) = 1.46, n_D^{25} (PMMA) = 1.49), the transparency is at least indicative of microdomain sizes smaller than about 150 nm, according to Okay (*18*).

In a comparative study, we assessed the average values of PLA domain diameters in IPNs by turbidimetry using UV-visible spectroscopy. The turbidity τ of an IPN sample was determined from the measurement of its transmittance *Tr* at 460 nm, and calculated according to the Beer-Lambert law as follows: $\tau = -\ln(Tr) / e$, where e is the sample thickness (2 mm). Then, following Blundell's pioneering study on a system constituted of domains of PMMA embedded in a polyurethane matrix (*19*), we applied his theoretical expression to our IPN systems to estimate the average size of PLA microdomains dispersed within the PMMA matrix. Thus, the t value led to the calculation of the parameter *B(y)* as shown in eq 1:

Downloaded by STANFORD UNIV GREEN LIBR on August 28, 2012 | http://pubs.acs.org
Publication Date: September 23, 2006 | doi: 10.1021/bk-2006-0939.ch009

$$L_{PLA}(nm) = \frac{\lambda \cdot y}{4\pi \cdot (1-\phi)} \tag{1}$$

where λ, ϕ and n are the wavelength used, the volume fraction of PLA and the refractive index of PMMA, respectively. The difference in refractive indices of phases, Δ_n, was determined from the difference of the values measured for pure PLA and PMMA network samples. The n values were measured at the wavelength of the sodium D ray (λ_0 = 589 nm) using a Prolabo refractometer connected to a thermostated bath operating at 25 °C.

Then, the parameter y was derived from the resolution of eq 2:

$$\tau = \frac{\left(2\pi \cdot \phi \cdot (1-\phi) \cdot (\Delta n)^2 \cdot B(y)\right)}{\lambda \cdot n^2} \tag{2}$$

The average equivalent diameter L_{PLA} of PLA microdomains was finally obtained from eq 3:

$$B(y) = \left[\frac{y^2+2}{y}\right] \cdot \left[\frac{y^2+2}{y^2+1} - \frac{2}{y^2} \cdot \ln\left(y^2+1\right)\right] \tag{3}$$

Figure 5 shows the dependence of PLA domain diameter on dimethacrylate nature and content. All IPN samples were characterized by PLA diameters smaller than 60 nm, and no major variation was noticed with varying the dimethacrylate nature or content. Hence, these results corroborated the conclusions inferred from the visual aspects.

Preparation of Mesoporous Networks by Partial Hydrolysis of IPNs

In order to design mesoporous networks with a narrow pore size distribution, we resorted to an original approach through the selective hydrolysis of the PLA sub-network associated with partially hydrolyzable PLA/PMMA IPNs. Advantage of the contrasted hydrolytic degradability of PLA and PMMA was thus taken. As specified in Figure 6, this degradation was conducted at 60 °C using a mixture of a phosphate buffer (pH = 8.2) and ethanol. It has to be stressed that the hydrolysis was performed at intermediate temperature between the T_g of PLA single network (40 °C) and those of PMMA single networks (110-160 °C) to avoid the collapse of the residual porous methacrylic structures, while allowing for an efficient degradation of PLA.

Downloaded by STANFORD UNIV GREEN LIBR on August 28, 2012 | http://pubs.acs.org
Publication Date: September 23, 2006 | doi: 10.1021/bk-2006-0939.ch009

Downloaded by STANFORD UNIV GREEN LIBR on August 28, 2012 | http://pubs.acs.org
Publication Date: September 23, 2006 | doi: 10.1021/bk-2006-0939.ch009

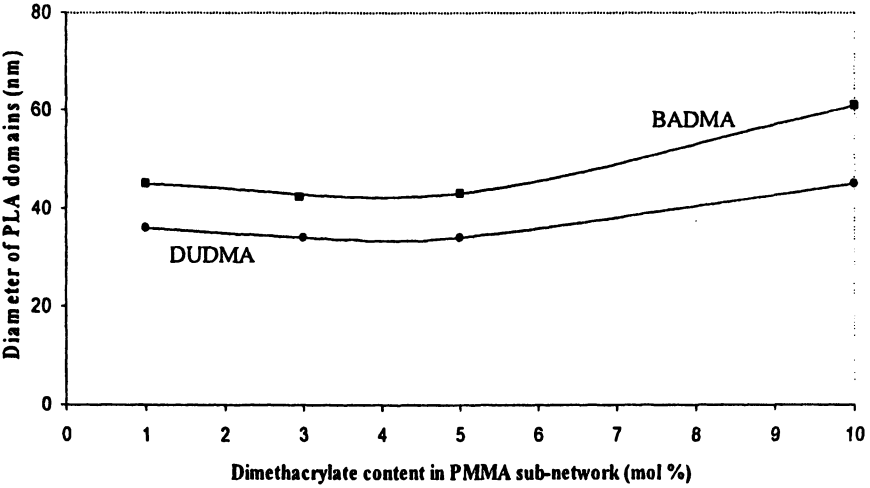

Figure 5. Average diameters of PLA microdomains in BADMA- and DUDMA-containing PLA/PMMA (50/50 wt %) IPNs as determined by turbidimetry.

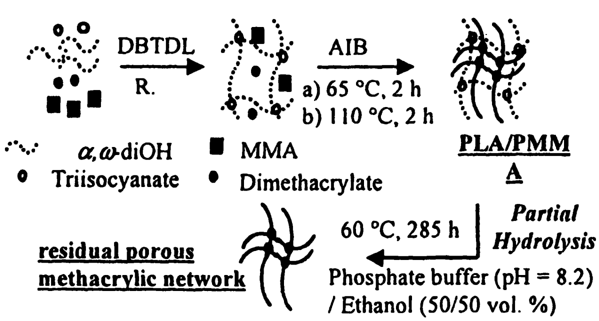
DBTDL
R.
AIB
a) 65 °C, 2 h
b) 110 °C, 2 h
α,ω-diOH
MMA
Triisocyanate
Dimethacrylate
PLA/PMMA
Partial Hydrolysis
60 °C, 285 h
Phosphate buffer (pH = 8.2) / Ethanol (50/50 vol. %)
residual porous methacrylic network

Figure 6. Design of mesoporous networks from PLA/PMMA IPNs.

Extracted IPNs as well as the corresponding single networks were subjected to hydrolysis under the same conditions, and the variations of mass loss were monitored as a function of the hydrolysis time (Figure 7 as an example). The PLA-based single network was completely degraded after 48 h. We observed a decrease of pH, due to the release of lactic acid in the hydrolysis medium. According to ^{1}H NMR and SEC analyses, the degradation products were constituted of oligolactides, lactic acid, and cross-linker residues, indicating that the hydrolysis affected both ester and urethane functions. As for IPN samples, regardless of the dimethacrylate nature and content, mass loss values higher than or close to 50 wt % were reached only after 285 h, and such values were associated with the quantitative degradation of PLA sub-network. The total disappearance of the characteristic bands associated with PLA sub-network (urethane and carbonyl groups) in the FTIR and solid-state ^{13}C NMR spectra of residual networks after hydrolysis confirmed their pure methacrylic structure. Furthermore, the T_g values of hydrolyzed IPNs were very close to those of corresponding PMMA single networks (110-160 °C). In order to understand how the conditions of PLA degradation affected the structure of PMMA subnetworks during the partial hydrolysis of IPNs, PMMA-based single networks were analyzed after undergoing the same experimental conditions. Even though mass loss decreased significantly when increasing dimethacrylate composition, values as high as 15 wt % were assessed for single networks based on 1 mol % dimethacrylate. On the other hand, water absorption increased when decreasing dimethacrylate content. Therefore, the concomitant variation of both parameters indicates a non-negligible degradation of PMMA which may be attributed to the partial hydrolysis of side-chain ester groups into carboxylic acid groups.

The morphologies of IPNs, before and after hydrolysis, were examined by SEM (Figure 8). Independently of the dimethacrylate nature and content, the non-degraded samples displayed compact and non-porous structures. This might arise from the good chain interpenetration of both constitutive sub-networks, as indicated by the transparency of IPN precursors. The corresponding PMMA single networks, after hydrolysis, did not exhibit a porous structure either, indicating a high compacity in this type of networks. In sharp contrast, the residual networks, after the hydrolysis of the PLA sub-network, exhibited porous structures with pore sizes ranging from 10 to 100 nm for BADMAcontaining systems, and from 10 to 60 nm for their DUDMA-derivatized homologues. Pore sizes minimally decreased when decreasing the dimethacrylate content (Table II). Thus, in such nanoporous materials, the dependence of pore size on dimethacrylate nature and content is not very significant.

Moreover, we determined pore sizes by thermoporometry through DSC measurements using water as the penetrant solvent. Thermoporometry has proved to be a reliable quantitative technique for the determination of pore size distributions in a wide range of (meso)porous materials, including porous silica, cellulose membranes, and hydrogels (*20*). It relies on the depression of melting

Downloaded by STANFORD UNIV GREEN LIBR on August 28, 2012 | http://pubs.acs.org
Publication Date: September 23, 2006 | doi: 10.1021/bk-2006-0939.ch009

Downloaded by STANFORD UNIV GREEN LIBR on August 28, 2012 | http://pubs.acs.org
Publication Date: September 23, 2006 | doi: 10.1021/bk-2006-0939.ch009

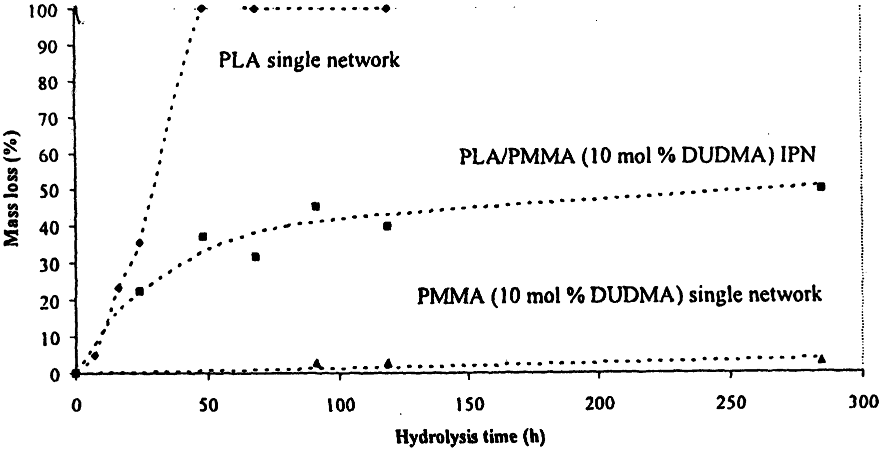

Figure 7. Dependence of mass loss on hydrolysis time for PLA- and/or PMMA-based networks.

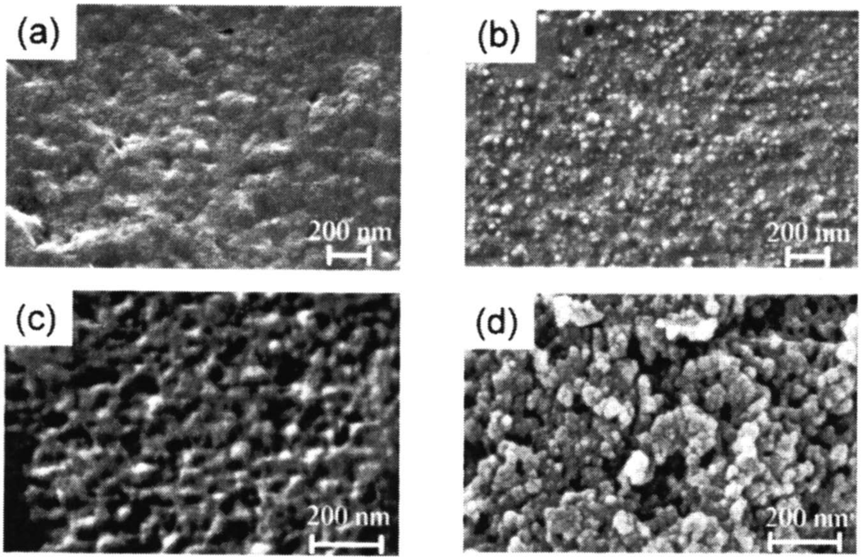

Figure 8. SEM micrographs of different PLA/PMMA (50/50 wt %) IPN systems: before hydrolysis: (a) 10 mol % DUDMA-based sample, (b) 10 mol % BADMA-based sample; after hydrolysis: (c) 10 mol % DUDMA-based sample, (d) 10 mol % BADMA-based sample.

Downloaded by STANFORD UNIV GREEN LIBR on August 28, 2012 | http://pubs.acs.org
Publication Date: September 23, 2006 | doi: 10.1021/bk-2006-0939.ch009

Table II. Pore Diameters (D_p) of Porous Methacrylic Networks as Determined by SEM and Thermoporometry

Dimethacrylate Content (mol %)	*D_p (nm) SEM* ***BADMA / DUDMA***	*D_p (nm) thermoporometry* ***BADMA / DUDMA***
10	10–100 / 10–60	30–100 / 20–80
5	10–50 / 10–50	15–60 / 15–60
3	10–50 / 10–50	15–60 / 15–60
1	10–50 / 10–50	15–50 / 15–50

temperature (T_m) and the Gibbs-Thompson effect shown by a solvent constrained within the pores. This technique is sensitive and precise to measure pore diameter smaller than 200–300 nm. As a matter of fact, from the melting thermograms of water contained in the porous methacrylic networks, the T_m depression could be correlated to the pore diameter D_p as follows (20): $D_p = 2 \cdot [0.68 - 32.33/(T_m - T_{m0})]$, where T_m and T_{m0} are the melting temperatures of confined and bulk water, respectively. The pore sizes thus determined are reported in Table II. We clearly observed relatively narrow pore size distributions, regardless of the dimethacrylate content. Overall, the estimates of pore diameters obtained by SEM and thermoporometry were in reasonable agreement; they were also in agreement with the average values of PLA microdomain diameters as determined by turbidimetry for IPN precursors (Figure 5). In these systems, the relatively small pore sizes and narrow pore size distributions of the methacrylic porous networks were essentially controlled by the good chain interpenetration of both PLA and PMMA sub-networks in the interlocking framework of IPN precursors.

Conclusions

This contribution has expanded the spectrum of frameworks based on hydrolyzable polyesters. Specifically, we have been interested in the design and synthesis of miscellaneous types of multifunctional polymer systems meant for specific applications. First, the controlled chemical modifications and polymerization processes from PHO have led to the effective formation of novel functional tailor-made biopolyesters, including PHO-*g*-PLA and PHO-*g*-PEG graft copolymers as well as PHO-*b*-PCL diblock copolymers. The semicrystalline copolyesters can be further used to prepare nanoparticles and encapsulate doxorubicin for controlled drug delivery devices. Second, a straightforward and versatile route toward mesoporous networks has been developed through the hydrolysis of the PLA sub-network from partially hydrolyzable PLA/PMMA-based IPNs as precursors. Cross-linked PLA subchains may effectively serve as porogen templates for the generation of such porous polymeric materials. The relatively small pore sizes and the narrow pore size distributions of the residual methacrylic networks seem to be controlled essentially by the high degree of chain interpenetration of both PLA and PMMA sub-networks in the interlocking configuration of IPNs. The potential applications of such porous networks are mainly expected in the areas of separation techniques, bioencapsulation, and chemistry in confined medium.

The development of multifunctional polymer systems with controlled degradability in the future will require diversification of the polyester structures, either by using novel monomers and/or precursors, or by varying the topology, the composition, and/or the functionality of macromolecular architectures. The aim of our investigations is to broaden the application portfolio: therapeutics, tissue engineering, biomacromolecule separation, and membrane catalysis.

Downloaded by STANFORD UNIV GREEN LIBR on August 28, 2012 | http://pubs.acs.org
Publication Date: September 23, 2006 | doi: 10.1021/bk-2006-0939.ch009

Acknowledgment

The authors thank the French Ministry of Research for providing G. R. and L. T. with Ph.D. grants. They are also indebted to Prof. F. Lauprêtre and Dr. S. Boileau for fruitful discussions concerning IPN systems.

References

1. Grande, D., Rohman, G.; Langlois, V.; Renard, E.; Timbart, L.; Guérin, Ph. *Polym. Prepr. (Am. Chem. Soc., Div. Polym. Chem.)* **2005**, *46(1)*, 285.
2. Steinbuchel, A.; Valentin, H. E. *FEMS Microbiol. Lett.* **1995**, *128*, 219.
3. Zinn, M.; Witholt, B.; Egli, T. *Adv. Drug Delivery Rev.* **2001**, *53*, 5.
4. (a) Odani, H.; Masuda, T. *Design of Polymer Membranes for Gas Separation;* VCH: New York, 1992. (b) Maier, G. *Angew. Chem. Int. Ed.* **1998**, *37*, 2960. (c) Buchmeiser, M. R. *Angew. Chem. Int. Ed.* **2001**, *40*, 3795. (d) Sykora, D.; Peters, E. C.; Svec, F.; Fréchet, J. M. J. *Macromol. Mater.* Eng. **2000**, *275*, 42.
5. Bachari, A.; Bélorgey, G.; Hélary, G.; Sauvet G. *Macromol. Chem. Phys.* **1995**, *196*, 411.
6. Bear, M. M.; Leboucher-Durand, M. A.; Langlois, V.; Lenz, R. W.; Goodwin, S.; Guérin, Ph. *React. Funct. Polym.* **1997**, *34*, 65.
7. Kurth, N.; Renard, E.; Brachet, F.; Robic, D.; Guérin, Ph.; Bourbouze, R. *Polymer* **2002**, *43*, 1095.
8. Renard, E.; Poux, A.; Timbart, L; Langlois, V.; Guérin, Ph. *Biomacromolecules* **2005**, *6*, 891.
9. Renard, E.; Walls, M.; Guérin, Ph.; Langlois, V. *Polym. Degrad. Stab.* **2004**, *85*, 779.
10. Renard, E.; Ternat, C.; Langlois,V.; Guérin, Ph. *Macromol. Biosci.* **2003**, *3*, 248.

11. Timbart, L.; Renard, E.; Langlois,V.; Guérin, Ph. *Macromol. Biosci.* **2004**, *4*, 1014.
12. Coulembier, O.; Degee, P.; Cammas-Marion, S.; Guérin, Ph.; Dubois, P. *Macromolecules* **2002**, *35*, 9896.
13. (a) Lee, J.S.; Hirao, A.; Nakahama, S. *Macromolecules* **1988**, *21*, 274. (b) Hashimoto, T.; Tsutsumi, K.; Funaki, Y. *Langmuir* **1997**, *13*, 6869. (c) Hedrick, J.L.; Carter, K.R.; Richter, R.; Miller, R.D.; Russell, T.P.; Flores, V.; Mecerreyes, D.; Dubois, P.; Jérôme, R. *Chem. Mater.* **1998**, *10*, 39. (d) Liu, G.J.; Ding, J.F.; Hashimoto, T.; Kimishima, K.; Winnik, F.M.; Nigam, S. *Chem. Mater.* **1999**, *11*, 2233. (e) Chan, V.Z.H.; Hoffman, J.; Lee, V.Y.; Iatrou, H.; Avgeropoulos, A.; Hadjichristidis, N.; Miller, R.D.; Thomas, E.L. *Science* **1999**, *286*, 1716. (f) Thurn-Albrecht, T.; Steiner, R.; DeRouchey, J.; Stafford, C.M.; Huang, E.; Bal, M.; Tuominen, M.; Hawker, C.J.; Russell, T.P. *Adv. Mater.* **2000**, *12*, 787. (g) Zalusky, A.S.; Olayo-Valles, R.; Taylor, C.J.; Hillmyer, M.A. *J. Am. Chem. Soc.* **2001**, *123*, 1519.
14. (a) Widmaier, J.M.; Sperling, L.H. *Macromolecules* **1982**, *15*, 625. (b) Du Prez, F.; Goethals, E.J. *Macromol. Chem. Phys.* **1995**, *196*, 903. (c) Hu, J.; Pompe, G.; Schulze, U.; Pionteck, J. *Polym. Adv. Technol.* **1998**, *9*, 746.
15. (a) Grande, D.; Pastol, J. L.; Guérin, Ph.; Boileau, S. *Polym. Prepr. (Am. Chem. Soc., Div. Polym. Chem.)* **2003**, *44(1)*, 44. (b) Balaji, R.; Boileau, S.; Guérin, Ph.; Grande, D. *Polym. News* **2004**, *29*, 205.
16. Sperling, L. H. *Interpenetrating Polymer Networks and Related Materials;* Plenum Press: New York, 1981.
17. Rohman, G.; Grande, D.; Lauprêtre, F.; Boileau, S.; Guérin, Ph. *Macromolecules* **2005**, *38*, 7274.
18. Okay, O. *Prog. Polym. Sci.* **2000**, *25*, 711.
19. Blundell, D. J.; Longman, G. W.; Wignall, G. D.; Bowden, M. J. *Polymer* **1974**, *15*, 33.
20. (a) Brun, M.; Lallemand, A.; Quinson, J.-F.; Eyraud, C. *Thermochim. Acta* **1977**, *21*, 59. (b) Hay, J. N.; Laity, P. R. *Polymer* **2000**, *41*, 6171.

Downloaded by STANFORD UNIV GREEN LIBR on August 28, 2012 | http://pubs.acs.org
Publication Date: September 23, 2006 | doi: 10.1021/bk-2006-0939.ch009

Downloaded by COLUMBIA UNIV on August 9, 2012 | http://pubs.acs.org
Publication Date: September 23, 2006 | doi: 10.1021/bk-2006-0939.ch010

Chapter 10

Poly(lactide)–Poly(ethylene oxide)–Poly(lactide) Triblock Copolymers: Synthesis and Thermal Properties

Naomi Sanabria-DeLong[1], Khaled A. Aamer[1], Sarvesh K. Agrawal[2], Surita R. Bhatia[2], and Gregory N. Tew[1]

[1]Department of Polymer Science and Engineering, University of Massachusetts at Amherst, 120 Governors Drive, Amherst, MA 01003
[2]Department of Chemical Engineering, University of Massachusetts at Amherst, 686 North Pleasant Street, Amherst, MA 01003

Poly (lactide) – poly (ethylene oxide) – poly (lactide) [PLA-PEO-PLA] triblock copolymers are of particular interest in the biomedical field due to their biocompatibility and their ability to form hydrogels in water. These hydrogels have potential applications in both drug delivery applications and tissue engineering. They are particularly interesting because their mechanical properties can be influenced by both the length of the PLA hydrophobic endblocks and by the ability of the PLA end-blocks to crystallize. Copolymers with crystallizable PLLA end-groups form stiffer gels, while copolymers with amorphous stereorandom PLA form weaker hydrogels. We investigate here the thermal properties of these triblock copolymers in their neat state to establish the presence of crystalline PLLA before incorporation into hydrogels and the effect of aging.

In Degradable Polymers and Materials; Khemani, K., et al.;
ACS Symposium Series; American Chemical Society: Washington, DC, 2006.

Polymer materials have attracted great interest in the area of regenerative medicine because of their great potential in both drug delivery and tissue engineering systems. However, the success of the common polyesters currently used has limitations because they do not accurately mimic the extracellular matrix of native tissue. Hydrogels are particularly attractive for use as polymer biomaterials because they have many similar properties to that of native tissue including a predominately aqueous environment, facile transport of cell metabolites, and tunable mechanical properties[1-3]. The issue of mechanical properties is particularly important, as it has been shown that cells sense their mechanical environment and will thrive or fail to mature accordingly. The processes that are affected by mechanical properties include cellular structure, metabolism, and viability[4-9]. Therefore, tunability in the mechanical properties is essential to the success of these hydrogel materials in order to match that of the target tissue.

Much work has been done on amphiphilic block copolymers that incorporate poly (lactide) [PLA] and poly (ethylene oxide) [PEO] due to their biodegradability and biocompatibililty, respectively. Both AB and ABA type structures have been used to form hydrogels[10-22]. However, these hydrogels exhibit low storage modulus and hence are less stiff than native tissue. We have already reported work on elastic hydrogels formed from PLA-PEO-PLA triblock copolymers that are much stiffer than previous studies with an elastic modulus in the kiloPascal range[23]. More importantly, it was shown that the mechanical integrity of the hydrogel could be controlled by both the block length and the crystallinity of the PLA end-blocks[24]. This shows that one can dial in the desired properties of the hydrogel.

There have been issues regarding reproducibility of the mechanical properties of PLA-PEO-PLA hydrogels formed at various times. We, therefore, wished to further investigate the thermal properties of the bulk copolymers to determine the extent of crystallization. This study focuses on the synthesis of these novel polymers as well as the crystalline and thermal characteristics of the neat PLAPEO-PLA triblock copolymer prior to hydrogel formation.

Materials and Methods

Materials

L-lactide and DL-lactide were purchased from Aldrich and purified by recrystallization in ethyl acetate, followed by sublimation prior to use in

Downloaded by COLUMBIA UNIV on August 9, 2012 | http://pubs.acs.org
Publication Date: September 23, 2006 | doi: 10.1021/bk-2006-0939.ch010

polymerization. Telechelic α, ω dihydroxy poly(ethylene oxide) macroinitiator was also purchased from Aldrich with a listed molecular weight of 8,000 Daltons. However, analysis by MALDI-TOF determined the number average molecular weight (M_n) to be 8,900 Daltons. PEO was dried under vacuum at room temperature prior to use for polymerization. Stannous (II) 2-ethyl hexanoate was purchased from Alfa Aesar and used without further purification.

Synthesis of PLA-PEO-PLA Triblock Copolymer

One equivalent of PEO was weighed into a dried round-bottom flask. The macroinitiator was then melted at 150°C and flushed with nitrogen for approximately thirty minutes (until no more bubbles are seen) to remove any remaining water. Half of an equivalent of Stannous (II) 2-ethyl hexanoate catalyst was added to the PEO, followed by immediate addition of either L-lactide monomer to create the stereoregular polymer or the meso-DL-lactide monomer to create the stereorandom polymer. The flask was then capped and the polymerization was carried out in the bulk at 150°C for 24 hours with stirring (Figure 1). When done, the mixture was quenched with methanol, dissolved in tetrahydrofuran, and precipitated in hexanes. Dissolution and precipitation was repeated three more times, and the polymer was dried under vacuum at room temperature for approximately 2 days.

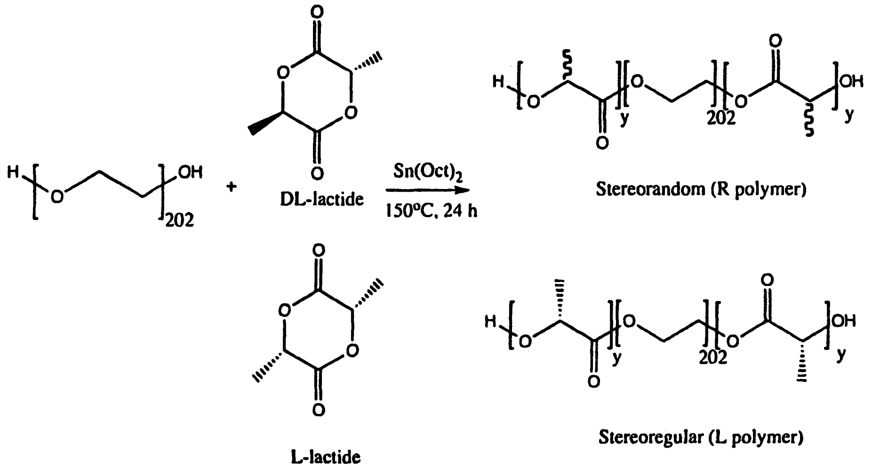

Figure 1. Synthesis of PLA-PEO-PLA triblock copolymer.

Downloaded by COLUMBIA UNIV on August 9, 2012 | http://pubs.acs.org
Publication Date: September 23, 2006 | doi: 10.1021/bk-2006-0939.ch010

Characterization and Instrumentation

The copolymer composition and degree of polymerization were characterized through ^{1}H NMR integration using a Bruker DPX300, 300MHz spectrometer in d-chloroform. Size exclusion chromatography [SEC] (PL GPC50) was used to determine the polydispersity of the synthesized copolymers versus PEO standards. Three Polymer Laboratories gel columns (5 μm 50Å guard column and three 5 μm MIXED-D) were used with N,N-dimethyl formamide (0.01M LiCl) as the eluting solvent at 1 mL/min at 50°C.

The copolymer samples were also analyzed thermally using thermogravimetric analysis (TGA TA Instruments Thermogravimetric Analyzer 2950) and differential scanning calorimetry (DSC 2910 DuPont Instrument). The samples were heated at 10°C/min from room temperature to 600°C in a platinum pan under a flow of nitrogen (to remove the volatiles) for TGA analysis. For DSC analysis, the samples were also heated at 10°C/min from room temperature to a maximum temperature of 200°C (in a hermetically sealed aluminum pan) then cooled at 10°C/min to remove any previous thermal history. The samples were then heated again at 10°C/min.

Wide angle X-Ray Diffraction (WAXD) experiments were performed using a Panalytical X'Pert Powder Diffractometer with a wavelength of radiation equal to 1.54Å. The voltage was set to 45kV and current to 40mA. The samples were scanned from $2\theta = 5°$ to $55°$ with a step size of 0.0167°.

Downloaded by COLUMBIA UNIV on August 9, 2012 | http://pubs.acs.org
Publication Date: September 23, 2006 | doi: 10.1021/bk-2006-0939.ch010

Results and Discussion

Block Copolymer Synthesis

PLA-PEO-PLA triblock copolymers were successfully synthesized with controlled molecular weights and molecular weight distributions. Figure 2 shows a ^{1}H NMR spectrum of a stereoregular triblock copolymer. The stereoregular copolymer shows a distinct quartet at ~5.17 ppm and a doublet at ~1.57 ppm corresponding to the one methine proton and the three methyl protons on the PLLA blocks of the copolymer, respectively. A distinct singlet is seen at ~3.64 ppm from the methylene protons of the PEO midblock. The spectrum for the stereorandom copolymer is quite similar except that the peak at ~5.17 ppm is no longer a distinct quartet but is now a multiplet. This is due to the increased number of conformations of that particular proton attached to the stereocenter carbon. Degrees of polymerization (DP) were determined through ^{1}H NMR integration of the methine proton peak of the PLA blocks as compared to the methylene peak of the PEO midblock (molecular weight/degree of polymerization of PEO is already known from MALDI-TOF measurements).

Almost all of the DPs were within plus or minus two repeat units of the targeted DP, and the polydispersity index (PDI) of all polymers are fairly low as determined through size exclusion chromatography. The reactions were only carried out to approximately 90% conversion (beyond this PDI broadens). A sampling of the polymers synthesized are listed in Table 1 and shows control over the DP of the PLA block, various molecular weights of PEO macroinitiator can be used, and both L and DL-lactide monomer can be used to create triblock copolymers.

Thermal Properties

These copolymers were tested using thermogravimetric analysis [TGA] and showed two transitions as expected for this type of copolymer system (degradation of PLA blocks and degradation of PEO block). Figure 3 shows that the first transition begins at approximately 200°C. The polymer continues to lose weight with increasing temperature until about 270°C, where the weight loss then levels off. This transition is attributed to the degradation of both PLA side chains of the triblock copolymer. A second transition occurs at approximately 350°C and weight loss increases with temperature until all the polymer is completely degraded (~400°C). This second weight loss is attributed to the degradation of the PEO middle block. The weight loss associated with the first and second transitions (PLA and PEO, respectively) agrees well with the calculated weight loss and further supports the assignments given. It is interesting to note that degradation of the polymer is completely quantitative with no leftover char material.

Further investigation of the copolymers' thermal properties were carried out using DSC analysis. Second heating cycles are shown in Figure 4 for L copolymers with different PLLA block lengths. The copolymers' first transition shows a melting endotherm of PEO between 50 and 53°C. As the temperature is increased a small melting endotherm can be seen at approximately 165°C due to crystalline PLLA. The L polymer can crystallize due to its stereoregular conformation. However, the intensity of the melting peak is dependent on the PLLA block length. Copolymers with short DPs do not show this melting endotherm at 165°C, suggesting that there may be a critical block length for crystallization of the PLLA blocks. Conversely, copolymers with long PLLA blocks show a very pronounced melting endotherm at 165°C. These results are intuitive, as one would expect larger crystals as the PLLA block length is increased, leading to a more pronounced melting peak.

A DSC thermogram of a stereorandom copolymer is shown in Figure 5. Similar to the L copolymers discussed above, the R polymers exhibit an endotherm between 50 and 53°C corresponding to melting of the crystalline PEO mid-block. However, there are no further phase changes over the sampled temperature range. In this case, the copolymers do not show melting of PLA because the stereocenter dictates amorphous PLA end blocks.

Downloaded by COLUMBIA UNIV on August 9, 2012 | http://pubs.acs.org
Publication Date: September 23, 2006 | doi: 10.1021/bk-2006-0939.ch010

Downloaded by COLUMBIA UNIV on August 9, 2012 | http://pubs.acs.org
Publication Date: September 23, 2006 | doi: 10.1021/bk-2006-0939.ch010

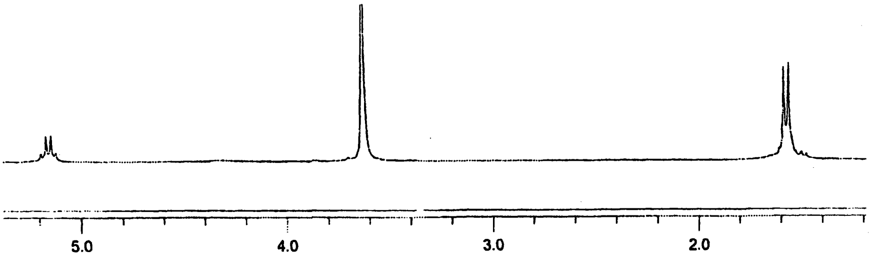

Figure 2. ^1H NMR spectra of PLLA-PEO-PLLA triblock copolymer.

Table 1. Molecular Weight Characterization of PLA-PEO-PLA.

Sample	M_{nPEO}*	M_{nPLA}**	M_{nTotal}	*PDI****	*Total* DP_{PLA}**	$Wt\%_{PEO}$	$Wt\%_{PLA}$
1	8,800	1,500	10,300	1.20	22L	84.7	15.3
2	8,900	3,200	12,100	1.21	44L	73.7	26.3
3	8,900	5,000	13,900	1.24	70L	63.8	36.2
4	8,900	6,300	15,200	1.12	87L	58.7	41.3
5	8,900	7,300	16,200	1.13	101L	55.0	45.0
6	8,900	4,000	12,900	1.14	56R	68.8	31.2
7	8,900	4,800	13,700	1.16	66R	65.2	34.8
8	8,900	5,600	14,500	1.14	78R	61.3	38.7
9	3,400	29,700	33,100	1.21	413L	10.3	89.7
10	12,000	19,500	31,500	1.33	271L	38.1	61.9
11	20,000	10,500	30,500	1.11	146L	65.5	34.5

*Determined by MALDI-TOF and SEC; **Determined by ^{1}H NMR; *** Determined by SEC.

Downloaded by COLUMBIA UNIV on August 9, 2012 | http://pubs.acs.org
Publication Date: September 23, 2006 | doi: 10.1021/bk-2006-0939.ch010

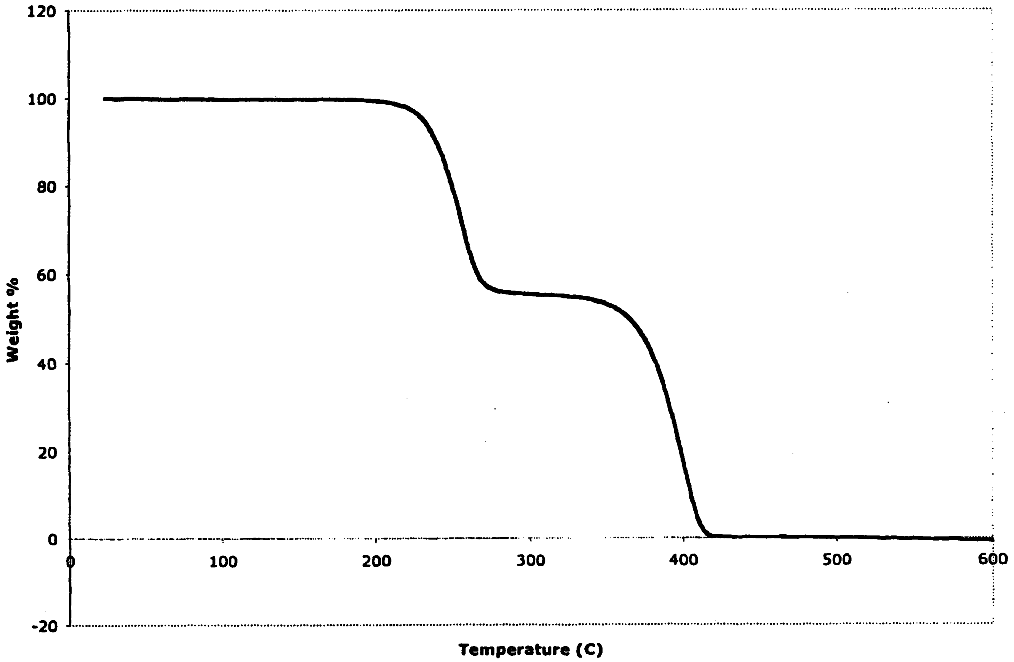

Figure 3. TGA of PLLA-PEO-PLLA triblock copolymer (M_{nPEO} = 8900, DP = 95L)

Downloaded by COLUMBIA UNIV on August 9, 2012 | http://pubs.acs.org
Publication Date: September 23, 2006 | doi: 10.1021/bk-2006-0939.ch010

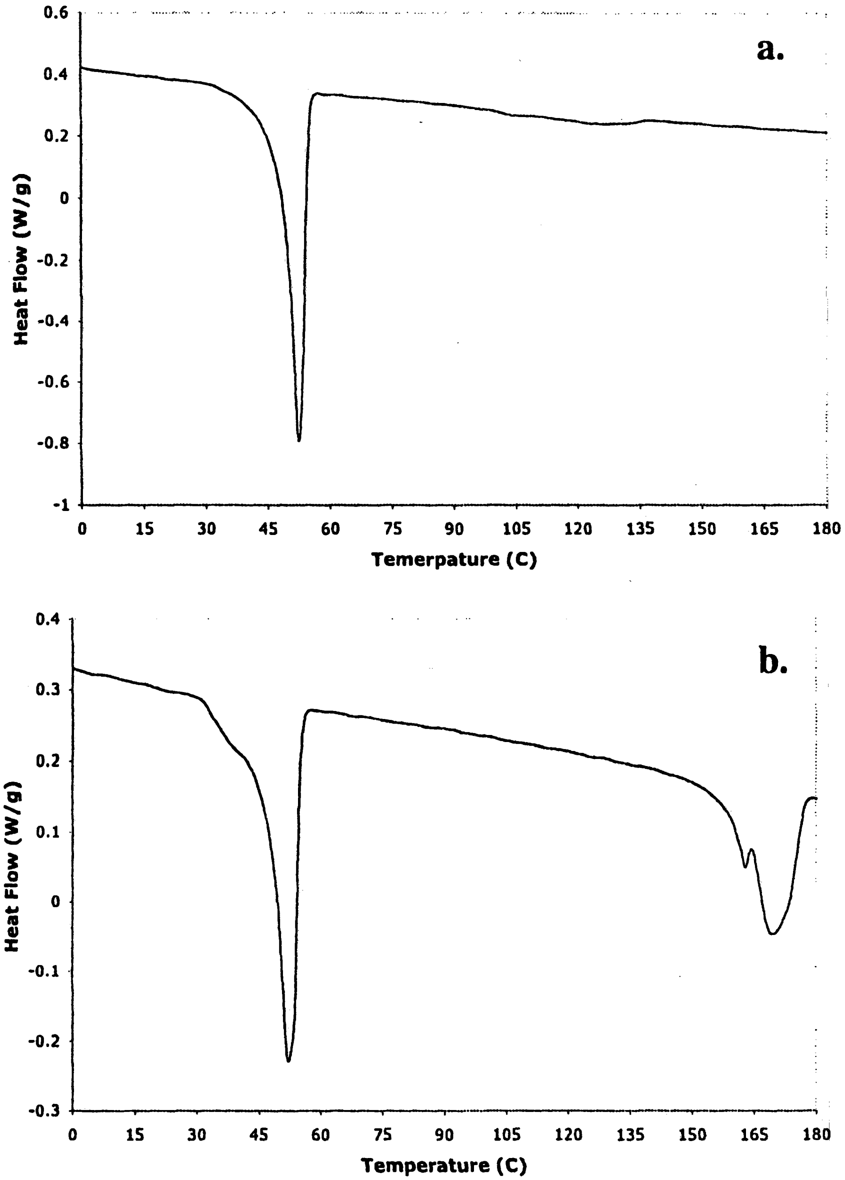

Figure 4. DSC of PLLA-PEO-PLLA with various PLLA block lengths, M_{nPEO} = 8900, a.) DP = 74L, b.) DP = 146L

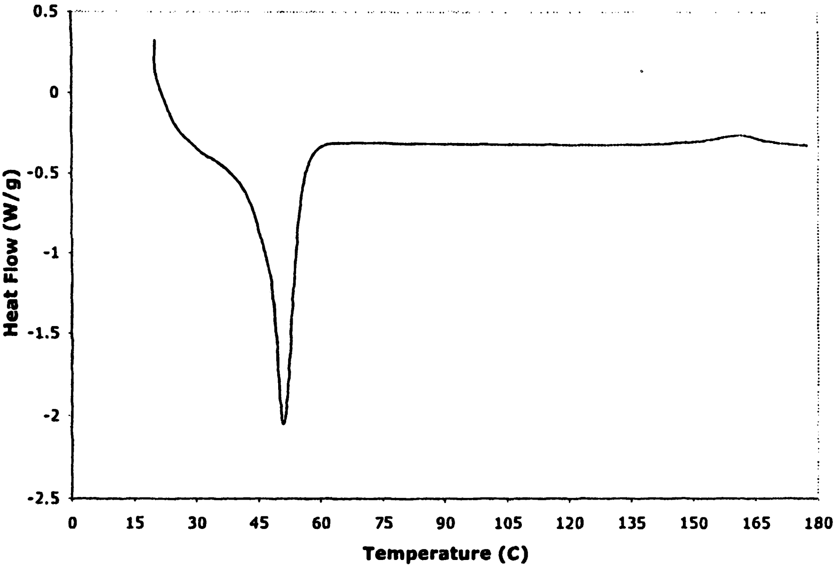

Figure 5. DSC of PLA-PEO PLA triblock copolymer, 1^{st} heating (M_{nPEO} = 8900, DP = 66R)

Aging of PLA-PEO-PLA Triblock Copolymers

It is important to characterize the crystalline properties of the neat polymer prior to hydrogel formation, as it has already been shown that the mechanical properties of the hydrogel are dependent on the ability of the PLA end–blocks to crystallize. Since there have been issues with reproducibility in mechanical properties of hydrogels formed from the same neat polymer, the crystallinity of the neat polymer (freshly precipitated and aged) was analyzed with both DSC and WAXD. However, DSC proved to be less sensitive to changes in crystallinity, so only WAXD data is presented here.

PLLA-PEO-PLLA copolymer (M_{nPEO} = 8900, DP = 77L) was allowed to age at room temperature for approximately 16 months. Half of this sample was redissolved in tetrahydrofuran and precipitated into excess hexanes drop-wise. The collected sample was then dried under vacuum for 2 days at room temperature at which point both samples (aged and reprecipitated) were analyzed with WAXD and the collected diffractograms are shown in Figure 6. The most prominent peaks are visible at $2\theta \approx 17°$, 19°, and 23°. Crystalline PEO is known to diffract at $2\theta \approx 19°$ and 23° [12]. However, crystalline PLLA also diffracts at $2\theta \approx 19°$ and 22°[25-28]. This overlap between the end-blocks and mid-blocks of the triblock copolymer means that these peaks cannot be used to

Downloaded by COLUMBIA UNIV on August 9, 2012 | http://pubs.acs.org
Publication Date: September 23, 2006 | doi: 10.1021/bk-2006-0939.ch010

Downloaded by COLUMBIA UNIV on August 9, 2012 | http://pubs.acs.org
Publication Date: September 23, 2006 | doi: 10.1021/bk-2006-0939.ch010

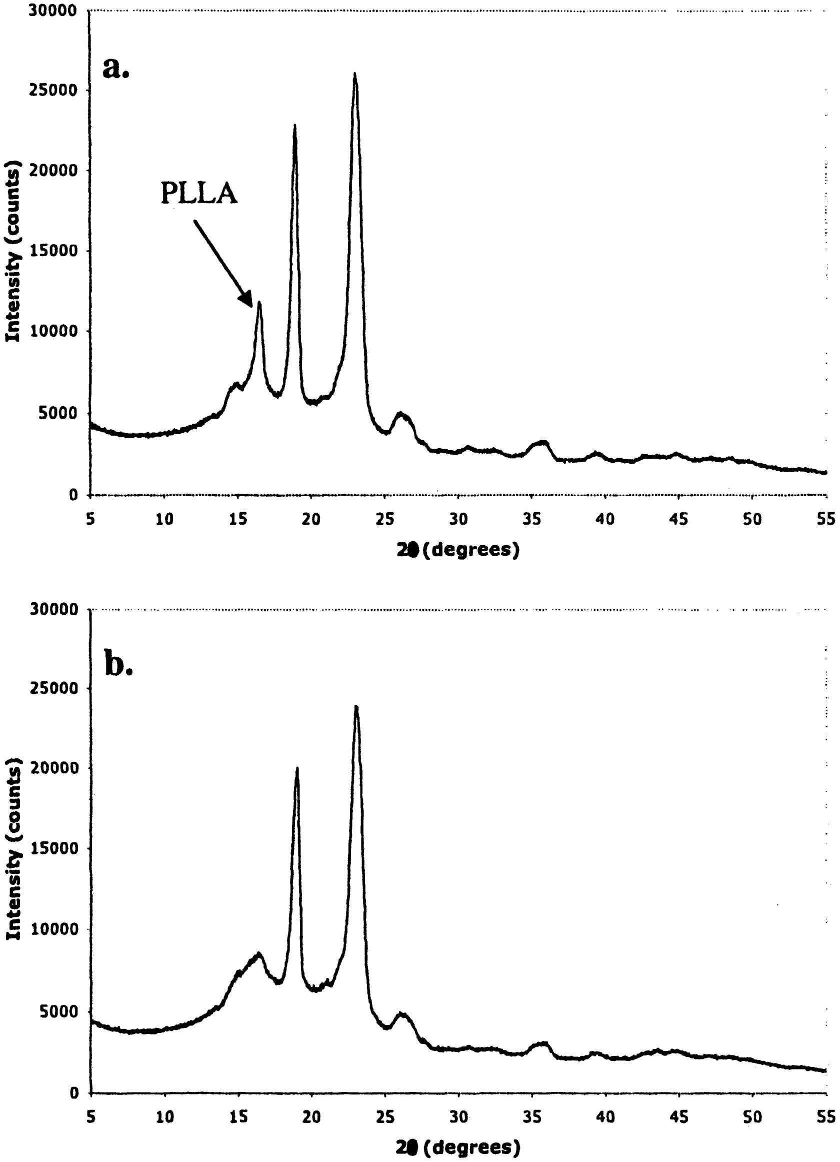

Figure 6. WAXD of PLLA-PEO-PLLA, M_{nPEO} = 8900, DP = 77L. a.) Aged for 16 months. b.) Freshly precipitated.

analyze the aging of the PLLA end-blocks. However, there is a distinct peak for crystalline PLLA at $2\theta \approx 17°$ that does not overlap with crystalline PEO diffraction, and this peak is clearly visible in the aged sample. The freshly precipitated polymer shows a much weaker and broadened peak at the scattering angle of $2\theta \approx 17°$. This data suggests that there is an effect of aging on this polymer, and further studies will be carried out to investigate how the initial crystallinity of the bulk polymer affects the overall crystallinity of the hydrogel.

Downloaded by COLUMBIA UNIV on August 9, 2012 | http://pubs.acs.org
Publication Date: September 23, 2006 | doi: 10.1021/bk-2006-0939.ch010

Conclusions

We have successfully synthesized PLA-PEO-PLA triblock copolymers with control of molecular weight. It was also demonstrated that the synthesis method used is applicable to various molecular weight PEO diol macroinitiators and to both L and DL-lactide. The thermal properties of these copolymers were further characterized to find the PLLA segments of copolymers made with L-lactide are crystallizable in the bulk above a critical length while copolymers made with DL-lactide are not. Furthermore, aging was found to promote PLLA crystallinity. We will continue to analyze the properties of the bulk copolymer, so that we may gain better insight into hydrogel formation and reproducibility.

Acknowledgements

This work utilized central facilities of the NSF-sponsored UMass MRSEC on Polymeric Materials (DMR-0213695). The authors gratefully acknowledge support from NIH (T32 GM08515), NSF, ONR, ARO, and various companies including 3M, DuPont, Bocton-Dickinson, Ethicon, General Electric, and Boston Scientific.

References

1. Hoffman, A. S., *Adv. Drug Deliv. Rev.* **2002**, 43, 3-12.
2. Kim, B.-S.; Mooney, D. J., *TIBTECH* **1998**, 16, 224-230.
3. Lee, K. Y.; Mooney, D. J., *Chem. Rev.* **2001**, 101, (7), 1869-1879.
4. Engler, A. J.; Griffin, M. A.; Sen, S.; Bonnemann, C. G.; Sweeney, H. L.; Discher, D. E., *J. Cell Bio.* **2004**, 166, (6), 877-887.
5. Ingber, D.; Karp, S.; Plopper, G.; Hansen, L.; Mooney, D., In *Physical Forces and the Mammalian cell,* ed.; Frangos, J. A., Academic Press: New York, 1993; 61-79.
6. Huang, S.; Ingber, D. E., *Nat. Cell Bio.* **1999**, 1, 131-138.
7. Lee, K. Y.; Peters, M. C.; Anderson, K. W.; Mooney, D. J., *Nature* **2000**, 408, 998-1000.

8. Choquet, D.; Felsenfeld, D. P.; Sheetz, M. P., *Cell* **1997**, 88, 39-48.
9. Wang, H. B.; Dembo, M.; Wang, Y. L., *Am. J. Physiol. Cell Physiol.* **2000**, 279, C1345-C1350.
10. Li, S. M.; Rashkov, I.; Espartero, J. L.; Manolova, N.; Vert, M., *Macromolecules* **1996**, 29, 57-62.
11. Rashkov, I.; Monolova, N.; Li, S. M.; Espartero, J. L.; Vert, M., *Macromolecules* **1996**, 29, 50-56.
12. Li, S.; Vert, M., *Macromolecules* **2003**, 36, 8008-8014.
13. Jeong, B.; Bae, Y. H.; Lee, D. S.; Kim, S. W., *Nature* **1997**, 388, 860-862.
14. Kissel, T.; Li, Y.; Unger, F., *Adv. Drug Deliv. Rev.* **2002**, 54, 99-134.
15. Lee, D. S.; Shim, M. S.; Kim, S. W.; Lee, H.; Park, I.; Chang, T., *Macromol. Rapid Commun.* **2001**, 22, 587-592.
16. Zhong, Z.; Dijkstra, P.; Feijen, J.; Kwon, Y. M.; Bae, Y. H.; Kim, S. W., *Macromol. Chem. Phys.* **2002**, 203, 1797-1803.
17. Lim, D. W.; Park, T. G., *J. Appl. Poly. Sci.* **2000**, 75, 1615-1623.
18. Fujiwara, T.; Mukose, T.; Yamaoka, T.; Yamane, H.; Sakurai, S.; Kimura, Y., *Macromolecular Bioscience* **2001**, 1, 204-208.
19. Mason, M. N.; Metters, A. T.; Bowman, C. N.; Anseth, K. S., *Macromolecules* **2001**, 34, 4630-4635.
20. Molina, I.; Li, S.; Martinez, M. B.; Vert, M., *Biomater.* **2001**, 22, 363-369.
21. Li, S.; Molina, I.; Martinez, M. B.; Vert, M., *Journal of Mat. Sci.: Mat. in Med.* **2002**, 13, 81-86.
22. Choi, S. W.; Choi, S. Y.; Jeong, B.; Kim, S. W.; Lee, D. S., *Journal of Polym. Sci.: Part A: Polym. Chem.* **1999**, 37, 2207-2218.
23. Aamer, K. A.; Sardinha, H.; Bhatia, S. R.; Tew, G. N., *Biomater.* **2004**, 25, 1087-1093.
24. Tew, G. N.; Sanabria-DeLong, N.; Agrawal, S. K.; Bhatia, S. R., *Soft Matter* **2005**, in press.
25. DeSantis, P.; Kovacs, A. J., *Biopoly.* **1968**, 6, 299-306.
26. Sarasua, J.-R.; Prud'homme, R. E.; Wisniewski, M.; LeBorgne, A.; Spassky, N., *Macromolecules* **1998**, 31, 3895-3905.
27. Pluta, M.; Galeski, A., *J. Appl. Poly. Sci.* **2002**, 86, 1386-1395.
28. Shin, D.; Shin, K.; Aamer, K. A.; Tew, G. N.; Russell, T. P.; Lee, J. H.; Jho, J. Y., *Macromolecules* **2005**, 38, 104-109.

Downloaded by COLUMBIA UNIV on August 9, 2012 | http://pubs.acs.org
Publication Date: September 23, 2006 | doi: 10.1021/bk-2006-0939.ch010

Downloaded by PENNSYLVANIA STATE UNIV on August 28, 2012 | http://pubs.acs.org
Publication Date: September 23, 2006 | doi: 10.1021/bk-2006-0939.ch011

Chapter 11

Degradable Poly(ethylene oxide)-*block*-Polycaprolactone Worm Micelles

Yan Geng and Dennis E. Discher

Department of Chemical and Biomolecular Engineering, University of Pennsylvania, Philadelphia, PA 19104–6391

Novel giant and flexible worm micelles were self-assembled from degradable copolymer poly (ethylene oxide)-*block*-polycaprolactone (OCL). Such worm micelles spontaneously shorten to spherical micelles, triggered by hydrolytic degradation of polycaprolactone. Unique degradation mechanism and kinetics in OCL worm micelles were elucidated, and key activating conditions of temperature, pH, and polymer molecular weight were quantitatively assessed. We have also demonstrated that degradable OCL worm micelles possess great potenial as novel controlled-release drug delivery vehicle: they are compatible with cultured cells and blood, capable of loading a model hydrophobic anti-cancer drug (taxol), easy storage, and the release of the drug is controlled by OCL worm micelle degradation rate.

In Degradable Polymers and Materials; Khemani, K., et al.;
ACS Symposium Series; American Chemical Society: Washington, DC, 2006.

Introduction

Degradable polymers are crucial to a number of fields ranging from agricultural, environmental to biomedical applications (*1*). Degradable homopolymers and random copolymers have been widely used as in bulk materials, micro/nano-particles, and films/ monolayers, and a great deal of study has focused on their degradation mechanism and kinetics. (*2-5*) In recent years, degradable self-assemblies of block copolymer amphiphiles are also emerging and have attracted considerable attentions. (*6-9*)

Self-assemblies of amphiphilic block copolymers with a hydrophilic block covalently connected to a hydrophobic block are a rapidly emerging subclass of colloids. Like conventional small-molecule surfactants (<1kD), amphiphilic block copolymers are capable of self-assembling into spherical and cylindrical micelles, as well as vesicles that define at least three stable morphologies. (*6*) Different self-assembly morphology is generally dictated by block proportions (*10*), and desired physical-chemical-mechanical properties can be tuned through molecular weight (Mn), structure of each block, modification and crosslinking (*11-14*). Such flexibility in design of copolymer "macro"-surfactant offers clear material advantages over small surfactants. Moreover, copolymer assemblies are much more stable systems compared to small surfactants, since they generally have much lower critical micellar concentration (CMC) and slower dissociation rate. (*6*) These features of diblock copolymers make them potentially useful in many applications, in particular drug delivery, where the outer hydrophilic corona, generally poly(ethylene oxide) (PEO), maximizes biocompatibility and helps micelles escape rapid reticuloendothelial system (RES) clearance after intravenous administration and prolongs their circulation in blood, and the hydrophobic micellar core can encapsulate the drugs with poor water solubility. (*15*) Compared to non-degradable polymer, using degradable polymer as the hydrophobic block of the copolymers offers advantages of being able to degrade into non-toxic low-molecular weight molecules that can be either absorbed by the body or removed by metabolism and mediate the release of the encapsulated drug as it degrades.

Attention on self-assemblies of degradable copolymers has thusfar been limited to spherical micelles, typically from copolymers of hydrophobic polyesters such as polylactides and polycaprolactone connected with hydrophilic PEO. (*7-9*) However, degradation has subtle if detectable effects on the spherical morphology, and degradation mechanisms and kinetics in spherical micelles have not been clearly distinguished in time scales or mechanisms from those in bulk or film. (*7-9*) In this book chapter, we described novel giant and flexible worm micelles self-assembled from degradable poly (ethylene oxide)-*b*-poly(ε-caprolactone copolymers (PEO-PCL, denoted OCL). Such OCL worm micelles spontaneously shorten to generate spherical micelles due to polycaprolactone hydrolytic degradation. Unique degradation mechanism and kinetics in OCL worm micelles are elucidated, and key activating conditions of temperature, pH,

Downloaded by PENNSYLVANIA STATE UNIV on August 28, 2012 | http://pubs.acs.org
Publication Date: September 23, 2006 | doi: 10.1021/bk-2006-0939.ch011

and polymer molecular weight are quantitatively assessed in this context of a microphase transition. (*16*)

Up to date, drug delivery vehicles are overwhelmingly spherical in shape. And worm micelles are just now emerging as a novel system that provides larger core volume to load drugs and is able to flow readily through capillary and pores, due to their cylindrical morphology and flexibility. (*17,18*) Recently, *in-vivo* injection of worm micelles into tail vein of rats has shown that they are able to circulate much longer than any spherical synthetics. (*19*) One useful and novel strategy for drug delivery is to start as worm micelles with larger drug loading capacity and longer circulation time and later degrade into spherical micelles, which are already proven to be extremely useful for therapeutic applications (*20*). With clarified mechanism/kinetics, such degradability of worm micelles could also be exploited to control drug release. In this book chapter, we also described the evaluation of of degradable OCL worm micelles as drug delivery vehicle: their biocompatibility with cultured cells as well as blood, loading of hydrophobic anti-cancer drug taxol, and how degradation influences the release kinetics of taxol. (*21*)

Downloaded by PENNSYLVANIA STATE UNIV on August 28, 2012 | http://pubs.acs.org
Publication Date: September 23, 2006 | doi: 10.1021/bk-2006-0939.ch011

Experimental

Materials

Diblock copolymers OCL of two molecular weights, OCL1 (M_n = 4770, polydispersity PD = 1.19) and OCL3 (M_n = 11,000, PD = 1.3) were from Polymerscource Inc. They were prepared by living anionic polymerization of ethylene oxide followed by ring-opening polymerization of *ε*-caprolactone. (*7*) Dialysis tubing, syringe filter, glass slides and coverslips were from Fisher, and all other chemicals were from Sigma-Aldrich.

Preparation of OCL Worm Micelles by Cosolvent/evaporation Method

100 µl of 10 mg/mL OCL1 or OCL3 stock solution in chloroform was added to a glass vial. Chloroform was removed under nitrogen. The remaining OCL film was then re-dissolved in 30µl chloroform, and 5 mL of water was added to the vial and stirred vigorously for 1-2 hours, yielding an opaque worm micelle dispersion (0.2mg/ml). Chloroform (~ 0.5% of solution volume) was then slowly removed by evaporation at 4°C to minimize OCL worm micelle degradation. After 24 hours, the OCL worm micelle solution turned clear and did not contain detectable chloroform, confirmed by gas chromatography (GC) with the detection limit of 0.01% volume fraction of chloroform. The CMC of OCL copolymers is around 1.2 µg/ml (*22*), therefore OCL copolymers are mainly in the form of micelles since its concentration exceeds CMC by a factor of 100.

Visualization of OCL Worm Micelles

Olympus IX71 inverted fluorescence microscope with a 60X objective and a Cascade CCD camera was used to visualize OCL worm micelles. A hydrophobic fluorophore dye (PKH 26) was added to the OCL worm micelles, and 2 μL sample was used in the glass slide-cover slip chamber and approximately 20 pictures were taken per sample. Analysis detail was described elsewhere (*23*). Cryo-TEM was also used to visualize OCL worm micelle morphological change. Sample preparation and analysis was described elsewhere. (*14*)

Downloaded by PENNSYLVANIA STATE UNIV on August 28, 2012 | http://pubs.acs.org
Publication Date: September 23, 2006 | doi: 10.1021/bk-2006-0939.ch011

Gel Permeation Chromatography (GPC) Studies on OCL Worm Micelle Degradation

At different times, 1 ml of 0.2 mg/ml OCL worm micelles was lyophilized, re-dissolved in 150 μl THF, passed through a 0.4 μm syringe filter and then analyzed by GPC. A Waters Breeze GPC equipped with Styragel HR2 and HR3 columns, connected with a refractive index detector was used. The mobile phase was THF and the flow rate was 1.0 mL/min. The copolymer peak was characterized by PEG standards. The predominant new peak generated with OCL worm micelle shortening was identified by "spiking" with standard monomer 6-hydroxycaproic acid (6-HPA) (Sigma-Aldrich: 6-HPA 80 wt%, mixed with other possible PCL hydrolysis products: dimmer, trimmer, tetramer and larger caprolactone oligomers). 6-HPA yield was estimated from its standard calibration curve that correlates peak area with amount.

^{1}H Nuclear Magnetic Resonance

^{1}H NMR was used to determine the loss of caprolactone units from OCL copolymer with worm micelle shortening. 20 ml of 0.2 mg/ml OCL worm micelles at different degradation time was lyophilized, after removing all possible degradation products by dialysis at 4°C, and re-dissolved in chloroform (*d*) for ^{1}H NMR analysis on a Bruker 300 MHz spectrometer. At different degradation time, caprolactone units (PCL_t) remained in the copolymer was estimated from comparing the summary of integral of PCL_t methylene peaks ($\delta \sim$ 4.0 ppm **t**, 2.3 ppm **t**, 1.6 ppm **m**, 1.3 ppm **m**, total proton = $10 \times \text{unit}_{PCLt}$) to the integral of PEO methylene peak ($\delta \sim$ 3.6ppm s, total proton = $4 \times \text{unit}_{PEO}$), which is non-degradable and remains constant with OCL worm micelle shortening.

Cell Culture

Bovine aortic endothelial cells and vascular smooth muscle cells were purchased from ATCC (American Type Culture Collection). Cells were plated and allowed to attach for 12 h, after which a measured dose of OCL worm micelles in PBS was added to each plate. Cell viability after exposure to OCL worm micelles for up to 5 days was assayed by Trypan Blue exclusion.

Hemolysis Study

Fresh whole blood was pelleted by centrifugation and 100 μl of the collected red blood cell (RBC) suspension was added to 900 μl of 10 mg/ml OCL worm micelles in PBS (RBC: 10% hematocrit in PBS). The samples were incubated for 24 hours at 37°C. The release of hemoglobin in the supernatant, collected by centrifugation, was measured by UV-Vis at 412 nm and compared to the complete hemolysis by 0.2% small surfactants Triton X-100.

Taxol Loading

Stock solutions of taxol in methanol (5mg/ml) was added with a weight ratio of 0.2:1 to 1 ml of OCL worm micellar solutions at different concentrations and vortexed for 5 minutes. The small amount of methanol was removed by dialysis at 4 °C for 2 hours. Unloaded taxol precipitate was centrifuged down at 3000 rpm for 5 min and further removed from the micelle supernatant by filtering with a 0.45 μm pore-sized syringe filter. The amount of taxol loaded into OCL worm micelles was then determined by HPLC. A Waters Breeze HPLC equipped with a diode array UV detector set at $\lambda = 220$ nm, connected with a Symmetry C-18 column, methanol as the mobile phase, and a flow rate of 0.8 mL/min was used. Taxol is well resolved from OCL peak, and the amount of taxol was estimated from its calibration curve that correlates peak area with amount.

Taxol Release

The release behavior of taxol from OCL worm micelles under different pH buffers (0.01 M PBS pH 7 and 0.01 M HEPES pH 5) was studied by dialysis at 37°C. 10 ml of taxol-encapsulated 0.2 mg/ml OCL worm micelle in a dialysis tubing (MWCO: 1000) was placed in a l L beaker filled with buffer solutions. At specific time intervals, a 150 μl aliquot was removed from the dialysis bag, lyophilized and re-dissolved in CHC13. Buffer salt was centrifuged down at 3000 rpm for 5 min and further removed from the micelle supernatant by filtering with a 0.45 μm pore-sized syringe filter. CHC13 was then evaporated under N2 and the mixture of taxol and OCL polymer was redissolved in 150 μl methanol and filtered through a 0.45 μm pore-sized syringe filter before injecting into HPLC. The amount of taxol remained in the dialysis bag was thus estimated from its

Downloaded by PENNSYLVANIA STATE UNIV on August 28, 2012 | http://pubs.acs.org
Publication Date: September 23, 2006 | doi: 10.1021/bk-2006-0939.ch011

calibration curve and the percentage of released taxol was calculated as % Release = (total taxol – taxol remained in dialysis bag)/total taxol × 100%.

Results and Discussion

Degradation Mechanism and Kinetics of OCL Worm Micelles

Downloaded by PENNSYLVANIA STATE UNIV on August 28, 2012 | http://pubs.acs.org
Publication Date: September 23, 2006 | doi: 10.1021/bk-2006-0939.ch011

Giant and flexible worm micelles were self-assembled from degradable copolymer OCL (OCL1 $Mn \sim 4700$, OCL3 $Mn \sim 11{,}000$) with weight fraction of PEO, $f_{EO} \sim 0.42$, that favors worm micelle formation (*10*), Figure 1a-0hr. The contour of the OCL worm is well resolved and considerable exceeds the optical resolution of the fluorescence microscope. Sequential snap-shots exhibiting thermal fluctuations of a single worm micelle, Figure 1b, demonstrate its flexibility. Overlays of skeletonized contours show that the distance R between worm ends fluctuates considerably, allowing evaluation of the thermal average $\langle R^2 \rangle = 2l_p^2[L/l_p - 1 + \exp(-L/l_p)]$ in terms of the measured contour length L of the worm and the flexibility as persistence length, l_p. (*23*) From analysis of ~ 100 worm micelles, we determine an average $l_p = 500 \pm 200$ nm for OCL1, and 5 ± 2 µm for OCL3 respectively. Both the persistence length l and diameter d of OCL worm micelles ($d \approx 11$ nm for OCL1 and 29 nm for OCL3 as measured by TEM) are essentially the same as those of worm micelles made from non-degradable PEO-PBD with similar M_n and likewise fit well to the scaling relation $l_p \sim d^{2.8}$ that is indicative of a fluid rather than a glassy aggregate. (*24*) Distribution of measurable contour lengths (> 1µm) of OCL worm micelles was plotted from ~ 200 worms measured by FM and fit with a Gaussian curve, Figure 1c at 0 hr. A mean contour length $<L> \sim 15$ µm for OCL1 and $<L> \sim 18$ µm for OCL3 is estimated from their distribution curves respectively.

On time scales of days, these giant OCL worm micelles spontaneously shorten to spherical micelles as observed by FM and Cryo-TEM, Figure 1a. The contour length shortening of OCL worm micelles can be quantitatively analyzed by tracing contour length distribution curves changing with time, Figure 1b. The mean contour length $<L>$ clearly shrinks from the initial long worms towards spheres with time, while the distribution curve narrows as well. It takes ~ 28 hours for OCL1 and ~ 200 hours for OCL3 worm micelles to completely transit into spherical micelles at 37°C in water.

As OCL worm micelles shorten to spherical micelles with time, the PCL hydrolysis monomer product, 6-hydroxycaproic acid (6-HPA), was found by GPC as the predominant new species generated, Figure 2. 6-HPA peak is well resolved from dimer, trimer, and larger caprolactone oligomers, and no other significant degradation products were detected, Figure2b. The polydispersity of

Downloaded by PENNSYLVANIA STATE UNIV on August 28, 2012 | http://pubs.acs.org
Publication Date: September 23, 2006 | doi: 10.1021/bk-2006-0939.ch011

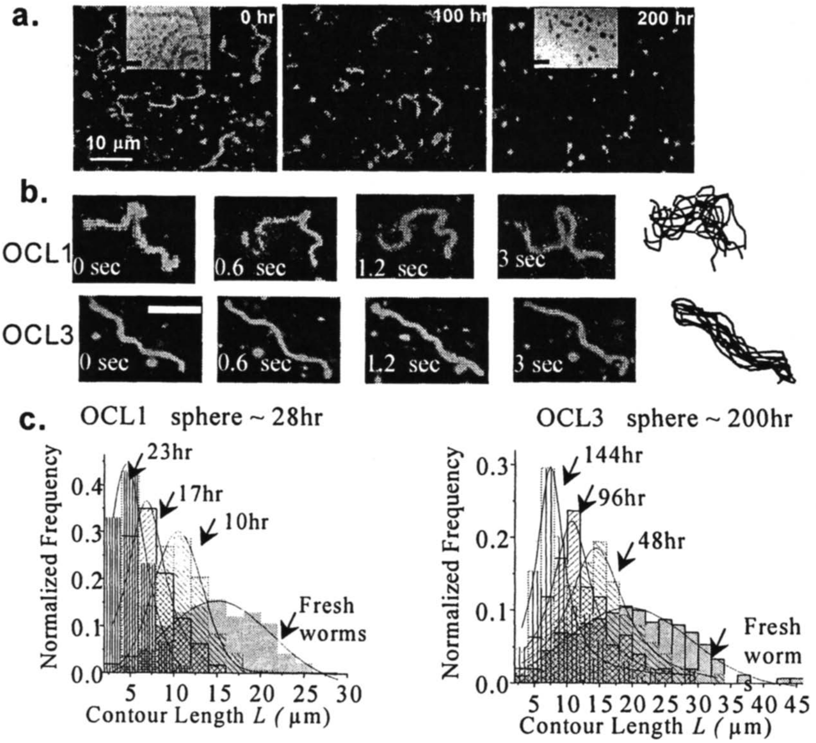

Figure 1. Self-assembled OCL worm micelles spontaneously shorten to spherical miceller. ***a.*** *Visualized by FM and cryo-TEM(inset, bar=100nm)* ***b.*** *Dynamic snapshots of single OCL worm micelle* ***c.*** *Contour length distributions. (Reproduced from reference 16. Copyright 2005 ACS)*

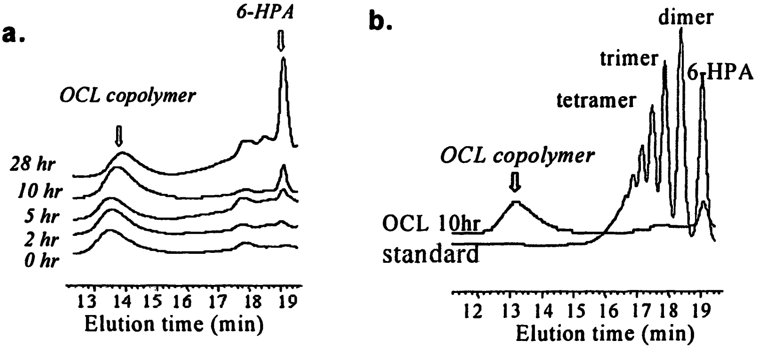

Figure 2. ***a.*** *GPC chromatograms of OCL1 worm micelle at different degradation times, at 37 °C.* **b.** *Identification of monomer 6-HPA with standards. (Reproduced from reference 16. Copyright 2005 ACS)*

OCL copolymer remained essentially the same, Figure 2a, and the loss of caprolactone units from OCL copolymer was further confirmed by NMR, Figure 3. Quantitative accumulation of 6-HPA, Figure 4a, parallels both in form and time-scales of the decays in mean contour length of OCL worm micelles for both copolymers, Figure 4b. The analytical results thus demonstrate that PCL in

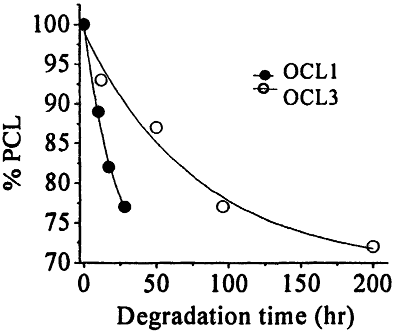

Figure 3. Percentage of caprolactone units remained in OCL copolymer with degradation by ^1H NMR. (Reproduced from reference 16. Copyright 2005 ACS)

these copolymers hydrolyzes from the end by "chain-end cleavage" rather than by "random-scission" that would yield various degradation products and broaden the polydispersity of the polymer far more than found here. (*25*)

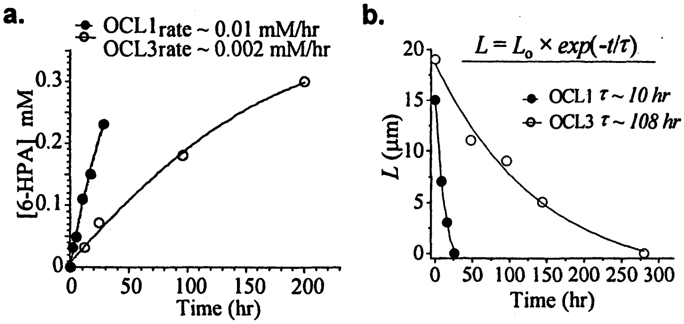

Figure 4. a. Cumulative production of PCL hydrolysis monomer, 6-HPA with b. the decay of OCL worm micelle mean contour length L (37 °C, pH 5 buffer). (Reproduced from reference 16. Copyright 2005 ACS)

End-hydrolysis of PCL increases f_{EO} and consequently shifts the preferred morphology towards a higher curvature structure. (*10*) By the time worms have

Downloaded by PENNSYLVANIA STATE UNIV on August 28, 2012 | http://pubs.acs.org
Publication Date: September 23, 2006 | doi: 10.1021/bk-2006-0939.ch011

disappeared, PCL chains have on average lost ~ 30% of their length by hydrolysis, Figure 4a, which corresponds to increases in f_{EO} from 0.42 to 0.55. Such f_{EO} above 0.5 favors spherical micelle formation. (*10*) This simple estimation highlights the reason why worm micelles are so susceptible to morphological transformation: only an extremely narrow range of f_{EO} favors the worm micelle structure, whereas spherical micelles are found with a much broader range of f_{EO} and are thus less sensitive to hydrolysis (*10*).

The worm-to-sphere transition occurs with bulb formation at the end of the worm, consistent with release of spherical micelles from the end, Figure 5. (*26*) Conservation of mass allows one to show that the hydrolysis kinetics is the rate-limiting step in worm shortening kinetics. The amount of monomer generated initially from OCL1 and OCL3 worm micelles, ~0.01 and 0.002 mM/hr, respectively, Figure 4a, gives the volume of spherical micelles generated from the worm micelles, based on the above changes in f_{EO} and PCL's volume density. The estimations yield respective shortening rates of ~1.0 and 0.1 μm/hr as observed in FM, Figure 4b. Such estimations apply equally well to the two copolymers that differ in *M*n and thus differ in molecular mobility within worms by far more than two-fold. (*13*) This suggests that the rate-limiting process is indeed hydrolysis rather than chain diffusion and segregation post-hydrolysis.

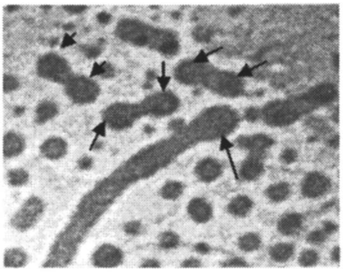

Figure 5. OCL worm-to-sphere transition occurs with bulb formation (arrow) at the end of the worm. (Reproduced from reference 16. Copyright 2005 ACS)

While the end-cleavage of PCL within worm micelles appears consistent with both the chemical and the nano-scale physical changes, it is also considerably faster than the slow hydrolysis reported for PCL homo/copolymer bulk, particle, or films, i.e. on the time scale of months-years under the same condition. (*2-5*) The distinction arises with the specific effect of OCL worm micelles on PCL hydrolysis. As speculated from studies on spherical micelles (*27*), the terminal -OH of the hydrophobic PCL block is not strictly sequestered in the 'dry', hydrophobic core but tends to be drawn into the hydrated corona. A 'micellar catalysis' effect involving interfacial water (*28*) plus the likely

Downloaded by PENNSYLVANIA STATE UNIV on August 28, 2012 | http://pubs.acs.org
Publication Date: September 23, 2006 | doi: 10.1021/bk-2006-0939.ch011

participation of the terminal -OH (*29*) collectively foster the attack by H_2O of the end-ester group nearest the terminus -OH. Following this ester hydrolysis, a new -OH is generated to restart the process of PCL end-cleavage. To provide direct evidence for the crucial role of the terminal -OH, -OH was modified in OCL1 to an acetate group by esterification. Worm micelles still formed with OCL1-acetate, but they showed no significant morphological change after more than 24 hrs at 37°C, by which time OCL1 worm micelles are completely degraded.

For both OCL1 and OCL3 worm micelles, shortening rate constants measured from FM increase exponentially with temperature, with minimal degradation at 4°C but considerable hydrolysis at the physiological temperature of 37°C. The temperature dependences fit classic Arrhenius behavior and yield activation energies E_a for the morphological transformations, Figure 6.

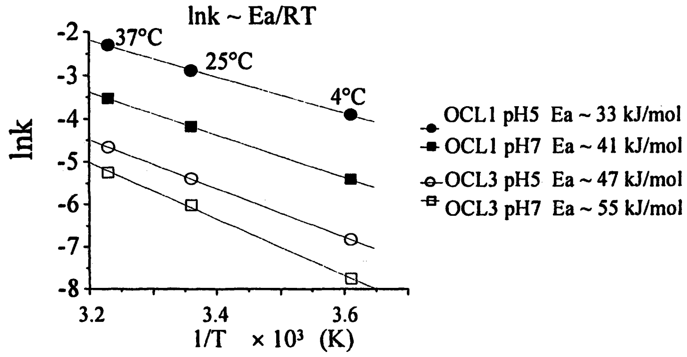

Figure 6. Arrhenius plots of OCL worm micelle shortening rate constants, k, with temperature. (Reproduced from reference 16. Copyright 2005 ACS)

Consistent with acid -catalyzed ester hydrolysis, acidic pH 5 (physiological HEPES buffer) enhances the shortening rate by 2-4 fold systematically and also lowers E_a by 7-8 kJ/mol, compared to neutral pH7 (PBS buffer). At either pH, the higher M_n OCL3 decreases the shortening rate by 3-4 folds and raises E_a by 10 kJ/mol compared to OCL1. This higher E_a is consistent with a larger entropic penalty for an activated reptation (*13*), i.e. entanglement release, of the terminal hydroxyl group of the longer OCL3 chain to the micellar interface. Moreover, the values for E_a (33-55 kJ/mol) of OCL worm micelle shortening are in good agreement with E_a of homogeneous hydrolysis of water-soluble polyester oligomers reported in literature (*30*). This adds to the proof that PCL hydrolysis is the driving force for worm micelle shortening and that such hydrolysis is surprisingly homogeneous rather than heterogeneous and limited – as seen in polyester degradation of bulk and particles – by the infiltration of water.

Downloaded by PENNSYLVANIA STATE UNIV on August 28, 2012 | http://pubs.acs.org
Publication Date: September 23, 2006 | doi: 10.1021/bk-2006-0939.ch011

Evaluation of Degradable OCL Worm Micelles for Drug Delivery

In-vitro Compatibility with Cultured Cells and Blood

Bovine aortic endothelial cells and vascular smooth muscle cells exposed to OCL worm micelles in PBS with a dose of 5 mg/ml showed no ill-effects for up to 5 days. OCL worm micelles and their degradation product, 6-hydroxycaproic acid are non-toxic and compatible with cultured cells. Incubating OCL worm micelles with whole blood for two days at 37°C shows that they don't stick to red blood cells (RBC) and remains suspended in plasma and retains their flexibility. Also, hemolysis study on OCL worm micelles (10mg/ml) shows negligible hemolytic activity (< 1%). (*21*)

The current clinical formulation of anti-cancer drug taxol is in a 50:50 mixture of Cremophore EL and ethanol, which is physically incompatible with intravenous infusion system and causes serious side effects such as hypersensitivity and neurotoxicity. (*31*) Here, degradable OCL worm micelles prove to be compatible with cultured cells and blood, offering great advantage over the conventionally surfactants as a potential alternative carrier for taxol.

Taxol Loading into OCL Worm Micelles

Like spherical polymeric micelles (7-9), the hydrophobic core of OCL worm micelles solubilizes and encapsulates the hydrophobic solute molecules. Taxol has very low water solubility of approximately 1 μg/ml (*32*), and is physically loaded into OCL worm micelles with a molar ratio of 1:7 for OCL1 and 1:2 OCL3 respectively, determined by HPLC. The loading molar ratio does not change with OCL worm micelle concentrations. Such loading capability of OCL worm micelles significantly enhances the solubility of taxol in water, e.g. 10–15 wt% OCL worm micelles can dissolve 3-7.5 mg taxol per ml, comparable to the maximum taxol solubility in Cremophore EL formulation (6mg/ml) (*31*). Another advantage of using worm micelles as carrier for taxol is that each micron-long worm micelles provide much larger core volume compared to the same-diametered spherical micelles and thus can load much more drug per carrier. Moreover, loading taxol into the core doesn't significantly change the flexibility, degradation kinetics of the OCL worm micelles (studied by FM).

In-vitro Release of Taxol from OCL Worm Micelles

Release kinetics of taxol from OCL worm micelles was studied by dialysis method under "sink condition". Figure 7 shows the percentage of taxol released from OCL1 and OCL3 worm micelles versus time at 37°C, under pH 5 Hepes and pH 7 PBS physiological buffers respectively. After an initial burst release, typical for polymeric micelle systems (*7*), a much slower and sustained release

Downloaded by PENNSYLVANIA STATE UNIV on August 28, 2012 | http://pubs.acs.org
Publication Date: September 23, 2006 | doi: 10.1021/bk-2006-0939.ch011

Downloaded by PENNSYLVANIA STATE UNIV on August 28, 2012 | http://pubs.acs.org
Publication Date: September 23, 2006 | doi: 10.1021/bk-2006-0939.ch011

was observed till completion: taxol was released over 10 hours period at pH 5 and 36 hours at pH 7 for OCL1, and for OCL3, taxol was released over 3 days period at pH 5 and 8 days period at pH 7 respectively. The initial burst release is probably due to the localization of some of the drug at the core-corona interface region, which doesn't have to diffuse through the large segments of the core to exit the micelle and its release is rapid. (*7*)

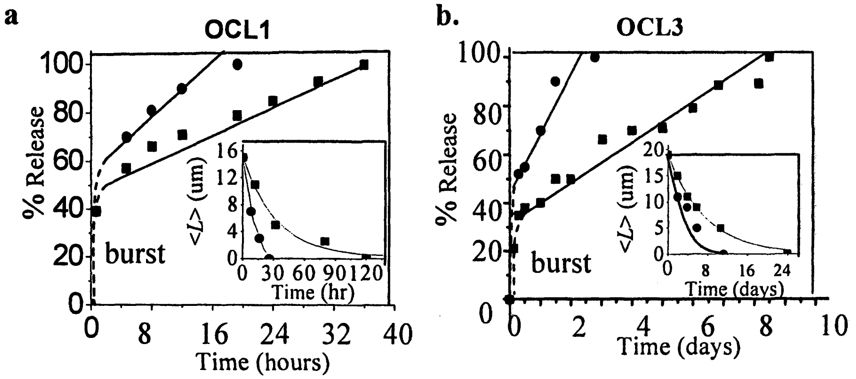

Figure 7. Release profiles of taxol from (a) OCL1 and (b) OCL3 worm micelles in pH 5 Hepes(●) and pH 7 PBS buffers (■) at 37 °C.Insets are the corresponding degradation-induced OCL worm micelle contour length shortening with time.

For both copolymer OCL1 or OCL3, the gradual release after the initial burst release is 2-4 fold faster in acidic pH 5 than in pH 7 buffer at 37°C, Figure 5. Controll experiment of taxol release from OCL1 worm micelles at 4°C, where degradation is negligible, show that the diffusivity-controlled release kinetics are similar under two buffers, demonstrating that the faster release in acidic buffer is not due to diffusivity but rather degradation. (*21*) Further comparison of taxol release rate with the corresponding OCL worm micelle shortening/degradation rate at 37° (inset) demonstrates that taxol release is indeed dominated by degradation. Taxol was released at ~3%/hour pH 5, ~1.5%/hour pH 7 for OCL1, and ~ 0.5%/hour pH 5, ~ 0.3%/hour pH 7 for OCL3 respectively. Whereas the corresponding degradation induced decay of mean contour length of OCL worm micelles are initially linear and the shortening rates, expressed as percentage of length shortened compared to initial length per hour: 3.8%/hour pH 5, 2%/hour pH 7 for OCL1, and ~ 0.5%/hour pH 5, ~ 0.3%/hour pH 7 for OCL3, are essentially the same as the taxol release rate. This implies a tight coupling between degradation and release.

Such degradation-dominant release behavior enables controlled drug release via tuning the degradation rate of OCL worm micelles. For example, low pH fosters degradation rate and release of the drug, which is especially interesting encapsulated inside OCL worm micelles with relatively slow release rate during circulation in blood plasma (pH 7), much faster release occurs once the micelles reach the tumor site where pH is lower than that in the normal tissue. (*33*) Furthermore, since polymeric micelles are usually internalized into the cells by endocytosis *(34),* the acidic environment of endosome/lysosome leads to accelerated drug release inside the cancer cells and faster therapeutic effect.

Downloaded by PENNSYLVANIA STATE UNIV on August 28, 2012 | http://pubs.acs.org
Publication Date: September 23, 2006 | doi: 10.1021/bk-2006-0939.ch011

Conclusion

In summary, worm micelles self-assemble from degradable PEO-*b*-PCL block copolymers and spontaneously shorten to spherical micelles. Such morphological transition is triggered by hydrolytic degradation of PCL, governed by an end-cleavage mechanism that is faster than in bulk/film. Degradation rate can be tuned by temperature, pH and M_n and quantitative assessment appears consistent with the molecular explanation whereby the hydroxyl end of the PCL chain localizes to the hydrated interface of the micelle. Degradable PEO-PCL worm micelles prove to be compatible with cultured cells and blood, capable of loading a model anti-cancer drug taxol into the hydrophobic core with convenient storage. Subsequent release of taxol is dominated by OCL worm micelle degradation, demonstrating great potential as a novel controlled-release drug delivery vehicle.

References

1. Scott, G.; Gilead, D. *Degradable Polymer;* Chapman & Hill: London 1995.
2. Gref, R.; Minamitake, Y.; Peracchia, M. T.; Trubetskoy, V.; Torchilin, V.; Langer, R. *Science* **1994**, 263, 5153.
3. Li, S.; Vert, M., Petrova, T.; Manolova, N.; Rashkov, I. *J. of Applied Polymer Science* **1998**, *68*, 989-998.
4. Lee, W-K; Gardella J. A. *Langmuir* **2000**, 16, 3401-3406.
5. Chen, D.; Chen, H.; Bei, J.; Wang, S. *Polym. Int.* **2000**, *49*, 269.
6. Alexandridis, P.; Lindman, B. Amphiphilic Block Copolymers: Self assembly and Applications; Elsevier: New York, 2000.
7. Soo, P.L.; Luo, L.; Maysinger, D.; Eisenberg, A. *Langmuir* **2002**, 18, 9996-10004.
8. Piskin, E.; Denkbas, E. B.; Kucukyavuz, Z. *Journal of Biomaterials Science. Polymer Ed.* **1995**, 7, 359-373.

9. Shin, IL G.; Kim, S. Y.; Lee, Y. M.; Cho, C. S.; Sung, Y. K. *J. Controlled Release* **1998**, 50, 79-92.
10. Jain, S.; Bates, F. S. *Science* **2003**, *300*, 460-464.
11. Discher, B. M.; Won, Y. Y.; Ede, D. S.; Lee, J. C. M.; Bates, F. S.; Discher, D. E.; Hammer, D. A. *Science* **1999**, *284*, 1143.
12. Discher, B. M.; Bermudez, H.; Hammer, D. A.; Discher, D. E. *J. Phys. Chem. B* **2002**, *106*, 2848-2854.
13. Lee, J. C. M.; Santore, M.; Bates, F. S.; Discher, D. E. *Macromolecules* **2002**, *35*, 323-326.
14. Bermudez, H.; Brannan, A. K.; Hammer D.A.; Bates F. S.; Discher D. E. *Macromolecules* **2002**, *35*, 8203
15. Discher, D. E.; Eisenberg, A. *Science* **2000**, *297*, 967.
16. "Hydrolytic Degradation of Poly(ethylene oxide)-*block*-Polycaprolactone Worm Micelles" Geng, Y.; Discher, D. E. *J. Am. Chem. Soc.* **2005,** *127 (37), 12780-12781.*
17. Dalhaimer, P.; Bates, F. S.; Discher, D. E. *Macromolecules* **2003**, 36, 6873.
18. Kim, Y.; Dalhaimer, P.; Christian, D. A.; Discher, D. E. *Nanotechnology* **2005**, 16 (7), S484
19. "Long Circulating Cylinder Micelles Demonstrate the Strong Effects of Morphology on Biological Transport and Interactions" Dalhaimer, P.; Geng, Y. and Discher, D. E. et. al. *to be submitted*
20. Kataoka, K.; Harada, A.; Nagasaki, Y. *Adv. Drug Deliv. Rev.* **2001**, *47*, 113-131.
21. "Visualization of Degradable Worm Micelle Breakdown and Relation to Drug Release" Geng, Y.;Discher, D. E. *Polymer*, **2005,** invited paper
22. Luo, L.; Tam, J.; Maysinger, D.; Eisenberg, A. *Bioconjugate Chem.* **2002,** *13,* 1259-1265
23. Geng Y, Ahmed F, Bhasin N, Discher, D. E. *J. Phys. Chem. B* **2005**, *109 (9)*: 3772-3779
24. Dalhaimer, P.; Bermudez, H.; Discher, D. *Journal of Polymer Science B: Polymer Physics* **2003,** *42*, 168-176.
25. Belbella, A.; Vauthier, C.; Fessi, H.; Defissaguet, J.P.; Puisieux F. *International Journal of Pharmaceutics* **1996**, *129*, 95-102.
26. Burke, S., Eisenberg, A. *Langmuir,* **2001**, 21, 6705
27. Nie, T.; Zhao, Y.; Xie, Z.; Wu, C. *Macromolecules* **2003**, 36, 8825-8829
28. Fendler, J. H.; Fendler, E. J. Catalysis in Micellar and Macromolecular Systems, Academic Press: New York, 1975
29. de Jong, S.J.; Arias, E.R.; Rijkers, D.T.S.; van Nostrum, C.F.; Kettenes-van Bosch, J.J.; Hennink, W. E. Polymer 2001, 42, 2795-2802

Downloaded by PENNSYLVANIA STATE UNIV on August 28, 2012 | http://pubs.acs.org
Publication Date: September 23, 2006 | doi: 10.1021/bk-2006-0939.ch011

30. Gesine, S.; Carsten, S.; Stefan, F.; Thomas, K. *Biomaterials* **2003,** 24 (21), 3835-3844.
31. Gelderblom, H.; Verweij, J.; Nooter, K.; Spareboom, A. *European Journal of Cancer* **2001,** *37,* 1590-1598
32. Liggins, R. T.; Hunter, W. L. *J. Pharm. Sci.* **1997,** *86,* 1458.
33. Shuai, X.; Ai, H.; Nasongkla, N.; Kim, S.; Gao, J. *J. Controlled Release,* **2004,** 98, 415
34. Kakizawa, Y.; Kataoka, K. *Adv. Drug Deliv. Rev.* **2002,** *54,* 203-222.

Downloaded by PENNSYLVANIA STATE UNIV on August 28, 2012 | http://pubs.acs.org
Publication Date: September 23, 2006 | doi: 10.1021/bk-2006-0939.ch011

Downloaded by STANFORD UNIV GREEN LIBR on August 9, 2012 | http://pubs.acs.org
Publication Date: September 23, 2006 | doi: 10.1021/bk-2006-0939.ch012

Chapter 12

Functional Degradable Polymeric Materials Prepared by Atom Transfer Radical Polymerization

Nicolay V. Tsarevsky, Ke Min, Nazeem M. Jahed, Haifeng Gao, and Krzysztof Matyjaszewski

Department of Chemistry, Carnegie Mellon University, 4400 Fifth Avenue, Pittsburgh, PA 15213

ATRP was applied to synthesize well-defined halogen-functionalized linear polymers and gels with disulfide groups. The disulfide groups were introduced by using a disulfide-containing alkyl halide initiator or a dimethacrylate with internal disulfide link. The synthesized biocompatible linear disulfide-containing poly(2-hydroxyethyl methacrylate) degraded quickly upon reaction with tributylphosphine yielding lower molecular weight polymers. The gels with disulfide crosslinks prepared either by solution ATRP or by ATRP in miniemulsion also degraded in the presence of reducing agents leading to the formation of soluble polymers. The high degree of Br-functionalization of the gels was demonstrated by chain extension reactions with styrene and analysis of the degradation products by 2D chromatography.

In Degradable Polymers and Materials; Khemani, K., et al.;
ACS Symposium Series; American Chemical Society: Washington, DC, 2006.

Introduction

(Bio)degradable polymers are of significant interest in soil treatment, tissue engineering, and drug delivery, which has stimulated the development of novel methods for their synthesis.*(1-3)* The past decade has witnessed the discovery of various strategies for the precise synthesis of novel, previously inaccessible, polymeric materials. Among the synthetic strategies, "living"/controlled radical polymerization (CRP)*(4)* and more specifically atom transfer radical polymerization (ATRP)*(5-7)* have found a wide application due to the easy experimental setup and tolerance towards functional groups, solvents and impurities. ATRP relies on the reversible reaction between a low oxidation state metal (often copper) complex and an alkyl halide (initiator) generating a high oxidation state metal complex with a coordinated halide ligand and radicals that can propagate in the presence of a monomer. An equilibrium between alkyl halide-type dormant polymeric species and active radicals is established which results in polymers of narrow molecular weight distribution and molecular weight or degree of polymerization (DP) predetermined by the ratio of the monomer to initiator. The polymers prepared by ATRP are halogen-capped which allows for further functionalization reactions.*(8)*

The use of functional alkyl halide initiators has been successfully applied to the preparation of various telechelic materials.*(8)* Disulfide is an example of a degradable group, which can be cleaved reversibly upon reduction to yield the corresponding thiols. The thiol-disulfide interconversion is widely utilized in nature, e.g., in the regulation of enzyme activity, in protein structure stabilization, and in various metabolic redox processes.*(9,10)* Thiols,*(11)* phosphines,*(12,13)* metal hydrides, and various metal / acid combinations are often employed as reducing agents. Disulfide groups can be introduced in a polymer by using an appropriate sulfur-containing initiator or monomer. The preparation of polymeric materials with internal disulfide bonds including linear polystyrene*(14)* or polymethacrylates,*(15-17)* polymer gels,*(17)* and miktoarm star copolymers*(18)* by ATRP was recently demonstrated. The degradation of these materials in the presence of dithiothreitol or tributylphosphine (Bu_3P) was reported. The degradation products were thiol-containing polymers which could be oxidized quantitatively back to the corresponding disulfides.*(14)*

Herein, we describe the ATRP of the biocompatible 2-hydroxyethyl methacrylate (HEMA) using a disulfide-containing alkyl halide initiator in protic media at near-ambient temperature. The reductive cleavage of this biocompatible

Downloaded by STANFORD UNIV GREEN LIBR on August 9, 2012 | http://pubs.acs.org
Publication Date: September 23, 2006 | doi: 10.1021/bk-2006-0939.ch012

polymer is studied as well. We also demonstrate that halogen-functionalized gels degradable in reducing environment can be prepared by ATRP in miniemulsion using a dimethacrylate with disulfide group as the crosslinker. This process is useful for the fabrication of fluid formulations containing gel nanoparticles that can release incorporated compounds (such as drugs or dyes) in a reducing environment.

Downloaded by STANFORD UNIV GREEN LIBR on August 9, 2012 | http://pubs.acs.org
Publication Date: September 23, 2006 | doi: 10.1021/bk-2006-0939.ch012

Experimental

Materials

Prior to use, the neat monomer (methyl methacrylate (MMA), HEMA, or styrene (Sty)) was passed through a column filled with basic alumina to remove the polymerization inhibitor. CuBr (98%, Aldrich) was purified by washing with glacial acetic acid followed by 2-propanol. The conventional radical initiators V-70 and AIBN (Wako) were recrystallized from methanol. The disulfide-containing ATRP initiator bis(2-bromoisobutyryloxethyl) disulfide ($(BiBOE)_2S_2$) and the disulfide-containing crosslinker bis(methacryloyloxyethyl) disulfide ($(MAOE)_2S_2$) were synthesized using a literature procedure.*(17)* The synthesis of bis(2-pyridylmethyl) octadecylamine (BPMODA) was described previously as well.*(19)* All other reagents (2,2'-bipyridine (bpy), N,N,N',N",N"-pentamethyldiethylenetriamine (PMDETA), ethyl 2-bromoisobutyrate (EBiB), and Bu_3P) and the solvents were used as received. PMDETA and $(BiBOE)_2S_2$ were deoxygenated prior to the experiments by bubbling with nitrogen for 2-3 h.

ATRP of HEMA

HEMA (3 mL, 3.219 g, 27.4 mmol) and methanol (3 mL) were mixed in a Schlenk flask to which a stir bar had been added, and the mixture was deoxygenated by 5 freeze-pump-thaw cycles. The mixture was then frozen, the flask was filled with nitrogen, and the solid catalyst consisting of CuBr, $CuBr_2$, and bpy was added. The flask was quickly closed, and was then evacuated and back-filled with nitrogen several times. The reaction mixture was allowed to thaw, the reaction flask was immersed in a water bath thermostated at 30 °C, and the initiator $(BiBOE)_2S_2$ was injected. In all experiments, the molar ratio of bpy to total copper (CuBr + $CuBr_2$) was 2:1, and the ratio of total copper to initiator was 2:1 (i.e., the ratio of total copper to bromine groups from the initiator was 1:1). Two different monomer-to-initiator ratios, namely 300 and 150 were used. The amount of $CuBr_2$ in the catalyst varied from 20 to 80% of the total copper. Samples were periodically withdrawn with a nitrogen-purged syringe and analyzed.

Preparation of degradable gels with disulfide groups (17)

MMA (5 mL, 0.0467 mol) and $(MAOE)_2S_2$ (0.15 mL, 0.57 mmol), were dissolved in 2 mL of acetone and the mixture was degassed as described above. The catalyst consisted of 0.0334 g (0.233 mmol) CuBr and 0.0727 g (0.4667 mmol) bpy. The reaction mixture was heated to 50 °C and deoxygenated $(BiBOE)_2S_2$ (150 μL, 0.491 mmol, 1/95 vs. MMA) was added. Gelation was observed in ca. 150 minutes (93 % monomer conversion determined by gravimetry). The obtained gel was washed repeatedly with acetone (4-5 times with 500-mL portions, keeping the gel in the solvent for ca. 12 h) to remove any free polymer. Gels with disulfide crosslinks were also synthesized from MMA and $(MAOE)_2S_2$ using conventional radical initiators such as V-70.

Chain extension of the disulfide-containing polyMMA-based "supermacroinitiator" gel with Sty (17)

0.3 g of the dried gel described above was mixed with 8 mL of Sty and the mixture was kept in a refrigerator overnight and then at room temperature for 2 hours to allow the gel to swell. The mixture was degassed as described above and 0.0286 g (0.20 mmol) of CuBr was added, followed by injection of 42 μL (0.20 mmol) of PMDETA. The reaction was carried out for 2.5 h at 90 °C. The product was washed repeatedly with THF to remove any free polymer that was not chemically attached to the gel.

Preparation of latexes degradable in reducing environment by ATRP

Simultaneous Reverse and Normal Initiation ATRP*(20,21)* was applied in miniemulsion to synthesize the degradable latex particles. $CuBr_2$ (0.0044 g, 0.020 mmol), BPMODA (0.0090 g, 0.020 mmol), MMA (2g, 20.0 mmol), EBiB (14.6 μL, 0.1 mmol), the degradable crosslinker ($(MAOE)_2S_2$, 0.1 g) and

Downloaded by STANFORD UNIV GREEN LIBR on August 9, 2012 | http://pubs.acs.org
Publication Date: September 23, 2006 | doi: 10.1021/bk-2006-0939.ch012

hexadecane (used as co-stabilizer, 0.10 mL) were added to a round-bottom flask, and heated upon stirring at 60 °C. After the formation of stable Cu^{II} complex, the mixture was cooled to room temperature, and AIBN (0.0020 g, 0.0125 mmol) was added. After the addition of the aqueous solution of surfactant Brij 98 (5 mM of polyoxyethylene(20) oleyl ether, 20 mL), the oil/water mixture was ultrasonificated (Heat Systems Ultrasonics W-385 sonicator; output control set at 8 and duty cycle at 70% for 1 min) in an ice bath to prevent a significant temperature rise. The resulting miniemulsion exhibited good shelf life stability at room temperature, as evidenced by a lack of visible creaming or phase separation over 1 day of aging. After homogenization and transfer to a 25 mL Schlenk flask, nitrogen was bubbled through the miniemulsion for 30 min at room temperature. The flask was then immersed in an oil bath thermostated at 80 °C, corresponding to time zero of the polymerization. After 4 h, the reaction was stopped by exposing the reaction mixture to air; the monomer conversion was 80%. The final miniemulsion was dried overnight.

Downloaded by STANFORD UNIV GREEN LIBR on August 9, 2012 | http://pubs.acs.org
Publication Date: September 23, 2006 | doi: 10.1021/bk-2006-0939.ch012

Reductive degradation of the disulfide-containing linear polymers and gels

0.01 g of the linear polymer was dissolved in 1 mL 50 mM solution of LiBr in DMF (same solution as the eluent for SEC) containing Ph_2O (SEC standard), and Bu_3P (10 μL) was added. The reaction mixture was analyzed by SEC after 30 min. The gels were degraded in a similar fashion: 0.02 g of the dry gel was kept in 3 mL of THF containing 0.05 mL of Ph_2O for 1 h to let it swell, and Bu_3P (50 μL) was added. The degradation was accompanied by complete dissolution and took several hours to days depending on the crosslink density. The disulfide-containing gel nanoparticles prepared by ATRP in miniemulsion were swelled (after removal of the surfactant) for 24 h in THF (12.3 g/L) and Bu_3P was added. The change of particle size was tracked by Dynamic Light Scattering (DLS) on High Performance Particle Sizer, Model HP5001 from Malvern Instruments, Ltd. The measurement took ca. 5 min. The particle size reported in this work is the one obtained at the end of each measurement.

2-Dimensional Chromatographic Analysis

After reductive degradation, the gels were analyzed by liquid chromatography under critical conditions (LCCC) for polyMMA. The chromatograph was equipped with a Waters 600 controller and pump. The mobile phase was a mixture of butanone and cyclohexane (74:26 by volume).

Downloaded by STANFORD UNIV GREEN LIBR on August 9, 2012 | http://pubs.acs.org
Publication Date: September 23, 2006 | doi: 10.1021/bk-2006-0939.ch012

The column used for separation was Macherey & Nagel, Nucleosil silica gel (particle size 5 µm, pore size 300 Å and column dimensions 250 × 4 mm i.d.). The column oven temperature was set at 32 °C. The mobile phase flow rate was 0.5 mL/min. An evaporative light scattering detector (ELSD, Polymer Laboratories, PL-ELS 1000, nitrogen flow 1.2 L/min, evaporator temperature 90 °C) was used. Dilute polymer solutions were prepared from 5 mg of degraded by reduction with Bu_3P gel (washed with methanol) in 1 mL mixture of butanone and cyclohexane (3:1 by volume). Each time a 5 µL sample was used for analysis. Data acquisition was accomplished with PSS-WINGPC 7 from Polymer Standards Service (PSS; Mainz, Germany). Following the LCCC analysis, the samples were analyzed by 2D liquid chromatography. For the first dimension (HPLC), the conditions were the same as for the LCCC, except that the flow rate was set to 0.08 mL/min. Sample fractions from the first dimension were transferred to the second dimension (SEC) via an eight-port valve system (VICI Valco EHC8W), which consisted of two 200-µL loops. The second dimension (SEC) consisted of a Waters 515 pump delivering THF at a flow rate of 5 mL/min. The column used was a PSS SDV linear M, high-speed column (pore size 5 µm, dimensions 50 × 20 mm i.d.). The same ELS detector was used as in HPLC analysis, and the second dimension was calibrated using polyMMA homopolymer standards. Data acquisition and processing were automatically performed by the WINGPC 7 and PSS-2D-GPC software, respectively.

Results and Discussion

Synthesis of degradable linear polyHEMA

PolyHEMA is a polymer that has attracted significant attention due to its biocompatibility; applications include hydrogels and contact lenses.*(22)* Well-defined polyHEMA with internal disulfide group was synthesized using $(BiBOE)_2S_2$ as the ATRP initiator as shown in Figure 1. The polymerizations were carried out in methanol at 30 °C and were relatively fast (high conversion was reached in 2-5 h depending on the conditions) similar to other ATRP reactions in protic media.*(23)* In all cases, the first order kinetic plots were linear or showed insignificant curvature (Figure 2a) indicating a constant number of active species throughout the reaction. It was recently shown*(23)* that in order to achieve satisfactory polymerization control in ATRP in protic media, a relatively large initial amount of deactivator ($CuBr_2$ / bpy) should be added to the reaction mixture. This is necessary because the Cu^{II} halide complexes are relatively unstable in protic solvents such as alcohols and water. Thus, a significant part of the deactivator may be lost, leading to inefficient deactivation and therefore to poor polymerization control. This process is especially pronounced in solutions dilute with respect to Cu^{II} and halide ions. Indeed, Figure 2b shows that although the polymer molecular weights increased linearly with conversion, the polydispersities (M_w/M_n) of the polymers isolated from a reaction mixture containing only 20% (with respect to the total copper) of initially added deactivator in the case of low total catalyst concentration (i.e., targeted DP of 300) were relatively large. The control over polymerization was largely improved when the amount of deactivator was increased to 40%. When the targeted DP was decreased twofold, the polymerization control was better due to the higher total concentration of catalyst and therefore of deactivator.

The degradation of polyHEMA in DMF was rather efficient and fast when Bu_3P was used as the reducing agent. Figure 3 shows the SEC traces of polymers obtained at two different monomer conversions before and after reductive degradation for 30 min at room temperature.

Downloaded by STANFORD UNIV GREEN LIBR on August 9, 2012 | http://pubs.acs.org
Publication Date: September 23, 2006 | doi: 10.1021/bk-2006-0939.ch012

Preparation and Degradation of Functional polyMMA-based Gels

The radical polymerization of a mixture of MMA and a difunctional monomer containing a disulfide bond, $(MAOE)_2S_2$, leads to the formation of a gel that can degrade in reducing environment yielding soluble linear polyMMA with thiol side groups. The polymerization was carried out in acetone at 50 °C using V-70 as the radical initiator in the presence of a dye, methyl violet. The gel with incorporated dye thus obtained was swollen in toluene and Bu_3P was added. Gradually, the disulfide links originating from the dimethacrylate crosslinker were cleaved and the gel degraded releasing the dye which precipitated in the solvent used (Figure 4).

The degradation rate can be adjusted by varying the crosslink density (i.e., by using various amounts of the dimethacrylate crosslinker). It also depends on

Downloaded by STANFORD UNIV GREEN LIBR on August 9, 2012 | http://pubs.acs.org
Publication Date: September 23, 2006 | doi: 10.1021/bk-2006-0939.ch012

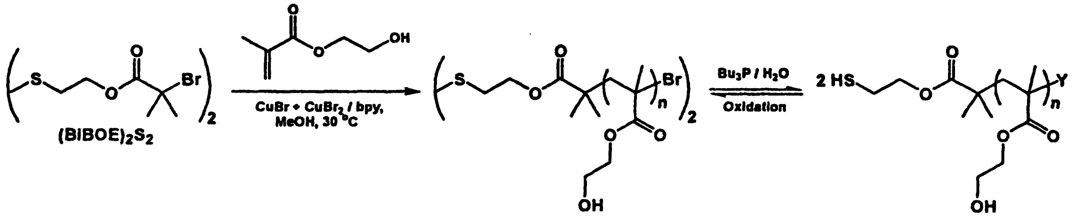
(BiBOE)$_2$S$_2$
CuBr + CuBr$_2$ / bpy, MeOH, 30 °C
Bu$_3$P / H$_2$O
Oxidation
2 HS
S
O
OH
Br
n
2
Y

Figure 1. Preparation of degradable polyHEMA by ATRP.

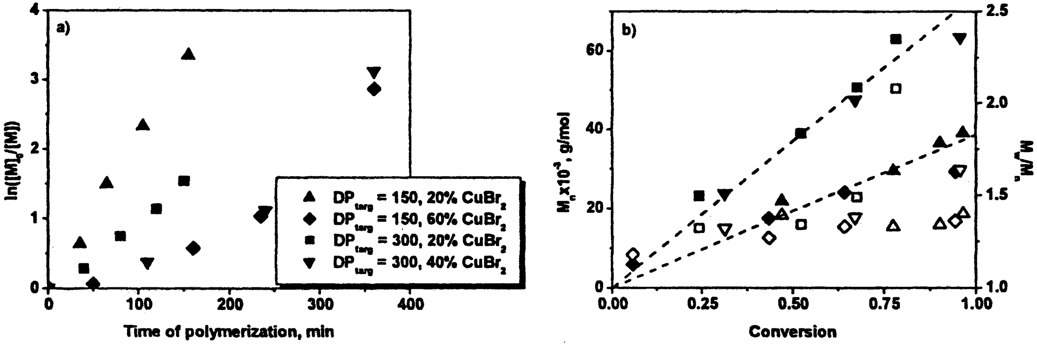

Figure 2. ATRP of HEMA using (BiBOE)$_2$S$_2$ as the initiator: a) kinetics and b) evolution of molecular weights (filled symbols with same shape as in graph a)) and polydispersity indices (open symbols) with monomer conversion.

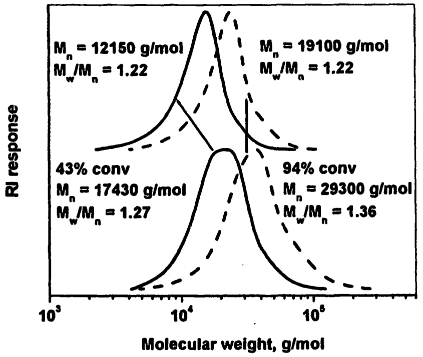

Figure 3. SEC traces of polyHEMA obtained at 43% and 94% monomer conversion using [HEMA]:[(BiBOE)$_2$S$_2$]:[CuBr]:[CuBr$_2$]:[bpy] = 150:1:0.8:1.2:4 before (bottom) and after (top) reductive degradation in the presence of Bu$_3$P (30 min).

the nature of the reaction medium. For instance, it is well documented that the redox potentials (and therefore the degradation efficiency) of disulfides depend significantly upon pH, solvent polarity and the presence of various reagents forming complexes with the free thiols or thiolate ions produced in the reduction.*(24)* The disulfide-based gels prepared by ATRP can be designed to degrade only in an environment with certain redox potential by changing the substituents at the disulfide group in the initiator and/or monomer. Gels with the potential to release incorporated compounds upon reduction are of significant interest for the biomedical sciences and engineering. Cancer tissues are hypoxic and the degradation of a gel accompanied with the release of a drug in such reducing environment is promising in cancer treatment.*(25)*

Once it was demonstrated that degradable crosslinked materials could be formed using the radical polymerization of (MAOE)$_2$S$_2$, the ATRP of MMA in the presence of this disulfide was studied. The reaction was initiated by the disulfide initiator (BiBOE)$_2$S$_2$ and yielded functional degradable gels (see the left-hand side of Figure 5). Both the initiator and the difunctional monomer served as sources of degradable disulfide groups in the gels. The high degree of chain end functionalization was demonstrated by a chain extension with a second monomer, Sty (Figure 5, right hand-side). This reaction was recently described in detail.*(17)*

In this work, we present further evidence that the bromide end groups in the gel remained intact during the synthesis and purification of the gel. The polyMMA-based gels were successfully degraded in THF using Bu$_3$P as the

Downloaded by STANFORD UNIV GREEN LIBR on August 9, 2012 | http://pubs.acs.org
Publication Date: September 23, 2006 | doi: 10.1021/bk-2006-0939.ch012

Downloaded by STANFORD UNIV GREEN LIBR on August 9, 2012 | http://pubs.acs.org
Publication Date: September 23, 2006 | doi: 10.1021/bk-2006-0939.ch012

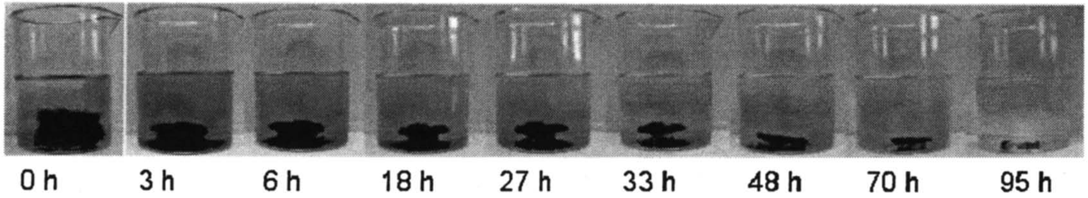

Figure 4. Degradation of polyMMA-based gel with disulfide groups in the presence of Bu_3P in toluene at room temperature producing soluble polyMMA. During the degradation, the incorporated dye (methyl violet) was released from the gel. (Synthesis: MMA (10 mL), $(MAOE)_2S_2$ (0.05 mL), acetone (4 mL), methyl violet (0.01 g), and V-70 (0.05 g), nitrogen atmosphere, 50 °C, 1.5 h.).

Downloaded by STANFORD UNIV GREEN LIBR on August 9, 2012 | http://pubs.acs.org
Publication Date: September 23, 2006 | doi: 10.1021/bk-2006-0939.ch012

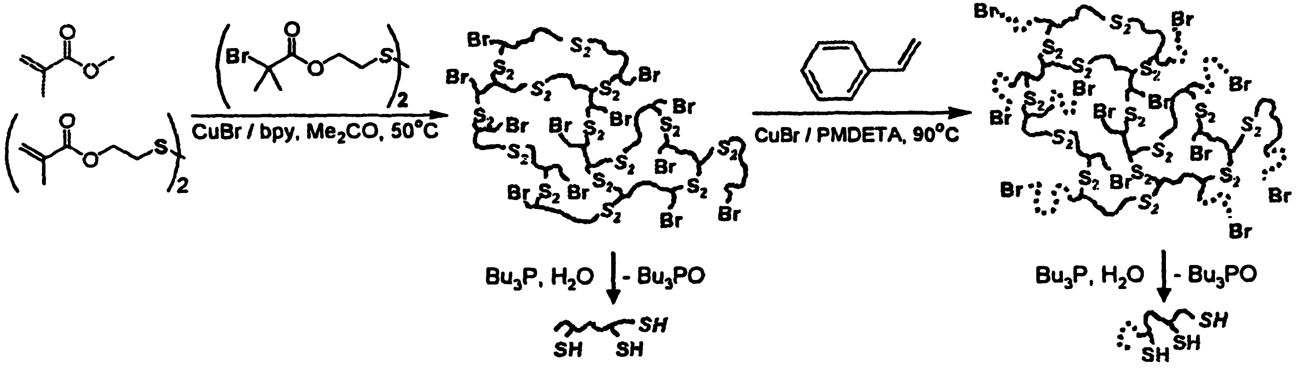

Figure 5. Preparation of degradable polyMMA-based gels by ATRP and their use as "supermacroinitiators". The disulfide and thiol groups originating from the functional initiator are shown in italics and the ones from the functional monomer in regular font. PolyMMA and polySty chains are represented with solid and dotted lines, respectively. (Reproduced from reference 17. Copyright 2005 American Chemical Society.)

Downloaded by STANFORD UNIV GREEN LIBR on August 9, 2012 | http://pubs.acs.org
Publication Date: September 23, 2006 | doi: 10.1021/bk-2006-0939.ch012

disulfide reducing agent, forming linear soluble polyMMA chains containing at least one thiol end-group originating from the disulfide initiator, and potentially one or more attached to the backbone originating from the disulfide-containing crosslinker $(MAOE)_2S_2$ (Figure 5). The soluble polymers formed by the reduction were analyzed by SEC. After the chain extension, the gel with pendant polySty chains was washed repeatedly with THF to remove any free polySty, generated by thermal initiation, and degraded using Bu_3P. The formed block copolymer was analyzed by SEC. The molecular weights of the products of reductive degradation of the gels demonstrate the efficient initiation from the polyMMA-based "supermacroinitiators". This is further verified from the symmetrical shift observed in the SEC traces of the soluble linear polymers formed after the reduction of the gels (Figure 6). No significant amount of homopolymer of MMA was observed in the products of degradation of the gels with segmented structures, indicating the high degree of functionalization of the gel prepared by ATRP.

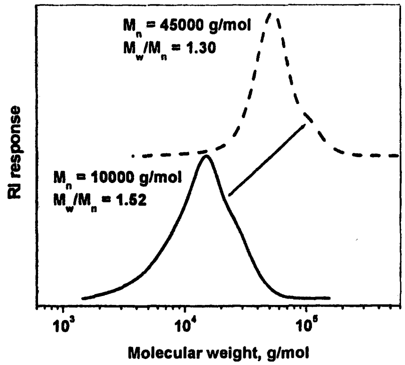

Figure 6. SEC traces of the products of reductive degradation of a disulfide-containing "supermacroinitiator" gel (bottom) and the gel prepared therefrom by chain extension with Sty (top).

The products of reductive degradation of polyMMA gel and the gel with "blocky" structure prepared from it were also analyzed by 2D chromatography. The analysis at the HPLC dimension was carried out at critical conditions for polyMMA. The position of the peak on the y-axis of the 2D plot (Figure 7) depends on the composition of the polymer. The second dimension (x-axis of the 2D plot) corresponds to SEC where the separation depends upon the molecular weight. The spot of the "supermacroinitiator" decomposition product (Figure 7a) is situated at molecular weight about 10^4 g/mol, which is in good agreement with the SEC trace from Figure 6. Some spreading is observed on the HPLC axis, most likely due to the variable number of thiol groups per polymer chain. The average number, based on monomer feed composition was 2.2 (one thiol group originating from the disulfide initiator and an average of 1.2 originating from the disulfide dimethacrylate). The gel with "blocky" structure degraded in the presence of Bu_3P (Figure 7b) forming a MMA-Sty block copolymer of molecular weight of about 5×10^4 g/mol (again, in good agreement with the data from Figure 6), which did not contain any detectable amount of free polyMMA (which would originate from chains in the "supermacroinitiator" which were not chain extended with Sty). This result clearly demonstrates the high degree of bromine-functionalization of the parent polyMMA-based "supermacroinitiator".

Downloaded by STANFORD UNIV GREEN LIBR on August 9, 2012 | http://pubs.acs.org
Publication Date: September 23, 2006 | doi: 10.1021/bk-2006-0939.ch012

Synthesis of Functional Degradable polyMMA-based Gels by ATRP in Miniemulsion

ATRP of various monomers can be successfully carried out in aqueous dispersed media yielding well-defined functional latexes.*(26,27)* Miniemulsion polymerization, including CRP in miniemulsion, is widely used for the preparation of latexes with particle sizes of the order of 100-500 nm. If the proper surfactant is used, the miniemulsions are stable for prolonged periods.

A degradable functional latex was prepared by the atom transfer copolymerization of MMA and $(MAOE)_2S_2$ in miniemulsion. The latex particles thus obtained, when swollen in THF, had a diameter of about 220 nm. The latex could be rapidly (20-30 min) degraded by Bu_3P. For the two experiments shown in Figure 8, 12 μL and 20 μL of Bu_3P was added to 2 mL of the particle suspension (12.3 g/L), respectively, to study the effect of the reducing agent amount on the degradation rate. As the reaction time progressed, the particle size increased due to the increasing amount of reductively cleaved disulfide crosslinks. The formed loosely crosslinked gel particles had higher swelling ratios than the starting material. At a certain moment which depended upon the amount of added reducing agent the gel degraded completely forming soluble linear polymer chains which was accompanied by a sharp decrease in the measured hydrodynamic volume.

In the future, surface modification of the degradable latex particles will be studied. Also, the possibility to incorporate various compounds in the degradable "nanocages" prepared by the atom transfer radical copolymerization of a disulfide-containing crosslinker and other monomers in miniemulsions, as well as the release of those compounds will be explored.

Downloaded by STANFORD UNIV GREEN LIBR on August 9, 2012 | http://pubs.acs.org
Publication Date: September 23, 2006 | doi: 10.1021/bk-2006-0939.ch012

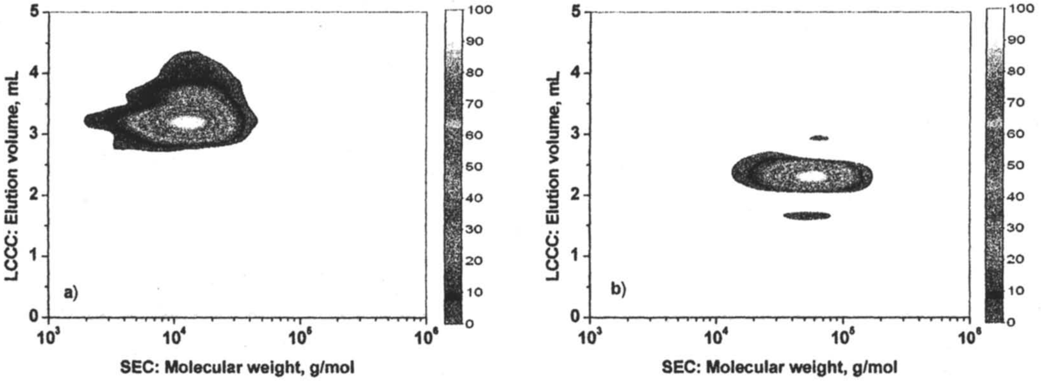

Figure 7. 2D chromatography plots of the products of reductive degradation of a) polyMMA-based "supermacroinitiator" gel and b) polyMMA-block-polySty-based gel.

Downloaded by STANFORD UNIV GREEN LIBR on August 9, 2012 | http://pubs.acs.org
Publication Date: September 23, 2006 | doi: 10.1021/bk-2006-0939.ch012

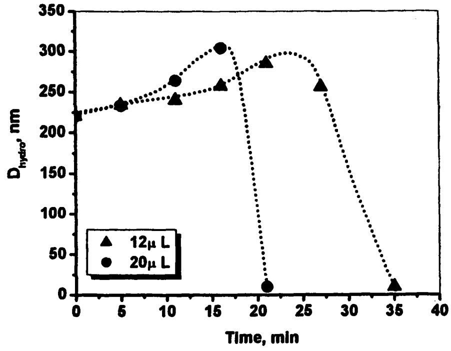

Figure 8. Reductive degradation of polyMMA-based latex crosslinked with $(MAOE)_2S_2$ in the presence of various amounts of Bu_3P in THF at ambient temperature.

Conclusions

Bis[2-(2-bromoisobutyryloxy)ethyl] disulfide was employed as an initiator for the ATRP of 2-hydroxyethyl methacrylate (HEMA) in methanol using CuBr + $CuBr_2$ / 2,2'-bipyridine as the catalyst to yield linear biocompatible polymers with internal disulfide bond. Sufficient deactivation rate and therefore satisfactory polymerization control in the protic reaction medium was observed only when the catalyst contained relatively large initial amount of deactivator (higher than 20% of the total catalyst). The reductive cleavage of the disulfide-containing polyHEMA with tributylphosphine in DMF at room temperature was complete in 30 min and produced polymers of lower molecular weight than the starting materials.

Mixtures of methyl methacrylate (MMA) and a difunctional methacrylate monomer with internal disulfide bond were copolymerized by ATRP both in an acetone solution and in an aqueous dispersed (miniemulsion) system to form functional degradable gels. The high degree of Br-functionalization of the gels was demonstrated by a chain extension reaction with styrene followed by reductive degradation and 2D chromatographic analysis of the degradation products which showed no significant amount of unextended polyMMA chains. The degradation of the degradable, disulfide-crosslinked, functional latex particles prepared by miniemulsion ATRP was monitored by DLS. At the early stages of degradation the particles showed increased swellability due to the decreasing crosslink density. Eventually, the particles degraded completely forming linear, soluble polyMMA chains with free thiol groups.

Acknowledgments

The authors thank the members of the ATRP/CRP Consortia at Carnegie Mellon University, NSF (grant DMR 0090409) and EPA (grant R82958001) for funding.

Downloaded by STANFORD UNIV GREEN LIBR on August 9, 2012 | http://pubs.acs.org
Publication Date: September 23, 2006 | doi: 10.1021/bk-2006-0939.ch012

References

1. Schnabel, W. *Polymer Degradation: Principles and Practical Applications*; Hanser International: Munich, 1981.
2. Hamid, S. H., Ed. *Handbook of Polymer Degradation*; Marcel Dekker: New York, 2000.
3. Edlund, U.; Albertsson, A.-C. *Adv. Polym. Sci.* **2002**, *157*, 67.
4. Matyjaszewski, K.; Davis, T. P., Eds. *Handbook of Radical Polymerization*; Wiley: Hoboken, 2002.
5. Wang, J.-S.; Matyjaszewski, K. *J. Am. Chem. Soc.* **1995**, *117*, 5614.
6. Matyjaszewski, K.; Xia, J. *Chem. Rev.* **2001**, *101*, 2921.
7. Kamigaito, M.; Ando, T.; Sawamoto, M. *Chem. Rev.* **2001**, *101*, 3689.
8. Coessens, V.; Pintauer, T.; Matyjaszewski, K. *Prog. Polym. Sci.* **2001**, *26*, 337.
9. Singh, R.; Whitesides, G. M. In *Supplement S: The chemistry of sulphur-containing functional groups*; Patai, S., Rappoport, Z., Eds.; Wiley: Chichester, 1993; pp 633-658.
10. Gilbert, H. F. *Bioelectrochemistry: Principles and Practice* **1997**, *5*, 256.
11. Singh, R.; Lamoureux, G. V.; Lees, W. J.; Whitesides, G. M. *Methods Enzymol.* **1995**, *251*, 167.
12. Humphrey, R. E.; Hawkins, J. M. *Anal. Chem.* **1964**, *36*, 1812.
13. Humphrey, R. E.; Potter, J. L. *Anal. Chem.* **1965**, *37*, 164.
14. Tsarevsky, N. V.; Matyjaszewski, K. *Macromolecules* **2002**, *35*, 9009.
15. Shah, R. R.; Merreceyes, D.; Husseman, M.; Rees, I.; Abbott, N. L.; Hawker, C. J.; Hedrick, J. L. *Macromolecules* **2000**, *33*, 597.
16. Bontempo, D.; Heredia, K. L.; Fish, B. A.; Maynard, H. D. *J. Am. Chem. Soc.* **2004**, *126*, 15372.
17. Tsarevsky, N. V.; Matyjaszewski, K. *Macromolecules* **2005**, *38*, 3087.
18. Gao, H.; Tsarevsky, N. V.; Matyjaszewski, K. *Macromolecules* **2005**, *38*, 5995.
19. Xia, J.; Matyjaszewski, K. *Macromolecules* **1999**, *32*, 2434.
20. Gromada, J.; Matyjaszewski, K. *Macromolecules* **2001**, *34*, 7664.
21. Li, M.; Min, K.; Matyjaszewski, K. *Macromolecules* **2004**, *37*, 2106.
22. Montheard, J.-P.; Chatzopoulos, M.; Chappard, D. *J. M. S. - Rev. Macromol. Chem. Phys.* **1992**, *C32*, 1.

23. Tsarevsky, N. V.; Pintauer, T.; Matyjaszewski, K. *Macromolecules* **2004,** *37,* 9768.
24. Gilbert, H. F. *Methods Enzymol.* **1984,** *107,* 330.
25. Brown, J. M.; Wilson, W. R. *Nature Reviews Cancer* **2004,** *4,* 437.
26. Qiu, J.; Charleux, B.; Matyjaszewski, K. *Prog. Polym. Sci.* **2001,** *26,* 2083.
27. Cunningham, M. F. *Prog. Polym. Sci.* **2002,** *27,* 1039.

Downloaded by STANFORD UNIV GREEN LIBR on August 9, 2012 | http://pubs.acs.org
Publication Date: September 23, 2006 | doi: 10.1021/bk-2006-0939.ch012

Downloaded by NORTH CAROLINA STATE UNIV on August 28, 2012 | http://pubs.acs.org
Publication Date: September 23, 2006 | doi: 10.1021/bk-2006-0939.ch013

Chapter 13

Assembly of Bioactive, Heparin-Derivatized Polymer Hydrogels for Protein Delivery

Nori Yamaguchi[1,2] and Kristi L. Kiick[1,2,*]

[1]Department of Materials Science and Engineering, University of Delaware,
201 DuPont Hall, Newark, DE 19716
[2]Delaware Biotechnology Institute, University of Delaware,
15 Innovation Way, Newark, DE 19711

Polymeric materials that can deliver therapeutic molecules and provide a desired biological response have proven critical in drug delivery and tissue engineering applications. Polysaccharide-derivatized polymers offer unique opportunities for the design of such materials, given the importance of polysaccharides in sequestering bioactive proteins in the extracellular matrix. Accordingly, we have synthesized low molecular weight heparin (LMWH)-modified star poly(ethylene glycol) (PEG-LMWH) that can undergo spontaneous association with heparin binding peptide (HBP)-modified star poly(ethylene glycol) (PEG-HBP) to form assembled hydrogels. Rheological characterization of the noncovalently assembled hydrogels shows that the hydrogels exhibit moderate storage moduli (ca. 200 Pa) that exceed the loss moduli from frequencies from 0.1 to 100 Hz and increase monotonically with increasing molar ratio of the PEG-HBP. The assembled hydrogels are demonstrated to be competent for the sequestration and delivery of bFGF.

Introduction

The study and manipulation of polysaccharide-derivatized polymeric materials have gained increasing attention owing to the importance of polysaccharide-protein interactions in applications such as wound healing, tissue engineering, protein therapeutics, and molecular diagnostics, coupled with the increasing understanding of and synthetic control over polysaccharide materials (*1-3*). Polysaccharide materials are used widely in biological applications owing to the generally low immunological response of the highly-hydrated polysaccharides, the prevalence of polysaccharides in mediating biological processes in vivo, and the availability of a variety of hydrogel-forming polysaccharides. The highly sulfated glycosaminoglycan heparin, while not intrinsically gel-forming, has also received an enormous amount of research attention because of its potent and important activities, such as binding to antithrombin III to mediate thrombosis, and binding to growth factors to stabilize their conformations, potentiate their activity, and protect them from degradation and thermal inactivation (*4*). There have therefore been a large number of studies that demonstrate the utility of incorporating heparin onto surfaces and into hydrogel matrices for the delivery of heparin-binding growth factors.

Heparin-containing delivery systems for the controlled application of growth factors have been reported by many investigators and have permitted delivery of growth factors for wound healing and tissue engineering applications. These delivery systems can rely on passive inclusion of heparin in hydrogel matrices (*5, 6*), noncovalent immobilization of the heparin in the matrix via affinity interactions with heparin-binding peptides (*7-11*), or covalent attachment of heparin to the drug delivery matrix (alginate, collagen, hyaluronate) (*12-16*). Immobilization of heparin via covalent and noncovalent methods has proven most successful for the delivery of bioactive growth factors over extended periods of time. Recent reports demonstrate the copolymerization of styrylated heparin with albumin to form surfaces capable of the delivery of bFGF (*17*) or to form three-dimensional structures (*18*). Silyl-heparin has also been produced to mediate adsorption of heparin to surfaces for delivery of bFGF (*19*). In other investigations, heparin and growth factors are transiently immobilized in a fibrin matrix via noncovalent interactions between growth factors, heparin, and covalently-incorporated heparin-binding peptides (*8*). In these cases, the affinity between heparin and the heparin-binding peptides has been shown to control the rate of growth factor delivery, with delivery also promoted by cell-mediated degradation of the fibrin matrix.

The objective of this work has been the synthesis of a new polymer-heparin conjugate and complementary polymer-heparin binding peptide conjugate for the formation of hydrogels. This investigation is motivated by the opportunities to utilize these and other related polymeric architectures as platforms for producing

Downloaded by NORTH CAROLINA STATE UNIV on August 28, 2012 | http://pubs.acs.org
Publication Date: September 23, 2006 | doi: 10.1021/bk-2006-0939.ch013

bioactive hydrogel materials for potential applications in wound healing and tissue engineering. We summarize here the synthesis of multifunctional poly(ethylene glycol)-low molecular weight heparin (PEG-LMWH), **1**, and poly(ethylene glycol)-heparin binding peptide (PEG-HBP), **2**, as well as the properties of their assembled hydrogels. The PEG-based star polymers (M_n = 10 000) offer advantages such as reported low immunogenicity, biocompatibility, lack of protein fouling, and hydrophilicity (*20*). As illustrated in Figure 1, the star polymer architecture in **1** mediates the formation of a noncovalently cross-linked hydrogel, **3**, when mixed with **2**. This multifunctional PEG-based polymer may also have additional uses where multivalent presentation of polysaccharides is relevant. The LMWH serves as a versatile assembly unit, as heparin binds a variety of biologically relevant proteins such as antithrombin III, laminin, fibronectin, and growth factors, and there are therefore many potential HBPs available for hydrogel assembly. Indeed, the multifunctional PEG-LMWH star copolymer discussed here has been shown to mediate the noncovalent assembly of hydrogel networks with tunable rheological properties via interactions with a variety of complementary PEG-HBP binding partners. In this summary we describe the assembly of PEG-LMWH with a PEG star polymer modified with the heparin binding domain of the heparin interacting protein (HIP) (PEG-HIP, **2**). The hydrogel networks formed are erodible and capable of binding and releasing bFGF.

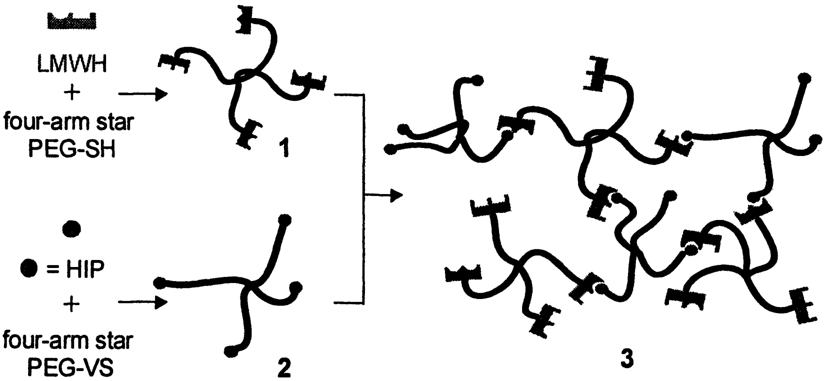

Figure 1. Schematic of the assembly of noncovalent hydrogel network, 3, from the individual constituent molecules 1 and 2. Potential HIP peptide and bFGF binding domains in LMWH are indicated by half circles and rectangles, respectively.

Downloaded by NORTH CAROLINA STATE UNIV on August 28, 2012 | http://pubs.acs.org
Publication Date: September 23, 2006 | doi: 10.1021/bk-2006-0939.ch013

Experimental

Materials and Methods

The syntheses of **1** and **2**, as well as the production of covalently cross-linked, nondegradable hydrogels and noncovalently assembled hydrogels, **3**, were reported previously (*21, 22*). The conditions used for all binding, release, and erosion experiments with the covalently cross-linked and noncovalently assembled hydrogels were described previously (*21*). ^{1}H NMR spectra were acquired, under standard quantitative conditions at ambient temperature, on a Bruker DRX-400 NMR spectrometer. All spectra were recorded in DMSO-d_6 and deuterium oxide and were referenced to TMS (tetramethylsilane) and DSS (sodium 2,2-dimethyl-2-silapentane-5-sulfonate), respectively. Dynamic mechanical measurements of the hydrogel linear viscoelastic response were performed using a Rheometrics ARES 100 strain-controlled rheometer. All sample preparation and testing conditions were described previously (*22*).

Results and Discussion

The synthesis of the PEG-LMWH offers opportunities for the production of noncovalently assembled, bioactive hydrogels capable of local and sustained release of therapeutically relevant proteins. Figure 1 illustrates the asssembly scheme and use of the PEG-LMWH conjugate for the assembly of hydrogel matrix, **3**, which may be useful for localized delivery of a variety of therapeutically relevant heparin-binding proteins and peptides. The individual constituent molecules, **1** and **2**, were synthesized, as previously described (*21*), via modification of the chain ends of four-arm star poly(ethylene glycol) (PEG) (M_n = 10 000) with either low molecular weight heparin (LMWH, M_r = 3000) or the heparin-binding domain of the heparin interacting protein (HIP) (*23*). Previous investigations (*24*) have demonstrated that heparin conjugated to PEG retains its ability to simultaneously bind antithrombin III (ATIII) and thrombin, suggesting that **1** would remain competent for binding to heparin-binding peptides and proteins. The use of the star PEG was motivated by the theoretical requirement that a minimum of three functional groups on one assembly partner and two functional groups on the complementary partner is necessary to permit physical cross-linking into a hydrogel network.

Downloaded by NORTH CAROLINA STATE UNIV on August 28, 2012 | http://pubs.acs.org
Publication Date: September 23, 2006 | doi: 10.1021/bk-2006-0939.ch013

Synthesis of 1

Reported methods for the conjugation of heparin to polymers and surfaces include reaction at the reducing terminus, modification of free amine groups, or coupling to free carboxylic acid groups on the polysaccharide. As surface plasmon resonance (SPR) studies of the interaction of heparin with various proteins (antithrombin III, avidin, thrombin, and lactoferrin) have shown that protein affinity for heparin is the highest when heparin is immobilized via its reducing terminus (25, *26*), our initial synthetic approach focused on the conjugation of LMWH to PEG via LMWH's reducing terminus. These reactions were unsuccessful, however, resulting in only 15-20% conversion, i.e., fewer than one in four arms was functionalized. The subsequent successful modification scheme included reaction of the free amines of LMWH, with 4-(*N*-maleimidomethyl)cyclohexanecarboxylic acid *N*-hydroxysuccinimide ester (SMCC) to produce maleimide-functionalized LMWH, which was then conjugated to the thiol-terminated four-arm star PEG to yield **1**. LMWH so modified was shown, via SPR assays, to bind to the HIP peptide employed in the synthesis of **2** (data not shown).

Hydrazinolysis of GlcNAc residues in LMWH was necessary to liberate a sufficient number of free amine groups for efficient conjugation to SMCC; deacetylation was confirmed via the disappearance of the acetyl group resonance at 2.13 ppm via ^{1}H NMR spectroscopy (in D_2O, indicating 1.2 free amine groups per LMWH chain) and via a positive ninhydrin assay result (*27*). Size exclusion chromatography (SEC) analysis on the isolated LMWH after the hydrazinolysis showed no reduction in molecular weight. Subsequently, the *N*-deacetylated LMWH was treated with SMCC to introduce maleimide functionality. The reaction between this product and the thiol-terminated four-arm star PEG was monitored via Ellman's assay, which indicated that 93% of the thiol groups had been consumed after 2 h. This value was not significantly increased by increasing the reaction time or the amount of the maleimide-functionalized LMWH added to the reaction, perhaps as a result of inaccessibility of the remaining thiol groups.

Analysis of the reaction mixture (after quenching and dialysis) via SEC yielded two broad fractions of different sizes, which were identified as **1** and unreacted maleimide-functionalized LMWH via ^{1}H NMR (data not shown). SEC also showed the absence of a peak at the expected elution volume for the thiol-terminated four-arm star PEG, indicating that the star PEG was completely consumed during the reaction. Characterization of the fraction with the largest hydrodynamic volume via ^{1}H NMR spectroscopy showed the expected resonance from the ethylene oxide protons of the star PEG backbone at 3.70 ppm, along with resonances from LMWH at 3.38-5.43 ppm in D_2O. Integration of the relevant peaks (PEG backbone vs. LMWH) in the NMR spectrum

Downloaded by NORTH CAROLINA STATE UNIV on August 28, 2012 | http://pubs.acs.org
Publication Date: September 23, 2006 | doi: 10.1021/bk-2006-0939.ch013

indicated an average of 73% functionalization in **1**, suggesting that on the average three out of four arms had been successfully functionalized with LMWH. The value of 73% functionalization is very likely underestimated due to overlapping of the PEG peak with the LMWH peaks. Nevertheless, since on average, a minimum of three arms of the star PEG were functionalized, **1** carries a necessary number of functional arms for the formation of a cross-linked network and was used in the assembly of noncovalent hydrogels with **2**.

Downloaded by NORTH CAROLINA STATE UNIV on August 28, 2012 | http://pubs.acs.org
Publication Date: September 23, 2006 | doi: 10.1021/bk-2006-0939.ch013

Synthesis of 2

The functionalization of hydroxy-terminated four-arm star PEG with vinyl sulfone (VS) groups (M_n = 10 300) was chosen for facile conjugation of the ATIII and HIP peptides as previously reported by Lutolf and Hubbell (*28*), since the reaction of peptides flanked by cysteine with VS groups has been demonstrated to proceed readily and provides a non-hydrolyzable linkage between the PEG and peptide termini (*11, 28*). The four-arm star PEG-VS was synthesized via previously reported methods (*21*). Characterization of the PEG-VS via ^{1}H NMR (in DMSO-*d6*) showed the expected vinyl resonances at 6.15-6.21 and 6.91-6.97 ppm for the PEG-VS, along with the ethylene oxide resonances of the star PEG backbone at 3.49 ppm. Integration of the appropriate resonances indicated up to 98% functionalization of four-arm star PEG with VS; the degree of functionalization depended on the specific synthetic strategy employed (*21*).

A short peptide derived from the heparin-binding domain of the heparin interacting protein (HIP), CRPKAKAKAKAKDQTK, was attached to the PEG-VS. The peptide sequence above was prepared via standard Fmoc solid phase peptide chemistry and was purified to > 99.5% purity via reverse-phase HPLC. An N-terminal cysteine residue was included to permit coupling to the PEG-VS via Michael-type addition as previously reported (*11, 28*). The reaction mixture was easily purified via SEC and the ^{1}H NMR spectrum (in D_2O) of the purified conjugate showed both the ethylene oxide resonances of the PEG at 3.70 ppm and the aliphatic resonances for the HIP peptide. The vinyl resonances at 6.80-7.36 ppm were of extremely low intensity, indicating that the majority of the VS group (ca. 95%) had reacted. Integration of appropriate peptide resonances (different HIP peptide resonances between 1.00 and 2.50 ppm), and comparison with the area of the PEG backbone resonance, revealed an average functionalization in **2** to be 77% (regardless of the mode of preparation of the PEG-VS), indicating that an average of three out of four arms had been functionalized in **2** with the peptide. Again, this degree of functionalization is likely underestimated due to errors in integration of the overlapping peptide and

PEG peaks in the ^{1}H NMR spectrum. A sufficient number of arms in **2** were functionalized with the HIP peptide, on average, to support the formation of **3** upon interaction with **1**.

Hydrogel Formation and Growth Factor Binding/Release

Downloaded by NORTH CAROLINA STATE UNIV on August 28, 2012 | http://pubs.acs.org
Publication Date: September 23, 2006 | doi: 10.1021/bk-2006-0939.ch013

Covalently Cross-linked Hydrogels

In order to demonstrate that the side chain modified LMWH, after a series of chemical reactions, is capable of binding/sequestering growth factors, **1** was chemically crosslinked into hydrogels with PEG methyl ether acrylate. Hydrogels were prepared via free radical polymerization of the acrylate monomer with potassium persulfate as the initiator. Propagating radicals abstract hydrogen atoms on ethylene glycol units of both the macromonomer PEG side chain and **1** and generate PEG free radicals that couple bimolecularly to crosslink the polymer solution into an insoluble hydrogel, **4** (*29, 30*). Such hydrogel matrices have covalently linked LMWH that cannot leach out and are therefore ideal substrates to analyze the ability of the PEG-LMWH to bind a variety of heparin binding peptides and proteins. Here, the binding and delivery of basic fibroblast growth factor (bFGF), which is known to induce the proliferation of a wide range of cells including endothelial cells, fibroblasts, smooth muscle cells, and chondrocytes (*16*), was investigated.

The chemically crosslinked hydrogels were washed thoroughly with PBS and then incubated in PBS to fully hydrate them prior to growth factor binding and release experiments. Toluidine blue assay (*21*) showed that the amount of immobilized LMWH was unchanged (ca. 22 μg per gel) after repeated washing and incubation. The growth factor binding of **4** and **5** (a gel which lacks covalent immobilization of **1** but contains the same amount of free LMWH (22 μg)) was evaluated via a sandwich ELISA assay. The LMWH immobilized hydrogel, **4**, exhibited significant bFGF binding compared to **5**, likely because the LMWH in **5** passively diffused out during the experiment (Figure 2). This observation agrees with results of toluidine blue assays, which showed no detectable amount of LMWH in **5** after washing with PBS overnight. Although the binding capacity and binding affinity of chemically modified LMWH may be altered versus free LMWH, this ELISA experiment unambiguously demonstrates that **1** retains binding and sequestering capabilities for bFGF. In addition, **4** was also capable of binding and sequestering VEGF (data not shown), suggesting the general utility of **1** for sequestration of heparin-binding proteins.

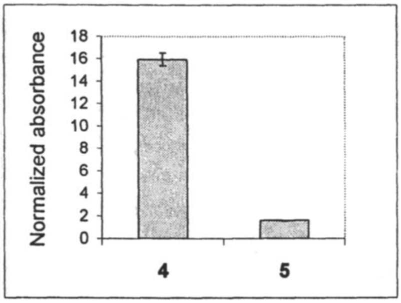

Figure 2. bFGF binding to covalently cross-linked hydrogels. Absorbance values reflect the amount of bFGF detected in the hydrogel via a standard ELISA assay. Values shown are an average of two separate experiments. These data were plotted from data in reference 21.

To provide insight into the kinetics of the growth factor release based on the diffusion of free bFGF from a heparinized matrix, a release profile of bFGF from **4** was constructed (Figure 3). Hydrogel **6**, a LMWH-free control, was prepared in the absence of **1** and was also used in the release assays (Table 1); thoroughly hydrated **4** and **6** were incubated with bFGF (10 ng) for 2 h prior to conducting the experiments. In the case of **4** where the mole ratio of immobilized LMWH to bFGF is 13,000:1, there is an essentially negligible burst release, after which the release was slowly sustained for up to 16 d with a cumulative release of less than 10%. As also seen in Figure 3 and Table 1, the LMWH-free hydrogel showed a significant burst release (nearly 80% of the initially loaded bFGF) within 1h. The observed results in this experiment show a good agreement with previous computational studies which suggest that heparin:bFGF ratios of 100:1 and 1000:1 reduce passive diffusion of bFGF from the ends of a cylindrical tube to

Table 1. Characteristics of Hydrogels Employed in bFGF Release Assays

Matrix	Crosslinker	Molar Ratio (LMWH:bFGF)	bFGF Binding	bFGF Release (%)
3	PEG-HIP, Noncovalent	1,340,000: 1	Yes	~20
4	PEG methyl ether acrylate, Covalent	13,000:1	Yes	< 10
5	"	N/A	No	N/A
6	"	0:1	No	~80

Downloaded by NORTH CAROLINA STATE UNIV on August 28, 2012 | http://pubs.acs.org
Publication Date: September 23, 2006 | doi: 10.1021/bk-2006-0939.ch013

4% and 1.4% relative to that due to simple diffusion (*8*). In the experiments here, bFGF release occurs from all surfaces of the hydrogel and is not limited dimensionally, which accounts for the greater LMWH:bFGF ratio required for substantial reduction of release. Nevertheless, the binding and slow release rate observed with **4** demonstrate not only that the covalently crosslinked hydrogel derived from **1** is capable of sustained delivery of bFGF but also that **1** may be utilized for the production of growth-factor releasing, noncovalently assembled hydrogel systems. The slow rate of release could be desirable for wound healing and/or tissue regeneration applications that require extended delivery of growth factors. The ability of **1** to form noncovalently assembled, erodible hydrogels was therefore explored to determine how broadly **1** could be used in materials design.

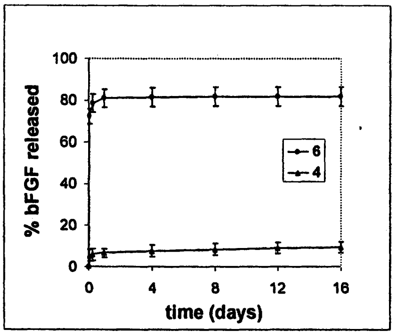

Figure 3. Profile of bFGF release from 4 and 6 as a function of time. Values shown are an average of three separate experiments. These data were plotted from data in reference 21.

Noncovalently Assembled Hydrogels

Rheological experiments were performed on **3** after the constituent molecules **1** and **2** were thoroughly mixed. In earlier reports by Seal and Panitch, the assembly, via noncovalent interactions, of high molecular weight polymers with gel-like properties was successfully demonstrated; a major difference from the investigations presented here was that PEG-peptide conjugates were mixed with high molecular weight heparin (*11*). In our experiments, solutions with 2.5 and 10wt% of **1** and **2** in PBS, respectively, were mixed to prepare a series of noncovalently assembled hydrogels, **3**, such that ligand mole ratios in **3** were 9:1, 8:2, and 6:4 (LMWH:HIP). The rheological properties of these hydrogels are shown in Figure 4. In all hydrogels assembled, excess LMWH was employed in order to produce hydrogels that would be able to bind and sequester additional heparin-binding proteins in future experiments.

Downloaded by NORTH CAROLINA STATE UNIV on August 28, 2012 | http://pubs.acs.org
Publication Date: September 23, 2006 | doi: 10.1021/bk-2006-0939.ch013

Figure 4 shows that the magnitude of $G'(\omega)$ and $G''(\omega)$ increases monotonically with increasing molar ratio of the HIP peptide component. As **2** is introduced to form the 9:1 and 8:2 molar ratio hydrogels, $G'(\omega = 0.1\text{Hz})$ exhibits a monotonic increase to 125Pa and 207Pa, respectively, with a corresponding increase in the loss moduli. Interestingly, in the case of the 6:4 molar ratio hydrogel, the storage modulus increases only moderately from that of the 8:2 hydrogel, to approximately 226Pa at 0.1Hz. The limitation in elastic modulus is presumably due to the saturation of the HIP peptide-binding sites in LMWH. Similar preliminary results have been suggested in rheological investigations of other hydrogels assembled via the interactions of PEG-LMWH and PEG-HBPs (data not shown).

Based on the combination of results from the binding experiments (Figure 2), which demonstrated that available PEG-LWMH can bind bFGF, and the bulk rheology (Figure 4), which suggested that a noncovalently assembled hydrogel with a LMWH:HIP ratio of 8:2 would have an elastic modulus potentially useful for soft tissue applications, the noncovalently assembled hydrogel **3**, formed at the ligand molar ratio of 8:2 (LMWH:HIP), was used to test the feasibility of sequestration and release of bFGF. A high ratio of LMWH:HIP (8:2) was employed in order to provide a significant amount of free LMWH to promote high levels of sequestration of the bFGF. With this ligand ratio, the overall mole ratio of LMWH to HIP peptide to bFGF (10 ng) is 1 800 000:460 000:1, indicating that the HIP peptide is limiting in the assembly process, and therefore excess LMWH should be free and available for binding to bFGF. With the assumption that one HIP peptide binds per LMWH chain, the theoretical mole ratio of free LMWH to bFGF in **3** is 1 340 000:1, which represents more than a 100-fold increase in mole ratio of free LMWH to bFGF when compared to **4** (Table 1) and may therefore slow the release of bFGF from **3** relative to **4**. That only a single HIP peptide would bind to each LMWH chain is suggested by the fact that the binding sequences of the HIP peptide (and those of bFGF) in heparin are proposed to be either hexa- or pentasaccharides (*31, 32*). As the mean molecular weight of LMWH corresponds to that of a dodecasaccharide, the LMWH can likely accommodate one molecule of the HIP peptide and/or bFGF. Furthermore, the HIP peptide and bFGF binding sequences in heparin are reported to be structurally different (*33*), suggesting that the HIP peptide and bFGF do not compete for the same binding sequence in heparin. The chemical heterogeneity of the LMWH termini of **1**, coupled with the large excess of LMWH employed in the formation of these hydrogels, will therefore permit loading of these hydrogels with multiple heparin-binding peptides and proteins (such as growth factors).

The amount of bFGF released from the 8:2 mole ratio hydrogels as a function of time is shown in Figure 5. Based on the release kinetics for the covalently crosslinked hydrogel **4**, which indicate that a large excess of LMWH

Downloaded by NORTH CAROLINA STATE UNIV on August 28, 2012 | http://pubs.acs.org
Publication Date: September 23, 2006 | doi: 10.1021/bk-2006-0939.ch013

Downloaded by NORTH CAROLINA STATE UNIV on August 28, 2012 | http://pubs.acs.org
Publication Date: September 23, 2006 | doi: 10.1021/bk-2006-0939.ch013

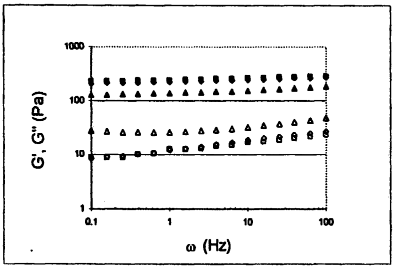

Figure 4. Storage moduli (closed symbols) and loss moduli (open symbols) of 3 at ligand molar ratios (LMWH:HIP) of 9:1 (triangles), 8:2 (diamonds), and 6:4 (squares). These data were plotted from data in reference 22.

can act to immobilize bFGF, the release kinetics of bFGF from **3** might be expected to be correspondingly slower relative to those for **4**, if the ratio of LMWH:HIP alone controlled the release of bFGF. As shown in Figure 5 and Table 1, however, the release of bFGF from **3** is much more rapid than that from **4**, suggesting that bFGF release from **3** is primarily associated with erosion of the noncovalently associated matrix. The matrix erosion kinetics of **3** were therefore examined to

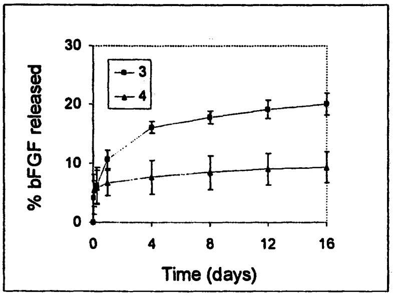

Figure 5. bFGF release profiles from 3 and 4 as a function of time. % bFGF released was determined via immunochemical assay and values shown are an average of three experiments. These data were plotted from data in reference 21.

determine the correlation between matrix erosion and the bFGF release profiles observed for **3**. Figure 6 illustrates the erosion profile for **3**, and as seen in the figure, matrix erosion resulted in a net mass loss of approximately 13% after 24 h. Assuming that **3** erodes uniformly to give the individual molecules **1** and **2** at a ligand mole ratio of 8:2 (LMWH:HIP), this 13% net mass loss represents a mass loss of 10.9wt% for **1**, which very closely matches the 10.6% of bFGF that was released from the hydrogel over the same time period. Provided that bFGF is evenly sequestered in **3**, these results suggest that the initially loaded bFGF is passively released in the form of a bFGF/**1** complex due to matrix erosion. Similarly, after 4 d the net losses of **1** (16.8wt%) due to matrix erosion still closely correlate with the cumulative release of bFGF (16.1%). A significant amount of bFGF continues to be released even after 8 d due to matrix erosion, although at slightly less than expected cumulative amounts based on the measured amount of matrix erosion. Furthermore, the diffusion-based release of bFGF from the highly heparinized hydrogel **4** over these timescales is insignificant (Figure 3), which provides additional support that the cumulative release of bFGF from **3** (Figure 5) results from matrix erosion. Other preliminary experiments indicate similar trends for the delivery of bFGF from other highly heparinized, noncovalent hydrogels (data not shown).

Downloaded by NORTH CAROLINA STATE UNIV on August 28, 2012 | http://pubs.acs.org
Publication Date: September 23, 2006 | doi: 10.1021/bk-2006-0939.ch013

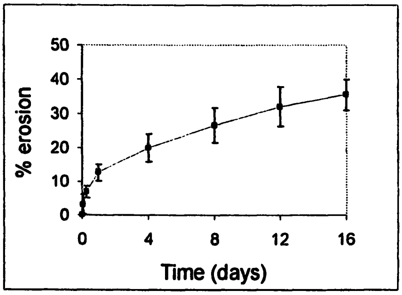

Figure 6. Matrix erosion profile of 3 as a function of time. Values shown are an average of three separate experiments. These data were plotted from data in reference 21.

Assays of human umbilical vein endothelial cell (HUVEC) adhesion and proliferation via optical microscopy and MTT assays indicate that bFGF released from **4** is bioactive (data not shown), based on the expected and observed increased adhesion and proliferation of this cell line in response to bFGF. There may be further improvements in bioactivity of the growth factor upon release from **3**, via stabilization of bFGF by PEG-LMWH in solution upon their co-release. Furthermore, the release rates of bFGF from **3** shown in this study are similar to those reported for other heparin-containing delivery systems (*6, 15, 16*), suggesting the utility of the hydrogels in mediating neovascularization and other biological events. The binding and release of bFGF by **1**, coupled with the successful noncovalent assembly of hydrogels upon interaction of **1** with **2**, indicate that **1** is capable of binding multiple types of heparin-binding molecules, and suggest that the bioconjugate may be generally useful for hydrogel assembly mediated by other heparin-binding peptides and

Downloaded by NORTH CAROLINA STATE UNIV on August 28, 2012 | http://pubs.acs.org
Publication Date: September 23, 2006 | doi: 10.1021/bk-2006-0939.ch013

proteins. Indeed, formation of noncovalent hydrogels via interactions between **1** and other PEG-HBPs and/or heparin-binding proteins has also been indicated (data not shown). The general use of **1** and other heparin-binding macromolecules offers a variety of opportunities for the production of bioactive, erodible matrices with tunable rheological, erosion, and delivery profiles that can be engineered based on designed heparin-peptide and heparin-protein interactions; such studies are currently under investigation.

Conclusions

The multifunctional PEG-LMWH bioconjugate offers multiple routes to materials that can sequester and release bioactive bFGF. Noncovalently assembled hydrogels with tunable elastic moduli can be produced via control of the ratio of PEG-LMWH and PEG-HBP in the hydrogel. The release of bFGF shows a close correlation with the release of PEG-LMWH, suggesting that bFGF is released from these hydrogels in conjunction with the PEG-LMWH. This approach may be generalized to produce bioactive materials that can deliver other therapeutically important heparin-binding peptides and proteins.

Acknowledgments

This work was supported in part by the National Institutes of Health (5 P20 RR15588 and 1 R01 EB003172-01), the Army Research Office (DAAD19-02-1-0173), and the Arnold and Mabel Beckman Foundation. Alyssa Panitch and Brandon Seal are thanked for helpful discussions. Cindy Farach-Carson and Weidong Yang are acknowledged for help with sandwich ELISA assays, Le Zhang for SPR data, Eric Furst and Byeong-Seok Chae for assistance with rheology experiments, and Robert Sikes and Nathaniel Brennan for HUVEC assay data.

References

1. Grande, D.; Baskaran, S.; Baskaran, C.; Gnanou, Y.; Chaikof, E. L. *Macromolecules* **2000**, *33*, 1123.
2. Grande, D.; Baskaran, S.; Chaikof, E. L. *Macromolecules* **2001**, *34*, 1640.
3. Shu, X. Z.; Liu, Y. C.; Palumbo, F. S.; Lu, Y.; Prestwich, G. D. *Biomaterials* **2004**, *25*, 1339.
4. Capila, I., Linhardt, R. J. *Angew. Chem. Int. Ed.* **2002**, *41*, 391.

5. Fujita, M.; Ishihara, M.; Simizu, M.; Obara, K.; Ishizuka, T.; Saito, Y.; Yura, H.; Morimoto, Y.; Takase, B.; Matsui, T.; Kikuchi, M.; Maehara, T. *Biomaterials* **2004**, *25*, 699.
6. Ishihara, M.; Obara, K.; Ishizuka, T.; Fujita, M.; Sato, M.; Masuoka, K.; Saito, Y.; Yura, H.; Matsui, T.; Hattori, H.; Kikuchi, M.; Kurita, A. *J. Biomed. Mater. Res. Part A* **2003**, *64A*, 551.
7. Schense, J. C.; Hubbell, J. A. *Bioconjugate Chem.* **1999**, *10*, 75.
8. Sakiyama-Elbert, S. E.; Hubbell, J. A. *J. Controlled Release* **2000**, *65*, 389.
9. Sakiyama-Elbert, S. E.; Hubbell, J. A. *Annu. Rev. Mater. Res.* **2001**, *31*, 183.
10. Halstenberg, S.; Panitch, A.; Rizzi, S.; Hall, H.; Hubbell, J. A. *Biomacromolecules* **2002**, *3*, 710.
11. Seal, B. L.; Panitch, A. *Biomacromolecules* **2003**, *4*, 1572.
12. Tanihara, M.; Suzuki, Y.; Yamamoto, E.; Noguchi, A.; Mizushima, Y. *J. Biomed. Mater. Res.* **2001**, *56*, 216.
13. Wissink, M. J. B.; Beernink, R.; Pieper, J. S.; Poot, A. A.; Engbers, G. H. M.; Beugeling, T.; van Aken, W. G.; Feijen, J. *Biomaterials* **2001**, *22*, 151.
14. Liu, L. S.; Ng, C. K.; Thompson, A. Y.; Poser, J. W.; Spiro, R. C. *J. Biomed. Mater. Res.* **2002**, *62*, 128.
15. Chinen, N.; Tanihara, M.; Nakagawa, M.; Shinozaki, K.; Yamamoto, E.; Mizushima, Y.; Suzuki, Y. *J. Biomed. Mater. Res. Part A* **2003**, *67A*, 61.
16. Wissink, M. J. B.; Beernink, R.; Poot, A. A.; Engbers, G. H. M.; Beugeling, T.; van Aken, W. G.; Feijen, J. *J. Controlled Release* **2002**, *64*, 103.
17. Magoshi, T.; Matsuda, T. *Biomacromolecules* **2002**, *3*, 976.
18. Matsuda, T.; Magoshi, T. *Biomacromolecules* **2002**, *3*, 942.
19. Zamora, P. O.; Tsang, R.; Pena, L. A.; Osaki, S.; Som, P. *Bioconjugate Chem.* **2002**, *13*, 920.
20. Harris, J. M.; Chess, R. B. *Nat. Rev. Drug Discovery* **2003**, *2*, 214.
21. Yamaguchi, N.; Kiick, K. L. *Biomacromolecules* **2005**, *6*, 121.
22. Yamaguchi, N.; Chae, B.-S.; Zhang, L.; Kiick, K. L.; Furst, E. M. *Biomacromolecules* **2005**, *6*, 131.
23. Raboudi, N.; Julian, J.; Rohde, L. H.; Carson, D. D. *J. Biol. Chem.* **1992**, *267*, 11930.
24. Tay, S. W.; Merrill, E. W.; Salzman, E. W.; Lindon, J. *Biomaterials* **1989**, *10*, 11.
25. Nadkarni, V. D.; Pervin, A.; Linhardt, R. J. *Anal. Biochem.* **1994**, *222*, 59.
26. Osmond, R. I. W.; Kett, W. C.; Skett, S. E.; Coombe, D. R. *Anal. Biochem.* **2002**, *310*, 199.
27. Kaiser, E.; Colescot, R. L.; Bossinge, C. D.; Cook, P. I. *Anal. Biochem.* **1970**, *34*, 595.
28. Lutolf, M. P.; Hubbell, J. A. *Biomacromolecules* **2003**, *4*, 713.

Downloaded by NORTH CAROLINA STATE UNIV on August 28, 2012 | http://pubs.acs.org
Publication Date: September 23, 2006 | doi: 10.1021/bk-2006-0939.ch013

29. Bo, G.; Wesslen, B.; Wesslen, K. B. *J. Polym. Sci. Part A-Polym. Chem.* **1992**, *30*, 1799.
30. Luo, N.; Hutchison, J. B.; Anseth, K. S.; Bowman, C. N. *Macromolecules* **2002**, *35*, 2487.
31. Liu, S. C.; Zhou, F. Y.; Hook, M.; Carson, D. D. *Proc. Natl. Acad. Sci. U.S.A.* **1997**, *94*, 1739.
32. Faham, S.; Hileman, R. E.; Fromm, J. R.; Linhardt, R. J.; Rees, D. C. *Science* **1996**, *271*, 1116.
33. Liu, S. C.; Hoke, D.; Julian, J.; Carson, D. D. *J. Biol. Chem.* **1997**, *272*, 25856.

Downloaded by NORTH CAROLINA STATE UNIV on August 28, 2012 | http://pubs.acs.org
Publication Date: September 23, 2006 | doi: 10.1021/bk-2006-0939.ch013

Downloaded by UNIV OF GUELPH LIBRARY on August 9, 2012 | http://pubs.acs.org
Publication Date: September 23, 2006 | doi: 10.1021/bk-2006-0939.ch014

Chapter 14

Thermo-Sensitive Gels: Biodegradable Hydrogels from Enantiomeric Copolymers of Poly(lactide) and Poly(ethylene glycol)

Tomoko Fujiwara[1] **and Yoshiharu Kimura**[2]

[1]**Department of Chemistry, Boise State University, 1910 University Drive, Boise, ID 83725**
[2]**Department of Polymer Science and Engineering, Kyoto Institute of Technology, Matsugasaki, Kyoto 600–8585, Japan**

Biodegradable hydrogels have been developed by using block copolymers of poly(lactide) (PLA) and poly(ethylene glycol) (PEG). Here, a novel thermo-sensitive formation of hydrogel is demonstrated by mixing micellar solutions of enantiomeric block copolymers of PLA and PEG in which the specific interaction of the enantiomeric PLA chains and that of the PEG chains connected with them are responsible for the hydrogel formation. This unique helix-induced gel is potentially useful for use as injectable drug carrier and implantable scaffold for tissue engineering.

In Degradable Polymers and Materials; Khemani, K., et al.;
ACS Symposium Series; American Chemical Society: Washington, DC, 2006.

Introduction

Polymer gels are classified by their crosslinking mechanism into two types – chemical and physical gels. The physical gels are crosslinked by physical bonds such as van der Waals interaction, hydrogen bond, hydrophobic interaction, and molecular entanglement. Poly(N-isopropylacrylamide) (PNIPAM), which is one of the most widely known physical gels, has a low critical solution temperature (LCST) around 32°C and forms a gel above the LCST as the both results of dehydration of the hydrophobic isopropyl groups and hydrogen bonding to the carbonyl groups (*1-4*). A triblock copolymer of poly(ethylene oxide) and poly(propylene oxide) (PEO-PPO-PEO), which is utilized as non-ionic surfactant by the trade names of Pluronic® and Poloxamer®, also exhibits sol-gel phase transition in water. Many researchers have studied the mechanism of this gelation (*5-9*) to conclude that the micelles are formed and packed to induce sol-to-gel transition near LCST and the PEO corona blocks shrink to lead gel-to-sol transition at higher temperature. In other cases, helix formation is responsible for the gel formation of gelatin and agarose in a cooled aqueous medium (*10*), while hydration of poly(oxyethylene) that grafted onto a substrate forms a gel (*11*).

Recently, these polymer gels have been applied as biomedical materials with achieving remarkable advances in medical science and biotechnology (*12*). The applications involve cell culture, tissue engineering, drug delivery system (DDS), medical sensing, and so on, for which the biocompatibility, biodegradability and safety of the gels are extremely important as well as the physicochemical properties. Particularly, biodegradability of the gels is essential in their *in vivo* use, and accordingly they must be prepared from biodegradable polymers having good biocompatibility. Among the biodegradable polymers thus developed, polylactides (PLA) have been receiving a special interest not only as eco-plastic materials (*13*) but also as biomedical materials (*14*). Since lactic acid, the starting material of PLA, can be derived from renewable natural resources such as cornstarch, PLA is regarded as one of the sustainable materials. The PLA consisting of the enantiomeric L- and D-lactic acids are called poly(L-lactide) (PLLA) and poly(D-lactide) (PDLA), respectively. Only PLLA is now being produced in industrial scale by ring-opening polymerization of L-lactide that can be synthesized from L-lactic acid, a renewable feedstock manufactured by large-scale fermentation. It is also known that the polymer blend of PLLA and PDLA forms a stereocomplex whose melting temperature (T_m) is 230°C, approximately 50°C higher than that of the respective PLLA and PDLA (*15-19*). Therefore, the improved properties are expected with the stereocomplex of PLLA and PDLA. Based on these backgrounds many trials have been done to obtain polymer gels from PLA derivatives.

Downloaded by UNIV OF GUELPH LIBRARY on August 9, 2012 | http://pubs.acs.org
Publication Date: September 23, 2006 | doi: 10.1021/bk-2006-0939.ch014

In this chapter, thermo-sensitive hydrogels of block copolymer systems consisting of enantiomeric PLA and poly(ethylene glycol) (PEG) will be described. Particularly, mechanistic studies will be stressed for the insight into the specific interaction of the enantiomeric PLA blocks and the role of PEG blocks in the hydrogel formation.

Hydrogels from various PLA-PEG block copolymers: ABA and BAB triblock and AB diblock

One of the preparative approaches to the hydrogels is to synthesize block copolymers consisting of the hydrophobic "hard" A-block, PLA and the hydrophilic "soft" B-block, PEG as the block components. Since both PLA and PEG are highly biocompatible and bioresorbable, the PLA-PEG block copolymers can provide various biomedical applications as temporary devices for clinical and pharmaceutical purposes. Zhu et al. first prepared a block copolymer, poly(DL-lactide)-*block*-polyoxyethylene (PDLLA-PEG) for use as a drug carrier in 80's (*20,21*). The typical chemical structures of ABA, BAB, and AB block copolymers are shown in Figure 1.

The ABA type block copolymer, PLA-PEG-PLA, has been most extensively studied since late 80's in regard to its synthesis (*22-27*), properties (*28,29*), and degradability (*30-34*). In the ABA system, PEG works as an intermolecular plasticizer in processing implant pastes, films, and scaffolds. Its hydrogels have also been studied mainly for their biomedical application (*35,36*). Vert et al. have recently reported the utilization of the hydrogels to the protein release (*37*). Microspheres have been prepared from the ABA block copolymers by W/O or W/O/W emulsion technique (*38-40*), and utilized for

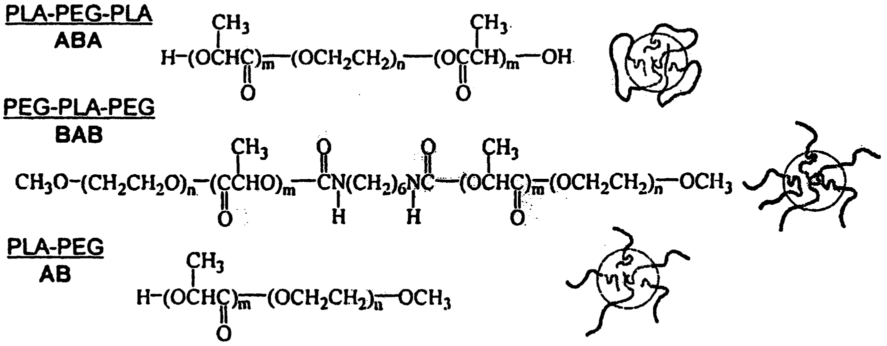
PLA-PEG-PLA
ABA
$H{-}(OCH(CH_3)C(=O))_m{-}(OCH_2CH_2)_n{-}(OC(=O)CH(CH_3))_m{-}OH$
PEG-PLA-PEG
BAB
$CH_3O{-}(CH_2CH_2O)_n{-}(C(=O)CH(CH_3)O)_m{-}C(=O)N(H)(CH_2)_6N(H)C(=O){-}(OCH(CH_3)C(=O))_m{-}(OCH_2CH_2)_n{-}OCH_3$
PLA-PEG
AB
$H{-}(OCH(CH_3)C(=O))_m{-}(OCH_2CH_2)_n{-}OCH_3$

Figure 1. Polymer structures and schematics of the micelles in aqueous medium.

Downloaded by UNIV OF GUELPH LIBRARY on August 9, 2012 | http://pubs.acs.org
Publication Date: September 23, 2006 | doi: 10.1021/bk-2006-0939.ch014

encapsulating hydrophilic macromolecular drugs. Nanoparticles with much smaller diameters (10~1000 nm) have been introduced for the drug targeting (*41*), and their properties have been analyzed for the practical biodegradable materials (*42-45*).

Recently, S. W. Kim et al. demonstrated the preparation of injectable microparticles for DDS from a BAB type triblock copolymer, poly(ethylene glycol)-*block*-poly(L-lactide)-*block*-poly(ethylene glycol) (PEG-PLLA-PEG) (*46,47*). The aqueous micellar solution containing BAB copolymers exhibited a sol-to-gel phase transition with decreasing temperature from higher temperature to the body temperature. The transition temperature varied depending on the block lengths and polymer concentration. The formation mechanism of this hydrogel is probably a simple swelling and hydration of the PEG layers. This group also developed the hydrogels by incorporating poly(L-lactide-coglycolide) (PLGA) as the A-block and observed a more complicated phase diagram having both sol-to-gel and gel-to-sol transitions with increasing temperature, just as the PEO-PPO-PEO system. It was believed from their small-angle light scattering (SLS) and dynamic light scattering (DLS) studies that an increase of aggregation number of the micelles causes the gelation (*46,48*).

AB diblock copolymers also have been used to create micelles which encapsulate drugs (*49,50*). Cohn and Younnes synthesized a family of PLAPEG block copolymers in their attempt to provide biodegradable elastomers for cardiovascular implants (*51*). AB diblock copolymers also form hydrogels by temperature change (*52*). The mechanism of this gelation is suggested to be similar to that of PEG-PLLA-PEG or other simple BAB triblock copolymers.

Downloaded by UNIV OF GUELPH LIBRARY on August 9, 2012 | http://pubs.acs.org
Publication Date: September 23, 2006 | doi: 10.1021/bk-2006-0939.ch014

Hydrogels from mixtures of enantiomeric PLA-PEG block copolymers: ABA and BAB triblock and AB diblock

Copolymer synthesis and gel formation

A number of PLA-PEG block copolymers having various molecular weights and block ratios have been synthesized thus far. Table I summarizes a set of copolymers of ABA, BAB, and AB types that have been demonstrated to induce thermo-sensitive gelation when L- and D-copolymers are mixed. Interestingly, the PLA/PEG ratio of the all different types is found to be near 0.5.

The ordinary ring-opening polymerization of L- or D-lactide initiated with PEG and MePEG gave the ABA and AB block copolymers, respectively, in high yields (*53,54*). The BAB triblock copolymers were obtained by the coupling of the AB diblock copolymers with hexamethylene diisocyanate (HMDI) (Figure 1) (*46*). These copolymers readily formed the core-shell type amphiphilic micelles in water as illustrated in Figure 1. The average hydrodynamic diameters of the micelles measured by DLS were in the range of 20-30 nm for 1 wt% solutions of all these copolymers. To obtain sol-to-gel or gel-to-sol transition, micellar solutions were prepared at various concentrations, and both solutions of L- and D-copolymers were mixed together at low temperature (typically at 4°C). Then the temperature increased up to 75 °C to observe the sol-gel behavior. All solutions were prepared in water.

The molecular weights of ABA, BAB and AB copolymers listed in Table I showed the best performance as a thermo-sensitive hydrogel. The authors have prepared a variety of length and composition of copolymers for each block type, and found that the PLA/PEG composition ratio and the size of appearance of PEG shell layer (since the PEG of ABA micelle makes a loop) were similar for three types of micelles rather than the molecular weights of PLA blocks.

Table I. Typical block copolymers and the molecular weight

Type	*Copolymers*	*PLA block (M_n)*	*PEG block (M_n)*	*total (M_n)*	*PLA/PEG*
ABA	PLLA-PEG-PLLA	1300	4600	7200	0.56
	PDLA-PEG-PDLA	1100	4600	6800	0.48
BAB	PEG-PLLA-PEG	2000	2000	6000	0.50
	PEG-PDLA-PEG	2000	2000	6000	0.50
AB	PLLA-PEG	1100	2000	3100	0.55
	PDLA-PEG	900	2000	2900	0.45

Hydrogels from micellar solutions of ABA triblock copolymers

At first, the spontaneous gel formation of the mixed micellar solution of the enantiomeric ABA triblock copolymers, PLLA-PEG-PLLA and PDLA-PEGPDLA, is discussed. This system is characterized by an interesting temperaturedependent sol-to-gel transition that is induced around 37°C by the stereocomplexation of the PLLA and PDLA block segments (*53*). The gel formation was successfully monitored by the rheological change of a micellar solution, and the stereocomplex formation was confirmed by wide-angle X-ray scattering (WAXS).

Figure 2 shows the sol-gel transition diagram of the mixed micellar solutions of PLLA-PEG-PLLA and PDLA-PEG-PDLA with respect to temperature and polymer concentration. Note that the single PLLA-PEG-PLLA micellar solution showed the only solution state at any temperature and concentration plotted in Figure 2 and all later phase diagrams. With the enantiomeric mixture having a concentration of 10 wt%, the so-to-gel transition

Downloaded by UNIV OF GUELPH LIBRARY on August 9, 2012 | http://pubs.acs.org
Publication Date: September 23, 2006 | doi: 10.1021/bk-2006-0939.ch014

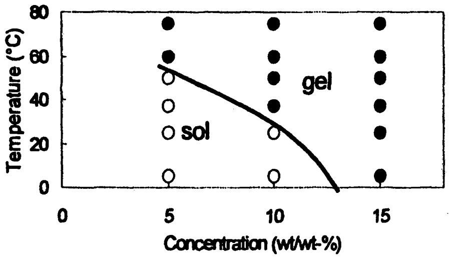

Figure 2. The phase diagram of mixed micellar solutions of PLLA-PEG-PLLA and PDLA-PEG-PDLA.

was observed between room temperature (25°C) and the body temperature (37°C) as shown in Figure 3A(d,e). While the single micellar solution of PLLAPEG-PLLA (control) turned white fluid after heating to 75°C (c) by the crystallization of homocrystals, the mixture became a white gel at 75°C (f).

We confirmed the responsibility of the stereocomplex formation of the enantiomeric polylactide blocks on the gelation by synchrotron WAXS measurement. Figure 3B shows the temperature-dependent WAXS profiles for the mixed solution. The measurement was started immediately after the 10 wt% micellar solutions of PLLA-PEG-PLLA and PDLA-PEG-PDLA were mixed at room temperature, and the data was collected every half minute by *in situ* heating at a rate of 2°C/min. Small diffraction peaks are confirmed at $2\theta = 16.8$ and 19.4° in the starting mixture, which means that the small amount of hexagonal crystals of PLLA and PDLA exist in the core of the micelles at room temperature. These diffractions are attributed to the (200) or (110) plane and the (203) or (113) plane of the hexagonal crystal lattice comprising the PLLA or PDLA 10/3-helices (*55*). With increasing temperature, the WAXS data show two different reflections at $2\theta = 12.1$ and 21.7° in addition to the small reflections of the hexagonal crystals. The formers are reasonably ascribed to the crystals of the stereocomplex of PLLA and PDLA (*53,54*). Around 37°C, these reflections are still weak, indicating that both the PLLA and PDLA chains may be mixed into a complexation state prior to the crystallization. At 75°C, the significant crystal growth of the stereocomplex is clearly shown.

In the single PLLA-PEG-PLLA micellar solution (control experiment), the hexagonal crystal growth was also observed with increasing temperature despite of its sol nature. The degree of crystallinity estimated from the WAXS was almost identical with that observed in the mixed solution at each temperature. Since the single and mixed solutions have same degree of crystallinity but mainly have different crystal forms which are hexagonal and stereocomplex, respectively, it is suggested that the gel formation in the mixed solution is closely related with the stereocomplexation of the enantiomeric PLA blocks.

Downloaded by UNIV OF GUELPH LIBRARY on August 9, 2012 | http://pubs.acs.org
Publication Date: September 23, 2006 | doi: 10.1021/bk-2006-0939.ch014

Downloaded by UNIV OF GUELPH LIBRARY on August 9, 2012 | http://pubs.acs.org
Publication Date: September 23, 2006 | doi: 10.1021/bk-2006-0939.ch014

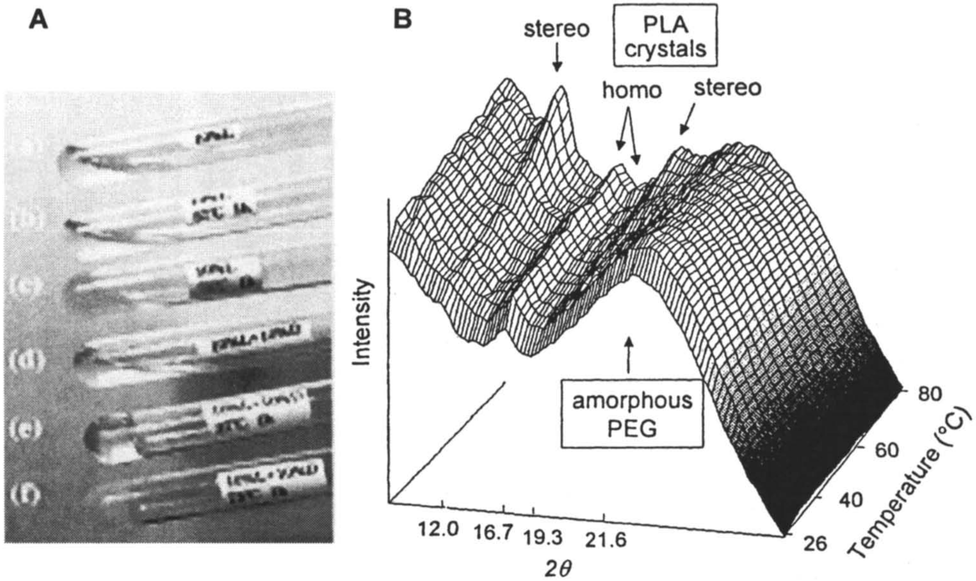

Figure 3. The appearances of 10wt% of ABA micellar solutions (A); PLLA-PEG-PLLA at room temperature(a), 37°C(b), 75°C(c), and enantio-mixture at room temperature(d), 37°C (e), 75°C (f). The temperature-dependent WAXS measurement of the mixture at a heating rate 2°C/min (B). (A:Reproduced from reference 53. Copyright 2001 Wiley-VCH.)

Hydrogels from BAB triblock copolymers

The second gel system consists of the enantiomeric BAB type triblock copolymers, PEG-PLLA-PEG and PEG-PDLA-PEG. The sol-gel transition of this system should be induced by the stereo interaction of L- and D-copolymers, being much different from that of the single BAB (PEG-PLLA-PEG) system that has previously been described to occur gelation by the ordinary hydrophobic/hydrophilic interaction (*46*).

The aqueous micellar solutions of PEG-PLLA-PEG (2000-2000-2000) or PEG-PDLA-PEG (2000-2000-2000) keep a "sol" phase at all temperatures in the concentration range of 10-40 wt%. Figure 4 is a sol-gel transition diagram plotted for 1:1 (v/v) mixed micellar solutions of PEG-PLLA-PEG and PEG-PDLA-PEG with respect to temperature and polymer concentration. It is found that the gel state cannot be formed at concentration lower than 30 wt% and that the gel state is preferentially kept below 75°C at concentration higher than 40 wt%. The gel-to-sol transition temperature increases up to 75°C at higher concentration. It should be noted here that in the present BAB system the gel and sol are formed at low and high temperatures, respectively, in a reversible manner. This is quite opposite to the above ABA system for which the gelation is induced with increasing temperature in an irreversible manner.

Figure 5A shows the typical changes of the mixed solution at a concentration of 35 wt% before and after the heat treatment from 37°C (c) to 75°C (d). This gel is formed immediately after the L- and D- solutions are mixed at room temperature.

It is observed that the mixed solution is in gel and sol states at 37 and 75°C, respectively, while the single solution remained fluid irrespective of the temperature (a,b). Since gel-to-sol transformation of the mixed solutions is reversible with the temperature change, sample (d) returns to gel after cooling to room temperature.

Downloaded by UNIV OF GUELPH LIBRARY on August 9, 2012 | http://pubs.acs.org
Publication Date: September 23, 2006 | doi: 10.1021/bk-2006-0939.ch014

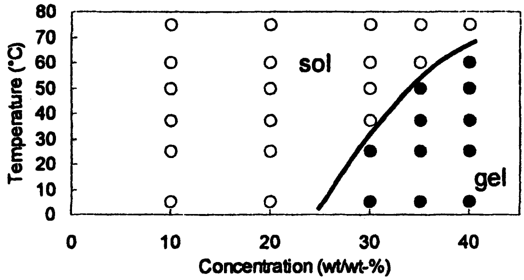

Figure 4. The phase diagram of mixed micellar solutions of PEG-PLLA-PEG and PEG-PDLA-PEG. (Reproduced from reference 54. Copyright 2004 Wiley-VCH.)

Downloaded by UNIV OF GUELPH LIBRARY on August 9, 2012 | http://pubs.acs.org
Publication Date: September 23, 2006 | doi: 10.1021/bk-2006-0939.ch014

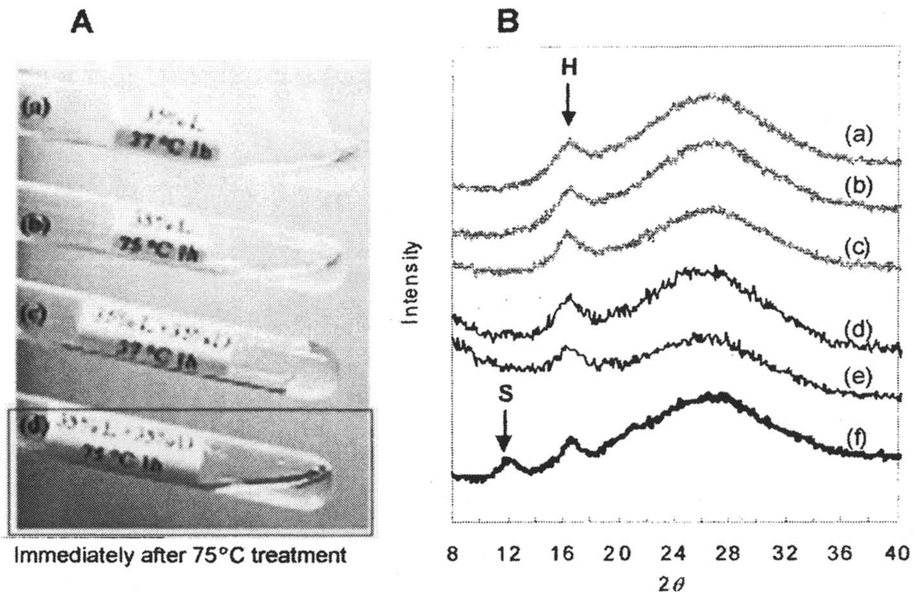

Figure 5. The appearance of 35wt% of BAB micellar solutions (A); PEG-PLLA-PEG at 37°C(a), 75°C(b), and enantio-mixture at 37°C(c), 75°C(d). The WAXS profiles of BAB micellar solutions (B); PEG-PLLA-PEG at room temperature(a), after 37°C(b), after 75°C(c), and enantio-mixture at room temperature(d), after 37°C(e), and after 75°C(f). (Reproduced from reference 54. Copyright 2004 Wiley-VCH.)

Figure 5B shows the WAXS profiles of the single and mixed solutions at different temperatures. The mixed solution shows very small reflections at 2θ = 12.1 and 21.7° in addition to the reflections of the hexagonal crystals (2θ =16.8°) of PLLA or PDLA only when heated at 75°C. This fact suggests that the stereocomplexation of the PLLA and PDLA blocks is induced even in the mixed solution heated at high temperature where the sol state is achieved. When this BAB sol is cooled, the gelation revives without significant change in the WAXS profile. Furthermore, the degree of crystallinity which was estimated by peak sepalation of each crystal and amorphous peaks. does not increase by the heat treatment, being obviously different from the ABA gel system. It is therefore concluded that the stereocomplexation is not directly related with the gel formation mechanism for the BAB system. The possible mechanism of this hyderogel is discussed in later section.

On the other hand, the Mechanical properties of the hydrogels are important for their practical application. From the time-dependent rheological change of the mixed micellar solutions of ABA and BAB copolymers at 37°C, the mechanical properties of the BAB system are dramatically higher than those of the ABA system (*53,54*). For the BAB system, the storage modulus (G') gradually rises up to reach 31 kPa after 60 min with the gelation occurring comparing to low G' of the ABA system, 400 Pa. This may be due to the increased polymer concentration in the micellar solution. The physical crosslinking though the PEG interaction can afford enough mechanical properties of the gel.

Downloaded by UNIV OF GUELPH LIBRARY on August 9, 2012 | http://pubs.acs.org
Publication Date: September 23, 2006 | doi: 10.1021/bk-2006-0939.ch014

Hydrogels from AB-diblock copolymers

Mixed micellar solutions of enantiomeric ABA or BAB block copolymers exhibited very different gelation behavior and crystal structure. As the third system, the micellar solutions of AB block copolymers, PLLA-PEG and PDLAPEG, were examined for the hydrogel formation. The AB system is similar to ABA in that the B-blocks form the corona shape in micelles as illustrated in Figure 1, while having a similarity with BAB because the mobility of the core A-blocks is similar to each other.

Figure 6 is a typical sol-gel phase diagram plotted for the mixed solutions of the enantiomeric AB diblock copolymers. This resembles the diagram of BAB system shown in Figure 4, indicating that the gel-to-sol transition occurs with increasing temperature. Figure 7A shows the typical phase changes of a mixed solution of the PLLA-PEG and PDLA-PEG (total 30 wt%) at 37°C (c) and 75°C (d) as compared with those of the corresponding single micellar solution of PLLA-PEG (30 wt%) (a,b). Although the latter solution does not form gel at any temperature, the mixed solution forms a gel on mixing at room temperature. The difference from the BAB system is that the sol formed at 75°C never turns to gel again when cooled. This irreversible nature suggests that the interaction of the micelles formed in the hydrogel at lower temperature may be changed after

Downloaded by UNIV OF GUELPH LIBRARY on August 9, 2012 | http://pubs.acs.org
Publication Date: September 23, 2006 | doi: 10.1021/bk-2006-0939.ch014

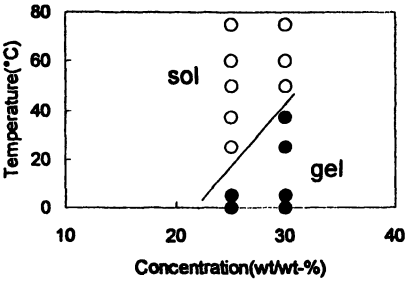

Figure 6. The phase diagram of mixed micelle solution of PLLA-PEG and PDLA-PEG.

turning to sol state by heating. Note that the normally synthesized AB diblock copolymer should involve a small amount of ABA triblock copolymer because MePEG is contaminated with dihydroxyterminated PEG (*56,57*). Kimura and his coworkers recently eliminated this impurity by high osmotic pressure chromatography and confirmed the same hydrogel formation for the pure enantiomeric AB system.

Figure 7B shows the WAXS profiles of the AB systems. They are significantly different from those of the BAB system. The single micellar solution of PLLA-PEG shows an increase in the crystallinity (a,b) with increasing temperature, while that of PEG-PLLA-PEG does not show such behavior. In the mixed AB solution, the gel state formed at lower temperature involves the hexagonal crystals as shown by the reflection at 2θ = 16.8° (c), and the sol state attained by heating at 75°C comprises the stereocomplex crystals (2θ = 12.1 and 21.7°) with most of the hexagonal crystals being lost (d). This feature is similar to that of the ABA system rather than the BAB system.

Mechanistic aspect of enantiomeric PLA-*b*-PEG hydrogels

In the micellar solutions of the enantiomeric ABA triblock copolymers, the hydrophobic PLLA and PDLA segments aggregate to form a core region around which the hydrophilic PEG segments settle to form a shell. Therefore, the PLLA and PDLA segments are isolated from each other when the micellar solutions of the enantiomeric block copolymers are mixed. When heated, the aggregation of the PLLA and PDLA segments in the core/shell interface is weakened to allow mixing of the segments outside the core. The shorter block length of PLLA and PDLA is favorable for this chain scrambling and mixing. Consequently, the stereocomplexation starts as evidenced by WAXS data (Fig. 3), and the micelles are wholly crosslinked with each other at 37°C to form a gel. With increasing temperature, the crosslinking state is changed by reorganization of the hydrophobic cores and increased crystallization of the stereocomplex. This

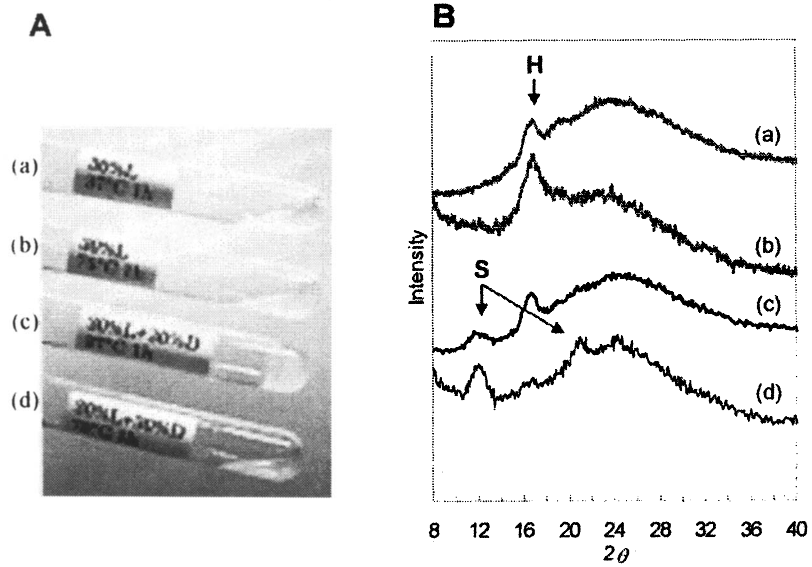

Figure 7. The appearance of 30wt% of AB micellar solutions (A); PLLA-PEG at 37°C(a), 75°C(b), and enantio-mixture at 37°C(c), 75°C(d). The WAXS profiles of AB micellar solutions (B); PLLA-PEG after 37°C(a), after 75°C(b), and enantio-mixture after 37°C(c), and after 75°C(d). (Reproduced from reference 54. Copyright 2004 Wiley-VCH.)

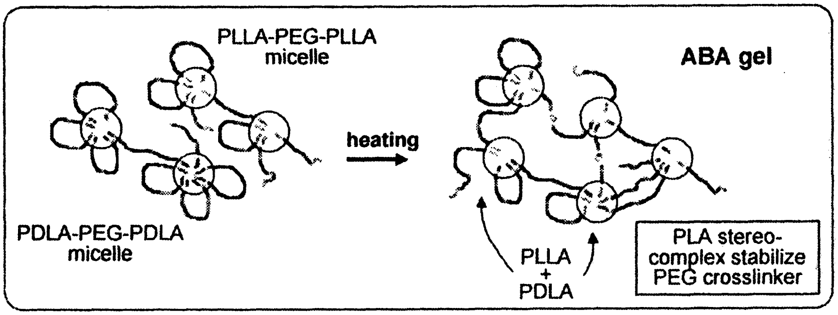
PLLA-PEG-PLLA micelle
PDLA-PEG-PDLA micelle
heating
ABA gel
PLLA + PDLA
PLA stereo-complex stabilize PEG crosslinker

Figure 8. Proposed gelation mechanism of enantiomeric mixture of ABA triblock copolymers.

Downloaded by UNIV OF GUELPH LIBRARY on August 9, 2012 | http://pubs.acs.org
Publication Date: September 23, 2006 | doi: 10.1021/bk-2006-0939.ch014

process was also supported by fluctuation of the storage modulus (G') curve in the rheology measurement (*54*). Figure 8 illustrates the schematic picture of the gelation of the ABA system. Since the stereocomplex formation depresses the mobility of the PLA chains and stabilizes the PEG crosslinkers, the gel formation is possible only for the enantiomeric mixture. This sol-gel transition is irreversible although the crosslinking is performed by the ordinary physical mechanism.

Gelation mechanism of the mixtures of enantiomeric BAB and AB block polymers is supposed to be much different from that of ABA system since the PEG blocks cannot act as direct crosslinkers between two micelles. The sol-gel transition diagrams and WAXS data suggest that the stereocomplexation between the PLLA and PDLA blocks is not directly correlated with the gelation of the mixed solution. Since in the BAB triblock copolymers the hydrophobic PLLA and PDLA are confined in the core of the micelles and surrounded by the hydrophilic PEG shell, a kind of macromolecular reorganization is needed to grow the stereocomplexation of PLLA and PDLA blocks in the micelles. Even heated at high temperature, the block chains are not easily exchanged among the micelles in the BAB system since PLLA and PDLA blocks are in the middle of copolymers (Figure 9A), so that the degree of stereocomplexation is limited. Even if the stereocomplex crystals could be formed, they are also confined in the micelle core and cannot bring such a strong interaction between the particles as to induce the gelation. It is therefore deduced that the interaction between the PEG chains surrounding the micellar cores is responsible for the gelation. Difficulty of the extensive molecular reorganization allows the sol-gel transition of the BAB system to be reversible by repeated heating and cooling.

The WAXS data (Figure 5) revealed that both PLLA and PDLA blocks of the BAB block copolymers form the hexagonal crystals in the micellar cores at room temperature. The IR spectra of the micellar solutions both in gel and sol states also showed absorption bands at 921 and 1210 cm^{-1}, supporting the presence of the 10/3 helical structure of the PLLA and PDLA blocks (*58*). This helix formation of the PLLA and PDLA blocks is possibly transmitted to the PEG chains through the block-linking bonds, because the PEG chain can readily take a similar helical conformation. In fact, the ordinary monoclinic crystals of PEG are known to consist of 7/2-helical chains. Since the helical senses of PLLA and PDLA are opposite to each other, the induced helices of the PEG chains should be right- and left-handed depending on the PLA chains connected with them. Those helical chains of PEG, having opposite senses, are allowed to aggregate probably through the chain interdigitation mechanism (or stereocomplexation of PEG), resulting in the change of hydrophilic/hydrophobic balance and leading the inter-chain cohesion of the PEG blocks even in the aqueous environment. With the helical conformation, the hydrophilic ether linkages are surrounded by the hydrophobic alkylene chains to make the whole chain hydrophobic. With a single BAB copolymer, the helices have an identical sense, and the chain interdigitation to cause gelation is impossible.

Downloaded by UNIV OF GUELPH LIBRARY on August 9, 2012 | http://pubs.acs.org
Publication Date: September 23, 2006 | doi: 10.1021/bk-2006-0939.ch014

Downloaded by UNIV OF GUELPH LIBRARY on August 9, 2012 | http://pubs.acs.org
Publication Date: September 23, 2006 | doi: 10.1021/bk-2006-0939.ch014

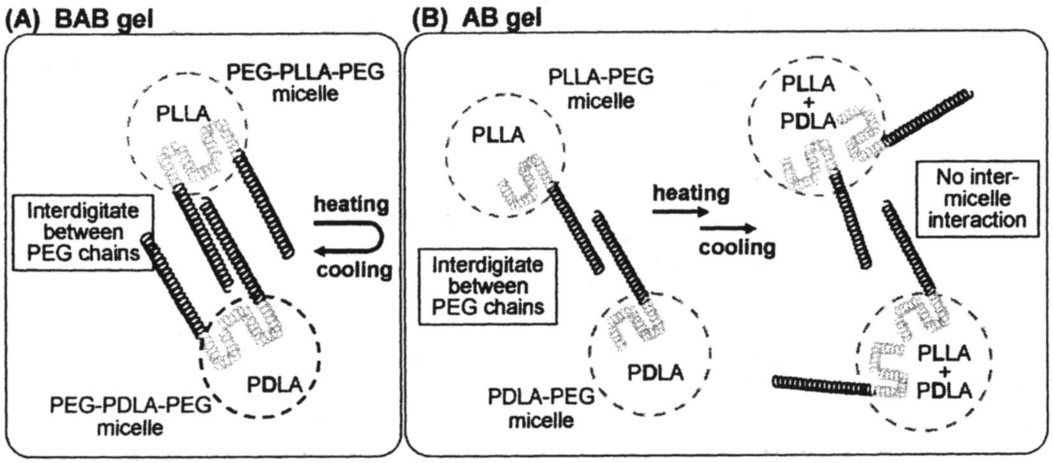
(A) BAB gel
PEG-PLLA-PEG micelle
PLLA
Interdigitate between PEG chains
heating
cooling
PDLA
PEG-PDLA-PEG micelle
(B) AB gel
PLLA-PEG micelle
PLLA
heating
cooling
Interdigitate between PEG chains
PDLA
PDLA-PEG micelle
PLLA + PDLA
No inter-micelle interaction
PLLA + PDLA

Figure 9. Proposed gelation mechanisms of enantiomeric mixture of BAB triblock (A) and AB diblock (B) copolymers.

Downloaded by UNIV OF GUELPH LIBRARY on August 9, 2012 | http://pubs.acs.org
Publication Date: September 23, 2006 | doi: 10.1021/bk-2006-0939.ch014

The interaction of the PEG chains in opposite helical senses was supported by the gelation behavior of the mixed micellar solution of the enantiomeric AB diblock copolymers (Figure 9B). In this case, the exchange of the core PLA blocks between micelles is much easier than in the BAB system, and in fact, the stereocomplex crystals grew with increasing the temperature of the mixed solution. At 75°C, most of the PLA crystals were replaced by the stereocomplex crystals. Therefore, most of the micelles comprise both PLLA and PDLA blocks in their core due to the exchange of PLA blocks at high temperature, and intermicelle interaction through the PEG in opposite helical senses is weakened even after cooling. The PEG interaction changed to intra-micellar instead of intermicellar. This is the reason why the gel of the AB system is irreversible.

Previously, we discovered an interesting band morphology formed from the nanoparticles of PLLA-PEG diblock and PLLA-PEG-PLLA triblock copolymers that were placed on a flat substrate surface (*59,60*). We verified that the band morphology is directed by crystallization of the PLLA segments and that the PLLA chains take a doubly twisted structure in it with the ordinary 10/3 helical conformation preserved. Prior to this PLLA band formation, the PEG blocks are phase-separated and play an important role. The two-dimensional network formed by the PLLA-PEG-PLLA bands on the surface well simulates the structure of the three-dimensional network systems observed in melt, concentrated solution, and hydrogel.

Figure 10 shows the atomic force microscopic (AFM) image of the nanobands prepared from a mixture of PLLA-PEG (5000-5000) and PDLA-PEG (5000-5000) micellar solutions. Each solution was 0.01 wt% in water, mixed at room temperature, cast on the mica surface, and then heated at 60 °C for 1 h. As observed from a single polymer system of PLLA-PEG, the mixed system also forms similar crystal nanobands. Extremely interesting is that they are aligned in pair (Figure 10). Analysis by TEM diffraction revealed that that both bands in pair consist of the single PLLA and/or PDLA crystals. These facts suggest that the PEG blocks connected with PLLA and PDLA interact so strongly prior to

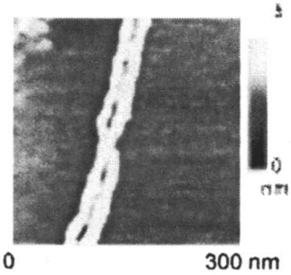

Figure 10. Typical AFM image of nanobands prepared from the enantiomeric mixture of AB block copolymers (MW: 5000-5000).

the band formation and guide the separate crystallization of the PLLA and PDLA blocks with opposite helical sense. This interaction is probably identical with that observed in the hydrogel formation of the mixture of the enantiomeric AB block copolymers.

Conclusions

Hydrogel formation of block copolymers consisting enantiomeric PLA and PEG was demonstrated. The reversible gel-sol transition occurred in the mixed micellar solution of the enantiomeric BAB triblock copolymers, PEG-PLLA-PEG and PEG-PDLA-PEG, depending on the polymer concentration and temperature. Since the stereocomplexation of the PLLA and PDLA is not responsible for the gelation, coagulation of micelles ought to be induced by the interaction of the PEG chains to which the helix formation of the PLLA and PDLA is transmitted. The PEG helices with opposite helical senses may interdigitate to lead the crosslinking of the system. The hydrogel of the mixed solution of the enantiomeric AB diblock copolymers also supported the PEG-crosslinking mechanism.

Downloaded by UNIV OF GUELPH LIBRARY on August 9, 2012 | http://pubs.acs.org
Publication Date: September 23, 2006 | doi: 10.1021/bk-2006-0939.ch014

References

1. Ringsdorf, H.; Venzmer, J.; Winnik, F. M. *Macromolecules* **1991**, *24*, 1678.
2. Takei, Y. G.; Aoki, T.; Sanui, K.; Ogata, N.; Sakurai, Y.; Okano, T. *Macromolecules* **1994**, *27*, 6163-6166.
3. Zareie, H. M.; Bulmus, E. V.; Gunning, A. P.; Hoffman, A. S.; Piskin, E.; Morris, V. J. *Polymer* **2000**, *41*, 6723-6727.
4. Maeda, Y.; Higuchi, T.; Ikeda, I. *Langmuir* **2000**, *16*, 7503-7509.
5. Vadnere, M.; Amidon, G.; Lindenbaum, S.; Haslam, J. L. *International Journal of Pharmaceutics* **1984**, *22*, 207-218.
6. Wanka, G.; Hoffmann, H.; Ulbricht, W. *Colloid and Polymer Science* **1990**, *268*, 101-117.
7. Jorgensen, E. B.; Hvidt, S.; Brown, W.; Schillen, K. *Macromolecules* **1997**, *30*, 2355-2364.
8. Deng, Y.; Yu, G. E.; Price, C.; Booth, C. *Journal of the Chemical Society-Faraday Transactions* **1992**, *88*, 1441-1446.
9. Alexandridis, P.; Holzwarth, J. F.; Hatton, T. A. *Macromolecules* **1994**, *27*, 2414-2425.
10. Rees, D. A. *Journal of the Chemical Society B-Physical Organic* **1969**, 217.
11. Hubbell, J. A.; L., W. J.; Chowdhury, S. M. In *Advanced Biomaterials in Biomedical Engineering and Drug Delivery Systems*; Springer: Tokyo, 1996; p 179.
12. Nagata, Y.; Kajiwara, K. *Gel Handbook*; NTS: Tokyo, 1997.

13. Steinbuechel, A. *Biopolymers*; Wiley-VCH: Weinheim, 2001; Vol. 3 and 4.
14. Tsuruta, T.; Hayashi, T.; Ishihara, K.; Kimura, Y. *Biomedical Applications of Polymeric Materials*; CRC Press: Boca Raton, 1993.
15. Okihara, T.; Tsuji, M.; Kawaguchi, A.; Katayama, K.; Tsuji, H.; Hyon, S. H.; Ikada, Y. *Journal of Macromolecular Science-Physics* **1991**, *B30*, 119.
16. Tsuji, H.; Horii, F.; Hyon, S. H.; Ikada, Y. *Macromolecules* **1991**, *24*, 2719.
17. Tsuji, H. *Polymer* **2000**, *41*, 3621-3630.
18. Brochu, S.; Prudhomme, R. E.; Barakat, I.; Jerome, R. *Macromolecules* **1995**, *28*, 5230-5239.
19. Brizzolara, D.; Cantow, H. J.; Diederichs, K.; Keller, E.; Domb, A. J. *Macromolecules* **1996**, *29*, 191-197.
20. Zhu, K. J.; Song, B. H.; Yang, S. L. *Journal of Polymer Science Part a-Polymer Chemistry* **1989**, *27*, 2151-2159.
21. Zhu, K. J.; Lin, X. Z.; Yang, S. L. *Journal of Applied Polymer Science* **1990**, *39*, 1-9.
22. Kricheldorf, H. R.; Boettcher, C. *Makromolekulare Chemie-Macromolecular Symposia* **1993**, *73*, 47-64.
23. Kricheldorf, H. R.; Kreisersaunders, I.; Boettcher, C. *Polymer* **1995**, *36*, 1253-1259.
24. Kricheldorf, H. R.; Meierhaack, J. *Makromolekulare Chemie-Macromolecular Chemistry and Physics* **1993**, *194*, 715-725.
25. Cerrai, P.; Tricoli, M. *Makromolekulare Chemie-Rapid Communications* **1993**, *14*, 529-538.
26. Jedlinski, Z.; Kurcok, P.; Walach, W.; Janeczek, H.; Radecka, I. *Makromolekulare Chemie-Macromolecular Chemistry and Physics* **1993**, *194*, 1681-1689.
27. Xie, W. H.; Chen, D. P.; Fan, X. H.; Li, J.; Wang, P. G.; Cheng, H. N.; Nickol, R. G. *Journal of Polymer Science Part a-Polymer Chemistry* **1999**, *37*, 3486-3491.
28. Younes, H.; Cohn, D. *Journal of Biomedical Materials Research* **1987**, *21*, 1301-1316.
29. Kubies, D.; Rypacek, F.; Kovarova, J.; Lednicky, F. *Biomaterials* **2000**, *21*, 529-536.
30. Li, Y. X.; Volland, C.; Kissel, T. *Journal of Controlled Release* **1994**, *32*, 121-128.
31. Rashkov, I.; Manolova, N.; Li, S. M.; Espartero, J. L.; Vert, M. *Macromolecules* **1996**, *29*, 50-56.
32. Shah, S. S.; Zhu, K. J.; Pitt, C. G. *Journal of Biomaterials Science-Polymer Edition* **1994**, *5*, 421-431.
33. Li, S. M.; Garreau, H.; Vert, M. *Journal of Materials Science-Materials in Medicine* **1990**, *1*, 123-130.
34. Hu, D. S. G.; Liu, H. J. *Polymer Bulletin* **1993**, *30*, 669-676.
35. Graham, N. B.; McNeill, M. E. *Biomaterials* **1984**, *5*, 27-36.
36. Li, S. M.; Rashkov, I.; Espartero, J. L.; Manolova, N.; Vert, M. *Macromolecules* **1996**, *29*, 57-62.

Downloaded by UNIV OF GUELPH LIBRARY on August 9, 2012 | http://pubs.acs.org
Publication Date: September 23, 2006 | doi: 10.1021/bk-2006-0939.ch014

37. Molina, I.; Li, S. M.; Martinez, M. B.; Vert, M. *Biomaterials* **2001**, *22*, 363.
38. Deng, X. M.; Li, X. H.; Yuan, M. L.; Xiong, C. D.; Huang, Z. T.; Jia, W. X.; Zhang, Y. H. *Journal of Controlled Release* **1999**, *58*, 123-131.
39. Perez, C.; Sanchez, A.; Putnam, D.; Ting, D.; Langer, R.; Alonso, M. J. *Journal of Controlled Release* **2001**, *75*, 211-224.
40. Beck, L. R.; Cowsar, D. R.; Lewis, D. H.; Gibson, J. W.; Flowers, C. E. *American Journal of Obstetrics and Gynecology* **1979**, *135*, 419-426.
41. Gref, R.; Domb, A.; Quellec, P.; Blunk, T.; Muller, R. H.; Verbavatz, J. M.; Langer, R. *Advanced Drug Delivery Reviews* **1995**, *16*, 215-233.
42. Sakurai, K.; Nakada, Y.; Nakamura, T.; Tudomi, R.; Matumoto, J.; Takahashi, Y. *Journal of Macromolecular Science-Pure and Applied Chemistry* **1999**, *36*, 1863-1877.
43. Matsumoto, J.; Nakada, Y.; Sakurai, K.; Nakamura, T.; Takahashi, Y. *International Journal of Pharmaceutics* **1999**, *185*, 93-101.
44. De Jaeghere, F.; Allemann, E.; Feijen, J.; Kissel, T.; Doelker, E.; Gurny, R. *Journal of Drug Targeting* **2000**, *8*, 143-153.
45. Mason, M. N.; Metters, A. T.; Bowman, C. N.; Anseth, K. S. *Macromolecules* **2001**, *34*, 4630-4635.
46. Jeong, B.; Bae, Y. H.; Lee, D. S.; Kim, S. W. *Nature* **1997**, *388*, 860-862.
47. Jeong, B.; Kim, S. W.; Bae, Y. H. *Advanced Drug Delivery Reviews* **2002**, *54*, 37-51.
48. Jeong, B.; Bae, Y. H.; Kim, S. W. *Macromolecules* **1999**, *32*, 7064-7069.
49. Miyamoto, S.; Takaoka, K.; Okada, T.; Yoshikawa, H.; Hashimoto, J.; Suzuki, S.; Ono, K. *Clinical Orthopaedics and Related Research* **1993**, 333.
50. Iijima, M.; Nagasaki, Y.; Okada, T.; Kato, M.; Kataoka, K. *Macromolecules* **1999**, *32*, 1140-1146.
51. Cohn, D.; Younes, H. *Journal of Biomedical Materials Research* **1988**, *22*, 993-1009.
52. Choi, S. W.; Choi, S. Y.; Jeong, B.; Kim, S. W.; Lee, D. S. *Journal of Polymer Science Part a-Polymer Chemistry* **1999**, *37*, 2207-2218.
53. Fujiwara, T.; Mukose, T.; Yamaoka, T.; Yamane, H.; Sakurai, S.; Kimura, Y. *Macromolecular Bioscience* **2001**, *1*, 204-208.
54. Mukose, T.; Fujiwara, T.; Nakano, J.; Taniguchi, I.; Miyamoto, M.; Kimura, Y.; Teraoka, I.; Lee, C. W. *Macromolecular Bioscience* **2004**, *4*, 361-367.
55. Fujiwara, T.; Miyamoto, M.; Kimura, Y.; Sakurai, S. *Polymer* **2001**, *42*, 1515-1523.
56. Lee, D.; Teraoka, I. *Polymer* **2002**, *43*, 2691-2697.
57. Lee, D.; Teraoka, I. *Biomaterials* **2003**, *24*, 329-336.
58. Kister, G.; Cassanas, G.; Vert, M. *Polymer* **1998**, *39*, 267-273.
59. Fujiwara, T.; Miyamoto, M.; Kimura, Y.; Iwata, T.; Doi, Y. *Macromolecules* **2001**, *34*, 4043-4050.
60. Fujiwara, T.; Kimura, Y. *Macromolecular Bioscience* **2002**, *2*, 11-23.

Downloaded by UNIV OF GUELPH LIBRARY on August 9, 2012 | http://pubs.acs.org
Publication Date: September 23, 2006 | doi: 10.1021/bk-2006-0939.ch014

Downloaded by UNIV MASSACHUSETTS AMHERST on August 28, 2012 | http://pubs.acs.org
Publication Date: September 23, 2006 | doi: 10.1021/bk-2006-0939.ch015

Chapter 15

Aromatic–Aliphatic Block Copolyesters Based on AA/BB Polymers and Poly(lactic acid)

Tim R. Cooper, Nathaniel Nix, and Robson F. Storey*

School of Polymers and High Performance Materials, Department of Polymer Science, The University of Southern Mississippi, Box 10076, Hattiesburg, MS 39406

Aromatic/aliphatic poly[L-lactide-*b*-(ethyleneoxyethylene terephthalate-*co*-adipate)-*b*-L-lactide] triblock copolymers were synthesized and characterized. Hydroxy-telechelic poly(ethyleneoxyethylene terephthalate-*co*-adipate) (PEOETA) was first prepared via polycondensation and then utilized as an initiator for the ring opening polymerization (ROP) of L-lactide (LLA) in the presence of stannous octanoate ($Sn(Oct)_2$). Formation of the block copolymer was confirmed by ^1H NMR spectroscopy, GPC, and AFM. The polymerization rate induced by the PEOETA macroinitiator was comparable to that of a small molecule initiator.

In Degradable Polymers and Materials; Khemani, K., et al.;
ACS Symposium Series; American Chemical Society: Washington, DC, 2006.

Poly(lactic acid) (PLA) has gained tremendous attention in the past decade due to its desirable characteristics, namely, degradability under biotic or abiotic conditions, non-toxicity of polymer and degradation by-products, and adequate mechanical properties for use in select applications.[1] Copolymerization of naturally occurring L-lactic acid with various polyester-forming monomers may potentially yield materials that display novel physical properties while maintaining reasonable degradation profiles. This approach also offers economical and environmental benefits due to the fact that L-lactic acid can be obtained from renewable resources, such as corn.[2]

A relatively new class of degradable polyesters contains both aromatic and aliphatic units within the chain. Research involving aromatic-aliphatic copolyesters has shown that an increase in the proportion of aromatic units causes an increase in mechanical properties and a decrease in biodegradability.[3] A family of aromatic-aliphatic polyesters that has grown to commercial-scale production is Ecoflex.[4] These biodegradable plastics are produced through a statistical polymerization of 1,4-butanediol, adipic acid, terephthalic acid, and a modular unit. A "modular unit" is defined by the manufacturer as a monomer system that produces branching and/or chain extension in the end polymer product. To date, relatively few reports have appeared that investigate aromatic-aliphatic copolyesters containing lactic acid segments.[5-8] The most common method of synthesis comprises a polycondensation polymerization in which hydroxy-terminated oligo(lactic acid) is used as a diol. Undesirable features common to the materials of these reports are high polydispersities and limited percentages of lactic acid within the final polyester.

Ring opening polymerization (ROP) of lactide from telechelic polymers has proven to be a successful method for synthesizing PLA-based block copolymers with relatively narrow polydispersities; we have previously reported several instances of using a macroinitiator in the ROP of lactides and lactones.[9-11] Ba and coworkers synthesized a unique block copolymer containing poly(butylene succinate) and poly(L-lactide) (PLLA). This was done by using hydroxy-terminated poly(butylene succinate) as a macroinitiator in the ROP of L-lactide (LLA), creating PLLA-*b*-PBS-*b*-PLLA.[12] The amount of PLLA could be regulated within the polymer with great precision.

In this chapter, we report the synthesis and characterization of ABA block copolyesters consisting of a poly(ethyleneoxyethylene terephthalate-co-adipate) center segment and PLLA outer segments: PLLA-*b*-PEOETA-*b*-PLLA. The method involves ROP of LLA using hydroxy-terminated PEOETA as the (macro)initiator and stannous 2-ethylhexanoate as the catalyst/coinitiator. A comparison of kinetic parameters is presented, focusing on rate constants of polymerization of a small molecule intiator and a macroinitiator, ethylene glycol (EG) and PEOETA, respectively. Atomic force microscopy (AFM) data suggest a phase-separated morphology.

Downloaded by UNIV MASSACHUSETTS AMHERST on August 28, 2012 | http://pubs.acs.org
Publication Date: September 23, 2006 | doi: 10.1021/bk-2006-0939.ch015

Experimental

Materials

Dimethyl adipate (99+%) and dimethyl terephthalate (99%) were used as received (Acros Organics). Diethylene glycol (DEG, 99%) was dried with $CaCl_2$ overnight and distilled under reduced pressure. Tin (II) 2-ethylhexanoate ($Sn(Oct)_2$, Aldrich) and L-lactide (Ortec, Inc., Easley, South Carolina) were used as received. Toluene was refluxed over sodium for 24 h and distilled under nitrogen before use.

Downloaded by UNIV MASSACHUSETTS AMHERST on August 28, 2012 | http://pubs.acs.org
Publication Date: September 23, 2006 | doi: 10.1021/bk-2006-0939.ch015

Characterization

Molecular weights and molecular weight distributions (MWD) of polymers were determined using a gel permeation chromatography (GPC) system consisting of a Waters Alliance 2695 Separations Module, an on-line multiangle laser light scattering (MALLS) detector (MiniDAWN™, Wyatt Technology Inc.) and an interferometric refractometer (Optilab DSP™, Wyatt Technology Inc.). Freshly distilled THF (dried over CaH_2) served as the mobile phase and was delivered at a flow rate of 1.0 mL/min through a PLgel 5μm guard (50×7.5mm) and two PLgel 5μm Mixed-D (300×7.5mm) columns in series. Sample concentrations were 5 mg/mL in freshly distilled THF, and the injection volume was 100 μL. The detector signals were simultaneously recorded using ASTRA™ software (Wyatt Technology Inc.). Absolute molecular weights were calculated from the MALLS detector signal and the dn/dc value, which was calculated from the signal response from the Optilab DSP, assuming 100% mass recovery from the columns.

Solution ^{1}H-NMR spectra were obtained on a Varian Unity 300 MHz spectrometer using 5 mm o.d. tubes with sample concentrations of 5-7% (w/w) in deuterated chloroform ($CDCl_3$) (Aldrich Chemical Co.) containing tetramethylsilane as an internal reference. Composition of the PEOETA prepolymer with respect to terephthalate/adipate ratio was determined by integration of the aromatic protons of the terephthalate units centered at 8.08 ppm and the α-carbon protons of the adipate units centered at 2.35 ppm.

A Bruker Equinox 55 FTIR spectrometer, equipped with an Axiom Analytical Diamond ATR Probe (DMD-270) and an external MCT mid-band detector, was used to collect infrared spectra of the polymerization components in real time. Each spectrum was an average of 8 scans, and spectra were acquired at 3.17 min intervals at a spectral resolution of 8 cm^{-1}. An interval as refered to here is the time period between the first scan of a spectrum and the first scan of the subsequent spectrum. The spectra were manipulated using OPUS NT software as described previously.[13] A toluene background spectrum was taken prior to each polymerization and subtracted from all subsequent spectra. LLA concentration was assumed to be proportional to peak height of the 1240 cm^{-1} absorbance, measured between the limits of 1248 and 1236 cm^{-1}, relative to a straight baseline from 1280 to 1010 cm^{-1} (OPUS method L). The initial monomer concentration ($[M]_0$) was set proportional to the average 1240 cm^{-1} peak height of the first few spectra taken before addition of the catalyst. As discussed previously,[13] due to a convoluting polymer peak centered at 1185 cm^{-1}, peak height at 1240 cm^{-1} leads to an over-estimation of LLA concentration at high conversion. The effect of this error was minimized by extrapolating apparent rate constants over a limited conversion range (< 0.15).

A MultiMode AFM (Digital Instruments) with an ultra sharp silicon cantilever (MicroMasch Silicon Cantilevers NSC16/AIBS/15) having a resonant frequency of 166.9 kHz and force constant of approximately 40 N/m was used to phase image the polymer sample in hard-tapping mode. The full tip cone angle was less than 30°, and the radius of curvature at the apex was less than 10 nm. To minimize artifacts, all bulk sample surfaces were smoothed using a diamond knife prior to acquiring the phase images. The sample was prepared by solvent (chloroform) casting.

Reaction mixtures were formulated within a Vacuum Atmospheres Company Dri-Lab glove-box under an inert N_2 atmosphere prior to reaction and data collection.

Synthesis

Synthesis of poly(ethyleneoxyethylene terephthalate-*co*-adipate) (PEOETA) macroinitiators. A polyester macroinitiator was produced using a 4-necked 250 mL round-bottom flask equipped with an overhead stirrer, nitrogen gas inlet tube, thermometer, and distillation head for removal of reaction by-products. A special stirrer bearing, of our own design, was employed to maintain a vacuum seal (< 0.20 mm Hg) at the stirrer shaft. The seal was created by compression, against the stir rod shaft, of two Viton-O rings housed within the stirrer bearing assembly. To the flask were charged 60.76 g (0.313 mole) dimethyl terephthalate, 62.21 g (0.357 mole) dimethyl adipate and 74.28 g (0.700 mole) diethylene glycol. No catalyst was used in the synthesis. Under nitrogen, the mixture was slowly heated, with stirring, until all components became molten (150-170°C). Heating and stirring were continued and methanol was continuously distilled as the transesterification reaction proceeded. When no further methanol could be removed under atmospheric pressure, a slight

Downloaded by UNIV MASSACHUSETTS AMHERST on August 28, 2012 | http://pubs.acs.org
Publication Date: September 23, 2006 | doi: 10.1021/bk-2006-0939.ch015

vacuum (100 mm Hg) was applied until the theoretical amount of methanol had been approximately collected. The vacuum was then gradually increased until a final vacuum of 0.200 mm Hg was achieved. The reaction was maintained under these conditions, and molecular weight of the final polyester was controlled by careful removal of a theoretical amount of DEG. When the targeted amount of DEG had been collected, heating was discontinued, and the contents were allowed to cool to ~100°C under nitrogen flow. The molten polymer was then carefully poured into a receiving vessel, cooled to room temperature, dissolved in chloroform (~325 mL), and precipitated into a 10-fold excess of cold (~0°C), dry methanol. The precipitated polymer was then dried under vacuum for 24 h until a constant weight was obtained.

Synthesis of PLLA-*b*-PEOETA-*b*-PLLA. The following is a representative procedure for the synthesis of a PLLA-*b*-PEOEAT-*b*-PLLA triblock copolymer. A 100 mL 3-necked round-bottom flask, equipped with a magnetic stir bar, a rubber septum, a Liebig condenser, and an ATR-FTIR probe, was charged with polyester prepolymer (4.99 g, 0.394 mol), LLA (20.13 g, 0.140 mol), and 61.8 mL of anhydrous toluene. The mixture was heated to 100°C using a silicone oil bath controlled with a Digi-Sense® 68900-01 temperature controller and held at this temperature for ~30 min under an argon purge. Then, 0.0042 g (1.04×10^{-5} mol) of $Sn(Oct)_2$ catalyst was introduced into the flask. FTIR spectroscopy was used to monitor the disappearance of the 1240-cm^{-1} peak associated with L-lactide monomer. The reaction was terminated by removal from the heat source upon attaining a specified monomer conversion as determined by real-time FTIR monitoring. Conversions and reaction times are listed in Table 1. The viscous liquid was allowed to cool to room temperature. The resulting solid crude polymer product was dissolved in 75 mL of chloroform and precipitated into a 10-fold volume excess of cold (~0°C), dry methanol. The precipitate was collected by filtration and washed with copious amounts of cold methanol and then dried under a vacuum at ambient temperature for 72 h until a constant weight was obtained.

Downloaded by UNIV MASSACHUSETTS AMHERST on August 28, 2012 | http://pubs.acs.org
Publication Date: September 23, 2006 | doi: 10.1021/bk-2006-0939.ch015

Results and Discussion

Synthesis of poly(ethyleneoxyethylene terephthalate-*co*-adipate). A macroinitiator containing a molar ratio of terephthalate/adipate of 1.14 was prepared via polycondensation. The polyester was purified by dissolution and precipitation in order to remove low-molecular weight components. The end groups of the low molecular weight macroinitiator were positively identified using ^1H NMR. The proton resonance signals for the end groups were observed at 3.59 and 1.82 ppm, as shown in Figure 1, representing the –

$CH_2CH_2OCH_2CH_2OH$ protons and the $-CH_2CH_2OCH_2CH_2OH$ proton of the PEOETA, respectively. A full assignment of the proton spectrum is found in Figure 1.

Downloaded by UNIV MASSACHUSETTS AMHERST on August 28, 2012 | http://pubs.acs.org
Publication Date: September 23, 2006 | doi: 10.1021/bk-2006-0939.ch015

ROP of LLA using PEOETA as macroinitiator. The synthesis of PLLA-*b*-PEOETA-*b*-PLLA (2) was done in solution (toluene) at 100°C using PEOETA (1) as the initiator and $Sn(Oct)_2$ as a catalyst (Scheme 1). Reaction conditions are listed in Table 1.

The conversion of LLA was monitored by following the disappearance of the 1240 cm^{-1} peak associated with the asymmetric C—O—C stretch of LLA. This was accomplished by using an ATR-FTIR probe inserted into the reaction flask. The reaction was stopped by removing from the heat and dissolving the resulting polymer product in chloroform. Reactions 2 and 4 (Table 1) displayed relatively rapid polymerization kinetics and were reacted to high conversion (80%). Reactions 1 and 3 were slower and arbitrarily terminated after 600 min (~22% conversion). GPC and ^1H-NMR spectroscopy were used to elucidate the structure of PLLA-*b*-PEOETA-*b*-PLLA triblock copolymers. Peak integration indicated a terephthalate/adipate ratio of 1.05.

First order apparent rate constants (k_{app}) for various PLLA polymerizations are shown in Table 1; k_{app} was obtained from the slope of a plot of ln ($[M]_0/[M]$) versus time (Figure 2).

Reactions 1 and 2 are control polymerizations carried out in the absence of purposefully added initiator (adventitious water only) and in the presence of ethylene glycol initiator, respectively. The k_{app} for Reaction 3 was found to be very close to that obtained in the presence of adventitious water only (Reaction 1). The low k_{app} for Reaction 3 was attributed to the presence of acid end groups within the macroinitiator. Carboxylic acid groups are well known to cause lower rates of polymerization in stannous octoate-catalyzed ROPs of lactones.[11]

Acid end groups within the macrointiator were quantified by measurement of acid number (ASTM 1639-90), as reported in Table 2. Using the acid number thus obtained, it was possible to calculate the moles of acid end groups contained in one gram of the macroinitiator. In Reaction 3 the concentration of acid end groups exceeded that of the catalyst, and a retardation of the polymerization rate was observed. Using this information and assuming that each acid end group removes one stannous octoate molecule, an adjustment of the catalyst concentration was made to provide a concentration of active sites that is equal to that used in Reaction 2. Once this was done, the k_{app} of the macroinitiator was very close the value obtained using the ethylene glycol as the initiator.

The hydroxy end groups associated with the PEOETA macroinitiator were no longer present in the proton NMR spectrum of PLLA-*b*-PEOETA-*b*-PLLA, which indicated successful initiation and formation of the block copolymer (Figure 4). In addition, the methine proton resonance of the ultimate repeat unit of the newly formed PLLA block was observed at 4.35 ppm.

Downloaded by UNIV MASSACHUSETTS AMHERST on August 28, 2012 | http://pubs.acs.org
Publication Date: September 23, 2006 | doi: 10.1021/bk-2006-0939.ch015

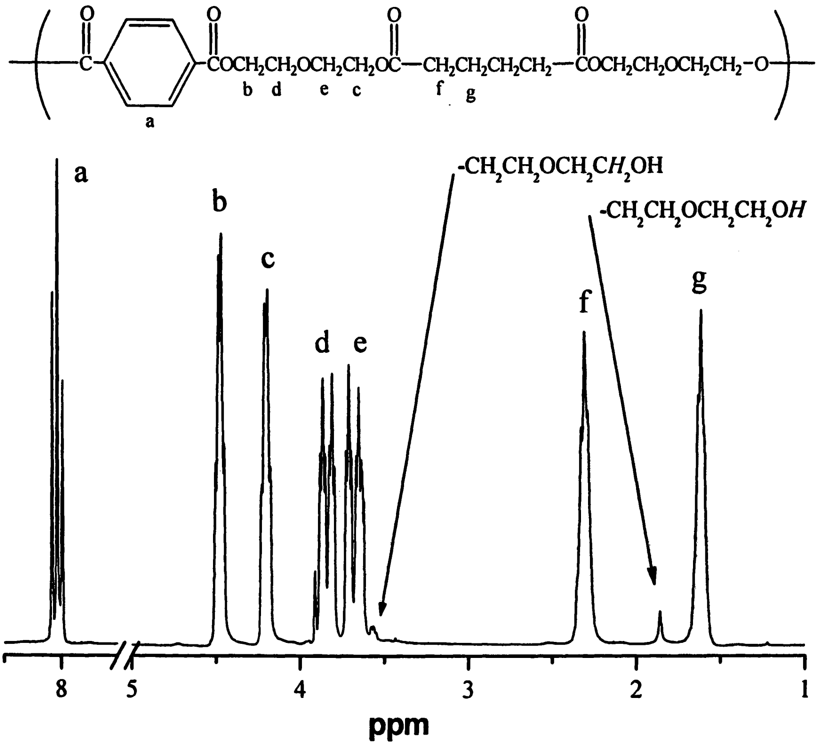

Figure 1. ^1H NMR assignment of PEOETA end groups and components.

Downloaded by UNIV MASSACHUSETTS AMHERST on August 28, 2012 | http://pubs.acs.org
Publication Date: September 23, 2006 | doi: 10.1021/bk-2006-0939.ch015

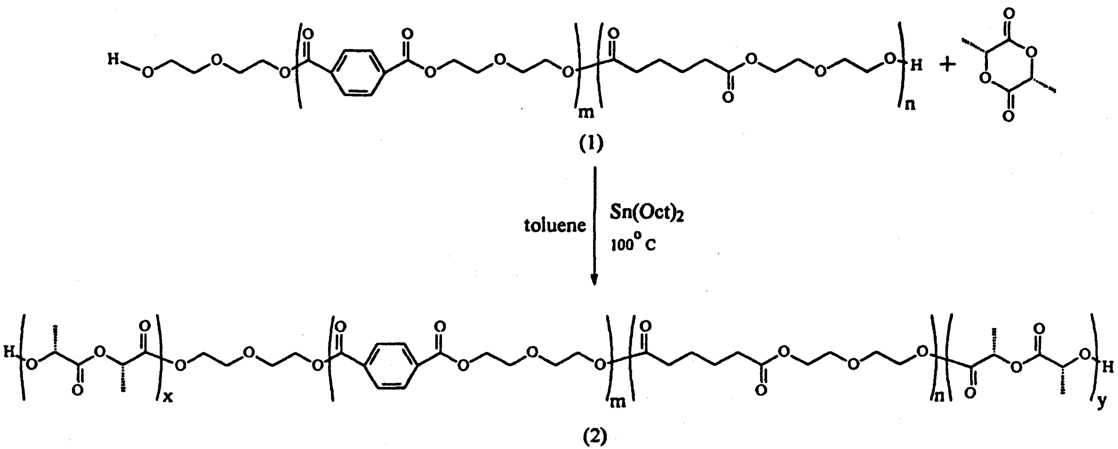

Scheme 1. Synthesis of triblock copolymer PLLA-b-PEOETA-b-PLLA. Sequence distribution of PEOETA is approximately random; m=51; n=49.

In Degradable Polymers and Materials; Khemani, K., et al.;
ACS Symposium Series; American Chemical Society: Washington, DC, 2006.

Downloaded by UNIV MASSACHUSETTS AMHERST on August 28, 2012 | http://pubs.acs.org
Publication Date: September 23, 2006 | doi: 10.1021/bk-2006-0939.ch015

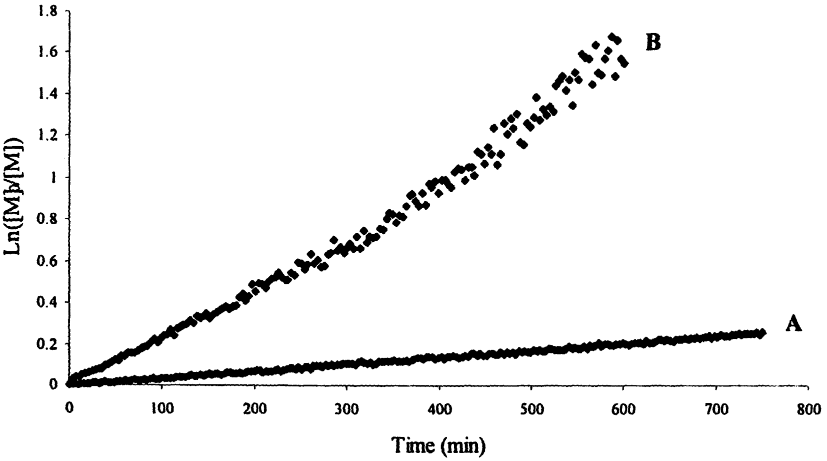

Figure 2. First order kinetic plots of LLA polymerizations initiated with PEOETA/Sn(Oct)$_2$, illustrating the effect of changing Sn(Oct)$_2$ to account for acid end groups of PEOETA: (A) Reaction 3, Table 1, k_{app}=3.2×10^{-6} s^{-1}; (B) Reaction 4, Table 1, k_{app}=1.47×10^{-5} s^{-1}.

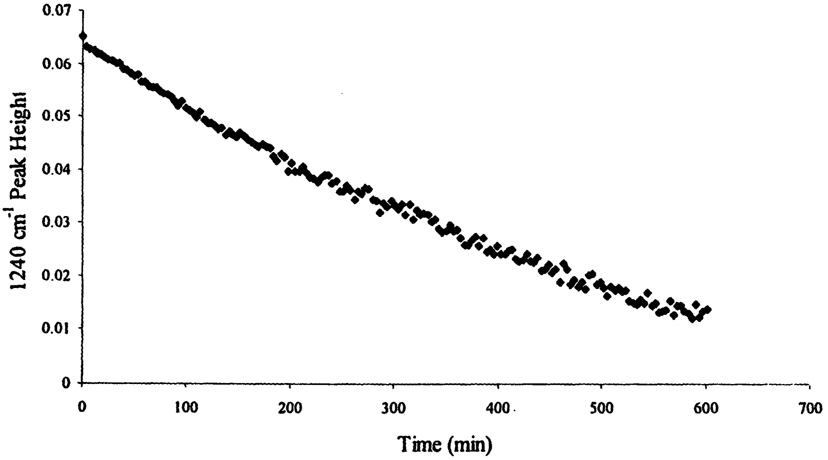

Figure 3. Reduction of the 1240 cm^{-1} peak height with time for LLA polymerization initiated with PEOETA/Sn(Oct)$_2$ (Reaction 4, Table 1).

Downloaded by UNIV MASSACHUSETTS AMHERST on August 28, 2012 | http://pubs.acs.org
Publication Date: September 23, 2006 | doi: 10.1021/bk-2006-0939.ch015

Table 1. Formulations and k_{app} values for LLA polymerizations

Reaction [a]	*Initiator*	*Initiator*[b] *(mol×10^3)*	*Sn(Oct)$_2$ Mass (g×10^3)*	*k_{app}*[c] *(s^{-1}×10^5)*	*Conv.*[d] *(%)*	*Mn (g/mol)*
1	H_2O [e]	------	4.2	0.30	22	3,100
2	EG	1.05	4.2	1.54	80	13,500
3	PEOETA	0.394	4.2	0.32	21	13,600
4	PEOETA	0.394	13.0	1.47	78	38,100

[a] Reaction 1 and 2 were performed under the same conditions as described for PLLA-*b*-PEOEAT-*b*-PLLA.

[b] 0.0618 liters of toluene and 20.13 (0.140 mols) grams of LLA were used in each reaction. Average number molecular weight of PEOETA 12,680 g/mol.

[c] Rate constant extraction was limited to conversion range of 0 to 15%.

[d] The corresponding reaction time to obtain the above monomer conversions was ~600 min.

[e] Adventitious water.

Table 2. Acid number determination of PEOETA macroinitiator

Sample	*Acid Number (mgKOH/gPEOETA)*	*Acid End Groups (mols/g) (x10^6)*
PEOETA	0.245	4.36

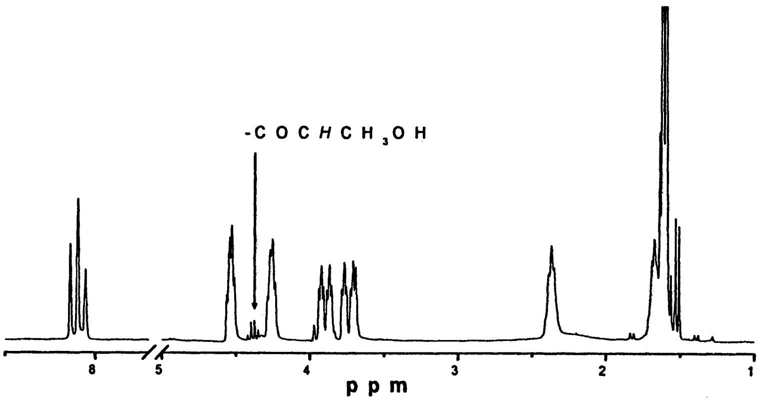

*Figure 4. Partial ^{1}H-NMR spectrum of PLLA-*b*-PEOEAT-*b*-PLLA.*

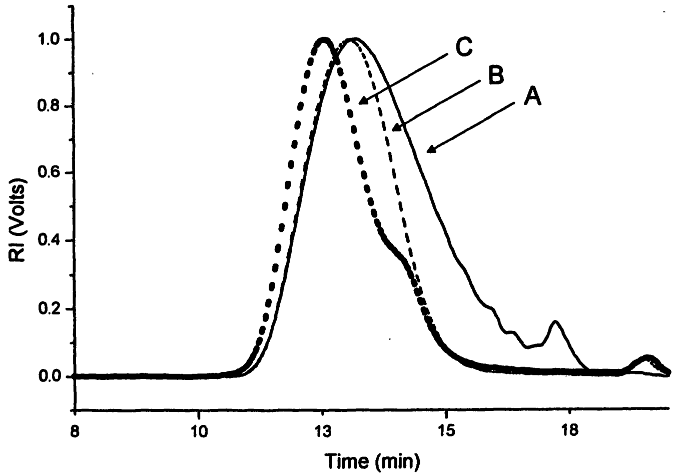

*Figure 5. GPC traces of PEOETA before (A) and after (B) precipitation, and of PLLA-*b*-PEOETA-*b*-PLLA block copolymer (C) (Reaction 4, Table 1). M_n PEOETA = 12,680 g/mol, PDI = 1.26; M_n PLLA-*b*-PEOETA-*b*-PLLA = 38,100 g/mol, PDI = 1.19.*

The GPC traces in Figure 5 show a clear shift to lower elution volume that occurred upon ROP of LLA from the PEOETA macroinitiator; however, the traces also reveal the presence of PLLA homopolymer. This is indicated by a shoulder on the high elution time side of the block copolymer trace. PLLA homopolymer is thought to be formed from water remaining in the PEOETA macroinitiator and/or the $Sn(Oct)_2$.

The morphology of the PLLA-*b*-PEOEAT-*b*-PLLA was examined using AFM in hard-tapping mode. This mode was deemed particularly appropriate since it interrogates morphology on the basis of local viscoelastic properties (hard vs. soft regions) and preserves the surface topography of the sample so that results are reproducible. The AFM image (Figure 6) suggests the presence of a continuous phase and a discontinuous phase, which would be typical of a block copolymer. Further studies are in progress to validate the two-phase morphology.

Conclusions

PLLA-*b*-PEOETA-*b*-PLLA triblock copolyester was synthesized by a combination of polycondensation and ROP polymerization techniques. The ROP polymerization of LLA using a well-defined PEOETA macroinitiator yielded a triblock copolyester within proximity of the targeted molecular weight

Downloaded by UNIV MASSACHUSETTS AMHERST on August 28, 2012 | http://pubs.acs.org
Publication Date: September 23, 2006 | doi: 10.1021/bk-2006-0939.ch015

Downloaded by UNIV MASSACHUSETTS AMHERST on August 28, 2012 | http://pubs.acs.org
Publication Date: September 23, 2006 | doi: 10.1021/bk-2006-0939.ch015

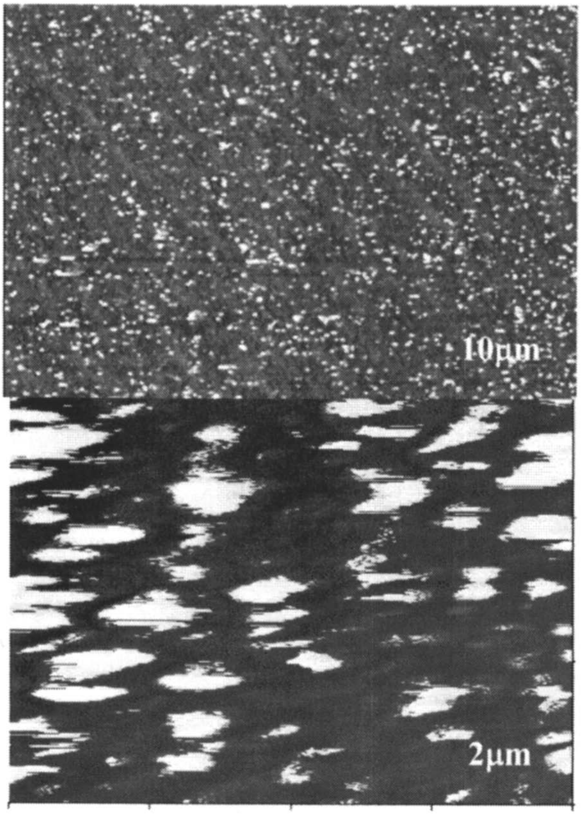

Figure 6. AFM images of PLLA-b-*PEOEAT*-b-*PLLA. The white areas were assigned to the PEOETA block (discontinuous phase) and the darker regions to the PLLA block (continuous phase). These phase assignments were based on composition.*

and a moderate PDI. The polymerization of LLA was retarded due to a presence of acid end groups contained in the PEOETA macroinitiator, consequently, a low k_{app} value was observed. Once the catalyst/coinitiator ($Sn(Oct)_2$) concentration was adjusted to account for the acid end groups the k_{app} of the macroinitiator resembled that of a small molecule initiator (EG). The triblock copolymer seems to form a two phase morphology, which can be partially confirmed from the AFM images.

Downloaded by UNIV MASSACHUSETTS AMHERST on August 28, 2012 | http://pubs.acs.org
Publication Date: September 23, 2006 | doi: 10.1021/bk-2006-0939.ch015

Acknowledgments

The research reported herein was funded by the Office of Naval Research, Grant No N00014-04-1-0703. The authors would also like to thank Ortec, Inc. (Easley, SC) for the generous donation of the L-lactide monomer and James Kopchik and Paul Jones for their assistance in obtaining the AFM micrographs. In addition the authors thank the Degradable Polymers and Materials A.C.S. Symposium Series organizers for the opportunity to present our work and for the preparation of this book.

References

1. Garlotta, D. *J. Polym. Environ.* **2001,** *9,* 63-84.
2. Gruber, P.; O'Brien, M.; In *Biopolymers*; Steinbüchel, A., Ed.; Wiley-VCH: New York, 2002; Vol. 4, pp 235-250.
3. Okada, M. *Prog. Polym. Sci.* **2002,** *27,* 87-133.
4. Yamamoto, M.; Witt, U.; Skupin, G.; Beimborn, D.; Mueller, R.-J., Biodegradable aliphatic-aromatic polyesters: "Ecoflex". In *Biopolymers*, Steinbüchel, A., Ed. Wiley-VCH: New York, 2002; Vol. 4, pp 299-313.
5. Haderlein, G.; Schmidt, C.; Wendorff, H.; Greiner, A. *Polym. Adv. Technol.* **1997,** *8,* 568-573.
6. Haderlein, G.; Petersen, H.; Schmidt, C.; Wendorff, H.; Schaper, A.; Jones, D. B. *Macromol. Chem. Phys.* **1999,** *200,* 2080-2087.
7. Chen, Y.; Wombacher, R.; Wendorff, H.; Visjager, J.; Smith, P.; Greiner, A. *Biomacromolecules* **2003,** *4,* 974-980.
8. Chen, Y.; Jia, Z.; Schaper, A.; Kristiansen, M.; Smith, P.; Wombacher, R.; Wendorff, H.; Greiner, A. *Biomacromolecules* **2004,** *5,* 11-16.
9. Storey, R. F.; Mullen, B. D.; Melchert, K. M. *J. Macromol. Sci.-Pure Appl. Chem.* **2001,** *A38,* 897-917.

10. Storey, R. F.; Mullen, B. D.; Desai, G.; Sherman, J.; Tang, C. *J. Polym. Sci.: Part A: Polym. Chem.* **2002,** *40,* 3434-3442.

11. Messman, J.; Storey, R. *J. Polym. Sci.: Part A: Polym. Chem.* **2004,** *42,* 6238-6247.

12. Chen, Y.; Wombacher, R.; Wendorff, H.; Visjager, J.; Smith, P.; Greiner, A. *Biomacromolecules* **2003,** 4, 974-980.

13. Messman, J.; Storey, R. F. *J. Polym. Sci. Part A: Polym. Chem.* **2004,** 42, 6238-6247.

Downloaded by UNIV MASSACHUSETTS AMHERST on August 28, 2012 | http://pubs.acs.org
Publication Date: September 23, 2006 | doi: 10.1021/bk-2006-0939.ch015

Downloaded by UNIV OF ARIZONA on August 9, 2012 | http://pubs.acs.org
Publication Date: September 23, 2006 | doi: 10.1021/bk-2006-0939.ch016

Chapter 16

Strategies in Aliphatic Polyester Synthesis for Biomaterial and Drug Delivery Applications

Bryan Parrish and Todd Emrick

Polymer Science and Engineering Department, Conte Center for Polymer Research, University of Massachusetts at Amherst, Amherst, MA 01003

Aliphatic polyesters are among the most important class of synthetic polymers for applications in biology due to their biodegradability. However, such polyesters are typically semi-crystalline, hydrophobic solids lacking in functionality, such that strategic tailoring of their structure and functionality carries the potential to expand their application base to a wide variety of particular applications. Various synthetic methods have been explored for introducing functional groups into aliphatic polyesters. This chapter will describe a number of these methods reported in the past several years, focusing primarily on examples of controlled ring-opening polymerization of functionalized lactones, and post-polymerization functionalization well-defined materials with controlled end-groups and narrow polydispersities.

In Degradable Polymers and Materials; Khemani, K., et al.;
ACS Symposium Series; American Chemical Society: Washington, DC, 2006.

Introduction

Early efforts to use synthetic polymers as biomaterials were based on high volume commodity polymers such as polyurethanes, polyacrylates, nylon, and poly(tetrafluoroethylene); polymers that clearly were designed initially for other purposes. Nevertheless, the wide availability and favorable physical properties of these polymers led to their use by surgeons in medical procedures that require durable and inert materials (*1,2*). However, the use of such polymer materials in surgical and other biological applications has been found to elicit significant problems, such as inflammation and even infection, due to the immune response of the body to the presence of foreign materials. Notable pioneering examples of polymer materials in biological applications include efforts of DeBakey and coworkers, who as early as the 1950's used Dacron™ (polyethylene terepthalate) for cardiovascular prostheses (*3*). These procedures were found to be successful in the repair of large arteries, but unfortunately failed in cases where the internal diameter was less than 5 mm. The breadth of expertise needed to solve such challenging problems in biomaterials, and effectively introduce synthetic materials to the body, includes chemistry, biology, engineering, and clinical surgery, thus generating a challenging interdisciplinary field that requires collaborative activity among these disciplines.

While many different types of polymers are of interest in biomaterial applications, aliphatic polyesters are particularly relevant to consider due to their degradable nature under physiologic conditions, thus making them desirable for resorbable applications. Aliphatic polyesters were initially used to fabricate degradable sutures in the 1960's, (*4*) and have since found use in a wide range of biomaterial applications including drug-delivery systems (*5*), tissue-engineering scaffolds (*6*), and temporary tissue/bone replacement (*7*) as depicted in Figure 1. Recent advances in the field include the work of Langer on aliphatic polyesters for tissue-engineering and drug-delivery (*8*), Fréchet and Grinstaff on drug-delivery (*9*) and surgical (*10*) applications of dendrimers, and Duncan in the area of drug-delivery systems and polymer therapeutics (*11*).

An effective approach to aliphatic polyesters of controlled molecular weight and potential medical importance entails a ring-opening polymerization of monomers shown in Figure 2, such as lactide, glycolide, ε-caprolactone (ε-CL), and δ-valerolactone (δ-VL). The ring-opening homo- and copolymerization of lactones and lactides is performed in the bulk or in solution using organometallic catalysts such as aluminum *iso*-propoxide ($Al(O^iPr)_3$), tin(II) 2-ethylhexanoate, ($Sn(Oct)_2$), tin(II) trifluoromethane sulfonate ($Sn(OTf)_2$), as well as organic catalysts based on *N*-heterocyclic carbenes (*12,13*). Primary and secondary alcohols and amines can be used to initiate polymerization and give aliphatic polyesters with control over end-group functionality, overall molecular weight, and polydispersity (PDI, defined as M_w/M_n).

Downloaded by UNIV OF ARIZONA on August 9, 2012 | http://pubs.acs.org
Publication Date: September 23, 2006 | doi: 10.1021/bk-2006-0939.ch016

Downloaded by UNIV OF ARIZONA on August 9, 2012 | http://pubs.acs.org
Publication Date: September 23, 2006 | doi: 10.1021/bk-2006-0939.ch016

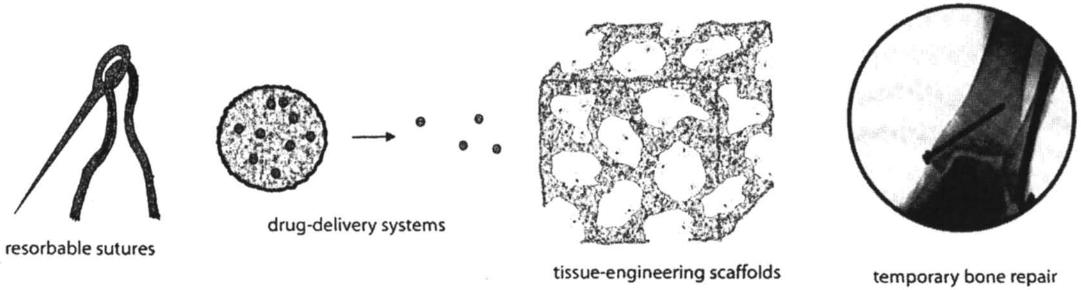
resorbable sutures
drug-delivery systems
tissue-engineering scaffolds
temporary bone repair

Figure 1. Examples of biomaterials applications using aliphatic polyesters

Downloaded by UNIV OF ARIZONA on August 9, 2012 | http://pubs.acs.org
Publication Date: September 23, 2006 | doi: 10.1021/bk-2006-0939.ch016

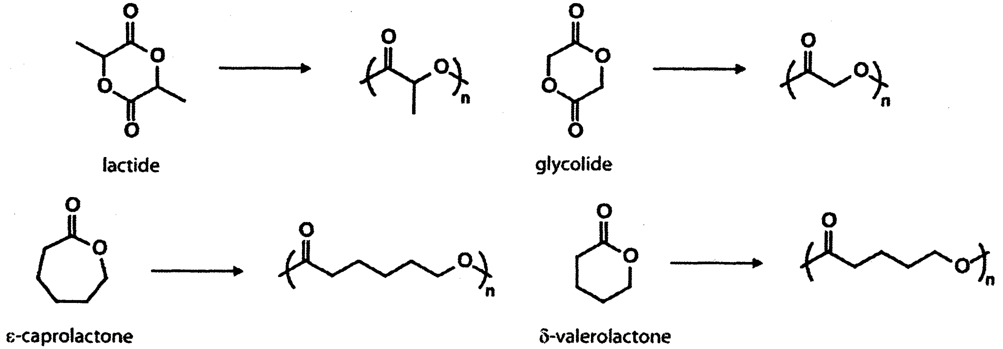
lactide
glycolide
ε-caprolactone
δ-valerolactone
n
n
n
n

Figure 2. Some aliphatic polyesters prepared by ring-opening polymerization

A range of mechanical properties and degradation rates can be achieved through copolymerization (*2*) of the monomers shown in Figure 2. However, many of these aliphatic polyesters are semi-crystalline, hydrophobic solids, and and all lack functionality that could otherwise be used to tailor their properties. Thus, methods to integrate functionality into aliphatic polyesters to to fine-tune their physical and biological properties have been sought. Water soluble polyesters are of particular interest for injectable applications, as are polyesters functionalized with drug moieties, cell-adhesion promoters, and targeting oligopeptide sequences for drug-delivery and tissue-engineering applications.

Downloaded by UNIV OF ARIZONA on August 9, 2012 | http://pubs.acs.org
Publication Date: September 23, 2006 | doi: 10.1021/bk-2006-0939.ch016

Strategies in Functionalization of Aliphatic Polyesters

Functionalization of aliphatic polyesters is a delicate challenge from the perspective of organic and polymer synthesis, as their degradable nature that makes them desirable as biomaterials also limits the types of chemistry that can be used for their modification. Consequently, mild synthetic strategies must be employed for controlled functionalization that can proceed in the absence of ester bond degradation. Functionalized aliphatic polyesters can be viewed from a macromolecular architecture perspective, including end-group functionalization of linear polyesters, non-linear polyesters such as dendritic and hyperbranched polymers that contain multiple functional groups as chain-ends, and the introduction of pendent functionality distributed as grafts on linear polyester backbones to give functional comb-type structures.

End-group Functionalization

The simplest functionalization strategy of aliphatic polyesters is at the chain-ends (examples shown in Figure 3). This can be achieved using functional initiators for ring-opening polymerization, or through end-capping reactions. Numerous reports describe initiation of lactone polymerization from the chain-end hydroxyl groups of poly(ethylene glycol) (PEG) -diols and -monomethyl ethers, to produce hydrophilic and often water soluble tri- and di-block copolymers, respectively, that can assemble into micellar structures in water with a polyester core and a PEG corona (*14,15*). Other examples of polyester functionalization by end-capping include esterification of the polyester hydroxyl chain-end with 4-azidobenzoyl chloride to give UV-photocurable polyesters (*16*), and end-capping with phosphorylcholine residues to give polyesters with phospholipid like moieties that reduce protein adsorption relative to non-functionalized polyesters (*17*).

Downloaded by UNIV OF ARIZONA on August 9, 2012 | http://pubs.acs.org
Publication Date: September 23, 2006 | doi: 10.1021/bk-2006-0939.ch016

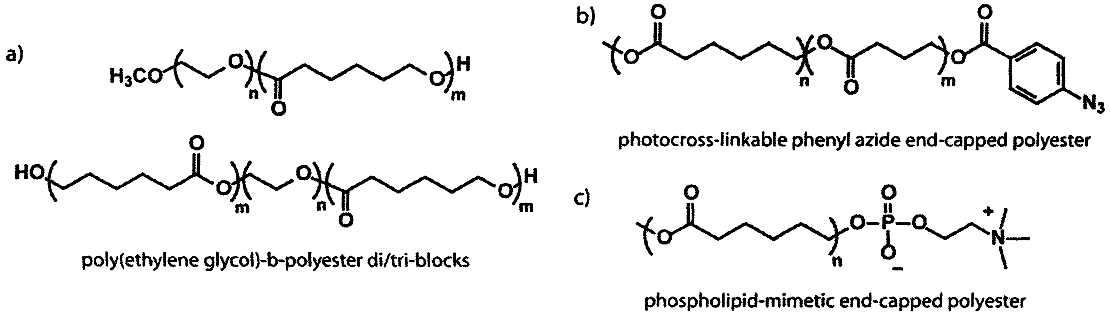

poly(ethylene glycol)-b-polyester di/tri-blocks

photocross-linkable phenyl azide end-capped polyester

phospholipid-mimetic end-capped polyester

Figure 3. End-functionalized polyesters a) poly(ethylene glycol)-b-polyester, b) phenyl azide end-capped, and c) phosphoryl choline end-capped

Chain-end functionalization has the advantage of simplicity, but clearly limits functional group incorporation to low levels (one or two groups per polyester molecule). Moreover, during polyester degradation by cleavage of ester bonds in the backbone, very little of the degraded material remains bound to the functional group of interest. Thus, methods to increase the level of functionality on polyesters have been pursued by several groups, for example by the synthesis of dendritic, hyperbranched and comb-like polyester-based structures.

Highly Functionalized Dendritic and Hyperbranched Aliphatic Polyesters

Non-linear polymer architectures including dendritic, hyperbranched, and linear-dendritic hybrid materials have been prepared as a means of altering polyester properties and introducing very high levels of functionality (Figure 4). In addition to the effect of branching on solid-state and solution properties, the large number of end-groups that result from this branching offer the opportunity to obtain very high levels of functional group loading. Dendrimers are especially attractive for their exceptionally high level of chain-end functionality, and thus are of interest in polymer-based drug delivery, where high drug loading per delivery vehicle can be particularly beneficial. Fréchet, Szoka, and coworkers recently put this concept into practice through the synthesis of aliphatic polyester dendrimers with covalently attached drugs such as the chemotherapy drug doxorubicin (Figure 4a) (*6,18*). *In vivo* evaluation of such conjugates demonstrated the effectiveness of the dendritic drug carrier relative to the direct use of free small molecule drugs. Hyperbranched polymers also provide considerable branching and chain-end functionality, but can be prepared by conventional polymerization chemistry rather than the somewhat tedious step-wise coupling approach to dendrimers. Hyperbranched aliphatic polyesters have been prepared by ring-opening polymerization of lactones bearing hydroxyl groups, as seen for example in reports of Hedrick and coworkers on bis(hydroxymethyl)-substituted ε-CL (Figure 4b) (*19*), as well as by Fréchet and coworkers on ring-opening polymerization of hydroxyethyl-substituted ε-CL (*20*). Hyperbranched poly-ε-CL samples of high molecular weight (65,000-85,000) were found to be soluble in polar solvents such as DMSO and methanol, due to the large number of hydroxyl end-groups in the structures. Hybrid copolymers consisting of linear and dendritic segments have also been prepared and evaluated as biomaterials, for example by Grinstaff and coworkers on photocross-linkable dendritic-linear-dendritic triblocks (Figure 4c) prepared for opthalmic tissue repair applications (*10*). After methacrylate end-capping, the hybrid copolymers were cross-linked to seal corneal lacerations and found to perform better than nylon sutures.

Downloaded by UNIV OF ARIZONA on August 9, 2012 | http://pubs.acs.org
Publication Date: September 23, 2006 | doi: 10.1021/bk-2006-0939.ch016

Downloaded by UNIV OF ARIZONA on August 9, 2012 | http://pubs.acs.org
Publication Date: September 23, 2006 | doi: 10.1021/bk-2006-0939.ch016

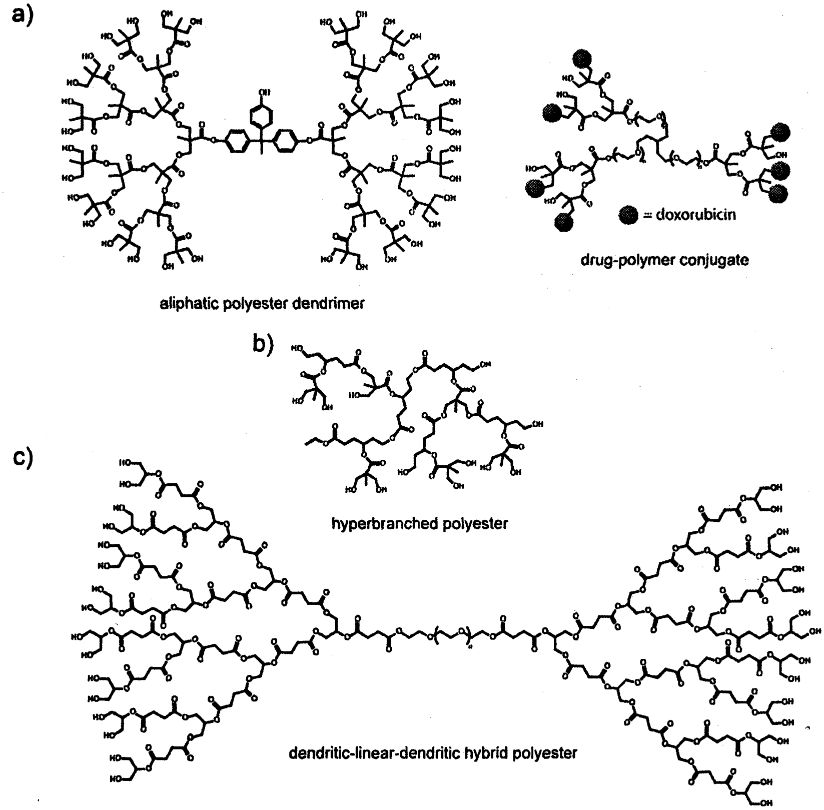
a)
aliphatic polyester dendrimer
= doxorubicin
drug-polymer conjugate
b)
hyperbranched polyester
c)
dendritic-linear-dendritic hybrid polyester

Figure 4. a) polyester dendrimer and drug conjugate; b) hyperbranched aliphatic polyester; and c) dendritic-linear-dendritic triblock copolymer

Aliphatic polyesters with pendent functionality

Functionalization of linear aliphatic polyesters with grafted moieties placed pendent to the polymer backbone has also been explored to integrate the desired functionality into the polymer material, while maintaining the linear backbone. As the introduction of pendent functionality to commercially available aliphatic polyesters presents few synthetic options and carries the risk of polymer degradation, recent work has focused on ring-opening polymerization of functionalized lactones. While simple functional groups that are compatible with lactone ring-opening polymerization conditions can be introduced with relative ease, many substituents present difficulties in lactone polymerization, indicated for example by Jérôme and coworkers where PEG-1,000 substituted ε-CL gave low PEG-grafting densities by ring-opening polymerization (21). Consequently, a stepwise approach is preferred, starting with the synthesis of functionalized lactones, followed by ring-opening polymerization, and finally post-polymerization modification of the functionalized polyester products. By copolymerization of the functionalized lactones with conventional lactone monomers, the functional group density can be tailored over a wide range. The conditions chosen for these post-polymerization reactions must be compatible with the polyester backbone to avoid degradation or cross-linking, but the ability to produce substituted polyesters for subsequent modification opens many options for further functionalization that are not possible in the case of unsubstituted polyesters. Indeed, quite a few functional polyester structures have been reported, including those with pendent alkyl bromides (*22,23*), ketones (*24*), alcohols (*25-27*), alkenes (*23,26,27*), alkynes (*28*), carboxylic acids (*25*), acrylates (*29*), 2-bromo-2-methylpropionates (*30*), PEG chains (21,*28,31*), dendrons (*32*), and oligopeptides (*28,33*). The remainder of this chapter provides a brief description of the synthetic accomplishments and potential applications for these pendent functionalized aliphatic polyesters.

Downloaded by UNIV OF ARIZONA on August 9, 2012 | http://pubs.acs.org
Publication Date: September 23, 2006 | doi: 10.1021/bk-2006-0939.ch016

Recent Studies on Pendent Functionalization of Aliphatic Polyesters as Degradable Synthetic Polymers for Biology

The synthetic versatility associated with lactone chemistry offers a number of methods for introducing functionality into the lactone ring. The most commonly employed methods for producing functionalized lactones that are amenable to ring-opening polymerization include: 1) Baeyer-Villiger ring-expansion of α-substituted cyclohexanones; 2) mono-substitution of 1,6-cyclohexane diol followed by oxidation with pyridinium chlorochromate (PCC), and subsequent ring-expansion using Baeyer-Villiger chemistry; and 3) substitution α to the carbonyl of the lactone, using for example lithium diisopropylamide (LDA) as a non-nucleophilic base, followed by addition of an appropriate electrophile. Taken together, these routes can be used to produce variously substituted ε-CL and δ-VL monomers, each having its own attractive features in terms of synthetic ease and versatility.

Hedrick, Jérôme, and coworkers provided early examples of pendent functionalized poly(ε-CL) by polymerization of allyl-functionalized ε-CL (**1**) (*23*). This new lactone monomer was prepared from 2-allyl cyclohexanone by Baeyer-Villiger oxidation with *meta*-chloroperoxybenzoic acid (*m*-CPBA) (Figure 5). This oxidative ring-expansion gives lactone **1**, with the expected oxygen insertion between the carbonyl and adjacent methine group. Olefin epoxidation by *m*-CPBA complicates the synthetic method to some degree, but lactone **1** can nonetheless be purified and used effectively in ring-opening polymerization.

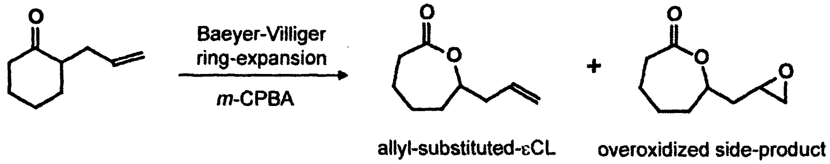

1

Figure 5. Synthesis of allyl-functionalized ε- CL (1) by Baeyer-Villiger oxidation of 2-allylcyclohexanone

Using a variety of hydroxyl containing initiators, lactone **1** was homopolymerized and copolymerized with both ε-CL and L,L-lactide using $Sn(Oct)_2$ as the catalyst to give allyl functionalized polyesters shown as **2**. In all cases, the experimental and theoretical molecular weights were in good agreement over the range of 3,000-12,000g/mol, and the polydispersities were fairly narrow (1.1-1.4), in accord with controlled/living ring-opening polymerization, and in clear contrast to typical polydispersity values of 2 for conventional polyesters prepared by polycondensation. Homopolymer **2** was found to be an amorphous material with a glass-transition temperature (T_g) of -62 °C, compared to -60 °C for poly(ε-CL). Chemical transformations performed on the pendent allyl groups of polymer **2** included bromination, epoxidation, and hydrosilation reactions to give polyesters **3-5** shown in Figure 6.

In all cases the transformations were achieved in the absence of degradation or cross-linking, as shown by comparing gel permeation chromatography traces of the starting polyesters and the products. This work nicely demonstrates the compatibility of unsaturated groups within the lactone monomer with controlled ring-opening polymerization, as well as a multi-step approach to polyester functionalization that can bring synthetic diversity to aliphatic polyesters upon post-polymerization modification.

Hedrick and coworkers further expanded the diversity of pendent polyester functionalization by the synthesis of hydroxyl and carboxyl derivatives (*25*). Incorporation of these moieties into the polyester structure required the synthesis and polymerization of novel lactones, for example the protected ε-CL derivatives shown in Figure 7. The protected hydroxyl derivative (**6**) was prepared from 1,6-cyclohexane diol, by mono-substitution with 2,2'-bis(phenyldioxymethyl) propionyl chloride, followed by oxidation with PCC, and Baeyer-Villiger ring expansion. The protected acid derivative (**7**) was synthesized from ethyl-4-hydroxycyclohexane carboxylate by oxidation with PCC, cleavage of the ethyl group with H_2SO_4, protection with benzyl bromide, and ring expansion with *m*-CPBA.

Downloaded by UNIV OF ARIZONA on August 9, 2012 | http://pubs.acs.org
Publication Date: September 23, 2006 | doi: 10.1021/bk-2006-0939.ch016

Downloaded by UNIV OF ARIZONA on August 9, 2012 | http://pubs.acs.org
Publication Date: September 23, 2006 | doi: 10.1021/bk-2006-0939.ch016

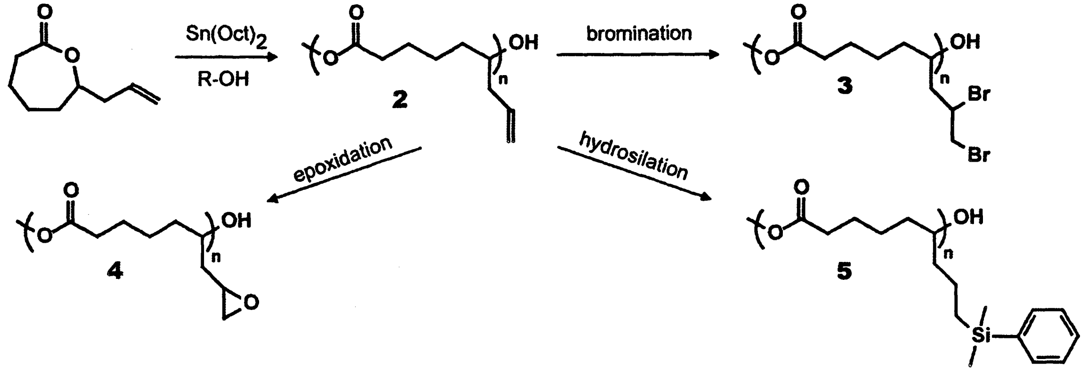
Sn(Oct)$_2$
R-OH
2
bromination
3
epoxidation
hydrosilation
4
5
OH
n
Br
Br
O
Si

Figure 6. Polymerization of lactone 1 and subsequent functional group transformations: bromination (3), epoxidation (4), and hydrosilation (5)

Downloaded by UNIV OF ARIZONA on August 9, 2012 | http://pubs.acs.org
Publication Date: September 23, 2006 | doi: 10.1021/bk-2006-0939.ch016

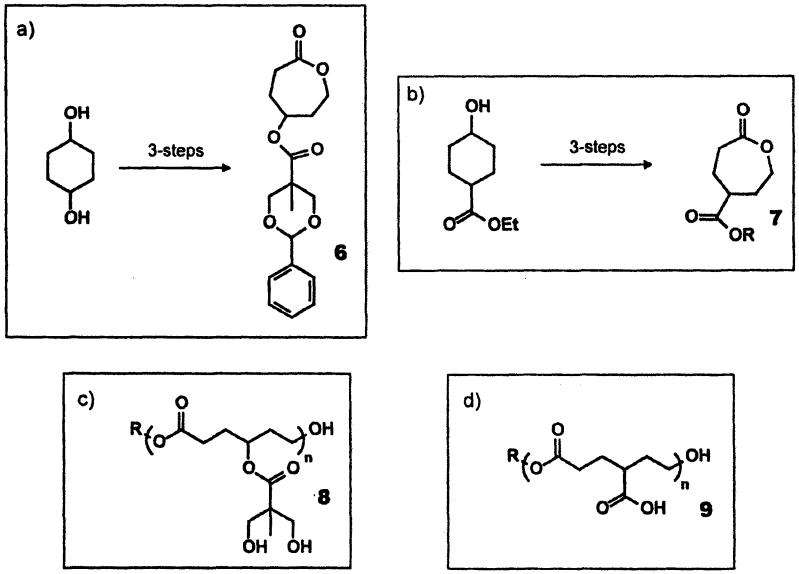

Figure 7. Protected hydroxyl and carboxyl monomers and deprotected polymers

Homo- and co-polymerizations of monomers **6** and **7** were performed using $Sn(Oct)_2$ catalysis, and ε-CL as the comonomer, to afford the corresponding aliphatic polyesters bearing protected pendent groups. Benzylidene groups were removed by catalytic hydrogenolysis to afford the desired hydroxyl (**8**) and carboxyl (**9**) pendent groups. Importantly, this deprotection strategy proved compatible with the aliphatic polyester backbone, such that the functionalized polymers could be prepared and isolated efficiently.

Emrick and coworkers have focused on the synthesis and polymerization of novel lactone monomers that are substituted α- to the carbonyl group. Treatment of δ-VL and ε-CL with non-nucleophilic bases such as LDA provides an effective strategy for lactone deprotonation (34); subsequent addition of an appropriate electrophile provides the functional lactones. Higher yields are obtained in these α-substitution reactions of δ-VL relative to ε-CL, due to greater stability of the six-membered ring, but either lactone can be substituted effectively and used in subsequent ring-opening polymerization. This strategy has led to novel aliphatic polyesters based on polymerization of δ-VL derivates substituted with allyl (*26*), cyclopentene (*27*), and acetylene (*28*) groups, as shown in Figure 8. Lactone monomers **10** and **11** were prepared by deprotonation of δ-VL with LDA, followed by quenching with allyl bromide or propargyl bromide to give the allyl and acetylene derivatives, respectively. Cyclopentene derivative **12** was prepared by two sequential allylation reactions, followed by a ring-closing metathesis reaction to give the desired cyclopentene substituent on the lactone ring.

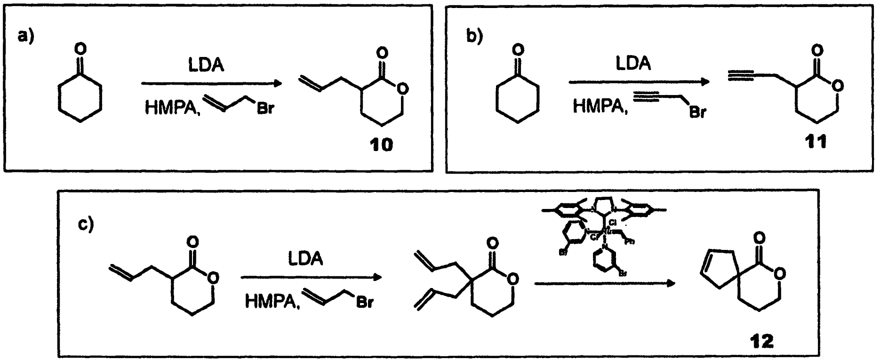

Figure 8. Synthesis of a) allyl, b) acetylene, and c) cyclopentene derivatives of d-valerolactone by substitution α to the carbonyl group.

Lactone **10** was homo- and copolymerized using $Sn(OTf)_2$ rather than $Sn(Oct)_2$ as the catalyst, following reports of Hedrick and coworkers that evaluated the effectiveness of a variety of Sn(II) catalysts in ring-opening polymerization of lactones and substituted lactones (12). Polymerizations of **10** in conjunction with comonomers ε-CL or δ-VL gave the aliphatic polyesters shown as **13** in Figure 9, with a controlled density of pendent allyl groups based on comonomer ratio, controlled molecular weights over the range of 3,000-15,000 g/mol (as estimated by gel permeation chromatography), and narrow polydispersities typically under 1.3, and in many cases as low as 1.1. The presence of greater than 15 mole percent allyl functionalized monomer in copolymers of type **13** sufficiently interrupted their semi-crystalline nature to give amorphous polymers that are liquids at room temperature. The allyl groups could be converted to 1,2-diols by reaction of the polymer with OsO_4 and N-methylmorpholine-N-oxide (NMO) to give 1,2-diol substituted polyesters shown as **14** in Figure 9.

Downloaded by UNIV OF ARIZONA on August 9, 2012 | http://pubs.acs.org
Publication Date: September 23, 2006 | doi: 10.1021/bk-2006-0939.ch016

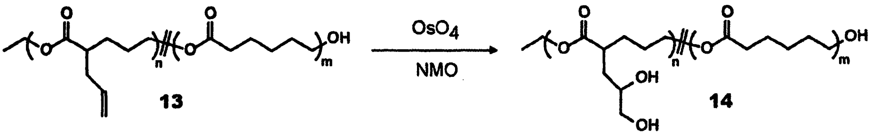

Figure 9. Preparation of pendent 1,2-diol substituted aliphatic polyesters

These hydroxyl functionalized polyesters, containing one primary and one secondary alcohol per functional monomer repeat unit, were found to degrade much more rapidly than unsubstituted polyesters; in cases of dense pendent functionalization (i.e., homopolymers of **10**), very rapid degradation was observed upon attempted isolation of the dihydroxylated product. This degradation can be expected to occur by the intramolecular transesterification (i.e., backbiting) of the primary hydroxyl group of the 1,2-diol with the nearby carbonyl group on the polymer backbone to give 6-membered lactones upon chain-cleavage. While rapidly degrading polyesters of this type would be of advantage in some applications, efforts towards shelf-stable 1,2-diol functionalized aliphatic polyesters led to the design, synthesis, and polymerization of cyclopentene-functionalized lactone **12**. While lactone **12** proved sluggish in attempted homopolymerization, it readily copolymerized with ε-CL to give copolymers, shown as **15** in Figure 10, with up to 20 mole percent **12** integrated into the polymer backbone, using $Sn(OTf)_2$ catalysis. This copolymerization chemistry displayed molecular weight (3,000-12,000 g/mol) and polydispersity (1.1-1.3) control similar to that of the allyl-substituted case. However, in the cyclopentene case, dihydroxylation of the pendent olefins with OsO_4 and NMO affords hydroxyl functionalized polyesters, shown as **16**, that do not degrade rapidly, and appear to have good shelf-life under normal storage conditions. This relative stability of **16** can be attributed to hindrance associated with intramolecular attack of the secondary alcohols on carbonyls on the polymer backbone, due to both the lower reactivity generally observed for secondary alcohols, and the steric constraints imposed by the cyclopentyl ring that limits the ability of these hydroxyl groups to approach the polymer backbone. These functionalized aliphatic polyesters can thus be prepared and stored conveniently for subsequent coupling to a range of aldehyde and carboxylic acid containing compounds through acetal formation and esterification (Figure 10). For example, dicyclohexylcarbodiimide (DCC) coupling of carboxylic acid terminated PEG monomethyl ether provided access to the first reported example of aliphatic polyester-*graft*-PEG copolymers (**17**) with substantial PEG-grafting (greater than 20 mol % for PEG-1100 g/mol) and narrow polydispersities. At high incorporations of PEG-1100, these graft copolymers polyesters are water-soluble, and envisioned to lead to new water-

Downloaded by UNIV OF ARIZONA on August 9, 2012 | http://pubs.acs.org
Publication Date: September 23, 2006 | doi: 10.1021/bk-2006-0939.ch016

based applications of polyesters where the functional group incorporation can be very high.

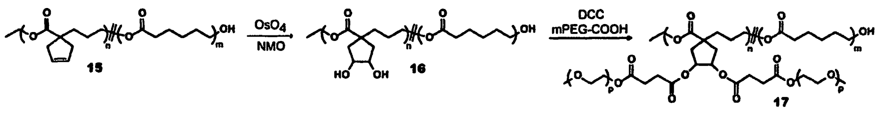

Figure 10. PEGylatation of 1,2-diol substituted aliphatic polyesters.

Further work by Emrick and coworkers has centered on aliphatic polyester functionalization by Cu(I)-catalyzed cycloaddition of azides and alkynes. This cycloaddition, a type of "click" chemistry that couples azides and alkynes to give triazoles, has proven extremely useful in recent years for the connection of small molecules, synthetic polymers, and biologically relevant materials (*35-37*). The preparation of acetylene-functionalized lactone **11** led to its homopolymerization, as well as copolymerization with ε-CL, using $Sn(OTf)_2$ catalysis. This gave novel aliphatic polyesters shown as **18** in Figure 11, with tunable degrees of acetylene substitution along the polyester backbone. Molecular weights and polydispersities could, as in prior examples, be controlled nicely over a range of about 3,000-12,000 g/mol, with PDI ~1.1-1.3. Key to the success of this concept was the stability of the pendent acetylenes to the click conditions, as the polymers proved amenable to a variety of click type reactions with organic azides. For example, water-soluble polyester-*graft*-PEG copolymers, depicted as **19** in Figure 11, could be prepared by reaction with azide-functionalized PEG-1100 monomethyl ethers to give grafting densities, (i.e., percentage functional monomer incorporation) ranging from 10-100 mole percent.

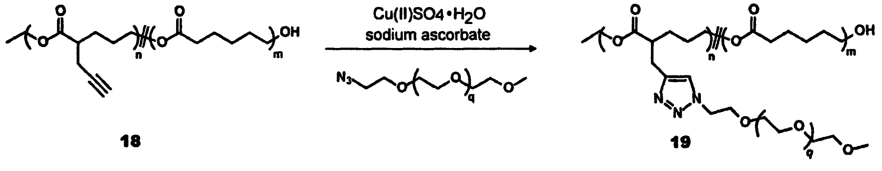

Figure 11. PEG-grafting by post-polymerization click chemistry of acetylene functionalized polyesters

Use of the pendent acetylene functionality and click chemistry carries a number of benefits relative to other methods discussed thus far, including the relatively easy one step monomer synthesis, the ability to homopolymerize or copolymerize the acetylene-functionalized lactone, and the single post-polymerization step that enables coupling of a very diverse range of azide-

Downloaded by UNIV OF ARIZONA on August 9, 2012 | http://pubs.acs.org
Publication Date: September 23, 2006 | doi: 10.1021/bk-2006-0939.ch016

functionalized moieties. The amphiphilicity of the polyester-*graft*-PEG copolymers prepared by this click chemistry is evident from their solution properties, and characteristic peaks in solution NMR experiments performed in both organic solvents and D_2O. Moreover, studies were initiated regarding the biocompatibility of these triazole-linked polyester-*graft*-PEG copolymers, by *in vitro* cytotoxicity testing using mouse fibroblast cells and human red blood cells. All of the polyester-*graft*-PEG samples tested were found to exhibit very low cytotoxicity, in accord with their polyester and PEG composition.

Emrick and coworkers extended the click coupling concept on acetylene-functionalized aliphatic polyesters to oligopeptide sequences. The polyester-*graft*-oligopeptide target is particularly challenging, due to the incompatibility of aliphatic polyesters with traditional solid-phase oligopeptide synthesis and deprotection conditions (*33*). Click chemistry provides a potentially unique solution to this problem, as the azide functionality can be incorporated easily into oligopeptide sequences by solid phase synthesis, and the click coupling can be performed in the presence of unprotected oligopeptides. For example, the preparation of azide-terminated oligopeptide sequences, such as the GRGDS cell-adhesion sequence, was followed by click coupling to acetylene-functionalized polyester **18**, as shown in Figure 12. Oligopeptide-*grafted*-polyesters shown as **20**, with 5 mole percent oligopeptide graft density, were prepared by this method, and the polymers were isolated without substantial degradation or cross-linking of the polyester backbone. Attempts to prepare samples with higher oligopeptide graft densities have been found to be much more challenging, and efforts in this area are in progress. However, the "bio-tailoring" concept driving the synthesis of these functionalized polyesters may prove useful for expanding polyesters in tissue engineering and drug-delivery applications where covalent attachment of oligopeptides can be of benefit, and where low grafting densities will be sufficient for the intended applications.

In summary, aliphatic polyesters, already an important class of synthetic degradable polymeric biomaterials, have been taken to unprecedented levels of synthetic diversity and tailoring through the efforts of many research groups in the U.S. and abroad. Some of these have been described in this brief review, with a focus on pendent or graft functionality by polymerization of functionalized lactones, and post-polymerization modification. Future efforts in this area must attempt to connect these synthetic advances to specific applications, through the collaborative efforts of experts in the chemistry, biology, and clinical use of synthetic polymer materials.

References

1. Ratner, B. D.; Hoffman, A. S.; Schoen, F. J.; Lemons, J. E. "Biomaterials Science: A Multidisciplinary Endeavor" In *Biomaterials Science: An*

Downloaded by UNIV OF ARIZONA on August 9, 2012 | http://pubs.acs.org
Publication Date: September 23, 2006 | doi: 10.1021/bk-2006-0939.ch016

Downloaded by UNIV OF ARIZONA on August 9, 2012 | http://pubs.acs.org
Publication Date: September 23, 2006 | doi: 10.1021/bk-2006-0939.ch016

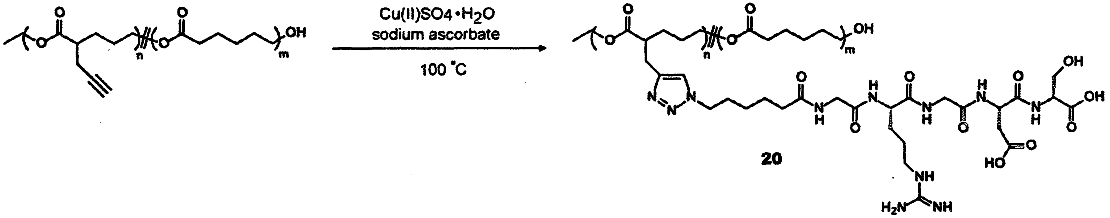
O
O
OH
n
m
Cu(II)SO4•H2O
sodium ascorbate
100 °C
O
O
OH
n
m
N
N
N
O
N
H
O
H
N
O
O
N
H
O
H
N
O
N
H
OH
OH
O
NH
H2N
NH
HO
O

20

Figure 12. Aliphatic polyester grafted with the GRGDS oligopeptide sequence

In Degradable Polymers and Materials; Khemani, K., et al.;
ACS Symposium Series; American Chemical Society: Washington, DC, 2006.

Introduction to Materials in Medicine 2nd edition; Ratner, B. D.; Hoffman, A. S.; Schoen, F. J.; Lemons, J. E.; Eds.; Elsevier Academic Press: San Diego, CA, **2004**, pp 1-9.

2. Albertsson, A. C.; Varma, I. K. *Biomacromolecules* **2003**, 4, 1466-1486.
3. DeBakey, M. E.; Jordan, G. L.; Abbott, J. P.; Halput, B.; O'Neill, R. M. *Arch. Surg.* **1964**, 89, 757-782
4. Postlethwait, R. W.; Dillon, M. L.; Reeves, J. W. *Am. J. Surg.* **1961**, 102, 706-709.
5. Nasongkla, N.; Shuai, X.; Ai, H.; Weinberg, B. D.; Pink, J.; Boothman, D. A.; Gao, J. *Angew. Chem. Int. Ed.* **2004**, 43, 6323-6327.
6. Han, D. K.; Hubbell, J. A. *Macromolecules* **1996**, 29, 5233-5235.
7. Orban, J. M.; Marra, K. G.; Hollinger, J. O. *Tissue Eng.* **2002**, 8, 529-539.
8. Langer, R. *Acc. Chem. Res.* **2000**, 33, 94-101.
9. Ihre, H. R.; Padilla De Jesús, O. L.; Szoka, F. C. Jr.; Fréchet, J. M. J. *Bioconjugate Chem.* **2002**, 13, 443-452.
10. Carnahan, M. A.; Middleton, C.; Kim, J.; Kim, T.; Grinstaff, M. W. *J. Am. Chem. Soc.* **2002**, 124, 5291-5293.
11. Andersson, L.; Davies, J.; Duncan, R.; Ferruti, P.; Ford, J.; Kneller, S.; Mendichi, R.; Pasut, G.; Schiavon, O.; Summerford, C.;Tirk, A.; Veronese, F. M.; Vincenzi, V.; Wu, G. *Biomacromolecules* **2005**, 6, 914-926.
12. Möller, M. Kånge, R. Hedrick, J. L. *J. Polym. Sci. Part A: Polym. Chem.* **2000**, 38, 2067-2074.
13. Nyce, G. W.; Glauser, T.; Conner, E. F.; Möck, A.; Waymouth, R. M.; Hedrick, J. L. *J. Am. Chem. Soc.* **2003**, 125, 3046-3056.
14. Savić, R.; Luo, L.; Eisenberg, A.; Maysinger, D. *Science* **2003**, 300, 615-618.
15. Bogdanov, B.; Vidts, A.; Van Den Bulcke, A.; Verbeeck, R. Schacht, E. *Polymer* **1998**, 39, 1631-1636.
16. Mizutani, M.; Arnold, S. C.; Matsuda, T. *Biomacromolecules* **2002**, 3, 668-675.
17. Nederberg, F.; Bowden, T.; Hilborn, J. *Macromolecules* **2004**, 37, 954-965.
18. Padilla De Jesús, O. L.; Ihre, H. R.; Gagne, L.; Fréchet, J. M. J. *Bioconjugate Chem.* **2002**, 13, 453-461.
19. Trollsås, M.; Löwenhielm, P.; Lee, V. Y.; Möller, M.; Miller, R. D.; Hedrick, J. L. *Macromolecules* **1999**, 32, 9062-9066.
20. Liu, M.; Vladimirov, N.; Fréchet, J. M. J. *Macromolecules* **1999**, 32, 6881-6884.
21. Rieger, J.; Bernaerts, K. V.; Du Prez, F. E.; Jérôme, R.; Jérôme, C. *Macromolecules* **2004**, 37, 9738-9745.
22. Detrembleur, C.; Mazza, M.; Halleux, O.; Lecomte, P.; Mecerreyes, D.; Hedrick, J. L.; Jérôme, R. *Macromolecules* **2000**, 33, 14-18.
23. Mecerreyes, D.; Miller, R. D.; Hedrick, J. L.; Detrembleur, C.; Jérôme, R. *J. Polym. Sci. Part A: Polym. Chem.* **2000**, 38, 870-875.

Downloaded by UNIV OF ARIZONA on August 9, 2012 | http://pubs.acs.org
Publication Date: September 23, 2006 | doi: 10.1021/bk-2006-0939.ch016

24. Latere, J. -P.; Lecomte, P.; Dubois, P.; Jérôme, R. *Macromolecules* **2002**, 35, 7857-7859.
25. Trollsås. M.; Lee, V. Y.; Mecerreyes, D.; Löwenhielm, P.; Möller, M.; Miller., R. D.; Hedrick, J. L. *Macromolecules* **2000**, 33, 4619-4627.
26. Parrish, B.; Quansah, J. K.; Emrick, T. *J. Polym. Sci. Part A: Polym. Chem.* **2002**, 40, 1983-1990.
27. Parrish, B.; Emrick, T. *Macromolecules* **2004**, 37, 5863-5865.
28. Parrish, B.; Breitenkamp, R. B.; Emrick, T. *J. Am. Chem. Soc.* **2005**, 127, 7404-7410.
29. Mecerreyes, D.; Humes, J.; Miller, R. D.; Hedrick, J. L.; Detrembleur, C.; Lecomte, P.; Jérôme, R.; San Roman, J. *Macromol. Rapid Commun.* **2000**, 21, 779-784.
30. Mecerreyes, D.; Atthoff, B.; Boduch, K. A.; Trollsås, M.; Hedrick, J. L. *Macromolecules* **1999**, 32, 5175-5182.
31. Taniguchi, I.; Mayes, A. M.; Chan, E. W. L.; Griffith, L. G. *Macromolecules* **2005**, 38, 216-219.
32. Lee, C. C.; Grayson, S. M.; Fréchet, J. M. J. *J. Polym. Sci. Part A: Polym. Chem.* **2004**, 42, 3563-3578.
33. Barrera, D. A.; Zylstra, E.; Lansbury, P. T.; Langer, R. *J. Am. Chem. Soc.* **1993**, 115, 11010-11011.
34. Molander, G. A.; Harris, C. R. *J. Am. Chem. Soc.* **1995**, 117, 3705-3716.
35. Kolb, H. C.; Finn, M. G.; Sharpless, K. B. *Angew. Chem., Int. Ed.* **2001**, 40, 2004-2021.
36. Wu, P.; Feldman, A. K.; Nugent, A.K.; Hawker, C. J.; Scheel, A.; Voit, B.; Pyun, J.; Fréchet, J. M. J.; Sharpless, K. B.; Fokin, V. V. *Angew. Chem., Int. Ed.* **2004**, 43, 3928-3932.
37. Link, A. J.; Vink, M. K. S.; Tirrell, D. A. *J. Am. Chem. Soc.* **2004**, 126, 10598-10602.

Downloaded by UNIV OF ARIZONA on August 9, 2012 | http://pubs.acs.org
Publication Date: September 23, 2006 | doi: 10.1021/bk-2006-0939.ch016

Downloaded by COLUMBIA UNIV on August 10, 2012 | http://pubs.acs.org
Publication Date: September 23, 2006 | doi: 10.1021/bk-2006-0939.ch017

Chapter 17

Degradable Polymers as Tools for Polyelectrolyte Complex Analysis

L. Leclercq, M. Boustta, and M. Vert

Research Centre for Artificial Biopolymers, UMR CNRS 5473, University of Montpellier 1, Faculty of Pharmacy, 15 Avenue Charles Flahault, B.P. 14491, 34093 Montpellier Cedex 5, France

As part of our investigations of the interest in degradable artificial biopolymers, attention was recently paid to other applications such as analysis of polyelectrolyte complexes or release of one of their polyelectrolyte component. The present work is aimed at comparing the enzymatic degradation of polyelectrolyte complexes formed when polyanions made of similar building blocks but having different chemical structures and charge densities are mixed with an enzyme sensitive polycation, namely poly(L-lysine). The two selected polyanions were poly(L-lysine citramide) and poly(L-lysine citramide imide) and the selected enzyme was trypsin. Fractions were prepared at different values of the degree of neutralization by adding the polycation in solution to a polyanion solution and vice-versa, according to a titration protocol. Dynamic light scattering was used to assess the size and stability of the complexes in the presence of salt at various concentrations. The molecular dimensions of the fractionated polyanions recovered after the degradation of the associated polycation molecules were determined by size exclusion chromatography. The influence of the chemical structure and charge density were discussed and the influence of the order of addition of the oppositely charged complex precursors was also discussed.

In Degradable Polymers and Materials; Khemani, K., et al.;
ACS Symposium Series; American Chemical Society: Washington, DC, 2006.

Introduction

The interest in degradable, biodegradable and/or bioresorbable polymers for time-limited applications is well known in various sectors of human activities, namely surgery, pharmacology and polymer waste management in relation to environmental protection. Polyionic systems of opposite charges interact electrostatically with each other to form complexes of the polyelectrolytic-type or PECs (*1, 2*). The formation and stability of PECs are affected by various factors including the strength of the polyelectrolytes in terms of acid or base, the charge density and concentration, the proportion of opposite charges, the molecular weight of the polyions, the pH and the ionic strength of the medium and even the addition order (*3-5*). At low polymer concentrations and far from charge stoichiometry, PECs are nanodispersed in solution, whereas they precipitate at high polymer concentrations, especially at charge stoichiometry. PECs can be re-dissolved at high salt concentrations, or in acid or basic medium, depending on the nature of the polyions (*3-5*). One of the major problems to analyze PECs is the separation of the complexed components. Two efficient methods using soft conditions were recently developed in our laboratory (*6, 7*). The two methods rely on the use of a salted medium to breakdown the PEC and thus separate their components. In the first method based on affinity chromatography, the resulting solution is percolated through an ion exchange column that retains either the polyanion or the polycation selectively, depending on the nature of the charged gel. Later on, the retained component is recovered using a more concentrated salted mobile phase (*6*). In the second method, the polycation or the polyanion is selectively degraded (hydrolytically or enzymatically), releasing the non-degraded component that can be analyzed easily by usual techniques or made available for further uses.

In the present article, we wish to complement our investigation by comparing the enzymatic degradation of polyelectrolyte complexes formed when polyanions made of similar building blocks but having different chemical structures and charge densities are mixed with a enzyme sensitive polycation, namely poly(L-lysine) (PLL). The two selected polyanions were polydispersed poly(L-lysine citramide) (PLCA) and poly(L-lysine citramide imide) (PLCAI) (*8*) and the selected enzyme was trypsin. Fractions were prepared at different values of the degree of neutralization by adding the polycation in solution to a polyanion solution and vice-versa, according to a titration protocol. The chemical formulae of PLCA, PLCAI and PLL are presented in Scheme 1. Dynamic light scattering was used to assess the size and stability of the complexes in the presence of salt at various concentrations. The molecular

Downloaded by COLUMBIA UNIV on August 10, 2012 | http://pubs.acs.org
Publication Date: September 23, 2006 | doi: 10.1021/bk-2006-0939.ch017

dimensions of the fractionated polyions recovered after the degradation of the associated polycation molecules were determined by size exclusion chromatography. The influence of the chemical structure and charge density on the complex formation during progressive blending of the oppositely charged complex precursors were discussed and the influence of the order of addition as well.

Materials and Methods

Downloaded by COLUMBIA UNIV on August 10, 2012 | http://pubs.acs.org
Publication Date: September 23, 2006 | doi: 10.1021/bk-2006-0939.ch017

Chemicals

Poly(L-lysine),HCl (PLL: $\overline{M_w}$ = 46,000 g/mol, I = 1.30) was purchased from Sigma.

Poly(L-lysine citramide),Na and poly(L-lysine citramide imide),Na, respectively PLCA ($\overline{M_w}$ = 21,000 g/mol) and PLCAI ($\overline{M_w}$ = 24,000 g/mol), were synthesized as previously described (*8*).

Trypsin (EC 3.4.21.4; from hog pancreas) and 2,4,6-trinitrobenzene-1-sulfonic acid (TNBS) were purchased from Fluka.

De-ionized water was obtained using a Milli-Q system from Millipore and then distilled once and filtered three times through a 0.22 µm filter from Millipore before use. Analytical grade NaCl was purchased from Merck.

Methods

Preparation of PEC fractions

Four PEC fractions were prepared by stepwise addition of a 1 M polycation solution to a strongly stirred polyanion solution (20 mg in 1 cm^3 water) in a plastic vial at room temperature. The first stage corresponded to a cationic charges to anionic charges N_{PC}/N_{PA} ratio of 0.3. A coacervate was formed and collected after centrifugation (fraction 1 or F1). The second stage corresponded to N_{PC}/N_{PA} = 0.6 (fraction 2 or F2). The third stage corresponded to a N_{PC}/N_{PA} =

Downloaded by COLUMBIA UNIV on August 10, 2012 | http://pubs.acs.org
Publication Date: September 23, 2006 | doi: 10.1021/bk-2006-0939.ch017

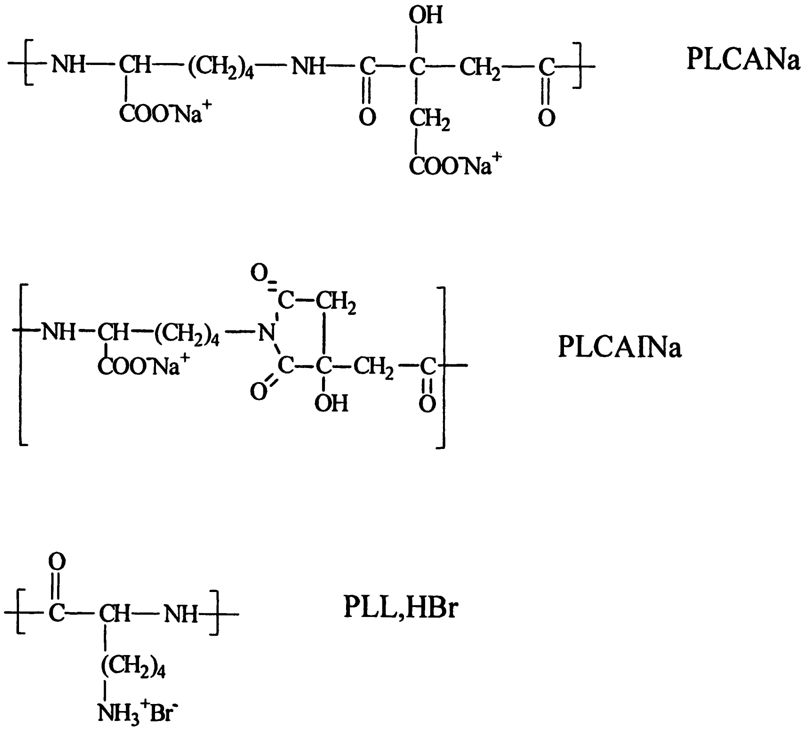

Scheme 1. Chemical formulae of PLCA, PLCAI and PLL.

1 (fraction 3 or F3). Coacervates were washed with de-ionized water. The solution collected after centrifugation at stage 3 was dialyzed against de-ionized water using a Spectra/por membrane with a cut-off of 1,000 Da and freeze-dried. The recovered solid constituted fraction 4 or F4.

Four PEC fractions were also prepared in the same way by changing the addition order, e.g. the polyanion was added to the polycation.

Centrifugation of the complexes was carried out using a Sigma 112 centrifuge at 6000 rpm for 5 min. A Christ LDC-1 apparatus was used for the freeze-drying steps.

Downloaded by COLUMBIA UNIV on August 10, 2012 | http://pubs.acs.org
Publication Date: September 23, 2006 | doi: 10.1021/bk-2006-0939.ch017

Size Exclusion Chromatography (SEC)

SEC experiments were carried out using a pump (P500) and a controller (LCC501 Plus) from Pharmacia and a UV-Visible detector from Waters (Model 486). The detector operated at 214 nm for all the experiments. As column material, a gel was purchased from Amersham Pharmacia Biotech that was composed of cellulose carrying carboxyl groups (CM Sepharose CL-6B). The mobile phase was a 0.15 M phosphate buffer and 1 M NaCl solution at pH=7.4. The elution rate was 0.25 cm^3/min.

Dynamic Light Scattering (DLS)

Vertically polarized DLS measurements (λ_0= 514.5 nm) were performed at 25°C with a commercial BI-200SM instrument (from Brookhaven Instrument Corporation) equipped with a BI-9000AT correlator. The values of the hydrodynamic radius R_H were determined in NaCl solutions using the Stokes-Einstein equation. The viscosity of the polymer solutions was determined using a Rheometer Rheostress RS 100 (from Haake) at 25°C.

The different PEC fractions were first dissolved in 2.5 M NaCl at a concentration of 0.4 mg/cm^3. 0.065 cm^3 of the resulting solution were then added in a Pyrex® tube to a strongly stirred NaCl solution whose concentration was calculated to be set at the appropriate final NaCl concentration, the final concentration of precipitates and the total volume being 13 μg/cm^3 and 2 cm^3, respectively. DLS measurements were performed 24 hours after PEC preparation.

Enzymatic degradation

Enzymatic degradation of PLL alone and within the various PEC fractions was carried out in a 0.1 M NaH_2PO_4 and 1.9 M NaCl solution at pH = 7.9 and at 25 °C using trypsin, known as active on poly(α-aminoacids) (*9*). Prior to introduction into a dialysis tube (Spectra/por membranes with a cut-off of 3,500 Da), the PEC fractions (at the concentration of 10 mg/cm^3) were dissolved in the buffer solution, to which 0.1 cm^3 of a 1 mg/cm^3 trypsin solution was added. Dialysis was carried out against 15 cm^3 of the buffer solution. At various time intervals, the dialyzed amine groups were determined by TNBS assay. Dialysis against fresh buffer solution was performed as long as no more amine was detected in the dialysis buffer solution. Dialysis against de-ionized water was then carried out to remove the salts, the degradation being considered as completed. The content of the dialysis tubes was finally freeze-dried.

TNBS assays

The amine groups released during PLL degradation were assessed by TNBS assay. This colorimetric method is commonly used in biology to determine contents in amine groups (*10*). 0.1 cm^3 of the solution containing the released amines were added into a 1 cm Hellma quartz cell containing 0.875 cm^3 of a 0.1 M borate buffer at pH = 9.3 and 0.025 cm^3 of a 0.03 M TNBS solution. After 120 min incubation, absorbance at λ = 420 nm using a Lambda 15 Perkin Elmer spectrophotometer was measured. A quartz cell containing 0.975 cm^3 borate buffer and 0.025 cm^3 TNBS solution was used as the reference.

Results and Discussion

The physicochemical behavior of the PECs was studied at low polyion concentrations that were in the range generally used in the case of the administration of macromolecular prodrugs or of complexes for drug delivery via nanodispersed amphiphilic systems and gene transfection (*11-13*).

Behavior of the various PEC fractions in the presence of NaCl

Four PLL/PLCA and PLL/PLCAI PEC fractions were collected, as described in the experimental section. The influence of NaCl on the interactions between the two polyanions and PLL was investigated by dilution starting from a NaCl concentration high enough to separate the polyelectrolytes forming the

Downloaded by COLUMBIA UNIV on August 10, 2012 | http://pubs.acs.org
Publication Date: September 23, 2006 | doi: 10.1021/bk-2006-0939.ch017

complex fractions, namely 2.5 M. It was thus not possible to decrease the salt concentration below 0.1 M NaCl according to the selected dilution protocol. DLS was used to monitor the presence of complex in the media of various salt concentrations keeping the 13 μg/cm^3 polymer concentration constant. At 2.5 M in NaCl, the measured sizes of scattering species were around 10 nm in agreement with dimensions obtained for separated polyions. Under these conditions, decreasing the salt concentration led sooner or later to the appearance of much greater scattering species with sizes larger than 100 nm. The salt concentration at which the formation of these rather large scattering species became detectable was named C_{recomp}, with "recomp" standing for recomplexation. The study was carried out using PEC dispersions in comparison with non-fractionated PECs. All the PEC fractions led to similar features with onsets and plateaux (Figure 1). In the case of the PEC fractions obtained from the mixtures of PLL and PLCA, recomplexation was detected for C_{recomp} values decreasing from 0.99 M for fraction 1 to 0.53 M for fraction 4. In the case of the PEC fractions obtained from the mixtures of PLL and PLCAI, the C_{recomp} values decreased from 0.76 M for fraction 1 to 0.38 M for fraction 4. When the salt concentration was decreased, a sharp size increase was observed for each fraction, followed by a zone where the size variations leveled off. It is interesting to note that no macroscopic flocculation was observed up to the salt limit of 0.1 M, as it was previously shown in literature for other systems (*14, 15*). This particular behavior can be assigned to the low charge density of the polyanions and to the presence of hydroxyl groups which stabilize the PEC particles against dramatic increase of hydrophobicity. For the PLL/PLCA couple and the PLL/PLCAI one, the curve corresponding to F1, F2 and F3 levelled off at almost the same R_H value, namely 780 nm and 650 nm, respectively. The plateau R_H values obtained for fractions 4 were much lower (325 nm in the case of PLL/PLCA and 310 nm in the case of PLL/PLCAI). It is worth noting that the C_{recomp} values for the non-fractionated systems decreased as compared to fractions 1. It is worthwhile to note that, PEC nanoparticles of almost constant size were stable in a broad range of ionic strength.

Downloaded by COLUMBIA UNIV on August 10, 2012 | http://pubs.acs.org
Publication Date: September 23, 2006 | doi: 10.1021/bk-2006-0939.ch017

Separation of the two components from the PEC fractions by selective degradation of the polycation component

It is interesting to study whether and how an enzyme degrades polycationic macromolecules in the presence of a polyanion. An endopeptidase, namely trypsin, that was previously shown to be capable of degrading preferentially PLL while keeping intact the PLCA and PLCAI nylon-type polyamides was selected (*7*). All the PEC fractions were destabilized in a 0.1 M NaH_2PO_4 and 1.9 M NaCl solution at pH = 7.9 and at 25°C, before introduction into a 1,000 Da cut-

Downloaded by COLUMBIA UNIV on August 10, 2012 | http://pubs.acs.org
Publication Date: September 23, 2006 | doi: 10.1021/bk-2006-0939.ch017

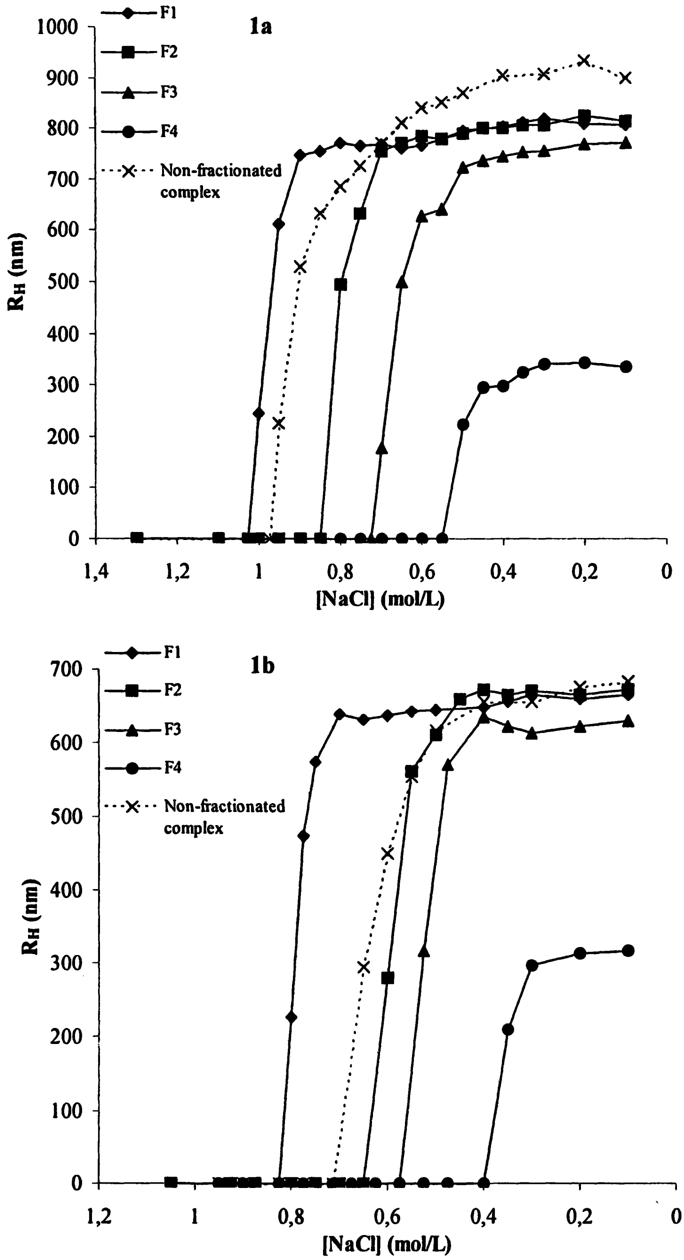

Figure 1. R_H dependence of the four PLL/PLCA (Figure 1a) and PLL/PLCAI (Figure 1b) PEC fractions and of the non-fractionated complexes on NaCl concentration. [PEC] = 13 $\mu g/cm^3$.

off dialysis tube together with trypsin. The same procedure was applied to PLL alone for comparison. The degradation of PLL led to the formation of lysine or small lysine oligomers which could diffuse through the dialysis membrane. The amount of amine-bearing degradation by-products that could pass the dialysis membrane was determined by the TNBS method. The degradation process was stopped and considered as complete when no more amine was released during two days. The content of the dialysis tubes was also checked and shown to be amine-free at the end. Figure 2 shows degradation data obtained for the PLL/PLCA and PLL/PLCAI PEC fractions. The enzymatic degradation by trypsin of PLL alone or within all PEC fractions showed the same profile and was completed in less than 24 hours according to the absence of amine in the dialysis tube. There was no significant difference in the degradation rate between the PLL/PLCAI PEC fractions and the PLL/PLCA ones in agreement with the salt-promoted decomplexation. The presence in the medium of a polyanion even of high charge density did not perturb the enzymatic degradation of the PLL. The final absorbance obtained by adding intermediate absorbance values observed at the various steps of the degradation process was compared to the absorbance value of an equivalent amount of lysine in the presence of TNBS. It was found that the ratio between the two values was almost 0.55 for each system, suggesting that degradation of the PLL by the trypsin endopeptidase led to dialyzable lysine oligomers and not monomers. This finding fully agrees with the mechanism of action of this enzyme. On another hand, the degradation of PLL issued from the PECs and that of the same quantity of free PLL gave the same final absorbance value, implying that oligolysine of similar length were formed and diffused through the dialysis membrane.

Downloaded by COLUMBIA UNIV on August 10, 2012 | http://pubs.acs.org
Publication Date: September 23, 2006 | doi: 10.1021/bk-2006-0939.ch017

Molecular weights determination

After isolating and recovering successfully the polyanion components from each PEC fraction, the polyanions were analyzed by SEC together with the initial PLCA and PLCAI (Figure 3). The SEC chromatogram of the initial PLCA and the chromatograms corresponding to PLCA fraction components recovered from the four PLL/PLCA PEC fractions are presented in Figure 3a. Similar data are reported in Figure 3b for the PLL/PLCAI fractions. The molecular weight of the PLCA and of the PLCAI components decreased from fraction 1 to fraction 4. All PLCA and PLCAI chromatograms were part of that of the initial PLCA or PLCAI, thus showing fractionation in molecular weight. Molecular weight of the polyanion components issued from fractions 4 could not be determined precisely because the retention times at the top of the corresponding SEC peaks were out of the calibration curves (Figure 3).

Downloaded by COLUMBIA UNIV on August 10, 2012 | http://pubs.acs.org
Publication Date: September 23, 2006 | doi: 10.1021/bk-2006-0939.ch017

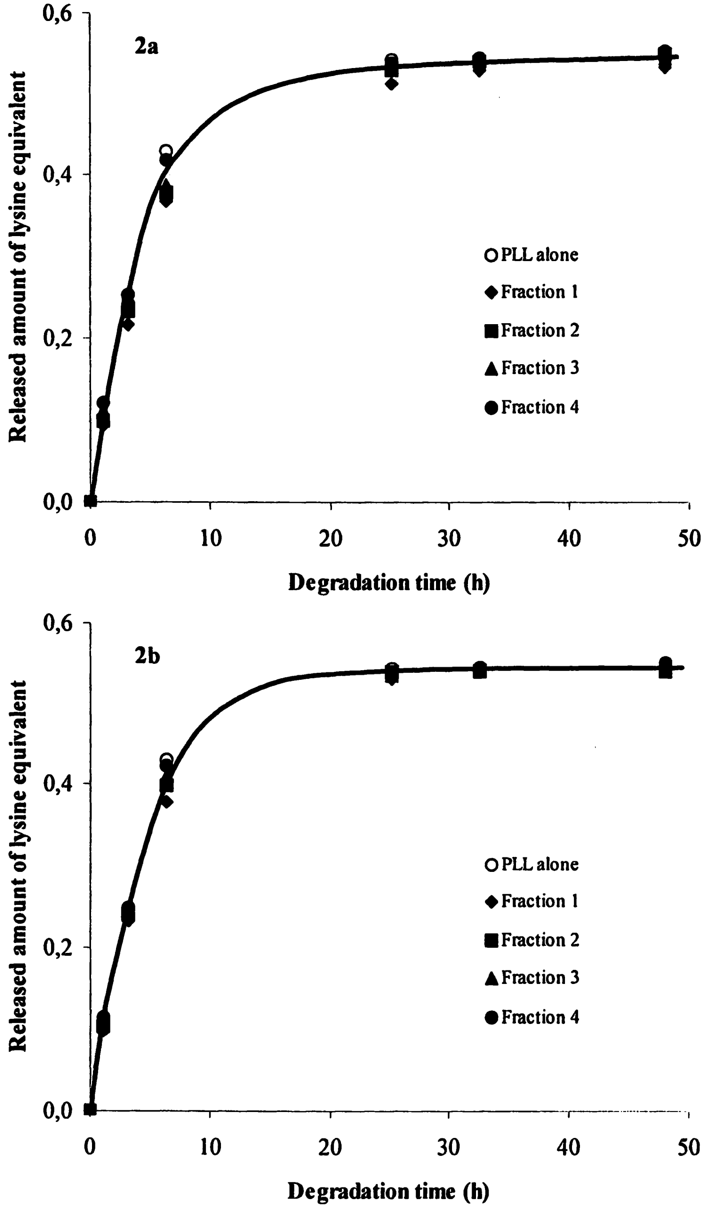

Figure 2. Released amount of aminated compounds in terms of lysine equivalent during the enzymatic degradation by trypsin of the PLL alone and of the PLL component in the four PLL / PLCA (Figure 2a) and PLL / PLCAI (Figure 2b) PEC fractions. [Trypsin] = 0.1 mg/cm^3; [PEC] = 10 mg/cm^3; degradation medium: 0.1 M phosphate buffer and 1.9 M of NaCl at pH = 7.9 and 25 °C.

Downloaded by COLUMBIA UNIV on August 10, 2012 | http://pubs.acs.org
Publication Date: September 23, 2006 | doi: 10.1021/bk-2006-0939.ch017

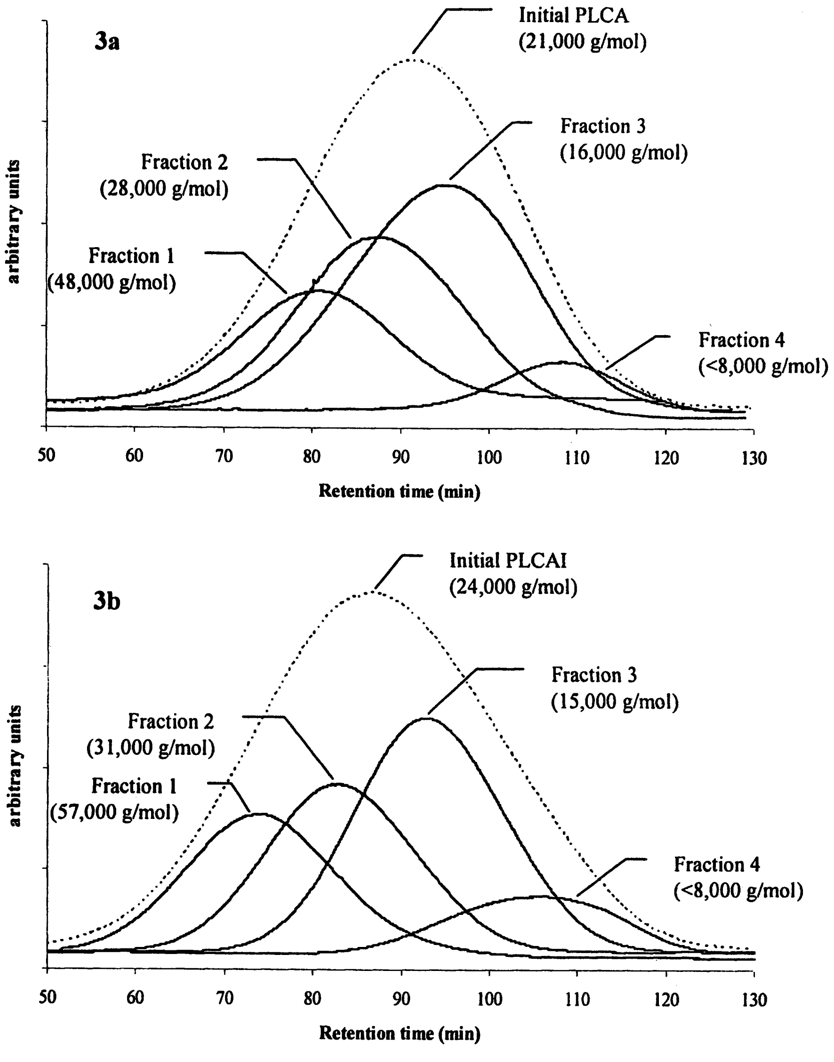

Figure 3. SEC chromatograms of the four PLCA (Figure 3a) and PLCAI (Figure 3b) components obtained from the four corresponding PLL/PLCA and PLL/PLCAI PEC fractions. Gel and elution conditions: anionic cellulose-based gel as the stationary phase and a 1 M NaCl and 0.15 M phosphate buffer solution at pH = 7.4 as the mobile phase.

Influence of the addition order

The influence of the addition order was considered in the case of the PLL/PLCA system. When PLCA was added to PLL, the behavior of the resulting PECs in the presence of NaCl did not change significantly. The plateau R_H and the C_{recomp} values were found close to those observed when adding PLL to PLCA. The molecular weight values for the PLCA within the four PEC fractions showed a little lower selectivity among the PLCA molecules (Table 1). These findings argue in favor of systems close to thermodynamic equilibriums, a situation that is not always observed for other PECs.

Table 1. Molecular weight of the PLCA components issued from each PLL/PLCA PEC fraction when PLL was added to PLCA (determined by SEC).

Fraction	*Mw of PLCA (g/mol)*
1	37,000
2	23,000
3	19,000
4	11,000

Conclusion

Enzymatic degradation of PLL was observed for all PLL/PLCA and PLL/PLCAI nanosized complexes that were formed under titration conditions. The nanodispersed particles remained stable in aqueous media, even in the presence of rather high salt concentrations provided the polyion concentration was kept very low. This finding could be explained by the presence of hydrophilic groups along the chains and the low charge density of the PLCA and PLCAI polyanions. The critical salt concentration C_{recomp} at which nanosized particles were formed was previously shown depending on the molecular weight. Herein it was shown that complex formation depended on the precipitated fraction and on the structure of the polyanion too. The higher the molecular weight, the higher the C_{recomp}.

Results showed that using a polyion which degrades rapidly can be a powerful tool to isolate and analyze the non-degraded partner. Fractionation in molar mass during progressive complex formation was confirmed. The influence of the addition order was relatively moderate.

Downloaded by COLUMBIA UNIV on August 10, 2012 | http://pubs.acs.org
Publication Date: September 23, 2006 | doi: 10.1021/bk-2006-0939.ch017

Acknowledgements

We thank very much Dr Tomas Etrych who contributed to the study of polyelectrolyte complexes by DLS and selective enzymatic degradation.

References

1. Kossel, A. *J. Physiol. Chem.* **1896,** *22*, 178-183.
2. Fuoss, R.M.; Sadek, H. *Science* **1949,** *110*, 552-573.
3. Tsuchida, E.; Abe, K. *Adv. Polym. Sci.* **1982,** *45*, 1-119.
4. Bekturov, E.A.; Bimendina, L.A. *Adv. Polym. Sci.* **1981,** *41*, 99-147.
5. Philipp, B.; Dautzenberg, H.; Linow, K.J.; Koetz, J.; Dawydoff, W. *Progr. Polym. Sci.* **1989,** *14*, 91-172.
6. Boustta, M.; Leclercq, L.; Vert, M. *J. Bioact. and Comp. Polym.* **2004,** *19*, 155-171.
7. Etrych, T.; Boustta, M.; Leclercq, L.; Vert, M. *J. Bioact. and Comp. Polym. in press*
8. Boustta, M.; Huguet, J.; Vert, M. *Makromol. Chem. Macromol. Symp.* **1991,** *47*, 345-355.
9. Huber, R.; Bode, W. *Acc. Chem. Res.* **1978,** *11*, 114-122.
10. Snyder, S.L.; Sobocinski, P.Z. *Anal. Biochem.* **1975,** *64*, 284-288.
11. Behr, J.P. *Bioconjug. Chem.* **1994,** *5*, 382-389.
12. Howard, K.A.; Dash, P.R.; Read, M.L.; Ward, K.; Tomkins, L.M.; Nazarova, O.; Ulbrich, K.; Seymour, L.W. *Biochim. Biophys. Acta* **2000,** *1475*, 245-255.
13. Abdellaoui, K.; Boustta, M.; Morjani, H.; Manfait, M.; Vert, M. *J. Drug Target.* **1997,** *5*, 193-206.
14. Dautzenberg, H.; Kötz, J.; Linow, K.J.; Philipp, B.; Rother, G. *Macromolecular complexes in chemistry and biology*; Springer-Verlag: Berlin, Germany, 1994; p 119.
15. Etrych, T.; Leclercq, L.; Boustta, M.; Vert, M. *Eur. J. Pharm. Sci.* **2005,** *25*, 281-288.

Downloaded by COLUMBIA UNIV on August 10, 2012 | http://pubs.acs.org
Publication Date: September 23, 2006 | doi: 10.1021/bk-2006-0939.ch017

Downloaded by UNIV MASSACHUSETTS AMHERST on August 9, 2012 | http://pubs.acs.org
Publication Date: September 23, 2006 | doi: 10.1021/bk-2006-0939.ch018

Chapter 18

Biobased and Biodegradable Polymer Materials: Rationale, Drivers, and Technology Exemplars

Ramani Narayan

Department of Chemical Engineering and Material Science, Michigan State University, East Lansing, MI 48824 (www.msu.edu/~narayan)

Biobased and biodegradable plastics can form the basis for an environmentally preferable, sustainable alternative to current materials based exclusively on petroleum feedstocks. These biobased materials offer value in the sustainability/life-cycle equation by being part of the biological carbon cycle, especially as it relates to carbon-based polymeric materials such as plastics, water soluble polymers and other carbon-based products like lubricants, biodiesel, and detergents. This global carbon cycle vis-à-vis managing carbon efficiently and in an environmentally responsible manner is discussed. Identification and quantification of biobased content uses radioactive C-14 signature. Biopolymers are generally capable of being utilized by living matter (biodegraded), and so can be disposed in safe and ecologically sound ways through disposal processes (waste management) like composting, soil application, and biological wastewater treatment. Single use, short-life, disposable products can be engineered to be biboased and biodegradable. The need for such products to be fully biodegradable in a defined time frame in the selected disposal infrastructure as opposed to degradable or partially biodegradable is reviewed. Emerging ASTM and International consensus standards on biobased content, and biodegradability is presented. The manufacture of starch foam and starch bioplastics is discussed as technology exemplars for biobased and biodegradable products.

In Degradable Polymers and Materials; Khemani, K., et al.;
ACS Symposium Series; American Chemical Society: Washington, DC, 2006.

Downloaded by UNIV MASSACHUSETTS AMHERST on August 9, 2012 | http://pubs.acs.org
Publication Date: September 23, 2006 | doi: 10.1021/bk-2006-0939.ch018

Why Biobased Polymeric Materials?

Sustainability, industrial ecology, ecoefficiency, and green chemistry are the new principles guiding the development of the next generation of products and processes. New polymeric materials have to be designed and engineered from "conception to reincarnation" incorporating a holistic "life cycle thinking approach". The ecological impact of raw material resources used in the manufacture of a product and the ultimate fate (disposal) of the product when it enters the waste stream has to be factored into the design of the product.

Carbon is the major basic element that is the building block of polymeric materials -- biobased products, petroleum based products, biotechnology products, fuels, even life itself. Therefore, discussions on sustainability, sustainable development, environmental responsibility centers on the issue of managing carbon (carbon based materials) in a sustainable and environmentally responsible manner. Natural ecosystems manages carbon through its biological carbon cycle, and so it makes sense to review how carbon based polymeric materials fit into nature's carbon cycle and address any issues that may arise.

Global Carbon Cycle – Biobased Products Rationale

Carbon is present in the atmosphere as CO_2. Photoautotrophs like plants, algae, and some bacteria fix this inorganic carbon to organic carbon (carbohydrates) using sunlight for energy.

$$CO_2 + H_2O \xrightarrow{\text{Sunlight energy}} (CH_2O)_x + O_2 \qquad \text{Equation 1}$$

Over geological time frames (>10^6 years) this organic matter (plant materials) is fossilized to provide our petroleum, natural gas and coal. We consume these fossil resources to make our polymers, chemicals & fuel and release the carbon back into the atmosphere as CO_2 in a short time frame of 1-10 years (see Figure 1). However, the rate at which biomass is converted to fossil resources is in total imbalance with the rate at which they are consumed and liberated (>10^6 years vs. 1-10 years). Thus, we release more CO_2 than we sequester as fossil resources – a kinetics problem. Clearly, this is not sustainable, and we are not managing carbon in a sustainable and environmentally responsible manner.

Downloaded by UNIV MASSACHUSETTS AMHERST on August 9, 2012 | http://pubs.acs.org
Publication Date: September 23, 2006 | doi: 10.1021/bk-2006-0939.ch018

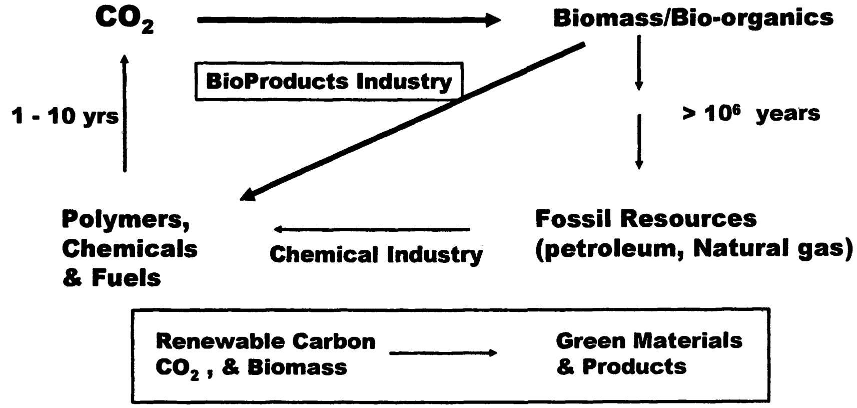
CO_2
Biomass/Bio-organics
BioProducts Industry
1 - 10 yrs
> 10^6 years
Polymers, Chemicals & Fuels
Chemical Industry
Fossil Resources (petroleum, Natural gas)
Renewable Carbon CO_2, & Biomass
Green Materials & Products

Figure 1. Global carbon cycle – sustainability driver

However, if we use annually renewable crops or biomass as the feedstocks for manufacturing our carbon based polymers, chemicals, and fuels, the rate at which CO_2 is fixed equals the rate at which it is consumed and liberated – this is sustainable and the use of annually renewable crops/biomass would allows us to manage carbon in a sustainable manner. Furthermore, if we manage our biomass resources effectively by making sure that we plant more biomass (trees, crops) than we utilize, we can begin to start reversing the CO_2 rate equation and move towards a net balance between CO_2 fixation/sequestration and release due to consumption. Thus, using annually renewable carbon feedstocks allows for:

- Sustainable development of carbon based polymer materials
- Control and even reduce CO_2 emissions and help meet global CO_2 emissions standards – Kyoto protocol
- Provide for an improved environmental profile

Biobased Materials Terminology

Based on the above discussion, and Equation 1, one can define biobased materials as follows:

Biobased Materials – organic material/s in which the carbon comes from contemporary (non-fossil) biological sources

Organic Material/s -- material(s) containing carbon based compound(s) in which the carbon is attached to other carbon atom(s), hydrogen, oxygen, or other elements in a chain, ring, or three dimensional structure (IUPAC nomenclature).

Therefore, to be classified as a biobased, the materials must be organic and contain recently fixed (new) carbon from biological sources.

The question then arises:

- How does one distinguish between new (contemporary) and old(fossil) carbon – i.e. identify biobased carbon?
- How does one quantify biobased carbon content?

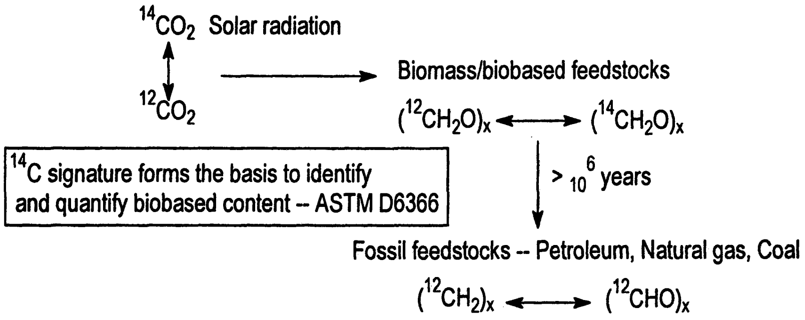
$^{14}CO_2$ Solar radiation
$^{12}CO_2$
Biomass/biobased feedstocks
$(^{12}CH_2O)_x \longleftrightarrow (^{14}CH_2O)_x$
^{14}C signature forms the basis to identify and quantify biobased content -- ASTM D6366
$> 10^6$ years
Fossil feedstocks -- Petroleum, Natural gas, Coal
$(^{12}CH_2)_x \longleftrightarrow (^{12}CHO)_x$

Figure 2. Carbon-14 method to identify and quantify biobased content

As shown in Figure 2, ^{14}C signature forms the basis for identifying and quantifying biboased content. The CO_2 in the atmosphere is in equilibrium with radioactive $^{14}CO_2$. Radioactive carbon is formed in the upper atmosphere through the effect of cosmic ray neutrons on ^{14}N. It is rapidly oxidized to radioactive $^{14}CO_2$, and enters the Earth's plant and animal lifeways through photosynthesis and the food chain. Plants and animals which utilise carbon in biological foodchains take up ^{14}C during their lifetimes. They exist in equilibrium with the ^{14}C concentration of the atmosphere, that is, the numbers of C-14 atoms and non-radioactive carbon atoms stays approximately the same over time. As soon as a plant or animal dies, they cease the metabolic function of carbon uptake; there is no replenishment of radioactive carbon, only decay. Since the half life of carbon is around 5730 years, the fossil feedstocks formed over millions of years will have no ^{14}C signature. Thus, by using this methodology one can identify and quantify biobased content. ASTM subcommittee D20.96 developed a test method (D 6866) to quantify biobased content using this approach (*1*).

D6866 test method involves combusting the test material in the presence of oxygen to produce carbon dioxide (CO_2) gas. The gas is analyzed to provide a measure of the products. $^{14}C/^{12}C$ content is determined relative to the modern carbon-based oxalic acid radiocarbon Standard Reference Material (SRM)

Downloaded by UNIV MASSACHUSETTS AMHERST on August 9, 2012 | http://pubs.acs.org
Publication Date: September 23, 2006 | doi: 10.1021/bk-2006-0939.ch018

4990c, (referred to as HOxII). Three different methods can be used for the analysis. The methods are:

Test Method A utilizes Liquid Scintillation Counting (LSC) radiocarbon (^{14}C) techniques by collecting the CO_2 in a suitable absorbing solution to quantify the biobased content. The method has an error from 5-10% depending on the LSC equipment used.

Test Method B utilizes Accelerator Mass Spectrometry (AMS) and Isotope Ratio Mass Spectrometry (IRMS) techniques to quantify the biobased content of a given product with possible uncertainties of 1 to 2 % and 0.1 to 0.5 %, respectively. Sample preparation methods are identical to Method A, except that in place of LSC analysis the sample CO_2 remains within the vacuum manifold and is distilled, quantified in a calibrated volume, transferred to a quartz tube, torch sealed. The stored CO_2 is then delivered to an AMS facility for final processing and analysis.

Test Method C uses LSC techniques to quantify the biobased content of a product. However, whereas Method A uses LSC analysis of CO_2 cocktails, Method C uses LSC analysis of sample carbon that has been converted to benzene. This method determines the biobased content of a sample with a maximum total error of ±2 % (absolute).

Although Test Method's A and C are less sensitive than that of using AMS/IRMS, they have two distinct advantages:

1. lower costs per evaluation, and
2. much greater instrument availability worldwide.

The 1950's nuclear testing programs resulted in a considerable enrichment of ^{14}C in the atmosphere. Although it continues to decrease by a small amount each year, the current ^{14}C activity in the atmosphere has not reached the pre 1950 level. Because all ^{14}C sample activities are referenced to a "pre-bomb" standard, and because nearly all new biobased products are produced in a post-bomb environment, all values (after correction for isotopic fractionation) must be multiplied by 0.93 (as of the writing of this standard) to better reflect the true biobased content of the sample.

It, therefore, follows that the biobased content of a material is based on the amount of biobased carbon present, and defined as follows:

Biobased content or gross biobased content -- Amount of biobased *carbon* in the material or product as fraction weight (mass) or percent weight (mass) of the total organic carbon in the material or product. **(ASTM D6866)**

Downloaded by UNIV MASSACHUSETTS AMHERST on August 9, 2012 | http://pubs.acs.org
Publication Date: September 23, 2006 | doi: 10.1021/bk-2006-0939.ch018

Biobased Products -- Product(s) made by transforming (chemically, biologically or physically blending) *biobased materials*, either exclusively or in combination with non-biobased materials.

Examples of biobased content determination

The following examples illustrate biobased content determinations.

Product 'O' is a fiber reinforced composite with the composition 30% biofiber (cellulose fiber) + 70% PLA (biobased material). The biobased content of Product 'O' is 100% -- all the carbon in the product comes from bioresources.

Product 'P' is a fiber reinforced composite with the composition 30% glass fiber + 70% PLA (biobased material. The biobased content of Product 'P' is 100%, not 70%. This is because the biobased content is on the basis of carbon, and glass fiber has no carbon associated with it. However, in all cases, one must define biobased content and organic content. Thus, the biobased content of Product 'P' is 100% but organic content is 70%, implying that the balance 30% is inorganic material. In the earlier example of Product 'O' the biobased content is 100% and organic content is 100%. Thus this allows the end-user/customer to clearly differentiate between two 100% biobased products and make their choice on additional criteria – looking at the LCA profile of the two products (using ASTM D 7075).

Product 'N' is a fiber reinforced composite with the composition 30% biofiber (cellulose) + 70% polypropylene (petroleum based organic). Product 'N' biobased content = 18.17% and not 30%. Again, biobased content is not based on weight (mass), but on a carbon basis i.e. amount of biobased *carbon* as fraction weight (mass) or percent weight (mass) of the total organic carbon. Therefore, biobased content = 0.3*44.4 (percent biocarbon; cellulose)/0.7*85.7 (percent carbon in polypropylene)+ 0.3*44.4 (percent biocarbon) * 100 which computes to 18.17%.

The justification and rationale for using carbon and not the weight or moles or other elements like oxygen, or hydrogen as the basis for establishing biobased content of products should now be very self evident. As discussed in earlier sections, the rationale for using biobased products is to manage carbon in a sustainable and efficient manner as part of the natural carbon cycle, therefore it makes sense to use carbon as the basis for determining biobased content. It is also fortituous that an absoloute method using ^{14}C is available to measure the biobased carbon present in a material. The theoretical calculations presented

Downloaded by UNIV MASSACHUSETTS AMHERST on August 9, 2012 | http://pubs.acs.org
Publication Date: September 23, 2006 | doi: 10.1021/bk-2006-0939.ch018

earlier have been validated in experimental observations using ASTM D6866 and are in agreement within +/- 2%.

The U.S. Congress passed the Farm Security and Rural Investment Act of 2002 (P.O. 107 – 171) requiring the purchase of biobased products by the Federal Government. The U.S. Department of Agriculture (USDA) was charged with developing guidelines for designating biobased products and publish a list of designated biobased product classes for mandated Federal purchase (*2*). In its rule-making the USDA adopted the methodology described above for identifying and quantifying biobased content and requires the use of ASTM D6866 to establish biobased content of products.

Material Design Principles for the Environment.

The focus of any product design and engineering has typically been on performance and cost in the product manufacturing stage. However, the impact of using a particular feedstock whether it be petroleum or biobased has not been factored into the equation except for cost. The question of what happens to a product after use when it enters the waste stream has, also, not been considered. Both these factors are beginning to play an increasingly important role in product design and engineering. Figure 3 schematically depicts these concepts.

In the earlier section, the use of biobased as opposed to petroleum feedstocks to manage our carbon based products in a sustainable and

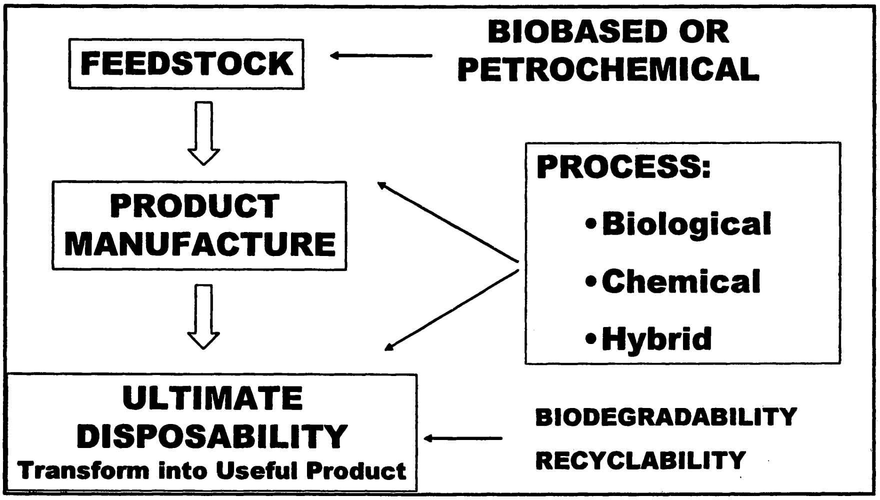

Figure 3. Material design principles for the environment; Life Cycle Assessment

Downloaded by UNIV MASSACHUSETTS AMHERST on August 9, 2012 | http://pubs.acs.org
Publication Date: September 23, 2006 | doi: 10.1021/bk-2006-0939.ch018

environmentally responsible manner has been discussed. However, that is onlypart of the equation, environmental responsibility requires us to look at the entire product cycle from feedstock to ultimate disposal from a holistic point of view --- in other words, one needs to conduct life cycle assessment (LCA) of the product. Towards meeting this goal, a new ASTM standard (D 7075) (*3*) has recently been published on evaluating and reporting on environmental performance of biobased products using LCA methodology.

As shown in Figure 3, disposal of a product after use using biodegradability, recyclability or other recovery options, is an important element of sustainability and environmental responsibility.

Biobased polymers are synthesized by many types of living matter - plants, animals and bacteria - and are an integral part of ecosystem function. Because they are synthesized by living matter, biopolymers are generally capable of being utilized by living matter (biodegraded), and so can be disposed in safe and ecologically sound ways through disposal processes (waste management) like composting, soil application, and biological wastewater treatment. Therefore, for single use, short-life, disposable, materials applications like packaging, and consumer articles, biobased materials can and should be engineered to retain its biodegradability functionality. For durable, long life articles biboased materials needs to be engineered for long-life and performance, and biodegradability may not be an essential criteria.

Biodegradable Materials

Currently, most products are designed with limited consideration to its ecological footprint especially as it relates to its ultimate disposability. Of particular concern are plastics used in single-use, disposable packaging and consumer goods. Designing these materials to be biodegradable and ensuring that they end up in an appropriate disposal system is environmentally and ecologically sound. For example, by composting our biodegradable plastic and paper waste along with other "organic" compostable materials like yard, food, and agricultural wastes, we can generate much-needed carbon-rich compost (humic material). Compost amended soil has beneficial effects by increasing soil organic carbon, increasing water and nutrient retention, reducing chemical inputs, and suppressing plant disease. Composting is increasingly a critical element for maintaining the sustainability of our agriculture system. The food wastes along with other biowastes are separately collected and composted to generate a good, valuable soil amendment that goes back on the farmland to re-initiate the carbon cycle (*4, 5*).

Downloaded by UNIV MASSACHUSETTS AMHERST on August 9, 2012 | http://pubs.acs.org
Publication Date: September 23, 2006 | doi: 10.1021/bk-2006-0939.ch018

Polymer materials have been designed in the past to resist degradation. The challenge is to design polymers that have the necessary functionality during use, but destruct under the stimulus of an environmental trigger after use. The trigger could be microbial, hydrolytically or oxidatively susceptible linkage built into the backbone of the polymer, or additives that catalyze breakdown of the polymer chains in specific environments. More importantly, the breakdown products should not be toxic or persist in the environment, and should be completely assimilated (as food) by soil microorganisms in a defined time frame. In order to ensure market acceptance of biodegradable products, the ultimate biodegradability of these materials in the appropriate waste management infrastructures (more correctly the assimilation/utilization of these materials by the microbial populations present in the disposal infrastructures) in short time frames (one or two growing seasons) needs to be demonstrated beyond doubt.

Polyethylene (PE) or PE-wax coated paper products are problematic in composting because the paper will fully biodegrade under composting conditions, but the PE or wax coating does not biodegrade and builds up in the compost. Paper products coated with fully biodegradable film can provide comparable water resistance, tear strength like the PE coating. However, it is completely biodegradable and non-interfering in recycling operations (unlike current polytheylene or PE-wax coated paper). These new packaging products along with other biowastes, including food wastes can be collected and composted to generate a good, valuable soil amendment that goes back on the farmland to re-initiate the carbon cycle.

Integration with Disposal Infrastructure

Making or calling a product biodegradable or recyclable has no meaning whatsoever if the product after use by the customer does not end up in a disposal infrastructure that utilizes the biodegradability or recyclability features. Recycling makes sense if the recyclable product can be easily collected and sent to a recycling facility to be transformed into the same or new product. Biodegradable products would make sense if the product after use ends up in a disposal infrastructure that utilizes biodegradation. Composting, waste water/sewage treatment facilities, and managed, biologically active landfills (methane/landfill gas for energy) are established biodegradation infrastructures Therefore, producing biodegradable plastics using annually renewable biomass feedstocks that generally end up in biodegradation infrastructures like composting is ecologically sound and promotes sustainability. Materials that cannot be recycled or biodegraded can be incinerated with recovery of energy (waste to energy). Landfills are a poor choice as a repository of plastic and

Downloaded by UNIV MASSACHUSETTS AMHERST on August 9, 2012 | http://pubs.acs.org
Publication Date: September 23, 2006 | doi: 10.1021/bk-2006-0939.ch018

organic waste. Today's sanitary landfills are plastic-lined tombs that retard biodegradation because of little or no moisture and negligible microbial activity. Organic waste such as lawn and yard waste, paper, food, biodegradable plastics, and other inert materials should not be entombed in such landfills. Figure 4 illustrates the integration of biodegradable plastics with disposal infrastructures that utilize the biodegradable function of the plastic product..

Amongst disposal options, composting is an environmentally sound approach to transfer biodegradable waste, including the new biodegradable plastics, into useful soil amendment products. Composting is the accelerated degradation of heterogeneous organic matter by a mixed microbial population in a moist, warm, aerobic environment under controlled conditions. Biodegradation of such natural materials will produce valuable compost as the major product, along with water and carbon dioxide. The CO_2 produced does not contribute to an increase in greenhouse gases because it is already part of the biological carbon cycle. Composting our biowastes not only provides ecologically sound waste disposal but also provides much needed compost to maintain the productivity of our soil and sustainable agriculture. Figure 4 shows disposal infrastructures that can receive biodegradable plastics.

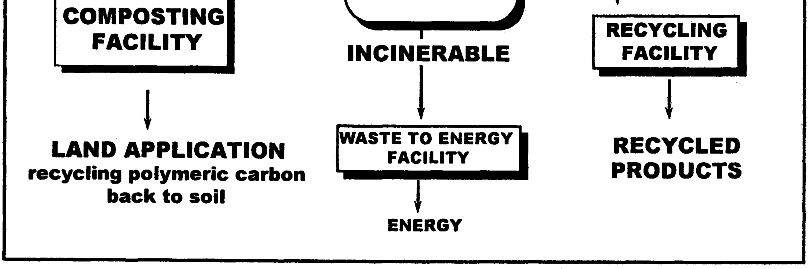
Anaerobic digestion facility
Marine environment
Biodegradable Plastics
Paper-biopolymer composite
COMPOSTING FACILITY
INCINERABLE
RECYCLING FACILITY
LAND APPLICATION recycling polymeric carbon back to soil
WASTE TO ENERGY FACILITY
ENERGY
RECYCLED PRODUCTS

Figure 4. Integration of biodegradable plastics with disposal infrastructures.

As discussed earlier, composting is an important disposal infrastructure because greater than 50% of the municipal soild waste (MSW) stream is biowastes like yard trimmings, food, non-recyclable paper products (see Figure 5).

Downloaded by UNIV MASSACHUSETTS AMHERST on August 9, 2012 | http://pubs.acs.org
Publication Date: September 23, 2006 | doi: 10.1021/bk-2006-0939.ch018

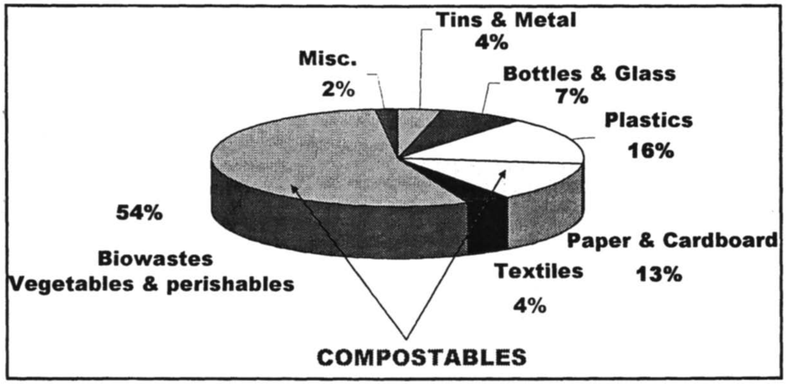

Figure 5. Typical MSW distribution by weight

Degradable vs Biodegradable – An Issue

Designing products to be degradable or partially biodegradable causes irreparable harm to the environment. Degraded products may be invisible to the naked eye. However, out of sight does not make the problem go away. One must ensure complete biodegradability in a short defined time frame (determined by the disposal infrastructure). Typical time frames would be up to one growing season or one year. As discussed earlier the disposal environments are composting, anaerobic digestion, marine/ocean, and soil.

Unfortunately, there are products in the market place that are designed to be degradable, i.e they fragment into smaller pieces and may even degrade to residues invisible to the naked eye. However, there is no data presented to document complete biodegradability within the one growing season/one year time period. It is assumed that the breakdown products will eventually biodegrade. In the meanwhile, these degraded, hydrophobic, high surface area plastic residues migrate into the water table and other compartments of the ecosystem causing irreparable harm to the environment. In a recent Science article (*6*) researchers report that plastic debris around the globe can erode (degrade) away and end up as microscopic granular or fiber-like fragments, and that these fragments have been steadily accumulating in the oceans. Their experiments show that marine animals consume microscopic bits of plastic, as seen in the digestive tract of an amphipod. The Algalita Marine Research Foundation (*7*) report that degraded plastic residues can attract and hold hydrophobic elements like PCB and DDT up to one million times background levels. The PCB's and DDT's are at background levels in soil, and diluted out so as to not pose significant risk. However, degradable plastic residues with these high surface area concentrate these highly toxic chemicals, resulting in a toxic time bomb, a poison pill floating in the environment posing serious risks.

Downloaded by UNIV MASSACHUSETTS AMHERST on August 9, 2012 | http://pubs.acs.org
Publication Date: September 23, 2006 | doi: 10.1021/bk-2006-0939.ch018

Downloaded by UNIV MASSACHUSETTS AMHERST on August 9, 2012 | http://pubs.acs.org
Publication Date: September 23, 2006 | doi: 10.1021/bk-2006-0939.ch018

Recently, Japanese researchers (*8*) confirmed these findings. They reported that PCBs, DDE, and nonylphenols (NP) were detected in high concentrations in degraded polypropylene (PP) resin pellets collected from four Japanese coasts. The paper documents that plastic residues function as a transport medium for toxic chemicals in the marine environment.

Therefore, designing hydrophobic polyolefin plastics, like polyethylene (PE) to be degradable, without ensuing that the degraded fragments are completely assimilated by the microbial populations in the disposal infrastructure in a very short time period poses more harm to the environment than if it was not made degradable. These concepts are illustrated in Figure 6. The Figure shows that heat, moisture, sunlight and/or enzymes shorten & weaken polymer chains, resulting in fragmentation of the plastic and some cross-linking creating more intractable persistent residues. It is possible to accelerate the breakdown of the plastics in a controlled fashion to generate these fragments, some of which could be microscopic and invisible to the naked eye, and some elegant chemistry has been done to make this happen as reported in some papers in this book.

However, this constitutes only degradation/fragmentation, and not biodegradation. As discussed earlier hydrophobic polymer fragments pose risk to the environment, unless the degraded fragments are completely assimilated as food and energy source by the microbial populations present in the disposal system in a very short period (one year). Microorganisms use the carbon substrates to extract chemical energy for driving their life processes by aerobic oxidation of glucose and other readily utilizable C-substrates as shown by the Equation 2.

AEROBIC

$$\text{C-substrate} + 6\,O_2 \longrightarrow 6\,CO_2\uparrow + 6\,H_2O;\ \Delta G^{0'} = -686\ \text{kcal/mol} \qquad \text{Equation 2}$$

$(CH_2O)_X$; $x = 6$

Thus, a measure of the rate and amount of CO_2 evolved in the process is a direct measure of the amount and rate of microbial utilization (biodegradation) of the C-polymer. This forms the basis for ASTM and International Standards for measuring biodegradability or microbial utilization of the test polymer/plastics. Thus, one can measure the rate and extent of biodegradation or microbial utilization of the test plastic material by using it as the sole carbon source in a test system containing a microbially rich matrix like compost in the presence of air and under optimal temperature conditions (preferably at 58^0 C – representing the thermophilic phase). Figure 7 shows a typical graphical output that would be obtained if one were to plot the percent carbon converted to CO_2 as a function of time in days.First, a lag phase during which the microbial

Downloaded by UNIV MASSACHUSETTS AMHERST on August 9, 2012 | http://pubs.acs.org
Publication Date: September 23, 2006 | doi: 10.1021/bk-2006-0939.ch018

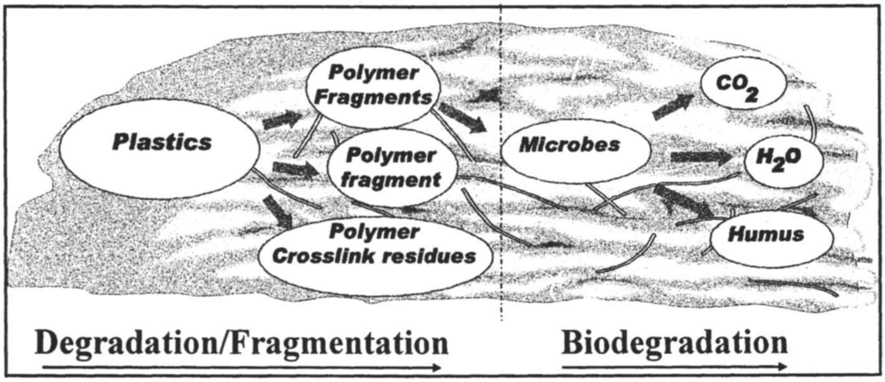
Plastics
Polymer Fragments
Polymer fragment
Polymer Crosslink residues
Microbes
CO_2
H_2O
Humus
Degradation/Fragmentation
Biodegradation

Figure 6. Degradation vs biodegradation

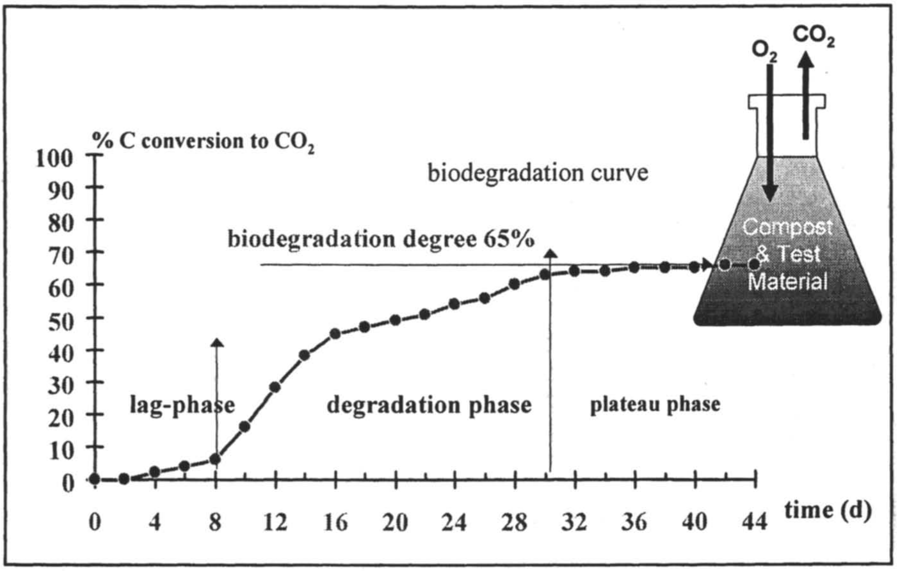

Figure 7. Test method to measure the rate and extent of microbial utilization (biodegradation) of biodegradable plastics

Downloaded by UNIV MASSACHUSETTS AMHERST on August 9, 2012 | http://pubs.acs.org
Publication Date: September 23, 2006 | doi: 10.1021/bk-2006-0939.ch018

population adapts to the available test C-substrate. Then, the biodegradation phase during which the adapted microbial population begins to utilize the carbon substrate for its cellular life processes, as measured by the conversion of the carbon in the test material to CO_2. Finally, the output reaches a plateau when all of the substrate is completely utilized.

Based on the above concepts, ASTM committee D20.96 (9) has developed a Specification Standard for products claiming to be biodegradable under composting conditions or compostable plastic. The specification standard ASTM D6400 identifies 3 criteria

- **Complete biodegradation (using ASTM D5338 test method):**
    - Conversion to CO_2, water & biomass via microbial assimilation of the test polymer material in powder, film, or granule form.
    - 60% carbon conversion of the test polymer to CO_2 for homopolymer & 90% carbon conversion to CO_2 for copolymers, polymer blends, and addition of low MW additives or plasticizers.
    - Same rate of biodegradation as natural materials -- leaves, paper, grass & food scraps
    - Time -- 180 days or less; if radiolabeled polymer is used 365 days or less.

Disintegration

- <10% of test material on 2mm sieve using the test polymer material in the shape and thickness identical to the product's final intended use – see ISO 16929 (*10)* and ISO 20200 (*11*).

Safety

- The resultant compost should have no impacts on plants, using OECD Guide 208, Terrestrial Plants, Growth Test
- Regulated (heavy) metals content in the polymer material should be less than 50% of EPA (USA, Canada) prescribed threshold.

The above specification standard is in harmony with standards in Europe, Japan, Korea, China, and Taiwan, for example EN13432 titled "Requirements for Packaging Recoverable through Composting and Biodegradation—Test Scheme and Evaluation Criteria for the Final Acceptance of Packaging" is the European standard (norm) and similar to D6400. At the International level, the International Standards Organization (ISO) is developing ISO 17088, "Specification for Compostable Plastics" which is in harmony with ASTM D 6400, and the European norms.

Figure 8 summarizes the current standards for the different disposal systems.

Downloaded by UNIV MASSACHUSETTS AMHERST on August 9, 2012 | http://pubs.acs.org
Publication Date: September 23, 2006 | doi: 10.1021/bk-2006-0939.ch018

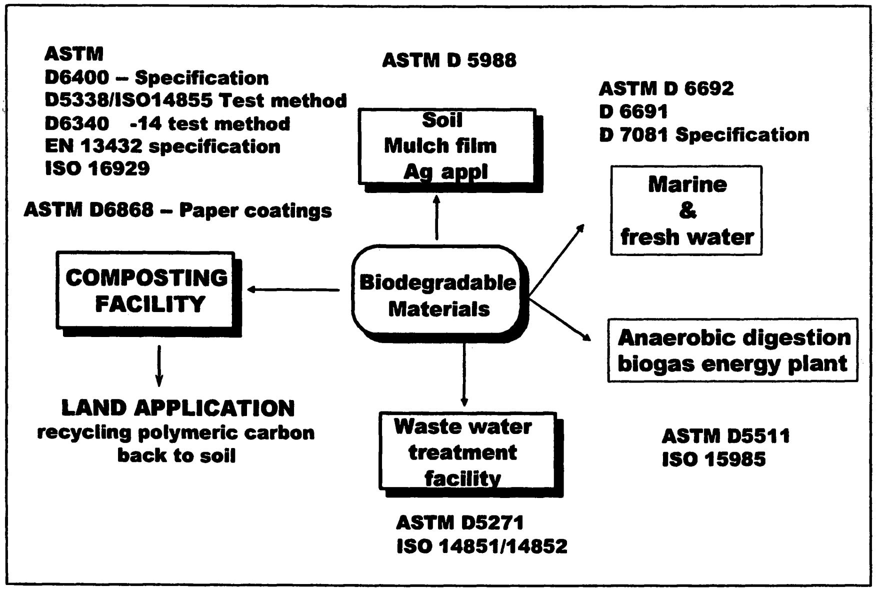
ASTM
D6400 – Specification
D5338/ISO14855 Test method
D6340 -14 test method
EN 13432 specification
ISO 16929
ASTM D6868 – Paper coatings
ASTM D 5988
Soil
Mulch film
Ag appl
ASTM D 6692
D 6691
D 7081 Specification
Marine
&
fresh water
COMPOSTING
FACILITY
Biodegradable
Materials
Anaerobic digestion
biogas energy plant
LAND APPLICATION
recycling polymeric carbon
back to soil
Waste water
treatment
facility
ASTM D5511
ISO 15985
ASTM D5271
ISO 14851/14852

Figure 8 ASTM and European (EN) Standards for biodegradable plastics in different disposal systems.

Technology Exemplars

Biobased and Biodegradable Polymer Materials

Polymer materials based on annually renewable agricultural and biomass feedstocks can form the basis for a portfolio of sustainable, environmentally preferable alternatives to current materials based exclusively on petroleum feedstocks. Two basic routes are possible. Direct extraction from biomass yields a series of natural polymer materials (cellulose, starch, proteins), fibers, and vegetable oils that can form the platform on which polymer materials and products can be developed as shown in Figure 9 , the bolded items in the Figure represents our work in this area.

Alternatively, the biomass feedstock (annually renewable resources) can be converted to bio-monomers by fermentation or hydrolysis. The biomonomers can be further modified by a biological or chemical route. As shown in Figure 10, the biomonomers can be fermented to give succinic acid, adipic acid, 1,3-propane diol – precursor chemicals for the manufacture of polyesters – example is DuPont's Sorona polyestyer made from a bio 1,3-propanediol.. Biomonomers

Downloaded by UNIV MASSACHUSETTS AMHERST on August 9, 2012 | http://pubs.acs.org
Publication Date: September 23, 2006 | doi: 10.1021/bk-2006-0939.ch018

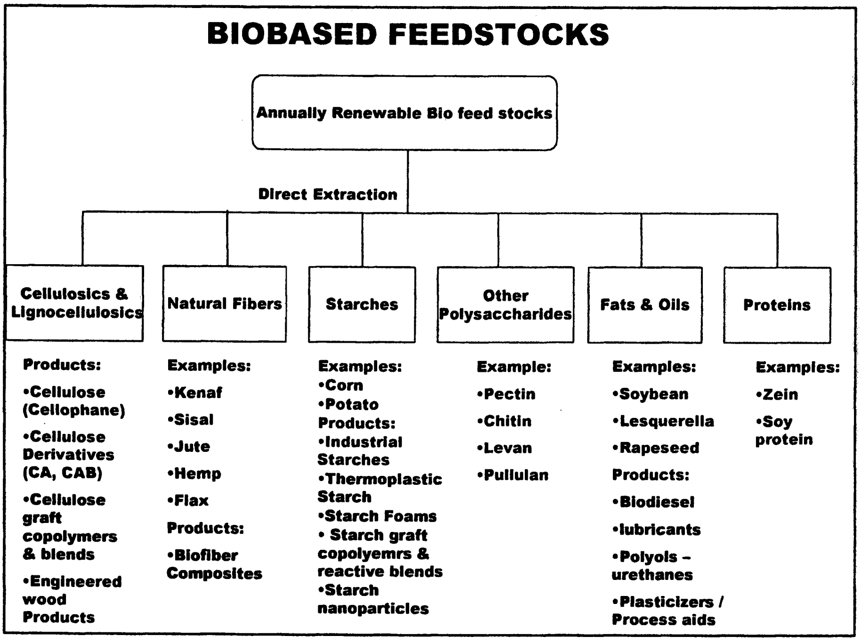
BIOBASED FEEDSTOCKS
Annually Renewable Bio feed stocks
Direct Extraction
Cellulosics & Lignocellulosics
Natural Fibers
Starches
Other Polysaccharides
Fats & Oils
Proteins
Products:
•Cellulose (Cellophane)
•Cellulose Derivatives (CA, CAB)
•Cellulose graft copolymers & blends
•Engineered wood Products
Examples:
•Kenaf
•Sisal
•Jute
•Hemp
•Flax
Products:
•Biofiber Composites
Examples:
•Corn
•Potato
Products:
•Industrial Starches
•Thermoplastic Starch
•Starch Foams
• Starch graft copolyemrs & reactive blends
•Starch nanoparticles
Example:
•Pectin
•Chitin
•Levan
•Pullulan
Examples:
•Soybean
•Lesquerella
•Rapeseed
Products:
•Biodiesel
•lubricants
•Polyols – urethanes
•Plasticizers / Process aids
Examples:
•Zein
•Soy protein

Figure 9. Direct extraction of biomass to provide biopolymers for use in manufacture of biobased products.

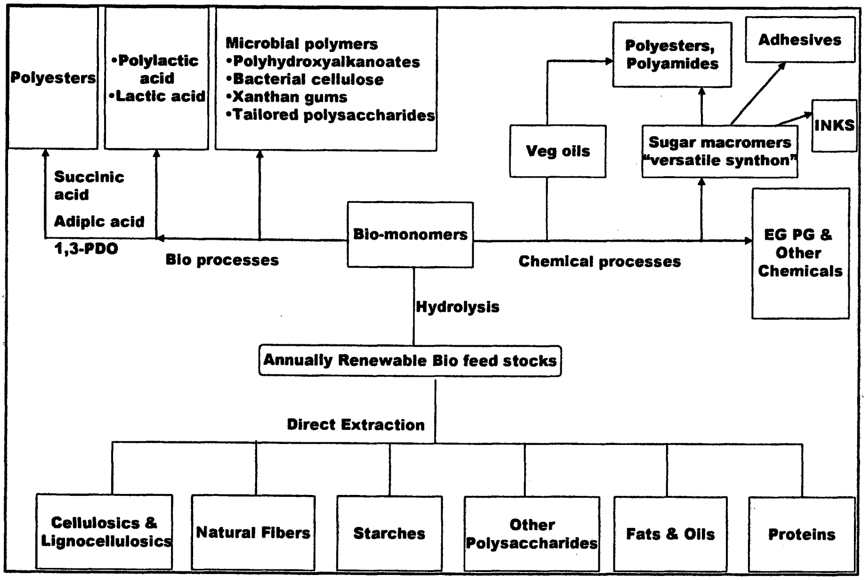
Polyesters
•Polylactic acid
•Lactic acid
Microbial polymers
•Polyhydroxyalkanoates
•Bacterial cellulose
•Xanthan gums
•Tailored polysaccharides
Polyesters, Polyamides
Adhesives
INKS
Veg oils
Sugar macromers "versatile synthon"
Succinic acid
Adipic acid
1,3-PDO
Bio processes
Bio-monomers
Chemical processes
EG PG & Other Chemicals
Hydrolysis
Annually Renewable Bio feed stocks
Direct Extraction
Cellulosics & Lignocellulosics
Natural Fibers
Starches
Other Polysaccharides
Fats & Oils
Proteins

Figure 10. Conversion to biomonomer and other chemicals and polymers.

can be fermented to lactic acid, which is then converted into poly(lactic acid) – currently being commercialized by NatureWorks LLC with a 300 MM lb manufacturing plant in Blair, Nebraska (*12*). Bio-monomers can also be microbially transformed to biopolymers like the polyhydroxyalkanoates (PHA's). Papers relating to PHA polymers can be found in other chapters in this book.

Instead of microbial fermentative processes, chemical conversion of biomonomers yields intermediate chemicals like ethylene, and propylene glycols. Vegetable oils offer a platform to make a portfolio of polyols, lubricants, polyesters, polyamides. In another chapter in this book, we report on ozone mediated transformation of vegetable oils to polyols, urethane foams, polyesters, and polyamides.

Surfactants, detergents, adhesives, and water-soluble polymers can be engineered from biomass feedstocks. As discussed earlier, biobased materials targeted for short-life, single use, disposable packaging materials and consumer products can and should be engineered to retain inherent biodegradability properties, thereby offering an environmentally responsible disposal option for such products.

Downloaded by UNIV MASSACHUSETTS AMHERST on August 9, 2012 | http://pubs.acs.org
Publication Date: September 23, 2006 | doi: 10.1021/bk-2006-0939.ch018

Starch Bioplastics. (*13-18*).

Starch is a polymer of anhydroglucose units linked by alpha-1,4 linkages, and is one of the most abundant renewable polymers found in nature. In the U.S. cereal grains, primarily corn, are the major sources of starch. They are found as granules ranging from 2 to 50 microns in diameter. The starch polymer present in the granules exists as a mixture of two polymers -- a predominantly linear α-1,4 glucan polymer called amylose, and an α-1,6- branched α-1,4 glucan polymer called amylopectin. Depending upon the origin and nature of the starch, the relative ratios of amylose and amylopectin vary.

Typical molecular weights of amylose are around one million and amylopectin around ten million. The amylose and amylopectin molecules are in an ordered arrangement within the granule and gives crystallinity to the granule.

Starch granules exhibit hydrophilic properties and strong inter-molecular association via hydrogen bonding due to the hydroxyl groups on the granule surface. This strong hydrogen bonding association and crystallization leads to poor thermal processing since the Tm is higher than the thermal decomposition temperature,and degradation sets in before thermal melting. The hydrophilicity and thermal sensitivity renders the starch molecule unsuitable for thermoplastic applications.

Downloaded by UNIV MASSACHUSETTS AMHERST on August 9, 2012 | http://pubs.acs.org
Publication Date: September 23, 2006 | doi: 10.1021/bk-2006-0939.ch018

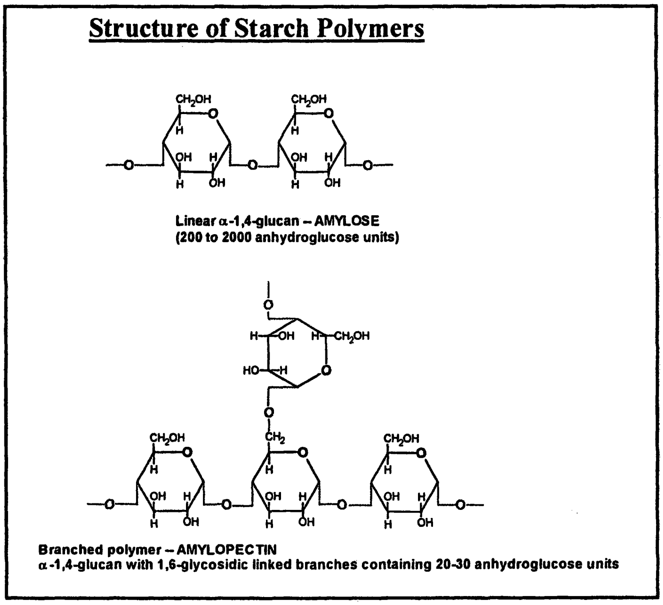
Structure of Starch Polymers
CH₂OH
O
H
OH
H
H
OH
Linear α-1,4-glucan – AMYLOSE
(200 to 2000 anhydroglucose units)
HO
CH₂
Branched polymer – AMYLOPECTIN
α-1,4-glucan with 1,6-glycosidic linked branches containing 20-30 anhydroglucose units

Figure 11. Structure of starch polymers

However, plastic starch can be synthesized by the use of appropriate plasticizers that break the hydrogen bonds, and allow the starch to flow like a thermoplastic. Plasticization of the starch in a twin screw extruder with appropriate screw elements, using glycerol as the plasticizer, with little or no water in a co-rotating twin screw extruder has been accomplished. The resultant material is brittle and does not offer suitable performance properties. Reactive compounding of these plastic starches with biodegradable polyesters in which the starch is the dispersed phase and the polyester is the continuous phase offers materials that can be processed into films with excellent performance properties. Figure 12 conceptualizes the reactive blend technology with plastic starch and biodegradable polyesters (*13-18*). Typical biodegradable polyesters are poly(butylene adipate-co-terephthalate); (PBAT, sold under the trade name EcoFlex by BASF), poly (ε-caprolactone), and our newly synthesized (*19*) three arm poly(ε-caprolactone), poly(lactic acid), PLA, and polyhydroxy alkanoates (PHA's).

Biodegradable Starch Esters

Modification of the starch -OH groups by esterification chemistry to form starch esters of appropriate degree of substitution (1.5 to 3.0 ds) imparts thermoplasticity and water resistance (*20*). Unmodified starch shows no thermal transitions except the onset of thermal degradation at around 260^0C. Starch

Downloaded by UNIV MASSACHUSETTS AMHERST on August 9, 2012 | http://pubs.acs.org
Publication Date: September 23, 2006 | doi: 10.1021/bk-2006-0939.ch018

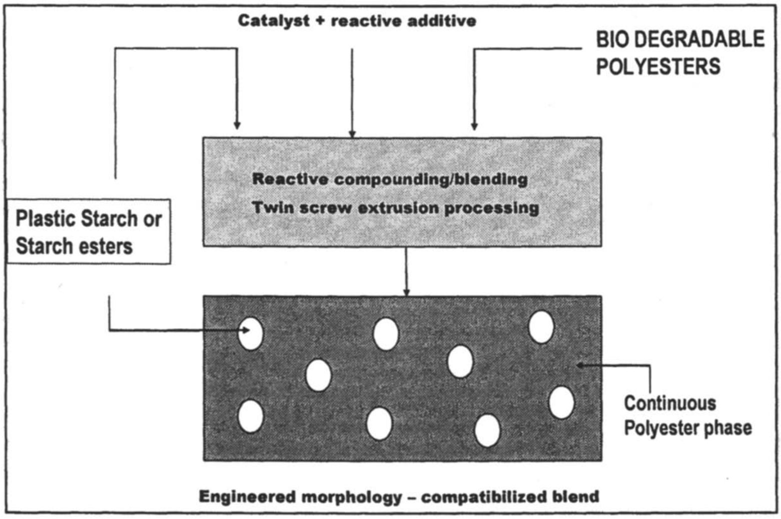
Catalyst + reactive additive
BIO DEGRADABLE POLYESTERS
Reactive compounding/blending
Twin screw extrusion processing
Plastic Starch or Starch esters
Continuous Polyester phase
Engineered morphology – compatibilized blend

Figure 12. Biobased and biodegradable reactive blend compositions

acetate of ds 1.5 shows a sharp glass transition at 155^{0}C and starch propionate of same ds had a Tg of 128^{0}C. Plasticizers like glycerol triacetate and diethyl succinate are completely miscible with starch esters and can be used to improve processability. Water resistance of the starch esters is greatly improved over the unmodified starch. The starch ester resin reinforced with biofibers (*22*) has properties comparable to general-purpose polystyrene.

Appropriately formulated starch esters with plasticizers and other additives provide resin compositions that can be used to make injection molded products and for direct lamination onto Kraft paper. Starch acetates up to ds=2.5 undergo complete and rapid biodegradation. In the case of starch triacetates, 70% of the carbon is converted to CO_2 at 58^{0}C in 45 days (*23*).

Starch Foam Technology

Our group at Michigan State University (MSU) has developed a one step, environmentally friendly extrusion process to manufacture biobased, biodegradable, foam sheets and blocks for packaging (*24-26*). The packaging foam is totally biobased non-toxic and biodegradable. After use, it can be completely disposed of in an environmentally responsible manner in soil or in compost operations, where it becomes a nutrient (food) for the soil. MSU's bioplastic foam has the performance characteristics of today's polyethylene-based foam in targeted applications, and supports a companies' ISO 1401 certification.

Downloaded by UNIV MASSACHUSETTS AMHERST on August 9, 2012 | http://pubs.acs.org
Publication Date: September 23, 2006 | doi: 10.1021/bk-2006-0939.ch018

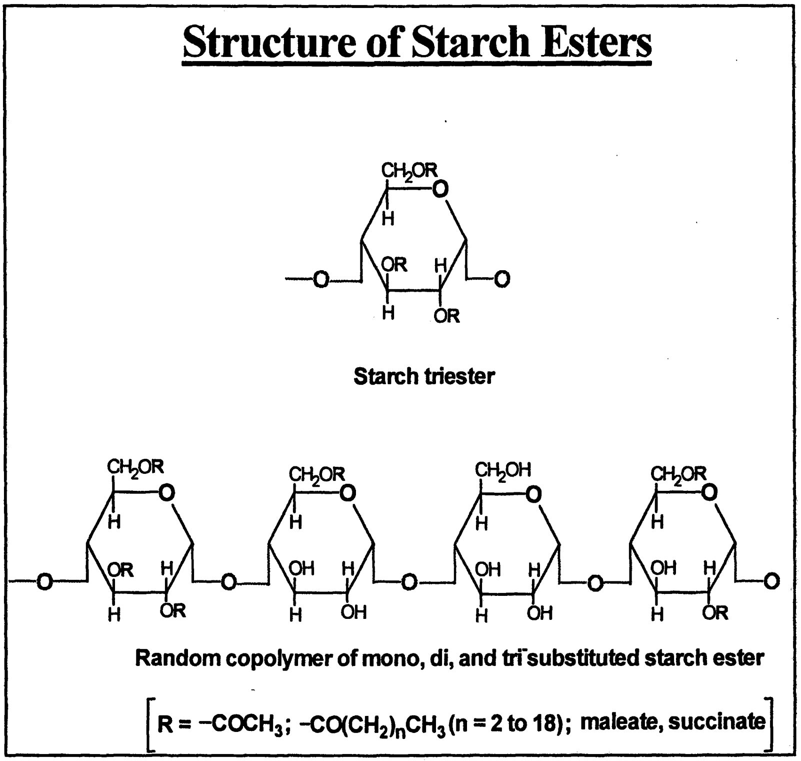
Structure of Starch Esters
CH$_2$OR
O
H
OR
H
O
O
H
OR
Starch triester
CH$_2$OR
CH$_2$OR
CH$_2$OH
CH$_2$OR
OR
OH
OH
OH
Random copolymer of mono, di, and tri-substituted starch ester
R = $-COCH_3$; $-CO(CH_2)_nCH_3$ (n = 2 to 18); maleate, succinate

Figure 13 Structure of biodegradable starch esters.

The MSU technology involves **using water as the plasticizer and blowing agent**. Water and the shear imparted in the extrusion process helps in breaking the hydrogen bonds holding the starch molecules in the granule state and release the polymer chains without significantly reducing the molecular weight of the amylose/amylopectin chains. Nucleating agents and process aids allows control of the cell structure, and maintain the flexibility of the foam material. Screw configurations are important to control the foaming process. In this project we are also developing process engineering parameters to make a portfolio of foam products with control of cell structure, resilience, and barrier properties. The cellular structure of the foam material is shown in Figure 14.

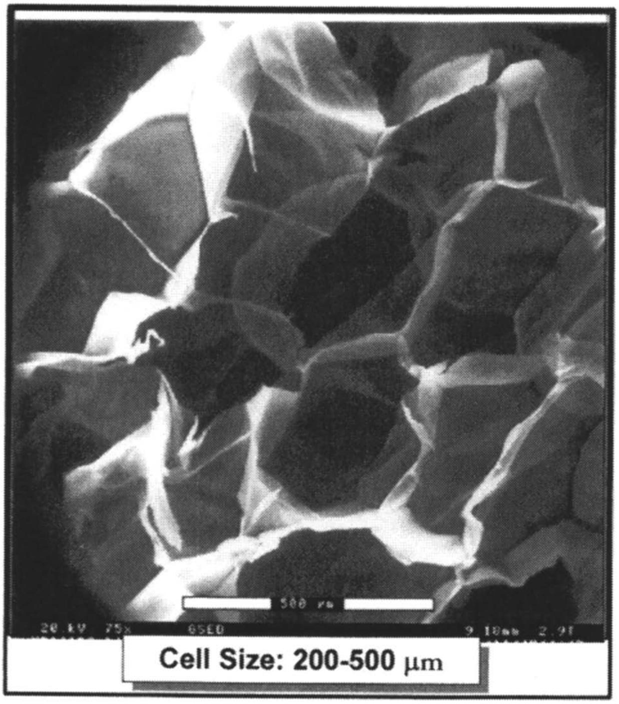

Figure 14. Closed cell structure of starch foams

Starch foam sheets have been manufactured and introduced to the market under the Green Cell trade name (*31*) (www.ktmindustries.com) for cushion packaging and insulation. The pictures in Figure 15 shows Green Cell protective packaging system designed for shipping an automotive video entertainment system, windshield, and end cap. Based on successful trials, this system has been used for over 12 months by a leading automotive parts manufacturer (Toyota) without any system failure. ***KTM*** Industries (*18*), has also cleverly exploited the light-weight, non-toxic, water wetable adhesive property of extrusion foamed

Downloaded by UNIV MASSACHUSETTS AMHERST on August 9, 2012 | http://pubs.acs.org
Publication Date: September 23, 2006 | doi: 10.1021/bk-2006-0939.ch018

Downloaded by UNIV MASSACHUSETTS AMHERST on August 9, 2012 | http://pubs.acs.org
Publication Date: September 23, 2006 | doi: 10.1021/bk-2006-0939.ch018

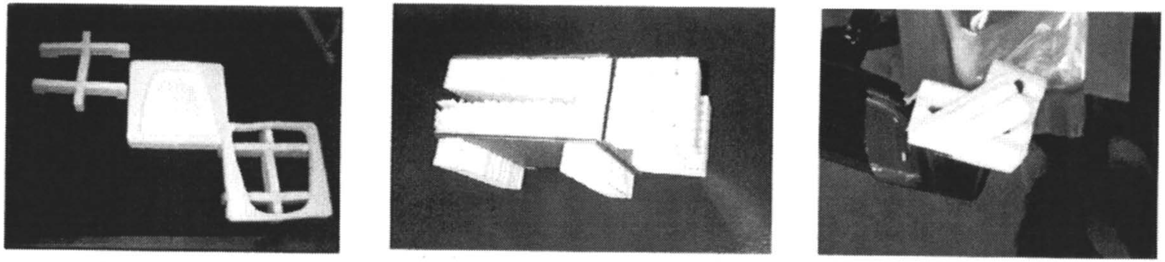

Figure 15. Starch foam sheets for protective cushion packaging

In Degradable Polymers and Materials; Khemani, K., et al.;
ACS Symposium Series; American Chemical Society: Washington, DC, 2006.

Downloaded by UNIV MASSACHUSETTS AMHERST on August 9, 2012 | http://pubs.acs.org
Publication Date: September 23, 2006 | doi: 10.1021/bk-2006-0939.ch018

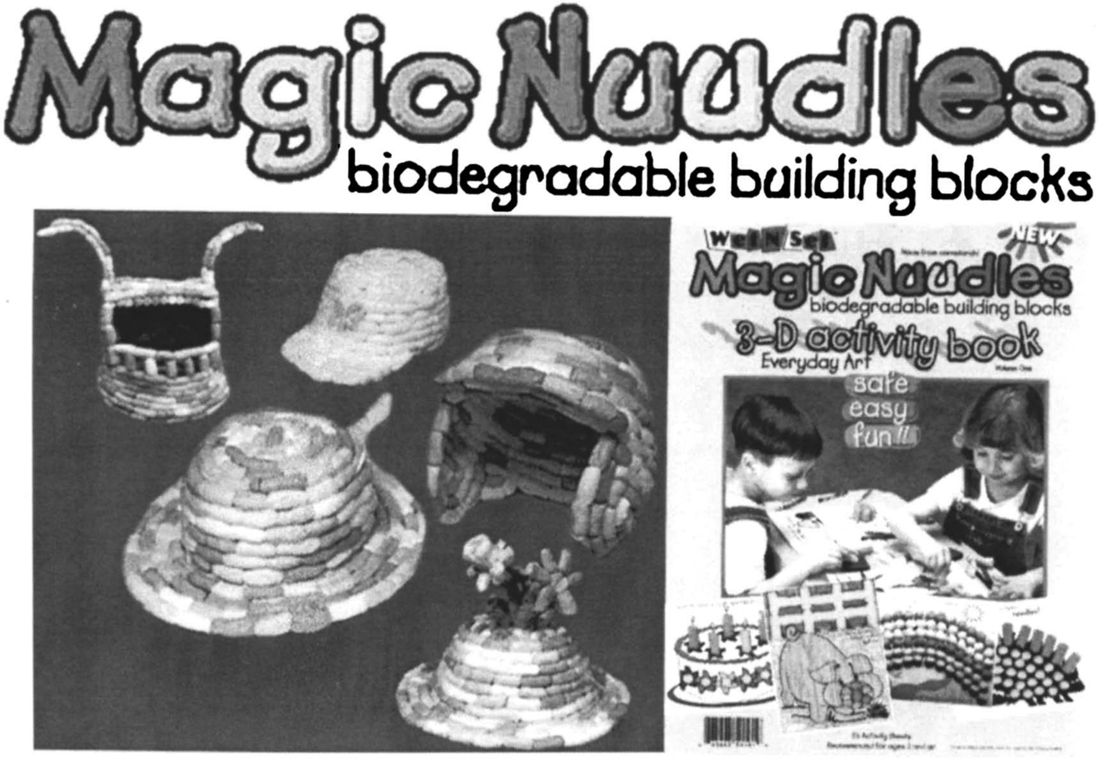
Magic Nuudles
biodegradable building blocks
WeNSet
NEW
Magic Nuudles
biodegradable building blocks
3-D activity book
Everyday Art
safe
easy
fun!!

Figure 16. Starch foam crafts and toys

starch to produce a new family of products for children -- a multi-colored foamed building block that is marketed under the brand name "Wet N' Set Magic Nuudles", see Figure 16.

References

---

1. Annual Book of Standards; Standard D 6866-04; ASTM International, Philadelphia, PA 2004, vol 8.03
2. About Federal Biobased Preferred Product Procurement Program (FB4P) www.biobased.oce.usda.gov
3. Annual Book of Standards; Standard D 7075, ASTM International, Philadelphia, PA 2004, vol 8.03.
4. Narayan, R. In: *Science and Engineering of Composting: Design, Environmental, Microbiological and Utilization Aspects;* Eds. H. A. J. Hoitink and H.M. Keener, Renaissance Publications, OH, 1993, pp. 339.
5. Narayan, R.. In: *Biodegradable Plastics and Polymers*, Eds., Y. Doi & K. Fukuda, Elsevier, New York, (1994), pp. 261.
6. Science 304, 838, 2004
7. From Algalita Marine Research Foundation – www.algalita.org/pelagic_plastic.html
8. Y. Mato, T. Isobe, H. Takada, H. Kahnehiro, C. Ohtake, and T. Kaminuma, *Environ. Sci. Technol.* 2001, *35*, 318-324
9. ASTM International, Committee D20 on Plastics, Subcommittee D20.96 on Biobased and Environmentally Degradable Plastics ; www.astm.org
10. Internationa Standards Organization (ISO) Plastics ISO 16929 -- Determination of the degree of disintegration of plastic materials under defined composting conditions in a pilot-scale test
11. International Standards Organization (ISO) Plastics ISO 202004 – Determination of the degree of disintegration of plastic materials under simulated composting conditions in a laboratory-scale test
12. About Nature works, PLA producer www.natureworks.com
13. Narayan, R., U.S. Patents 5,540,929, 5,462,983, 5,500,465, 5,578,691, 5,616,671, 5,969,089
14. Narayan R, Mohan Krishnan Polymer Preprints, American Chemical Society, 186, 1996
15. Narayan, R. In: *Paradigm for Successful Utilization of Renewable Resources*, Eds: D.J. Sessa and J.L. Willett, AOCS Press, Champaign, IL, 1998, pp. 78
16. Narayan, R. In: *Polymers from Agricultural Coproducts*, Ed., M.L. Fishman, R.B. Friedman, and S.J. Huang, *Am. Chem. Soc. Symp. Ser.*, (1994), vol 2 pg 575.

Downloaded by UNIV MASSACHUSETTS AMHERST on August 9, 2012 | http://pubs.acs.org
Publication Date: September 23, 2006 | doi: 10.1021/bk-2006-0939.ch018

17. Shin, B.Y., Lee, S. I., Shin, Y.S., Balakrishnan, S., and Narayan, R., *Polymer Eng. & Sci., 2004 44(8), 1429-1438*
18. Dubois, P., Narayan, R., *Macromolecular Symposia 198, 233-243, 2003.* (7th European Symposium on Polymer Blends, 2002)
19. Balakrishnan, S., Krishnan, M., Dubois, P., and Narayan, R., Polymer Eng. & Sci., (2006) In press
20. Narayan, R.,Bloembergen, S., and Lathia, A., U.S. Patent 5,869,647, 1999
22. Narayan, R. U.S. Patent 5,728,824,1998
23. Bloembergen, S., David, J., Geyer, D.,Gustafson, A., Snook J., and Narayan R. In Biodegradable Plastics and Polymers, Eds., Y. Doi & K. Fukuda, Elsevier, New York, 1994, pg. 601
24. Nabar Y, and Narayan R. Polymer Eng. & Science, 2006, In press
25. Nabar, Y; Raquez, J-M; Dubois, P; and Narayan, R, Biomacromolecules 2005, 6(2), 807-817.
26. Nabar, Y. U., Draybuck, D, Narayan, R., J. Appl. Polm. Sci., In press, 2005
31. About KTM Industries in manufacture of starch foam sheets and toys, www.ktmindustries.com

Downloaded by UNIV MASSACHUSETTS AMHERST on August 9, 2012 | http://pubs.acs.org
Publication Date: September 23, 2006 | doi: 10.1021/bk-2006-0939.ch018

Downloaded by CORNELL UNIV on August 10, 2012 | http://pubs.acs.org
Publication Date: September 23, 2006 | doi: 10.1021/bk-2006-0939.ch019

Chapter 19

Chromatographic Analysis and Total Luminescence Intensity as Tools for Early Degradation Detection and Degradation State Estimation

Minna Hakkarainen, Lina Burman, and Ann-Christine Albertsson*

Department of Fibre and Polymer Technology, School of Chemical Science and Engineering, Royal Institute of Technology (KTH), Teknikringen 56–58, 100 44 Stockholm, Sweden

Indicator product concept, chromatographic fingerprinting in combination with multivariate data analysis and total luminescence intensity (TLI) are presented as tools for product evaluation, quality control and testing of degradable polymers. A correlation was shown between the number of chain scission and the release of dicarboxylic acids during photo-and thermo-oxidation of polyethylene. This opens for degradation state prediction from the amount of indicator products released. Multivariate data analysis of chromatographic fingerprints of dicarboxylic acids allowed classification of polyethylene materials both with respect to the degradation state and pro-oxidant system. Total luminescence intensity proved to be an excellent tool for early degradation detection and classification of polyethylene materials. Further applications could include classification of materials with respect to durability or degradability, evaluation of antioxidant or pro-oxidant packages, longterm property and lifetime predictions.

In Degradable Polymers and Materials; Khemani, K., et al.;
ACS Symposium Series; American Chemical Society: Washington, DC, 2006.

Introduction

The demands on polymeric products are growing both with respect to their function and purity. One major topic is the design of materials to controlled lifetimes or degradation rates. There is a need for new sensitive characterization tools to rapidly evaluate and test materials. Techniques that allow the detection of initial small changes during the early degradation will lead to more precise service-life predictions and enable the design of service-life and degradation time to suit a specific application. Gas chromatographic analysis of degradation products and chemiluminescence are two sensitive techniques that have large potential in this area. We have earlier shown that differences are detected in the degradation product patterns before changes are observed in e.g. molecular weight (1) or mechanical properties (2). Total luminescence intensity (TLI), on the other hand can be related to the amount of hydroperoxides present in the sample after the specific time of ageing given an estimation of the degree of oxidation (3)

The desired lifetime for different polyethylene materials range from months to many years. Degradable polyethylene films are used worldwide in applications ranging from disposables to mulch films. The susceptibility to oxidation is a crucial part of the function of these materials. For example the purpose of mulch films is to increase the production. They shall protect the crops in the beginning of the season but be brittle enough after 4 to 6 weeks for the crops to puncture the films without being damaged. However, the films must still be sufficiently resistant so that they are not torn into pieces by wind and normal weather conditions during the time when the plants are still small. In such applications it is very valuable to be able to monitor the degradation process during the early stages of degradation in order to develop improved degradable materials or to choose between already existing ones. A rapid degradation state prediction and classification method based on the initial degradation rate is a valuable tool for determination of long-term properties and for the development of polyethylene materials with tailored degradation rates. Early degradation state detection is also a key issue in order to effectively stabilize materials for long lifetimes *(4)*. The evaluation of the long-term efficiency of antioxidants under non-accelerated conditions takes too much time to be practical. The accelerated tests currently in use are made under unrealistic physical conditions, which leads to unreliable results *(5,6,7)*. Early degradation detection is an essential component in the efforts to reduce the acceleration needed to reach practical test times and more reliable results. This paper summarises our recent results in early degradation detection and degradation state estimation in different

Downloaded by CORNELL UNIV on August 10, 2012 | http://pubs.acs.org
Publication Date: September 23, 2006 | doi: 10.1021/bk-2006-0939.ch019

polyethylene materials by using the indicator product concept, chromatographic fingerprinting and total luminescence intensity measurements.

Experimental

Indicator product analysis: The studied materials consisted of two starch based blends consisting of 70wt-% corn starch and either 30wt-% of polyethylene (PE) or 30wt-% ethylene vinyl acetate copolymer (EVA) prepared according to Ramkumar et al (8), three polyethylene films containing photosensitising or stabilising additives (iron dimethyldithiocarbamate, 0.8% carbon black and nickel dibutyldithiocarbamate) and one polyethylene film without additives. Thermo-oxidation was performed in closed 20 ml glass vials at 190°C (30 min or 3 hours) or at 230°C (30 min). Photo-oxidation for 300 h was done in an Atlas UVCON weatherometer equipped with UV-lamps (FS-40 fluorescent sunlamp).

The thermo-oxidation products were extracted according to a method described by Hakkarainen et al. (9). After the thermo-oxidation 0.5 ml diethyl ether was added to each vial. After 1 hour the diethyl ether was separated from the remaining polymeric material and evaporated to dryness with a gentle stream of nitrogen. The hexane soluble products were dissolved in 1ml hexane and subjected to solid phase extraction (SPE) to separate the products into three fractions. The SPE column was silica bonded to aminopropyl chains (NH_2) from Varian. The column was activated with 2 ml hexane, then the hexane fraction with degradation products was passed through the column. The column was first washed with 1 ml hexane, then with 1 ml chloroform and finally with 2% acetic acid in diethyl ether (1ml). The fractions were concentrated to 50 µl and subjected to GC-MS analysis.The remaining hexane insoluble fraction containing the dicarboxylic acids was dissolved in 2% HCl in methanol (100µl) and analysed separately. The degradation products from the photo-oxidized films were extracted according to the method described by Hakkarainen et al. (10) 1 ml diethyl ether was added to cover the films. After 1 hour the diethyl ether was separated from the remaining polymer films and evaporated to dryness. The products were then dissolved in 50 µl hexane. The hexane fraction was removed and the hexane insoluble products were dissolved in 50 µl 0.1% HCl in methanol. Before GC-MS analysis the methanol fraction was warmed for 15 minutes at 60°C to methylize the keto-and dicarboxylic acids.

Downloaded by CORNELL UNIV on August 10, 2012 | http://pubs.acs.org
Publication Date: September 23, 2006 | doi: 10.1021/bk-2006-0939.ch019

For the gas chromatographic analysis of thermo-oxidation products a Perkin Elmer 8500-model connected to a Perkin Elmer Ion-trap detector (ITD) mass spectrometer was used. The GC was equipped with a DB-1 (dimethyl polysiloxane) capillary colonn for the analysis of hexane, chloroform and methanol fractions and A DB-FFAP (nitroterephthalic acid modified polyethylene glycol) capillary columns for the analysis of the ether/acetic acid fractions. Both columns were from J&W (30 m x 0.32 mm I.D.). The samples were introduced in the splitless injection mode at 250°C. The photo-oxidized samples were analysed with a Varian gas chromatograph coupled to a Finnigan SSQ7000 mass spectrometer Equipped with DB-WAX capillary column from J&W (30 m x 0.32 mm I.D.). The samples were introduced in the splitless injection mode at 225°C. Helium was used as a carrier gas. A Waters 150C high-temperature SEC apparatus equipped with two PLgel 10 μm mixed-B columns and an RI detector was used to measure changes in molar mass and distributions. The mobile phase was 1,2,4-trichlorobenzene (TCB) at 135°C and the flow rate was 1 ml/min.

Downloaded by CORNELL UNIV on August 10, 2012 | http://pubs.acs.org
Publication Date: September 23, 2006 | doi: 10.1021/bk-2006-0939.ch019

Chromatographic fingerprinting and total luminescence intensity anlysis: The studied materials were 15 μm films of polyethylene, three of the films contained prooxidants, 1) 10% Fe(II)-stearate master batch, 2) 10% Fe(II)-stearate master batch and 10% polyoctylene, and 3) 7.5% Ampacet MB, a commercial prooxidant. The amount of Ampacet MB was chosen to get the same amount of iron as in the Fe(II)-stearate master batch. The films were kindly provided by Tenova AB. Degradation of the films were performed in open containers in air at 80 °C. The processing and analyses are described in more details elewere (3,11).

For chromatographic fingerprinting, carboxylic acids were extracted, from the degraded polymer samples, and methylated using a 0.1 vol% HCl/MeOH solution containing 5-phenylvaleric acid and 4-phenylbutyric acid as internal standards. The vials were thereafter opened for slow evaporation to dryness. A second extraction was made using a hexane solution that contained decanoic acid ethyl ester as internal standard. The evaporation of the acids, due to the change of extraction solvent, was compensated for by calculation using quotient analoguos to the individual degree of evaporation of the acids as described by Burman et.al. (3). The extracts were analysed using a GCQ GC-MS from ThermoFinnigan equipped with a CP-Sil 8 CB/MS column, 30 m * 0.25 mm * 0.25 μm, from Varian, scanning in the range of 35 to 650 m/z. The analyes were performed with splitless injection and Helium of 99.9999% purity was used as carrier gas.

Fourier transform infrared spectroscopy (FTIR) measurements were performed using a Perkin-Elmer 2000X FTIR spectrometer equipped with a

Golden Gate single reflection ATR unit. The final spectra was an average of 20 scans at a 4 cm^{-1} resolution. Total luminescence intensity (TLI) measurements were performed under nitrogen using a Lumipol-2 chemiluminescence instrument. The temperature were, after an initial 10 min at 60 °C, ramped up to 180 °C at a rate of 2.5 °C/min. The crystallininty was calculated based on measured using a Mettler Toledo 820 differential scanning calorimeter (DSC). The samples were heated and cooled at 10 °C/min in two cycles from 0 °C to 180 °C with 3 min isothermally at each turning point.

Downloaded by CORNELL UNIV on August 10, 2012 | http://pubs.acs.org
Publication Date: September 23, 2006 | doi: 10.1021/bk-2006-0939.ch019

Indicator products as a tool to degradation state prediction

Analysis of volatiles is frequently utilised in food industry to quality control food products and to determine shelf-life for various products. Some recent examples are the use of sensor arrays to differentiate milk products according to their aging times (12) and the use of solid phase microextraction-mass spectrometry-multivariate data system to predict the shelf-life of pasteurised milk (13). Volatiles emitted by plants have also been correlated to abiotic or biotic stress and the degree of damage caused by the stress (14). Similar principles should be applicable to polymeric materials i.e. the formation of certain volatiles or indicator products during degradation of the polymer is related to the changes in the polymer matrix (Fig. 1).

We have in several studies by gas chromatography-mass spectrometry identified more than 100 low molar mass degradation products formed during thermo-and photo-oxidation of different photo-and biodegradable polyethylenes (9,10,15). These compounds included different alkanes, alkenes, aldehydes, ketones, carboxylic acids, dicarboxylic acids, ketoacids and lactones. These studies showed that during thermo-oxidation especially the amount of dicarboxylic acids and lactones increased as the degree of degradation in the polymer matrix increased, while the degree of degradation in photo-oxidized polyethylene correlated with the amount of dicarboxylic acids. Recently we further investigated the correlation between the amount of dicarboxylic acids and lactones formed during thermo-and photo-oxidation and the matrix changes. This revealed a linear relationship between the number of chain scissions during thermo-oxidation and the formation of dicarboxylic acids and lactones (16). As shown by Figure 2 a relationship was also observed between the relative amount of dicarboxylic acids and the remaining molecular weight after photo-oxidation.

Downloaded by CORNELL UNIV on August 10, 2012 | http://pubs.acs.org
Publication Date: September 23, 2006 | doi: 10.1021/bk-2006-0939.ch019

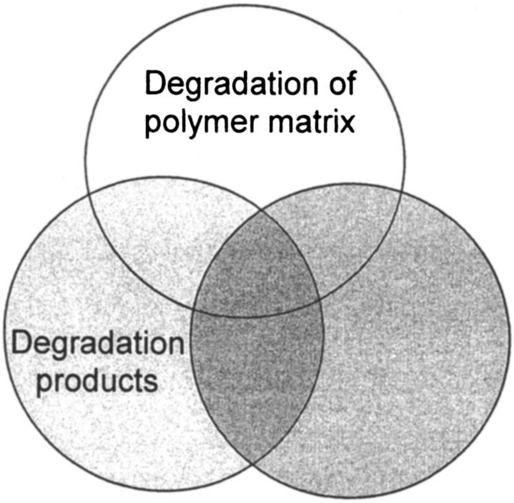

Figure 1. If there is a connection between the molecular, macromolecular and macroscopic scale changes in polymeric materials, then macromolecular and macroscopic scale changes can be predicted from the molecular scale events.

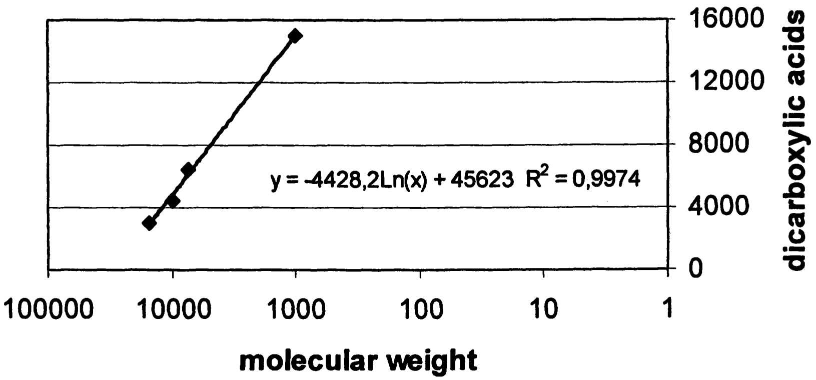

Figure 2. The logarithmic relationship between the relative amount of dicarboxylic acids in the different photo-degradable polyethylenes and the remaining molecular weight after photo-oxidation for 300 hours.

We have also shown that the emission of certain low molecular weight degradation products during thermo-oxidation of virgin and in-plant recycled polyamide-66 was in clear correlation with changes in mechanical properties (*2*). The results also clearly showed a shorter induction time for recycled materials i.e. more degradation products and in larger quantities were formed in recycled materials. This correlation between the formation of certain volatiles, indicator products, and the deterioration of solid-state polymer, opens for totally new types of test methods, where the "condition" of the polymeric material can be assessed by measuring the content or emission of indicator products.

Downloaded by CORNELL UNIV on August 10, 2012 | http://pubs.acs.org
Publication Date: September 23, 2006 | doi: 10.1021/bk-2006-0939.ch019

Classification and product control using chromatographic fingerprinting

We have in earlier studies seen that the chromatographic fingerprints from gas chromatographic analyses of the emitted volatiles change depending on the degree of oxidation in the polyethylene matrix (9,10). Chromatographic fingerprinting and volatile component analysis has also been applied for identification of different polyethylene and polypropylene samples (17). Electronic nose system was recently applied in the car industry to analyse the "new car odour". Two MS-based devices were evaluated to analyse the compounds emitted from different plastic parts present in car interior (18). Metal oxide semiconductor chemical sensors have also been used to estimate the oxidative stability of polypropylene during processing (19). Chromatographic fingerprinting is also applicable as a tool to differentiate between abiotic and biotic degradation of polymers (20,21). While different carboxylic acids or hydroxyacids dominated the chromatographic fingerprints after abiotic degradation, these compounds were assimilated during the biotic degradation and were almost completely absent in the chromatographic fingerprints obtained after biotic aging.

Degradable polyethylene films show different degradation behaviour depending on the prooxidant system incorporated in them. We had the hypothesis that different prooxidant systems would lead to differences in the patterns of degradation products, and that it thereby would be possible to classify these systems using product patterns. Four samples were included in the investigation. One was a reference sample without prooxidants. The other three all contained a metal stearate as prooxidant, and one also contained a polymer with unsaturations to increase the number of sites sensitive to degradation. Classification was performed successively using chromatographic fingerprints from Gas Chromatography – Mas Spectrometry of volatile dicarboxylic acids (11), the main group of volatile degradation products from polyethylene (22,23,24).

The samples were clearly divided into different groups depending on the type of prooxidant system, at multivariate data analysis based on the amount of diacids. The type of prooxidant system was described by the second principal component (PC2) in a Principal Component Analysis (PCA) model over the diacids. The materials were grouped at opposite sides of the mid point of PC2 depending on if their prooxidant systems contained double bonds.

It also was shown that patterns of diacids are useful for estimation of the degradation state of degradable polyethylene films, provided the compared materials contain the same type of prooxidant system. The state of degradation was described by PC1 in the PCA model of the diacids. Estimations of degradation states were performed using partial least square (PLS) analysis. Figure 3 show estimated degradation times of oxidised samples of a commercial degradable polyethylene calculated using a PLS model obtained from oxidised samples of a material containing only Fe(II)-stearate as prooxidant.

Downloaded by CORNELL UNIV on August 10, 2012 | http://pubs.acs.org
Publication Date: September 23, 2006 | doi: 10.1021/bk-2006-0939.ch019

Early degradation state prediction and classification using total luminescence intensity measurements

Polyolefins emit a weak light, luminescence, when heated in air. In the early 1960's this luminescence effect was linked to the oxidation of the polymer (25). Ashby noted differences in the intensity of the light emitted from PP that contained different antioxidant concentrations and types, which suggested that the phenomenon could be used to study polymer stability. The number of photons emitted from a polyolefin can be counted during the degradation time and this number can be related to the amount of hydroperoxides and thereby the degree of aging. Hydroperoxides are the first group of degradation products formed during the oxidation of polyolefins, which makes measurements of them interesting for early degradation detection.

In chemiluminescence studies, the sample is most often aged by thermal oxidation in the sample chamber during the measurement. This procedure is unfortunately ineffective for large quantities of sample, and it means that the degradation must take place at high temperatures to make emission detection possible since the emission per time unit decreases rapidly with decreasing temperature. Evaluation of the long-term performance requires measurements below the melting temperature to obtain relevant data. The measurement of total luminescence intensity make it possible to investigate degradation outside the instrument at low temperatures. The pre-aged sample is analysed in an atmosphere of nitrogen to avoid further oxidation. The temperature is increased at a constant rate and the area under the curve of the CL intensity versus the temperature, i.e. the total luminescence intensity (TLI), can be related to the amount of hydroperoxides present in the sample after the specific time of ageing (26,27). The TLI value can thereby be correlated to the degree of degradation of

Downloaded by CORNELL UNIV on August 10, 2012 | http://pubs.acs.org
Publication Date: September 23, 2006 | doi: 10.1021/bk-2006-0939.ch019

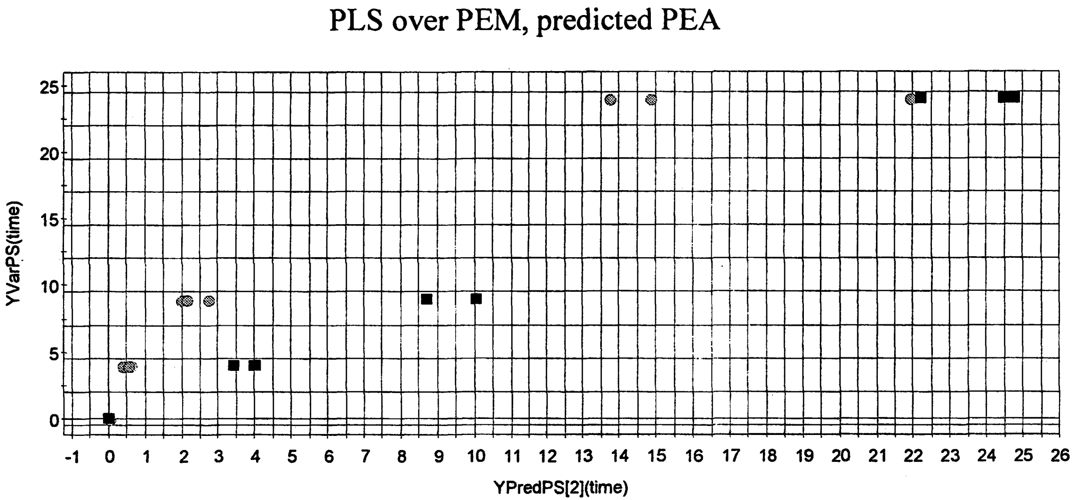

Figure 3. Y predicted plot for a partial least square model obtained from oxidised samples of a material containing Fe(II)-stearate as prooxidant (black) with predicted corresponding degradation states for a material with a commercial prooxidant (grey). (Reproduced with permission from reference 20. Copyright 2005 by Authors.)

the sample. The luminescence measured using chemiluminescence technique is considered as a result of termination or decomposition of peroxides (28,29). We have shown that TLI measurements give earlier degradation detection for degradable polyethylene films than carbonyl index, Table 1, and crystallinity measurements (30).

Table 1. Total luminescence intensisty (TLI) and carbonyl index for polyethylene films containing Fe(II)-stearate and polyoctylene (PE-MO), Fe(II)-stearate (PE-M) or a commercial prooxidant system (PE-A) aged in air at 80°C.

Aged, days	TLI, counts/mg			Carbonyl index, %		
	PE-MO	PE-M	PE-A	PE-MO	PE-M	PE-A
0	31127	30988	75903	0	0	0
2	925265	491319	523943			
4	1387256	942561	619896	24	0	0
7	2215709	579030	837645			
9	1772701	509992	996066	28	12	11
11	2999267	380521	838262			
14	2360702	349040	475916	34	26	26
17	2263230	413284	620847	27	38	29
19	2750287	341016	485567			
22	2512629	462561	668443	58	43	38

Classification of the films according to the type of prooxidant system was possible also using TLI measurements. Higher TLI values were noted for the materials containing double bounds compared to the other two prooxidant containing materials. Differences between the materials were furthermore seen in the change in activiation energies needed for decomposition of hydroperoxides in the materials. The temperatures corresponding to the peaks of the TLI-curves were compared. The needed activation energy decreased for the materials containing prooxidant systems without double bounds. The same behaviour has been noted by others for different polymer materials and been explained as an effect of fast and slowly decomposing hydroperoxides, were the fast decomposing hydroperoxides originate from further oxidation of primary oxidation products (31). The opposite trend was seen for the material containing double bounds, indicating the formation of more stable hydroperoxides or hindered catalysis of the decomposition.

Downloaded by CORNELL UNIV on August 10, 2012 | http://pubs.acs.org
Publication Date: September 23, 2006 | doi: 10.1021/bk-2006-0939.ch019

Comparison of the techniques in early degradation detection

In comparison with using indicator products for estimation of the degradation state, a larger number of degradation products are used with the chromatographic fingerprinting method. The use of indicator products provide easier analyses data due to the focusing on only one or a few products. Chromatographic fingerprinting, however, also provides information for classifications purposes. The relative degradation rates of the materials estimated by chemiluminescence and carbonyl index measurements were in accordance to the results obtained by using chromatographic fingerprinting. Chemiluminescence provides a fast and easy measurement without need of time consuming preparation of samples, such as extractions. However, there are still uncertainties about the chemical reactions involved in the chemiluminescence analyses. Therefore, using a complimentary technique is wiseful at evaluation of samples containing new types of additives. The complexity of the involved chemical reactions is reflected in the techniques potential for material classification based on differences in the activation energies of the decomposition of the present peroxides.

Downloaded by CORNELL UNIV on August 10, 2012 | http://pubs.acs.org
Publication Date: September 23, 2006 | doi: 10.1021/bk-2006-0939.ch019

Conclusions

We have shown a correlation between matrix changes and formation of certain degradation products. Analysis of these indicator products is a way to predict the degree of degradation in the polymer matrix and further a tool to predict the remaining lifetime of the polymer product. Chromatographic fingerprints over dicarboxylic acids formed during oxidation of degradable polyethylene films were an excellent tool to classify materials according to the type of prooxidant system in the films and the relative state of degradation in the films. Total luminescence intensity (TLI) measurements allowed earlier degradation detection than other commercial methods such as FTIR. TLI was furthermore shown to be sensitive to relative differences in the degradation processes and gave complimentary information regarding changes in activation energies. The shown sensitivity of TLI to differences in the degradation processes of the films signifies its potential for material classification.

References

1. Lindström, A.; Albertsson, A.-C.; Hakkarainen M. *Polym. Degrad. Stab.* **2004**, *83*, 487-493.
2. Gröning, M.; Hakkarainen, M. *J. Appl. Polym. Sci.* **2002**, *86*, 3396-3407.
3. Ragnarsson, L.; Albertsson, A.-C. *Biomacromolecules* **2003**, *4*, 900-907.
4. Burman, L.; Albertsson, A.-C. *J. Polym. Sci. Part A Polym. Chem.* **2005**, 43, 4537-4546.
5. Billingham, N.C.; Calvert, P.D. *Dev. Polym. Stab.* **1980**, 3, 139-190.
6. Allen, N.S. In Fundamentals of Polymer Degradation and Stabilisation; Allen, N.S.; Edge, M., Eds.; Elsevier Applied Science: London, 1992; Ch. 2.
7. Pospisil, J.; Horak, Z.; Pilar, J.; Billingham, N.C.; Zweifel, H.; Nespurek, S. *Polym. Degrad. Stab.* **2003**, 82, 145-162.
8. Ramkumar, D.; Vaidya, U. R.; Bhattacharya, M.; Hakkarainen, M.; Albertsson A.-C.; Karlsson, S. *Eur. Polym. J.,* **1996**, 32, 999-1010.
9. Hakkarainen, M.; Albertsson, A.-C.; Karlsson, S. *J. Chromatogr. A,* **1996**, *741*, 251-263.
10. Karlsson S.; Hakkarainen, M.; Albertsson, A.-C. *Macromolecules* **1997**, *30*, 7721-7728.
11. Burman, L.; Albertsson, A.-C. *Polym. Degrad. Stab.* **2005**, 89, 50-63.
12. Capone, S.; Epifani, M.; Quaranta, F.; Siciliano, P.; Taurino, A.; Vasanelli, L. *Sens. Actuators B,* **2001**, *78*, 174-179.
13. Marsili, R.T. *J. Agric. Food Chem.* **2000**, *48*, 3470-3475.
14. Maes, K.; Debergh, P.C. *Plant Cell, Tissue and Organ Culture* **2003**, *75*, 73-78.
15. Hakkarainen, M.; Albertsson, A.-C.; Karlsson, S. *J. Environm. Polym. Degrad.* **1997**, *5*, 67-73.
16. Hakkarainen, M.; Albertsson, A.-C. *Biomacromolecules* **2005**, *6*, 775-779.
17. Willoughby, B.G.; Golby, A.; Davies, J.; Cain, R. *Polym. Test.* **2003**, *22*, 553-570.
18. Garrigues, S.; Talou, T.; Nesa, D.; Gaset, A. *Sens. Actuators B,* **2001**, *78*, 337-344.
19. Potyrailo, R. A.; Wroczynski, R.J.; Morris, W.G.; Bradtke, G.R. *Polym. Degrad. Stab.* **2004**, *83*, 375-381.
20. Albertsson, A.-C.; Barenstedt, C.; Karlsson, S.; Lindberg, T. *Polymer,* **1995**, *36*, 3075-3083.
21. Albertsson, A.-C.; Erlandsson, B.; Hakkarainen, M.; Karlsson, S. *J. Environ. Polym. Degrad.* **1998**, *6*, 187-195.
22. Hoff, A.; Jacobsson, S. *J. Appl. Polym. Sci.* **1981**, *26*, 3409-3423.
23. Albertsson, A.-C.; Barenstedt, C.; Karlsson, S. *Acta Polym.* **1994**, *45*, 97-103.
24. Hakkarainen, M.; Albertsson, A.-C.; Karlsson, S. *J. Appl. Polym. Sci.* **1997**, *66*, 959-967.

Downloaded by CORNELL UNIV on August 10, 2012 | http://pubs.acs.org
Publication Date: September 23, 2006 | doi: 10.1021/bk-2006-0939.ch019

25. Ashby, G.E. *J. Polym. Sci.* **1961**, *50*, 99-106.
26. Billingham, N. C.; Then, E. T. H.; Gijsman, P. *Polym. Degrad. Stab.* **1991**, *34*, 263-277.
27. Ahlblad, G.; Reitberger, T.; Terselius, B.; and Stenberg, B. *Polym. Degrad. Stab.* **1999**, *65(2)*, 179-184.
28. Russell, G. A. *J. Am. Chem. Soc.* **1957**, *79*, 3871-3877.
29. Reich, L.; Stivala, S. S. *Makromol. Chem.* **1967**, *103*, 74-82.
30. Ragnarsson, L.; Albertsson, A.-C. *Biomacromolecules* **2003**, *4*, 900-907.
31. Gijsman, P.; Verdun, F. *Polym. Degrad. Stab.* **2001**, *74*, 533-542.

Downloaded by CORNELL UNIV on August 10, 2012 | http://pubs.acs.org
Publication Date: September 23, 2006 | doi: 10.1021/bk-2006-0939.ch019

Chapter 20

Characterization of Biodegradable Polymer Blends by Inverse Gas Chromatography: Amylopectin and Its Blends

Zeki Y. Al-Saigh

Department of Chemistry, State University of New York, Buffalo State College, 1300 Elmwood Avenue, Buffalo, NY 14222

Downloaded by NORTH CAROLINA STATE UNIV on August 9, 2012 | http://pubs.acs.org
Publication Date: September 23, 2006 | doi: 10.1021/bk-2006-0939.ch020

Amylopectin (AP), as a potato starch based polymer, with a molar mass of six million gram/mol was blended with several biodegradable polymers: poly(ε-caprolactone) (PCL), Poly (3-hydroxy butyric acid) (PHBA), poly (DL-lactide-co-glycolide) (PLG) and three different molar mass of poly (acrylic acid) (PAA). All pure polymers and the blends were characterized using the Inverse Gas Chromatography Method (IGC), Differential Scanning Calorimetry (DSC) and X-Ray Diffraction (XRD) over a wide range of temperatures (80-260 °C). Nineteen solutes (solvents) were injected into five chromatographic columns containing AP-biodegradable polymer blends. These solutes probed the dispersive, dipole-dipole, H-bonding interactions, acid-base characterstics, the wettability and water uptake of AP-PCL blends. Retention diagrams of these solutes in a temperature range of 80-260 °C revealed at least two zones, crystalline and amorphous. T_g and T_m of the pure polymers and the blends were measured using these zones. The two zones were used to calculate the degree of crystallinity of the pure AP and its blends below the melting temperature which ranged from 81% at 104 °C to 0% at the T_m values. IGC has complimented the DSC method in obtaining the T_g and T_m values of the pure AP and the AP-PCL blends.

In Degradable Polymers and Materials; Khemani, K., et al.;
ACS Symposium Series; American Chemical Society: Washington, DC, 2006.

Downloaded by NORTH CAROLINA STATE UNIV on August 9, 2012 | http://pubs.acs.org
Publication Date: September 23, 2006 | doi: 10.1021/bk-2006-0939.ch020

These values were unexpectedly elevated for the blends from that of the pure AP, and ranged from 105 °C to152 °C for T_g values, and 166°C to 210 °C for T_m values. The T_m values agreed well with the XRD analysis data. This elevation in T_g and T_m values may be due to the change in heat capacity at T_g, and the dependence of T_g on various variables including molar mass, and the blend composition. Tg values for AP- PHBA, PLG and PAA were also elevated in contrary to the Tm values which showed a depression in the melting points.

Polymer blend–solvent interaction parameters were measured using a variety of solutes at a wide range of temperatures which determined the solubility of the blends in these solutes. It was also able to determine the blends compatibility over a wide range of temperatures and weight fractions. χ_{23} and B_{23} parameters agreed well on the partial miscibility of the blends studied. The dispersive component of the surface energy of the pure polymers and the blends were measured using alkanes which ranged from 16.00 mJ/m^2 for the pure AP to 55.46 mJ/m^2 when AP was mixed with PHBA in a 50-50% ratio. This reveals the increase of the surface energy of AP when it was blended with other biodegradable polymers. IGC was effective and versatile in measuring the degree of crystallinity of the pure polymers and the blends at any single temperature below AP's T_m, unlike the DSC method which provides a range of the degree of crystallinity.

Introduction

Most of the physico-chemical knowledge of macromolecules comes from studies in dilute solution where the polymer molecules are more or less isolated from each other. Since the viscosity of polymers is high, most practical applications of polymers, the polymer is highly concentrated and usually represents 90% or more of the bulk phase. In particular, when two polymers are mixed to form a polymer blend, the resulting mixture is highly viscous. Experimental techniques developed for dilute solution studies are often inapplicable under these conditions. Furthermore, there is a category of polymers that insoluble, or partially soluble in known solvents and hence cannot be studied at all in a dilute solution. The inverse gas chromatographic procedure (IGC) (sometimes called the molecular probe technique) eliminates both of these difficulties. Gas chromatographic equipment is generally available at a reasonable cost, the experimental simplicity, and the ease which large amounts of data can be collected using the IGC, is becoming the method of choice for the study of thermodynamic interactions of small molecules with polymers in the solid phase. It can also be used to measure surface areas and adsorption isotherms, glass and other solid phase transitions in polymers, degrees of crystallinity, crosslink density and diffusion constants for small molecules in polymeric materials. Since 1969, Inverse Gas Chromatography (IGC) has been used for the characterization of polymers, blends and materials. During this period, it has undergone extensive development and received considerable interest in its application to polymers and blends (*1-12*). The IGC technique utilizes conventional gas chromatography, with minor modifications, to measure the interaction between pure solute (mobile phase) and the polymers or blends (stationary phase) in terms of the retention time of the solute. The term "solute" is used to represent the low-molar mass volatile solvent that is usually injected onto the chromatographic column. Solute is dispersed in a mobile phase and the polymer blend is stationary in the column as a liquid phase. Volatility of solutes insures the availability of a vanishing small amount of solute in the mobile phase which leads to fast establishment of equilibrium between the gas and the stationary phases. The term "inverse" refers to the fact that the stationary phase (the polymeric system) is the phase to be studied in IGC experiments, in contrast to the objective of the separation of components in traditional gas chromatography (GC). The stationary phase is prepared by dissolving the polymer or polymer blend in the appropriate solvent and depositing the resulting mixture onto a solid support using a specific technique developed by us (*1*). There have been excellent reviews on IGC during the past three decades outlining the methodology and technique. Reviews on this work have been given by Guillet and co-workers (*3,4*), Munk (*5*), Al-Saigh (*2,14*), and Guillet and Al-Saigh (*13*).

There have been several applications of IGC to the determination of surface interactions (*15-24*). In particular, IGC was applied to several studies of natural polymers. Among them are: cellulose (*25*), wood (*26*), potato starch as Amylopectin (*27*) and lignocellosic surfaces (*28*). In these studies, the surface thermodynamic characteristic of wood fiber and its relationship to the fiber's water vapor adsorption was determined by IGC (*26*) Also, the surface energy, surface acid-base free energy, enthalpy of desorption of acid-base probes, surface acid-base acceptors, and donor parameters were determined by IGC (*26*). Cellulose was also found by IGC to be sensitive to the presence of adsorbed water which possibly disorders its surface structure.

Starch and its blends have attracted much attention as environmentally biodegradable polymers (*29-31*). However they suffer from disadvantages as compared with conventional polymers and blends such as brittleness and a narrow processability window (*32*). The thermal behavior and phase morphology of starch-blend systems have been studied by differential scanning calorimetry (DSC), Fourier Transform Infrared (FTIR) spectroscopy, scanning electron microscopy solvent extraction, X-ray diffraction, optical rotation, nuclear magnetic resonance (NMR) and polarizing optical microscopy (*33-36*). Like polymer blends wide applications starch-based blends have the potential to be

Downloaded by NORTH CAROLINA STATE UNIV on August 9, 2012 | http://pubs.acs.org
Publication Date: September 23, 2006 | doi: 10.1021/bk-2006-0939.ch020

Downloaded by NORTH CAROLINA STATE UNIV on August 9, 2012 | http://pubs.acs.org
Publication Date: September 23, 2006 | doi: 10.1021/bk-2006-0939.ch020

used in the environmental and biomedical fields as they are easily obtained in a large quantity by an inexpensive route and are totally biodegradable. New areas of applications of starch-based blends in the biomedical field are emerging such as drug delivery systems, hydrogels, bone cements and bone replacements. Most of these applications require accurate control of polymer water up-take ability, degradation rate and mechanical performance in various media. To improve these properties of starch-based polymers, blending the natural polymer with a homo biodegradable polymer can be utilized, and the characterization of the new resulting properties will be the subject of this chapter. Special attention will be devoted to surface, physical, and chemical properties of the new blends. The blending process is expected to have an impact on the surface and mechanical properties of the blends. The mechanical properties of such materials with two or more components are strongly influenced by the properties of the components and by the properties of the interface. In case there is no chemical bonding within the components, and the surface of the material is smooth, the interaction between the components is of a physical nature and the strength of dispersive and acid base interaction forces is essential for the adhesion between the components and, therefore, the properties of the material. From studies carried out in the past decades, we believe that blends of biodegradable polymers can combine highly mechanical properties along with the physical properties such as: stability, low gas permeability, environmental safety and easy processing and modeling. Since the properties of starch-based polymers depend on the compatibility of the blend and the structure of the system, the thermodynamic and energetic characteristics of the interaction of the starch with synthetic polymers within the blend and the structure of such blends need further exploration. It has been shown (*37*) by Bertuzzi et al. that when corn starch film was blended with glycerol, a negative exponential dependence on the blend's concentration had occurred. In addition, a decrease in in tensile strength (TS) from 26.84 MPa to 1.52 MPA was observed. In another study, Ramkumar and Bhattacharya (*38*) showed that when a starch was blended with a synthetic polymer such as polyolefin, the tensile properties of the blend increased and the crystallinity of the starch was considerably decreased. Even if the starch is not compatible with the synthetic polymer, the mechanical properties can be significantly improved by adding a functional group, such as maleic acid, or phenolic group on the synthetic polymer. It has been reported that the blending process resulted in inferior mechanical properties, and the biodegradability of the blend was increased (*39*). Averous et al. (*40*) observed a significant improvement in the properties of the blend due to the presence of PCL which decreased the material modulus but the impact resistance improved.

This chapter will explore the characterization of several Amylopectin-biodegradable polymer blends using the IGC method. These blends are: Amylopectin–Poly(ε-caprolactone) (PCL), Amylopectin-Poly(DL-lactide-Co-glycolide) (PLG), Amylopectin-Poly(3-hydroxy butyric acid) (PHBA), and Amylopectin-Poly (acrylic acid) (PAA). A series of molar mass of PAA will be used ranging from 2,000 to 750,000 g/mol. This series will explore the dependence of the molar mass of the polymer diluent (PAA in this case) on the interaction of the two polymers melting and glass transition temperatures, the degree of crystallinity and the surface energy. Blending two biodegradable polymers is a cost effective method. The rate of biodegradation is correlated with morphology, crystallinity, surface area, and additives. To accomplish this goal, the physical properties of the blends need to be investigated with precision. Such properties will evolve the determination of the blend's compatibility over a range of temperatures and compositions.

Analysis of Polymer Blends

A series of pure low molar mass solutes with different polarities, such as alkanes, acetates, alcohols, formic acid, dimethyl amine and water were injected into the chromatographic column that contains the polymer blend. Their interaction with the stationary phase will reveal the effect of the chemical nature of the injected solutes on their miscibility with the blend. Several chromatographic quantities, illustrated in Equation 1 are precisely measured directly from the IGC experiment. These quantities will yield the specific retention volume, V_g^o. V_g^o is the key term in the calculation of thermodynamic parameters and is commonly used to describe the chromatographic elution behavior of solutes. It is defined as:

$$V_g^o = \frac{273.15\Delta t F J}{w T_{room}} \tag{1}$$

Here, $\Delta t = t_p - t_m$ is the difference between the retention time of the solute, t_p and of the marker, t_m. Air is usually used as a marker, when the Thermal Conductivity (TC) detector is used, to account for the dead volume in the chromatographic column. The retention time of the marker has to be subtracted from the solute retention time to reflect the absolute value of the solute retention time as t_p. F is the flow rate of the carrier gas measured at room temperature T_r, w is the mass of the stationary phase, and J is a pressure correction factor which depends on P_i and P_o, the inlet and outlet pressures respectively. P_i and P_o are measured using electronic transducers which are interfaced at the inlet and outlet of the column. These transducers are usually calibrated using a mercury manometer. To calculate the interaction parameter, χ_{12}, of the polymer-solute system, V_g^o from Eqn 1 is utilized as follows:

$$\chi_{12} = \ln\left[\frac{273.15 R v_2}{V_g^o V_1 P_1^o}\right] - 1 + \frac{V_1}{M_2 v_2} - \frac{B_{11} - V_1}{RT} P_1^o \tag{2}$$

Downloaded by NORTH CAROLINA STATE UNIV on August 9, 2012 | http://pubs.acs.org
Publication Date: September 23, 2006 | doi: 10.1021/bk-2006-0939.ch020

1 denotes the solute and 2 denotes the polymer; υ_2 is the specific volume of the polymer at the column temperature *T; M_1* is the molar mass of the solute; P_1^o is the saturated vapor pressure of the solute; V_1 is the molar volume of the solute; *R* is the gas constant; and B_{11} is the second virial coefficient of the solute in the gaseous state. For polymer blend systems, the key term in the miscibility of a polymer-polymer pair is the free energy of mixing, ΔG_m as

$$\Delta G_m = \Delta H_m - T\Delta S_m \tag{3}$$

where ΔS_m is the combinatorial entropy of mixing and ΔH_m is the molar heat of mixing. A complete analysis of the thermodynamics of polymer blends was given in our earlier publications (*1*). Utilizing the specific retention volume, V_g^0, the polymer-polymer interaction coefficient, χ_{23} can be derived. When a polymer pair is used as a stationary (liquid) phase in a chromatographic column, subscripts 2 and 3 will be used to represent polymers 2 and 3, respectively. Subscript 1 refers to the test solute. The interaction between two polymers is expressed in terms of the free energy of mixing ΔG_{mix} in Equation 4. Subscripts 2 and 3 refer to polymer 1 and 2, respectively. The first two (entropic) terms in this equation are negligible for polymer blends. Thus, for the polymer blend to be miscible (ΔG_{mix} being negative), χ_{23} must be negative. When considering the IGC of polymer blends, the free energy of mixing must be written for a three-component system. It is usually expressed as

$$\Delta G_{mix} = \mathrm{RT}[n_1 \ln\phi_1 + n_2 \ln\phi_2 + n_3 \ln\phi_3 + n_1 \phi_2 \chi_{12} + n_1 \phi_3 \chi_{13} + n_2 \phi_3 \chi_{23}] \tag{4}$$

Recognizing that for a polymer blend containing polymer 2 and polymer 3, υ_2 in Eqn 2 should be replaced by ($w_2\,\upsilon_2 + w_3\,\upsilon_3$), where w_2 and w_3 are the weight fractions and υ_2 and υ_3 are the specific volumes of the two polymers in the blend. Thus one can Easily derive Equation 5:

$$\ln\frac{273.15R(w_2v_2 + w_3v_3)}{V_g^{\,o}V_1P_1^o} - 1 - \frac{B_{11} - V_1}{RT}P_1^o = \phi_2\left[\chi_{12} - \frac{V_1}{M_2v_2}\right] + \phi_3\left[\chi_{13} - \frac{V_1}{M_3v_3}\right] - \frac{V_1}{V_2}\phi_2\phi_3\chi_{23} \tag{5}$$

where φ_2 and φ_3 are the volume fractions of the two polymers in the blend. Comparison of Equations 2 and 5 suggest that to obtain χ_{23} for a polymer blend, utilizing IGC, χ_{12} and χ_{13} have to be known. Three columns are usually prepared; two from the homopolymers and the third prepared from a blend of the two

Downloaded by NORTH CAROLINA STATE UNIV on August 9, 2012 | http://pubs.acs.org
Publication Date: September 23, 2006 | doi: 10.1021/bk-2006-0939.ch020

Downloaded by NORTH CAROLINA STATE UNIV on August 9, 2012 | http://pubs.acs.org
Publication Date: September 23, 2006 | doi: 10.1021/bk-2006-0939.ch020

samples used for the homopolymer columns. A further three columns containing different compositions of the blend can also be prepared if the effect of the weight fraction of the blend on miscibility needs to be explored. These columns should be studied under identical conditions of column temperature, carrier gas flow rate and inlet pressure of the carrier gas, and with the same solutes. This keeps all auxiliary parameters (P_1^o, T, M_2, M_3, V_1, v_2, v_3 and B_{11}) identical for the three experiments, and a combination of Equation 2 (taken twice for two homopolymers) and Equation 5 for the blend, the parameter χ_{23} can be derived

$$\chi_{23} = \frac{\ln \frac{V^o_{g,blend}}{W_2 v_2 + W_3 v_3} - \phi_2 \ln \frac{V^o_{g,2}}{v_2} - \phi_3 \ln \frac{V^o_{g,3}}{v_3}}{\phi_2 \phi_3} \tag{6}$$

Equation 6 is routinely used in IGC experiments particularly when for solutes for which the Parameters P_1^o, V_1 and B_{11} are not known with sufficient accuracy. χ_{23} can also be related to B_{23} which is another indicator of the blend miscibility with negative value being necessary for mixing.

$$B_{23} = RT\left(\frac{\chi_{23}}{V_1}\right) \tag{7}$$

For high molar mass polymer, The second term in Equation become negligible, and the equation can be reduced to a better practical form that can be used routinely in IGC experiments.

$$\chi_{12} = \ln\left[\frac{273.15 R v_2}{V_g^o V_1 P_1^o}\right] - 1 - \frac{B_{11} - V_1}{RT} P_1^o \tag{8}$$

Analysis of Semicrystalline Polymer-Containing Blends

For polymer blends containing complex mixtures such as amylopectin and semicrystalline homopolymers, the morphology of the blend will be more complex as compared with the amorphous-amorphous polymer pair. In this case, it is possible to obtain the polymer-polymer interaction coefficient χ_{23} and the interaction energy parameter (B_{23}) experimentally by measuring the melting point-depression of a polymer mixture (blend) experimentally in a different way than explained earlier. This technique involves measuring the melting point depression of a polymer mixture (blend) containing a semicrystalline polymer to quantify the heat of mixing of the polymer pair. When crystals of the semicrystalline polymer are in equilibrium with the amorphous part of the semicrystalline and the amorphous counter-polymer, the melting point of the semicrystalline polymer is lower than when the equilibrium is with the amorphous part of the semicrystalline polymer only. This is known as a melting point depression, resulting in mixing amorphous polymer with a semicrystalline polymer. In most cases, the amount of the depression of the melting point depends on the weight fraction of the diluent polymer. The melting point depression can be used as an indicator for the polymer blend miscibility. Most of the work performed thus far using melting point depression is based on calorimetry, and there have only been a few studies using IGC (*41*). The thermodynamic analysis of polymer-polymer mixtures using melting point depression can be based on Flory-Huggins theory (*41,43*). Information can only be obtained a temperature close to the pure semicrystalline polymer melting point. However, a number of factors influence the measured melting point (perfection, size, and environment of crystals) which must be accounted for. The depression in the melting point can be used as an indicator for the polymer blend miscibility. Equation 9 is usually used for the calculation of the melting point depression:

$$\frac{1}{T_m} - \frac{1}{T_m^o} = -R\left(\frac{V_{2u}}{\Delta H_{2u}}\right)\left[\frac{\rho_2 \ln\phi_2}{M_2} + \left(\frac{\rho_2}{M_2} - \frac{\rho_3}{M_3}\right)v_3 + \left(\frac{B_{23}}{RT_m}\right)\phi_3^2\right] \qquad (9)$$

The quantities φ_2, φ_3, ρ_2, ρ_3, M_2 and M_3 are the volume fractions, densities and molar masses of the semicrystalline (2) and the diluent amorphous polymer (3), respectively, in the blend. T_m^o is the melting point of the pure semicrystalline polymer before mixing. T_m is the melting point of the semicrystalline polymer after mixing. The quantity. H_{2u}/V_{2u} is the heat of fusion of the semicrystalline polymer (2), (u being the symbol for the fusion). The first two terms in Equation 9 are the entropic contribution to the mixing process while the third term is the enthalpic contribution. If the molar mass of the semicrystalline (amylopectin in this case) and the diluent polymers are high, then the entropic contribution represents less than 1 °C which would play a minor role in the melting point depression. Therefore, the values of the first two terms can be neglected and Equation 9 can be reduced to the following form:

$$\frac{1}{T_m} - \frac{1}{T_m^o} = -\left(\frac{V_{2u}}{\Delta H_{2u}}\right)\left(\frac{B_{23}}{T_m}\right)\phi_3^2 \qquad (10)$$

Downloaded by NORTH CAROLINA STATE UNIV on August 9, 2012 | http://pubs.acs.org
Publication Date: September 23, 2006 | doi: 10.1021/bk-2006-0939.ch020

Where. T_m is the depression in the melting point of the semicrystalline polymer. B_{23}, as defined above, is related to the Flory-Huggins interaction parameter χ_{23} as in the following equation:

$$B_{23} = RT_m^o\left(\frac{\chi_{23}}{V_3}\right) \tag{11}$$

Where V_3 is the molar volume of the diluent polymer. Equation 10 can be rearranged to reflect the depression in the melting point as follows:

$$\Delta T = T_m^{\,o} - T_m = -T_m^{\,o}\left[\frac{V_{2u}}{\Delta H_{2u}}\right]B_{23}\phi_3^{\,2} \tag{12}$$

Equation 12 will be used routinely in IGC experiment as an indicator of the blends miscibility. B_{23} can be obtained by plotting ΔT versus φ_3^2 of the diluent polymer.

Surface Energy of Polymers

For the case of bulk absorption, when the retention volume is independent of probe sample size, the equilibrium concentrations of the probe in the polymer and gas phase are linearly related for low concentrations of the sample. When surface adsorption is present, the isotherm relating these two concentrations is often curved due to surface teterogeneity and saturation of available sites. In addition, the experimental concentrations used may not be low enough to ensure a linear isotherm. Under these conditions the shape of the isotherm can be used to investigate the adsorbate - adsorbant interaction. There are two approaches using GC to reveal adsorption isotherms. The "frontal" technique takes into account kinetic factors and gas phase volume changes due to vapor adsorption. Here the sample is continuously fed into the column. For substances with a Langmuir isotherm (adsorption) the result is a single sharp step, produced at the first exit of the substance. From the time needed for breakthrough, the amount of substance retained can be determined. The second approach is the "elution" technique, where a pulse of material is injected and the shape of the isotherm is found from a single unsymmetrical peak. Using the gas phase concentration of eluted probe vapor, the retention volume may be calculated.

Downloaded by NORTH CAROLINA STATE UNIV on August 9, 2012 | http://pubs.acs.org
Publication Date: September 23, 2006 | doi: 10.1021/bk-2006-0939.ch020

To quantify the interaction of solute in the gaseous form with the polymer blend layer, the surface energy, γ_s, may be obtained. The dispersive component of the surface energy describes the interactions due to dispersive forces or a combination of dispersive forces with H-bonding or with dipole-dipole forces. Fowkes (*44*) first reported this method of characterization. Fowkes (*44*) determined the surface energy of several components. Generally, the contribution of dispersive forces and all other types of forces can be expressed as the energy of adhesion, as follows:

$$\gamma_a = \gamma^d + \gamma^{sp} \tag{13}$$

Where γ^d is the contribution of dispersive forces and γ^{sp} is the contribution of specific interaction forces such as H-bonding, dipole-dipole, acid-base, etc. The IGC method was successfully applied in recent years to determine the surface properties of divided solids (*45,46*). From gas chromatographic measurements, V_g^o is determined by using equation (1). V_g^o relates to the equilibrium constant K between the adsorbed solute and the polymer surface as follows:

$$V_g^o = KA \tag{14}$$

Where K is the surface partition coefficient and A is the total surface area of the polymer powder in the chromatographic column. Thermodynamically, the molar free energy of adsorption,.ΔG_l^a, of solute on the polymer layer can be related to V_g^o by the following relationship:

$$\Delta G_l^a = -RT \ln V_g^o + C \tag{15}$$

Where C is a constant depending on A. Equation (16) relates the energy of adhesion to the free energy of adsorption as follows:

$$RT \ln V_g^o + C = 2Na\sqrt{\gamma_s^d \gamma_l^d} \tag{16}$$

Where γ_s^d and γ_l^d are the dispersive components of the solid surface and the interactive solutes phase, respectively. N is Avogadro's number and a is the area of the adsorbed molecules (solutes). In IGC experiments a series of interactive solutes, such as alkanes, can be injected into the chromatographic column in order to determine the dispersive surface energy, γ_s^d. A plot of ΔG_l^a or (RT ln V_g^o) versus the number of carbons in the alkane chain can be meaningful, since such a plot is linear and the slope of the straight line will account for the incremental contribution of ΔG_l^a. The molar enthalpy of adsorption can also be calculated from ΔG_l^a as follows:

Downloaded by NORTH CAROLINA STATE UNIV on August 9, 2012 | http://pubs.acs.org
Publication Date: September 23, 2006 | doi: 10.1021/bk-2006-0939.ch020

$$\Delta H_1{}^a = -T^2\left(\frac{\partial}{\partial \mathrm{T}}{}^{(\frac{\Delta G_1{}^a}{T})}\right) \quad (17)$$

Combining equations (16) and (17) yield the dispersive surface energy as follows:

$$\gamma_S{}^d = \left[\frac{1}{4\,\gamma_{CH_2}}\right] \left[\frac{(\Delta G_a{}^{CH2})^2}{(N.\,a_{CH_2})^2}\right] \quad (18)$$

Where γ_{CH2} is the surface energy of a hydrocarbon consisting only of n-alkanes, a_{CH2} is the area of one -CH2- group. Equation (18) usually tests the IGC method for obtaining the dispersive surface energy of polymers.

Experimental

MATERIALS: Amylopectin (AP) and four biodegradable polymers (poly(ε-caprolactone) (PCL), poly(DL-lactide-Co-glycolide) (PLG), poly(3-hydroxy butyric acid) (PHBA), and poly(acrylic acid)(PAA)) were selected for this study. Blends of AP and the selected biodegradable polymers were made in the laboratory. In order to establish the strength of the solubility (compatibility) of AP-Polymer blends and the type of interaction forces between the blends and the gaseous mobile phase we have selected a series of chemically different families of solutes in addition to formic acid, dimethyl amine and water to interact with the blends. Vanishing small amounts (0.02 μL) of a series of the selected solutes were injected into the chromatographic column. These solutes will probe the dispersive, dipole, hydrogen bonding, acid-base interactions as well as the wettability of the blends. A total of nineteen solutes, chromatographic grade, were purchased as HPLC grade. Their purity was checked by gas chromatography prior to use. AP was obtained from Aldrich Chemical Co. in a powder form. Its molar mass was determined as 6.60 million gram/mol. The four selected biodegradable polymers mentioned above were also purchased from Aldrich and their average molar masses are listed in Table I. Chromatographic support, Chromosorb W (AW-DMCS treated, 60/80 mesh) was obtained from Analabs. Chromatographic columns were made in the laboratory from 5-ft-long, copper tubing, 1/4 inch in o.d. All copper columns were washed with methanol and annealed for several hours before use. Fifteen chromatographic columns were prepared, eight of which were blends of AP-biodegradable polymer and seven were pure biodegradable polymers including AP. Five weight fractions of

Downloaded by NORTH CAROLINA STATE UNIV on August 9, 2012 | http://pubs.acs.org
Publication Date: September 23, 2006 | doi: 10.1021/bk-2006-0939.ch020

Downloaded by NORTH CAROLINA STATE UNIV on August 9, 2012 | http://pubs.acs.org
Publication Date: September 23, 2006 | doi: 10.1021/bk-2006-0939.ch020

Table I. Description of Biodegradable Polymers and Blends Studied

Polymer or Blend	*Amount Used, g*	*Dissolved in*	*Column Loading*	*Av. Molar Mass, g/mol*
100% Amylopectin	0.4870	Hot Water	7	6.6 x 10^6
100% Poly(ε-caprolactone) (PCL)	0.4680	Hot Water	7	80.0 x 10^3
25 – 75% AP-PCL	0.125/0.375	Hot Water	7	6.6 x 106/ 80.0 x 10^3
50 -50% AP-PCL	0.249/0.250	Hot Water	7	6.6 x 106/ 80.0 x 10^3
75 – 25% AP-PCL	0.369/0.126	Hot Water	7	6.6 x 106/ 80.0 x 10^3
100% Poly(DL-lactide-Co-glycolide) (PGL)	0.4000	Acentonitrile	7	1.00 x 10^5
50 – 50% AP-PLG	0.200/0.200	Water/ Acetonitrile	7	6.6 x 106/ 1.00 x 10^5
100% Poly(3-hydroxy butyric acid) (PHBA)	0.4000	Hot Chloroform	7	4.37 x 10^4
50 – 50% AP-PHBA	0.20/0.20	Hot Chloroform	7	6.6 x 106/ 4.37 x 10^4
100% Polyacrylic Acid (2000)(PAA)	0.4980	Methanol	7	2.00 x 10^3
100% Polyacrylic Acid (450000)(PAA)	0.4980	Methanol	7	4.5 x 10^5
100% Polyacrylic Acid (750000)(PAA)	0.4980	Methanol	7	7.5 x 10^5
50 – 50% AP-PAA (2000)	0.249/0.252	Methanol	7	6.6 x 10^6/ 4.50 x 10^3
50 – 50% AP-PAA (450000)	0.249/0.246	Methanol	7	6.6 x 10^6/ 4.5 x 10^5
50 – 50% AP-PAA (750000)	0.250/0.251	Methanol	7	6.6x10^6/ 7.5 x 10^5

each blend were prepared, ranging from 0 to 100% amylopectin. The resulting load of the blend on the column was maintained at 7% in all columns. Blending was achieved by dissolving a certain amount of AP and a certain amount of biodegradable polymer in the appropriate solvent and then depositing the solution onto the solid support using the method reported earlier (*1*). Table I shows the description of each polymer used with their amounts, solvents, column loading and the average molar mass.

Instrumentation and Procedure

Chromatographic measurements were made using three IGC Stations. Each IGC station includes two modified Hewlett Packard GC's (model 5890) and one Varian 3800 gas chromatograph equipped with a thermal conductivity detector. The three chromatographs were modified to allow continuous monitoring of the carrier gas flow rate, the inlet and outlet pressure, and the column temperature. These modifications, along with the complete chromatographic procedure and IGC setup were reported in our earlier publication (*1*, *33*). Continuous monitoring is important because it reduces experimental error significantly in the four measurable parameters mentioned in equation (*1*). This procedure yielded better controlled measurable quantities. The monitored parameters are usually measured over a period of seven hours and then their values are averaged. Each IGC station is equipped with an electronic monitoring device for an accurate determination of the flow rate, the inlet and the outlet pressure. Varian 3800 GC is further equipped with the capability of correcting the flow rate electronically should a fluctuation occur. In addition, the flow rate and the inlet pressure will be checked and calibrated periodically using external conventional devices. Since the blend used in this study contains semicrystalline AP, every effort was made to avoid recrystallization of AP by keeping the chromatograph operational at all times. During the course of the experiments, the oven temperature was uniformly increased until a complete set of data were obtained. Control of the mass of the blend in the stationary phase has been modified and a new method for coating the polymer was developed and recently reported (*1*). A flow rate of 8 ml/minute will be used throughout this work in order to eliminate the effect of flow rate (kinetic) on V_g^o values. From our previous experiments, it has been demonstrated that the flow rate of the carrier gas, helium, between 0 - 10 ml/minute had no significant effect on the retention volumes. Flow rates above 10 ml/minute may cause a considerable error in the retention volumes, particularly if helium is used as a carrier gas (*47*).

Seven pure polymer and eight blend solutions were made, one blend solution was made with different weight fractions. The seven solutions contain only pure (100%) AP, PCL, PLG, PHBA and a series of different molar mass of PAA, while the other eight solutions contain a composition of the blend ranging from 0% to 100% by weight. A total of fifteen chromatographic columns were prepared which yielded information regarding the effect of the weight fraction of each polymer on the miscibility of the polymer blend. The proposed blends were prepared by weighing the appropriate amount of polymer components, as illustrated in Table I, at ratios of 0/100, 25/75, 50/50, 75/25 and 100/0 AP-

Downloaded by NORTH CAROLINA STATE UNIV on August 9, 2012 | http://pubs.acs.org
Publication Date: September 23, 2006 | doi: 10.1021/bk-2006-0939.ch020

counter biodegradable polymer. These mixtures were prepared by dissolving the proposed blends in the appropriate solvent and the resulting mixtures were deposited onto the solid support using the soaking method developed by us (*1*). After evaporating the solvent, blends were dried under a vacuum for 48 hours prior to use. To obtain information about the miscibility of solvents on these chromatographic columns, a series of pure solvents with a different chemical nature (such as alkanes, acetates, alcohols, formic acid, ethylamine and water) were injected onto these columns. Their retention times were measured as an indicator of their interactions with the pure polymers and blends.

Thermal Analysis

Potato starch containing amylopectin (AP) was purchased from Aldrich with an estimated molar mass of 6.60 million g/mol. It is estimated to contain 25% of amylose. The branching in the starch molecule may contain on the average, twenty glucose residues (*48*). Amylopectin molecules also form helices; the shorter side chains form double helices (*49,50*). Amylopectin was thermally characterized by the melting point determination of DSC and TGA methods. These analyses were carried out by the USDA Forest Service in Madison, WI. The polymer was decomposed at approximately 343 °C with approximately 80% weight loss. The polymer also showed two transitions at approximately 105 °C, accompanied by 6% weight loss and at approximately 166 °C with no measurable weight loss. The temperature of 166 °C was later identified to be the T_m and 105 °C to be the T_g of Amylopectin. IGC has confirmed the findings of the DSC technique.

Retention Diagrams

Nineteen solutes were injected into fifteen separate chromatographic columns containing AP and its blends. From chromatographic retention times of solutes, the specific retention volumes V_g^0 of all solutes were calculated according to Equation (1). From V_g^0 values, retention diagrams for all solutes were generated by plotting ln V_g^0 versus 1/T, similar to Figures 1 (AP-PCL blends using acetates series as solutes). Curvatures in phase diagrams were observed, indicating the change in the morphology of the polymers used as a function of temperature. A minimum of two regions were identified: crystalline (region D) and amorphous (region A-B). A third region (A) can also be identified above 235 °C, as the polymer starts to decompose. The alkane series showed an isotherm with a maximum of 160 °C which can be identified as the melting point of AP, in agreement with the DSC data. Above 160 °C, a straight line (region A-B) can be observed due to the establishment of the equilibrium between the solutes and the AP, an indication that the polymer is in an amorphous state. This region,

Downloaded by NORTH CAROLINA STATE UNIV on August 9, 2012 | http://pubs.acs.org
Publication Date: September 23, 2006 | doi: 10.1021/bk-2006-0939.ch020

Downloaded by NORTH CAROLINA STATE UNIV on August 9, 2012 | http://pubs.acs.org
Publication Date: September 23, 2006 | doi: 10.1021/bk-2006-0939.ch020

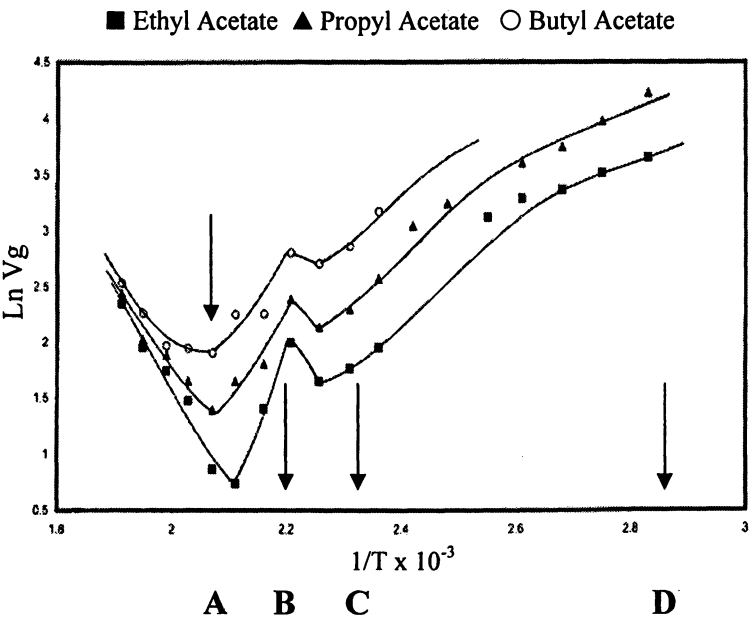

Figure 1: Retention Diagram, Blend of 50-50% AP- PCL-Acetate Systems at (80 – 260 °C)

represents the next transition that occurs in crystalline polymers – the melting process. Since the crystalline phase (region C-D) is usually impermeable, this section of the plot can give information about the size, shape and distribution of crystalline regions. The final, linear section of the plot represents the wholly amorphous polymer. Extrapolation of this line to lower temperatures and comparison of these values with the true experimental values gives information about the percentage crystallinity of the sample at any temperature, reflected by the difference in specific volume (due to bulk sorption) between a totally amorphous and partially crystalline product.

Below 160 °C (region B-D) , AP and its blends are mostly crystalline and, in some cases, the isotherm could not clearly identify the glass transition temperature (T_g) (C). Retention of the solute in this region arises from condensation and adsorption onto the next region, corresponding to a change in the slope of the diagram, and represents a non-equilibrium absorption of the solute into the bulk phase. The diffusion rate is slow in this region, hence the molecules injected as a pulse at this temperature would not penetrate through the entire bulk of the polymer during the time of passage of the solute peak. The solute does not have time to reach an equilibrium partition between polymer and carrier gas, hence the V_g value obtained is flow rate dependent. Bulk contribution to the retention volume increases as temperature increases toward the melting point (C-B), which is a function of the film thickness. This maximum temperature is reached when the increase in bulk sorption due to the increase in the probe diffusion constant is balanced by the decrease in retention due to increased volatility of the probe. In this non-equilibrium region it is possible to obtain information about the probe diffusion coefficient and its dependence on temperature. For pure AP, when solutes changed from alkanes to more interactive solutes such as alcohols and diethyl amine, T_m is shifted from 160 °C to 151.50 °C. This is due to the strong hydrogen bonding developed between these solutes and AP. It is interesting to note that alcohols, acetates, formic acid, and water did not exit the 100% AP column in a period of 20 minutes. This can be explained by the strong interaction of these probes with the polymer surface and may lead to a chemical reaction in the column. It is also interesting to note that the retention volumes of water are very high; an indication of the strong interaction, as expected, with the polymer surface.

When AP was blended with PCL, PLG and a series of different molar mass of PAA, both T_m and T_g values were shifted from the equilibrium values of pure AP. Table II shows the values of both T_m and T_g of all pure polymers and the blends used. These values for AP-PCL showed an interesting trend, an elevation, rather than the expected depression. T_g values ranged from 152 °C for 25-75%, 148 °C for 50-50% to 120 °C for 75-25% AP-PCL. T_m values for the same blends ranged from 210 °C for 25-75%, 181 °C for 50-50 and 185 °C for 75-25% AP-PCL. The T_m values agreed well with the XRD analysis data (Figure 2). T_m values were consistent among all retention diagrams of all AP-PCL compositions and were clearly recognizable due to the sharp change in the isotherms. These

Downloaded by NORTH CAROLINA STATE UNIV on August 9, 2012 | http://pubs.acs.org
Publication Date: September 23, 2006 | doi: 10.1021/bk-2006-0939.ch020

high values are unexpected as compared with those of the pure AP. The blends behavior can be explained by Gibbs-DiMarzio theory that offers predictions including the change in heat capacity at T_g, and the dependence of T_g on various variables including molar mass, cross-link density, mechanical deformation, plasticizer content and the blend composition (*47,51*). It has been shown that an unusual compositional variation of miscible polymer blends with strong specific interaction Tg. Painter and co-workers (*52*) had proposed a modified classical thermodynamics theory to explain such behavior around Tg with numerous composition.

Where * in Table II denotes parameters measured by the IGC, others are reported by the suppliers. When AP was blended with PLG and PHBA the T_g values were elevated while the T_m values showed a depression. Blends containing AP and various MW of PAA showed a similar trend, a depression in the T_m values while the T_g values were elevated.

Downloaded by NORTH CAROLINA STATE UNIV on August 9, 2012 | http://pubs.acs.org
Publication Date: September 23, 2006 | doi: 10.1021/bk-2006-0939.ch020

Polymer-Solute Interaction Parameters

Interaction parameters, χ_{12}, of all pure biodegradable polymers-solute and some blends-solute systems were calculated using Equation (8). Table III shows the values of χ_{12} for selected solutes. Only alkanes and alcohols were used for χ_{23} calculations, other solutes could not be used due to the lack of Antoine constants in the literature. Generally, χ_{12} showed more exothermic values as a number of carbons (n) in both alkane, acetate and alcohol series increased. Dodecane, butyl acetate and butanol showed the most exothermic values among alkanes, acetates and alcohols. Values of χ_{12} become more exothermic as temperature increased as expected. The exothermic values are indicators for the solubility of these polymers in solutes. The dispersive forces among the three families played a major role in determining the solubility.

Polymer-Polymer Interaction Parameters

Polymer-Polymer Interaction Parameters, χ_{23}, for blend systems were calculated using IGC and equation (6) at a temperature range of 80 -160 °C. χ_{23} revealed mixed results, partially negative values for AP-PCL at a range of weight fractions (0 -100% AP), extremely exothermic for AP-PAA (for all molar mass).

Table II. Measured Physical parameters of Biodegradable polymers and their Blends

Name of Polymers or Blends	*ΔHs, KJ/mol*	T_g *°C*	T_m *°C*	*Degree of Crystallinity at 110 °C*	*Surface Energy, mJ/m^2 (160 °C)*
100% Amylopectin (AP)	-40.87	105*	166*	81	16.00
100% Poly (ε-caprolactone) (PCL)	--------	-62	60	------	------
100% Poly (3-hydroxy butyric acid) (PHBA)	-47.23	48	130*	93	------
100% Poly(DL-lactide-Co-glycolide) (PLG)	-59.59	119*	172	45	48.90
25-75% AP-PCL	----------	152*	210*	40	18.55
50-50% AP-PCL	-20.04	148*	181*	86	38.26
75-25% AP-PCL	----------	120*	185*	75	6.50
50-50% AP-PLG	-51.68	140*	150*	77	46.30
50-50% AP-PHBA	-19.38	120*	130*	78	55.46
Poly acrylic acid (PAA) (MW:2000)	-14.52	105	124*	69	19.08
Poly acrylic acid (PAA) (MW:450000)	-12.07	105	133*	67	36.54
Poly acrylic acid (PAA) (MW:750000)	-7.50	105	129*	74	42.36
50-50% AP-PAA (2000)	-6.60	126*	138*	73	31.89
50-50% AP-PAA (450000)	-5.90	117*	142*	71	36.54
50-50% AP-PAA (750000)	-4.5	117*	141*	59	42.36

Downloaded by NORTH CAROLINA STATE UNIV on August 9, 2012 | http://pubs.acs.org
Publication Date: September 23, 2006 | doi: 10.1021/bk-2006-0939.ch020

Downloaded by NORTH CAROLINA STATE UNIV on August 9, 2012 | http://pubs.acs.org
Publication Date: September 23, 2006 | doi: 10.1021/bk-2006-0939.ch020

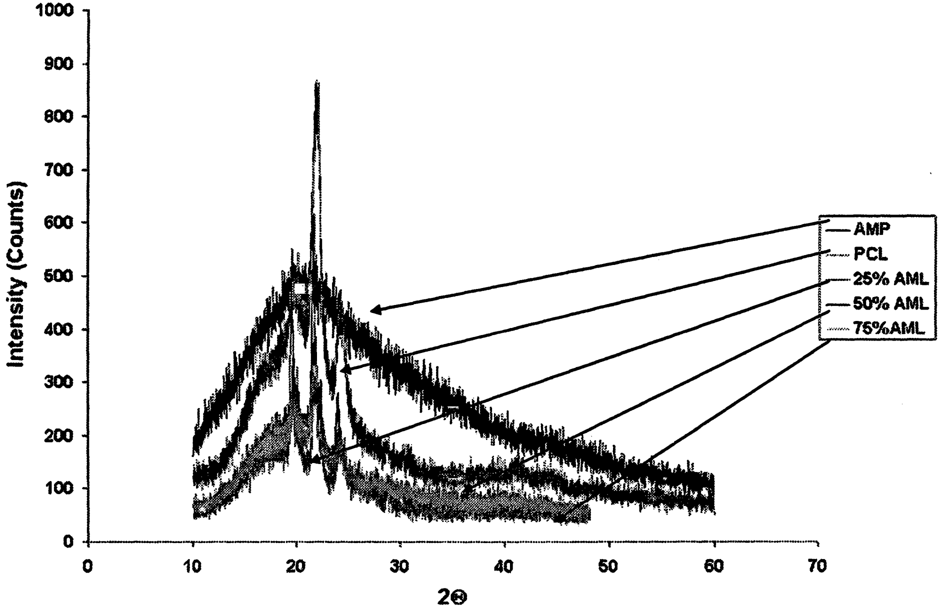

Figure 2. XRD spectra of Amylopectin (AP), Poly(ε-caprolactone) (PCL) and Blends of AP and PCL

Downloaded by NORTH CAROLINA STATE UNIV on August 9, 2012 | http://pubs.acs.org
Publication Date: September 23, 2006 | doi: 10.1021/bk-2006-0939.ch020

Table III. Polymer-Solvent and Polymer-Polymer Interaction Coefficients

Polymer or Blends	*Solute*	χ_{12}	χ_{23}
Poly acrylic acid (PAA) (MW:2000)	Pentane	0.52	
	Dodecane	-0.46	
	Methyl Acetate	-0.24	
Poly acrylic acid (PAA) (MW:450000)	Pentane	4.45	
	Dodecane	-10.37	
Poly acrylic acid (PAA) (MW:750000)	Pentane	3.17	
	Dodecane	-10.33	
50-50% AP-PAA (2000)	Pentane	2.22	-2.86
	Dodecane	-9.97	-2.06
	Methyl Acetate	1.06	-3.29
	Butyl Acetate	-2.54	-4.55
50-50% AP-PAA (450000)	Pentane	4.95	2.25
	Dodecane	-9.36	-10.01
	Methyl Acetate	1.25	-1.14
	Butyl Acetate	-2.22	-5.53
50-50% AP-PAA (750000)	Pentane	2.37	2.04
	Dodecane	-9.64	-9.61
	Methyl Acetate	1.52	-1.78
	Butyl Acetate	-2.49	-5.39
Amylopectin (AP)	Pentane	-1.56	
	Heptane	0.36	
25-75% AP-PCL	Heptane		-0.15
	Methyl Alcohol		-1.42
	Butyl Alcohol		-1.39
50-50% AP-PCL	Heptane		-0.18
	Methyl Alcohol		-0.29
	Butyl Alcohol		-0.05
75-25% AP-PCL	Heptane		-0.26
	Methyl Alcohol		-0.33
	Butyl Alcohol		-0.26

χ_{23} were not calculated for AP-PLG and AP-PHBA. Table III shows the values of χ_{23} of three AP-PCL blends with compositions of 25-75%, 50-50% and 75-25%. The negative values obtained varied with the weight fraction from close to zero to -1.42. These values indicate a partial compatibility of AP and PCL. However, in case of 50-50% AP and PAA (all molar masses) showed more exothermic χ_{23} values, an indication of a strong compatibility of AP and PAA for all molar masses and at 50-50% composition. The effect of the molar mass of PAA did not show any marked affect on the compatibility of the two polymers, however, the compatibility becomes more exothermic as temperature increased as expected. It is also interesting to note that χ_{23} values become more exothermic, as number of carbons in the alkanes and acetates series increased, demonstrating again the effect of the dispersive forces on the polymer-polymer compatibility. Inspection of Table III confirms our previous observation (*53*), χ_{23} values depended on the chemical nature of the solutes. Similar observations were made by several IGC researchers in the past and it was attributed to the deficiency of Flory-Huggins theory. Prolongo et al (*54*) reported that the equation of state does not yield the true polymer-polymer parameters for polymer blend systems. They developed a method that took into account several types of interactions, such as dispersive forces, dipole-dipole and H-bonding, to obtain polymer-polymer parameters independent of the chemical nature of the solute. The reported results were in agreement with those obtained from other methods used for polymer characterization.

Crystallinity

Measurements of polymer crystallinity can be readily made using the IGC method. However, with many polymers, the thermal history of the coating process may alter the crystallinity of the sample. In this case, cryogenic grinding of the polymer, followed by screening to remove particles larger than about 0.1 mm will give particles which can be blended mechanically with the support prior to packing the chromatography column. Also, the chromatograph is kept continuously running for the entire studies and the temperature was raised in increments to avoid the re-crystallization of the polymer, and thus, the change in morphology. The degree of crystallinity of all pure biodegradable polymers and blends in the temperature range of 80 – 220 °C was achieved by extrapolating the linear portion of the retention diagrams (similar to figure 3) to the crystalline region, two retention volumes can be measured: $V_{g,sample}$ is the retention volume of the solute along the curvature line in the crystalline region, and $V_{g,amorphous}$ is the retention volume of the solute along the extrapolated line of the amorphous region. By using the following relationship, the degree of the crystallinity was assessed.

Downloaded by NORTH CAROLINA STATE UNIV on August 9, 2012 | http://pubs.acs.org
Publication Date: September 23, 2006 | doi: 10.1021/bk-2006-0939.ch020

Downloaded by NORTH CAROLINA STATE UNIV on August 9, 2012 | http://pubs.acs.org
Publication Date: September 23, 2006 | doi: 10.1021/bk-2006-0939.ch020

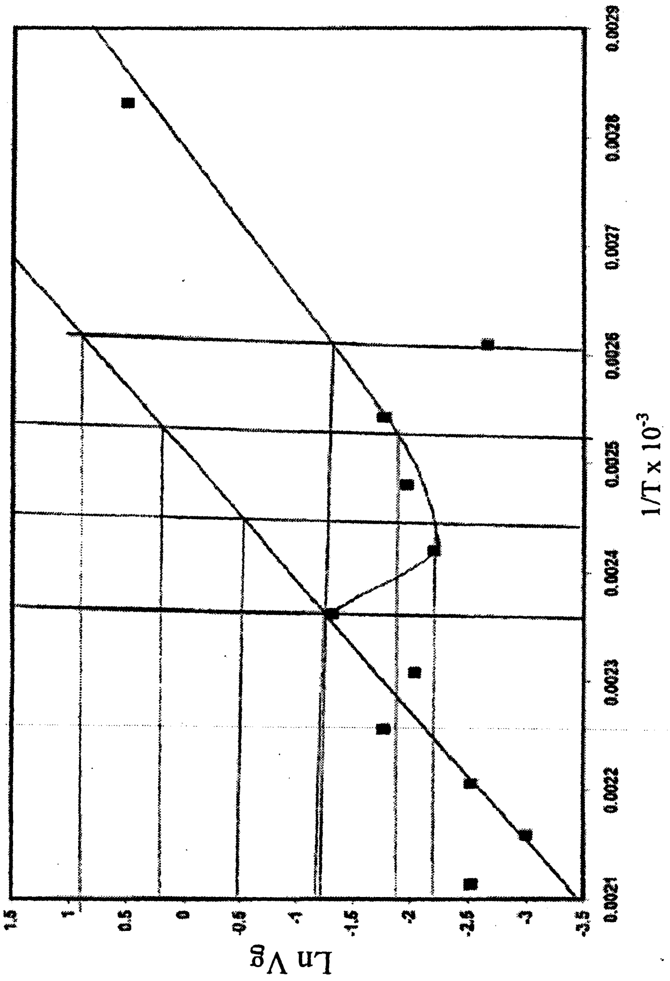

Figure 3: Retention Diagram of Poly Acrylic Acid (MW; 2000)-Pentane System

$$\%X_c = 100\left(1 - \left(\frac{V_{g,sample}}{V_{g,amorphous}}\right)\right) \tag{19}$$

Table II shows the degree of crystallinity of all polymers and blends below the melting temperature. Figure (4) shows the degree of crystallinity of AP-PCL blends which also can easily determine the melting point of these blends as the intersection of the curve with the X-axis (Table II). Figure (4) shows the versatility of the IGC method by determining the degree of crystallinity at any single temperature below the T_m value, unlike the DSC method. It has been shown (*44*) a significant reduction in the degree of crystallinity when corn starch was blended with ethylene-co-vinyl acetates. The degree of crystallinity observed for 50-50% and 75-25% AP-PCL blend did not show any reduction as compared to that of the pure AP. This observation is unusual which caused an elevation in T_m and T_g values. IGC has agreed with XRD measurements in regards to the degree of crystallinity and T_m and T_g values of the blends. However, when AP was blended with PLG, PHBA and different molar masses of PAA, a slight reduction in the degree of crystallinity of AP was observed. The $\%X_c$ ranged from 59 – 78% at 110 °C as compared to 81% for the pure AP.

For polymer blends containing complex mixtures such as amylopectin and semicrystalline biodegradable polymers like PCL, the morphology of the blend will be more complex as compared with the amorphous-amorphous polymer pair. In this case, it is possible to obtain the polymer-polymer interaction coefficient χ_{23} and the interaction energy parameter (B_{23}) experimentally by measuring the melting point-depression (or elevation) of a polymer mixture (blend) (Equations 11 and 12). In the past (*1*), we related the depression in the melting point of PVF_2-PEMA blend to the polymer blend miscibility successfully.

$\Delta H_{2u}/V_{2u}$ is the heat of fusion of the AP (2) (Equation 9), (u being the symbol for the fusion). It was taken from reference (55) as 35.90 cal/g or 45.23 cal/mL. The first two terms in Equation (9) are the entropic contribution, and the third term is the enthalpic contribution. Since the molar mass of both AP and PCL is above 80,000 g/mol, the entropic contribution is envisioned to play a minor role in the melting point depression. A plot of ΔT_m versus the volume fraction of PCL (φ^2) yielded a straight line (Figure 5). The slope of the line yielded a value of B_{23} of +9.84 Cal/mL and an intercept of +10.31 °C. This intercept may be attributed to an entropic contribution to the mixing process. Thus, we can conclude the mixing of AP and PCL was driven by enthalpic and entropic effects and the first two terms in Equation (9) have a role in the mixing process. The values of B_{23} and the intercept suggest the partial incompatibility of AP and PCL. These values explain the fact that χ_{23} values were partially exothermic; values were close to zero, except for 25-75% AP-PCl composition.

Downloaded by NORTH CAROLINA STATE UNIV on August 9, 2012 | http://pubs.acs.org
Publication Date: September 23, 2006 | doi: 10.1021/bk-2006-0939.ch020

Downloaded by NORTH CAROLINA STATE UNIV on August 9, 2012 | http://pubs.acs.org
Publication Date: September 23, 2006 | doi: 10.1021/bk-2006-0939.ch020

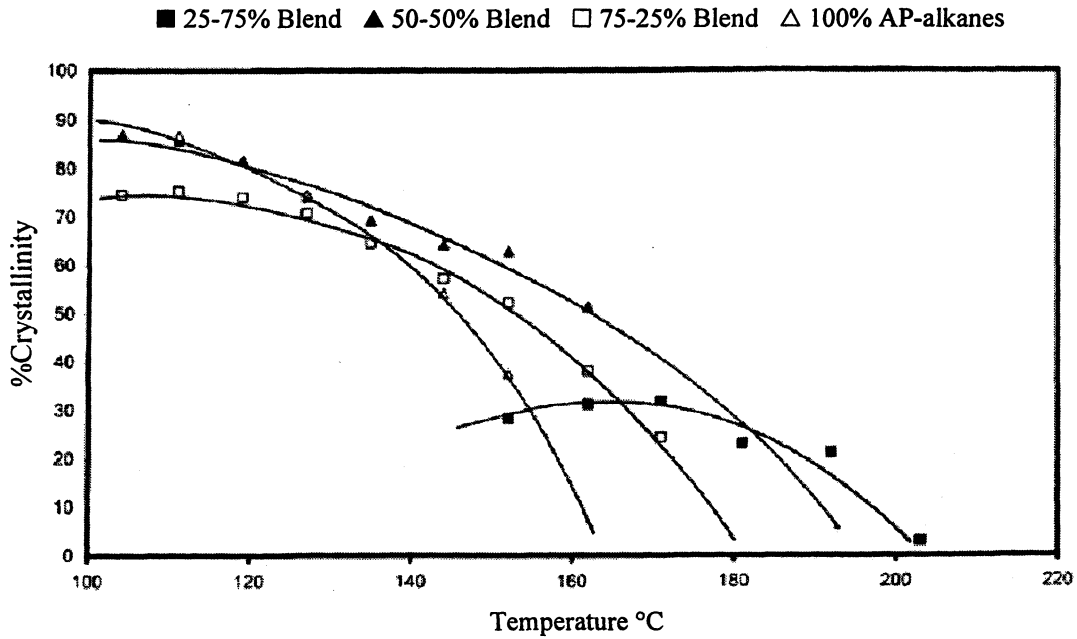

Figure 4: Degree of Crystallinity of Amylopectin and Blends (0 - 100% AP) (105 -210 °C)

Downloaded by NORTH CAROLINA STATE UNIV on August 9, 2012 | http://pubs.acs.org
Publication Date: September 23, 2006 | doi: 10.1021/bk-2006-0939.ch020

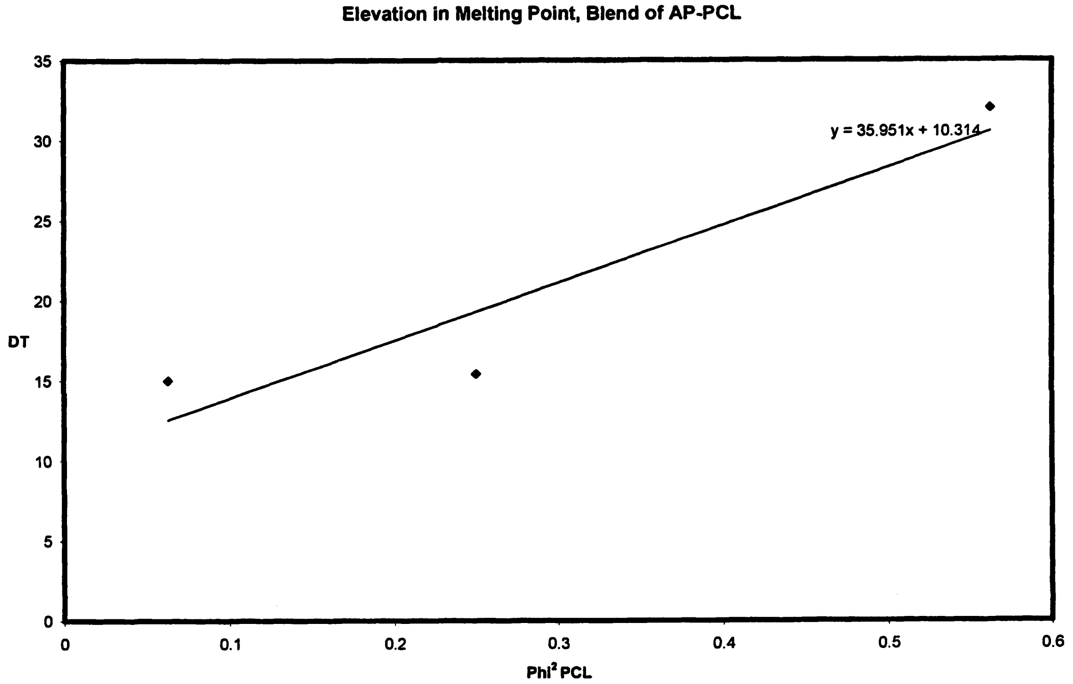

Figure 5: Elevation in Melting Point, Blends of AP-PCL

mixing process of AP and PCL is a significant molar mass dependent. The sizes and shapes of the two polymers may generate a small ratio of molecular volumes which affect the free volume variation with blending the two polymers which may cause an entropy contribution to the mixing process (56). The entropic effect on the mixing process may explain the observed elevation in T_m and T_g values of the blend. This implies the change in entropy of mixing at the glass transition of the blend in relation to the changes in heat capacities of the blend at T_g.

Downloaded by NORTH CAROLINA STATE UNIV on August 9, 2012 | http://pubs.acs.org
Publication Date: September 23, 2006 | doi: 10.1021/bk-2006-0939.ch020

Surface Energy

The dispersive component of the surface energy of AP and its blends was calculated using only the alkane series in the temperature range of 80 – 200 °C. According to equation (16), plots of (RT ln Vg^o) versus the number of carbons in the alkane series were generated for each temperature. A linear relationship was obtained in all of these plots and the slopes of the straight lines were computed as the free energy of desorption of a CH_2 group, ΔG_a^{CH2}. Utilizing equation (18), the dispersive component of the surface energy of these two polymers was calculated as a function of temperature. The cross-sectional area of an adsorbed CH_2 group, a_{CH2} is estimated to be 6 (A^o) (21). The surface-free energy of a solid containing only CH_2 groups,. γ_{CH2}, is computed as a function of temperature as follows:

$$\gamma_{CH2} = 36.80 - 0.058\ T \qquad (20)$$

Where T is the temperature in °C. Table II shows the dispersive component of the dispersive surface energy of the AP and its blends. γ^s_d ranged from 6.50 mJ/m^2 to 55.46 mJ/m^2 at 160 °C . The low values of γ^s_d for the pure AP is expected, since AP surface is highly crystalline below 160 °C and mechanically weak. An increase in temperature lowered the values of γ^s_d significantly which may be caused by the expansion of the surface above the melt. Blending AP with PCL resulted in doubling the value of γ^s_d when the composition of the blend is at 50 – 50 %. At a composition of 25 – 75% of the blend, the γ^s_d value was slightly increased. This slight increase in γ^s_d values reveal the contribution of PCL to the surface energy upon mixing. However, when the composition of the blend is mostly AP (75-25%), the value of γ^s_d was considerably decreased, contrary to the 25 -75% composition. Blending AP with PLG, PHBA and PAA has resulted in an increase in γ^s_d values, particularly for AP-PHBA.

References

1. Al-Saigh, Z.Y. and Chen, P., *Macromolecules*, **1991**, 24, 3788-3795
2. Al-Saigh, Z.Y, *Polymer News* , **1994**, 19, 269-279
3. Lipson, J.E.G. and Guillet, J. E. ***Developments in Polymer Characterization-3***, Dawkins, J. V., ed; pp. 1-266, Applied Science Publisher, Essex, England, **1982**
4. Braun, J.M. and Guillet, J.E., *Adv. Polym. Sci.,* **1976**, 21, 107-145.
5. Munk, P. ***Modern Methods of Polymer Characterization***, (Barth, H., and Mays, J.W., Eds.) Chemical Analysis: A Series of Monographs on Analytical Chemistry and its Applications, vol 113; Winefordner, J. D. Series Ed., **1991**, pp. 151-200, Wiley
6. Munk, P., Hattam, P., Abdual-Azim, A. and Du, Q., *Makromol. Chem.,Macromol. Symp.,* **1990**, 38, 205-220
7. El-Hibri, M.J., Cheng, W. and Munk, P., *Macromolecules,* **1988**, 21, 3458-3468
8. Hildebrand, J.H. and Scott, R. L., ***the Solubility of Non-electrolytes (3rd edn),*** Dover Publications, New York, **1964**
9. DiPaola-Baranyi, G. ***Inverse Gas Chromatography, Characterization of Polymers and Other Materials*** (Lloyd, D.R., Ward, T. C. and Schreiber, H. P., eds) (ACS *Symposium Series No. 391), pp.* 108-120, *American Chemical Society,* **1989**
10. Prolongo, M.G., Masegosa, R.M. and Horta, A., *Macromolecules,* **1989**, 22, 4346-4351
11. Shi, Z.H. and Schreiber, H.P., *Macromolecules,* **1991**, 24, 3522-3527
12. Etxeberria, A., Uriarte, C., Fernandez-Berridi, M.J. and Iruin, J.J., *Polymer,* **1994**, 35, 2128-2132
13. Al-Saigh, Z.Y. and Guillet, J., in "***Inverse Gas Chromatography in Analysis of Polymers and Rubbers***", *Encyclopedia of Analytical Chemistry*: **Instrumentation and Applications**, R. Meyers, Editor, Vol. 9, PP. 7759-7792, John Wiley & ons Ltd, Chichester, **2000**
14. Al-Saigh, Z. Y., Int. *J. Polym. Charact. Anal.*, **1997**, 3, 249-291
15. Al-Saigh, Z. Y., *Polym. Int.*, **1996**, 40, 25- 32
16. Al-Saigh, Z. Y, *Polymer*, **1999**, 40, 3479-3485
17. Chehimi, M.M. Pigois-Landureau, E. & Delamar, M. M., *J. Chim., Phys.*, **1992**, 89, 1173-1178
18. Pigois-Landureau , E., and Chehimi, M.M., *J. Appl. Polym. Sci.*, **1993**, 49, 183-186
19. Chehimi, M.M., Abel, M.L., Perruchot, C., Delamar, M., Lascelles, S. F., Armes, S.P., *Synth. Met.*, **1999**, 104, 51-59
20. Lundqvist, A., and Odberg, L., *J. of Pulp and Pap. Sci.*, **1997**, 23, J298-J302

Downloaded by NORTH CAROLINA STATE UNIV on August 9, 2012 | http://pubs.acs.org
Publication Date: September 23, 2006 | doi: 10.1021/bk-2006-0939.ch020

21. Papirer, E., Ligner, G., Vidal, A., Balard, H. & Mauss, F. in ***"Chemically Modified Oxide Surfaces"***, E. Leyden & W.T.Collins, Editors, Gordon and Breach, New York, **1990,** 361- 26
22. Papirer, E., Balard, H. & Vidal, A., *Eur. Polym. J.*, **1988,** 24, 783-790
23. Papirer, E., Roland, P., Nardin, M. & Balard, H., *J. Colloid Interface Sci.*, **1986,** 113, 62-66
24. Al-Gahmdi, A. and Al-Saigh, Z. Y, *J. of Polym. Sci., Part B: Polym. Phys.*, **2000,** B38, 1155-1166
25. Papirer, E, Brendle, E, Ballard, H, and Vergelati, C, *J. Adhesion Sci. Technol.*, **2000,** 14, 321-337
26. Tshabalala, M.A., Denes, A.R., Williams, R. S., *J. Appl. Polym. Sci.,* **1999,** 73, 399-407
27. Al-Ghamdi, A., Melibari, M., and Al-Saigh, Z.Y, *J. Polym. Environm.*, **2005,** 13, 319-327
28. Tshabalala, M.A., *J. Appl. Polym. Sci.,* 1997, **65**, 1013-1020
29. Holmes, P.A., ***in Developments in Crystalline Polymers***, Vol. 2, ed. D.C. Bassett Elsevier, London, **1988,** pp.1-65.
30. Doi, Y. Microbial, ***Polyesters***, VCH Publishers, New York, **1990**
31. Holmes, P.A., *Phys. Technol.*, **1985,** 16, 32-36
32. Barham, P.J., & Keller, A. A., *J. Polym. Sci. Polym. Phys. Edn.*, **1986,** 24, 69-77
33. Zhang, L., Deng, X., Zhao, S., & Huang, Z., *Polym. Int.*, **1997,** 44, 104-110
34. Fanta, G.F., Swanson, C.L., Doane, W.M, *J. Appl. Polym. Sci.*, **1990,** 40, 811-821
35. Shogren, R.L., Thompson, A.R., *J. Appl. Polym. Sci.*, **1992,** 44, 1971- 1978
36. Shogren, R.L., Greene, R.V., Wu, Y. V., *J. Appl. Polym. Sci.,* **1991,** 42, 1701.
37. Bertuzzi, M. A., Vidaurr, E. F., Armada, M. and Gottifredi, J. C., *International Materials, Research Congress, XIII,* Symp., **2004, 7,** 36-37
38. Ramkumar, D. H. S., Battacharya, M., *J. Mater. Sci.*, **1997,** 32, 2565-2572
39. Bastioli, C., Cerrutti, A., Guanella, L., Romano, G. C., Tosin, M., *J. Env. Polym. Deg.*, **1995,** 3, 81-95
40. Averous, L., Moro, L., Dole, P., Fringant, C., *Polymer*, 2000, 41, 4157-4167
41. Lipatov, Y. S., Nesterov, A. E., *Macromolecules*, **1975,** 8, 889-694
42. Flory, P. J., Principles of Polymer Chemistry; Cornell University Press; Ithaca, NY, **1953**
43. Tyagi, O. S., Sajjiad, S. M., Husain, S., *Polymer*, **1987,** 28, 2329-2334
44. Fowkes, F.M., J. *Adhesion Sci. Technol.*, **1990,** 4, 669-691
45. Balard, H. & Papirer, E., *Progress in Organic Coating*, **1993** 22, 1-17
46. Ligner, G., Vidal, A., Balard, H. & Papirer, *J. Colloid Interface Sci.*, **1989,** 133, 200-210
47. Card, T.W., Al-Saigh, Z.Y., Munk, P., *J. Chromatog.*, **1984,** 301, 261-264

Downloaded by NORTH CAROLINA STATE UNIV on August 9, 2012 | http://pubs.acs.org
Publication Date: September 23, 2006 | doi: 10.1021/bk-2006-0939.ch020

48. Suvorova, A.I., Tyukova, I.S., Trufanova, E.I., *Russ. Chem. Rev.*, **2000**, 69, 451-459
49. Blanshard, J. M. W., "Starch granule structure and function": A Physicochemical Approach, in *Starch: Properties and Potentials, Critical Reports on Applied Chemistry* (Ed. T. Galliard), Wiley, New York, **1987**, pp. 16–54.
50. Poutanen, K., Forssel, P.,*Trends Polym. Sci.*, **1996**, 4, 128-132
51. Gibbs, J. H., and DiMarzio, E. A., *J. Chem. Phys.*, **1958**, 28, 373-383
52. Coleman, M. M., Xu, Y., Painter, P. C., *Macromolecules*, **1994**, 27, 127-137
53. Al-Saigh, Z. Y., and Munk, P., *Macromolecules*, **1984**, 17, 803-809
54. Prolongo, M.G., Masegosa, R.M. and Horta, A., *Macromolecules*, **1989**, 22, 4346-4351
55. Ramkumear, D.H.S., Yang, Z., Bhattachrya, M., *Polymer Networks Blends*, 1997, 7, 31-41
56. Pesci, A., I., and Freed, K. F., *J. Chem. Phys.*, **1989**, 90, 2017-2026

Downloaded by NORTH CAROLINA STATE UNIV on August 9, 2012 | http://pubs.acs.org
Publication Date: September 23, 2006 | doi: 10.1021/bk-2006-0939.ch020

Downloaded by UNIV MASSACHUSETTS AMHERST on August 10, 2012 | http://pubs.acs.org
Publication Date: September 23, 2006 | doi: 10.1021/bk-2006-0939.ch021

Chapter 21

Dependence of In Vitro Degradation of an Experimental Poly(glycolide-*co*-L-lactide) Multifilament on Preloading and Temperature

Meng Deng, Jack J. Zhou, Gavin G. Chen, and Daniel Burkley

Research and Technology Development, Ethicon, Inc., a Johnson & Johnson Company, P.O. Box 151, Somerville, NJ 08876

In this work, we investigated the in vitro degradation behavior of an experimental poly(glycolide-*co*-L-lactide) multifilament braid. The experiment was conducted in phosphate buffer solution at pH 7.4 with varying pre-loading and temperature. The dependence of material properties on experimental conditions during degradation was evaluated by mechanical tensile tests, gel permeation chromatography analysis, and scanning electron microscopy. The interrelationships between material properties, exposure time, pre-load and temperature were explored. The results indicated that the polymer multifilament braids gradually lost their tensile strength and molecular weight with the increasing in vitro exposure. It was found that the pre-load levels did not change the degradation behavior of the materials. However, high temperatures significantly accelerated the degradation. There exists a well-defined relationship between molecular weight and tensile strength. Microscopy analysis revealed visible change in the surface morphology of the materials during in vitro degradation.

Polylactide, polyglycolide and their co-polymers are the most-widely used biodegradable polymers. They have been used for sutures, bone fixture pins and screws, soft tissue anchors, tissue scaffolds, wound dressing and drug carriers. As a result, many studies on the in vitro degradation of these polymers have been published in the past (*1-20*). These studies investigated the dependence of degradation on different parameters such as composition, molecular weight, morphology, processing, pH value, etc. However, there are still two under-explored areas, the role of pre-load and temperature during the degradation of these polymers. More importantly, it would be very useful, if a relationship could be established between mechanical properties and molecular weight for a polymeric biomaterial during degradation. It is well known that external stresses influence an implanted medical device. As for temperature, fever and local inflammation may cause the temperature at the implantation site to deviate from normal body temperature. The effects of these extrinsic factors on material degradation need to be more clearly understood. In a series of on-going studies, we conducted experiments to evaluate the effects of pre-load and temperature on physical properties of an experimental poly(glycolide-co-L-lactide) multifilament braid during in vitro degradation. The relationships between tensile properties, external loading, temperature, molecular weight, time, and the surface morphology for the polymer braid samples were investigated.

Downloaded by UNIV MASSACHUSETTS AMHERST on August 10, 2012 | http://pubs.acs.org
Publication Date: September 23, 2006 | doi: 10.1021/bk-2006-0939.ch021

Experimental

Materials

Experimental multifilament braids based on oriented 2.0 dpf continuous yarns made from a partially-crystalline copolymer of ~90 mol% glycolide and ~10 mol% L-lactide (PGLL 90/10) were tested. All materials were produced in-house. The braids were not surface-coated, nor were they sterilized. The filament braid had an initial average molecular weight (M_w) of 57,000 g/mol, polydispersity index (PDI) = 3.04, tensile breaking strength = 1020 MPa, Young's modulus = 10.7 GPa, tensile breaking strain = 16.7%, and a nominal diameter of 0.304 mm. These parameters were used as baseline at degradation time 0. For the purpose stored in a nitrogen box before use.

Methods

Phosphate buffer solution (PBS) was prepared, according to the supplier's instruction, by dissolving phosphate buffer GAL-PAC (Sigma Scientific, USA) in deionized water, resulting in a buffer solution of 0.1 mol/L and pH 7.4 at 25°C. Braid specimens were immersed into the PBS and kept at a constant temperature. The pH values of the PBS were closely monitored during the experiments and the fluid was changed once every three days. Three temperatures (27.5, 37.5 and 47.5°C) were selected to evaluate the effects of temperature change on degradation behavior of the material. To investigate the dependence of degradation on pre-load, two constant load levels (0.2 and 0.8 Newton) were applied to the lower end of the braid specimens by applying a dead weight during the in vitro experiments. At each pre-determined time period, 5 specimens were removed from PBS and tested.

Downloaded by UNIV MASSACHUSETTS AMHERST on August 10, 2012 | http://pubs.acs.org
Publication Date: September 23, 2006 | doi: 10.1021/bk-2006-0939.ch021

The tensile mechanical tests were performed on an Instron 4501 tester with a 500-N load cell (Instron Corporation, USA). The braid specimens were tested at room temperature immediately following their removal from PBS. The gauge length was 80 mm and the crosshead speed was 127 mm/min. The breaking strength, Young's modulus and breaking strain were determined.

Molecular weight and polydispersity were determined by gel permeation chromatography (GPC) analysis with a Waters GPC system (comprising a 515 HPLC pump, a 717 autosampler, a 2410 RI detector, a column heater and two Styragel HT6E columns), with a mobile phase of HFIP with 0.01M LiBr at the flow rate of 0.5 ml/min. The specimens were dissolved in hexafluoroisopropanol (HFIP) at a concentration of 2 mg/ml. The solution was filtered with a 5 ml polypropylene (PP) syringe equipped with a 0.45 µm PP filter to remove any insoluble materials prior to GPC injection. Polymethyl methacrylate standards with narrow polydispersity were used for calibration. The data was analyzed by Millennium version 3.05.01 software.

Changes of braid surface morphology during degradation were evaluated by a JEOL JSM-5900LV scanning electron microscope (SEM) under high vacuum at 5 kV. The specimens were mounted on a carbon stub with carbon paint and gold-coated with an EMS 550 sputter coater.

Results and Discussion

Effect of Pre-load on Tensile Properties

Changes of tensile properties with pre-loading and time during in vitro conditioning at 37.5°C are illustrated in Figures 1 to 3. These figures show that the tensile properties as a function of time and pre-loading followed a similar trend and therefore the degradation behavior of the material did not change significantly after a pre-load was applied during in vitro study. Figure 1 shows dependence of breaking strength on load and in vitro exposure time. Clearly, the strength decreased gradually with time. Although a slightly higher strength was observed at a few time intervals for the samples not subjected to pre-load, there are no statistically significant differences in strength between the control and pre-loaded samples. Within the first two weeks, the samples lost their strength slowly. The strength decrease during this period was less than 20%. Then, the strength started to decrease at a faster rate. By day 27, the materials had retained only 20% of their initial strength. The time for half strength loss was about 20 days. It is believed that the initial strength loss was largely due to absorption and/or diffusion of water into amorphous regions of the polymer, leading to swelling and plasticization and a limited decrease in molecular chain orientation. Then, the hydrolytic scission of the polymer chains in the amorphous regions results in more strength loss, and the generation of polar chain ends. This in turn caused even more water absorption, initiating a cycle resulting in the rapid loss of tensile strength.

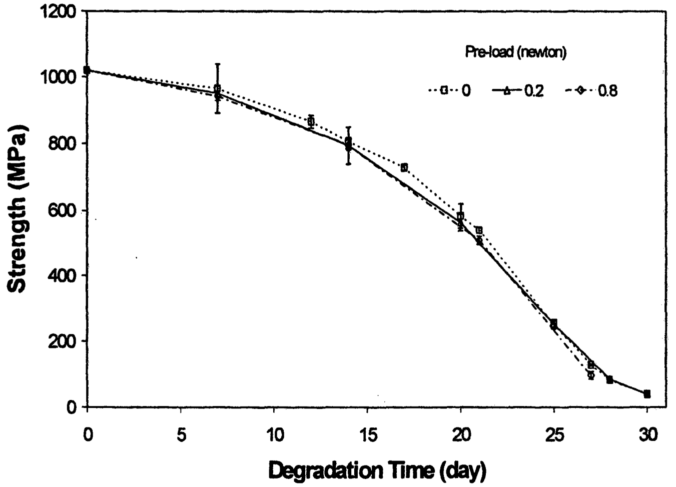

Figure 1. Change of tensile breaking strength as a function of pre-load and in vitro time at 37.5 °C

Figure 2 displays the experimental results for tensile modulus. It is obvious from this figure that pre-loading did not significantly affect the modulus of the polymer braids during in vitro degradation. However, in comparison to strength loss, the modulus changed in a different manner, with a period of stabilization during in vitro conditioning. At the very beginning (less than seven days), there was a 40% sharp drop in modulus. Although this could have been caused by a combined effect of polymer hydrolysis and water absorption, we believe that the reduction in modulus in this time period was mainly due to the water absorption, leading to swelling, relaxation and plasticization of the filaments and braid. After this initial reduction, the modulus remained almost unchanged for about 25 days when the braids had lost about 75% of their tensile strength. This might have been the result of an increase in percent crystallinity and chain scission of the polymer with increasing exposure time. While strength is dependent on crystallinity, long chains, chain entanglement, and orientation, modulus with elastic response is largely dependent on crystallinity. Finally, there was another significant reduction in modulus in the late stage of in vitro degradation process. It is possible that during this short time period, hydrolysis had cleaved most of the tie molecules holding the crystals together, leading to another sharp drop in modulus.

Downloaded by UNIV MASSACHUSETTS AMHERST on August 10, 2012 | http://pubs.acs.org
Publication Date: September 23, 2006 | doi: 10.1021/bk-2006-0939.ch021

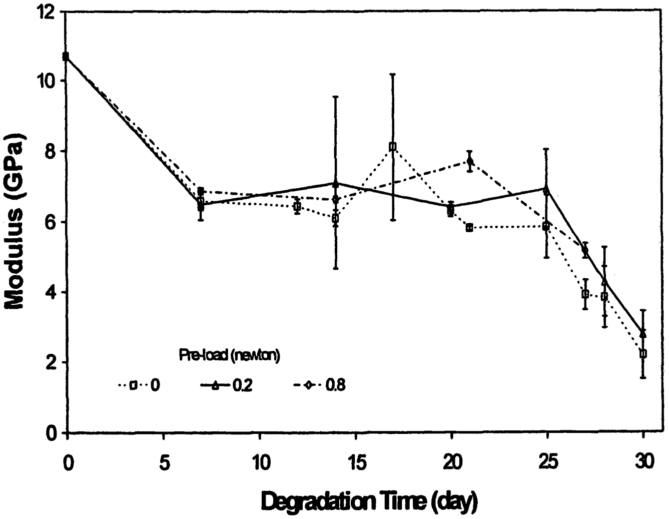

Figure 2. Change of tensile modulus as a function of pre-load and in vitro time at 37.5°C

Figure 3 shows the effects of pre-loading on tensile breaking elongation during the degradation process. The experimental results indicated that pre-loading tended to reduce the elongation of the braid. The higher the pre-load, the greater the elongation reduction. A small increase in elongation at the beginning of the degradation process might have been caused mainly by filament and braid relaxation as the result of water absorption (swelling and plasticization effects). After having reached its peak around 7 days, the elongation started to decrease gradually as a result of polymer hydrolysis. At day 30, the fibers exhibited a very limited stretch-ability with a breaking elongation of less than 4%.

The above results and analyses show that pre-loading up to 0.8 Newton had a very limited effect on the changes of tensile mechanical properties of PGLL 90/10 multifilaments during in vitro degradation processes. This is because on one hand, the load may accelerate degradation; on the other hand, it may help recrystallization (drawing effect and stress-induced recrystallization), therefore slowing down degradation. Additionally, the stress created by the external load may retard the loss of molecular orientation allowing more of the strength to be retained. The trade-off of these effects was that there was no significant net effect at the load levels of this study.

Downloaded by UNIV MASSACHUSETTS AMHERST on August 10, 2012 | http://pubs.acs.org
Publication Date: September 23, 2006 | doi: 10.1021/bk-2006-0939.ch021

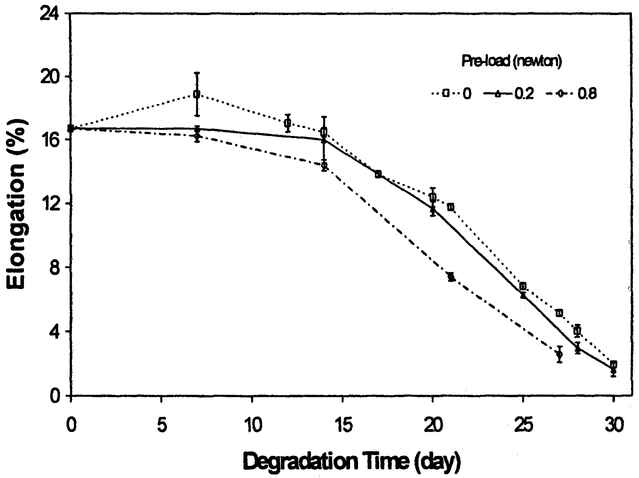

Figure 3. Change of tensile breaking elongation as a function of pre-load and in vitro time at 37.5 °C

Downloaded by UNIV MASSACHUSETTS AMHERST on August 10, 2012 | http://pubs.acs.org
Publication Date: September 23, 2006 | doi: 10.1021/bk-2006-0939.ch021

Effect of Temperature on Tensile Properties

Variation of tensile properties at three temperatures and zero load during in vitro aging is illustrated in Figures 4 to 6. It is obvious from these figures that an elevated temperature significantly accelerated the degradation process and therefore shortened the time needed to degrade the materials. The dependence of tensile strength on temperature is displayed in Figure 4. This figure clearly indicates that the higher temperature led to a much faster decrease of the strength. Quantitatively, at 37.5°C, it took about 30 days for the braid to lose about 90% of its strength. But, at 27.5°C, it took about 100 days for the braid to lose the same amount of strength. At 47.5°C, less than 10 days were required to degrade the material. So, the higher the temperature, the shorter the time needed to degrade the polymer. The significance of the temperature effect is that the in vitro degradation time needed to degrade the biodegradable polymers to a given strength can be substantially reduced if the in vitro studies are performed at elevated temperatures. Therefore, the experimental time could be greatly saved.

Figure 5 shows the effect of temperature on tensile modulus during in vitro degradation processes. Again, temperature had a significant effect on the modulus of the materials during in vitro degradation. The higher the temperature was, the shorter the time needed to reduce the modulus. The maximum reduction in modulus was less than 80%. All three temperatures yielded similar trends for modulus change, i.e., initial drop, followed by a plateau, and then another drop at or near the end of degradation process. Figure 6 illustrates the effects of temperature on tensile breaking elongation during in vitro degradation. Unlike

Downloaded by UNIV MASSACHUSETTS AMHERST on August 10, 2012 | http://pubs.acs.org
Publication Date: September 23, 2006 | doi: 10.1021/bk-2006-0939.ch021

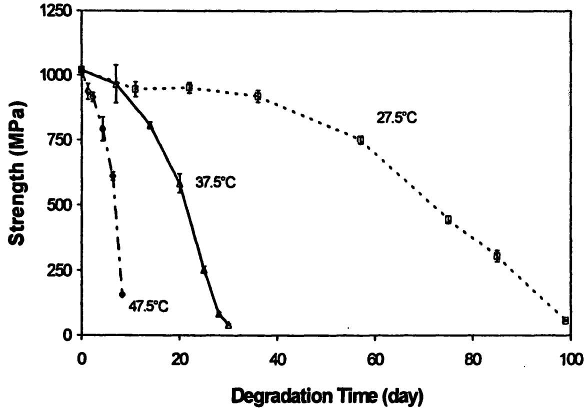

Figure 4. Effects of temperature on breaking strength during in vitro degradation

strength and modulus, the elongation showed some increase at the initial stages of the degradation process for all three temperatures. Generally, the higher the temperature, the larger the initial elongation increase and the shorter the time for the increase to occur. This may be because high temperature helped accelerate fiber relaxation, resulting in an increased ability to stretch. However, the elevated temperature caused the elongation to decrease much faster with time.

Change of Molecular Weight during In Vitro Degradation

The change of weight-average molecular weight at three temperatures during in vitro degradation is shown in Figure 7. The higher the temperature, the faster the molecular weight decreased. When the molecular weight dropped below 10,000, the polymer braid virtually lost most of its strength. The PDI decreased with increasing in vitro exposure time, changing from about 3.5 to about 1.5. Such results suggested a non-random chain scission process and a great likelihood of large molecules undergoing chain breakage.

Relationship between Molecular Weight and Tensile Properties

In the field of biomaterials, the dependence of mechanical performance on molecular weight for biodegradable polymers is seldom investigated during their degradation. Nevertheless, it would be very useful if the mechanical strength

Downloaded by UNIV MASSACHUSETTS AMHERST on August 10, 2012 | http://pubs.acs.org
Publication Date: September 23, 2006 | doi: 10.1021/bk-2006-0939.ch021

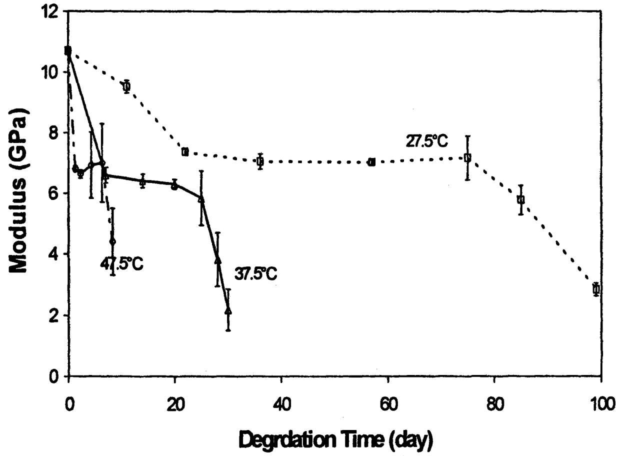

Figure 5. Effects of temperature on modulus during in vitro degradation

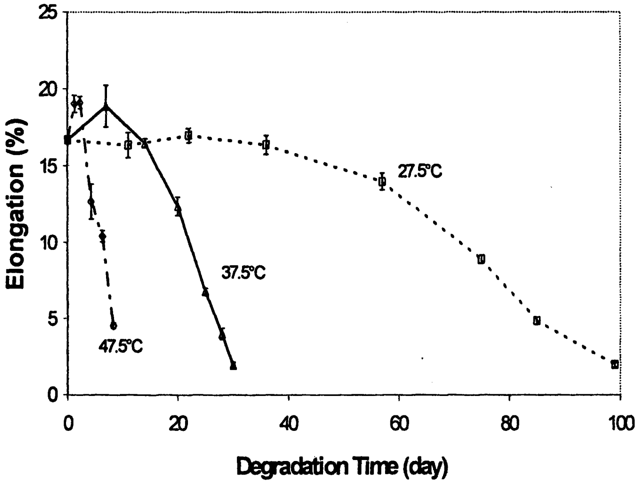

Figure 6. Effects of temperature on breaking elongation during in vitro degradation

Downloaded by UNIV MASSACHUSETTS AMHERST on August 10, 2012 | http://pubs.acs.org
Publication Date: September 23, 2006 | doi: 10.1021/bk-2006-0939.ch021

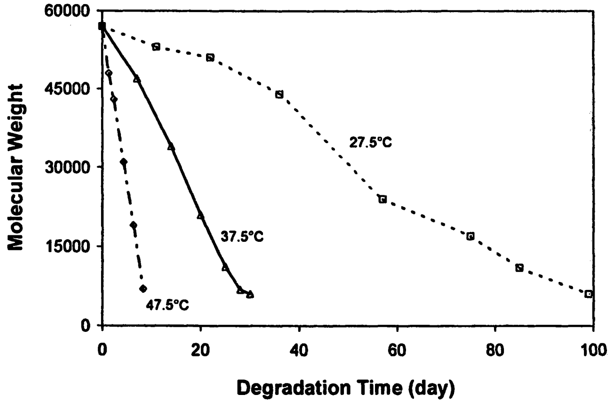

Figure 7. Effects of temperature on weight average molecular weight during in vitro degradation

could be related to the polymer molecular weight, or vice versa. To explore the relationship between molecular weight and tensile strength, the experimental data is plotted in Figure 8. Since the data points were taken from all three temperatures, the results suggest that there exists a good correlation between strength and molecular weight, and temperatures does not affect this relationship. Further analysis showed that the following formula illustrates the experimental data very well,

$$\sigma = c_1 + c_2 \ln M_w \qquad (1)$$

where σ is tensile strength, M_w weight average molecular weight, c_1 and c_2 constants. The above equation can be rewritten as

$$\sigma = \sigma_{\max} \frac{\ln M_w - \ln M_{\min}}{\ln M_{\max} - \ln M_{\min}} \qquad (2)$$

Where $M_{\max}$ is the molecular weight before degradation (with corresponding strength $\sigma_{\max}$) and $M_{\min}$ is the molecular weight after the polymer has completely degraded (strength is 0). By curve-fitting the experimental data, c_1 and c_2 were determined as –3792 and 440, respectively. The fitted curve is also plotted in Figure 8, as the solid line. Based on the above relationship, one will be able to predict strength from molecular weight at a given in vitro time, or vice versa. Letting σ be 0 (completely degraded) or 1020 MPa (no degradation) yields the corresponding M_w of 5,500 or 56,200, respectively. Thus, one could infer from that a minimum M_w of about 5,500 would be a pre-condition for the polymer braid to have any load-bearing capability.

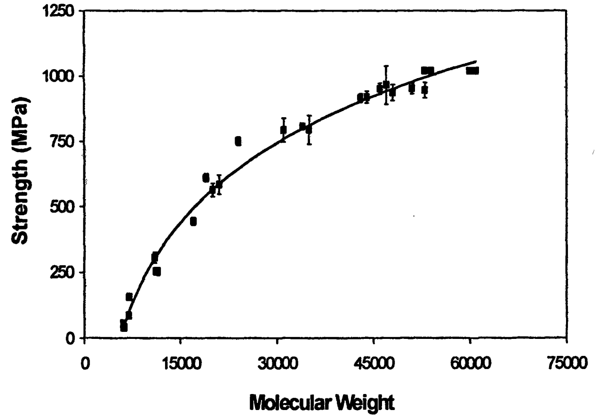

Figure 8. Strength as a function of M_w for polymer braid during degradation

Figure 9 shows the modulus as a function of M_w. Since the data from all three temperatures fell on essentially the same curve in this figure, clearly molecular weight was the important factor, and not the degradation temperature to achieve a particular modulus value, assuming the morphology is constant. This graph indicates that after an initial drop in modulus, the braids maintained their moduli until the M_w decreased to about 15,000 where another significant reduction occurred. The initial reduction in modulus was mainly due to the effects of fluid absorption, leading to relaxation and plasticization of the braided fibers. The relatively stable and/or slight increase in crystallinity was responsible for the flattened regions of modulus, which may have counter-balanced the effect of molecular weight reduction. Figure 10 displays the relationship between breaking elongation and molecular weight. Again, the temperature did not have profound effects on the relationship.

Morphology Change during Degradation

During in vitro degradation, the surfaces of the polymer braids and the individual filaments did not show significant change in appearance after SEM examination up to 500X magnification until after an approximate 50% decrease

Downloaded by UNIV MASSACHUSETTS AMHERST on August 10, 2012 | http://pubs.acs.org
Publication Date: September 23, 2006 | doi: 10.1021/bk-2006-0939.ch021

Downloaded by UNIV MASSACHUSETTS AMHERST on August 10, 2012 | http://pubs.acs.org
Publication Date: September 23, 2006 | doi: 10.1021/bk-2006-0939.ch021

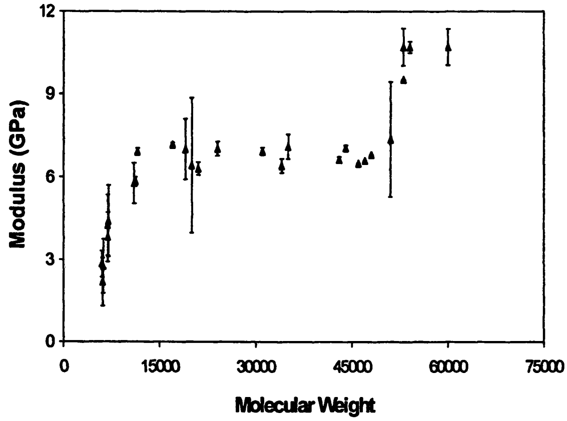

Figure 9. Modulus as a function of M_w for polymer braid during degradation

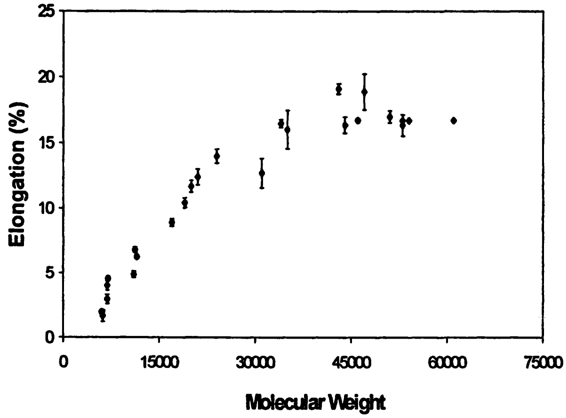

Figure 10. Elongation as a function of M_w for polymer braid during degradation

in strength was observed. Then, surface erosion or material loss could be clearly seen on individual filaments. Figures 11 and 12 illustrate the typical surface morphology of polymer braids during degradation at 37.5°C. At day 7, there was hardly any visible surface erosion, and at day 17 a few focal regions of degradation could be observed. At day 30, the increased focal regions and a large amount of more diffuse degradation was evident on the fiber surface. It is possible that the diffuse regions were the result of propagation of the focal regions along the fiber longitudinal axis. It seems from Figure 11 that the diameter of the braid increased slightly during in vitro degradation, probably due to the relaxation effect caused by the fluid diffusion.

Downloaded by UNIV MASSACHUSETTS AMHERST on August 10, 2012 | http://pubs.acs.org
Publication Date: September 23, 2006 | doi: 10.1021/bk-2006-0939.ch021

Conclusions

The dependence of in vitro degradation behaviors of an experimental poly(glycolide-co-L-lactide) multifilament braid on pre-load and temperature was investigated in phosphate buffer solution at pH 7.4. While the pre-loading did not affect significantly the degradation of the braid, the changes of tensile mechanical properties and molecular weight at any given time were strongly temperature-dependent. High temperature led to the fast degradation and therefore shortened degradation time. There exists a well-defined relationship between strength and molecular weight for the polymer braid during in vitro degradation. The surface morphology of the filaments showed visible changes during in vitro conditioning.

Acknowledgements

The authors want to thank Dr. Mark Storch, Dr. Robert Scott, Robert Tannhauser, Dr. Edward Dormier and Dr. John Sheets for their review of the manuscript.

References

1. Gilding, D. K.; Reed, A. M. *Polymer*; **1979**, *20*, 1459–1464.
2. Reed, A. M.; Gilding, D.K. *Polymer*; **1981**, *22*, 494-498.
3. Fredericks, R. J.; Melveger, A. J.; Dolegiewitz, L. J. *J. Polym. Sci. Phys. Ed.* **1984**, *22*, 57-66.

Downloaded by UNIV MASSACHUSETTS AMHERST on August 10, 2012 | http://pubs.acs.org
Publication Date: September 23, 2006 | doi: 10.1021/bk-2006-0939.ch021

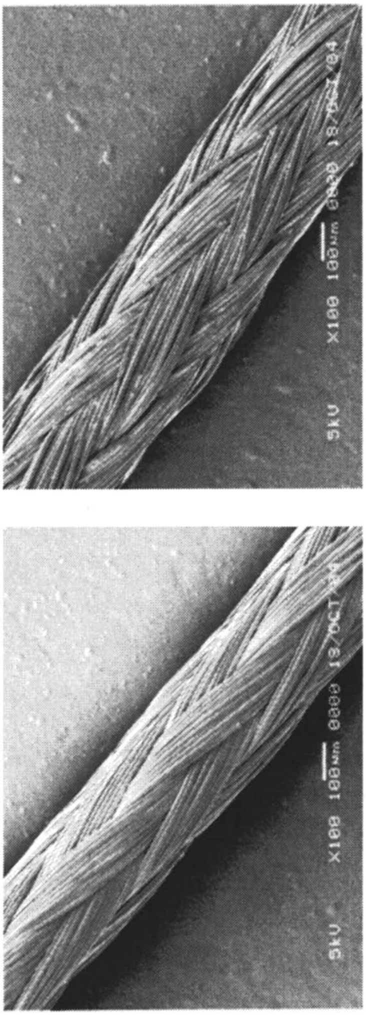
5kU X100 100µm 0000 13/OCT/04
5kU X100 100µm 0000 18/OCT/04

0 day

7 days

Downloaded by UNIV MASSACHUSETTS AMHERST on August 10, 2012 | http://pubs.acs.org
Publication Date: September 23, 2006 | doi: 10.1021/bk-2006-0939.ch021

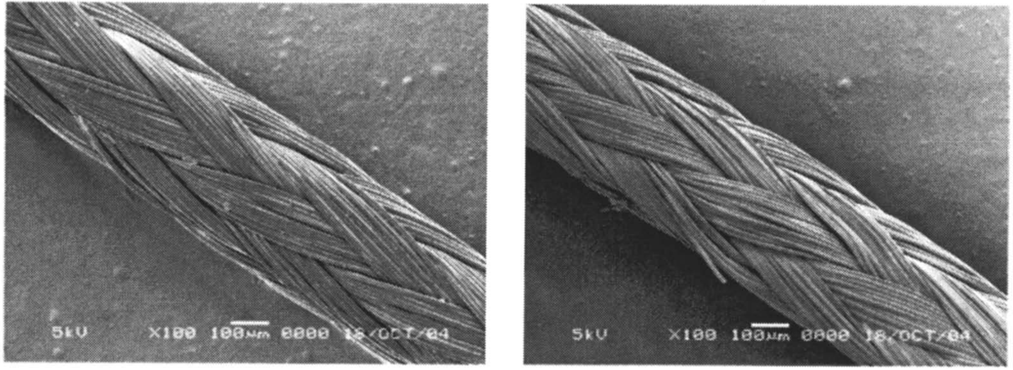
5kV X100 100μm 0000 18/OCT/04
5kV X100 100μm 0000 18/OCT/04

17 days

30 days

Figure 11. Surface morphology of the braid samples during degradation (original magnification 100X)

Downloaded by UNIV MASSACHUSETTS AMHERST on August 10, 2012 | http://pubs.acs.org
Publication Date: September 23, 2006 | doi: 10.1021/bk-2006-0939.ch021

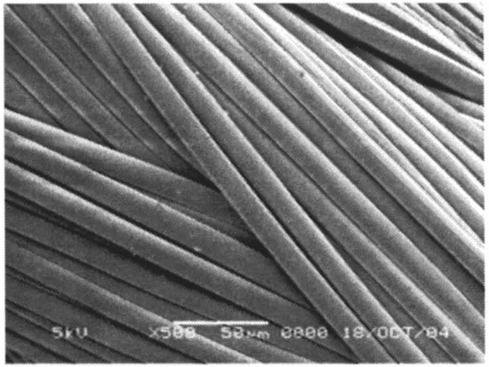
5kV X500 50µm 0000 18/OCT/04

0 day

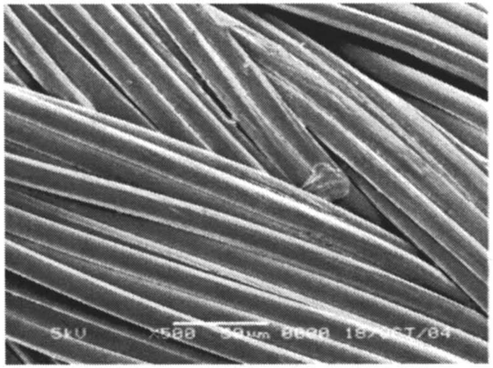
5kV X500 50µm 0000 18/OCT/04

7 days

Downloaded by UNIV MASSACHUSETTS AMHERST on August 10, 2012 | http://pubs.acs.org
Publication Date: September 23, 2006 | doi: 10.1021/bk-2006-0939.ch021

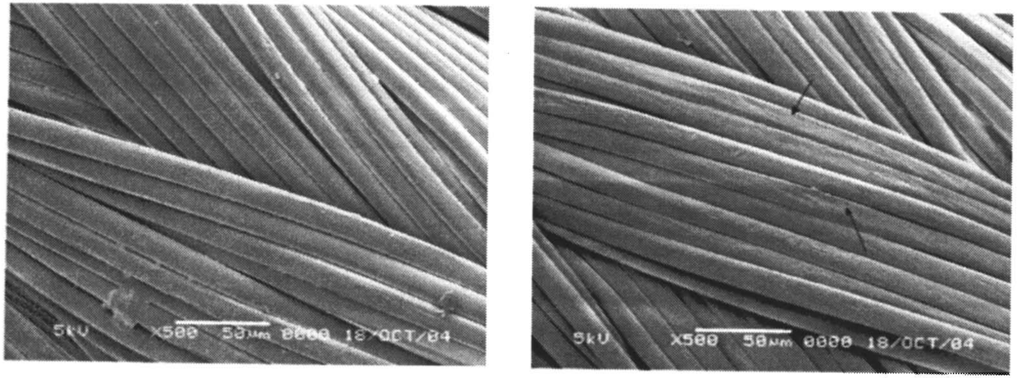
5kV X500 50µm 0000 18/OCT/04
5kV X500 50µm 0000 18/OCT/04

17 days

30 days

Figure 12. Surface morphology of the braid samples during degradation. Arrows indicate significant eroded areas (original magnification 500X)

Downloaded by UNIV MASSACHUSETTS AMHERST on August 10, 2012 | http://pubs.acs.org
Publication Date: September 23, 2006 | doi: 10.1021/bk-2006-0939.ch021

4. Miller, N. D.; Williams, D. F. *Biomaterials*; **1984**, *5*, 365-368.
5. Nakamura, T.; Hitomi, S.; Watanabe, S.; Shimizu, Y.; Jamshidi, K.; Hyon, S. H.; Ikada, Y. *J. Biomed. Mater. Res.* **1989**; 23,1115–1130.
6. Zhang, L.; Loh, I. H.; Chu, C. C. *J. Biomed. Mater. Res.* **1993**, *27*, 1425-1431.
7. *Biomedical Polymers: Designed-to-Degrade Systems*, Shalaby, S. W.; Burg, K., Eds., Carl Hanser Verlag, New York, 1994.
8. Schmitt, E. A.; Flanagan, D. R.; Linhardt, R. *Macromolecules*, **1994**, *27*, 743–748.
9. *Degradable Polymers—Principles and Applications*; Scott, G.; Gilead. D., Eds.; London, Chapman and Hall, 1995.
10. Grizzi, I.; Garreau, H.; Li, S.; Vert, M. *Biomaterials*, **1995**, *16*, 305–311.
11. Zong, X. H.; Wang, Z. G.; Hsiao, B. S. Chu, B.; Zhou, J.; Jamiolkowski, D. D.; Muse, E.; Dormier. E. *Macromolecules*; **1999**, *32*, 8107-14.
12. Kim, K. S.; Chung, S.; Chin, I. J.; Yoon, J. S. *J. Appl. Polym. Sci.* **1999**, *72*, 341–348.
13. Lu, L.; Garcia, C. A.; Mikos, A. G. *J. Biomed. Mater. Res.* **1999**, *46*, 236–244.
14. Li, S. *J. Biomed. Mater. Res.* **1999**, *48*, 342–353.
15. Li, S.; McCarthy. S. *Biomaterials*, **1999**, *20*, 35–44.
16. Kangas, J.; Paasimaa, S.; Makela, P.; Leppilahti, J.; Tormala, P.; Waris, T.; Ashammakhi, N. *J. Biomed. Mater. Res.* **2001**, *58*, 121-126.
17. Tomihata, K.; Suzuki, M.; Ikada, Y. *J. Biomed. Mater. Res.* **2001**, *58*, 511-518.
18. Yuan, X. Y.; Mak, A. F. T.; Yao, K. D. *J. Appl. Polym. Sci.* **2002**, *85*, 936-943.
19. Deng, M.; Uhrich, E. K., *J. Mater. Sci. Mater. Med.* **2002**, *13*, 1091-1096.
20. *Absorbable and Biodegradable Polymers*, Shalaby, S. W.; Burg, K., Eds., CRC Press, New York, 2004.

Downloaded by PENNSYLVANIA STATE UNIV on August 9, 2012 | http://pubs.acs.org
Publication Date: September 23, 2006 | doi: 10.1021/bk-2006-0939.ch022

Chapter 22

Organization and Expression of the Genes Involved in the Metabolism of Poly(ethylene glycol) and Poly(vinyl alcohol)

Fusako Kawai, Akio Tani, and Kazuhide Kimbara

Research Institute for Bioresources, Okayama University, Kurashiki, Okayama 710–0046, Japan

Because of the large-scale production and widespread use of poly(ethylene glycol) (PEG) and poly(vinyl alcohol) (PVA), these products eventually find their way into the natural environment. Their microbial metabolic pathways have been well studied. Our laboratory has cloned the relevant genes involved in the degradation of PEG and PVA from *Sphingomonas* sp. strains 103 and 113P3, respectively. A 13.3 kb DNA fragment containing the PEG dehydrogenase gene was cloned and sequenced. This report presents data about the operon related to PEG degradation and the regulation of this operon. Similar gene structures were found in other PEG-utilizing sphingomonads. In addition, the PVA degradation operon, which includes genes for PVA dehydrogenase and oxidized PVA hydrolase, was also investigated. These genes were located in tandem with little intergenic space between them, suggesting that both genes are expressed constitutively and polycistronically.

In Degradable Polymers and Materials; Khemani, K., et al.;
ACS Symposium Series; American Chemical Society: Washington, DC, 2006.

Downloaded by PENNSYLVANIA STATE UNIV on August 9, 2012 | http://pubs.acs.org
Publication Date: September 23, 2006 | doi: 10.1021/bk-2006-0939.ch022

Past intensive studies have clarified the biodegradability of xenobiotic polymers and the factors required for their biodegradation. The biodegradability of polymers is verified by the existence of either enzymes involved in their metabolism or microorganisms, which can assimilate them as a sole carbon source. Depolymerization processes are crucial for the degradation of polymers, which are categorized into two classes: exogenous and endogenous. Examples of exogenously degraded polymers include polyethylene glycol (PEG) and polyethylene, where polymers are depolymerized step by step by cleaving a small molecule from the terminus of the molecule. Examples of polymers that are degraded by an endogenous mechanism include polyvinyl alcohol (PVA) and other hydrolysable polymers including polyesters, polylactide and polycaprolactone, where polymers are rapidly depolymerized by hydrolysis at random.

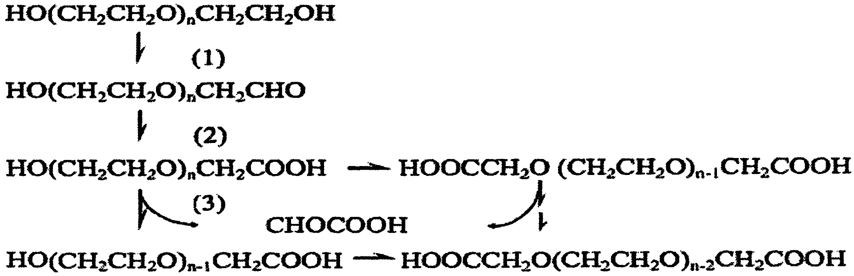
$HO(CH_2CH_2O)_nCH_2CH_2OH$
(1)
$HO(CH_2CH_2O)_nCH_2CHO$
(2)
$HO(CH_2CH_2O)_nCH_2COOH$
$HOOCCH_2O\,(CH_2CH_2O)_{n-1}CH_2COOH$
(3)
CHOCOOH
$HO(CH_2CH_2O)_{n-1}CH_2COOH$
$HOOCCH_2O(CH_2CH_2O)_{n-2}CH_2COOH$

(1) PEG dehydrogenase
(2) PEG-aldehyde dehydrogenase
(3) PEG-carboxylate dehydrogenase

Figure 1. Aerobic metabolic pathway of PEG degradation.

PEG and PVA are water-soluble polymers, which are produced on a large scale and used in various areas, eventually entering natural streams after use. Their metabolic pathways have been well studied and major metabolic enzymes purified and characterized (*1*). PEG is depolymerized exogenously at the molecular end, and a product, glyoxylic acid, is produced step by step, which is metabolized through the central metabolic pathway. PVA, however, is depolymerized endogenously at random, and a final product, acetic acid, is metabolized through the central metabolic pathway. Prior to depolymerization PEG is oxidized to PEG-carboxylate by PEG dehydrogenase (PEGDH) and PEG-aldehyde dehydrogenase (PEGALDH) and then an ether-bond is split by PEG-carboxylate dehydrogenase (PEGCaDH), as shown in Figure 1 (*2*). PVA is

Downloaded by PENNSYLVANIA STATE UNIV on August 9, 2012 | http://pubs.acs.org
Publication Date: September 23, 2006 | doi: 10.1021/bk-2006-0939.ch022

first oxidized by PVA dehydrogenase (PVADH) at hydroxyl groups and then adjacent dicarbonyl groups are subject to hydrolysis by oxidized PVA hydrolase (OPH) (*3*), as shown in Figure 2. The focus of this paper is to characterize enzymes and their genes relevant to the degradation of PEG and PVA.

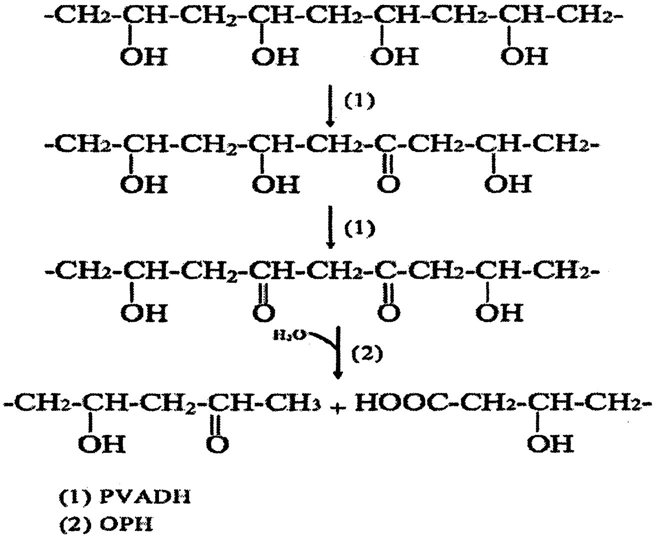
-CH2-CH-CH2-CH-CH2-CH-CH2-CH-CH2-
OH OH OH OH
(1)
-CH2-CH-CH2-CH-CH2-C-CH2-CH-CH2-
OH OH O OH
(1)
-CH2-CH-CH2-CH-CH2-C-CH2-CH-CH2-
OH O O OH
H2O
(2)
-CH2-CH-CH2-CH-CH3 + HOOC-CH2-CH-CH2-
OH O OH
(1) PVADH
(2) OPH

Figure 2. Metabolic pathway of PVA degradation.

Characterization of Genes Relevant to the Metabolism of PEG

Gene Cluster Conserved in PEG-Utilizing Sphingomonads

The metabolism of PEG has been reported for several sphingomonads, either in an axenic (e.g., *S. macrogoltabidus*) or mixed culture (e.g., *S. terrae* with *Rhizobium* sp.) (*4*). The first step in the degradation pathway is catalyzed by PEGDH. A gene for PEGDH (*pegA*) was cloned from *Sphingomonas terrae* and sequenced (*5*). Characterization of the cloned enzyme suggested that the enzyme is a novel type of flavoprotein alcohol dehydrogenase belonging to the

Downloaded by PENNSYLVANIA STATE UNIV on August 9, 2012 | http://pubs.acs.org
Publication Date: September 23, 2006 | doi: 10.1021/bk-2006-0939.ch022

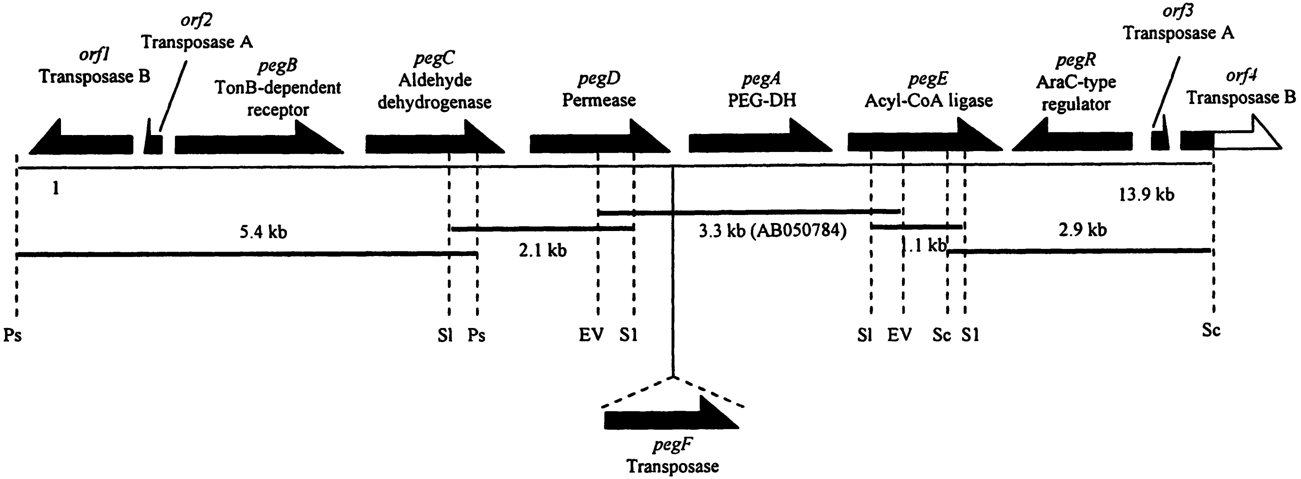
orf1
Transposase B
orf2
Transposase A
pegB
TonB-dependent receptor
pegC
Aldehyde dehydrogenase
pegD
Permease
pegA
PEG-DH
pegE
Acyl-CoA ligase
pegR
AraC-type regulator
orf3
Transposase A
orf4
Transposase B
1
13.9 kb
5.4 kb
2.1 kb
3.3 kb (AB050784)
1.1 kb
2.9 kb
Ps
Sl
Ps
EV
Sl
Sl
EV
Sc
Sl
Sc
pegF
Transposase

Figure 3. Gene cluster of peg operon in Sphingomonas macrogoltabidus sp. strain 103.Cloned DNA fragments were illustrated as thick lines and primers.. Open reading frames and their orientations were indicated as thick arrows with gene and protein names. The structure of the operons was the same among three strains except that one transposon gene (pegF) was found in the intergenic region between pegD and pegA, in strain 203. Restriction sites used for cloning were indicated by dashed lines: Ps, Pst I; SI, SalI; EV, EcoRV; and Sc, SacI~~s~~.

group of glucose-methanol-choline (GMC) flavoprotein oxidoreductases. As strain 103 had *pegA* identical to that of *S. terrae,* the upstream and downstream regions of *pegA* (13.3 kb) were cloned and sequenced, as shown in Figure 3. Five putative ORFs encoding transposases A and B, TonB-dependent receptor (*pegB*), aldehyde dehydrogenate (*pegC*) and permease (*pegD*) were found in the upstream region, while acyl-CoA ligase (*pegE*), AraC-type transcription regulator (*pegR*, in an opposite orientation) and transposases A and B were posited in the downstream region. The nucleotide sequences of these were deposited in the DDBJ, EMBL and GenBank nucleotide sequence databases under accession number AB196775. The same gene structure was conserved in the *S. terrae* and *S. macrogoltabidus* strain 203 (6). In strain 203, another transposase gene was inserted in the intergenic region between *pegD* and *pegA*. These conserved genes shared a very high homology of more than 99%.

Downloaded by PENNSYLVANIA STATE UNIV on August 9, 2012 | http://pubs.acs.org
Publication Date: September 23, 2006 | doi: 10.1021/bk-2006-0939.ch022

Expression of Genes Involved in the Conserved Gene Cluster in *S. macrogoltabidus* sp. strain 103

To find out whether the conserved genes among three sphingomonads are inducibly expressed by PEG and whether they are monocistronic or polycistronic, mRNAs for *pegB* ~ *pegE* were detected by dot-blot hybridization and reverse transcription PCR (RT-PCR). The strain was grown on PEG and ethylene glycol (EG) media, and the total RNAs extracted. The total RNAs were spotted on nylon membrane and the genes-specific probes were hybridized to detect the transcripts of each gene. RT-PCR technique was used to detect transcripts including the intergenic regions.

Dot-blot hybridization exhibited that all of *pegB~R* were induced by PEG, but not by EG, which showed inductive expression of these 6 genes. RT-PCR showed that *pegB* ~ *pegE* and their intergenic regions were expressed polycistronically in PEG medium, as shown in Figure 4. These results showed that the PEG-induced expression of the five genes (*pegB~E)* occurred polycistronically. A promoter for *pegB* ~ *pegE* was thought to exist in the upstream region of *pegB*. Although the expression of *pegR* was also inducible in PEG medium, its role in PEG degradation still remains to be elucidated. We designated this gene cluster including *peg B* ~ *peg R* as *peg* operon.

Our previous work suggested that the PEGDH activity of strain 203 was constitutively expressed while those from strain 103 and *S. terrae* were inducible by PEG (7). Enzyme activity and Western blotting with the anti-PEGDH antibody were compared in strains 103 and 203. Enzyme activity was induced by

Downloaded by PENNSYLVANIA STATE UNIV on August 9, 2012 | http://pubs.acs.org
Publication Date: September 23, 2006 | doi: 10.1021/bk-2006-0939.ch022

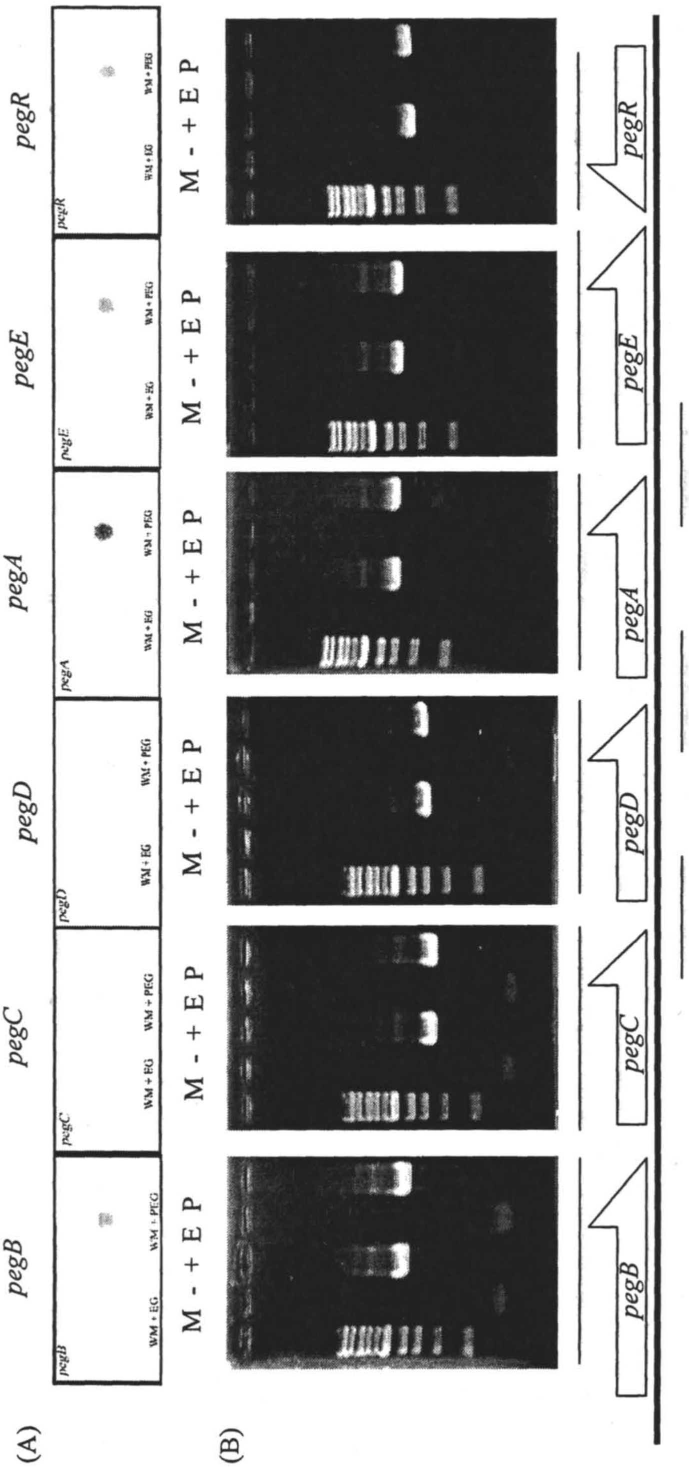
(A)
pegB
pegC
pegD
pegA
pegE
pegR
WM + EG
WM + PEG
(B)
M - + E P
M - + E P
M - + E P
M - + E P
M - + E P
M - + E P
pegB
pegC
pegD
pegA
pegE
pegR

Downloaded by PENNSYLVANIA STATE UNIV on August 9, 2012 | http://pubs.acs.org
Publication Date: September 23, 2006 | doi: 10.1021/bk-2006-0939.ch022

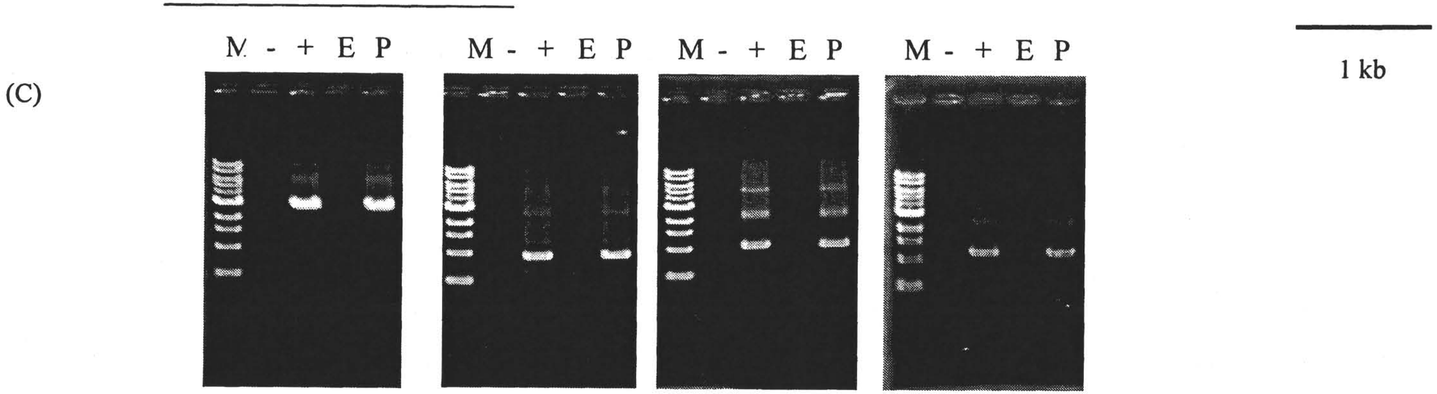

Figure 4. Dot-blot hybridization and RT-PCR analysis of peg operon in strain 103. (A) Dot-blot hybridization was performed using gene-specific probes generated by PCR. The sizes of the probes were identical to products obtained by RT-PCR analyses (B). (B) RT-PCR analyses of each gene and (C) RT-PCR analyses of each intergenic region were performed. The sizes of the detected PCR bands were illustrated by thin lines under or above the picture of each gel; M, 1 kb ladder marker; (-), negative control prepared by skipping the reverse-transcription step and RNA sample was prepared from PEG-grown cells; (+), positive control using total DNA from strain 103 as a template; E and P, RNAs were isolated from EG-grown and PEG-grown cells, respectively.

PEG in strain 103, but constitutively formed in strain 203. Western blotting showed the same results as the enzyme activity (Figure 5). Thus the insertion of a transposon (*pegF*) between *pegD* and *pegA* must cause the constitutive expression of *pegA* in strain 203, suggesting another promoter in the upstream region of *pegA*.

Role of *pegC* Conserved in *peg* Operon

A gene (*pegC*) encoding aldehyde dehydrogenase (ALDH) was located 3.4 kb upstream of *pegA* in *S. macrogoltabidus* strain 103. The ORF of *pegC* consisted of 1344 bp corresponding to 447 amino acid residues. The gene was expressed in *E. coli* and the recombinant enzyme tagged with hexahistidines was purified on a Ni-nitrilotriacetic acid agarose column (*8*). The recombinant enzyme was a homotetramer consisting of four 46.1-kDa subunits. The alignment of the putative amino acid sequence of ALDH showed high similarity with a group of NAD (P)-dependent ALDHs (identity 36-52%). Contrary to NAD (P)-dependent ALDHs in general, the cofactor was tightly bound to the enzyme, as shown in Figure 6. The extracted cofactor was identified as NADP and the enzyme contained approximately one mole NADP per subunit. The enzyme acted on *n*-aldehydes (C_2-C_{14}) (Table I) and PEG-aldehydes (Figure 7). Thus the enzyme was concluded to be a novel nicotinoprotein (NADP-containing) ALDH, which is the second metabolic enzyme (PEGALDH) involved in PEG degradation.

The roles of the TonB-dependent receptor, permease, acyl-CoA ligase and AraC-type transcription regulator remain to be clarified.

Genes Involved in the Metabolism of PVA

Purification and Characterization of OPH

PVADH and OPH were constitutively present in the periplasm of *Sphingomonas* sp. strain 113P3 (formerly *Pseudomonas* sp. 113P3 (*9*)) (Table II). The OPH from strain 113P3 was purified to homogeneity and characterized for the first time (*10*). The enzyme was a homodimer consisting of 35-kDa subunits. Enzymatic activity was inhibited by phenylmethylsulfonyl fluoride, Hg^{2+} and Zn^{2+}. The enzyme hydrolyzed oxidized PVA and *p*-nitrophenyl acetate (PNPA), but did not hydrolyze any of the mono- or diketones tested. K_m and V_{max} values for oxidized PVA and PNPA were 0.2 and 0.3 mM, and 0.1 and 3.4 μmol min^{-1} mg^{-1}, respectively. Whether the OPH was really active toward oxidized PVA was confirmed by a decrease in A_{300} (for diketone structure) (*11, 12*) and the shift of the average molecular weight (Mn) of oxidized PVA. An increase in

Downloaded by PENNSYLVANIA STATE UNIV on August 9, 2012 | http://pubs.acs.org
Publication Date: September 23, 2006 | doi: 10.1021/bk-2006-0939.ch022

Downloaded by PENNSYLVANIA STATE UNIV on August 9, 2012 | http://pubs.acs.org
Publication Date: September 23, 2006 | doi: 10.1021/bk-2006-0939.ch022

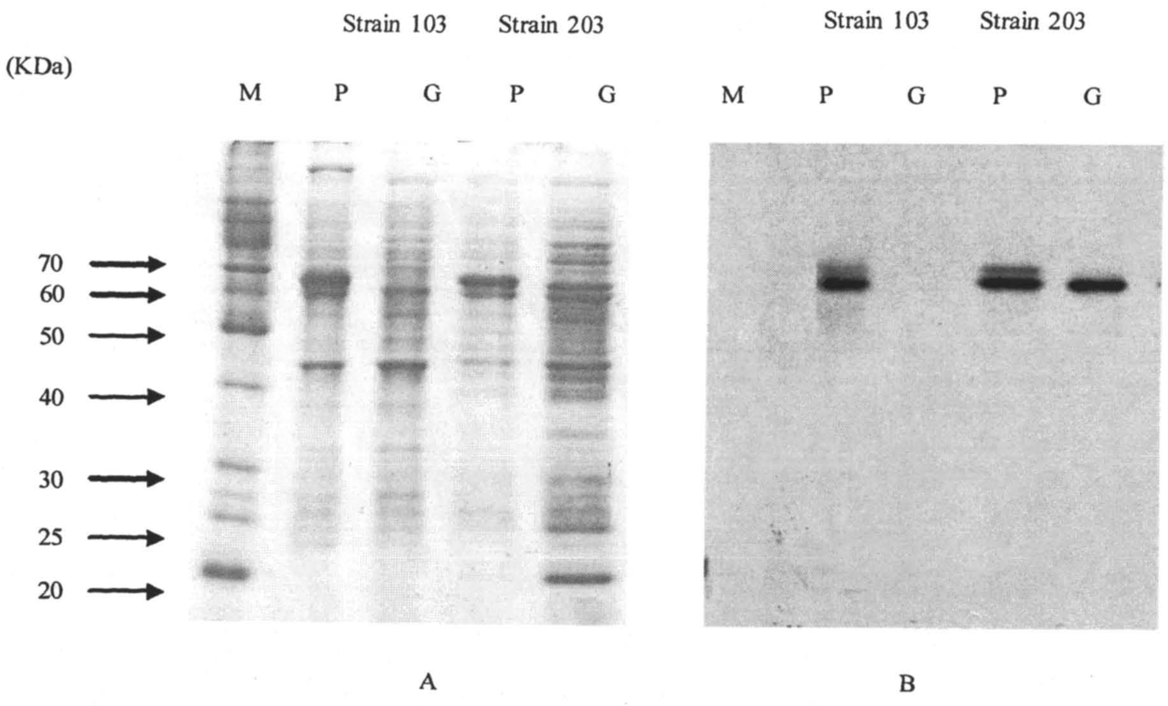
Strain 103
Strain 203
(KDa)
M
P
G
P
G
70
60
50
40
30
25
20
A
Strain 103
Strain 203
M
P
G
P
G
B

Figure 5. Expression of PEGDH. (A) SDS-PAGE of cell-free extracts from strains 103 and 203 grown on PEG or glucose; (B) Western blotting with anti-PEGDH antibody. M, protein markers; P, PEG-grown cells and G, glucose-grown cells.

Downloaded by PENNSYLVANIA STATE UNIV on August 9, 2012 | http://pubs.acs.org
Publication Date: September 23, 2006 | doi: 10.1021/bk-2006-0939.ch022

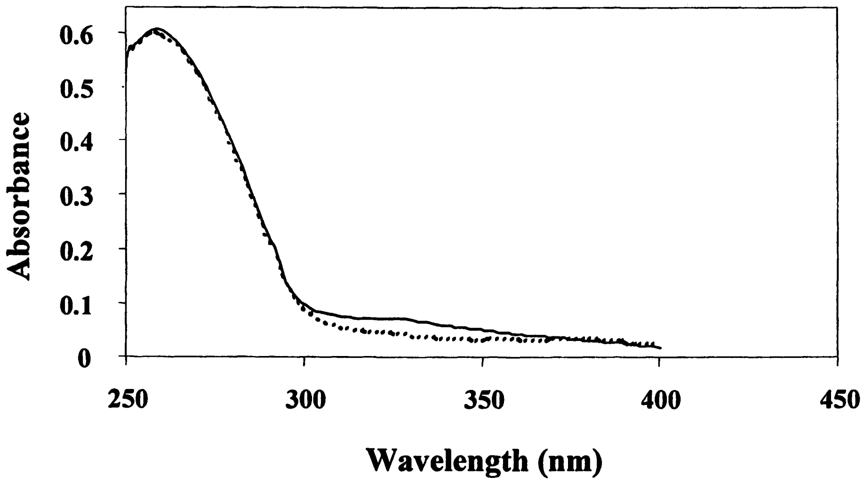

Figure 6. Absorption spectra of the purified recombinant ALDH from E. coli harboring pegC. Dashed line, the purified enzyme; solid line, the reduced form of the purified enzyme in the presence of n-decanal. (Reproduced from reference 8. Copyright 2005 Springer-Verlag GmbH.)

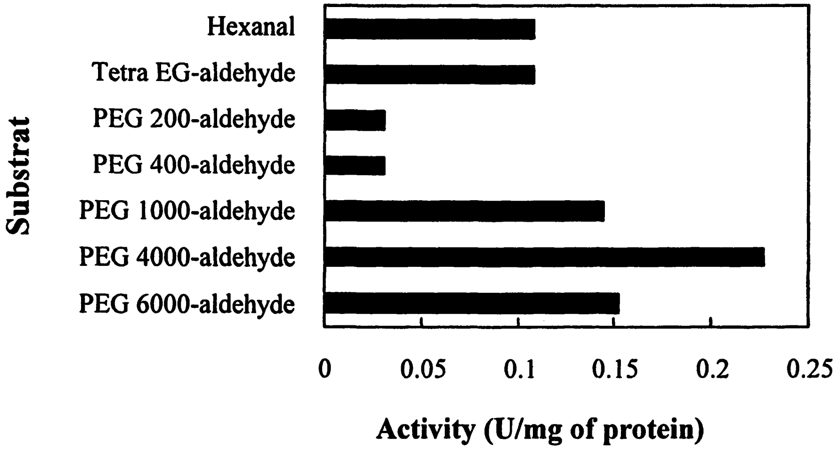

Figure 7. Substrate specificity of the recombinant ALDH against PEG-aldehyde. (Reproduced from reference 8. Copyright 2005 Springer-Verlag GmbH.)

Downloaded by PENNSYLVANIA STATE UNIV on August 9, 2012 | http://pubs.acs.org
Publication Date: September 23, 2006 | doi: 10.1021/bk-2006-0939.ch022

Table I. Comparison of the Substrate Specificities of Yeast ALDH and the Recombinant ALDH

Substrate	*Conc. (mM)*	*ALDH (S. cerevisiae)*		*PEGALDH (S. macrogoltabidus strain 103)*	
		Activity		*Activity*	
		(U/mg of protein)	*(%)*[a]	*(U/mg of protein)*	*(%)*[b]
Formaldehyde	1	0.89	40	0.27	49
Acetaldehyde	1	2.2	100	0.42	78
n-Propanal	1	1.8	80	0.35	64
n-Butanal	1	0.99	44	0.32	58
n-Pentanal	1	0.88	39	0.30	56
n-Hexanal	1	1.1	50	0.28	51
n-Heptanal	1	1.5	67	0.37	68
n-Octanal	1	1.6	70	0.39	72
n-Nonanal	1	0.71	32	0.43	79
n-Decanal	1	0.22	9.7	0.47	86
n-Undecanal	1	n.d.	-----	0.47	87
n-Dodecanal	1	n.d.	-----	0.49	91
n-Tridecanal	1	n.d.	-----	0.52	97
n-Tetradecanal	1	n.d.	-----	0.54	100

n.d.: not detected

[a]: The activity on acetaldehyde was defined as 100%.

[b]: The activity on *n*-tetradecanal was defined as 100%.

The values were expressed on average of three repeated experiments.

SOURCE: Reproduced from Reference 8. Copyright 2005 Springer-Verlag GmbH.

A_{300} up to 60 min due to PVADH and then a decrease due to OPH were found (Figures 8a, 8b). Oxidized PVA was hydrolyzed by OPH, which was analyzed by HPLC (Figure 8c). The oxidized PVA prepared by PVADH showed two peaks on HPLC, corresponding to Mn values of approximately 11,000 (47%) and 1400 (53%). The former peak was shifted to Mn values ranging from 7,500 to 3,700 and the latter peak increased in height after hydrolysis by OPH.

Table II. Localization of OPH and PVADH in *Sphingomonas* sp. strain 113P3

Enzyme preparation	*Total activity (%)*	
	PVADH	*OPH*
Culture supernatant	1.0	21
Periplasm	87	63
Cytoplasm	12	16
Membrane	0	0

SOURCE: Reproduced from Reference 10. Copyright 2005, The Society for General Microbiology.

Downloaded by PENNSYLVANIA STATE UNIV on August 9, 2012 | http://pubs.acs.org
Publication Date: September 23, 2006 | doi: 10.1021/bk-2006-0939.ch022

Gene Structure of PVA-Degradative Operon in Strain 113P3

Based on the N-terminal and internal amino acid sequences of OPH, nested PCR with degenerate primers was performed and a fragment of 500 bp was amplified. The region surrounding *oph* was amplified by inverse PCR. A further downstream region was cloned by colony hybridization. Thus, a DNA sequence (3827 bp) containing three ORFs, encoding OPH (*oph*), PVADH (*pvaA*) and a putative cytochrome *c* (*cytC*) was obtained (Figure 9). The ORF of *oph* consisted of 1095 bp corresponding to 364 amino acid residues, encoding a signal peptide and a mature protein of 34 and 330 amino acids residues, respectively. The deduced amino acid sequence was in accordance with the N-terminal and internal amino acid sequences of the purified OPH. The presence of a serine-hydrolase motif (a lipase box; Gly-X-Ser-X-Gly) strongly suggested that the enzyme belongs to the serine-hydrolase family. The putative amino acid sequence of *oph* exhibited homology to OPH from *Pseudomonas* sp. strain VM15C (63% identity) and the polyhydroxybutyrate (PHB) depolymerases from *Mesorhizobium loti*, *Rhizobium* sp., and *Sinorhizobium meliloti* (29-32% identity). The gene was overexpressed in cell-free extracts of *E. coli* but the protein formed inclusion bodies. The molecular weight of the recombinant protein was approximately 35 kDa, corresponding to the same size as that of the purified OPH. The recombinant enzyme did not exhibit any activity toward

Downloaded by PENNSYLVANIA STATE UNIV on August 9, 2012 | http://pubs.acs.org
Publication Date: September 23, 2006 | doi: 10.1021/bk-2006-0939.ch022

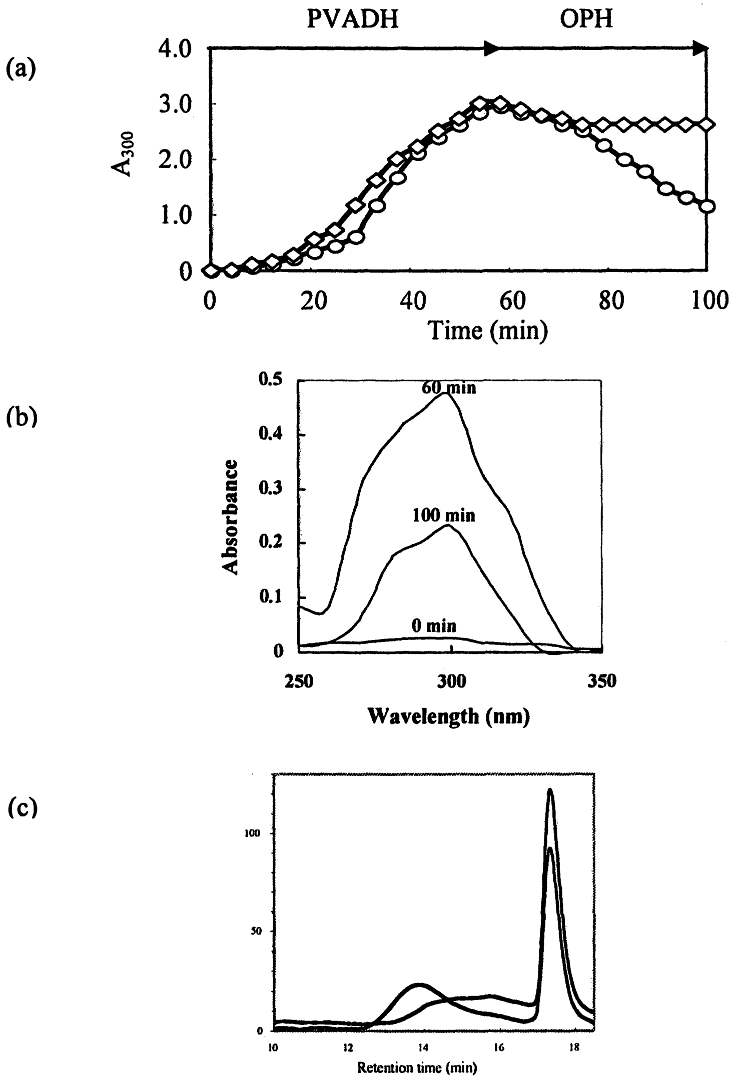

Figure 8. In vivo degradation of PVA by PVADH and OPH from Sphingomonas sp. strain 113P3. (a) Spectrophotometric analysis of oxidized PVA formation and hydrolysis. Open circle, in the presence of OPH, and open diamond, in the absence of OPH. (b) Absorption spectra of oxidized PVA formed in the reaction mixture. (c) HPLC analysis of molecular shift by hydrolysis of oxidized PVA; solid line, oxidized PVA; dashed line, hydrolyzed oxidized PVA. (Reproduced from reference 10. Copyright 2005 The Society for General Microbiology.)

PNPA or oxidized PVA but its N-terminal amino acid sequence was the same as the purified OPH. In the downstream region of *oph*, *pvaA* was located. The putative amino acid sequence of the gene exhibited homology with PVADH from strain VM15C (53% identity). As *oph* and *pvaA* are located in tandem and little space was found between them, both genes must be expressed polycistronically. Furthermore, a putative cytochrome *c* gene located downstream of *pvaA* was found, suggesting a PVADH-cytochrome complex. These three genes possibly compose the major part of a *pva* operon.

PHB depolymerases share common structural domains conserved in the group as a whole: in the N-terminus, the signal peptide, and the catalytic domain including the lipase box, threonine-rich region and the substrate-binding site. The primary structure of the catalytic domain of PHB polymerases conserved an oxyanion hole (histidine) and a triad of three amino acids residues (serine, aspartate and histidine), which is conserved among the serine proteases. These structures are putatively conserved in the OPHs as well (Figure 10), although further work still remains to analyze the catalytic residues. It may be possible that PHB depolymerases act on oxidized PVA, a topic which is currently under investigation.

Downloaded by PENNSYLVANIA STATE UNIV on August 9, 2012 | http://pubs.acs.org
Publication Date: September 23, 2006 | doi: 10.1021/bk-2006-0939.ch022

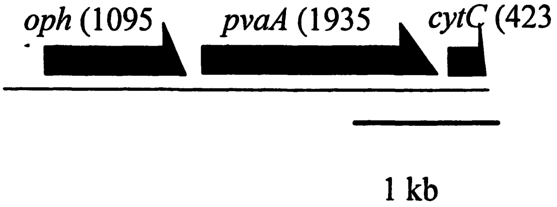

Figure 9. Gene organization of the cloned regions including oph, PVADH gene (pvaA) and a putative cytochrome c gene (cytC). (Reproduced from reference 10. Copyright 2005 The Society for General Microbiology.)

Discussion

The PEG-degradative gene cluster including 10 genes from *S. macrogoltabidus* strain 103 was sequenced. Except for the putative transposase genes located at both ends of the cloned sequence, all six genes were expressed in the presence of PEG, suggesting that these genes are related to the metabolism of PEG (designated as *peg* operon). The *peg* operons were highly conserved among three PEG-utilizing sphingomonads. Whether the upstream and downstream regions of the *peg* operon are conserved as well as the *peg* operon

Downloaded by PENNSYLVANIA STATE UNIV on August 9, 2012 | http://pubs.acs.org
Publication Date: September 23, 2006 | doi: 10.1021/bk-2006-0939.ch022

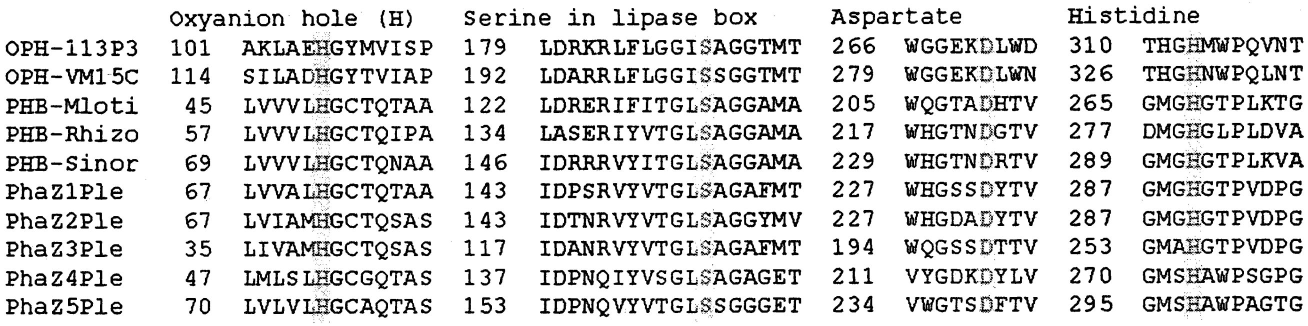

	Oxyanion hole (H)		Serine in lipase box		Aspartate		Histidine	
OPH-113P3	101	AKLAEHGYMVISP	179	LDRKRLFLGGISAGGTMT	266	WGGEKDLWD	310	THGHMWPQVNT
OPH-VM15C	114	SILADHGYTVIAP	192	LDARRLFLGGISSGGTMT	279	WGGEKDLWN	326	THGHNWPQLNT
PHB-Mloti	45	LVVVLHGCTQTAA	122	LDRERIFITGLSAGGAMA	205	WQGTADHTV	265	GMGHGTPLKTG
PHB-Rhizo	57	LVVVLHGCTQIPA	134	LASERIYVTGLSAGGAMA	217	WHGTNDGTV	277	DMGHGLPLDVA
PHB-Sinor	69	LVVVLHGCTQNAA	146	IDRRRVYITGLSAGGAMA	229	WHGTNDRTV	289	GMGHGTPLKVA
PhaZ1Ple	67	LVVALHGCTQTAA	143	IDPSRVYVTGLSAGAFMT	227	WHGSSDYTV	287	GMGHGTPVDPG
PhaZ2Ple	67	LVIAMHGCTQSAS	143	IDTNRVYVTGLSAGGYMV	227	WHGDADYTV	287	GMGHGTPVDPG
PhaZ3Ple	35	LIVAMHGCTQSAS	117	IDANRVYVTGLSAGAFMT	194	WQGSSDTTV	253	GMAHGTPVDPG
PhaZ4Ple	47	LMLSLHGCGQTAS	137	IDPNQIYVSGLSAGAGET	211	VYGDKDYLV	270	GMSHAWPSGPG
PhaZ5Ple	70	LVLVLHGCAQTAS	153	IDPNQVYVTGLSSGGGET	234	VWGTSDFTV	295	GMSHAWPAGTG

Figure 10. Alignment of the deduced amino acid sequences of OPHs from Sphingomonas sp. strain 113P3 and Pseudomonas sp. stain VM15C with PHB depolymerases (13,14). OPH-113P3, OPH from strain 113P3; OPH-VM15C, OPH from strain VM15C; PHB-Mloti, PHB depolymerase from Mesorhizobium loti; PHB-Rhizo, PHB depolymerase from Rhizobium sp.; PHB-Sinor, PHB depolymerase from Sinorhizobium meliloti strain 1021; PhaZ1Ple to PhaZ5Ple, PHB depolymerases from Pseudomonas lemoignei. The regions surrounding the putative active sites are aligned. The amino acids serine (S), aspartate (D), and histidine (H) of the catalytic triad and the putative oxyanion hole are shaded (Reproduced from reference10. Copyright 2005 The Society for General Microbiology.)

and involved in PEG degradation still remains to be elucidated, but the conserved *peg* operon beyond species barrier indicates the horizontal transfer of the gene cluster over different species. Although PEGDH, PEGALDH and PEGCaDH were suggested as metabolic enzymes, a putative acyl-CoA ligase gene was strongly expressed, suggesting that this gene might be involved in the metabolism as a new possible step or another pathway. The roles of the TonB-dependent receptor, permease and AraC-type transcription regulator still remain to be clarified: they might suggest a special transport system for PEG and regulation of the *peg* operon.

PEGDH belongs to a GMC group of flavoprotein oxidoreductases, and its reaction mechanism was well characterized by 3D modeling based on glucose oxidase (unpublished data). PEGALDH is the first nicotinoprotein aldehyde dehydrogenase possessing a tightly bound NADP, keeping high similarity with general NAD (P)-dependent ALDHs. OPH was purified for the first time and characterized to show that the enzyme was a serine hydrolase. The amino acid sequence of the recombinant OPH also indicated a lipase box unique to a serine hydrolase and suggested similarity with PHB depolymerases. This finding suggests that OPH, PHB depolymerases and serine hydrolases have a common origin. It appears that nature has adapted already existing enzymes to xenobiotic polymers within a short period of time, at most a few decades since their production began.

To date, many biochemical and molecular biological studies have been performed on the degradation of polymers, natural or synthetic. Our work, however, is unique in that we aim to clarify not only the enzymes and genes involved in degradation, but also the regulation of genes by macromolecules (non-penetrable into cells). We also aim to clarify how and where macromolecules are degraded to enter the central metabolic pathway.

Acknowledgments. We are grateful for financial support from JSPS, the Oohara Foundation, and the Yakumo Foundation for Environmental Science and the Wesco Scientific Promotion Foundation. We would like to thank our many collaborators for their efforts throughout this work. We are thankful to publishers for giving us the copyright use permissions and KN International (http://www.kninter.com) for editing the paper.

References

1. Kawai, F. In *Advances in Biochemical Engineering/Biotechnology*; Fiechter, A., Ed.; Springer-Verlag: Heidelberg, Germany, 1995; Vol. 52, pp.151-194.
2. Kawai, F. In *Biopolymers*; Matsumura, S.; Steinbüchel, A., Eds.; Wiley-VCH: Weinheim, Germany, 2003; Vol. 9, pp.267-298.

Downloaded by PENNSYLVANIA STATE UNIV on August 9, 2012 | http://pubs.acs.org
Publication Date: September 23, 2006 | doi: 10.1021/bk-2006-0939.ch022

3. Matsumura, S. In *Biopolymers*; Matsumura, S.; Steinbüchel, A., Eds.; Wiley-VCH: Weinheim, Germany, 2003; Vol. 9, pp.329-362.
4. Takeuchi, M.; Kawai, F.; Shimada, Y.; Yokota, A. *Syst. Appl. Microbiol.* **1993**, *16*, 227-238.
5. Sugimoto, M.; Tanabe, M.; Hataya, S.; Enokibara, S.; Duine, J. A.; Kawai, F. *J. Bacteriol.* **2001**, *183*, 6694-6698.
6. Tani, A, et al. *J. Bacteriol.* Submitted for publication.
7. Kawai, F.; Yamanaka, H. *J. Ferment. Bioeng.* **1989**, *67*, 300-302.
8. Ohta, T.; Tani, A.; Kimbara, K.; Kawai, F. *Appl. Microbiol. Biotechnol.* **2005**, *68,*639-646
9. Hatanaka, T.; Asahi, N.; Tsuji, M. *Biosci. Biotech. Biochem.* **1995**, *59*, 1813-1816.
10. Klomklang, W.; Tani, A.; Kimbara, K.; Mamoto, R.; Ueda, T.; Shimao, M.; Kawai, F. *Microbiology* **2005**, *151*, 255-1262.
11. Silverstein, R. M.; Basier, G. C.; Morrill, T. C. In *Spectrometric identification of organic compounds*; Ed.; Wiley-VCH: New York, NY, 1991.
12. Shimao, M.; Tamogami, T.; Kishida, S.; Harayama, S. *Microbiology* **2000**, *146*, 649-657.
13. Jendrosseck, D; Backhaus, M; Andermann, M. *Can. J. Microbiol.* **1995**, *41*, 160-169.
14. Jendrosseck, D; Frisse, A; Behrens, A; Andermann, M; Kratzin, H.D.; Stanislawski, T.; Schlegel, H. G. *J. Bacteriol.* **1995**, *177*, 596-607.

Downloaded by PENNSYLVANIA STATE UNIV on August 9, 2012 | http://pubs.acs.org
Publication Date: September 23, 2006 | doi: 10.1021/bk-2006-0939.ch022

Downloaded by STANFORD UNIV GREEN LIBR on August 10, 2012 | http://pubs.acs.org
Publication Date: September 23, 2006 | doi: 10.1021/bk-2006-0939.ch023

Chapter 23

Factors Controlling the Rate of Photodegradation in Polymers

Bevin C. Daglen and David R. Tyler*

Department of Chemistry, University of Oregon, Eugene, OR 97403

The effects of the glass transition temperature and of radical trap concentration on the quantum yields of polymer photochemical degradation were studied. Special polymers with metal-metal bonded units incorporated into the polymer backbone were synthesized in order to investigate these effects because these polymers photodegrade in a relatively straightforward reaction involving metal-metal bond photolysis without complicating side-reactions. Using these polymers, it was shown that when polymers are irradiated above their glass transition temperatures (T_g) their quantum yields of degradation are similar to their quantum yields in solution. When irradiated below their glass transition temperatures, the photochemical degradation reactions are much less efficient. When irradiation takes place above the glass transition temperature there is no dependence of the quantum yields on the radical trap concentration. However, when irradiation occurs below the glass transition temperature, the quantum yields are dependent on the concentration of radical trap. These results are explained in terms of polymer chain mobility. It is suggested that, when irradiation takes place above T_g, chain mobility is facile enough that a metal-radical trap is encountered before metal radical - metal radical coupling occurs. In contrast, when irradiation takes place below T_g, chain mobility is limited and metal radical - metal radical coupling occurs in many instances before a metal radical encounters a trap. Chain mobility also explains the affect of radical trap concentration on the efficiency of photodegradation. When the irradiation takes place above T_g,

In Degradable Polymers and Materials; Khemani, K., et al.;
ACS Symposium Series; American Chemical Society: Washington, DC, 2006.

the reaction of the metal radicals with radical traps is kinetically saturated with trap at the concentrations of trap used in these experiments. In contrast, when irradiation occurs below the glass transition temperature then, because of limited chain mobility, the reaction kinetics are not saturated in trap concentration and the quantum yields are dependent on the concentration of radical trap.

Downloaded by STANFORD UNIV GREEN LIBR on August 10, 2012 | http://pubs.acs.org
Publication Date: September 23, 2006 | doi: 10.1021/bk-2006-0939.ch023

Introduction

Considerable research is being devoted to devising new photodegradable polymers with improved performance because there are compelling economic and social reasons for using degradable plastics in certain applications (*1-4*). The biggest use for photodegradable plastics is in agriculture, specifically in the burgeoning subdiscipline called plasticulture. In plasticulture, the ground is covered with plastic sheeting (typically a polyolefin), which acts as a mulch to prevent the growth of weeds (thus requiring the use of fewer herbicides), to decrease water demand, and to extend the growing season by keeping the ground warmer. By making these agricultural films out of degradable plastics, considerable labor and money can be saved in the plastics recovery phase of the technique. In the environmental area, photodegradable plastics are finding increased use as packaging materials in items that have a high probability of becoming litter. The idea is that if such materials should end up as litter they will degrade rather quickly and not be an eyesore.

There are two basic methods for making polymer materials photochemically degradable (*2,3*). One method is to chemically incorporate a chromophore into the polymer chains. Although numerous chromophores have been evaluated, the most commercially successful chromophore is the carbonyl group (*2,3,5*). Absorption of UV radiation leads to degradation by the Norrish Type I and II processes or by an atom abstraction process (Scheme 1), all of which are typical photoreactions of the carbonyl chromophore. Note that once radicals are introduced into the system, chain degradation can occur by the autooxidation mechanism (Scheme 2).

The second general method for making polymer materials photochemically degradable is to mix a radical initiator into the polymer. Once carbon-based radicals have formed, the chains degrade by the autooxidation cycle (Scheme 2). Numerous radical initiators have been investigated, and a partial list includes metal oxides (e.g., TiO_2, ZnO, CuO), metal chlorides (e.g., LiCl, $FeCl_3$), $M(acac)_n$ complexes, $M(stearate)_n$ complexes, benzophenone, quinones, and peroxides (*2,3*).

Downloaded by STANFORD UNIV GREEN LIBR on August 10, 2012 | http://pubs.acs.org
Publication Date: September 23, 2006 | doi: 10.1021/bk-2006-0939.ch023

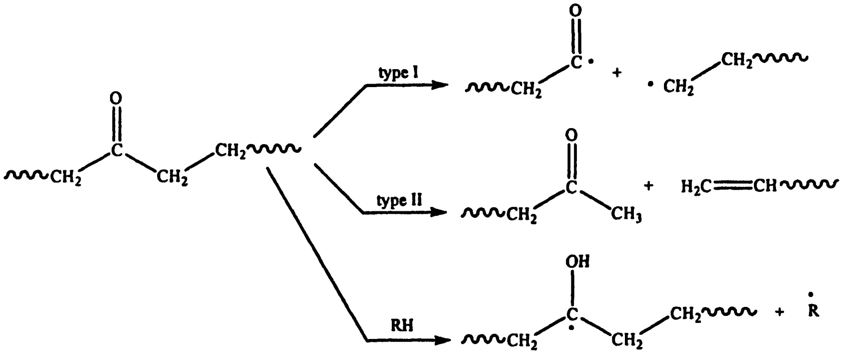

Scheme 1. Photochemical Degradation Pathways for Polymers Containing Carbonyl Groups

Initiation

$\text{Initiator} \longrightarrow R_i\bullet$

$R_i\bullet + O_2 \longrightarrow R_iOO\bullet$

$R_iOO\bullet + R{-}H \longrightarrow R_iOOH + R\bullet$

Propagation

$R\bullet + O_2 \longrightarrow ROO\bullet$

$ROO\bullet + R{-}H \longrightarrow R_iOOH + R\bullet$

Termination

various radical-radical coupling or
disproportionation reactions

Scheme 2. The Autooxidation Mechanism for Hydrocarbon Materials

Downloaded by STANFORD UNIV GREEN LIBR on August 10, 2012 | http://pubs.acs.org
Publication Date: September 23, 2006 | doi: 10.1021/bk-2006-0939.ch023

The ideal photodegradable polymer has (at least) three ideal properties. First, the onset of degradation should be reliably predictable. Although it is obvious why this property is desirable for practical applications, it is noted that it is difficult to predict polymer lifetimes in practice because light intensities vary, as do temperatures and a host of other mechanistic variables that control degradation rates and degradation onsets. Second, the onset of degradation should be tunable. Photodegradable polymers have different applications and each application will generally require different polymer lifetimes. Methods must be found for manipulating polymer lifetimes. Third, the polymer should degrade completely and quickly once degradation starts. This characteristic is important for practical reasons because most polymer mechanical properties are related to molecular weight (*6*). Small amounts of degradation can drastically decrease the molecular weight (and thus mechanical properties) of a plastic, yet to all appearances the plastic piece is visually unchanged. In essence, the plastic is still present but it is not structurally sound – and hence useless and perhaps dangerous. Under such circumstances, it may as well be completely degraded.

In order to predict polymer lifetimes, to control when a polymer starts to degrade, and to control the rate of degradation, it is necessary to identify the experimental parameters that affect polymer degradation rates and to understand how these parameters affect degradation. Among the parameters that have been identified as affecting polymer lifetime are temperature, exposure to ultraviolet radiation, light intensity and wavelength, oxygen diffusion rates in the polymer, tensile stress, compressive stress, chromophore concentration, molecular weight, humidity, and polymer morphology (*2-4,7*). In this manuscript, we add to this list by reporting that the glass transition temperature and the radical trap concentration also affect polymer photodegradation rates.

Results and Discussion

Experimental Approach to the Problem

Several challenging experimental problems hinder the rigorous experimental mechanistic exploration of polymer photodegradation. One of the difficulties is that polymer degradations are mechanistically complicated (*8*). This is not to say that the mechanisms are not understood; in fact, they are understood in detail (*8*). Rather, the mechanisms are intricate, often involving multiple steps, cross-linking, and side-reactions; this makes pinpointing the effects of stress difficult. Another complication is that oxygen diffusion is the rate-limiting step in photooxidative degradations, the primary degradation mechanism in most polymers (*9,10*). This can add to the intricacy of the kinetics analysis because cracks and fissures develop in the polymer as

Downloaded by STANFORD UNIV GREEN LIBR on August 10, 2012 | http://pubs.acs.org
Publication Date: September 23, 2006 | doi: 10.1021/bk-2006-0939.ch023

degradation proceeds; these fractures provide pathways for direct contact of the polymers with oxygen, which will then no longer degrade at a rate controlled by oxygen diffusion. To circumvent these experimental and mechanistic complexities and therefore make it less difficult to interpret data and obtain fundamental insights, we use three key experimental strategies in our investigations. First, we study the problem using special photodegradable polymers of our own design that contain metal-metal bonds along the backbone (*11-16*). These polymers are photodegradable because the metal-metal bonds can be cleaved with visible light (eq 1) and the resulting metal radicals captured with an appropriate radical trap, typically an organic halide or molecular oxygen; Scheme 3 (*17,18*).

$$
\begin{gathered}
L_nM-ML_n \xrightarrow{h\nu} L_nM\bullet + \bullet ML_n \\
\bullet ML_n = CpMo(CO)_3\ (Cp = \eta^5-C_5H_5), CpW(CO)_3, \\
Mn(CO)_5, Re(CO)_5, CpFe(CO)_2
\end{gathered}
\qquad (1)
$$

By studying these "model" systems, we are able to extract information without the mechanistic complications inherent in the degradation mechanisms of organic radicals. (For example, metal radicals do not lead to crosslinking, so we can avoid this complicating feature found with organic radicals.) The second key experimental strategy is to use polymers that have built-in radical traps, namely C-Cl bonds (*19,20*). By eliminating the need for external oxygen to act as a trap, we excluded the complicating kinetic features of rate limiting oxygen diffusion. The third experimental strategy is to use the distinctive M-M bond chromophore to spectroscopically monitor the photodegradation reactions of the polymers. This allows us to compare the efficiencies of the photodegradations by measuring the quantum yields of the reactions. (The quantum yield, Φ, is defined as the rate of a photoreaction divided by the absorbed light intensity; i.e., Φ = rate/absorbed intensity.) The use of quantum yields to quantify and compare the various degradation rates is a crucial advance because polymer degradation reactions have typically been monitored by stress testing, molecular weight measurements, or attenuated total reflection (ATR) spectroscopy (*21*), all of which can be laborious and time consuming. Relative to these techniques, quantum yield measurements are straightforward. (Note that quantum yields in regular carbon-chain polymers cannot be measured conveniently by UV-vis spectroscopy because there are generally no suitable chromophores.) To further expedite our quantum yield measurements, we use a computerized apparatus that automatically measures the quantum yields on thin film polymer samples (*22*).

Downloaded by STANFORD UNIV GREEN LIBR on August 10, 2012 | http://pubs.acs.org
Publication Date: September 23, 2006 | doi: 10.1021/bk-2006-0939.ch023

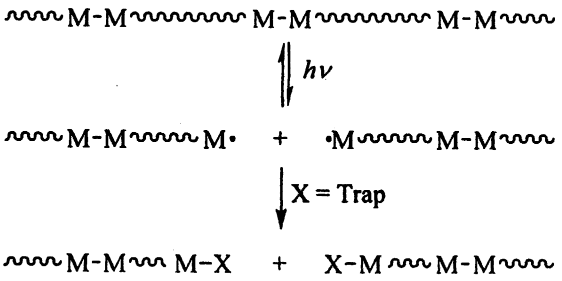

Scheme 3. Photochemical reaction of a polymer with metal-metal bonds along its backbone.

Polymer synthesis strategy

Our general synthetic route for incorporating metal-metal bonds into polymer backbones is based on the step polymerization techniques for incorporating ferrocene into polymer backbones (*6,23-28*). Step polymers of ferrocene can be made by substituting the cyclopentadienyl (Cp) rings with appropriate functional groups, followed by reaction with appropriate difunctional organic monomers (e.g., eq 2) (*29-31*).

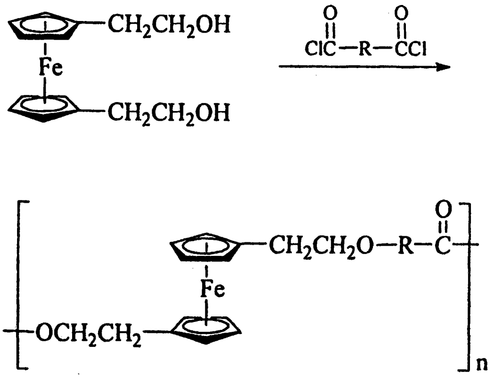

(2)

The analogous strategy for synthesizing metal-metal bond-containing polymers also uses difunctional, cyclopentadienyl-substituted metal dimers. A sample polymerization reaction is shown in eq 3, which illustrates the reaction of a metal-metal bonded "diol" with hexamethylene diisocyanate (HMDI) to form a polyurethane (*13*). This step polymerization strategy is quite general, and a number of metal-metal bond-containing polymers have been made from monomers containing functionalized Cp ligands (*11,32*).

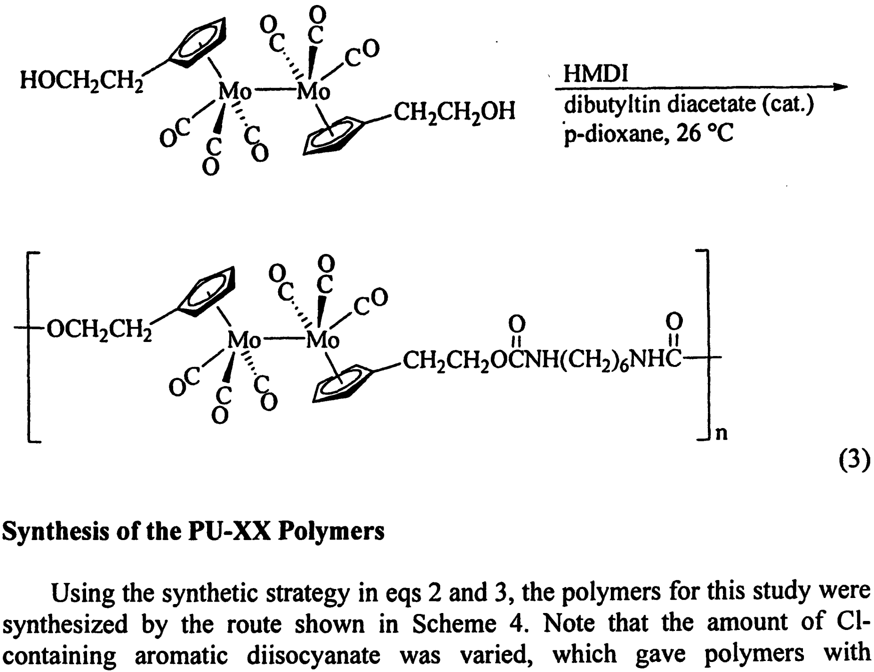

(3)

Synthesis of the PU-XX Polymers

Using the synthetic strategy in eqs 2 and 3, the polymers for this study were synthesized by the route shown in Scheme 4. Note that the amount of Cl-containing aromatic diisocyanate was varied, which gave polymers with different glass transition temperatures as well as polymers that have different metal-radical trap to metal atom ratios. For example, PU-90 has a T_g of 35 °C and a 9:1 [C-Cl]:[Mo] ratio, and PU-70 has a T_g of -44 °C and a 7:1 [C-Cl]:[Mo] ratio. (The XX number in the PU-XX nomenclature indicates the mole fraction of aromatic diisocyanate in the overall amount of diisocyanate used in the formulation.)

Photodegradation Occurs in the Absence of O_2.

As expected, polymers containing C-Cl bonds photochemically degraded in the absence of oxygen. Spectroscopic monitoring of the reactions showed the disappearance of the $Cp_2Mo_2(CO)_6$ chromophore (λ_{max} = 390 and 510 nm;

Downloaded by STANFORD UNIV GREEN LIBR on August 10, 2012 | http://pubs.acs.org
Publication Date: September 23, 2006 | doi: 10.1021/bk-2006-0939.ch023

Downloaded by STANFORD UNIV GREEN LIBR on August 10, 2012 | http://pubs.acs.org
Publication Date: September 23, 2006 | doi: 10.1021/bk-2006-0939.ch023

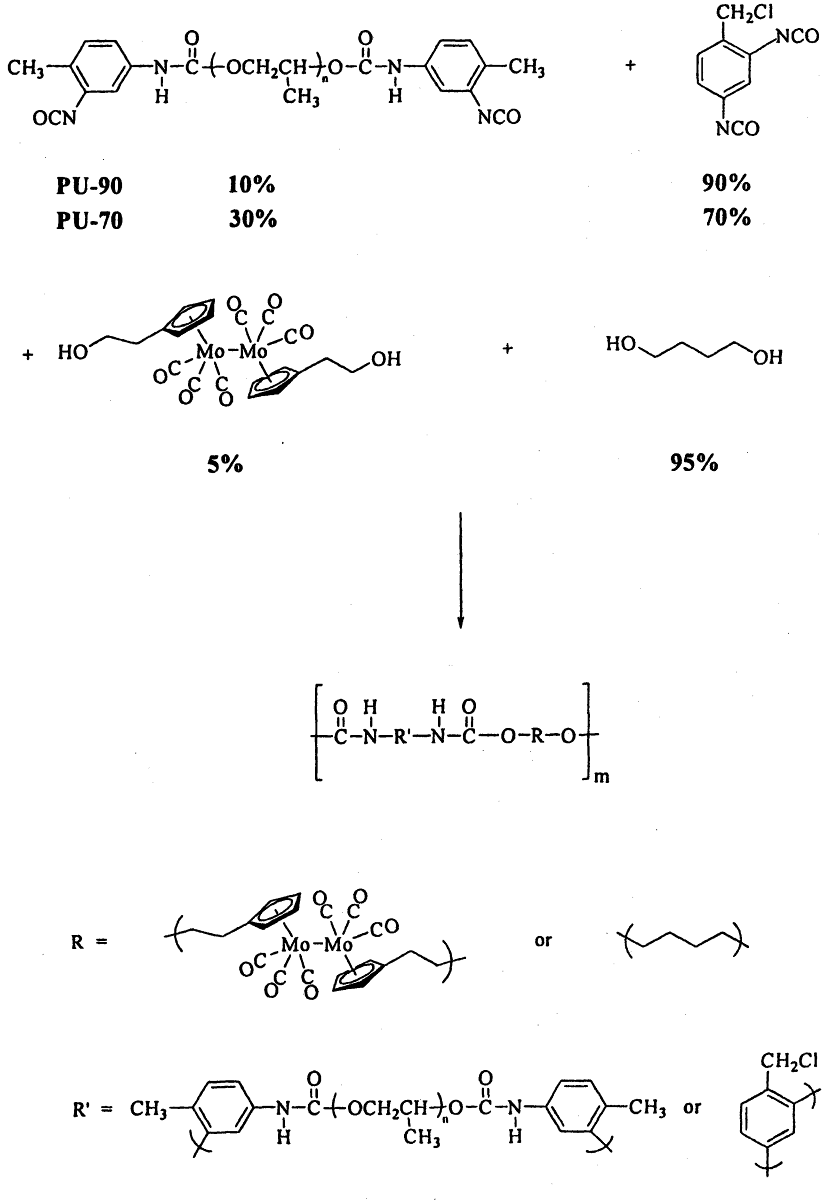
PU-90
PU-70
10%
30%
90%
70%
+
5%
95%
R =
or
R' =
or
CH₂Cl
NCO
OCN
HO
OH
Mo
m

Scheme 4. Synthesis of the PU-XX polymers.

$\nu(C \equiv O)$ 2009, 1952, and 1913 cm^{-1}) and the appearance of the $CpMo(CO)_3Cl$ unit ($\nu(C \equiv O)$ = 1967 and 2048 cm^{-1}). In addition, the number average molecular weight decreased steadily during the course of the reaction. The reaction in Scheme 5 is suggested.

Effect of T_g on the Efficiency of Photodegradation.

The quantum yields for PU-90 and PU-70 at 26 °C are shown in Table I. In addition, the quantum yields for PVC-Mo_2 and PVC-Mo_2 plasticized with DOP (20 %) are shown. PVC-Mo_2 is poly(vinylchloride) with $Cp_2Mo_2(CO)_6$ units along the backbone shown below.

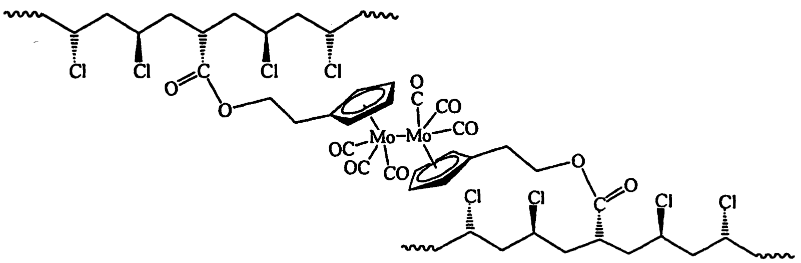

The quantum yields were measured at 26 °C. Note in the table that the quantum yields are 0.35 for the two polymers with $T_g < 26$ °C, while the two polymers with $T_g > 26$ °C have considerably smaller quantum yields of degradation.

The quantum yields for the polymers with $T_g < 26$ °C are close to the quantum yields for model complexes (e.g., $\phi = 0.43$ for model complex **1** at 0.38 cP; eq 4). This result suggests that, when the irradiation takes place above T_g, chain mobility is facile enough that a metal-radical trap (i.e., a C-Cl bond) is encountered before metal-radical–metal-radical coupling occurs. In contrast, when irradiation takes place below T_g, chain mobility is limited and metal-radical–metal-radical recombination occurs in many instances before a metal-radical encounters a C-Cl bond. The quantum yields above T_g are similar to those in solution because, in solution, chain mobility is quite facile and radical traps are readily encountered.

Downloaded by STANFORD UNIV GREEN LIBR on August 10, 2012 | http://pubs.acs.org
Publication Date: September 23, 2006 | doi: 10.1021/bk-2006-0939.ch023

Downloaded by STANFORD UNIV GREEN LIBR on August 10, 2012 | http://pubs.acs.org
Publication Date: September 23, 2006 | doi: 10.1021/bk-2006-0939.ch023

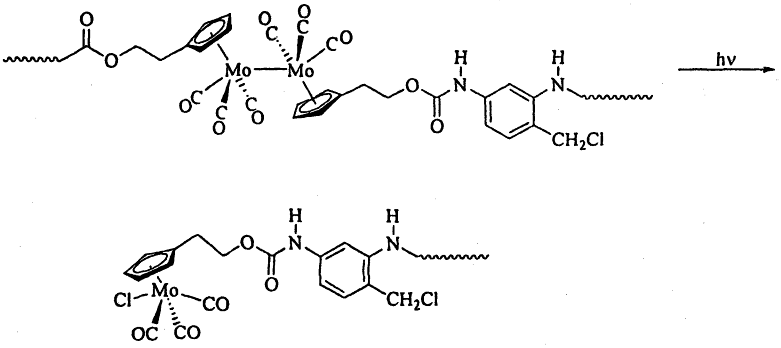

Scheme 5. Photochemical reaction of the PU-XX polymers.

Table I. Quantum yields for various polymers with different glass transition temperatures and for a model complex.

Polymer	T_g *(°C)*	*Quantum Yield (ϕ) at 26 °C*
PVC-Mo_2	75	0.15 ± 0.03
PU-90	35	0.05 ± 0.02
PU-70	-44	0.35 ± 0.04
PVC+DOP	<< RT	0.35 ± 0.07
model complex **1**	solution phase	0.43 ± 0.03

Downloaded by STANFORD UNIV GREEN LIBR on August 10, 2012 | http://pubs.acs.org
Publication Date: September 23, 2006 | doi: 10.1021/bk-2006-0939.ch023

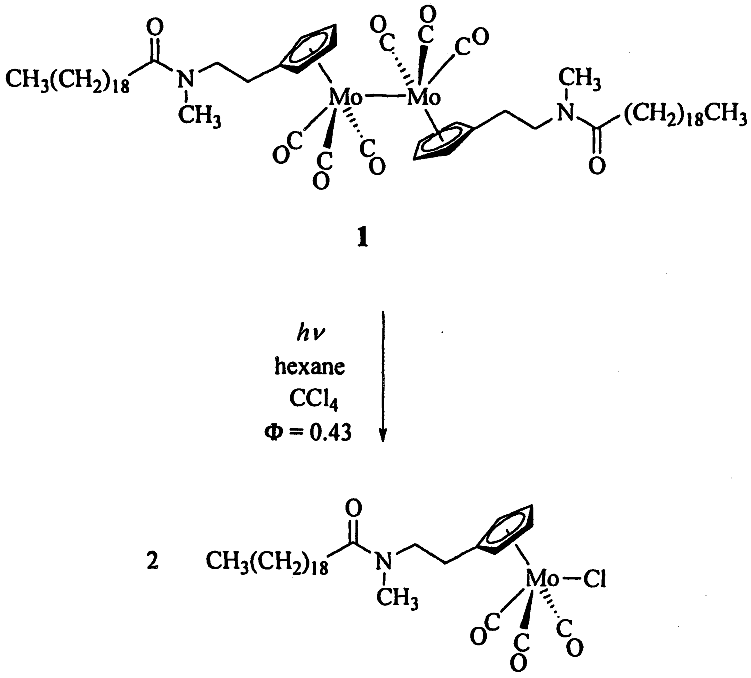

(4)

The Effect of Trap Concentration

The effect of radical trap concentration on the quantum yields of polymer degradation was studied using the polymers PU-35, PU-50, PU-60, PU-70, and PU-90. The results are shown in Table II and can be summarized as follows: If $T_g < T_{irradiation}$ then the quantum yield (ϕ) is independent of trap concentration. Thus, $\phi = 0.35$ for PU-35, PU-50, PU-60, and PU-70. In contrast, if $T_g > T_{irradiation}$ then the quantum yield is dependent on trap concentration. Thus, $\phi = 0.05$ for PU-90 ($T_g = 35$ °C) under an N_2 atmosphere but $\phi = 0.10$ for PU-90 under an O_2 atmosphere. (The O_2 is a radical trap so the experiment under an O_2 atmosphere has a larger concentration of radical trap.) The explanation for these observations again lies in chain mobility. When the irradiation takes place above T_g then the radical chain ends are relatively mobile, and the reaction of the metal radicals with radical traps is kinetically saturated with trap at the concentrations of trap used in these experiments. In contrast, when irradiation occurs below the glass transition temperature then, because of limited chain mobility, the reaction kinetics are not saturated in trap concentration and the quantum yields are dependent on the concentration of radical trap.

Table II. Quantum yields for polymer degradation for polymers with different concentrations of metal-radical trap.

Polymer (N_2 or O_2 atmosphere)	*T_g (°C)*	*Quantum Yield (ϕ) at 26 °C*
PU-35 (N_2)	-47	0.35 ± 0.04
PU-50 (N_2)	-46	0.35 ± 0.01
PU-60 (N_2)	-46	0.35 ± 0.02
PU-70 (N_2)	-44	0.35 ± 0.04
PU-90 (N_2)	35	0.05 ± 0.02
PU-90 (O_2)	35	0.10 ± 0.03

Summary and Conclusions

The photochemical reactivity of polymers is of considerable interest because photodegradable plastics have a number of applications. Additional interest in polymer photoreactivity stems from the need to limit and control "weathering" in polymer materials. Photodegradation is an important component of polymer weather, and a proper understanding of degradation processes and of the experimental factors that affect degradation is necessary for the accurate estimation of polymer lifetime and for the development of stabilizing systems.

Among the experimental parameters that have been shown to affect polymer degradation rates are light intensity, temperature, oxygen diffusion, chromophore concentration, polymer morphology and stress. This study added two more experimental parameter to this list, namely the glass transition temperature and the concentration of radical trap. To investigate the effects of T_g and trap concentration on degradation efficiencies, specially designed polymers with metal-metal bonds along their backbones were synthesized. These polymers degrade by a straightforward mechanism that makes it possible to extract meaningful information. Using these polymers, it was shown that when polymers are irradiated above their glass transition temperatures their quantum yields of degradation are similar to their quantum yields in solution. When irradiated below their glass transition temperatures, the quantum yields of photodegradation are small, i.e., the degradations are inefficient. The explanation suggested is that when the irradiation takes place above T_g, chain mobility is facile enough that a metal-radical trap is encountered before radical-

Downloaded by STANFORD UNIV GREEN LIBR on August 10, 2012 | http://pubs.acs.org
Publication Date: September 23, 2006 | doi: 10.1021/bk-2006-0939.ch023

radical recombination occurs. In contrast, when irradiation takes place below T_g, chain mobility is limited and metal-radical–metal-radical recombination occurs in many instances before a metal-radical encounters a trap. The quantum yields above T_g are similar to those in solution because, in solution, chain mobility is facile and radical traps are readily encountered. Chain mobility also explains the affect of radical trap concentration on the efficiency of photodegradation. When the irradiation takes place above T_g then the radical chain ends are relatively mobile, and the reaction of the metal radicals with radical traps is kinetically saturated with trap at the concentrations of trap used in these experiments. In contrast, when irradiation occurs below the glass transition temperature then, because of limited chain mobility, the reaction kinetics are not saturated in trap concentration and the quantum yields are dependent on the concentration of radical trap.

Downloaded by STANFORD UNIV GREEN LIBR on August 10, 2012 | http://pubs.acs.org
Publication Date: September 23, 2006 | doi: 10.1021/bk-2006-0939.ch023

Acknowledgments

Acknowledgment is made to the National Science Foundation (DMR-0096606), to the NSF GK-12 grant to the University of Oregon, and to the Petroleum Research Fund, administered by the American Chemical Society, for the support of this research.

References

1. Guillet, J. E. In *Degradable Materials*; Barenberg, S. A., Brash, J. G., Narayan, R., Redpath, A. E., Eds.; CRC Press: Boston, 1990, p 55-97.
2. Grassie, N.; Scott, G. *Polymer Degradation and Stabilization*; Cambridge University Press: New York, 1985.
3. Guillet, J. *Polymer Photophysics and Photochemistry: An Introduction to the Study of Photoprocesses in Macromolecules*; Cambridge University Press: New York, 1985.
4. Hamid, S. H.; Editor *Handbook of Polymer Degradation: Second Edition, Revised and Expanded. [In: Environ. Sci. Pollut. Control Ser., 2000; 21]*, 2000.
5. Hocking, P. J. *J. Macromol. Sci., Rev. Macromol. Chem. Phys.* **1992**, *C32*, 35-54.
6. Pittman, C. U., Jr.; Rausch, M. D. *Pure Appl. Chem.* **1986**, *58*, 617-22.
7. Rabek, J. F. *Mechanisms of Photophysical Processes and Photochemical Reactions in Polymers*; Wiley: New York, 1987.
8. Geuskens, G. *Compr. Chem. Kinet.* **1975**, *14*, 333-424.
9. Huvet, A.; Philippe, J.; Verdu, J. *Eur. Polym. J.* **1978**, *14*, 709-13.

10. Cunliffe, A. V.; Davis, A. *Polym. Degrad. Stab.* **1982**, *4*, 17-37.
11. Tyler, D. R. *Coord. Chem. Rev.* **2003**, *246*, 291-303.
12. Tenhaeff, S. C.; Tyler, D. R. *Organometallics* **1991**, *10*, 1116-23.
13. Tenhaeff, S. C.; Tyler, D. R. *Organometallics* **1991**, *10*, 473-82.
14. Tenhaeff, S. C.; Tyler, D. R. *Organometallics* **1992**, *11*, 1466-73.
15. Nieckarz, G. F.; Tyler, D. R. *Inorg. Chim. Acta* **1996**, *242*, 303-10.
16. Nieckarz, G. F.; Litty, J. J.; Tyler, D. R. *J. Organomet. Chem.* **1998**, *554*, 19-28.
17. Meyer, T. J.; Caspar, J. V. *Chem. Rev. (Wash., D. C.)* **1985**, *85*, 187-218.
18. Geoffroy, G. L.; Wrighton, M. S. *Organometallic Photochemistry*; Academic Press: New York, 1979.
19. Chen, R.; Yoon, M.; Smalley, A.; Johnson, D. C.; Tyler, D. R. *J. Am. Chem. Soc.* **2004**, *126*, 3054-3055.
20. Chen, R.; Tyler, D. R. *Macromolecules* **2004**, *37*, 5430-5436.
21. Krisyuk, B. E.; Popov, A. A.; Zaikov, G. E. *Vysokomolekulyarnye Soedineniya, Seriya A* **1980**, *22*, 329-34.
22. Male, J. L.; Lindfors, B. E.; Covert, K. J.; Tyler, D. R. *J. Am. Chem. Soc.* **1998**, *120*, 13176-13186.
23. Gonsalves, K.; Zhan-Ru, L.; Rausch, M. D. *J. Am. Chem. Soc.* **1984**, *106*, 3862-3.
24. Gonsalves, K. E.; Lenz, R. W.; Rausch, M. D. *Appl. Organomet. Chem.* **1987**, *1*, 81-93.
25. Knobloch, F. W.; Rauscher, W. H. *J. Polym. Sci.* **1961**, *54*, 651-6.
26. Pittman, C. U., Jr. *J. Polym. Sci., Polym. Chem. Ed.* **1968**, *6*, 1687-95.
27. Gonsalves, K. E.; Rausch, M. D. *J. Polym. Sci., Part A: Polym. Chem.* **1988**, *26*, 2769-75.
28. Patterson, W. J.; McManus, S. P.; Pittman, C. U., Jr. *J. Polym. Sci., Polym. Chem. Ed.* **1974**, *12*, 837-50.
29. Nguyen, P.; Gomez-Elipe, P.; Manners, I. *Chem. Rev. (Wash., D. C.)* **1999**, *99*, 1515-1548.
30. Manners, I. *Adv. Organomet. Chem.* **1995**, *37*, 131-68.
31. Manners, I. *Coord. Chem. Rev.* **1994**, *137*, 109-29.
32. Moran, M.; Pascual, M. C.; Cuadrado, I.; Losada, J. *Organometallics* **1993**, *12*, 811-22.

Downloaded by STANFORD UNIV GREEN LIBR on August 10, 2012 | http://pubs.acs.org
Publication Date: September 23, 2006 | doi: 10.1021/bk-2006-0939.ch023

Chapter 24

Biodegradable Polymers: Are Sources and Structures Important?

Graham Swift[1] and Radu Baciu[2]

[1]GS Polymer Consultants, Chapel Hill, NC 27517,
[2]EPI Environmental Products Inc. Vancouver, BC, Canada

Downloaded by CORNELL UNIV on August 9, 2012 | http://pubs.acs.org
Publication Date: September 23, 2006 | doi: 10.1021/bk-2006-0939.ch024

This general review article is meant to be a constructive critical broad overview of the development of biodegradable polymers for industrial and commercial applications. It draws upon diverse sources of information and publications and from many years of personal experience in all areas of the field of biodegradable polymers. Interest in these polymers began when they were identified as one of several possible solutions to the management of pollution of the environment by discarded synthetic polymeric materials. Plastics used in agricultural films, packaging materials and fast food utensils were and still are widely visible as litter; whereas, water-soluble polymers used in detergents and superabsorbent, for example, were never recognized as pollutants by the layman as they are invisible after use and on disposal. Plastic wastes were, of course, the major focal point with their instant visibility and ready culpability to all. However, water-soluble polymers, which pass unseen into the wastewater streams after use and thence are capable of rapidly pervading the environment, were recognized by scientists in industries that produced and used them as an equally troublesome environmental issue. The approaches and issues surrounding both targets: the development of viable commercial

In Degradable Polymers and Materials; Khemani, K., et al.;
ACS Symposium Series; American Chemical Society: Washington, DC, 2006.

biodegradable polymers to replace existing recalcitrant analogues, were not unalike and are discussed and summarized in this review. Needs and issues that had to be focused and then resolved such as definitions, methods for estimating biodegradability in selected diposal or use environments, and specifications for acceptable performance are identified and critiqued as to how successful and appropriate the current solutions are; and, importantly, what remains to be done to ensure a vibrant successful future commercial reality for these polymers.

Downloaded by CORNELL UNIV on August 9, 2012 | http://pubs.acs.org
Publication Date: September 23, 2006 | doi: 10.1021/bk-2006-0939.ch024

Introduction

Biodegradable polymers were recognized as one response to the developing problem of polymer wastemanagement during the middle of the last century when the severity of the issue became obvious to all. Polymers, particularly those widely used in the fabrication of disposable packaging, utensils in the fast food industry and in agricultural land covers, were a fast developing litter issue and an eyesore to the general public as they scarred the landscape and rapidly filled landfill sites. This was due in large part to their designed longevity and resistance to degradation and biodegradation, but, also, to a cultural laxity towards littering. Water-soluble polymers, designed for one time use as in detergents and superabsorbent polymers for diapers, on the other hand, entered wastewater streams unseen after use and eventually entered streams and permeated water-tables and held the potential for environmental damage as they, too, were developed for their resistance to degradation properties without regard for disposal issues that might develop after use.

Alternative options for disposal of fabricated polymers and plastics included biodegradable analogues of currently used polymers for controlled biodegradation in use sites, such as soil in agriculture, litter sites such as land, oceans and rivers, and selected disposal sites such as compost facilities. Other potential wastemanagement options introduced included recycle, incineration, and landfill. Recycle was considered for recovered plastic either as virgin unused material (factory waste) or collection after use. Virgin plastic recovered from factory waste was easily, and continues to be, recycled in the streams it came from. After use waste requires collection, separation from other plastics and cleaning for re-use as the original plastic, or cleaning and no separation for use in polymer blends. Recovery and reuse of plastics in recycle has issues to be resolved, in addition to those mentioned, including collection and transportation, and these have held up progress and wide adoption of this option. Recycle is also recognized to include recovery of the monomers comprising the polymer and then reusing them to rebuild similar or different polymers. Currently, opportunities are being pursued for condensation polymers through hydrolysis to monomers and recovery; and, also, by thermal cracking of certain addition polymers, acrylics are one example, to monomers.

Incineration of waste is not a currently favored solution to polymer wastemanagement since the combustion of mixed plastics produces, in some cases, toxic gases and leaves residues that may also be toxic and still require careful disposal. An advantage it does have, though, is that the waste plastics are returned to the energy stream, oil, from which their raw materials were diverted. Hence, this approach to wastemanagement may be worth reconsidering as energy prices increase and incineration engineering improves.

Landfilling is regarded as a last and least desirable option as the net result is loss of landfill space and loss of potentially valuable resources.

Water-soluble polymers with few exceptions, such as poly(vinyl alcohol) used in packaging, are difficult to recover after use and present environmental issues that are still not adequately addressed. There have, fortunately, been no serious environmental incidents with traditional water-soluble polymers attributed to their disposal and they still stay below the recognition threshold of the general public. Manufacturers and end users are aware of the potential problem they present and are still working to find acceptable solutions through new polymerization chemistries and polymer compositions.

This general review of biodegradable polymers as a practical approach to wastemanagement of polymers endeavors to cover problem identification and definition; definitions, testing protocols and specifications for environmentally degradable and biodegradable polymers; and chemical approaches for new biodegradable polymers as viable commercial replacements for currently used polymers. Included in this review is a comparison and impact of polymer origins, natural or fossil resources, and polymer types and structures, condensation and addition, and how these have affected developments to date. The evolution of biodegradable polymers is not yet complete, or greatly commercially successful. However, biodegradable polymers are available, growing in volume in the market place and, with the growth of renewable resources to replace declining and increasingly expensive fossil resources as a source for monomers and polymers, the light at the end of the tunnel to wide adoption may just be visible. But, there are issues that still need to be addressed and resolved before we have really cost and performance competitive biodegradable polymers in the market as alternatives to currently used

Downloaded by CORNELL UNIV on August 9, 2012 | http://pubs.acs.org
Publication Date: September 23, 2006 | doi: 10.1021/bk-2006-0939.ch024

commodities based on addition polymers such as polyolefins and polyvinyls, and condensation polymers such as polyesters, and polyamides. These issues will be indicated with the intention of focusing attention and expectation that they will be addressed.

Development of Biodegradable Polymers

Goals

Downloaded by CORNELL UNIV on August 9, 2012 | http://pubs.acs.org
Publication Date: September 23, 2006 | doi: 10.1021/bk-2006-0939.ch024

Development of commercially viable biodegradable polymers, as with other products, must meet certain demands and requirements, not all of which are technical, and these are set by "Gatekeepers" who control issues such as described below:

- Consumers have purchasing power and polymers need to meet their expected cost / performance expectations to be successful.
- Regulatory Authorities set regulations for products and monitor claims for environmental safety (risk) and biodegradation in contact environments on disposal or use such as soil, water, compost, landfill, etc.
- Standards Organizations develop accepted standard definitions for products, standard methodologies for testing products and specifications for their acceptance.
- Polymer Industries determine whether a polymer is to be added to their product lines based on expected profitability.

A major concern in this technical endeavor to develop commercially viable biodegradable polymers which still needs resolution, as will become obvious later, is the differentiation of the terms environmental safety and biodegradation. The terms are related but have been somewhat confused and misunderstood in the rush to develop the wastemanagement of polymers by developing biodegradable polymers. This misunderstanding has lead to limitations in test methodology development and, in turn, to a limit in the creativity of polymer development. Some question that still need to asked, include:

> Are we developing polymers that rapidly biodegrade in the environment or environmentally degradable and biodegradable polymers that are not environmentally toxic?
>
> How do we select the time period for biodegradation in the environment?
>
> How do we measure biodegradation and toxicity in sequential degradation environments, such as compost and then land application?
>
> How can we measure long term toxicity affects on the environment?

Downloaded by CORNELL UNIV on August 9, 2012 | http://pubs.acs.org
Publication Date: September 23, 2006 | doi: 10.1021/bk-2006-0939.ch024

Biodegradation is really a significant factor in establishing environmental safety with regards to the introduction of xenophobic materials into a given environment. The rate of biodegradation certainly relates to environmental accumulation, fast biodegradation signifies slow accumulation and complete biodegradation no accumulation. Hence, as a corollary, low or no environmental risk is associated with fast or complete biodegradation. Conversely, it cannot be claimed that slow biodegradation leads to environmental risk concerns, unless the accumulation is demonstrated to be toxic. It should be noted that natural materials biodegrade at greatly different rates, some are fast and some are very slow, such as lignins, and yet pose no environmental concerns—in fact slow is beneficial in the sense of top soil build and retention of vital elements for plant growth.

Hence, we have reached a critical point where there is a very real need to reassess what we have accomplished, are developing and categorically specifying as biodegradable and, therefore, environmentally acceptable polymers.

> Should we be trying to develop environmentally benign polymers regardless of time to biodegrade in a given environment and, of course standard test methods to confirm acceptance ? An acceptance would mean more work and difficult test methods developments, but the outcome could be very beneficial to everyone.
>
> A clear example of this dilemma will be discussed later when comparing so-called hydrobiodegradable polymers, those with

hydrolysis as a first stage degradation prior to biodegradation, and oxobiodegradable polymers, those with an oxidation as a first stage degradation prior to biodegradation.

Synthetic and Other Approaches to Biodegradable Polymers

The general structural characteristics that facilitate the biodegradation of polymers were defined many years ago in preliminary work using unsophisticated testing protocols which, nevertheless, proved to be adequate for establishing guidelines for future synthesis programs. Indications were that biodegradation was enhanced by characteristics such as linear polymer chain structures, low molecular weight, hydrophilicity, non-crystallinity, heteroatom backbone polymers (condensation polymers) and low levels of functional groups such as amines and carboxylic acids. These guidelines have been widely applied in the development of biodegradable polymers, particularly plastics, which are emerging today. The guidelines are, it should be emphasized, equally applicable to polymers based on fossil or renewable resources.

Polymers from fossil resources are still the staple of the dominant non-biodegradable commercial polymer industry in the production of plastics and water-soluble polymers in both condensation and addition polymerizations, as exemplified by oil in the schematic in Figure 1. From one resource, oil, monomers suitable for condensation and addition polymers are readily available. Condensation polymers, because of their structures with hydrophilic backbone linkages such as esters and amides are susceptible to hydrolytic degradation; whereas, addition polymers with hydrocarbon backbones (carbon chain) are susceptible to oxidative degradation. In the development of commodity commercial polymers used widely today, these inherent weaknesses wererecognized and minimized by making condensation polymers as hydrophobic as possible consistent with performance, and addition polymers were bolstered against oxidation by compounding with anti-oxidants.

Based on these limitations, overcome, as indicated, in the development of the recalcitrant commodity polymers used widely today, the options for the development of biodegradable polymers were simply (1) to modify existing condensation polymers by making them more hydrophilic, (2) to develop new hydrophilic condensation polymers from different monomers with similar cost and performance profiles, and (3) to develop controlled oxidation degradation chemistry for addition polymers by modifying the stabilizing influence of antioxidants used widely today. Almost all approaches chosen were to develop new more hydrophilic condensation polymers rather than to develop modifications of existing polymers. This approach, given the learning profile of new developments, has resulted in relatively expensive biodegradable polymers.

Downloaded by CORNELL UNIV on August 9, 2012 | http://pubs.acs.org
Publication Date: September 23, 2006 | doi: 10.1021/bk-2006-0939.ch024

A few approaches followed the tack of modifying the very inexpensive commodity addition polymers, polyolefins, to control and increase the rate of oxidation and hence hydropilicity of the polymer which enhanced degradation and biodegradation rates.

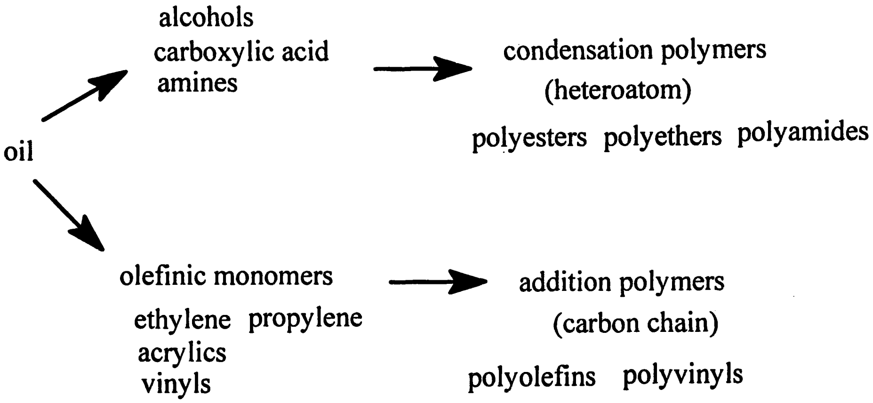
alcohols
carboxylic acid
amines
condensation polymers
(heteroatom)
polyesters polyethers polyamides
oil
olefinic monomers
ethylene propylene
acrylics
vinyls
addition polymers
(carbon chain)
polyolefins polyvinyls

Figure 1. Pathways to condensation and addition polymers from fossil resources

Polymers from renewable resources have become more attractive in the last few years as the interest in alternate lower cost feedstocks to fossil fuels has grown both for energy and for chemicals. Figure 2 indicates routes to condensation and addition polymers from renewable resources.

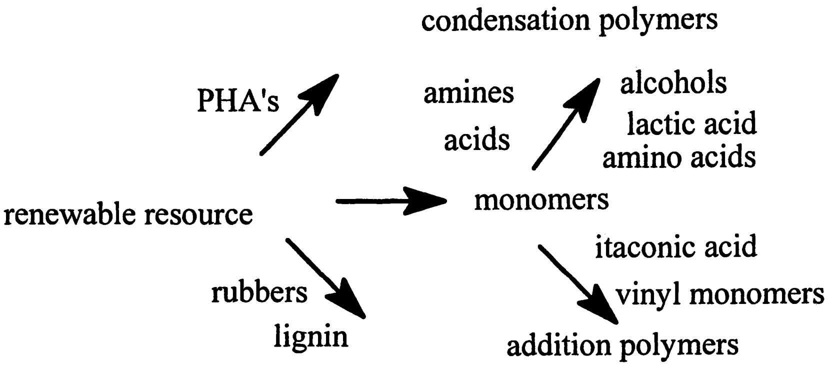
condensation polymers
PHA's
amines
acids
alcohols
lactic acid
amino acids
renewable resource
monomers
itaconic acid
rubbers
vinyl monomers
lignin
addition polymers

Figure 2. Pathways to addition and condensation polymers from renewable resources

Downloaded by CORNELL UNIV on August 9, 2012 | http://pubs.acs.org
Publication Date: September 23, 2006 | doi: 10.1021/bk-2006-0939.ch024

New natural polymers have emerged such as polyhydroxyalkanoates (PHA's) to augment available and widely used starches and celluloses, etc. The production of monomers from natural resources, some with structures identical to or similar to those from fossil resources, is growing in number and attractiveness. Because of synthetic flexibility already established industrially in addition and condensation polymers, these new monomers from renewable resources, amines, alcohols, acids, vinyls etc. permit the design of new biodegradable polymers using well established and understood polymerization technologies. Lactic acid monomer as a precursor to its polymer, poly(lactic acid) is a great example of this approach pioneered by Natureworks, LLC (formerly Cargill-Dow Corporation) and others with limited commercialization established.

Natural polymers such as starch and cellulose are chemically modified or blended with other degradable and biodegradable synthetic and natural polymers for a wide variety of application such as, packaging, films, detergents, etc. and the composites retain their biodegradation.

Environmental Degradation Processes

Identifying and understanding environmental degradation processes is essential in developing environmentally degradable and biodegradable polymers and in establishing standard definitions, methods, and specifications for these polymers. This is key for establishing whether polymers are indeed degradable and biodegradable in a given environment.

Environmental degradation processes for polymers may be hydrolyitic or oxidative in character and they may both be promoted biotically, in biological pathways, or abiotically, in non-biological pathways. Regardless, the first stage of each pathway leads to fragments of low molecular weight polymers, simple organic molecules or oligomers. These fragments may then either penetrate microbial organisms rapidly or slowly and biodegrade rapidly or slowly, respectively. Slowly means they remain in the environment for an extended period of time and they may be regarded as recalcitrant or very slowly biodegradable. Figure 3 depicts these processes.

Oxidation in the environment is usually a slower degradation process than hydrolysis. Hence, when comparing polymers designed for environmental degradation and biodegradation, polymers that require oxidation as the first stage of degradation are generally slower in the overall measured biodegradation rate process than those requiring hydrolysis as a first stage. This, even though the degradation intermediates are similar in chemical composition, has lead to problems and issues with respect to standard methods developed for estimating the extent of biodegradation of condensation and addition polymers in a given time period in a given environment. This difference in first stage degradation

Downloaded by CORNELL UNIV on August 9, 2012 | http://pubs.acs.org
Publication Date: September 23, 2006 | doi: 10.1021/bk-2006-0939.ch024

rate, and consequently overall rate of biodegradation, is particularly important when deciding what polymers are and what are not acceptable for environmental disposal. As to be expected, this has resulted in sharp diffences in opinion among scientists and manufacturers of different polymer types as to why and how different polymers are labeled biodegradable or not biodegradable.

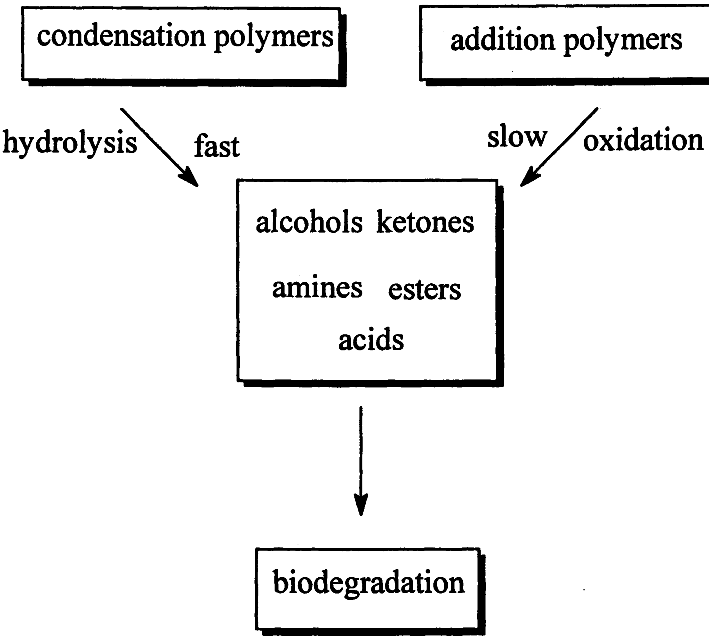

Figure 3. Environmental degradation processes for addition and condensation polymers

Standards Development

Definitions are at this time generally agreed throughout the industrial world. Biodegradation is understood to be degradation promoted by living organisms and environmental degradation may be by both biotic and abiotic mediation, both resulting in loss of properties and loss of molecular weight. They can be independent processes, consecutive processes or concurrent processes. Abiotic and biotic degradation are easily distinguished by comparison of polymer degradation in an environment that has been sterilized, where abiotic degradation cannot occur. Biodegradation is a biotic degradation process in vivo which leads to carbon dioxide and mixtures of carbon dioxide and methane evolution in

Downloaded by CORNELL UNIV on August 9, 2012 | http://pubs.acs.org
Publication Date: September 23, 2006 | doi: 10.1021/bk-2006-0939.ch024

aerobic and anaerobic environments, respectively, as the intermediate degradation products are consumed and used by living organisms. The extent of evolution and rate of evolution of gases is the basis of all current standard test methodology for establishing biodegradation and specifications for products to be designated biodegradable.

The standards developed for biodegradation testing in all environments including compost, soil, fresh and seawater are heavily biased towards fast degradation and biodegradation; therefore, hydrophilic polymers, which are typically condensation polymers, where hydrolysis is the first stage of degradation, more readily meet test specifications than do addition polymers. This test method development is understandable since laboratory testing cannot be prolonged with accuracy when measuring low levels of gas evolution without the use of expensive radiolabels. In addition, there is also a tendency for speeding the design and developement of new polymers, and fast biodegradation satisfies this need. Therefore, it is unfortunate that we do not have better and more reasonable long term standard test methods for biodegradation coupled with environmental toxicity which could measure the acceptability of polymers in the environment over prolonged time periods The current standard test methods for biodegradable polymers do, nevertheless, intentionally or not, discriminate by their tendency to fail polymers designed to degrade by oxidation and then biodegrade, polyolefins, even though there may be no toxicological issues with the polymers and their degradation products in the environment. Hence, many polymers that are quite clearly degradable and then slowly biodegradable in the environment are currently discriminated against and new testing protocols need to be developed to accommodate this difference. Indeed, this is reinforced by the fact that many natural polymers would fail the current standard testing methods.

> A good example of this is in the standard test method for polymers disposed of in compost facilities (and subsequently soil). The standards calls for complete biodegradation as measured by carbon dioxide evolution in 90 days (CEN) or 180 days(ASTM) in the compost, prior to land application. This totally disregards the fact that compost is intended as a soil amending additive and incomplete biodegradation in the compost stage may be completed in soil. This method, therefore, essentially rules that polymers degrading by oxobiodegradation(oxidation followed by biodegradation) are not acceptable for disposal in composting. Yet, there are numerous examples in the literature where such polymers, notably those degrading by oxidation and then biodegradation, have been composted to provide non-toxic and acceptable compost by every other measurement than carbon dioxide evolution. Data available from EPI Environmantal Products, Inc. for compost and soil, shown below, clearly supports the need for new

Downloaded by CORNELL UNIV on August 9, 2012 | http://pubs.acs.org
Publication Date: September 23, 2006 | doi: 10.1021/bk-2006-0939.ch024

standards development. The data are for degradation in compost, laboratory and real world and in soil. All are indicative of the stated need for additional standards to augment those we already have.

EPI Data on Degradation of Polyethylene with Prodegradants

Biodegradation in fullscale Municipal Compost facility in Vienna, Austria

- Polyethylene with TDPA™ prodegradant additive
- No discernable plastic residue
- Compost toxicity testing (DIN V549900-3): no adverse effects on plant growth (equivalent to compost without the polyethylene TDPA™)

Biodegradation in Mature Compost by Biometer testing

	Days to 60% CO_2 evolution (theory)
Polyethylene with TDPA™	ca. 600
Cellulose standard for activity check	ca.160 (meets ASTM Standard)
Oak leaves (OWS data)	ca. 350 (natural material)

Biodegradation in Forest Soil

	Days to 60% CO_2 evolution (theory)
Cellulose standard for activity check	ca. 160
Polyethylene / TDPA™ prodegradant	ca. 720

The time frame for total degradation of polyethylene with prodegradant, which is oxidation plus biodegradation, is measurable reaching the ASTM prescribed 60% of theoretical carbon conversion to carbon dioxide in a much longer time than current standards allow. Interestingly, the oak leaf, which is a natural product, is not biodegradable by current standards, and this surely is not the case.

Steps topwards resolving this issue of oxidation followed by biodegradation are underway with the recently developed ASTM Standard Guidline, D 6954-04, which clearly indicates how to test polymers that degrade with oxidation preceeding biodegradation in all environments. The next steps are to extend the

Downloaded by CORNELL UNIV on August 9, 2012 | http://pubs.acs.org
Publication Date: September 23, 2006 | doi: 10.1021/bk-2006-0939.ch024

standard guide to standard methods for different use and disposal environments and then to standard specifications.

Progress to Commercial Reality

Based on current standard testing methods and specifications, several renewable resource polymers may be considered biodegradable, the foremost being starch blends, cellulosic derivatives, polyhydroxyalkanoates and poly(lactic acid). Several new and old condensation polymers based on monomers obtained from fossil resources, such as polycaprolactone and the Bionolle series from Japan (Showa High Polymers) based on suucinic acid, are also acceptable by current standards, as are there blends with natural polymers such as starch.

In stark contrast to the above examples of condensation polymers, addition polymers, including natural polymers such as rubber, lignin, and blends fail current standard methods for establishing biodegradation and are not acceptable on the basis of time to biodegrade in a chosen environment. Likewise, standard traditional polyolefins do not meet these tests requirements. However, there are activated olefins such as poly(vinyl alchol), which may be considered a partially oxidized polyolefin, that meet the tests requirements. Also, there are non-oxidized activated polyolefins containing catalytic quantities of prodegradants to control the rate of oxidative degradation of the polymer backbone and subsequent biodegradation. The oxidation and biodegradation of these polymers can be controlled to fit a disposal environment requirements such as compost and subsequent soil application. However, in this example, biodegradation of the oxidized polymer fragments occurs over an extended period of time, longer than the compost cycle and, therefore, beyond the specifications currently in place. Such anomalies need to be addressed with further standard test method development in biodegradation and environmental toxicity.

Downloaded by CORNELL UNIV on August 9, 2012 | http://pubs.acs.org
Publication Date: September 23, 2006 | doi: 10.1021/bk-2006-0939.ch024

Conclusions

Biodegradable polymers are an attractive solution to aspects of polymer wastemanagement regardless of structure or source, condensation or addition polymers and fossil or renewable resource based. Some are more advanced than others and rates of degradation and biodegradation differ significantly, the slower degrading often being labeled unacceptable by current standard testing methods. This difference in rate as a measure of rapid biodegradation versus slow biodegradation and potential environmental impact must be resolved from an environmental risk perspective with better and more thorough toxicity testing to augment gas evolution as the sole environmental measure of acceptance.

It should be remembered that a variety of polymers are needed for different application and property balances to satisfy different needs and we should not be excluding new polymers based on simplistic standard testing methodology. Additionally, it must be recognized and remembered that slow biodegradation is a well established evolved natural process to accompany fast degradation which benefits the environment in soil accumulation and fertility. We still have far to go and much to learn! We are not finished. There are new polymers to discover and develop, and new test methods to establish.

> Remember the words of Einstein: "The only thing worse than ignorance is arrogance"

Downloaded by CORNELL UNIV on August 9, 2012 | http://pubs.acs.org
Publication Date: September 23, 2006 | doi: 10.1021/bk-2006-0939.ch024

Author Index

Aamer, Khaled A., 156
Adachi, Norihito, 45
Agrawal, Sarvesh K., 156
Albertsson, Ann-Christine, 307
Al-Saigh, Zeki Y., 320
Baciu, Radu, 398
Bhatia, Surita R., 156
Bora, Emilia, 14
Boustta, M., 267
Braun, B., 102
Budde, H., 61
Burkley, Daniel, 350
Burman, Lina, 307
Busse, K., 61
Castro, Guillermo R., 14
Chen, Gavin G., 350
Cooper, Tim R., 234
Daglen, Bevin C., 384
Deng, Meng, 350
Discher, Dennis E., 168
Doi, Yoshiharu, 30, 45
Dorgan, J. R., 102
Emrick, Todd, 248
Farminer, Ken, 76
Fujiwara, Tomoko, 216
Gao, Haifeng, 184
Geng, Yan, 168
Graiver, Daniel, 76
Grande, Daniel, 140
Guérin, Philippe, 140
Hakkarainen, Minna, 307
Hasegawa, Masashi, 45
Hayes, Douglas G., 126
Iwata, Tadahisa, 45
Jahed, Nazeem M., 184
Kaplan, David L., 14
Kawai, Fusako, 367
Khemani, Kishan, 2
Kiick, Kristi L., 201
Kimbara, Kazuhide, 367
Kimura, Yoshiharu, 216
Knauss, D. M., 102
Kressler, J., 61
Langlois, Valérie, 140
Leclercq, L., 267
Matyjaszewski, Krzysztof, 184
Min, Ke, 184
Narayan, Ramani, 76, 282
Nix, Nathaniel, 234
Nomura, Christopher T., 30
Panilaitis, Bruce, 14
Parrish, Bryan, 248
Patrick, Laura, 76
Renard, Estelle, 140
Rohman, Géraldine, 140
Sanabria-DeLong, Naomi, 156
Scholz, Carmen, 2, 61
Storey, Robson F., 234
Swift, Graham, 398
Tanaka, Toshihisa, 45
Tani, Akio, 367
Teramachi, Shinya, 45
Tew, Gregory N., 156
Timbart, Laurianne, 140
Tran, Phuong, 76
Tsarevsky, Nicolay V., 184
Tyler, David R., 384
Vert, M., 267
Wegner, J. R., 102
Yamaguchi, Nori, 201
Zhou, Jack J., 350

Downloaded by 89.163.35.42 on August 9, 2012 | http://pubs.acs.org
Publication Date: September 23, 2006 | doi: 10.1021/bk-2006-0939.ix001

Subject Index

Downloaded by 89.163.35.42 on August 9, 2012 | http://pubs.acs.org
Publication Date: September 23, 2006 | doi: 10.1021/bk-2006-0939.ix002

A

Accelerator mass spectrometry, biobased content method, 286
Addition polymers
  environmental degradation processes, 405–406
  pathways from renewable resources, 404*f*
  pathways to, from fossil resources, 404*f*
Agriculture, photodegradable plastics, 385
Alcaligenes eutrophus
  fermentation, 63
  See also Poly(β-hydroxybutyrate) (PHB)
Alginate
  adsorption of bovine serum albumin (BSA) by microspheres, 23, 25*f*
  blue dextran release profile, 22, 23*f*
  chemical structure, 16*f*
  crosslinking and gelation, 22
  energy dispersive X-ray (EDX) analysis of micropheres, 23, 24*f*
  linear polysaccharide, 15
  stabilizing, gels, 15
  See also Emulsan-alginate microspheres (EAMs)
Aliphatic polyesters
  allyl, acetylene, and cyclopentene derivatives of δ-valerolactone, 259–260
  allyl-functionalized ε-caprolactone (ε-CL), 256, 257*f*
  biomaterials applications, 249, 250*f*
  click chemistry, 262–263
  copolymerization to fine-tune properties, 252
  degradation of hydroxyl functionalized, 261
  dendrimer and doxorubicin drug conjugate, 254, 255*f*
  1,2-diol substituted with poly(ethylene glycol) (PEG), 261–262
  end-group functionalization, 252, 254
  grafted with oligopeptide sequence, 264*f*
  highly functionalized dendritic and hyperbranched, 254, 255*f*
  hydroxyl and carboxyl derivatives, 257, 259*f*
  lactone monomers and substitution α- to carbonyl group, 259–260
  methods for producing functionalized lactones, 256
  PEG-*b*-polyester, 253*f*
  PEG-grafting by post-polymerization click chemistry of acetylene functionalized, 262*f*
  pendent acetylene functionality and click chemistry, 262–263
  pendent functionality, 255–256
  pendent functionalized poly(ε-CL), 256–257, 258*f*
  phenyl azide end-capped, 253*f*
  phosphoryl choline end-capped, 253*f*
  polymerization of allyl-functionalized ε-CL and functional group transformations, 257, 258*f*
  preparation of pendent 1,2-diol substituted, 261*f*
  protected hydroxyl and carboxyl monomers and deprotected polymers, 257, 259*f*

Downloaded by 89.163.35.42 on August 9, 2012 | http://pubs.acs.org
Publication Date: September 23, 2006 | doi: 10.1021/bk-2006-0939.ix002

  - ring-opening polymerization of monomers, 249, 251*f*
  - Sn(II) catalysts in ring-opening polymerization of lactones, 260
  - *See also* Aromatic-aliphatic block copolyesters
- Alizarin dye, nuclear magnetic resonance of, and oligoethoxylated product, 67, 68*f*
- Aluminum alkoxides, catalysts and initiators for polylactic acids (PLA), 111
- Amylopectin (AP) and blends
  - analysis of polymer blends, 324–326
  - analysis of semicrystalline polymer-containing blends, 326–328
  - blend solutions preparation, 332–333
  - characterization of AP-biodegradable polymer blends, 323–324
  - crystallinity, 340, 342, 345
  - degree of crystallinity of, 343*f*
  - description of biodegradable polymers and blends, 331*t*
  - development of inverse gas chromatography (IGC), 321–322
  - elevation in melting point of AP-PCL blends, 344*f*
  - experimental, 330–345
  - free energy of mixing, 325
  - instrumentation and procedure, 332–345
  - interaction energy parameter, B_{23}, 326, 328
  - interaction parameter, χ_{12}, 324
  - materials, 330–332
  - measured physical parameters of biodegradable polymers and blends, 337*t*
  - melting point depression, 328
  - molecular probe technique, 321–322
  - polymer-polymer interaction parameters, 336, 340
  - polymer-solute interaction parameters, 336
  - polymer-solvent and polymer-polymer interaction coefficients, 339*t*
  - retention diagram of poly(acrylic acid)-pentane system, 341*f*
  - retention diagrams, 333–336
  - specific retention volume, 324
  - starch-based polymers, 322–323
  - surface energy, 345
  - surface energy of polymers, 328–330
  - surface interactions by IGC, 322
  - thermal analysis, 333
  - thermodynamic analysis of polymer-polymer mixtures by melting point depression, 327–328
  - XRD spectra of AP, poly(ε-caprolactone) (PCL) and AP-PCL blends, 338*f*
  - *See also* Inverse gas chromatography (IGC)
- Architectural variation, polylactic acids (PLA), 112–113
- Aromatic-aliphatic block copolyesters
  - ABA block of poly(ethyleneoxyethylene terephthalate-*co*-adipate) and poly(L-lactide) segments (PLLA–PEOETA–PLLA), 235
  - acid number determination of PEOETA macroinitiator, 243*t*
  - atomic force microscopy (AFM) images of PLLA-*b*-PEOETA-*b*-PLLA, 237, 244, 245*f*
  - characterization methods, 236–237
  - experimental, 236–238
  - first order kinetic plots of L-lactide (LLA) polymerizations, 242*f*

Downloaded by 89.163.35.42 on August 9, 2012 | http://pubs.acs.org
Publication Date: September 23, 2006 | doi: 10.1021/bk-2006-0939.ix002

  - formulations and apparent rate constants (k_{app}) for LLA polymerizations, 243*t*
  - gel permeation chromatography (GPC) traces of PEOETA and PLLA-*b*-PEOETA-*b*-PLLA, 244*f*
  - ^{1}H NMR of PEOETA end groups and components, 240*f*
  - monitoring LLA conversion by 1240 cm^{-1} peak, 239, 242*f*
  - morphology of PLLA-*b*-PEOETA-*b*-PLLA by AFM, 244, 245*f*
  - partial ^{1}H NMR spectrum of PLLA-*b*-PEOETA-*b*-PLLA, 243*f*
  - ring opening polymerization of LLA using PEOETA macroinitiator, 239, 244
  - synthesis of PEOETA, 238–239
  - synthesis of PEOETA macroinitiators, 237–238
  - synthesis of PLLA-*b*-PEOETA-*b*-PLLA, 238, 241
  - *See also* Aliphatic polyesters
- ASTM D5338, biodegradation test method, 294–295
- ASTM D6866, quantifying biobased content, 285–286
- Atomic force microscopy (AFM), aromatic-aliphatic block copolyester, 237, 244, 245*f*
- Atom transfer radical polymerization (ATRP)
  - ATRP of 2-hydroxyethyl methacrylate (HEMA), 186–187
  - ATRP of HEMA using bis(2-bromoisobutyryloxethyl) disulfide [$(BiBOE)_2S_2$] initiator, 191*f*
  - chain extension of disulfide-containing poly(methyl methacrylate) (PMMA)-based "supermacroinitiator" gel with styrene (Sty), 187
  - 2-dimensional chromatographic analysis, 188–189
  - experimental, 186–189
  - functional group tolerance, 185
  - materials, 186
  - preparation and degradation of functional PMMA-based gels, 190, 192–196
  - preparation of degradable gels with disulfide groups, 187
  - preparation of degradable polyHEMA by, 191*f*
  - preparation of latexes degradable in reducing environment, 187–188
  - reductive degradation of disulfide-containing linear polymers and gels, 188
  - size exclusion chromatography (SEC) traces of polyHEMA, 192*f*
  - synthesis of degradable linear polyHEMA, 189–190
  - synthesis of functional degradable PMMA-based gels by, in miniemulsion, 196, 198*f*
  - *See also* Poly(methyl methacrylate) (PMMA)-based gels
- Autooxidation mechanism, hydrocarbon materials, 385, 386
- *Azotobacter vinelandii*
  - fermentation, 63
  - *See also* Poly(β-hydroxybutyrate) (PHB)

B

- Bans, non-degradable plastics, 6
- Basic fibroblast growth factor (bFGF)
  - binding and release from covalently crosslinked hydrogels, 207–209
  - binding and release from noncovalently assembled hydrogels, 209–213

Downloaded by 89.163.35.42 on August 9, 2012 | http://pubs.acs.org
Publication Date: September 23, 2006 | doi: 10.1021/bk-2006-0939.ix002

See also Heparin-derivatized polymer hydrogels
Beer–Lambert law, turbidity calculation using, 148–149
Biobased content
  examples of determination, 287–288
  method identifying and quantifying, 285–286
  terminology, 286
Biobased feedstocks, biopolymers, 297*f*
Biobased materials, terminology, 284
Biobased polymeric materials
  biobased content, 286
  biobased materials, 284
  biobased products, 287
  biodegradable materials, 289–291
  biodegradable starch esters, 300
  biomass feedstock, 296
  carbon-14 method for quantifying biobased content, 285*f*
  chemical energy for driving life processes by aerobic oxidation of glucose, 293
  closed cell structure of starch foams, 301*f*
  complete biodegradation (ASTM D5338 method), 294–295
  conversion to biomonomer and others, 297*f*
  D6866 method quantifying biobased content, 285–286
  degradable vs. biodegradable, 292–295
  designing hydrophobic polyolefin plastics to be degradable, 293
  direct extraction of biomass providing biopolymers for use in biobased products, 297*f*
  disintegration, 295
  examples of biobased content determination, 287–288
  global carbon cycle, 283–284
  integration with disposal infrastructure, 290–291
  justification and rationale for using carbon, 287–288
  life cycle assessment, 288*f*
  material design principles for environment, 288–289
  measure of rate and amount of evolved CO_2, 293
  municipal solid waste (MSW) distribution by weight, 292*f*
  organic materials, 284–286
  percent carbon conversion to CO_2 as function of time, 294*f*
  polyethylene (PE) and PE-wax coated paper, 290
  product 'N', 287
  product 'O', 287
  product 'P', 287
  rationale, 283–284
  reactive blend compositions, 299*f*
  safety, 295
  standards for disposal systems, 295, 296*f*
  starch bioplastics, 298–299
  starch foam crafts and toys, 303*f*
  starch foam sheets for protective cushion packaging, 302*f*
  starch foam technology, 301, 304
  sustainability driver, 284*f*
  technology exemplars, 295–304
  terminology, 284–287
Biobased products, terminology, 287
Biochemical pathways, polymer degradation, 3
Biocompatible gels, applications, 15
Biodegradable, degradable vs., 292–295
Biodegradable materials
  carbon dioxide evolution, 407–408
  consumers, 401
  degradation of polyethylene (PE) with prodegradants, 408–409
  disposability, 289–291

  environmental degradation processes, 405–406
  environmental safety, 402
  forest soil, 408
  goals in development of, 401–403
  integration with disposal infrastructure, 290–291
  landfilling, 400
  mature compost, 408
  municipal compost facility, 408
  natural polymers, 7–8, 405
  pathways to addition and condensation polymers from renewable resources, 404*f*
  pathways to condensation and addition polymers from fossil resources, 404*f*
  plastics recovery and reuse, 399–400
  polymer industries, 401
  polymers and manufacturers, 5*t*
  polymer waste management, 399–401
  production, 4
  progress to commercial reality, 409
  regulatory authorities, 401
  standards development, 406–409
  standards organizations, 401
  synthetic and other approaches, 403–405
  See also Biobased polymeric materials
Biodegradation, standard criteria, 294–295
Biodiesel, soy-based
  catalytic ozonation, 93–94
  composition of methyl soyate biodiesel after catalytic ozonation with methanol, 94*f*
  differential scanning calorimetry of methyl soyate, 96, 97*f*, 98
  expected composition of, after ozonolysis, 95*t*
  properties, 95–98
  Rancimat tests of biodiesel and treated biodiesel, 97*f*
  stability of ozone treated, toward oxidation, 96, 97*f*
  thermogravimetric analysis of methyl soyate, ozone treated methyl soyate, and diesel fuel, 95, 96*f*
  See also Soybean oil modifications
Biolubricants
  lubricant-related properties of mineral oils and poly(hydroxy acid) esters, 129*t*
  market, 127–128
  potential market size, 128*t*
  ricinoleic acid oligomers, 127–129
  See also Lubricants, soy-based; Ricinoleic acid polymers
Biomaterials, aliphatic polyesters, 249, 250*f*
Biomedical materials
  development of degradable, 10
  poly(3-hydroxybutyrate) [P(3HB)] and copolymer with 3-hydroxyvalerate [P(3HB-*co*-3HV)], 34
Bioplastics
  Fourier transform infrared (FTIR) spectra of soy oil and soy polyol, 91, 92*f*
  nuclear magnetic resonance (NMR), 91, 92*f*, 93
  possible inter- and intramolecular side reactions, 90*f*, 91
  soy polyol preparation by catalytic ozonation, 89–90
  See also Biobased polymeric materials; Polylactic acids (PLA); Soybean oil modifications
Biopol™. *See* Poly[(R)-3-hydroxybutyrate-*co*-(R)-3-hydroxyvalerate]
Biosynthesis. *See* Polyhydroxyalkanoates (PHAs)

Downloaded by 89.163.35.42 on August 9, 2012 | http://pubs.acs.org
Publication Date: September 23, 2006 | doi: 10.1021/bk-2006-0939.ix002

Downloaded by 89.163.35.42 on August 9, 2012 | http://pubs.acs.org
Publication Date: September 23, 2006 | doi: 10.1021/bk-2006-0939.ix002

Blends. *See* Amylopectin (AP) and blends
Block copolymers
  polylactic acids (PLA), 112–113
  See also Aromatic-aliphatic block copolyesters; Poly(β-hydroxybutyrate) (PHB); Poly(3-hydroxyoctanoate) (PHO); Thermo-sensitive gels
Blood, poly(ethylene glycol)-*b*-poly(ε-caprolactone) worm micelles, 172, 178
Blue dextran, release profiles from alginate and emulsan-alginate microspheres, 22, 23*f*
Bovine serum albumin (BSA)
  adsorption to alginate microspheres, 23, 25*f*
  effect of emulsan on BSA adsorption, 23, 25*f*
  See also Emulsan-alginate microspheres (EAMs)
Branched polymers, polylactic acids (PLA), 113

C

Candida antarctica
  immobilized lipase from, 130
  See also Lipase-catalyzed synthesis
ε-Caprolactone (CL)
  ring opening polymerization (ROP), 249, 251*f*
  See also Poly(ethylene oxide)-*b*-poly(ε-caprolactone) (PEO–PCL) (OCL); Poly(3-hydroxyoctanoate) (PHO)
Carbon cycle, biobased products rationale, 283–284
Carbonyl groups, photochemical degradation pathways for polymers with, 385, 386
Carbonyl index, polyethylene films, 316*t*
Cargill Corporation, potential of polylactic acids (PLA), 103
Catalytic ozonation
  calculated composition of soy oil before and after, with methanol, 80, 81*t*
  double bonds in soy oil, 79–80
  initial attach of ozone on double bond, 78*f*
  methyl oleate in sodium methoxide solution, 79*f*
  methyl soyate biodiesel after, with methanol, 94*f*
  olefin conversion in single-step reaction, 78–79
  set-up, 81–82
  soy-based biodiesel, 93–94
  soy-based lubricants, 84–86
  soy polyol preparation by, 89–90
  thermally stable lubricant from soy oil and MPEG 350, 79*f*
  See also Biodiesel, soy-based; Soybean oil modifications
Chain extension, oligomeric polylactic acid (PLA), 109
Chromatographic fingerprinting
  analysis method, 310–311
  classification and product control, 313–314
  comparison of early detection techniques, 317
Chromophore
  chemical incorporation into polymer, 385
  distinctive M–M bond, monitoring photodegradation, 388
Circular dichroism (CD)
  bovine serum albumin (BSA) structure before and after release, 27, 28*f*
  method, 18–19
Classification
  chromatographic fingerprinting, 313–314

- early degradation, by total luminescence intensity, 314, 316

Click chemistry, aliphatic polyesters, 262–263
Coatings for paper, applications for polylactic acids (PLA), 108
Co-gelation, stabilizing alginate gels, 15
Composting
- biodegradable or recyclable products, 290–291
- biodegradation, 408
- biodegradation in municipal compost facility, 408

Condensation polymerization, polylactic acids (PLA), 109–110
Condensation polymers
- environmental degradation processes, 405–406
- pathways from renewable resources, 404*f*
- pathways to, from fossil resources, 404*f*

Consumers
- biodegradable polymers, 401
- environmentally friendly products, 4, 6

Coordination insertion, mechanism for polymerization of lactide, 111
Copolymers
- polylactic acids (PLA), 112–113
- *See also* Aromatic-aliphatic block copolyesters; Poly(glycolide-*co*-L-Lactide) (PGLL); Poly(β-hydroxybutyrate) (PHB); Thermo-sensitive gels

Corn, source to polylactic acids (PLA), 103, 104*f*, 105
Covalently crosslinked hydrogels
- formation and growth factor binding/release, 207–209
- *See also* Heparin-derivatized polymer hydrogels

Crosslinking
- alginate, and gelation, 22
- stabilizing alginate gels, 15

Crystallinity
- amylopectin (AP) and blends, 340, 342, 343*f*, 345
- inverse gas chromatography (IGC) method, 340
- retention diagram of poly(acrylic acid)-pentane system, 341*f*

Crystallization
- atomic force microscopy (AFM) measurement, 71, 72*f*
- poly(β-hydroxybutyrate) (PHB), 69–73
- process of PHB, by polarized light microscope, 71, 72*f*
- small-angle X-ray scattering (SAXS) of modified PHB, 70, 71*f*

Cyclopentadienyl rings, incorporation into polymer backbones, 389–390

D

Degradability
- graft and block copolyesters for controlled, 141
- time and pathways, 2–3
- *See also* Multifunctional polyester-based materials

Degradable, biodegradable vs., 292–295
Degradable materials
- natural polymers, 7–8
- petroleum as source, 9–10
- polyesters containing both aromatic and aliphatic units, 235
- polymers from renewable resources, 8–9

Degradation
- exogenous and endogenous mechanisms, 368
- *See also* Photodegradation in polymers; Poly(ethylene glycol) (PEG); Poly(glycolide-*co*-L-

Downloaded by 89.163.35.42 on August 9, 2012 | http://pubs.acs.org
Publication Date: September 23, 2006 | doi: 10.1021/bk-2006-0939.ix002

lactide) (PGLL); Poly(vinyl alcohol) (PVA)
Degradation, early detection
  chromatographic fingerprinting, 310–311
  classification and product control, 313–314
  demands of polymeric products, 308–309
  early degradation state prediction and classification using total luminescence intensity (TLI), 314, 316
  electronic nose system, 313
  estimation of degradation times, 314, 315*f*
  experimental, 309–311
  gas chromatography/mass spectrometry (GC/MS) of degradable polyethylene films, 313
  indicator product analysis, 309–310
  indicator products as tool to predicting degradation, 311, 313
  molecular, macromolecular, and macroscopic scale changes, 312*f*
  partial least square (PLS) analysis, 314, 315*f*
  principal component analysis (PCA) model, 313–314
  relationship between dicarboxylic acid content in photo-degradable polyethylenes, 312*f*
  technique comparison, 317
  TLI and carbonyl index for polyethylene films, 316*t*
  TLI method, 310–311
  See also Total luminescence intensity (TLI)
Degradation mechanism, worm micelles, 173–177
Dendritic aliphatic polyesters, highly functionalized, 254, 255*f*
Detection. *See* Degradation, early detection
Developed nations, laws for non-degradable plastic products, 6
Diesel. *See* Biodiesel, soy-based
Differential scanning calorimetry (DSC)
  methyl soyate, 96, 97*f*, 98
  triblock copolymer of poly(lactide) (PLA) and poly(ethylene oxide) (PEO), 160, 163*f*, 164*f*
Disintegration, standard criteria, 295
Disposability, biodegradable materials, 289–291
Disposal infrastructure, biodegradable or recyclable products, 290–291
Disposal tax, non-degradable plastic products, 6
Disulfide-containing polymers
  atom transfer radical polymerization (ATRP) of 2-hydroxyethyl methacrylate (HEMA), 186–187, 191*f*
  functional poly(methyl methacrylate) (PMMA)-based gels, 190, 192–196
  reductive degradation, 188
  tolerance of ATRP, 185
  See also Atom transfer radical polymerization (ATRP); Poly(methyl methacrylate) (PMMA)-based gels
Dow Chemical, potential of polylactic acids (PLA), 103
Doxorubicin, drug-polymer conjugate, 254, 255*f*
Drug delivery
  biocompatible gels, 15
  evaluation of degradable worm micelles, 178–180
  worm micelles, 170

E

Early detection. *See* Degradation, early detection

Downloaded by 89.163.35.42 on August 9, 2012 | http://pubs.acs.org
Publication Date: September 23, 2006 | doi: 10.1021/bk-2006-0939.ix002

Downloaded by 89.163.35.42 on August 9, 2012 | http://pubs.acs.org
Publication Date: September 23, 2006 | doi: 10.1021/bk-2006-0939.ix002

Ecoefficiency, biobased polymeric materials, 283
Electronic nose system, analysis of new car odor, 313
Emulsan
  chemical structure, 17*f*
  composition, 15
  See also Emulsan-alginate microspheres (EAMs)
Emulsan-alginate microspheres (EAMs)
  absorption of bovine serum albumin (BSA), 23, 25*f*
  alginate crosslinking and gelation, 22
  bacterial cultures and emulsan purification, 17
  blue dextran release profile, 22, 23*f*
  circular dichroism (CD), 18–19
  EDX (energy dispersive X-ray) mapping, 18
  EDX spectra of alginate and EAMs, 23, 24*f*
  effect of emulsan on BSA absorption by microspheres, 23, 25*f*
  enzymatic cleavage from, 26–27
  enzymatic release of azo-BSA from EAMs, 26*f*, 27*t*
  enzyme triggered release methods, 26
  experimental, 17–19
  materials, 17
  microsphere formation, 18
  OM (optical microscopy), 18
  OM of alginate and emulsan-alginate microspheres , 20*f*
  release studies, 19
  scanning electron microscopy (SEM), 18
  SEM of alginate and emulsan-alginate microspheres , 21*f*
  structure of BSA by CD before and after release from, 27, 27*f*
  surface morphologies, 19, 20*f*, 21*f*
  time release of tracer molecules, 22
Enantiomeric copolymers
  blend of poly(D-lactide) (PDLA) and poly(L-lactide) (PLLA), 217
  hydrogels from AB-diblock copolymers, 225–226
  hydrogels from BAB triblock copolymers, 223–225
  hydrogels from micellar solutions of ABA triblock copolymers, 220–221
  hydrogels from mixtures of, PLA–PEG block copolymers, 219–230
  mechanisms of enantiomeric PLA-*b*-PEG hydrogels, 227–230
  See also Thermo-sensitive gels
End-group functionalization
  aliphatic polyesters, 252, 253*f*, 254
  See also Functionalization
Endogenous degradation. *See* Poly(vinyl alcohol) (PVA)
Energy dispersive X-ray (EDX) mapping, emulsan-alginate microspheres (EAMs), 18, 23, 24*f*
Energy requirements, polylactic acids (PLA), 105, 106*f*
Environment
  degradation of polymerics materials in, 105
  material design principles for, 288–289
  plastic materials damaging, 3
Environmental degradation processes, addition and condensation polymers, 405–406
Environmentally friendly products, consumers worldwide, 4, 6
Environmental Protection Act 1986, non-biodegradable plastics, 6
Environmental safety, biodegradation, 402
Enzymatic cleavage, azo-BSA (bovine serum albumin) from microspheres, 26–27

Downloaded by 89.163.35.42 on August 9, 2012 | http://pubs.acs.org
Publication Date: September 23, 2006 | doi: 10.1021/bk-2006-0939.ix002

Enzymatic degradation
  poly[(R)-3-hydroxybutyrate-*co*-(R)-3-hydroxyvalerate] films, 48, 56–58
  polyelectrolyte complexes (PECs), 272–273, 275
Escherichia coli
  conditions for polyhydroxyalkanoate (PHA) production, 31–32
  medium-chain-length PHA from recombinant, 37*t*
  model strain for PHA production, 31
  short-chain-length PHA from recombinant, 33*t*
  See also Polyhydroxyalkanoates (PHAs)
European countries, laws for non-degradable plastic products, 6
Exogenous degradation. *See* Poly(ethylene glycol) (PEG)
Expression. *See* Gene expression

F

Fatty acid biosynthesis, polyhydroxyalkanoate (PHA) production, 36*f*, 38
Feedstocks, biopolymers, 297*f*
Fermentation, lactic acid formation, 103, 104*f*, 105
Fibers
  melt- and solution-spun polylactic acids (PLA), 108
  See also Poly[(R)-3-hydroxybutyrate-*co*-(R)-3-hydroxyvalerate]
Films. *See* Poly[(R)-3-hydroxybutyrate-*co*-(R)-3-hydroxyvalerate]
Fingerprinting. *See* Chromatographic fingerprinting
Foam technology, starch, 301, 304
Forest soil, biodegradation, 408
Fossil resources
  biodegradable natural polymers, 409
  See also Biodegradable materials
Free energy of mixing, polymer blends, 325
Friction, soy-based lubricants, 87–88
Functionalization
  aliphatic polyesters with pendent, 255–256
  dendritic and hyperbranched aliphatic polyesters, 254, 255*f*
  end-group, of aliphatic polyesters, 252, 254
  phenyl azide end-capped polyester, 252, 253*f*
  phosphoryl choline end-capped polyester, 252, 253*f*
  poly(ethylene glycol)-*b*-polyester, 252, 253*f*
  See also Aliphatic polyesters; Pendent functionalization

G

Gas chromatography (GC). *See* Inverse gas chromatography (IGC)
Gas chromatography/mass spectrometry (GC/MS), degradable polyethylene films, 313
Gelation, alginates, 15
Gels. *See* Heparin-derivatized polymer hydrogels; Poly(methyl methacrylate) (PMMA)-based gels; Thermo-sensitive gels
Gene expression. *See* Poly(ethylene glycol) (PEG); Poly(vinyl alcohol) (PVA)
Glass transition temperature (Tg), efficiency of photodegradation, 392, 393*t*
Global carbon cycle, biobased products rationale, 283–284

Glycolide, ring opening polymerization (ROP), 249, 251*f*
Graft copolyesters. *See* Multifunctional polyester-based materials
Green chemistry, biobased polymeric materials, 283
Gross biobased content, terminology, 286

H

Hemolysis study, blood in poly(ethylene glycol)-*b*-poly(ε-caprolactone) (OCL) worm micelles, 172, 178
Heparin binding peptide (HBP). *See* Heparin-derivatized polymer hydrogels
Heparin-derivatized polymer hydrogels
  basic fibroblast growth factor (bFGF) binding, 207, 208*f*
  bFGF release profiles from noncovalently assembled hydrogels, 211–212
  binding and release of bFGF, 212–213
  biological applications of polysaccharide materials, 202
  characteristics of hydrogels in bFGF release assays, 208*t*
  conjugate poly(ethylene glycol)–low molecular weight heparin (PEG–LMWH) for assembly of, 204
  covalently crosslinked hydrogels, 207–209
  experimental, 204
  heparin-containing delivery systems, 202
  human umbilical vein endothelial cell (HUVEC) adhesion and proliferation, 212
  materials and methods, 204
  matrix erosion profile of noncovalently assembled hydrogel vs. time, 212*f*
  noncovalently assembled hydrogels, 209–213
  PEG–heparin binding peptide (PEG–HBP) synthesis, 206–207
  PEG–LMWH synthesis, 205–206
  profile of bFGF release vs. time, 209*f*
  schematic of assembly of noncovalent hydrogel network, 203*f*
  storage and loss moduli of noncovalently assembled hydrogel, 210, 211*f*
High-tech applications, plastic materials, 3
Hydrogels. *See* Heparin-derivatized polymer hydrogels; Thermo-sensitive gels
Hydrolysis. *See* Interpenetrating polymer networks (IPNs)
Hydrolytic degradability. *See* Multifunctional polyester-based materials
Hydroxy acids, polymers of (PHAs) applications, 127
  See also Ricinoleic acid polymers
3-Hydroxybutyrate (3HB)
  common short-chain-length monomer in polyhydroxyalkanoates (PHAs), 33*t*, 34
  copolymer with 3-hydroxyvalerate [P(3HB-*co*-3HV)], 34
  monomer supply for P(3HB), 35*f*
  See also Polyhydroxyalkanoates (PHAs)
4-Hydroxybutyrate (4HB), monomer supply for poly(4HB), 35*f*
2-Hydroxyethyl methacrylate (HEMA). *See* Atom transfer radical polymerization (ATRP)

Downloaded by 89.163.35.42 on August 9, 2012 | http://pubs.acs.org
Publication Date: September 23, 2006 | doi: 10.1021/bk-2006-0939.ix002

3-Hydroxyvalerate (3HV)
  copolymer with 3-hydroxybutyrate [P(3HB-*co*-3HV)], 34
  monomer supply for poly(3HV), 35*f*
Hyperbranched aliphatic polyesters, highly functionalized, 254, 255*f*

I

Incineration, waste, 400
Indicator product analysis
  comparison of early detection techniques, 317
  method, 309–310
  tool of degradation state prediction, 311, 313
  See also Degradation, early detection
Industrial ecology, biobased polymeric materials, 283
Interaction parameters, polymer blends, 324, 326
Interpenetrating polymer networks (IPNs)
  average equivalent diameter of poly(lactide) (PLA) microdomains, 149, 150*f*
  dependence of mass loss on hydrolysis time, 151, 152*f*
  mesoporous networks design from PLA/poly(methyl methacrylate) (PLA/PMMA) IPNs, 150*f*
  morphologies before and after hydrolysis by scanning electron microscopy (SEM), 151, 152*f*
  partial hydrolysis of IPNs, 142
  pore sizes by SEM and thermoporometry, 151, 153*t*
  preparation of mesoporous networks by partial hydrolysis of IPNs, 149, 151, 153
  synthesis and characterization of PLA-based IPNs, 148–149
  synthesis of PLA/PMMA IPNs, 142
  turbidity using Beer–Lambert law, 148–149
  See also Multifunctional polyester-based materials
Inverse gas chromatography (IGC)
  crystallinity of amylopectin (AP) and blends, 340, 342, 345
  degree of crystallinity of amylopectin and blends, 343*f*
  development, 321–322
  instrumentation and procedure, 332–333
  polymer-polymer interaction parameters, 336, 340
  polymer-solute interaction parameters, 336, 339*t*
  polymer-solvent and polymer-polymer interaction coefficients, 339*t*
  retention diagrams, 333–336
  See also Amylopectin (AP) and blends
In vitro degradation. *See* Poly(glycolide-*co*-L-Lactide) (PGLL)
Irradiation
  photodegradation of polymers, 395–396
  See also Photodegradation in polymers
Isotope Ratio Mass Spectrometry (IRMS), biobased content method, 286

K

Kinetics, worm micelles, 173–177

Downloaded by 89.163.35.42 on August 9, 2012 | http://pubs.acs.org
Publication Date: September 23, 2006 | doi: 10.1021/bk-2006-0939.ix002

Downloaded by 89.163.35.42 on August 9, 2012 | http://pubs.acs.org
Publication Date: September 23, 2006 | doi: 10.1021/bk-2006-0939.ix002

L

Lactide
  ring opening polymerization (ROP), 109–110, 235, 249, 251*f*
  See also Poly(lactide) (PLA)
Landfill disposal, packaging materials, 6–7
Landfilling, biodegradable or recyclable products, 290–291, 400
Laws, non-degradable plastic products, 6
Life cycle analysis, polylactic acids (PLA), 105, 106*f*
Life cycle assessment, material design principles for environment, 288–289
Lipase-catalyzed synthesis
  Candida antarctica as lipase source, 130
  eco-friendly biocatalytic synthesis of poly(hydroxy acids), 129–130
  poly(hydroxy acid) esters, 131–133, 137
  See also Ricinoleic acid polymers
Liquid Scintillation Counting (LSC), biobased content method, 286
Lubricant market
  mineral oils, 127
  See also Biolubricants
Lubricants, soy-based
  approaches to thermal stability, 83–84
  catalytic ozonolysis of triglycerides with alcohol, 84*f*
  cold flow properties, 87*f*
  consumption of double bonds during ozonolysis, 86*f*
  Fourier transform infrared (FTIR) of reaction progress, 85–86
  friction and wear, 87–88
  lubrication properties, 86–88
  partial FTIR showing double bond disappearance, 85*f*
  scanning Brookfield technique (SBT), 86–87
  thermally stable, from soy oil and mono-methoxy poly(ethylene glycol) (MPEG), 85*f*
  thermo-oxidation engine oil simulation test (TEOS), 86
  wear plot, 88*f*
  See also Biolubricants; Soybean oil modifications

M

Macromolecular architecture, well-defined, 141
Manufacturers, biodegradable polymers, 5*t*
Medical applications, polylactic acids (PLA) and PLA copolymers, 107
Medium-chain-length polymers. *See* Polyhydroxyalkanoates (PHAs)
Melting point
  depression in polymer-polymer mixtures, 327, 328
  elevation in, for amylopectin–poly(ε-caprolactone) (AP–PCL) blends, 344*f*
Melt-spun fibers, polylactic acids (PLA), 108, 114
Mesoporous networks
  dependence of mass loss on hydrolysis time, 151, 152*f*
  design from poly(lactide)/poly(methyl methacrylate) (PLA/PMMA) interpenetrating polymer networks (IPNs), 150*f*
  morphologies of IPNs before and after hydrolysis, 151, 152*f*
  partial hydrolysis of IPNs, 149–153
  pore sizes, 151, 153
  See also Interpenetrating polymer networks (IPNs)
Metal-metal bonds

Downloaded by 89.163.35.42 on August 9, 2012 | http://pubs.acs.org
Publication Date: September 23, 2006 | doi: 10.1021/bk-2006-0939.ix002

  incorporation into polymer backbones, 389–390
  photodegradable polymers, 388, 389
  See also Photodegradation in polymers
Methyl soyate. *See* Biodiesel, soy-based
Micelles. *See* Poly(ethylene oxide)-*b*-poly(ε-caprolactone) (OCL) worm micelles
Michigan State University (MSU), starch foam technology, 301, 304
Microbeam X-ray diffraction. *See* X-ray diffraction
Minerals
  lubricants, 127
  See also Biolubricants
Molecular probe technique. *See* Inverse gas chromatography (IGC)
Molecular weight, tensile properties and, during poly(glycolide-*co*-L-lactide) (PGLL) degradation, 356, 358–359
Morphology
  aromatic-aliphatic block copolyester by atomic force microscopy, 237, 244, 245*f*
  degradation of poly(glycolide-*co*-L-lactide) (PGLL), 352, 359, 361, 362*f*, 363*f*, 364*f*, 365*f*
Multifilament braids. *See* Poly(glycolide-*co*-L-lactide) (PGLL)
Multifunctional polyester-based materials
  bacterial graft copolymers from poly(3-hydroxyoctanoate-*co*-9-carboxy-3-hydroxydecanoate) (PHOD), 144, 145*f*
  characteristics of PHO-*b*-PCL diblock copolyesters, 147*t*
  controlled drug delivery, 141
  copolyesters with pendant carboxylic groups (PHOD), 144, 145*f*
  design and properties of graft copolyester poly(3-hydroxyoctanoate-*co*-3-hydroxyundecenoate) (PHOU), 143–144
  design of polyhydroxyalkanoate (PHA)-based, 143–146
  diblock copolymer synthesis with poly(3-hydroxyoctanoate) (PHO) oligomer, 142
  experimental, 141–143
  functional polyesters by chemical modifications on PHOU, 145*f*
  instrumentation, 143
  nanostructure stability in presence of different salt concentrations as function of PHO-based structure, 146*f*
  PHO methanolysis, 141–142
  porous networks from partially hydrolyzable IPNs, 147–153
  synthesis and properties of block copolyesters, 146–147
  synthesis of PHO-*b*-PCL (poly(3-hydroxyoctanoate)-*b*-poly(ε-caprolactone) diblock copolymers, 147*f*
  See also Interpenetrating polymer networks (IPNs)
Municipal compost facility, biodegradation, 408
Municipal solid waste (MSW), typical distribution, 291, 292*f*
Municipal waste, packaging materials, 6–7

N

Natural polymers, biodegration, 405
Networks. *See* Interpenetrating polymer networks (IPNs);

Downloaded by 89.163.35.42 on August 9, 2012 | http://pubs.acs.org
Publication Date: September 23, 2006 | doi: 10.1021/bk-2006-0939.ix002

Mesoporous networks
Noncovalently assembled hydrogels
  formation and growth factor binding/release, 209–213
  See also Heparin-derivatized polymer hydrogels
Non-degradable plastics, laws and taxes, 6
Nuclear magnetic resonance (NMR)
  alizarin dye and oligoethoxylated product, 67, 68*f*
  bioplastics from chemically modified soy oil, 91, 92*f*, 93
  determination of PHA composition, 32
  polyhydroxyalkanoate (PHA) from *Escherichia coli*, 40*f*, 41*f*
  triblock stereoregular copolymer of poly(L-lactide) (PLA) and poly(ethylene oxide) (PEO), 159–160, 161*f*

O

Optical microscopy, emulsan-alginate microspheres (EAMs), 18, 19, 20*f*
Organic materials, terminology, 284–286
Oxidation agent, ozone, 78
Ozone
  catalytic ozonation process, 78–83, 93–94
  initial attach on double bond, 78*f*
  oxidation agent, 78
  ozonolysis of methyl oleate in sodium methoxide solution, 79*f*
  See also Catalytic ozonation

P

Packaging industry
  applications for polylactic acids (PLA), 108, 115
  biodegradable production, 4
  development of degradable biomedical materials, 10
  starch foam technology, 302*f*, 304
  worldwide production, 4
Paper products, applications for polylactic acids (PLA), 108
Partial least square (PLS) analysis, degradable polyethylene films with prooxidants, 314, 315*f*
Pendent functionalization
  acetylene functionality and click chemistry, 262–263
  aliphatic polyesters with, 255–256
  allyl, acetylene, and cyclopentene derivatives of δ-valerolactone, 260*f*
  allyl-functionalized ε-caprolactone (ε-CL), 256, 257*f*
  functionalized lactones for ring-opening polymerization, 256
  hydroxyl functionalized polyesters, 261
  lactone monomers with substitution α- to carbonyl group, 259–260
  oligopeptide-grafted polyesters, 263, 264*f*
  poly(ethylene glycol) (PEG) grafting, 261–262
  polymerization of allyl-functionalized ε-CL, 257, 258*f*
  protected hydroxyl and carboxyl monomers and deprotected polymers, 257, 259*f*
  See also Aliphatic polyesters; Functionalization
Pentaerythritol ethoxylate (PEE)
  ester bond linkage to poly(β-hydroxybutyrate (PHB), 62
  See also Poly(β-hydroxybutyrate) (PHB)
Permeation, polylactic acids (PLA) in packaging, 115
Petroleum, degradable materials from, 9–10
Photodegradation in polymers

Downloaded by 89.163.35.42 on August 9, 2012 | http://pubs.acs.org
Publication Date: September 23, 2006 | doi: 10.1021/bk-2006-0939.ix002

- agriculture, 385
- autooxidation mechanism for hydrocarbon materials, 386
- basic methods, 385
- built-in radical traps, 388
- distinctive M–M bond chromophore, 388
- effect of glass transition temperature (Tg) on efficiency, 392, 393*t*
- effect of trap concentration, 394–395
- experimental approach, 387–388
- experimental parameters affecting rates, 395–396
- ideal properties, 387
- incorporating ferrocene into polymer backbone, 389–390
- metal-metal bonds, 388, 389
- occurring in absence of oxygen, 390, 392
- photochemical degradation pathways for polymers with carbonyl groups, 386
- photochemical reaction of polymer with metal-metal bonds along backbone, 389
- photochemical reaction of PU-XX polymers, 392
- plasticulture, 385
- polymer synthesis strategy, 389–390
- quantum yields for polymers with different concentrations of metal-radical trap, 395*t*
- quantum yields for various polymers and model complex, 393*t*
- synthesis of PU-XX polymers, 390, 391
- weathering, 395

Physical pathways, polymer degradation, 3

Plastic materials
- applications, 3
- *See also* Biobased polymeric materials

Plasticulture, photodegradable plastics, 385

Plastic waste, landfill disposal vs. recycling, 6–7

Poly(acrylic acid) (PAA)
- blend solution preparation, 332–333
- description and blends, 331*t*
- physical parameters of, and blends, 337*t*
- polymer-solvent and polymer-polymer interaction coefficients, 339*t*
- retention diagram of PAA-pentane system, 341*f*
- *See also* Amylopectin (AP) and blends

Poly(ε-caprolactone) (PCL)
- blend solution preparation, 332–333
- description and blends, 331*t*
- polymer-solvent and polymer-polymer interaction coefficients, 339*t*
- retention diagram of 50:50% AP-PCL-acetate systems, 333, 334*f*
- X-ray diffraction (XRD) spectra of amylopectin, PCL, and blends, 335–336, 338*f*
- *See also* Amylopectin (AP) and blends; Poly(ethylene oxide)-*b*-poly(ε-caprolactone) (OCL) worm micelles; Poly(3-hydroxyoctanoate) (PHO)

Polyelectrolyte complexes (PECs)
- assays of 2,4,6-trinitrobenzene-1-sulfonic acid (TNBS), 272
- behavior of PEC fractions in presence of NaCl, 272–273, 274*f*
- dynamic light scattering (DLS) measurement, 271

Downloaded by 89.163.35.42 on August 9, 2012 | http://pubs.acs.org
Publication Date: September 23, 2006 | doi: 10.1021/bk-2006-0939.ix002

  enzymatic degradation, 272, 275, 276*f*
  enzyme sensitive poly(L-lysine) (PLL) and polyanions poly(L-lysine citramide) (PLCA) and poly(L-lysine citramide imide) (PLCAI), 268
  formation and stability, 268
  influence of addition order, 278
  influence of NaCl on interactions of polyanions with PLL, 272–273, 274*f*
  materials and methods, 269, 271–272
  molecular weight of PLCA components from PLL/PLCA, 278*t*
  molecular weights determination, 275, 277*f*
  PLCA, PLCAI and PLL chemical formulae, 270
  preparation of PEC fractions, 269, 271
  selective degradation of polycation component, 273, 275
  size exclusion chromatography (SEC) analysis, 271
  use of salted medium to breakdown PEC, 268

Polyester materials
  biodegradable polymers and manufacturers, 5*t*
  renewable resources for, 9
  See also Aromatic-aliphatic block copolyesters; Multifunctional polyester-based materials

Poly(ethylene glycol) (PEG)
  absorption spectra of purified recombinant aldehyde dehydrogenase (ALDH) from *Escherichia coli* harboring *pegC*, 376*f*
  aerobic metabolic pathway of PEG degradation, 368*f*
  comparison of substrate specificities of yeast ALDH and recombinant ALDH, 377*t*
  dot-blot hybridization and reverse transcription PCR (RT-PCR) of *peg* operon in strain 103, 372*f*, 373*f*
  exogenous degradation, 368–369
  expression of genes in conserved gene cluster in *Springomonas macrogoltabidus* sp. strain 103, 371, 374
  expression of PEG dehydrogenase (PEGDH), 375*f*
  gene cluster conserved in PEG-utilizing sphingomonads, 369, 371
  gene cluster of peg operon in *S. macrogoltabidus* sp. strain 103, 370*f*
  oligomer linkage to poly(β-hydroxybutyrate) (PHB), 62
  PEG-degradative gene cluster, 380, 382
  role of gene *pegC* conserved in *peg* operon, 374
  substrate specificity of recombinant ALCH against PEG-aldehyde, 376*f*
  See also Heparin-derivatized polymer hydrogels; Poly(ethylene oxide)-*b*-poly(ε-caprolactone) (OCL) worm micelles; Poly(β-hydroxybutyrate) (PHB); Poly(vinyl alcohol) (PVA); Thermo-sensitive gels

Poly(ethylene oxide)-*b*-poly(ε-caprolactone) (OCL) worm micelles
  cell culture, 171–172
  chain-end cleavage, 175
  cumulative production of PCL hydrolysis monomer 6-

Downloaded by 89.163.35.42 on August 9, 2012 | http://pubs.acs.org
Publication Date: September 23, 2006 | doi: 10.1021/bk-2006-0939.ix002

- hydroxycaproic acid (6-HPA), 175*f*
- degradation mechanism and kinetics of, 173–177
- drug delivery vehicles, 170
- end-cleavage of PCL within worm micelles, 176–177
- evaluation of OCL worm micelles for drug delivery, 178–180
- experimental, 170–173
- gel permeation chromatography (GPC) of OCL worm micelle degradation, 171
- GPC of OCL worm micelle at different degradation times, 173, 174*f*, 175
- hemolysis study, 172
- ^{1}H nuclear magnetic resonance (NMR), 171
- in-vitro compatibility with cultured cells and blood, 178
- in-vitro release of taxol from OCL worm micelles, 178–180
- OCL worm-to-sphere transition, 176*f*
- percentage caprolactone units in OCL with degradation, 175*f*
- preparation by cosolvent/evaporation method, 170
- self-assemblies of degradable copolymers, 169
- taxol loading, 172
- taxol loading into OCL worm micelles, 178
- taxol release, 172–173
- taxol release profiles, 179*f*
- thermal fluctuations of worm micelle, 173, 174*f*
- visualization of OCL worm micelles, 171

Poly(ethylene oxide) (PEO). *See* Poly(lactide)-poly(ethylene oxide)-poly(lactide) (PLA-PEO-PLA)

Poly(ethyleneoxyethylene terephthalate-*co*-adipate) (PEOETA)
- acid number determination, 243*t*
- gel permeation chromatography (GPC) traces of, before and after precipitation, 244*f*
- ^{1}H NMR assignments, 240*f*
- ring opening polymerization (ROP) of L-lactide (LLA) with PEOETA, 239, 244
- synthesis of PEOETA macroinitiator, 237–239
- *See also* Aromatic-aliphatic block copolyesters

Polyethylene (PE)
- chromatographic fingerprinting analysis, 310–311
- chromatographic fingerprinting of degradable films, 313
- designing to be degradable, 293
- films containing prooxidants, 310, 311
- lifetime of degradable PE films, 308–309
- problematic PE or PE-wax coated paper, 290
- relationship between dicarboxylic acid content in photodegradable, 311, 312*f*
- TLI analysis (total luminescence intensity), 310–311
- TLI and carbonyl index for PE films, 316*t*
- *See also* Degradation, early detection

Poly(glycolide-*co*-L-lactide) (PGLL)
- change of molecular weight during in vitro degradation, 356, 358*f*
- change of tensile breaking elongation as function of pre-load and in vitro time, 354, 355*f*

Downloaded by 89.163.35.42 on August 9, 2012 | http://pubs.acs.org
Publication Date: September 23, 2006 | doi: 10.1021/bk-2006-0939.ix002

  change of tensile breaking strength as function of pre-load and in vitro time, 353*f*
  change of tensile modulus as function of pre-load and in vitro time, 353, 354*f*
  effect of pre-load on tensile properties, 352–354
  effect of temperature on tensile properties, 355–356
  effects of temperature on breaking elongation during in vitro degradation, 357*f*
  effects of temperature on breaking strength during in vitro degradation, 356*f*
  effects of temperature on modulus during in vitro degradation, 357*f*
  elongation as function of Mw for polymer braid during degradation, 360*f*
  experimental, 351–352
  in vitro degradation studies, 350–351
  medical uses, 350
  modulus as function of Mw for polymer braid during degradation, 360*f*
  morphology change during degradation, 359, 361
  multifilament braid, 351
  relationship between molecular weight and tensile properties, 356, 358–359
  strength as function of Mw for polymer braid during degradation, 359*f*
  surface morphology of braid samples during degradation, 362*f*, 363*f*, 364*f*, 365*f*
Poly(hydroxy acids) (PHAs)
  applications, 127
  eco-friendly biocatalytic synthesis, 129–130
  lipase-catalyzed synthesis of PHA esters, 131–133, 137
  lubricant-related properties, 129*t*
  pentaerythritol (PE)- and dimer diol (DD)-poly(ricinoleic acid) (pRA) star polymers, 132*f*
  selected hydroxy fatty acids from nature, 128*t*
  See also Ricinoleic acid polymers
Polyhydroxyalkanoates (PHAs)
  alternatives to petroleum-based plastics, 31
  bacterial strains, plasmids, and culture conditions for PHA production, 31–32
  biomedical applications, 34
  classifying medium-chain-length (MCL) as elastomers, 31
  classifying short-chain-length (SCL) as thermoplastics, 31
  copolymer poly(3-hydroxybutyrate-*co*-4-hydroxybutyrate) [P(3HB-*co*-4HB)], 34
  copolymer poly(3-hydroxybutyrate-*co*-3-hydroxyvalerate) [P(3HB-*co*-3HV)], 34
  determination of PHA polymer composition by nuclear magnetic resonance (NMR), 32
  differential scanning calorimetry (DSC) endotherm profiles for P(3HB) homopolymer and copolymer, 39, 42*f*
  Escherichia coli model strain for PHA production, 31
  experimental, 31–32
  fatty acid biosynthesis, 36*f*, 38
  gel permeation chromatography (GPC) analysis, 32
  3HB as common SCL monomer, 33*t*, 34
  incorporation of MCL monomers into PHA, 36

  MCL-PHA from recombinant *E. coli*, 37*t*
  MCL-PHA monomer supplying pathways, 36*f*
  MCL-PHA production from non-related carbon sources, 36*f*
  molecular weight by GPC, 39
  new natural polymers, 405
  NMR spectra of SCL-MCL PHA polymer, 40*f*, 41*f*
  P(3HB) monomer supply, 35*f*
  P(3HV) monomer supply, 35*f*
  P(4HB) monomer supply, 35*f*
  physical characterization of SCL-MCL PHA copolymer, 38–39
  production from non-related carbon sources in recombinant *E. coli*, 32–38
  SCL-PHA from recombinant *E. coli*, 33*t*
  SCL-PHA production, 35*f*
  thermal property determination of SCL-MCL PHA polymers by recombinant *E. coli*, 32
  tricarboxylic acid cycle, 35*f*
  See also Biodegradable materials; Multifunctional polyester-based materials; Poly(β-hydroxybutyrate) (PHB); Poly[(R)-3-hydroxybutyrate-*co*-(R)-3-hydroxyvalerate]

Poly(β-hydroxybutyrate) (PHB)
  alizarin dye and oligoethoxylated product, 67, 68*f*
  atomic force microscopy (AFM) experiments, 66
  contact angle measurements, 67
  crystallization, 69–73
  description of investigated samples, 66*t*
  ester bond linkage of pentaerythritol ethoxylate (PEE) to, 62*f*
  experimental, 63–67
  fermentation of PHB in presence of dye, 67, 69
  formation of various ω-hydroxy-oligoethoxy-9,10-anthraquinones, 64*f*
  gel permeation chromatography (GPC) for molecular weight analysis, 65–66
  ^{1}H NMR spectrum of PEE-modified PHB, 69*f*
  initiation and growth of modified PHB spherulites, 69
  isothermal crystallization, 70
  isothermal crystallization by AFM, 71, 72*f*
  light microscope for annealing experiments, 67
  materials, 63–64
  modification of PHB during fermentation, 67
  observing crystallization process in polarized light microscope, 71, 72*f*
  polymer analyses, 65–67
  small-angle X-ray scattering (SAXS) analysis of, and PEE modified, 66, 70, 71*f*
  surface tension studies, 73
  synthesis of block copolymers, 64–65
  UV-vis spectrum of colored PHB, 70*f*
  water contact angle and surface tension, 73*t*

Poly[(R)-3-hydroxybutyrate-*co*-(R)-3-hydroxyvalerate]
  Biopol™, 46
  crystallinity of films, 50*t*
  crystal orientation of films, 50*f*, 50*t*
  effect of storage time on film mechanical properties, 56
  enzymatic degradation, 48, 56, 57*f*
  experimental, 46–49
  materials, 46–47
  mechanical properties of films, 50*t*

Downloaded by 89.163.35.42 on August 9, 2012 | http://pubs.acs.org
Publication Date: September 23, 2006 | doi: 10.1021/bk-2006-0939.ix002

Downloaded by 89.163.35.42 on August 9, 2012 | http://pubs.acs.org
Publication Date: September 23, 2006 | doi: 10.1021/bk-2006-0939.ix002

- microbeam X-ray diffraction, 48
- microbeam X-ray fiber diagrams, 53, 55*f*
- processing of fibers with high tensile strength, 47
- processing of films with high tensile strength, 47
- scanning electron microscopy (SEM), 49
- SEM of film after partial enzymatic degradation, 57*f*, 58
- small-angle X-ray scatterings (SAXS) of films, 48, 50, 51*f*
- small- (SAXS) and wide-angle (WAXD) X-ray diffraction, 48
- stress-strain test, 47–48
- structure and mechanical properties of fibers, 52
- structure and mechanical properties of films, 49–50
- tensile strength of films, 50*f*
- WAXD and SAXS patterns of fibers, 52, 54*f*, 55*f*
- WAXD and SAXS patterns of films, 51*f*

Poly(3-hydroxybutyric acid) (PHBA)
- blend solution preparation, 332–333
- description and blends, 331*t*
- physical parameters of, and blends, 337*t*
- *See also* Amylopectin (AP) and blends

Poly(2-hydroxyethyl methacrylate) (polyHEMA)
- atom transfer radical polymerization (ATRP) of HEMA, 186–187
- experimental, 186–189
- kinetics and molecular weight evolution of ATRP of HEMA, 190, 191*f*
- preparation of degradable, by ATRP, 191*f*
- size exclusion chromatography (SEC) traces, 192*f*
- synthesis of degradable linear polyHEMA, 189–190
- *See also* Atom transfer radical polymerization (ATRP)

Poly(3-hydroxyoctanoate) (PHO)
- block copolyester of PHO and poly(ε-caprolactone) (PCL), 146–147
- characteristics of PHO-*b*-PCL diblock copolyesters, 147*t*
- design of graft copolyester poly(3-hydroxyoctanoate-*co*-3-hydroxyundecenoate) (PHOU), 143–144
- diblock copolymer synthesis, 142
- functional polyester design by chemical modification on PHOU, 145*f*
- methanolysis, 141–142
- PHO-*b*-PCL synthesis from PHO oligomers, 147*f*
- poly(3-hydroxyoctanoate-*co*-9-carboxy-3-hydroxydecanoate) (PHOD), 144, 145*f*
- *See also* Multifunctional polyester-based materials

Polyisoprene, natural degradable polymers, 7

Polylactic acids (PLA)
- aluminum alkoxides catalysts and initiators for PLA polymerization, 111
- applications, 107–108
- architectural variations, 112–113
- assessing environmental impact, 105, 106*f*
- attention for degradability, 235
- block copolymers, 112–113
- chain extension of oligomeric PLA, 109
- commercial route to biobased PLA, 104*f*

Downloaded by 89.163.35.42 on August 9, 2012 | http://pubs.acs.org
Publication Date: September 23, 2006 | doi: 10.1021/bk-2006-0939.ix002

condensation polymerization, 109–110
coordination insertion mechanism, 111
extrusion coating of paper products, 108
fibers, 108
fundamental chain properties, 113
highly branched polymers, 113
history of development, 103
lactide formation, 109–110
life cycle analysis for energy content, 105, 106*f*
mechanisms for lactide polymerization, 110–111
medical applications, 107
packaging, 108
permeation properties, 115
physical properties, 105, 107
potential as commodity polymer, 103
processing properties, 114
process with corn as feedstock, 103, 104*f*, 105
random copolymers, 112
renewable resources, 9
ring-opening polymerization, 109, 112–113, 235
single-site catalysts, 112
synthesis, 109–112
tin octoate as coordination insertion catalyst, 111
types of lactide and corresponding polymers, 110*f*
See also Aromatic-aliphatic block copolyesters; Bioplastics

Poly(DL-lactide-*co*-glycolide) (PLG)
blend solution preparation, 332–333
description and blends, 331*t*
physical parameters of, and blends, 337*t*
See also Amylopectin (AP) and blends

Poly(lactide) (PLA). *See* Amylopectin (AP) and blends; Interpenetrating polymer networks (IPNs); Poly(glycolide-*co*-L-lactide) (PGLL); Thermo-sensitive gels

Poly(lactide)–poly(ethylene oxide)–poly(lactide) (PLA–PEO–PLA)
aging of, 164, 166
amphiphilic block copolymers, 157
block copolymer synthesis, 159–160
characterization and instrumentation, 159
differential scanning calorimetry (DSC) analysis for L copolymers with different PLLA block lengths, 160, 163*f*
DSC of stereorandom copolymer, 160, 164*f*
^{1}H NMR spectrum of stereoregular PLLA–PEO–PLLA, 161*f*
materials, 157–158
materials and methods, 157–159
molecular weight characterization, 161*t*
synthesis with DL-lactide or L-lactide, 158
thermal properties, 160
thermogravimetric analysis (TGA), 160, 162*f*
wide-angle X-ray diffraction of freshly precipitated and aged, 159, 164, 165*f*

Poly(L-lactide) (PLLA). *See* Aromatic-aliphatic block copolyesters

Poly(L-lysine citramide imide) (PLCAI)
chemical formula, 270
molecular weight determination, 275, 277*f*
selected polyanion, 268–269
See also Polyelectrolyte complexes (PECs)

Poly(L-lysine citramide) (PLCA)
  chemical formula, 270
  molecular weight determination, 275, 277*f*
  molecular weight of PLCA components, 278*t*
  selected polyanion, 268–269
  See also Polyelectrolyte complexes (PECs)
Poly(L-lysine) (PLL)
  chemical formula, 270
  enzyme sensitive polycation, 268–269
  See also Polyelectrolyte complexes (PECs)
Polymer blends
  analysis, 324–326
  free energy of mixing, 325
  interaction parameters, 324, 326
  specific retention volume, 324
  See also Amylopectin (AP) and blends
Polymer hydrogels. *See* Heparin-derivatized polymer hydrogels
Polymeric materials
  connection between molecular, macromolecular and macroscopic scale changes, 311, 312*f*
  See also Biobased polymeric materials; Photodegradation in polymers
Polymer industries, biodegradable polymers, 401
Polymer-polymer interaction parameters, amylopectin (AP) and blends, 336, 340
Polymer-solute interaction parameters, amylopectin (AP) and blends, 336
Poly(methyl methacrylate) (PMMA). *See* Interpenetrating polymer networks (IPNs)
Poly(methyl methacrylate) (PMMA)-based gels
  atom transfer radical polymerization (ATRP), 192, 194*f*
  bromide end groups remaining intact, 192, 195
  functional degradable, by ATRP in miniemulsion, 196, 198*f*
  gel by extension with styrene (Sty), 192, 195*f*
  preparation of degradable, and use as "supermacroinitiators", 194*f*
  products of reductive degradation by 2D chromatography, 195–196, 197*f*
  reductive degradation of PMMA-based latex, 196, 198*f*
  size exclusion chromatography (SEC) traces of products of reductive degradation of disulfide-containing "supermacroinitiator" gel, 195*f*
  See also Atom transfer radical polymerization (ATRP)
Polyphenols, natural degradable polymers, 7
Polysaccharides, natural degradable polymers, 7–8
Poly(vinyl alcohol) (PVA)
  alignment of deduced amino acid sequences of oxidized PVA hydrolase (OPH), 381*f*
  endogenous degradation mechanism, 368–369
  gene organization of cloned regions, 380*f*
  gene structure of PVA-degradative operon in strain 113P3, 378, 380
  localization of OPH and PVA dehydrogenase (PVADH) in *Springomonas* sp. strain 113P3, 378*t*
  metabolic pathway of PVA degradation, 369*f*

Downloaded by 89.163.35.42 on August 9, 2012 | http://pubs.acs.org
Publication Date: September 23, 2006 | doi: 10.1021/bk-2006-0939.ix002

Downloaded by 89.163.35.42 on August 9, 2012 | http://pubs.acs.org
Publication Date: September 23, 2006 | doi: 10.1021/bk-2006-0939.ix002

  purification and characterization of oxidized PVA hydrolase (OPH), 374, 378, 379*f*
Porous networks. *See* Interpenetrating polymer networks (IPNs)
Prediction
  early degradation, by total luminescence intensity, 314, 316
  See also Degradation, early detection
Pre-loading. *See* Poly(glycolide-*co*-L-lactide) (PGLL)
Principal component analysis (PCA), prooxidant system by PCA model, 313–314
Processing, polylactic acids (PLA), 108, 114
Prodegradants, biodegradation of polyethylene, 408–409
Production, biodegradable materials, 4
Prooxidants
  dicarboxylic acids in photodegradable polyethylenes, 311, 312*f*
  partial least square model of, in polyethylene films, 314, 315*f*
  photo- and thermo-oxidation of polyethylene films, 311, 313
  See also Degradation, early detection
1,3-Propanediol, building block for Sorona polyester, 9
Protein delivery
  combining alginate with emulsan, 15, 17
  See also Emulsan-alginate microspheres (EAMs); Heparin-derivatized polymer hydrogels
Proteins, natural degradable polymers, 7

Q

Quantum yields photodegradation in polymers, 393*t*, 395*t*

R

Radical traps
  built-in radical traps, 388
  concentration effect, 394–395
  mixing radical initiator into polymer, 385
  See also Photodegradation in polymers
Random copolymers, polylactic acids (PLA), 112
Recycling
  biodegradable polymers, 400
  disposal of fabrication polymers, 399–400
  plastic waste, 6
Regulatory authorities, biodegradable polymers, 401
Renewable resources
  approaches, 8
  poly(lactic acid), 9
  polymers from, 8–9
  Sorona polyester, 9
  vegetable oils, 77
Retention diagrams, amylopectin (AP) and polymer blends, 333–336
Ricinoleic acid polymers
  Andrade Equation plot, 133, 134*f*
  catalysis by lipase from *Candida antarctica* (CAL), 130
  current research on copolymers, 133–136
  elongation of pRA by ω-pentadecyl lactone or lauric acid, 135*f*
  future research, 137
  GPC chromatograms of CAL-catalyzed polymerization of

Downloaded by 89.163.35.42 on August 9, 2012 | http://pubs.acs.org
Publication Date: September 23, 2006 | doi: 10.1021/bk-2006-0939.ix002

    homopolymers and copolymers, 136*f*
  hydroxy fatty acids from nature, 128*t*
  oligomers as biolubricants, 127–129
  plot of molecular weight vs. viscosity, 134*f*
  reaction of RA and pRA with pentadecyl lactone (PDL) and lauric acid, 135*t*
  See also Poly(hydroxy acids) (PHAs)
Ring opening polymerization (ROP)
  aliphatic polyesters by, 249, 251*f*
  lactide, 109, 112–113, 235
  See also Aromatic-aliphatic block copolyesters

S

Safety
  biodegradation, 402
  standard criteria, 295
Scanning Brookfield technique (SBT), soy-based lubricants, 86–87
Scanning electron microscopy (SEM), emulsan-alginate microspheres (EAMs), 18, 19, 21*f*
Self-assembly
  amphiphilic block copolymers, 169–170
  See also Poly(ethylene oxide)-*b*-poly(ε-caprolactone) (OCL) worm micelles
Semicrystalline polymer-containing blends, analysis, 326–328
Short-chain-length polymers. *See* Polyhydroxyalkanoates (PHAs)
Small-angle X-ray diffraction. *See* X-ray diffraction
Solution-spun fibers, polylactic acids (PLA), 108, 114
Sorona polyester, renewable resources, 9
Soybean
  U.S. production and consumption, 77
  See also Catalytic ozonation
Soybean oil modifications
  approaches for improving, 83–84
  bioplastics from chemically modified soy oil, 88–93
  catalytic ozonation process, 78–83
  catalytic ozonation with di- and tri-alcohols, 89–90
  catalytic ozonolysis of triglycerides in presence of alcohol, 84*f*
  ^{13}C NMR of soy oil and soy polyol, 91, 92*f*
  cold flow properties, 87*f*
  consumption of double bonds during ozonolysis, 86*f*
  Fourier transform infrared (FTIR) spectra of soy oil and soy polyol, 91, 92*f*
  friction and wear by modified Falex pin and V-block test, 87–88
  lubrication properties, 86–88
  methods for polyols from vegetable oils, 88–89
  partial infrared spectrum for double bond disappearance, 85*f*
  possible inter- and intramolecular side reactions, 90*f*
  preparation of soy polyol by catalytic ozonation in ethylene glycol, 90*f*
  scanning Brookfield technique (SBT), 86–87
  schematic of ozonolysis process, 82*f*
  statistical analysis of product mixture, 90–91
  thermally stable lubricant from, 85*f*
  thermally stable soy-based lubricants, 83–88

- thermo-oxidation engine oil simulation test (TEOS), 86
- typical procedure, 82–83
- wear plot of modified soy oil, 88*f*
- *See also* Biodiesel, soy-based

Soy polyol. *See* Bioplastics

Specific retention volume, polymer blends, 324

Stability, ozone treated biodiesel, 96, 97*f*

Standards, biodegradable plastics, 295, 296*f*

Standards organizations, biodegradable polymers, 401

Standard testing
- biodegradation testing, 407
- carbon dioxide evolution, 407–408
- degradation of polyethylene (PE) with prodegradants, 408–409
- development, 406–409
- *See also* Biodegradable materials

Starch
- biodegradable, esters, 300
- bioplastics, 298–299
- closed cell structure of foams, 301*f*
- foam crafts and toys, 303*f*
- foam sheets for protective cushion packaging, 302*f*
- foam technology, 301, 304
- indicator product analysis of blends with polyethylene or ethylene vinyl acetate (EVA) copolymer, 309–310
- reactive blend compositions, 299*f*
- structure of polymers, 298*f*
- thermal behavior and phase morphology of starch-blend systems, 322–323
- *See also* Amylopectin (AP) and blends; Degradation, early detection

Stereoblocks, polylactic acids (PLA), 112

Storage, poly[(R)-3-hydroxybutyrate-*co*-(R)-3-hydroxyvalerate] films, 56

Stress-strain testing
- poly[(R)-3-hydroxybutyrate-*co*-(R)-3-hydroxyvalerate] fibers, 52
- poly[(R)-3-hydroxybutyrate-*co*-(R)-3-hydroxyvalerate] films, 49, 50*f*
- poly[(R)-3-hydroxybutyrate-*co*-(R)-3-hydroxyvalerate] films and fibers, 47–48
- poly[(R)-3-hydroxybutyrate-*co*-(R)-3-hydroxyvalerate] films and storage, 56

Supermacroinitiators
- chain extension of disulfide-containing poly(methyl methacrylate) PMMA-based, gel with styrene, 187
- 2-dimensional chromatography of PMMA-based, gel, 197*f*
- preparation of degradable PMMA-based gels, 192, 194*f*
- *See also* Atom transfer radical polymerization (ATRP); Poly(methyl methacrylate) (PMMA)-based gels

Surface energy
- amylopectin (AP) and blends, 345
- polymers, 328–330

Surface morphology
- degradation of poly(glycolide-*co*-L-lactide) (PGLL), 352, 359, 361, 362*f*, 363*f*, 364*f*, 365*f*
- emulsan-alginate microspheres (EAMs), 19, 20*f*, 21*f*

Surface tension, polymer samples, 73

Sustainability, biobased polymeric materials, 283

Downloaded by 89.163.35.42 on August 9, 2012 | http://pubs.acs.org
Publication Date: September 23, 2006 | doi: 10.1021/bk-2006-0939.ix002

Downloaded by 89.163.35.42 on August 9, 2012 | http://pubs.acs.org
Publication Date: September 23, 2006 | doi: 10.1021/bk-2006-0939.ix002

T

Taxol
  degradable poly(ethylene glycol)-*b*-poly(ε-caprolactone) (OCL) worm micelles for delivery, 178–180
  loading into OCL worm micelles, 172, 178
  release from worm micelles, 172–173
  release profiles from worm micelles, 179*f*
  in vitro release from OCL worm micelles, 178–180
  See also Poly(ethylene oxide)-*b*-poly(ε-caprolactone) (OCL) worm micelles
Temperature
  tensile properties of poly(glycolide-*co*-L-lactide) (PGLL) degradation, 355–356, 357*f*, 358*f*
  See also Poly(glycolide-*co*-L-lactide) (PGLL)
Tensile properties
  effects of pre-load on poly(glycolide-*co*-L-lactide) (PGLL) degradation, 352–354, 355*f*
  effects of temperature on PGLL degradation, 355–356, 357*f*, 358*f*
  elongation as function of Mw, 360*f*
  modulus as function of Mw, 360*f*
  molecular weight and, during PGLL degradation, 356, 358–359
  strength as function of Mw, 359*f*
  See also Poly(glycolide-*co*-L-lactide) (PGLL)
Terminology, biobased materials, 284–287
Thermogravimetric analysis (TGA)
  ozone treated and untreated biodiesel, 95, 96*f*
  triblock copolymer of poly(lactide) (PLA) and poly(ethylene oxide) (PEO), 160, 162*f*
Thermo-oxidation engine oil simulation test (TEOS), soy-based lubricants, 86
Thermoplastic polymers, life cycle analysis, 105, 106*f*
Thermo-sensitive gels
  ABA poly(L-lactide)–poly(ethylene glycol)–poly(L-lactide) (PLLA–PEG–PLLA) micellar solutions and temperature, 221, 222*f*
  AB micellar solutions of PLLA–PEG, 226, 227*f*
  atomic force microscopy of enantiomeric mixture of PLLA–PEG and poly(D-lactide)–PEG (PDLA–PEG) diblock copolymers, 230
  BAB triblock (PEG–PLLA–PEG and PEG–PDLA–PEG) micellar solutions, 223, 224*f*, 225
  biomedical materials, 217
  gelation mechanism, 227, 229
  hydrogels from AB-diblock copolymers, 225–226
  hydrogels from BAB triblock copolymers, 223, 225
  hydrogels from micellar solutions of ABA triblock copolymers, 220–221
  hydrogels from mixtures of enantiomeric PLA–PEG block copolymers, 219–230
  hydrogels from PLA-*b*-PEG, 218–219
  mechanistic aspect of enantiomeric PLA-*b*-PEG hydrogels, 227–230
  molecular weight of typical block copolymers, 220*t*

Downloaded by 89.163.35.42 on August 9, 2012 | http://pubs.acs.org
Publication Date: September 23, 2006 | doi: 10.1021/bk-2006-0939.ix002

- phase diagram of mixed micellar solutions of PEG–PLLA–PEG and PEG–PDLA–PEG, 223*f*
- phase diagram of mixed micellar solutions of PLLA–PEG–PLLA and PDLA–PEG–PDLA, 221*f*
- phase diagram of mixed micelle solution of PLLA–PEG and PDLA–PEG, 226*f*
- PLA–PEG block copolymer synthesis and gel formation, 219–220
- polymer structures and schematics of micelles in aqueous medium, 218*f*
- proposed gelation mechanism of enantiomeric mixture of ABA triblock copolymers, 227*f*
- proposed gelation mechanisms of enantiomeric mixture of BAB triblock and AB diblock copolymers, 228*f*
- temperature-dependent wide-angle X-ray scattering (WAXS) of ABA triblock, 221, 222*f*

Time frame, degradability, 2–3
Time release, tracer molecules retained or absorbed in microspheres, 22, 23*f*
Tin octoate, polymerization of polylactic acids (PLA), 111
Total luminescence intensity (TLI)
- analysis method, 310–311
- comparing early degradation detection techniques, 317
- early degradation state prediction and classification, 314, 316
- hydroperoxide content with aging, 308
- polyethylene films, 316*t*

Triblock copolymers. *See* Poly(lactide)–poly(ethylene oxide)–poly(lactide) (PLA–PEO–PLA); Thermo-sensitive gels
Tricarboxylic acid cycle, short-chain-length polyhydroxyalkanoate production, 35*f*
Trypsin for degradation. *See* Polyelectrolyte complexes (PECs)
Turbidity, calculation using Beer–Lambert law, 148–149

U

United States, plastics production, 4

V

δ-Valerolactone (δ-VL), ring opening polymerization (ROP), 249, 251*f*
Vegetable oil, renewable biomaterials, 77

W

Waste management of polymers
- biodegradable polymers, 399–401
- developing biodegradable
  - polymers, 401–402

Waste water/sewage treatment, biodegradable or recyclable products, 290
Water contact angles, polymer samples, 73*t*
Wautersia eutropha
- fermentation, 63
- *See also* Poly(β-hydroxybutyrate) (PHB)

Wear, soy-based lubricants, 87–88
Weathering, polymer materials, 395
Wide-angle X-ray diffraction
- aged and fresh triblock copolymer of poly(lactide) (PLA) and poly(ethylene oxide) (PEO), 159, 164, 165*f*

See also X-ray diffraction
Worldwide production, plastics, 4
Worm micelles. *See* Poly(ethylene oxide)-*b*-poly(ε-caprolactone) (OCL) worm micelles

X

X-ray diffraction
poly[(R)-3-hydroxybutyrate-*co*-(R)-3-hydroxyvalerate] fibers by micro-beam, 53, 55*f*
poly[(R)-3-hydroxybutyrate-*co*-(R)-3-hydroxyvalerate] fibers by wide- and small-angle, 52, 54*f*, 55*f*
poly[(R)-3-hydroxybutyrate-*co*-(R)-3-hydroxyvalerate] films by wide- and small-angle, 48, 49–50, 51*f*

Downloaded by 89.163.35.42 on August 9, 2012 | http://pubs.acs.org
Publication Date: September 23, 2006 | doi: 10.1021/bk-2006-0939.ix002